Beiträge zur *Zintl*-Chemie der Elemente der 6. Periode im Festkörper und in Lösung

Kumulative Dissertationsschrift

zur Erlangung des akademischen Grades eines
Doktors der Naturwissenschaften
(Dr. rer. nat.)

dem
Fachbereich Chemie der Philipps-Universität Marburg
(Hochschulkennziffer 1180)
vorgelegt von

Niels Lichtenberger, M. Sc.
aus Bremen

Marburg, 2018

Erstgutachterin:	Prof. Dr. Stefanie Dehnen
Zweitgutachter:	Prof. Dr. Michael Gottfried
Promotionsverfahren eröffnet:	23.11.2018
Annahme der Dissertation:	18.12.2018
Disputationstermin:	19.12.2018

A philosopher once said:
'It is necessary for the very existence of science that the same conditions always produce the same results.'
Well, they do not.

Richard P. Feynman

Lizenzierung

Inhaltsverzeichnis

Tabellenverzeichnis

Abbildungsverzeichnis

Abkürzungsverzeichnis

μ-RFA	Micro-Röntgenfluoreszenzanalyse
A	Alkalimetall
cod	1,5-Cyclooctadien
cp	Cyclopentadienyl-Anion $(C_5H_5)^-$
cp*	Pentamethylcyclopentadienyl-Anion $(C_5Me_5)^-$
DMF	*N,N*-Dimethylformamid
EA	Erdalkalimetall
E	p-Block-Element
en	Ethylendiamin
ESI-MS	Elektrospray-Ionisations-Massenspektrometrie
GA	genetischer Algorithmus
GE	Gerüstelektronen
I	Kernspin
18-Krone-6	1,4,7,10,13,16-Hexaoxacyclooctadekan
Krypt-222	4,7,13,16,21,24-Hexaoxa-1,10-diazabicyclo[8.8.8]hexacosan
LMO	lokalisiertes Molekülorbital
MPA	Mulliken-Populationsanalyse
n	Atomanzahl
NMR	Kernmagnetische Resonanz
NPA	Natural Population Analysis
PABOON	Population Analysis Based on Occupation Numbers
Pn	Pnictogen/Pentelelement

q . . . . . .Ladung

RP . . . . . .Neuzuordnung von Atompositionen durch Störungstheorie

seq . . . . . .Sequestrierungsmittel

THF . . . . . .Tetrahydrofuran

Tr . . . . . .Trielelement

Tt . . . . . .Tetrelelement

VE . . . . . .Valenzelektronen

ZKB-Konzept . *Zintl-Klemm-Busmann*-Konzept

Erklärung

Ich erkläre, dass eine Promotion noch an keiner anderen Hochschule als an der Philipps-Universität Marburg, Fachbereich Chemie, versucht wurde.

Ich versichere, dass ich meine vorgelegte Dissertation:

„Beiträge zur *Zintl*-Chemie der Elemente der 6. Periode im Festkörper und in Lösung“

selbst und ohne fremde Hilfe verfasst, nicht andere als die in ihr angegebenen Quellen oder Hilfsmittel benutzt, alle vollständig oder sinngemäß übernommenen Zitate als solche gekennzeichnet sowie die Dissertation in der vorliegenden oder einer ähnlichen Form noch bei keiner anderen in- oder ausländischen Hochschule anlässlich eines Promotionsgesuchs oder zu anderen Prüfungszwecken eingereicht habe.

Marburg, 8. Januar 2019 Niels Björn Lichtenberger

Erstgutachterin:	Prof. Dr. Stefanie Dehnen
Zweitgutachter:	Prof. Dr. Michael Gottfried
Promotionsverfahren eröffnet:	23.11.2018
Annahme der Dissertation:	18.12.2018
Disputationstermin:	19.12.2018

Die vorliegende Arbeit wurde im Zeitraum von Dezember 2013 bis Dezember 2018 unter der Leitung von Prof. Dr. Stefanie Dehnen am Fachbereich Chemie der Philipps-Universität Marburg angefertigt.

1 Einleitung

1.1 Die p-Block-Elemente der 6. Periode

Im Rahmen dieser Arbeit wurden unterschiedlichste Elemente der Gruppen 13 bis 15 für die Studien eingesetzt, wobei der größte Anteil der dargestellten Verbindungen mindestens ein Atom eines Elements der 6. Periode, also Thallium, Blei oder Bismut enthielt. Aus diesem Grund sollen im Folgenden einige Eigenschaften dieser Elemente zunächst näher betrachtet werden, bevor in Kapitel 1.2 eine allgemeine Einleitung in die *Zintl*-Chemie und im Anschluss daran in Kapitel 1.3 in intermetalloide und heterometallische Cluster gegeben wird.

1.1.1 Thallium

Dsa Element Thallium ist das schwerste stabile Element der Gruppe 13 und ist hauptsächlich aufgrund seiner Giftigkeit bekannt.[1] Der Name Thallium stammt aus dem altgriechischen $\theta\alpha\lambda\lambda\acute{o}\varsigma$ („thallus“) für „grüner Zweig“, welchen das Element seiner charakteristischen grünen Spektrallinie wegen erhielt. Es findet im Vergleich zu seinen leichteren Homologen wenig Anwendung, hat jedoch einige Applikationen in Spezialbereichen. Die Giftigkeit beruht auf der Ähnlichkeit der Ionenradien von Tl^+ und K^+ bei gleichzeitiger Präferenz der Oxidationsstufe +1 des Tl unter physiologischen Bedingungen. So wird elementares Tl schnell in Gegenwart von Luft und Wasser zu TlOH oxidiert, während Tl(III)-Verbindungen leicht reduziert werden.

Elementares Tl wird entweder unter Wasser oder trockenem Argon aufbewahrt. In Wasser bildet sich in Gegenwart von Sauerstoff TlOH, welches wasserlöslich ist und durch Waschen mit entgastem Wasser leicht entfernt werden kann. Anschließendes Trocknen in inerter Atmosphäre liefert dann das reine Metall. Die Gewinnung erfolgt großtechnisch aus den Röstgasen von Blei- und Zinkhütten, wobei es zunächst als Tl_2SO_4 anfällt. Dieses wird in TlCl überführt, welches sich zur elektrolytischen Gewinnung des reinen Metalls eignet.

Ein Aspekt, der Tl insbesondere für biochemische Forschungen interessant macht, ist die Isotopenzusammensetzung. Thallium kommt mit den Isotopen ^{203}Tl (29.5%) und ^{205}Tl (70.5 %) in der Natur vor, welche die einzigen stabilen Isotope dieses Elements darstellen. Beide Atomkerne sind NMR-aktiv (NMR: Kernmagnetische Resonanz), haben einen Kernspin von $I = +1/2$ und weisen äußerst hohe Empfindlichkeiten auf.[2] Aufgrund der Ähnlichkeit zu K^+-Ionen kann somit die Rolle dieser durch Substitution mit Tl^+ in biologischen Systemen durch NMR-Spektroskopie verfolgt werden. Eine große Herausforderung stellt in diesem Bereich allerdings das extrem große spektrale Fenster dar, in dem Tl-Verbindungen beobachtet werden. Neben der hauptsächlich auftretenden Oxdiationsstufe +I kommt das Element weiterhin in den Oxidationsstufen +II und +III vor, wobei Tl(II)-Verbindungen exotischer sind und spezielle Ligandensysteme zur Stabilisierung erfordern.[3]

Ähnlich wie seine leichteren Homologen kann Tl zudem reduziert werden, wonach es in den formalen Oxidationsstufen −I und −II vorliegt. Eine der vermutlich bekanntesten Verbindungen, in der Tl-Atome eine negative Ladung tragen, ist das NaTl. Hierbei handelt es sich um einen Prototyp der *Zintl*-Phasen, die oftmals als Lehrbuchbeispiel für die Erklärung des *Zintl-Klemm-Busmann*-Konzepts (auch Pseudo-Elementkonzept) herangezogen wird (siehe Kapitel 1.2.2). Die formal vorliegenden Tl^--Ionen sind isovalenzelektronisch zu Kohlenstoff und bilden dementsprechend ein Diamantgitter, in dessen Lücken die Na^+-Ionen eingebaut sind. Neben dieser ausgedehnten Festkörperstruktur weist Tl zudem die Fähigkeit auf isolierte Clusteranionen im Festkörper zu bilden.[4] Bislang wurde über die Charakterisierung der Anionen Tl_4^{8-}, Tl_5^{7-}, Tl_6^{6-}, Tl_6^{8-}, Tl_7^{7-}, Tl_9^{9-} und Tl_{11}^{7-} berichtet. Zudem existiert eine Reihe substituierter und intermetalloider Cluster. Allen ist gemein, dass diese eine extrem hohe Ladung aufweisen, die nur durch enge Kationen-Anionen-Kontakte mit entsprechenden Alkalimetallen stabilisiert werden können. Diese Verbindungsklasse erinnert stark an die elektronendefizitären Cluster der Gruppe 14, es fehlen jedoch bis zu acht Gerüstelektronen (GE, $2n - 6$) zur Erfüllung der entsprechenden Elektronenzahlen (siehe Kapitel 1.2.2). Dies äußert sich in den beobachteten Clustergeometrien, welche sich häufig von typischen Wade-Clustern unterscheiden.

1.1.2 Blei

Das Element Blei ist der Menschheit bereits seit ungefähr 6400 v. Chr. bekannt und wurde schon früh zur Herstellung von Gegenständen verwendet.[1a, 5] Der deutsche Name leitet sich aus dem indogermanischen Wort *bhlei* ab, was mit schim-

mern, glänzen oder leuchten zu übersetzen ist. Sein Elementsymbol *Pb* erhielt das Element durch seinen latenischen Namen *plumbum*, was eigentlich eine Sammelbezeichnung für weiche Metalle war. Es wurde zwischen *plumbum nigrum* (schwarzes Blei: Pb) und *plumbum candidum* oder *plumbum album* (weißes Blei: Sn) unterschieden.

Blei besitzt vier natürlich vorkommende, stabile Isotope: ^{204}Pb (1.4%), ^{206}Pb (24.1 %), ^{207}Pb (22.1%) und ^{208}Pb (52.4 %), von denen nur ^{207}Pb ($I = +1/2$) für NMR-Spektroskopie geeignet ist. Die großtechnische Produktion des Elements erfolgt zumeist durch Röstreduktion von PbS.

Blei ist für den Menschen giftig und reichert sich, anders als Thallium, im Körper an. Trotzdem findet das Metall auch heute noch eine Vielzahl von Anwendungen im Alltag, beispielsweise in Bleiakkumulatoren. Auch im Strahlenschutz wird Blei häufig in Form von Bleiblöcken oder Schürzen eingesetzt. Auf die Verwendung von Blei zur Herstellung von Rohrleitungen oder als Kraftstoffzusatz in Form von $PbEt_4$ wird jedoch inzwischen verzichtet, um Vergiftungen zu vermeiden.

In der Natur tritt das Element zumeist in der Oxidationsstufe +2 auf, es kann aber auch als +4 in Verbindung mit starken Donoren stabilisiert werden. Organobleiverbindungen enthalten üblicherweise Pb(IV)-Atome. Viele Eigenschaften des Bleis sind stark durch den relativistischen Effekt geprägt, was sich insbesondere in der bevorzugten Oxidationsstufe bemerkbar macht.[6] Auch eine Reduktion von Pb-Atomen mit Alkalimetallen in intermetallischen Verbindungen und in Lösung ist möglich. Die klassischen Polyanionen des Bleis in Lösung werden im Kapitel 1.2.4 behandelt. Neben dem Element Antimon ist das Blei eines von zwei Elementen anhand derer *Joannis* zum ersten Mal die Bildung solcher Polyanionen beobachtete.[7]

1.1.3 Bismut

Der Herkunft des Namens des Elementes Bismut (alt: Wismut) ist nicht abschließend geklärt.[1a, 8] So wird beispielsweise angenommen, dass sich der Name auf den Ort „in den Wiesen“ am Schneeberg im Erzgebirge bezieht, den Ort an dem das Element erstmals genutzt wurde. Eine Alternative dazu stellt die Annahme dar, dass sich der Name aus dem Wort „wismuth“ für weiße Masse ableitet. Das Element tritt sowohl gediegen, als auch in Form von Oxiden und Sulfiden in der Natur auf und besitzt lediglich das natürliche Isotop ^{209}Bi. Im Jahr 2003 gelang der Nachweis, dass auch dieses Isotop nicht stabil ist sondern eine extrem lange Halbwertszeit von $\tau_{1/2} = 1,9 \cdot 10^{19}$ Jahren besitzt.[9]

Die Gewinnung erfolgt üblicherweise durch (Röst)Reduktion der entsprechenden Oxide und Sulfide. Während die übrigen Elemente in diesem Bereich des Periodensystems in größeren Dosen giftig sind, sticht das Bismut in diesem Aspekt heraus. Es ist nicht nur ungiftig, sondern wird in Kosmetika verarbeitet und sogar als Medikament gegen Magenbeschwerden sowie einer Reihe weiterer medizinischer Anwendungen eingesetzt.

Bismut bildet in Kombination mit anderen Metallen häufig niedrigschmelzende Legierungen, deren gängige Anwendung der Einsatz als Lot ist. Bekannt ist Bismut auch für die Form und Farbe seiner Einkristalle. Das Element kristallisiert mit stufenartigen Kanten und erscheint silbrig grau. Werden die Kristalle aus einer Schmelze an Luft gezogen so bildet sich schnell eine Oxidschicht, die passivierend wirkt und das Metall vor nichtoxidierenden Säuren schützt. Weiterhin verleiht sie dem Metall seinen berühmten golden-regenbogenartigen Glanz. In Verbindungen tritt Bismut häufig in den Oxidationsstufen +3 und +5 auf, wobei erstere bevorzugt ist. Weiherhin sind auch Bi(I)-Verbindungen bekannt.[10] Ähnlich wie Blei durch Reduktion mit Alkalimetallen zur Bildung polyanionischer Cluster verwendet werden kann, ist die Bildung polykationischer Cluster des Bismuts durch dessen Oxidation möglich.[11] Diese folgen wiederum den Wade-Mingos-Regeln für elektronendefizitäre Cluster (siehe Kapitel 1.2.2): beispielsweise ist Bi_9^{5+} isoelektronisch zu Pb_9^{4-} und beide nehmen eine einfach überkappte, quadratisch antiprismatische Struktur ein. Auch die Reduktion mit Alkalimetallen zu (Poly)Bismuthiden ist möglich. Diese Polyanionen treten sowohl in intermetallischen Verbindungen als auch in Lösung auf und werden in den Kapiteln 1.2.3 und 1.2.4 ausführlicher diskutiert.

1.2 Einführung in die *Zintl*-Chemie

Zintl-Phasen und -Anionen bilden die Basis dieses Promotionsprojektes, weshalb zunächst eine kurze Einführung in dieses Forschungsgebiet gegeben werden soll.

1.2.1 Begriffe und Historisches

Unter dem Begriff *Zintl*-Anionen werden Polyanionen der p-Block-Elemente E_n^{q-} (E: p-Block-Element, n: Atomanzahl, q: Ladung) verstanden.[12] Hierbei spielt es keine Rolle, ob die Anionen in intermetallischen Verbindungen oder als molekulare Anionen in Salzen vorliegen. *Zintl*-Phasen werden erhalten, wenn Elemente der Gruppen 13 bis 15 mit (Erd)Alkalimetallen ((E)A) reduziert werden.[13] In diesen

können, müssen aber nicht zwangsläufig isolierte *Zintl*-Anionen vorliegen. Weiterhin können sowohl eindimensionale Polyanionenketten als auch zwei- oder dreidimensionale Polyanionennetzwerke gebildet werden.[4] *Zintl*-Phasen sind salzartig, spröde, haben oftmals Halbleitereigenschaften und sind in den meisten Fällen sehr oxidationsempfindlich – häufig sogar pyrophor. Oftmals werden auch die Salze der *Zintl*-Anionen mit komplexierten Gegenionen $[A(seq)]_qE_n$ (seq: Sequestrierungsmittel) als *Zintl*-Phasen bezeichnet, was jedoch falsch ist und zur besseren Unterscheidung streng getrennt voneinander behandelt werden sollte. Auch wird der Begriff *Zintl*-Phase häufig synonym für alle Verbindungen von (Erd)Alkalimetallen mit Elementen der Gruppen 13 bis 15 verwendet, ohne das die Eigenschaften der Verbindungen näher untersucht wurden.

Die ersten in der Literatur beschriebenen Berichte über die Bildung von *Zintl*-Anionen erfolgten im Jahr 1891 durch *Joannis*, der das Verhalten von Blei und Antimon in Lösungen der Alkalimetalle Natrium und Kalium in flüssigem Ammoniak untersuchte.[7] Hierbei stellte er fest, dass sich die Metalle unter Bildung tief gefärbter Lösungen vollständig auflösen, eine weitere Charakterisierung der resultierenden Produkte gelang jedoch nicht. Vierzig Jahre später widmete sich *Zintl* solchen Lösungen und den entsprechenden binären intermetallischen Verbindungen.[14] Ihm gelang der Nachweis, dass in den Lösungen Polyanionen der entsprechenden p-Block-Elemente vorliegen. Die Zusammensetzung des Polyanions des Bleis, welches seinen Ammoniaklösungen eine tiefgrüne Farbe verleiht, bestimmte er korrekterweise zu Pb_9^{4-}, die strukturelle Charakterisierung der ersten *Zintl*-Anionen erfolgte jedoch erst im Jahr 1975 durch *Corbett*.[15] *Laves* schlug nach dem frühen Ableben *Zintls* zu dessen Ehren die Begriffe zur Diskussion der entsprechenden Verbindungen vor.[12]

Seit den ersten Arbeiten von *Corbett* wurde insbesondere die Chemie von *Zintl*-Anionen in Lösung durch mehrere Gruppen weiterentwickelt, aber auch binäre *Zintl*-Phasen fanden Aufmerksamkeit. So wurde Na_4Ge_9 in einer Reaktion mit einer ionischen Flüssigkeit oxidiert, was zur Bildung einer neuen Elementmodifikation des Germaniums ($cF136$) führte.[16] Umsetzungen von *Zintl*-Anionen mit Übergangsmetallkomplexen öffneten weitere Forschungsfelder, die seither rege Beachtung finden.[13, 17]

1.2.2 Wichtige Bindungskonzepte und Methoden

In *Zintl*-Phasen und -Anionen und den daraus darstellbaren intermetalloiden und heterometallischen Clustern werden häufig Clusterverbindungen mit komplexen

Bindungssituationen erhalten. Mit der Molekülorbitaltheorie existiert ein quantenchemischer Ansatz, der die elektronischen Strukturen innerhalb dieser sehr präzise beschreibt, oftmals sind die Ergebnisse dieser Theorie jedoch zunächst unintuitiv und erfordern eine aufwendige und ausgiebige Analyse. Um die geometrischen und elektronischen Strukturen der Clusterverbindungen besser verstehen und schnell interpretieren zu können, wurden daher vereinfachte Modelle entwickelt, die dies ermöglichen sollen. Die relevantesten werden im Folgenden kurz vorgestellt, bevor im Anschluss daran auf die quantenchemische Analyse von Bindungssituationen und die dafür verwendeten Methoden eingegangen wird. An dieser Stelle muss ausdrücklich erwähnt werden, dass es sich bei den *Wade-Mingos*-Regeln und dem *Zintl-Klemm-Busmann*-Konzept um einfache Modelle handelt und diese schnell an ihre Grenzen stoßen, auch wenn dies nicht auf den ersten Blick ersichtlich ist. Nach einer ersten Analyse von Clusterverbindungen mit den im Folgenden präsentierten Ansätzen sollte also stets noch eine detaillierte Analyse mit quantenchemischen Methoden erfolgen, um ein vollständiges Bild zu erhalten. Einige Fälle, in denen quantenchemische Analysen zum besseren Verständnis intermetalloider Cluster beigetragen haben, sind im Kapitel 1.3.5 aufgeführt.

Die Wade-Mingos-Regeln

Im Jahr 1972 publizierte *Wade* Regeln zur Beschreibung der Bindungssituationen in elektronendefizitären Clusterverbindungen, die durch *Mingos* erweitert wurden.[18] Die Regeln lassen eine Vorhersage von Strukturen anhand von Gesamtelektronenzahlen zu, wobei ein Zusammenhang zwischen den Valenzelektronen (VE), den Gerüstelektronen (GE) und der Clustergeometrie gebildet wird. Zur Berechnung der Valenzelektronenzahl einer Verbindung wird über alle Valenzelektronen ($e(A_i)$) aller Atome n_i und der Clusterladung q summiert.

$$VE = \sum^{i} n_i \cdot e(A_i) + q \tag{1.1}$$

Um die Gerüstelektronenzahl, also die Anzahl an Elektronen, die tatsächlich zur Bindung im Clustergerüst beitragen, zu erhalten, müssen alle übrigen Elektronen von der Valenzelektronenzahl subtrahiert werden. Im Fall der Borane sind dies die exo-H-Bindungen, wohingegen im Fall von *Zintl*-Clustern von einem freien Elektronenpaar an jedem Hauptgruppenelement ausgegangen wird. Die Gerüstelektronen ergeben sich somit aus den Valenzelektronen gemäß Formel 1.2, wobei n_{exo} die Anzahl der exo-H-Bindungen bzw. der freien Elektronenpaare ist.

$$GE = VE - 2n_{exo} \tag{1.2}$$

Die Clustergeometrie folgt nun aus der Gerüstelektronenzahl anhand von Beziehung 1.3, worin n die Anzahl der Atome im Clustergerüst angibt. Durch die Variable x wird bestimmt, um welchen Clustertyp es sich handelt.

$$GE = 2n + x \tag{1.3}$$

Für das vollständig geschlossene Clustergerüst eines *closo*-Clusters beträgt x = 2. Durch das Entfernen eines Atoms aus dem Gerüst entsteht ein *nido*-Cluster mit x = 4, wobei die ehemals durch das Atom zur Bindung beigetragenen Elektronen nun durch zwei zusätzliche Elektronen zur Verfügung gestellt werden müssen. Eine Übersicht über die gängigsten Wade-Clustertypen mit den entsprechenden Bezeichnungen und Beispielen ist in Tabelle 1.1 gegeben. Die Variable x wird immer in 2-Elektronenschritten variiert, da das BH-Fragment, welches zunächst für die Entwicklung der Wade-Mingos-Regeln betrachtet wurde, zwei Elektronen zur Clusterbindung zur Verfügung stellt. Es kann weiterhin der Fall eintreten, dass x kleinere Werte als 2, bis hin zu negativen Zahlen, annimmt. Solche Cluster werden als hypoelektronische Cluster bezeichnet und treten in der Festkörperchemie der Trielelemente auf. Sie bilden nach wie vor deltaedrische Gerüste, jedoch werden in diesen mitunter Geometrien realisiert, die sonst nicht beobachtet werden. Die Chemie dieser Cluster wurde ausführlich von *Corbett* untersucht und in einem Übersichtsartikel zusammengefasst.[4]

Tabelle 1.1: Beispiele für Arten von Wade-Clustern.

Clustertyp	Gerüstelektronen	Beispiel	GE	Referenz
hypo	$2n - x$ $(x \leq 0)$	Tl_7^{7-}	$2 \cdot 7 = 14$	[19]
closo	$2n + 2$	$(Tl_4Bi_3)^{3-}$	$2 \cdot 7 + 2 = 16$	[20]
nido	$2n + 4$	$(Tl_4Bi_5)^{3-}$	$2 \cdot 9 + 4 = 22$	[21]
arachno	$2n + 6$	Bi_8^{2+}	$2 \cdot 8 + 6 = 22$	[22]
hypho	$2n + 8$	$(Sn_3Bi_3)^{5-}$	$2 \cdot 6 + 8 = 20$	[23]

Das *Zintl-Klemm-Busmann*-Konzept

Es wird das Verhalten der Atome in Bezug auf ihre tatsächliche Valenzelektronenzahl betrachtet. Das Modell beruht auf der Annahme, dass sich die Atome in

den Verbindungen entsprechend ihrer Valenzelektronenzahl verhalten und durch Oxidation oder Reduktion ihr Bindungsverhalten entsprechend verändern.[14a, 24] So führt die Aufnahme eines Elektrons durch ein Atom dazu, dass sich dieses Atom entsprechend eines Elements der benachbarten Gruppe mit Z+1 verhält. Gleiches gilt für eine entsprechende Oxidation, wodurch das Valenzverhalten des Atoms nun dem eines Elements mit Z−1 entspricht. Aus diesem Grund wird häufig auch der Begriff Pseudo-Element-Konzept synonym mit dem *Zintl-Klemm-Busmann*(ZKB)-Konzept verwendet. Hierbei ist zu beachten, dass häufig nur das Verhalten eines Elements der benachbarten Gruppe und nicht zwangsläufig das des direkt benachbarten Elements repliziert wird. Die Verbindung NaTl lässt sich im Rahmen des ZKB-Konzepts beschreiben und wurde bereits kurz im Kapitel 1.1.1 diskutiert. Sie stellt ein Beispiel für die Anwendung des Modells in einem ausgedehnten Festkörper dar. Es besteht auch die Möglichkeit diskrete Moleküle mithilfe des Modells zu interpretieren. Die Anionen Pn_7^{3-} (Pn = P - Bi) weisen allesamt eine nortricyclanartige Käfigstruktur auf, so wie es auch für das Tetraphosphortrisulfid P_4S_3 der Fall ist.[17c, 25, 26] Drei der sieben Pn-Atome in den Käfigen tragen eine negative Ladung und verhalten sich dementsprechend gemäß eines Chalkogens. Hieraus folgt die Strukturverwandtschaft zwischen den beiden Verbindungen, die in Abbildung 1.1 zur Veranschaulichung dargestellt sind.

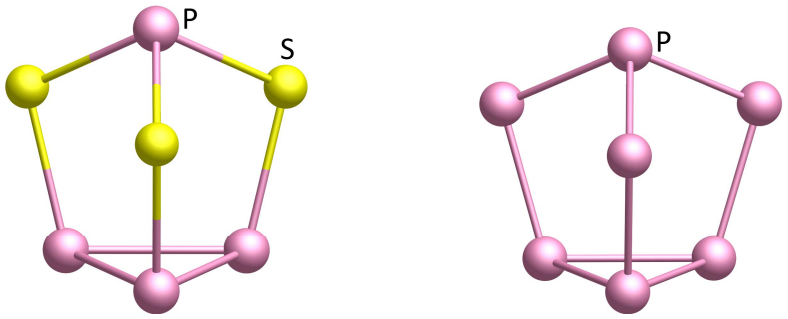

(a) P_4S_3 **(b)** P_7^{3-}

Abbildung 1.1: Vergleich der Strukturen von P_4S_3 und des isoelektronischen *Zintl*-Anions P_7^{3-}.[25a, 26a]

Quantenchemische Methoden

In diesem Abschnitt soll ein kurzer Überblick darüber gegeben werden, wie quantenchemische Untersuchungen von Hauptgruppenmetallclustern dazu beitragen können, die Bindungssituationen in diesen besser zu verstehen und diesen Verbindungen inhärente Probleme zu lösen. Es folgt eine Zusammenfassung der gängigs-

ten Methoden, mit denen diese Fragestellungen typischerweise adressiert werden. Für die Grundlagen zur Dichtefunktionaltheorie sei der Leser an dieser Stelle auf entsprechende Literatur verwiesen.

Die Analyse von Bindungssituationen beruht auf den etablierten Methoden, die auch für andere Verbindungsklassen eingesetzt werden. Oftmals liefert die Betrachtung lokalisierter Molekülorbitale (LMOs) bereits einen tieferen Einblick in die elektronische Situation innerhalb der Clusterverbindungen.[27] Hierbei kann, basierend auf den entsprechenden Orbitalbeiträgen und den Formen der LMOs, eine Aussage darüber getroffen werden, ob es sich um kovalente, ionische oder Mehrzentrenbindungen handelt. Zur genaueren Beantwortung dieser Fragen werden ergänzend Bindungsanalysen, typischerweise die Natural Population Analysis (NPA), eine Mulliken-Populationsanalyse (MPA) sowie die Population Analysis Based on Occupation Numbers (PABOON), durchgeführt.[28]

Insbesondere binäre Cluster, die Atome mit sehr ähnlichen Ordnungszahlen enthalten, verursachen einige Probleme bei deren Charakterisierung. So ist die Unterscheidung dieser Atome auf den Schweratomlagen in Kristallstrukturen, die mit gängigen Einkristalldiffraktometern bestimmt wurden, oftmals nicht möglich. Der Einsatz von Mo-K_α oder Cu-K_α Strahlung erlaubt in diesen keine Unterscheidung zwischen den Atomen, da die Unterschiede in den Beiträgen der jeweiligen Atomformfaktoren direkt proportional zur Anzahl der Elektronen des jeweiligen Atoms und damit für benachbarte Elemente verschwindend gering sind.[29]

Ein experimenteller Ansatz zur Lösung dieses Problems ist die Aufnahme von Röntgenbeugungsdaten bei der Wellenlänge einer Absorptionskante eines der schweren Elemente. So ist es mitunter möglich, einen signifikanten Unterschied in den imaginären Beiträgen der Atomformfaktoren herbeizuführen, der letztendlich eine Differenzierung der Atomsorten im finalen Strukturmodell erlaubt. Dies erfordert jedoch eine Strahlungsquelle mit durchstimmbarer Wellenlänge, häufig Synchrotronstrahlung, und ist somit nur in wenigen Fällen praktikabel. Zusätzlich gibt jede Kristallstrukturbestimmung nur einen Mittelwert über die reale Atomverteilung in den Kristallen wieder und liefert damit nur dann aussagekräftige Ergebnisse, wenn ein Isomer gegenüber allen restlichen möglichen deutlich stabiler ist. Häufig sind jedoch mehrere Isomere mit sehr ähnlichen Energien für die Clusteranionen zugänglich. Dies ist die herausragende Stärke der quantenchemischen Untersuchungen, da diese einen Einblick in die energetische Potentialhyperfläche von Verbindungen erlauben. Zur Auffindung des energetisch günstigsten Isomers einer gegebenen Verbindung gibt es mehrere Ansätze, die verfolgt werden können.

Aus einer Kristallstrukturanalyse werden Atompositionen ohne genaue Informationen über Elementzuordnung erhalten. Beschränkt sich die Anzahl möglicher Isomere auf eine überschaubare Anzahl, werden diese üblicherweise alle individuell optimiert und abschließend deren Energien und finale Strukturen mit den experimentellen Daten verglichen.

Für eine größere Anzahl möglicher Isomere bietet die Methode „reassignment of positions by perturbation theory“ (RP) einen eleganten Ansatz. Hierbei wird allem Atompositionen zunächst ein gemitteltes Kernpotential, basierend beispielsweise auf bekannten Zusammensetzungen, zugewiesen.[30] Dieser Parameter wird nun im Zuge der elektronischen und strukturellen Optimierungszyklen mit freigegeben und für jede Position optimiert. Ist so die erste optimierte Atomposition gefunden, wird allen übrigen Atompositionen wiederum ein aktualisiertes mittleres Kernpotential zugewiesen und der Prozess beginnt erneut.

Ein alternativer Ansatz zur Auffindung einer energetischen Minimumsstruktur für eine gegebene Zusammensetzung bei gleichzeitig bekannter Ladung stellt der Einsatz eines genetischen Algorithmus dar.[31] Hierbei werden eingangs keine strukturellen Parameter festgelegt, das Programm startet mit einer zufällig gewählten Struktur und bekannter Summenformel und führt anschließend anhand einer evolutionären Strategie Optimierungen durch. Die Atompositionen werden wiederum durch die Verwendung des RP-Algorithmus zugewiesen - die Methode wird als GA-RP bezeichnet.

1.2.3 Intermetallische Verbindungen

In diesem Kapitel werden ausschließlich solche intermetallischen Verbindungen der Tetrel (Tt)- und Pentelelemente (Pn) vorgestellt, die für eine weitere Folgechemie mit *Zintl*-Anionen in Lösung relevant sind. Hierfür ist eine Löslichkeit der Festkörper in geeigneten Lösungsmitteln erforderlich, welche nur für solche Festkörper gegeben ist, die Alkalimetalle enthalten. Zwar existiert auch eine Reihe an Verbindungen mit Erdalkalimetallen, diese sind jedoch aufgrund starker Coulomb-Wechselwirkungen nur sehr mäßig bis gar nicht in den Lösungsmitteln Ethylendiamin (en) oder *N,N*-Dimethylformamid (DMF) löslich. Gleiches gilt für die intermetallischen Verbindungen der Trielelemente (Tr), deren Clusterverbindungen derart hohe Ladungen tragen, dass diese nicht mehr in gängigen Lösungsmitteln stabilisiert werden können. Eine kurze Übersicht über die verschiedenen Clustertypen der Trielelemente wurde bereits in Kapitel 1.1.1 gegeben. Die Festkörperchemie dieser Elemente wurde zudem ausführlich in einem Übersichtsartikel

zu diesem Thema diskutiert.[4]

Binäre intermetallische Verbindungen der Gruppe 14

In den Phasensystemen A/Tt sind drei verschiedene Zusammensetzungen besonders relevant, da die Verbindungen isolierte Clusteranionen Tt_4^{4-} und, beziehungsweise oder, Tt_9^{4-} enthalten, die durch Auflösen der Verbindungen in flüssigem NH_3 oder en in Gegenwart von Komplexierungsmitteln wie 4,7,13,16,21,24-Hexaoxa-1,10-diazabicyclo[8.8.8]hexacosan (Krypt-222) oder 1,4,7,10,13,16-Hexaoxacyclooctadekan (18-Krone-6) in Lösung überführt und weiter umgesetzt werden können. Die Zusammensetzungen sind ATt (genauer A_4Tt_4; Tt = Si - Pb),[32] A_4Tt_9 (Tt = Ge - Pb)[33] und $A_{12}Tt_{17}$ (Tt = Si - Sn).[33a, 33c, 34] In den Verbindungen ATt und A_4Tt_9 liegen jeweils ausschließlich die tetraedrischen Anionen Tt_4^{4-} respektive 9-Atomkäfige Tt_9^{4-} vor, während in den Verbindungen $A_{12}Tt_{17}$ beide Arten von Anionen in einem 2:1-Verhältnis vorhanden sind. Im Falle des Siliciums existiert keine Verbindung A_4Si_9, sondern nur A_4Si_4 und $A_{12}Si_{17}$. Hierdurch wird die *Zintl*-Chemie des Elementes limitiert, da $A_{12}Si_{17}$ nicht in dem typischerweise verwendeten Lösungsmittel en löslich ist sondern nur in flüssigem NH_3. Aus diesem Grund ist, im Vergleich zu den restlichen Tetrelelementen, ein erheblich größerer experimenteller Aufwand nötig, um die Reaktivität der Anionen zu untersuchen. Es existieren vereinzelte Berichte über entsprechende Untersuchungen, in denen allerdings immer nur über Koordinationsverbindungen berichtet wird, in denen die Silicium-Polyanionen als Liganden an Übergangsmetallen fungieren.[35, 36, 49e] Intermetalloide Cluster mit Siliciumatomen im Clustergerüst sind bislang nicht bekannt.

Binäre intermetallische Verbindungen der Gruppe 15

Im Fall der Pentelelemente sind sechs verschieden Verbindungstypen bekannt, die für die *Zintl*-Chemie relevant sind. Durch eine vollständige Reduktion der Pentelelemente entstehen die Verbindungen A_3Pn, in der isolierte Pn^{3-}-Anionen (Pn = P - Bi) vorliegen.[37] Diese Verbindungen werden häufig als Quelle für isolierte Pentelatome eingesetzt, beispielsweise zur Synthese von $Pn(SiMe_3)_3$, aber auch die Darstellung heterometallischer Cluster, wie $[Sb_6\{Ru(cp^*)\}_2]^{2-}$ (cp^*: Pentamethylcyclopentadienyl-Anion), ist möglich.[38, 39] Neben den vollständig reduzierten Pentelatomen Pn_3^{3-} in A_3Pn existieren eine Reihe weiterer binärer Verbindungen mit niedrigeren A:Pn-Verhältnissen. Die Verbindungen A_3Bi_2 und A_5Pn_4 weisen hiervon die höchsten Alkalimetallgehalte auf und enthalten isolierte Bi_2^{2-}-Hanteln re-

spektive Pn_4^{4-}-Ketten.[40, 41] Aus beiden lassen sich durch Extraktion mit en in Gegenwart von Krypt-222 die Salze $[A(Krypt{-}222)]_2Bi_2$ und $[A(Krypt{-}222)]_2Pn_4$ (Pn = Sb, Bi) herstellen.[42, 43] Eine weitere Verringerung des Alkalimetallgehalts liefert die Verbindungen APn mit einer 1D-Pn^--Kettenstruktur, vergleichbar mit den Elementstrukturen von Selen und Tellur.[44] Den größten Pentelgehalt weisen die Verbindungen ABi_2 auf, die eine kubische Laves-Phase mit einem dreidimensionalen Bi-Polyanionennetwerk bilden.[37a, 45]

Für die Elemente Phosphor bis Antimon sind weiterhin die Verbindungen A_3Pn_7 (Pn = P - Sb) und A_3Pn_{11} (Pn = P, As) bekannt, die im Festkörper vorgeformte Anionen Pn_7^{3-} und Pn_{11}^{3-} enthalten.[44b, 46, 47] Diese lassen sich durch Extraktion unzersetzt aus dem Festkörper herauslösen. Bisher wurde jedoch nur der Anionentyp Pn_7^{3-} für weitere Umsetzungen mit Übergangsmetallkomplexen eingesetzt. Stattdessen wird häufig ein alternativer Zugang zu Polypnictiden gewählt. Insbesondere die Verbindungen K_5Pn_4 (Pn = Sb, Bi) werden darin als *in-situ* Quelle für Polyantimonide und Polybismuthide verwendet.[48]

Ternäre intermetallische Verbindungen der Gruppen 13/14 und 13/15

Während für die binären Verbindungen der Alkalimetalle mit Triel-, Tetrel- und Pentelelementen große Teile der Phasendiagramme bekannt sind und die Kristallstrukturen der entsprechenden Verbindungen aufgeklärt wurden, verhält es sich für entsprechende ternäre Systeme anders. In diesen Fällen gibt es nur vereinzelte Berichte über Einkristallstrukturen solcher Festkörper und relevante ternäre Phasendiagramme sind nicht bekannt. Dies erschwert die Suche nach geeigneten Ausgangsverbindungen zur Darstellung binärer *Zintl*-Anionen, ausgehend von wohldefinierten Edukten. Anders als im Fall homoatomarer *Zintl*-Anionen der Gruppe 14 existiert keine ternäre Verbindung mit vorgeformten Anionen, die durch Extraktion unverändert in Lösung überführt werden könnten. Alle in der Literatur beschriebenen Synthesen legen nahe, dass eine Reihe von Bindungsbrüchen und -bildungen während der Auflösung des Edukts im Lösungsmittel geschieht, bevor die *Zintl*-Anionen als finale Produkte gebildet werden. Mitunter müssen komplexe dreidimensionale Anionennetzwerke aufgebrochen werden, um daraus einfache molekulare Anionen zu bilden. Dies wurde beispielsweise bei der Bildung von $(TlBi_3)^{2-}$, ausgehend von KTlBi und KBi_2 beobachtet.[20] Eine Übersicht über die bisher für solche Synthesen eingesetzten Verbindungen und die dadurch erhaltenen Produkte folgt in Kapitel 1.2.5.

Insgesamt ist das Feld der ternären Eduktverbindungen zur Synthese binärer

Zintl-Anionen vergleichsweise wenig erforscht, was mitunter auf experimentelle Herausforderungen zurückzuführen ist. Die Züchtung qualitativ hochwertiger Einkristalle ist mit den verwendeten Synthesemethoden anspruchsvoll und die Aufnahme von Pulverdiffraktogrammen ebenfalls eine Herausforderung. Die Oxidationsempfindlichkeit und starke Reduktionskraft der Verbindungen erschwert die Auswahl zur Strukturaufklärung geeigneter Einkristalle und die oftmals hohen Absorptionskoeffizienten der Verbindungen erfordern besondere Maßnahmen bei der Präparation von Pulverdiffraktometrieproben. Häufig wird bei der Synthese zusätzlich ein Gemisch verschiedener Verbindungen erhalten, die optisch nicht unterschieden werden können. Durch den Mangel an bekannten Verbindungen zum Abgleich simulierter Pulverdiffraktogramme mit den experimentellen Daten fällt die initiale Charakterisierung von Reaktionsprodukten schwer. Insgesamt besteht noch ein großer Forschungsbedarf in diesem Bereich, der aber letztendlich die Grundlage für alle weitere Folgechemie binärer *Zintl*-Anionen darstellt und aus diesem Grund eine wichtige Rolle spielt.

1.2.4 Homoatomare *Zintl*-Anionen in Lösung

Die Elemente der Gruppe 14 bilden in Verbindung mit (Erd-)Alkalimetallen im Festkörper Clusteranionen, wie bereits in Kapitel 1.2.3 ausgeführt. In Lösungsmitteln wie en oder DMF lassen sich diese Anionen unter Zusatz von Komplexierungsagenzien aus den Festkörpern herauslösen und auch als entsprechende Salze kristallisieren. Auf diesem Weg sind die Anionen Tt_4^{4-}, Tt_9^{q-} (q = 2 - 4) und in eingeschränktem Maße auch Tt_5^{2-} (Tt = Si - Pb) zugänglich und stehen für Umsetzungen zur Verfügung.[49–51] Eine Limitierung besteht im Fall des Elementes Silicium, da die entsprechenden Verbindungen nur in flüssigem Ammoniak löslich sind. *Fässler* stellte jüngst einen Umweg zur Untersuchung der Si_9^{4-}-Cluster vor, indem die Cluster nach Extraktion mit flüssigem NH_3 *in-situ* zu $(Si_9R_3)^-$ und $(Si_9R_2)^{2-}$ in Tetrahydrofuran (THF) (R = $Si(^tBu)_2H$) umgesetzt wurden.[52]

Während im Fall der Tetrelelemente wohldefinierte Anionen als Ausgangsverbindungen zur Verfügung stehen, werden im Fall der Pentelelemente oftmals binäre Festphasen eingesetzt, aus denen ein Gemisch verschiedener Polypnictide dargestellt und direkt *in-situ* umgesetzt wird. Der prominenteste Anionentyp der Polypnictide, welcher auch am häufigsten für Umsetzungen verwendet wird, ist Pn_7^{3-}. Diese Anionen werden durch Extraktion aus A_3Pn_7 gewonnen und sind für die Elemente Phosphor bis Antimon auf diesem Weg zugänglich.[53] In Abbildung 1.2 sind die Strukturmotive der beschriebenen Anionen dargestellt.

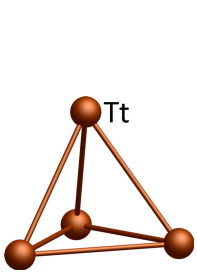

(a) Tt_4^{4-} (Tt = Si - Pb)

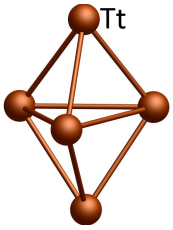

(b) Tt_5^{2-} (Tt = Si - Pb)

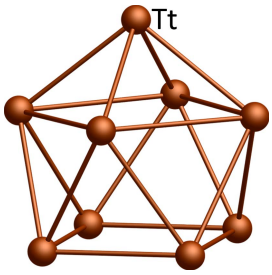

(c) Tt_9^{q-} (C_{4v}; Tt = Si - Pb)

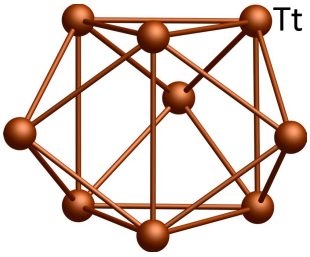

(d) Tt_9^{q-} (D_{3h}; Tt = Si - Pb)

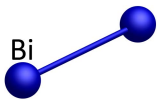

(e) Bi_2^{2-}

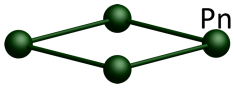

(f) Pn_4^{2-} (Pn = As - Bi)

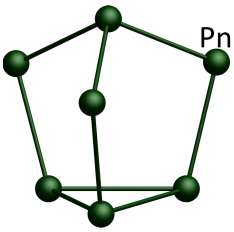

(g) Pn_7^{3-} (Pn = P - Bi)

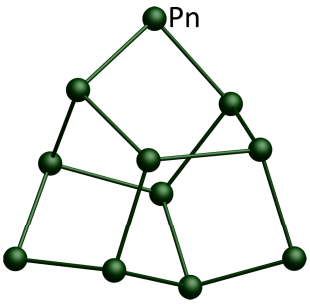

(h) Pn_{11}^{3-} (Pn = P - Bi)

Abbildung 1.2: Strukturmotive homoatomarer *Zintl*-Anionen. Referenzen für a: [49], b: [50a, 51], c,d: [50], e: [42], f: [43, 54], g: [26b, 53], h: [17c, 55].

1.2.5 Heteroatomare *Zintl*-Anionen in Lösung

Durch die Extraktion ternärer Festkörper oder Mischungen zweier binärer Festkörper können binäre *Zintl*-Anionen synthetisiert werden. Sofern diese zur Darstellung intermetalloider Cluster eingesetzt werden sollen, ist der Erhalt tetraedrischer Anionen erwünscht, da diese sich als besonders reaktiv herausgestellt haben.

Während die Synthesen homoatomarer Polyanionen in den allermeisten Fällen durch ein einfaches Herauslösen der bereits im Festkörper vorliegenden Cluster erfolgt, ist dies im Fall binärer Anionen wesentlich komplexer. Die hierbei verwendeten Edukte weisen entweder Festkörperstrukturen mit zum Teil ausgedehnten Anionennetzwerken auf, enthalten binäre Anionen mit hohen Ladungen oder sind überhaupt nicht näher charakterisiert. Im Folgenden sind die Fälle aufgeführt, in denen wohldefinierte Edukte eingesetzt wurden.

Eine Studie berichtet von der Verwendung von K_8SnSb_4 in unterschiedlichen Lösungsmitteln und den darin jeweils erhaltenen Produkten.[56] Es wird hierbei nicht das im Edukt vorliegende Anion $(SnSb_4)^{8-}$ erhalten, sondern verschiedene binäre Anionen mit einer reduzierten Ladung. So liefert die Extraktion mit en das tetraedrische Anion $(Sn_2Sb_2)^{2-}$, während in flüssigem Ammoniak $(Sn_3Sb_4)^{6-}$ mit nortricyclanartigier Käfigstruktur erhalten wird. In einer weiteren Arbeit wird die Bildung des binären Anions $(Sn_2Bi_2)^{2-}$ durch den Einsatz zweier binärer Edukte, KSn_2 und K_3Bi_2, beschrieben.[57] Weiterhin kann selbiges Anion auch durch Auflösen von formal ternärem „KSnBi“ gewonnen werden, wobei diese Verbindung nicht näher untersucht wurde, und möglicherweise ebenfalls ein Gemisch zweier binärer Verbindungen ist. Die Bildung eines binären Anions, ausgehend von einem Gemisch zweier unterschiedlicher Edukte, wurde ebenfalls für das Anion $(TlBi_3)^{2-}$ beobachtet.[20] In diesem Fall entsteht das Anion aus der ternären Verbindung KTlBi in einer Reaktion mit KBi_2 - bei beiden handelt es sich um *Laves*-Phasen mit ausgedehnten Polyanionennetzwerken. Wird für diese Elementkombination die Zusammensetzung des Edukts variiert und „K_2TlBi“ eingesetzt, dessen Hauptkomponente $K_6Tl_2Bi_3$ mit darin vorliegenden $^1_\infty[Tl_4Bi_6]^{12-}$-Strängen ist, entsteht das Anion $(Tl_4Bi_3)^{3-}$. Mit der Darstellung von $(Sn_3Bi_3)^{5-}$ durch Extraktion eines Gemisches von „$RbSn_2$“ und „$RbBi_2$“ in flüssigem Ammoniak existiert ein weiterer Bericht über die Bildung eines binären Anions durch den Einsatz zweier binärer Eduktverbindungen.[23] Über die der binären Anionenbildung zugrunde liegenden Mechanismen ist bisher nichts bekannt und es besteht noch ein großer Aufklärungsbedarf.

Für viele Elementkombinationen lassen sich die gewünschten Anionen $(TrBi_3)^{2-}$

(Tr = Ga, In) oder $(Tt_2Pn_2)^{2-}$ (Tt/Pn = Sn/Bi, Pb/Bi) ausgehend von Verbindungen mit den nominellen Zusammensetzungen „$K_5Tr_2Bi_4$“ oder „$K_2Tt_2Pn_2$“ darstellen.[57–59] Ferner werden die Verbindungen „K_2TlBi_3“ und „K_2TtPn“ (Tt/Pn = Ge/As, Sn/Sb, Pb/Sb) zur Synthese der Anionen $(TlBi_3)^{2-}$ oder $(Tt_2Pn_2)^{2-}$ (Tt/Pn = Ge/As, Sn/Sb, Pb/Sb) eingesetzt.[20, 60] Eine Übersicht über alle bekannten binären *Zintl*-Anionen, die aus Lösung kristallisiert werden können, ist zusammen mit den entsprechenden Edukten in Tabelle 1.2 gegeben. Die Strukturmotive der beschriebenen Anionen sind in Abbildung 1.3 veranschaulicht.

Tabelle 1.2: Bekannte binäre *Zintl*-Anionen, die aus Lösung als $[A(seq)]^+$-Salze kristallisiert werden können. Mit * markierte Anionen sind bisher nicht auf direktem Weg durch Extraktion zugänglich, sondern entstehen als Nebenprodukte in Reaktionen. Mit ◇ markierte Anionen sind nur in flüssigem NH_3 darstellbar.

Elemente	Anion 1	Anion 2	Edukte	Ref.
Tl/Sn	$(TlSn_9)^{3-}$	$(TlSn_8)^{3-}$	Na_5TlSn_3	[20]
Tl/Pb	$(TlPb_9)^{3-}$	$(TlPb_{11})^{3-}$	„Na_5TlPb_3“	[20]
Ga/Bi	$(GaBi_3)^{2-}$		„$K_5Ga_2Bi_4$“	[58]
In/Bi	$(InBi_3)^{2-}$	$(In_4Bi_5)^{3-}$	„$K_5In_2Bi_4$“	[58]
Tl/Sb	$(Tl_4Sb_5)^{3-}$		„$K_6Tl_2Sb_3$“	[61]
Tl/Bi	$(TlBi_3)^{2-}$	$(Tl_4Bi_5)^{3-}$	„$K_5Tl_2Bi_4$“	[20, 21]
	$(TlBi_3)^{2-}$		„K_2TlBi_3“	[20]
	$(Tl_4Bi_3)^{3-}$		„K_2TlBi“	[20]
Ge/P	$(Ge_2P_2)^{2-}$	$*(Ge_7P_2)^{2-}$	„$K_2Ge_2P_2$“	[62]
Ge/As	$(Ge_2As_2)^{2-}$	$(Ge_7As_2)^{2-}$	„KGeAs:Ta“	[63]
	$(Ge_2As_2)^{2-}$	$(Ge_7As_2)^{2-}$	„KGeAs“	[63]
	$(Ge_2As_2)^{2-}$		„K_2GeAs“	[60c]
Ge/Sb	$(Ge_7Sb_2)^{4-}$	$[(Ge_8Sb)_2]^{4-}$	Ge_9^{4-} + $SbPh_3$	[64]
Ge/Bi	$(Ge_4Bi_{14})^{4-}$		„K_2GeBi“	[65]
	$[(Ge_8Bi)_2]^{4-}$		Ge_9^{4-} + $BiPh_3$	[64]
Sn/As	$(SnAs_{14})^{4-}$		„K_3SnAs_7“	[66]
Sn/Sb	$(Sn_2Sb_2)^{2-}$	$◇(Sn_3Sb_4)^{6-}$	K_8SnSb_4	[56]
	$(Sn_2Sb_2)^{2-}$		„K_2SnSb“	[60a]
Sn/Bi	$(Sn_2Bi_2)^{2-}$	$*(Sn_7Bi_2)^{2-}$	„$K_2Sn_2Bi_2$“	[87a]
	$◇(Sn_3Bi_3)^{5-}$		„$RbSn_2$“ + „$RbBi_2$“	[23]
	$◇(Sn_3Bi_5)^{3-}$		„RbSnBi“	[23]
	$◇(Sn_4Bi_4)^{4-}$		„CsSnBi“	[67]
Pb/Sb	$(Pb_2Sb_2)^{2-}$		„K_2PbSb“	[60b]
Pb/Bi	$(Pb_2Bi_2)^{2-}$	$*(Pb_7Bi_2)^{2-}$	„$K_2Pb_2Bi_2$“	[59]

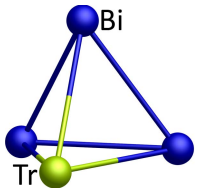

(a) $(TrBi_3)^{2-}$ (Tr = Ga - Tl)

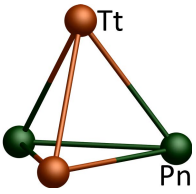

(b) $(Tt_2Pn_2)^{2-}$*

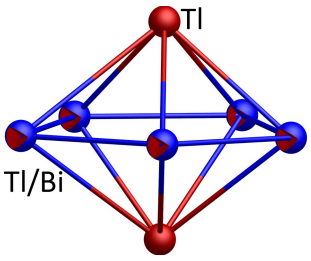

(c) $(Tl_4Bi_3)^{2-}$

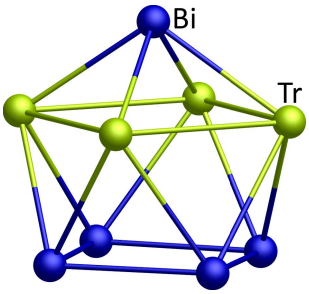

(d) $Tr_4Pn_5^{3-}$ (Tr = In, Tl)

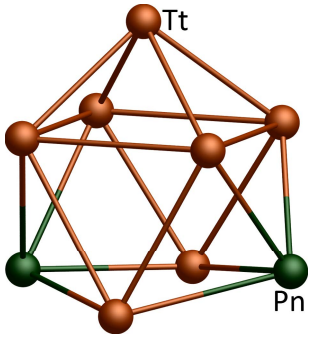

(e) $Tt_7Pn_2^{2-}$ (Tt/Pn = Ge/P-Sb, Sn/Bi, Pb/Bi)

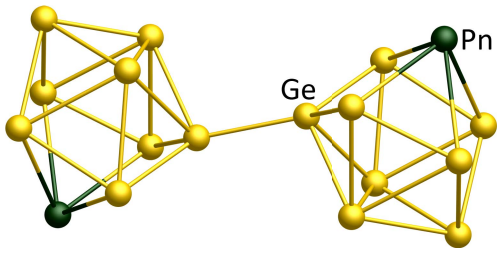

(f) $[(Ge_8Pn)_2]^{4-}$ (Pn = Sb, Bi)

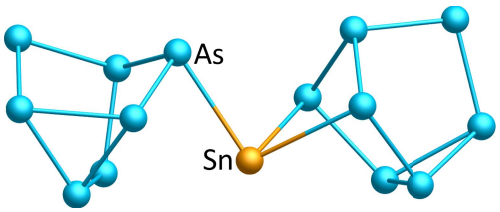

(g) $(SnAs_{14})^{4-}$

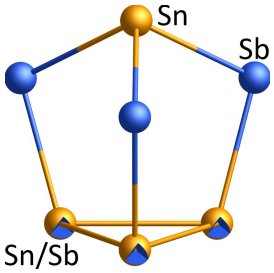

(h) $(Sn_3Sb_4)^{6-}$

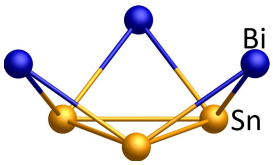

(i) $(Sn_3Bi_3)^{5-}$

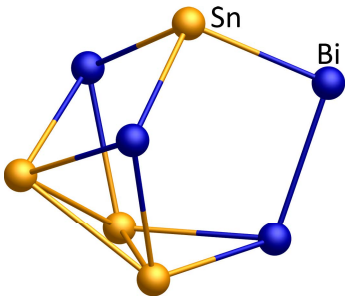

(j) $(Sn_4Bi_4)^{4-}$

Abbildung 1.3: Strukturmotive binärer *Zintl*-Anionen. *Für eine Liste aller bekannten Zusammensetzungen siehe Tabelle 1.2. $(Sn_3Bi_5)^{3-}$ ist isostrukturell zu $(Sn_4Bi_4)^{4-}$ und nicht abgebildet. Referenzen für a: [58], b: [20, 56, 59, 60a, 60b, 60c, 62, 63, 87a], c: [20], d: [21, 58], e: [59, 62–64, 87a], f: [64], g: [66], h: [56], i: [23], j: [67].

1.3 Intermetalloide und heterometallische Cluster

Ein Hauptziel dieses Promotionsprojektes bestand in der Darstellung neuer intermetalloider und heterometallischer Cluster, ausgehend von zuvor neu dargestellten binären *Zintl*-Anionen. Zur Einordnung der diskutierten Ergebnisse soll zunächst eine kurze Übersicht über diese Verbindungsklassen gegeben werden. Zu diesem Thema wurden bereits mehrere Übersichtsartikel verfasst, auf die an dieser Stelle als weiterführende Literatur verwiesen werden soll.[13, 17]

1.3.1 Begriffsfindung

Der Begriff der metalloiden Cluster wurde 1999 durch *Schnöckel* geprägt und beschreibt Clusterverbindungen, in deren Kern formal neutrale Metallatome vorliegen, die von einer Hülle aus positiv geladenen Metallatomen mit entsprechenden Schutzgruppen umgeben sind.[68] Hierbei soll die Anzahl von Metall-Metall-Kontakten die an Metall-Ligand-Kontakten übersteigen und zusätzlich Metallatome mit reinen Metall-Metall-Kontakten vorliegen.

Nach den ersten Berichten über Reaktionen homoatomarer *Zintl*-Anionen mit Übergangsmetallkomplexen und deren Reaktionsprodukten sowie der Synthese des ersten ligandenfreien, endohedralen Clusters $[Pt@Pb_{12}]^{2-}$ im Jahr 2004, wurde von *Fässler* noch im selben Jahr der Begriff intermetalloide Cluster vorgeschlagen und in die Diskussion dieser Verbindungen aufgenommen.[13, 69] Die Definition des Begriffs „intermetalloid“ nach *Fässler* soll zum Ausdruck bringen, dass in einem diskreten Cluster der allgemeinen Formel $[M_x@E_y]^q$ (M = Übergangsmetall, E = Element(e) der Gruppe(n) 13 - 15, q = Ladung) ein oder mehrere Zentralatome M enthält, die von einer Schale aus p-Block-Elementen umschlossen sind. In diesen ist die Koordinationszahl des(/der) Zentralatom(e) ähnlich groß, wie in intermetallischen Phasen, woraus sich die Ableitung des Begriffs intermetalloid ergibt. Der bereits eingangs erwähnte Cluster $[Pt@Pb_{12}]^{2-}$ stellt somit einen solchen intermetalloiden Cluster dar, in dem sich ein Platinatom im Zentrum einer ikosaedrischen Pb_{12}^{2-} Schale befindet. Es wurde eine alternative Interpretation der Definition des Begriffs nach *Fässler* durch *Kempe* vorgeschlagen, anhand derer die Spanne an Verbindungen, die dadurch beschrieben werden, deutlich erweitert wird.[70] So ist nach dieser Auffassung jede metallzentrierte Clusterverbindung ein intermetalloider Cluster, wobei in diesem Fall der Clusterbegriff nach *Cotton* verwendet wird.[71] Hierdurch werden auch Metallkomplexe mit einem zentralen Metallatom ohne hohe Koordinationszahlen in die Verbindungsklasse mit aufgenommen. Dies

soll nur der Vollständigkeit halber erwähnt werden, spielt jedoch für alle im Nachfolgenden diskutierten Verbindungen keine Rolle. Es findet ausschließlich die Interpretation nach *Fässler* Anwendung.

Zur Abgrenzung von den intermetalloiden Clustern werden jene, in denen die Übergangsmetallatome nicht in das Zentrum eines Clusters eingebaut, sondern mit in die Clusterschale integriert werden, als heterometallische Cluster bezeichnet. Hierbei können die ursprünglich an den Übergangsmetallatomen vorhandenen Liganden zum Teil an diesen verbleiben oder vollständig abgestreift werden.

1.3.2 Binäre intermetalloide Cluster

Die ersten Studien zur Reaktivität homoatomarer *Zintl*-Anionen beschäftigten sich zum Großteil mit den leicht zugänglichen Anionen Tt_9^{4-}. Aus deren Umsetzungen mit Komplexen elektronenreicher Übergangsmetalle gehen häufig deltaedrische intermetalloide Cluster hervor, die den Wade-Mingos-Regeln folgen und aus 9, 10 oder 12 Atomen aufgebaut sind.[69, 72] Der Aufbau von Käfigen mit relativ flexiblen Gerüsten ist für die Elemente der Gruppe 14 durch die Bildung von Mehrzentrenbindungen sehr günstig, woraus eine Vielzahl unterschiedlicher intermetalloider Cluster resultiert. Durch den Einbau von Übergangsmetallatomen, insbesondere solchen mit einer abgeschlossenen d^{10}-Schale, können größere Clustergerüste ohne eine Veränderung der Gerüstelektronenzahl stabilisiert werden.[13, 69, 72b, 73, 89c] So sind die größten bekannten, leeren *closo*-Wade-Cluster Tt_{10}^{2-} (Tt = Ge, Pb), durch den Einbau von Übergangsmetallatomen können jedoch auch die entsprechenden 12-Atomkäfige $[M@Tt_{12}]^{q-}$ dargestellt werden.[74] Weiterhin sind noch größere intermetalloide Clusteranionen darstellbar, die nach wie vor strukturell an klassische, deltaedrische Wade-Cluster erinnern, deren Elektronenzählregeln jedoch nicht mehr erfüllen.[75] Auch nicht-deltaedrische Cluster wurden inzwischen durch den Einbau von endohedralen Eisen-, Cobalt- und Rutheniumatomen in die Clustergerüste synthetisiert.[76]

Anders als Tetrelatome bilden Pentelatome in Clusterverbindungen bevorzugt lokalisierte 2e-2c-Bindungen und dementsprechend sind diese zumeist elektronenpräzise (VE = $5n$). Insgesamt sind nur wenige intermetalloide Cluster der Pentelelemente bekannt - weitaus häufiger werden Koordinationsverbindungen der Polyanionen erhalten.[17c, 38, 48b, 48c, 77–79] In der Abbildung 1.4 sind beispielhaft einige intermetalloide Clusteranionen dargestellt.

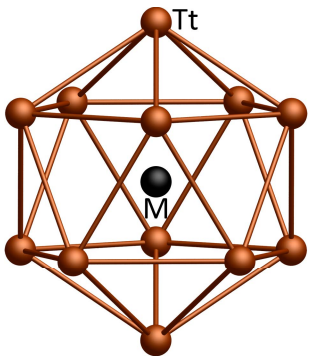

(a) $[M@Tt_{12}]^{q-}$ (M/Tt/q = Ni-Pt/Pb/2, Ir/Sn/3, Au/Pb/3)

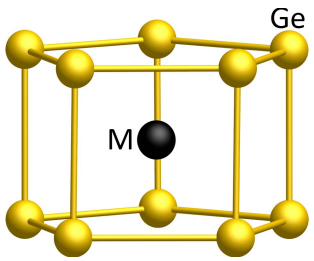

(b) $[M@Ge_{10}]^{3-}$ (M = Fe, Co)

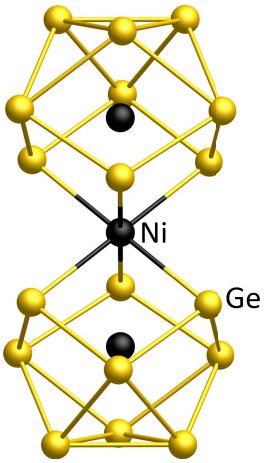

(c) $[(Ni@Ge_9)Ni(Ni@Ge_9)]^{4-}$

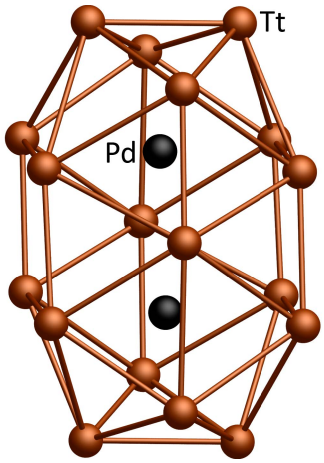

(d) $[Pd_2@Tt_{18}]^{4-}$ (Tt = Ge, Sn)

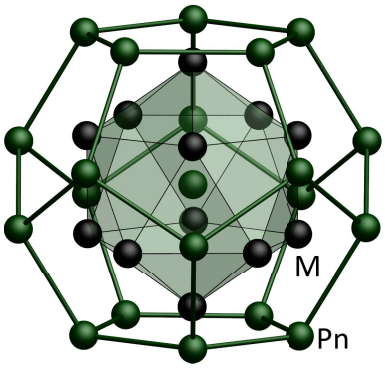

(e) $[Pn@M_{12}@Pn_{20}]^{q-}$

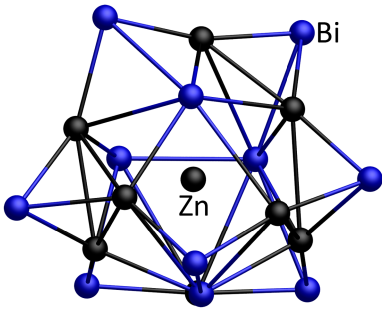

(f) $[Zn@Zn_8Bi_{11}]^{3-}$

Abbildung 1.4: Beispiele für binäre intermetalloide Cluster mit Elementen der Gruppen 14 und 15. Referenzen für a: [69, 72b, 73, 89c], b: [76a, 76b], c: [80], d: [75a, 75c], e: [77], f: [78a].

1.3.3 Binäre heterometallische Cluster

Während der Begriff „intermetalloid“ eine scharfe Abgrenzung der Verbindungen erlaubt, so gestaltet sich eine entsprechende Unterscheidung für heterometallische Cluster wesentlich schwieriger. In diesen Fällen muss zunächst die Frage beantwortet werden, ob eine Verbindung als Cluster oder als einfache Koordinationsverbindung zu betrachten ist. Für Polyanionen der Tetrelelemente ist dies noch problemlos möglich, da sowohl die Anzahl zu bewertender Verbindungen als auch deren strukturelle Vielfalt wesentlich geringer ist, als im Fall der Pentelelemente. Tetrelide treten in der Regel in Form von Vier-, Fünf-, oder Neunatomkäfigen auf, neigen nicht zur Bildung isolierter Anionen Tt^{4-} und nur in seltenen Fällen zur Bildung neuer Polyanionengerüste.[81] Sofern ein intakter Vier-, Fünf-, oder Neunatomkäfig in den Verbindungen vorliegt, werden diese als Koordinationsverbindungen verstanden und nur in den Fällen, in denen neue Polyanionengerüste gebildet werden, als heterometallische Cluster.

Im Gegensatz dazu fungieren (Poly)Pnictide häufig als Liganden für ein- und mehrkeringe Übergangsmetallkomplexe, wobei eine wesentlich größere strukturelle Vielfalt auftriff, als es für die Polytetrelide der Fall ist. Neben den in Kapitel 1.2.4 vorgestellten Pn_7^{3-}-Anionen, wird eine Vielzahl weiterer Polypnictide beobachtet, die eine umfangreiche Koordinationschemie ermöglichen. Ein sehr ausführlicher Übersichtsartikel von *Whitmire* behandelt alle Verbindungen mit einer Übergangsmetall-Pnictogen-Bindung und verdeutlicht, wie groß die Gruppe an Verbindungen ist, aus denen in diesem Fall zwischen heterometallischen Clustern und reinen Koordinationsverbindungen unterschieden werden muss.[82] In vielen Fällen sind die Grenzen zwischen heterometallischen Clustern und Koordinationsverbindungen fließend und die Zuordnung zu einer der beiden Verbindungsklassen gestaltet sich als Glaubensfrage. So kann beispielsweise die Verbindung $[Pd_7As_{16}]^{4-}$ (Abbildung 1.5d) entweder als heterometallischer Cluster betrachtet werden oder als siebenkerniger Palladium-Komplex mit einem Pd^{2+}, sechs Pd^{+}-Ionen und unterschiedlichen (Poly)Arsenidliganden: 2 planare As_5^{-}-Ringe, 2 As_2^{2-}-Hanteln und zwei isolierten As^{3-}-Ionen.[83]

In der Abbildung 1.5 sind exemplarisch einige heterometallische Clusteranionen mit und ohne an den Übergangsmetallatomen gebundenen Liganden dargestellt.

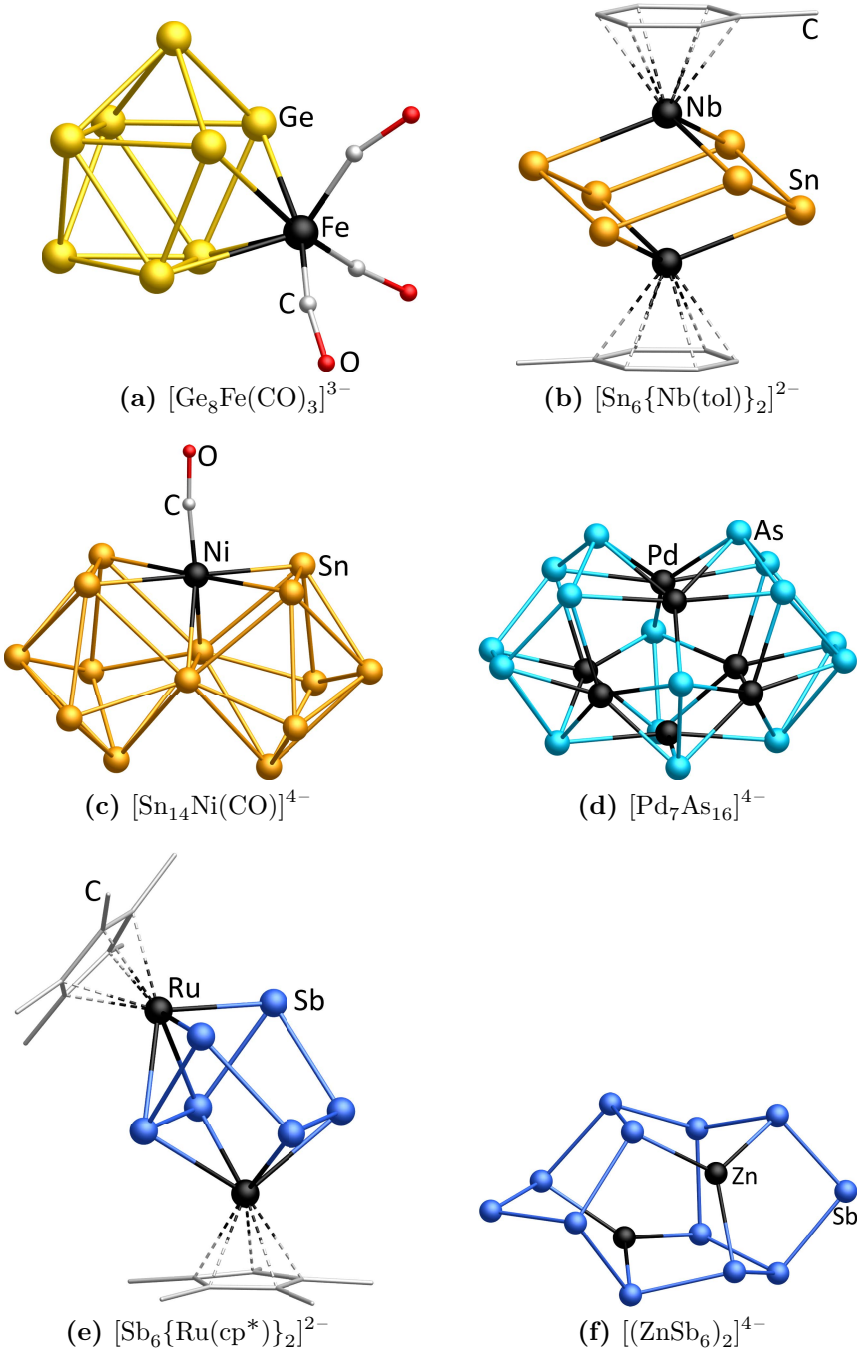

(a) $[Ge_8Fe(CO)_3]^{3-}$ **(b)** $[Sn_6\{Nb(tol)\}_2]^{2-}$

(c) $[Sn_{14}Ni(CO)]^{4-}$ **(d)** $[Pd_7As_{16}]^{4-}$

(e) $[Sb_6\{Ru(cp^*)\}_2]^{2-}$ **(f)** $[(ZnSb_6)_2]^{4-}$

Abbildung 1.5: Beispiele für heterometallische Cluster mit Elementen der Gruppen 14 und 15 - mit und ohne an den Übergangsmetallatomen gebundenen Liganden. Referenzen für a: [84], b: [81a], c: [85], d: [83], e: [38], f: [86].

1.3.4 Ternäre intermetalloide und heterometallische Cluster

Alle bisher vorgestellten und diskutierten Verbindungen sind binärer Natur und wurden aus Reaktionen homoatomarer Polyanionen mit Übergangsmetallkomplexen erhalten. Eine Erweiterung des Produktspektrums wird durch den Einsatz binärer *Zintl*-Anionen realisiert, in denen Elemente zweier unterschiedlicher Hauptgruppen (13 - 15) kombiniert sind. Dies ermöglicht die „Verdünnung“ von Ladungen der Anionen und eine Erhöhung der Löslichkeit im Vergleich zu den homoatomaren Analoga. So sind die Anionen Tt_4^{4-} zwar bekannt, allerdings nur in flüssigem Ammoniak stabilisierbar. Durch die Beimischung von Pentelatomen können die Anionen $(Tt_2Pn_2)^{2-}$ erhalten werden, in denen die Ladung um 2 reduziert wurde und die dadurch in Ethylendiamin löslich sind. Mit diesem Ansatz können Elemente in Clusterverbindungen eingebaut werden, für die es andernfalls keinen Zugang durch lösliche homoatomare Polyanionen gibt. Werden beide Elementsorten in das Clustergerüst inkorporiert, so müssen im Produkt auch konsequenterweise die elektronischen Bedürfnisse beider befriedigt werden. Aus diesem Grund werden häufig neuartige Clusteranionen erhalten, die andernfalls nicht darstellbar wären.[60a, 87] Durch den Einsatz binärer *Zintl*-Anionen konnten so erstmals auch f-Block-Elemente in intermetalloide Cluster eingebaut werden.[88] Weiterhin öffnet der Einsatz binärer Anionen alternative Reaktionspfade. Für Anionen $(E_x^A E_y^B)^{q-}$ ist es möglich, dass unter Verlust der Atome von Sorte E^A ein neues Polyanion $(E_z^B)^{w-}$ entsteht, welches andernfalls nicht zugänglich wäre. Dieses Polyanion kann anschließend entweder unverändert in Lösung verbleiben oder als Ligand für Übergangsmetallkomplexe dienen. Beispiele hierfür sind die erstmalige Darstellung des Bi_{11}^{3-} durch Oxidation von $(GaBi_3)^{2-}$ in Pyridin und die Bildung von $[Bi_9\{Ru(cod)\}_2]^{3-}$ aus $(TlBi_3)^{2-}$ und $[Ru(cod)(Me-Allyl)_2]$ (cod: 1,5-Cyclooctadien).[21, 55d]

Neben der Bildung intermetalloider Cluster können auch binäre *Zintl*-Anionen als Komplexliganden fungieren. Dies wurde sowohl für tetraedrische Anionen als auch den nortricyclanartigen Siebenatomkäfig $(Sn_2Sb_5)^{5-}$ und das *nido*-Clusterfragment $(Sn_3As_3)^{5-}$ beobachtet.[56, 62, 89] Der Cluster $[Tl_2Bi_6\{Ru(cod)\}]^{2-}$ stellt wiederum einen Grenzfall dar, in dem die Verbindung entweder als heterometallischer Cluster oder als Koordinationsverbindung aufgefasst werden kann.[21]

In Abbildung 1.6 sind einige ternäre intermetalloide und heterometallische Cluster dargestellt.

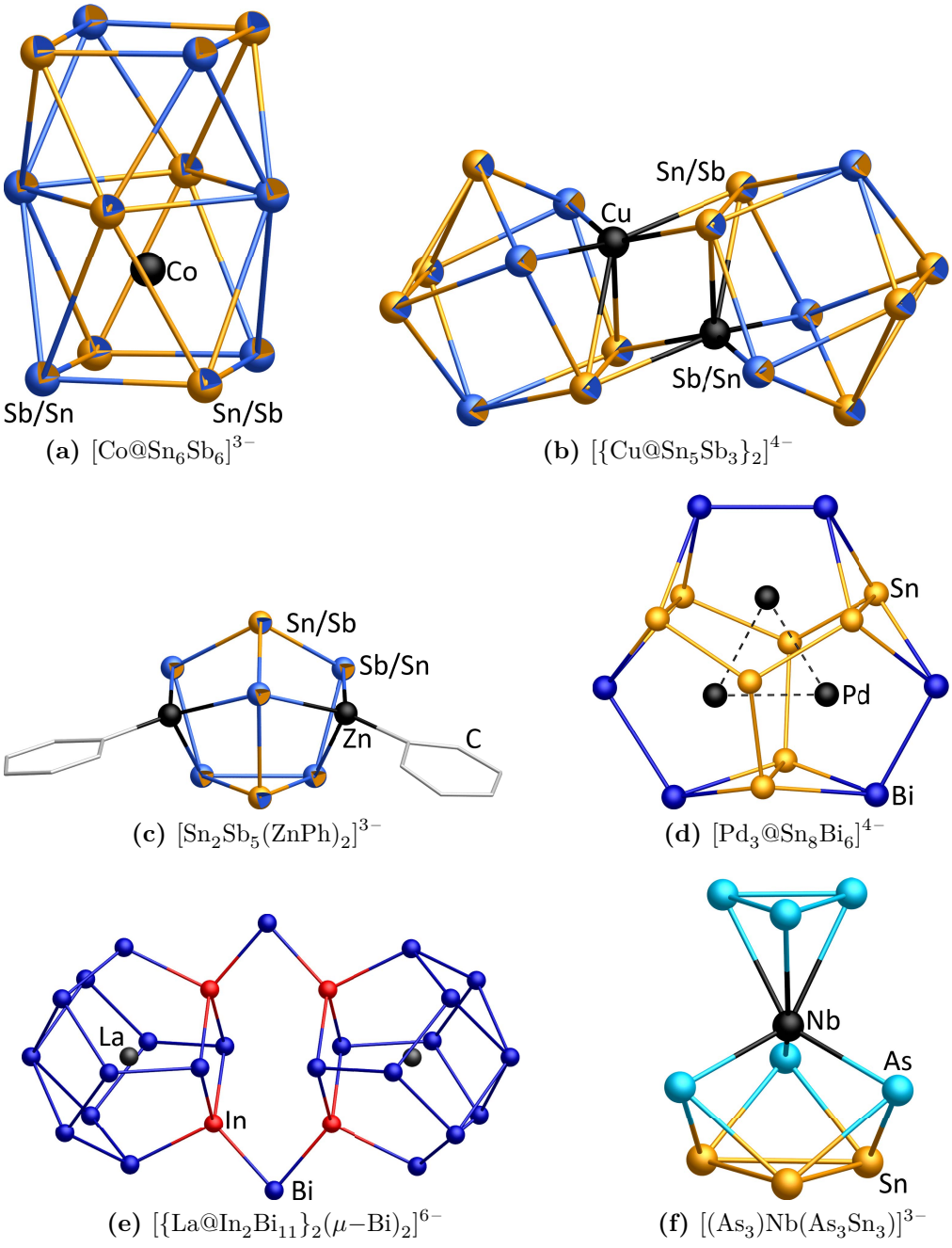

(a) $[Co@Sn_6Sb_6]^{3-}$ **(b)** $[\{Cu@Sn_5Sb_3\}_2]^{4-}$

(c) $[Sn_2Sb_5(ZnPh)_2]^{3-}$ **(d)** $[Pd_3@Sn_8Bi_6]^{4-}$

(e) $[\{La@In_2Bi_{11}\}_2(\mu{-}Bi)_2]^{6-}$ **(f)** $[(As_3)Nb(As_3Sn_3)]^{3-}$

Abbildung 1.6: Beispiele für ternäre intermetalloide und heterometallische Cluster und Koordinationsverbindungen mit *Zintl*-Anionen. Für in den Kristallstrukturen nicht unterscheidbare Elementkombinationen sind energetisch präferierte Isomere durch Oktandendarstellung in den jeweiligen Farben hervorgehoben. Referenzen für a: [87c], b: [60a], c: [56], d: [90], e: [88c], f: [91].

1.3.5 Elektronische Strukturen intermetalloider Cluster

Die Bindungssituationen in intermetalloiden und heterometallischen Clustern decken einen breiten Bereich ab. Anhand dieser Verbindungen können somit interessante und kuriose elektronische Situationen untersucht werden.

Wie bereits angeführt folgen insbesondere kleinere intermetalloide Cluster der Gruppe 14 häufig den Wade-Mingos-Regeln. Eine nähere Betrachtung dieser ist jedoch bereits lohnenswert und zeigt schnell die Grenzen des Modells auf. So liegt im Anion $[Ir@Sn_{12}]^{3-}$ eine nahezu perfekt ikosaedrische Clusterschale vor, während $[Pd@Pb_{12}]^{2-}$ bereits eine leichte Verzerrung aufweist, die in $[Co@Ge_{12}]^{3-}$ noch deutlich ausgeprägter ist.[72b, 73, 92] Alle Cluster weisen jedoch mit 50 VE gleiche Elektronenzahlen auf und erfüllen die Wade-Mingos-Regeln für einen 12-Atom *closo*-Käfig. In einer Reihe quantenchemischer Studien wurde gezeigt, dass für die Käfige $[M@Tt_n]^{q-}$ (n = 10, 12, 14) eine Reihe von Faktoren die Geometrie der Clusterhülle beeinflussen.[93] So spielt, neben den Radienverhältnissen von M:Tt, insbesondere die Wechselwirkung zwischen dem Zentralatom und der Clusterhülle eine entscheidende Rolle. Mitunter agieren die Zentralatome mit formal geschlossenen d^{10}-Schalen als Elektronendonoren für das Clustergerüst, was zu signifikanten Verzerrungen dessen führen kann.

Im Gegensatz dazu exisitieren Cluster, die vollständig mit einem elektronenpräzisen Modell beschrieben werden können. Dies ist beispielsweise für den 14-Atomcluster $[U@Pb_7Bi_7]^{3-}$ der Fall, in dem jede Position in der Clusterschale drei Bindungen aufweist und sich somit alle Atome wie ein Pentelelement verhalten.[88f] Hierfür sind insgesamt $5n = 70$ VE nötig, da jedes Atom zusätzlich ein freies Elektronenpaar aufweist. Gemäß des ZKB-Konzepts muss jedes Pb-Atom hierfür zu einem formalen Pb^--Ion reduziert werden. Im Zentrum des Clusters befindet sich ein U^{4+}-Ion, wodurch sich für die Clusterschale die Formel $(Pb_7Bi_7)^{7-}$ mit den nötigen 70 VE ergibt.

Es werden in einigen Fällen allerdings auch solche Cluster erhalten, die sich weder mit den Wade-Mingos-Regeln noch in einem vollständig elektronenpräzisen Bild erklären lassen. So kann es zu einem vollständigen Abweichen von diesen beiden Konzepten kommen, obwohl die Elektronenzahlen eine deltaedrische Struktur erwarten lassen würden, wie in $[M@Ge_{10}]^{3-}$ (M = Fe, Co), oder $[Fe@Sn_{10}]^{3-}$.[76a, 76b, 93a] Die Cluster $[M@Ge_{10}]^{3-}$ (M = Fe, Co) bilden pentagonale Prismen trotz 41 bzw. 42 VE, die eigentlich eine *closo*-Struktur in Form eines zweifach überkappten quadratischen Antiprismas erwarten lassen würden. Ein Intermediat zwischen diesen beiden Strukturen wird im Fall von $[Fe@Sn_{10}]^{3-}$

beobachtet, welches ebenfalls 41 VE und eine stark verzerrte, zweifach überkappte quadratisch antiprismatische Struktur besitzt. Die Ausbildung dieser Strukturtypen wird auf signifikante Wechselwirkungen zwischen den Zentralatomen und dem Clustergerüst zurückgeführt.

Ebenso kann es dazu kommen, dass durch die Verwendung binärer Edukte Clustergerüste mit Valenzelektronenzahlen gebildet werden, die weder die Wade-Mingos-Regeln erfüllen noch vollkommen elektronenpräzise Interpretationen erlauben. So liefert die Reaktion von $(Sn_2Sb_2)^{2-}$ mit $[Co(cod)_2]^-$ die intermetalloiden Cluster $[Co_{2-x}@Sn_{5+x}Sb_{7-x}]^{3-}$ (x = 0, 1) mit 56 VE.[87c] Diese Elektronenzahl liegt zwischen den für einen Wade-Cluster benötigten 50 VE und 60 VE für einen elektronenpräzisen Cluster und das Gerüst besteht aus zwei flächenverknüpften quadratischen Antiprismen. Eine quantenchemische Studie legt nahe, dass in diesen Clustern eine Kombination von elektronenpräzisen 2e-2c-Bindungen in den äußeren Vierringen und Mehrzentrenbindungen zu den endohedralen Atomen und dem zentralen Vierring vorliegt.

Diese kurze Übersicht zeigt bereits, wie komplex die elektronischen Strukturen intermetalloider Cluster sein können.

1.3.6 Alternative Reaktionspfade: Koordinationschemie

An dieser Stelle soll noch einmal explizit auf den zur Clusterbildung alternativen Reaktiospfad der Bildung von Koordinationsverbindungen von *Zintl*-Anionen mit Übergangsmetallkomplexen eingegangen werden. Die Anionen können in vielen Fällen Liganden der Metallkomplexe verdrängen und selber deren Rolle einnehmen, woraus Koodinationsverbindungen hervorgehen.

Insbesondere ligandstabilisierte $(Ge_9R_3)^-$-Cluster (R = sperrige Silylgruppen, insbesondere Hypersilyl: $Si(SiMe_3)_3$) eignen sich für solche Reaktionen - die Anbindung sperriger Substituenten R scheint nach bisherigem Kenntnisstand die Bildung intermetalloider Cluster zu unterdrücken.[94] Erst kürzlich wurde über einen synthetischen Zugang zu den entsprechenden $(Si_9R_3)^-$- und $(Si_9R_2)^{2-}$-Clustern (R = $Si(^tBu)_2H$) berichtet, so dass auch deren Reaktionsverhalten in naher Zukunft erforscht werden wird.[52]

Die Grenze zwischen Koordinationsverbindungen und heterometallischen Clustern ist fließend und in vielen Fällen sind beide Begriffe zutrefend. Anhand der Verbindungen $[(Ge_9)Sn(Ge_9)]^{4-}$ und $[(Ge_9)Zn(Ge_9)]^{4-}$ wurde die Natur der Wechselwirkungen zwischen Clustergerüst und koordiniertem Metallatom auf Basis quantenchemischer Analysen näher betrachtet.[95] Hierbei wurde eine Abhängigkeit der

Art der Wechselwirkung zwischen dem vom Clustergerüst koordinierten Metallatom und der koordinierenden Fläche gefunden. Wird das Metallatom durch die Atome in einer quadratische Fläche des Käfigs koordiniert, so kann es als Teil des Käfigs betrachtet werden, während eine Koordination über eine Dreiecksfläche als Donor-Akzeptor-Wechselwirkung zu verstehen ist.

In der Abbildung 1.7 sind die Strukturen ausgewählter Beispiele von Koordinationsverbindungen homoatomarer *Zintl*-Anionen gezeigt.

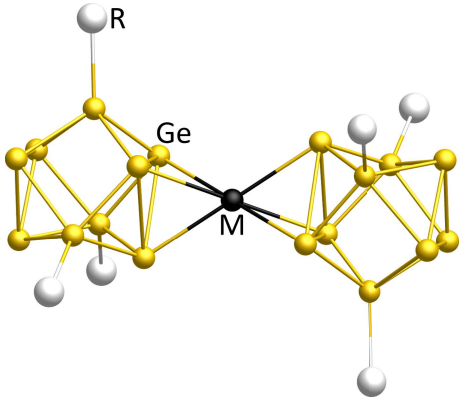

(a) Strukturmotiv: $[(Ge_9R_3)M(Ge_9R_3)]^q$ (R = sperrige Silylgruppen).

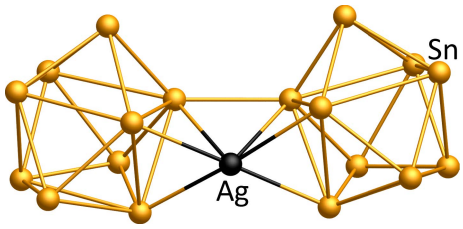

(b) $[Ag(Sn_9{-}Sn_9)]^{5-}$

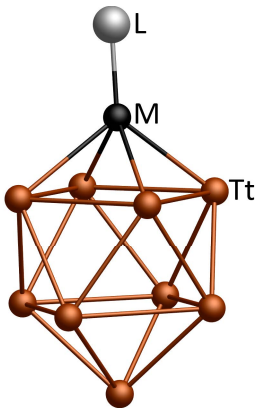

(c) Strukturmotiv: $[(Tt_9)M(L)]^{q-}$ (L = Ligand).

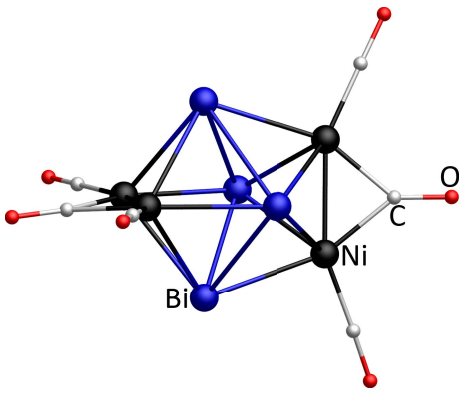

(d) $[Bi_4\{Ni_2(CO)_3\}_2]^{2-}$

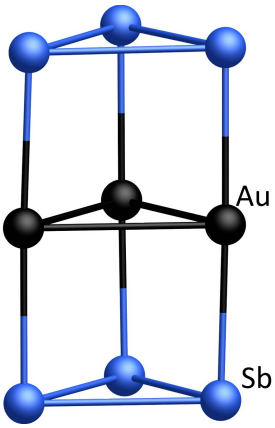

(e) $[(Sb_3)Au_3(Sb_3)]^{3-}$

Abbildung 1.7: Koordinationsverbindungen homoatomarer *Zintl*-Anionen. Bei (a) und (c) handelt es sich um Strukturmotive und es sind ausgewählte Beispiele zitiert. Referenzen für a: [94d], b: [96], c: [73], d: [48b], e: [79a].

2 Motivation

Zintl-Anionen und deren Folgeprodukte stellen Verbindungsklassen dar, die auf den ersten Blick zunächst sehr kurios wirken, da sich die (Halb)Metalle in den Clustern nicht in einer Art verhalten, die für (Halb)Metalle üblich wäre. Dies allein ist bereits ein Grund diese Verbindungen näher zu untersuchen und somit möglicherweise einen tieferen Einblick in das Verhalten der jeweiligen Atomsorten zu erhalten, die in anderen Bereichen der Chemie nicht zu Tage treten.

Binäre *Zintl*-Anionen bieten hierbei einen besonderen Reiz bei der Synthese intermetalloider Cluster, da durch die unterschiedlichen Atomsorten mitunter unterschiedliche Reaktivitäten an einem Clustergerüst erzielt werden können. Weiterhin schafft die Anwesenheit zweier Elemente mit unterschiedlichen Elektronenzahlen einen zusätzlichen Freiheitsgrad für die Bildung neuer Clustergerüste, die mit homoatomaren Reagenzien nicht zugänglich sind. Die Untersuchung homoatomarer Trielelementcluster ist auf deren Charakterisierung in intermetallischen Festkörpern beschränkt, da diese Clusteranionen eine hohe Ladung tragen, welche nicht in konventionellen Lösungsmitteln stabilisiert werden kann. Durch die Verwendung binärer Anionen ist es allerdings möglich Trielelemente in die Clustergerüste einzuführen, indem die hohe negative Ladung dieser Atome durch die Anwesenheit von Gruppe 14 oder Gruppe 15 Elementen „verdünnt“ wird. Hierbei stellt die Synthese neuer Anionen dieser Klasse eine große Herausforderung dar, da sie entsprechende ternäre Ausgangsmaterialien erfordert. Die ternären Phasendiagramme der allermeisten der relevanten Elementkombinationen sind bisher nicht untersucht worden und auch Berichte über ternäre Verbindungen sind rar.

Ziel dieser Arbeit war es, neue Zugänge zu binären *Zintl*-Anionen mit Trielelementen zu erforschen, die zur Synthese eingesetzten Edukte näher zu charakterisieren und im Anschluss daran die Reaktivität zu beleuchten. Das Reaktionsverhalten von Anionen des Typs $(Tt_2Pn_2)^{2-}$ wurde im Arbeitskreis *Dehnen* bereits vergleichsweise ausgiebig studiert, während entsprechende Untersuchungen für *Zintl*-Anionen mit Trielelementen sich auf ausgewählte Umsetzungen der Anionen $(TrBi_3)^{2-}$ (Tr = Ga, In) mit Lanthanoidkomplexen beschränkten. Im

Rahmen meiner Masterarbeit gelang mir die erstmalige Synthese von $(TlBi_3)^{2-}$ als Gemisch mit $(Tl_4Bi_5)^{3-}$.[97] Ein Hauptziel des Promotionsprojektes lag in der Syntheseoptimierung des $(TlBi_3)^{2-}$-Anions und der damit möglichen Reaktivitätsstudien. Weiterhin sollten entsprechende Untersuchungen für neue Elementkombinationen der Triel- und Tetrelelemente durchgeführt werden.

3 Kumulativer Teil

Aus den Forschungen im Rahmen des Promotionsprojektes sind bislang vier veröffentliche Publikationen erschienen.[1] Zusätzlich zu diesen bin ich Co-Autor eines eingeladenen Übersichtsartikels zu dem Themengebiet der intermetalloiden und heterometallischen Cluster, der derzeit begutachtet wird.

Die elektronischen Zusatzinformationen der Publikationen sind im Anhang C in den Abschnitten C.1 bis C.4 zu finden. Anhang D enthält die zum Abdruck und zur Verwendung der Publikationen benötigen Genehmigungen der Verlage.

Inhalt

[1] Zum Zeitpunkt der mündlichen Prüfung befand sich das Manuskript 3.4 noch im Begutachtungsprozess. Es wurde am 28.12.2018 zur Publikation angenommen und ist seit dem 05.01.2019 online zugänglich. Im Folgenden ist die vom Verlag akzeptierte, nicht editierte Version abgedruckt.

3.1 Main Group Metal-Actinide Magnetic Coupling and Structural Response Upon U^{4+} Inclusion Into Bi, Tl/Bi, or Pb/Bi Cages

Zitat: N. Lichtenberger, R. J. Wilson, A. R. Eulenstein, W. Massa, R. Clérac, F. Weigend, S. Dehnen, *J. Am. Chem. Soc.* **2016**, *138*, 9033–9036.

Abstract

The encapsulation of actinide ions in intermetalloid clusters has long been proposed but was never realized synthetically. We report the isolation and experimental, as well as quantum chemical, characterization of the uranium-centered clusters $[U@Bi_{12}]^{3-}$, $[U@Tl_2Bi_{11}]^{3-}$, $[U@Pb_7Bi_7]^{3-}$, and $[U@Pb_4Bi_9]^{3-}$, upon reaction of $(EE'Bi_2)^{2-}$ (E = Ga, Tl, E' = Bi; E = E' = Pb) and $[U(C_5Me_4H)_3]$ or $[U(C_5Me_4H)_3Cl]$ in 1,2-diaminoethane. For $[U@Bi_{12}]^{3-}$, magnetic susceptibility measurements rationalize an unprecedented antiferromagnetic coupling between a magnetic U^{4+} site and a unique radical $Bi_{12}{}^{7-}$ shell.

Zusammenfassung

In dieser Publikation wird über die Synthese der ersten actinoidzentrierten intermetalloiden Cluster $[U@Bi_{12}]^{3-}$, $[U@Tl_2Bi_{11}]^{3-}$, $[U@Pb_7Bi_7]^{3-}$ und $[U@Pb_4Bi_9]^{3-}$ berichtet. Diese wurden durch Umsetzungen binärer *Zintl*-Anionen $(EE'Bi_2)^{2-}$ (E = Ga, Tl, E' = Bi; E = E' = Pb) mit $[U(C_5Me_4H)_3]$ oder $[U(C_5Me_4H)_3Cl]$ in en erhalten und als deren $[K(Krypt{-}222)]^+$-Salze kristallisiert. Alle Salze wurden mittels Einkristall-Röntgenstrukturanalyse untersucht und die Strukturen der Clusteranionen bestimmt. Weitere Charakterisierungsmethoden umfassen Elektrospray-Ionisations-Massenspektrometrie (ESI-MS), Micro-Röntgenfluoreszenzanalyse (μ-RFA), magnetische Suszeptibilitätsmessungen und quantenchemische Studien. Zunächst wurden alle Synthesen ausgehend von der U(III)-Verbindung $[U(C_5Me_4H)_3]$ durchgeführt, da die Ionenradien von U^{3+} und La^{3+} nahezu identisch sind und für alle verwendeten *Zintl*-Anionen bereits intermetalloide Clusteranionen mit La^{3+}, ausgehend von $[La(C_5Me_4H)_3]$, erhalten wurden. Für die binären Anionen $(TlBi_3)^{2-}$ und $(Pb_2Bi_2)^{2-}$ wurden die Clusteranionen $[U@Tl_2Bi_{11}]^{3-}$, $[U@Pb_7Bi_7]^{3-}$ und $[U@Pb_4Bi_9]^{3-}$ mit bereits aus den entsprechenden Lanthanoidverbindungen bekannten Strukturmotiven erhalten. Die Ladung

des $[U@Tl_2Bi_{11}]^{3-}$ ist jedoch im Vergleich zu den analogen Lanthanoidverbindungen um 1 reduziert, was auf eine Oxidation der Uranatome von +3 in der Startverbindung zu +4 im finalen Produkt hinweist. Auch die Cluster $[U@Pb_7Bi_7]^{3-}$ und $[U@Pb_4Bi_9]^{3-}$ enthalten zentrale U^{4+}-Ionen. In Fall dieser Cluster kann die Ladung des Zentralatoms nicht aus der Gesamtladung abgeleitet werden, da sinch die Zusammensetzung der Clusterschale entsprechend der Ladung des Zentralatoms ändern kann, was für eine entsprechende Ladungskompensation sorgt. Die durch eine Kombination von ESI-MS und μ-RFA bestimmten Zusammensetzungen sowie die magnetischen Suszeptibilitätsmessungen sind klar mit der Anwesenheit von U^{4+}-Ionen in den Clustern im Einklang. Zur weiteren Bestätigung der Oxidationsstufe der Uranatom wurden alle Synthesen nochmals ausgehend von der U(IV)-Verbindung $[U(C_5Me_4H)_3Cl]$ durchgeführt und verliefen mit gleichbleibenden oder besseren Ausbeuten.

Wird $(GaBi_3)^{2-}$ mit $[U(C_5Me_4H)_3]$ zur Reaktion gebracht, so entsteht das Clusteranion $[U@Bi_{12}]^{3-}$. Entsprechende $[Ln@Sb_{12}]^{3-}$-Verbindungen (Ln = Y, La, Ho, Er, Lu) wurden kurz vor der Veröffentlichung unserer Publikation von *Sun* berichtet.[78b] Da für die Lanthanoide in den meisten Fällen nur die Oxidationsstufe +3 zugänglich ist, besteht in diesen Verbindungen kein Zweifel über die Oxidationsstufe der Zentralatome. Die für die Tl/Bi und Pb/Bi-Cluster erhaltenen Ergebnisse ließen allerdings Zweifel daran aufkommen, ob es sich bei $[U@Bi_{12}]^{3-}$ um $[U^{3+}@{Bi_{12}}^{6-}]^{3-}$ handelt, oder ob nicht $[U^{4+}@{Bi_{12}}^{7-}]^{3-}$ in Betracht gezogen werden muss. Eine genaue Betrachtung der Strukturparameter des $[U@Bi_{12}]^{3-}$ und ein Vergleich mit den $[Ln@Sb_{12}]^{3-}$-Clustern zeigt auffällige Diskrepanzen, die nicht durch die unterschiedlichen Atomsorten allein erklärt werden können, sondern auf eine Veränderung in der elektronischen Struktur innerhalb des Clusteranions hinweisen. Durch quantenchemische Studien konnten wir zeigen, dass $[U^{4+}@{Bi_{12}}^{7-}]^{3-}$ tatsächlich die zutreffende Beschreibung darstellt und nur so die experimentell bestimmten Strukturparameter reproduziert werden können. Hierfür wurden zwei Rechnungen mit unterschiedlichen Basissätzen durchgeführt. In einer wurden die f-Elektronen des Uranatoms in das effektive Kernpotential inkludiert, wodurch diese nicht mehr für Bindungen zur Verfügung stehen und die maximale Oxidationsstufe des Uranatoms virtuell auf +3 beschränkt wird. Der zweite Basissatz umfasst explizit alle Elektronen und stellt somit die f-Elektronen für Bindungswechselwirkungen zur Verfügung. Hierdurch sind für das Uranatom höhere Oxidationsstufen als +3 zugänglich und nur diese Rechnung reproduziert die Strukturparameter des Clusteranions korrekt. Die Veränderung der elektroni-

schen Struktur im Vergleich zu den Ln-Verbindungen wurden auf die Ausbildung einer bindenden Uran-Bismut-Wechselwirkung zurückgeführt, wofür ein sonst unbesetztes Orbital populiert werden muss. Dies ruft die strukturellen Veränderungen in der Clusterschale hervor. Weiterhin konnte die Verbindung wiederum von der U(IV)-Verbindung ausgehend synthetisiert werden. In den magnetischen Messungen wurde ein gegenüber den anderen Verbindungen reduziertes magnetisches Moment gemessen, was auf eine starke antiferromagnetische Kopplung zwischen der paramagnetischen Clusterschale und dem U^{4+}-Ion hindeutet.

Es gelang uns, die ersten actinoidzentrierten intermetalloiden Cluster darzustellen und die Bindundssituationen in diesen näher zu beleuchten. Die Ergebnisse zeigen, dass es deutliche Unterschiede zu den entsprechenden Lanthanoidverbindungen gibt und dass eine weitere Untersuchung dieser Verbindungsklasse lohnenswert ist. Abbildung 3.1 zeigt die Strukturen der in der Publikation präsentierten Clusteranionen.

Eigener Anteil

Die Idee für die Umsetzungen binärer *Zintl*-Anionen mit Actinoidkomplexen entwickelte ich auf einer Konferenz im Jahr 2014 zusammen mit *Stosh A. Kozimor* vom Los Alamos National Laboratory. Ziel war es, Verbindungen herzustellen, an denen die Wechselwirkungen zwischen f-Block- und Hauptgruppenelementen studiert werden können. Um die Umsetzbarkeit dieser Idee zu testen habe ich zunächst die Verbindung $[U(cpMe_4H)_3]$ (cp: Cyclopentadienyl-Anion) hergestellt und mit meinem primär verwendeten Edukt $[K(Krypt{-}222)]_2(TlBi_3)\cdot 0.5en$ umgesetzt. Die Einkristallstrukturbestimmung des Produktes $[K(Krypt{-}222)]_2[K(Krypt{-}222)(en)][U@Tl_2Bi_{11}]\cdot tol$ habe ich selbst durchgeführt, ebenso wie einen Großteil der Strukturlösung und Verfeinerung. Anhand dieses Strukturmodells konnte bereits die Oxidation von U(III) zu U(IV) geschlussfolgert werden. Aufgrund ausgeprägter Fehlordnungen in der Struktur sowie einer schlechten Kristallqualität wurde die endgültige Verfeinerung durch Prof. Dr. *Werner Massa* abgeschlossen. Um ein umfassenderes Bild der Reaktivität binärer *Zintl*-Anionen gegenüber $[U(cpMe_4H)_3]$ zu erhalten stellte ich die Verbindung meinen Kollegen Dr. *Robert J. Wilson* und *Armin Eulenstein*, der zu dieser Zeit seine Masterarbeit in unserem Labor anfertigte, zur Verfügung. Die entsprechenden Umsetzungen mit den von Ihnen bearbeiteten binären Edukten $(GaBi_3)^{2-}$ und $(Pb_2Bi_2)^{2-}$ sowie die entsprechenden Einkristallstrukturanalysen führten Sie eigenständig durch, wobei alle finalen Strukturverfeinerungen durch Prof. Dr. *Werner Massa* erfolgten. Alle

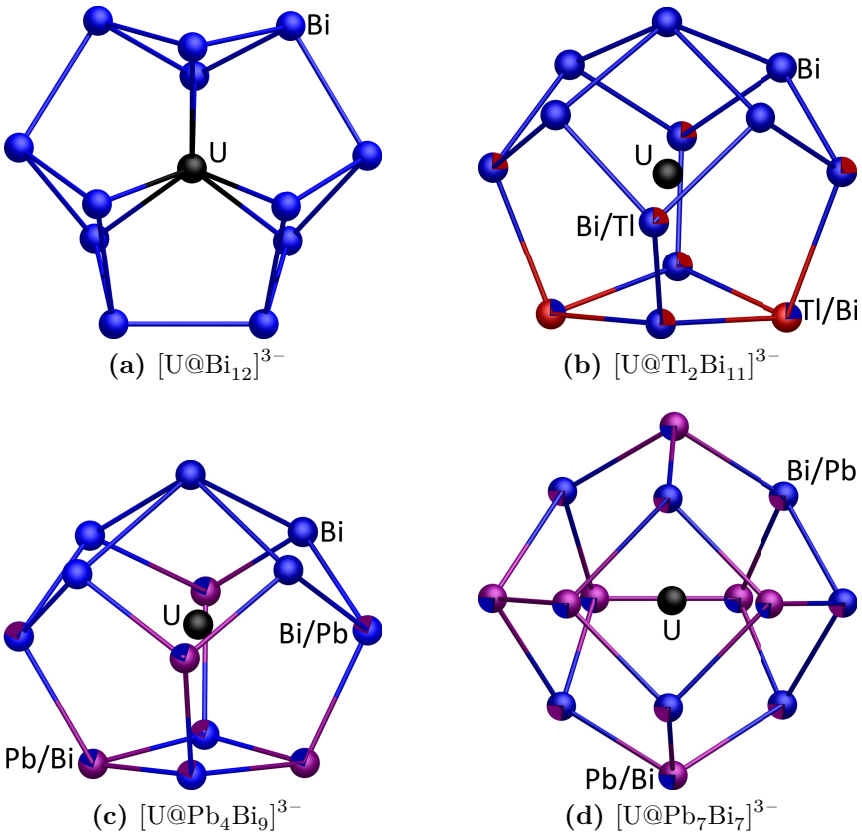

(a) $[U@Bi_{12}]^{3-}$ **(b)** $[U@Tl_2Bi_{11}]^{3-}$

(c) $[U@Pb_4Bi_9]^{3-}$ **(d)** $[U@Pb_7Bi_7]^{3-}$

Abbildung 3.1: Strukturen der ersten actinoidzentrierten intermetalloiden Cluster.[88f] Für in den Kristallstrukturen nicht unterscheidbare Elementkombinationen sind energetisch präferierte Isomere durch Oktandendarstellung in den jeweiligen Farben hervorgehoben.

massenspektrometrischen Analysen wurden in Zusammenarbeit mit der zentralen Abteilung für Massenspektrometrie und Elementanalytik durchgeführt, wobei der jeweilige Experimentator die Probenvorbereitung übernahm und die Messungen durch *Jan Bamberger* und Dr. *Uwe Linne* in unserem Beisein erfolgten. Die Anfertigung der Proben für die magnetischen Messungen wurden ebenfalls durch den jeweiligen Experimentator durchgeführt - die Messungen selbst wurden in einer Kooperation durch Dr. *Rodolphe Clérac* vorgenommen. PD. Dr. *Florian Weigend* übernahm alle quantenchemischen Rechnungen. Das Verfassen des Manuskripts erfolgte im Dialog und alle Personen trugen zu allen Teilen der Veröffentlichung bei. Insbesondere das tiefere Verständnis der Bindungsverhältnisse im ungewöhnlichen Clusteranion $[U@Bi_{12}]^{3-}$ entstand durch Diskussionen zwischen allen beteiligten Autoren.

JACS
JOURNAL OF THE AMERICAN CHEMICAL SOCIETY

Communication

pubs.acs.org/JACS

Main Group Metal–Actinide Magnetic Coupling and Structural Response Upon U^{4+} Inclusion Into Bi, Tl/Bi, or Pb/Bi Cages

Niels Lichtenberger,[†,∥] Robert J. Wilson,[†,∥] Armin R. Eulenstein,[†,∥] Werner Massa,[†] Rodolphe Clérac,[§,⊥] Florian Weigend,[‡] and Stefanie Dehnen*[,†]

[†]Fachbereich Chemie und Wissenschaftliches Zentrum für Materialwissenschaften (WZMW), Philipps-Universität Marburg, Hans-Meerwein-Straße, 35043 Marburg, Germany

[‡]Institut für Nanotechnologie, Karlsruher Institut für Technologie, Hermann-von-Helmholtz Platz 1, D-76344 Eggenstein-Leopoldshafen, Germany

[§]CNRS, CRPP, UPR 8641, F-33600 Pessac, France

[⊥]Univ. Bordeaux, CRPP, UPR 8641, F-33600 Pessac, France

Supporting Information

ABSTRACT: The encapsulation of actinide ions in intermetalloid clusters has long been proposed but was never realized synthetically. We report the isolation and experimental, as well as quantum chemical, characterization of the uranium-centered clusters $[U@Bi_{12}]^{3-}$, $[U@Tl_2Bi_{11}]^{3-}$, $[U@Pb_7Bi_7]^{3-}$, and $[U@Pb_4Bi_9]^{3-}$, upon reaction of $(EE'Bi_2)^{2-}$ (E = Ga, Tl, E′ = Bi; E = E′ = Pb) and $[U(C_5Me_4H)_3]$ or $[U(C_5Me_4H)_3Cl]$ in 1,2-diaminoethane. For $[U@Bi_{12}]^{3-}$, magnetic susceptibility measurements rationalize an unprecedented antiferromagnetic coupling between a magnetic U^{4+} site and a unique radical Bi_{12}^{7-} shell.

Ligand-free metal clusters, often described as superatomic systems,[1] show intriguing size-dependent electronic properties, which define their optoelectronic behavior, reactivity, and magnetism.[2] Moreover, multimetallic clusters can be viewed as nanosized alloys or as doped (semi)metal particles, making them attractive to experimentalists as well as theorists in this field.[3] They are regarded as promising catalysts and as precursors to novel intermetallic phases with new structural patterns. Here, intermetalloid clusters $[M@E_n]$ that are obtained by encapsulation of transition and lanthanide metal atoms (M) in main group element clusters (E_n) turned out to be ideal candidates for such systems. They have been intensely studied over the past two decades by a variety of synthetic approaches[4] and by spectroscopy[5] and quantum chemistry.[6]

In contrast, stable actinide-centered main group metal clusters have been predicted theoretically but heretofore not confirmed experimentally.[7] The realization of such clusters would be of great interest in regard to their structural, bonding, and magnetic properties, and would further complement the dynamic research taking place in the field of actinide chemistry.[8] Binary main group metal shells display remarkable flexibility of composition, nuclearity, and charge and thus represent ideal systems for trapping metal atoms with flexible oxidation states.

Herein we report the successful transfer of a synthetic approach, formerly applied to the syntheses of ternary lanthanide-centered main group metal clusters,[9] to their first actinide-centered analogs $[K(crypt\text{-}222)]_3[U@Bi_{12}]\cdot tol\cdot 1.5en$ (**1**), $[K(crypt\text{-}222)]_2[K(crypt\text{-}222)(en)][U@Tl_2Bi_{11}]\cdot tol$ (**2**), and $[K(crypt\text{-}222)]_3[U@Pb_7Bi_7]_{0.66}[U@Pb_4Bi_9]_{0.34}\cdot 2tol$ (**3**). Compounds **1**–**3** exhibit unique structural and electronic peculiarities not observed in the Ln congeners. They were first synthesized by reactions of $[K(crypt\text{-}222)]_2(EE'Bi_2)\cdot en$ (E = Ga, Tl, E′ = Bi; E = E′ = Pb)[10] with $[U(C_5Me_4H)_3]$[11] (denoted as $[UCp^{\#}_3]$ in the following) in 1,2-diaminoethane (en) and were characterized by means of X-ray diffraction, electrospray ionization (ESI) mass spectrometry, micro X-ray fluorescence spectroscopy (μ-XFS), quantum chemistry, and magnetic measurements.

Compound **1** was obtained as black crystalline prisms in ~13% yield upon using $(GaBi_3)^{2-}$ as the binary precursor. In the anion in compound **1** (Figure 1), a U atom is surrounded by an unprecedented polybismuthide architecture (U–Bi_B 3.119(3)–3.167(3) Å; U–Bi_A 3.463(3)–3.545(3) Å). The doughnut-like Bi_{12} shell may be described as an assembly of three Bi_4 butterfly-like moieties (Bi_A–Bi_B 3.051(4)–3.109(4) Å), which are linked by three shorter Bi_A–Bi_A contacts along

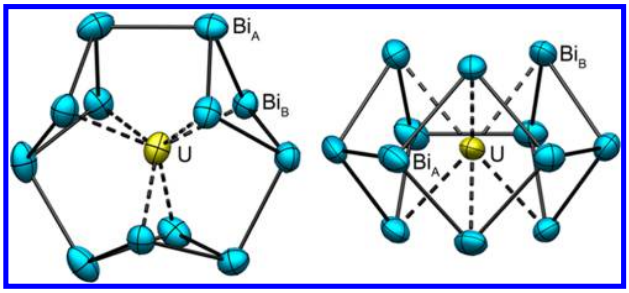

Figure 1. Top (left) and side (right) views of the molecular structure of one of the two individual anions, $[U@Bi_{12}]^{3-}$, in **1** (thermal ellipsoids at 50% probability). Structural details are given in Table S2.

Received: May 6, 2016
Published: July 8, 2016

DOI: 10.1021/jacs.6b04363
J. Am. Chem. Soc. 2016, 138, 9033–9036

the molecular "equator" (3.018(4)−3.046(4) Å). The structure is related to that of known lanthanide-centered 14-atom cages (Figure S13). However, the $[U@Bi_{12}]^{3-}$ anion lacks two atoms at the molecular "poles" that would otherwise complete a spherical cluster shell like that of $[Ln@Sn_7Bi_7]^{4-}$ or the oblate cluster $[Pd_3@Sn_8Bi_6]^{4-}$.[9b,12] The relatively large number of 69 valence electrons in **1** precludes the adoption of any known 12-atom topology, like an icosahedron, a recently reported D_{2d} symmetric structure, or a hexagonal prism.[6b,13]

Despite reacting a binary anion, $(GaBi_3)^{2-}$, we did not obtain a ternary cluster anion. However, it is known that $(GaBi_3)^{2-}$ is sensitive to disproportionation into elemental Ga^0 and polybismuthides, cf. the formation of Bi_{11}^{3-} and Bi_4^{2-} from $(GaBi_3)^{2-}$ in pyridine.[14] The structure of the anion in **1** suggests that $(GaBi_3)^{2-}$ again undergoes disproportionation and concomitant formation of Ga^0 beside Bi_4^{2-}, the latter of which successively replace precursor ligands. As illustrated in Scheme 1, organic 6π Hückel aromatic systems are thus replaced with inorganic ones.

Scheme 1. Calculated Minimum Structures Showing Folding and Coupling of Bi_4^{2-} Rings (turquoise) As They Replace $Cp^{\#}$ Ligands Around the U Ion during Formation of $[U@Bi_{12}]^{3-}$

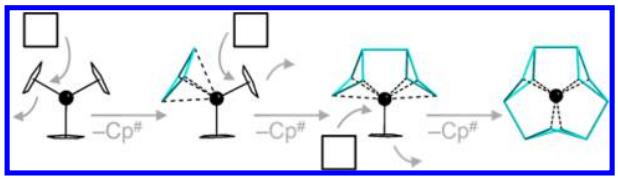

Quantum chemical calculations reproduce the folding and thus dearomatization of the Bi_4^{2-} rings upon substitution of the second and third ligand and subsequent Bi−Bi bond formation. The third exchange step produces the unique $[U@(Bi_4)_3]^{3-}$ = $[U@Bi_{12}]^{3-}$ anion in **1**. We consider the shown pathway to be chemically more plausible than trapping of a U ion by an anionic Bi_{12} shell preformed without a (templating) metal atom.

One might assume that the cluster anion in **1** consists of a U^{3+} ion that is surrounded by a diamagnetic Bi_{12}^{6-} shell. However, magnetic measurements of **1** (*vide infra*) indicate the presence of U^{4+}. The anion in **1** should thus be formally described as $[U^{4+}@Bi_{12}^{7-}]^{3-}$, with a radical Bi_{12}^{7-} shell. An odd electron number is a very uncommon feature of main group polyanions and has so far only been observed for the polygermanide shell of the intermetalloid cluster anion $[Ru@Ge_{12}]^{3-}$.[13a] To confirm the findings, we produced compound **1** directly from a U^{4+} precursor, $[UCp^{\#}_3Cl]$,[11a] thus corroborating the preference for this oxidation state in the present system.

DFT calculations[15] helped to rationalize the experimental findings of an oxidation state higher than U^{3+} and shorter Bi−Bi distances between the Bi_4 rings than within them. The most favorable orbital occupation (in D_{3h} symmetry) is a doublet state (with slight spin contamination, $\langle S^2\rangle$ = 0.79) at level ECP78,[15c,h] TZVP,[15f,h] B3LYP,[15b,d] COSMO.[15e] Bi−Bi distances are 3.090 Å within the Bi_4 rings and 2.971 Å between them, reproducing the experimental trend. Notably, this is reverse of calculations of a bare Bi_{12}^{6-} unit with respective values of 3.043 and 3.138 Å. This indicates that the f electrons are involved in the bonding (otherwise a quartet state would be expected), leading to strengthening of the Bi_A−Bi_A bonds. For elucidation, we considered the frontier orbitals of the bare Bi_{12}^{6-} unit and inspected the changes upon inserting a U atom (Figure 2). The LUMO of Bi_{12}^{6-} (a_2'') is a combination of p_z

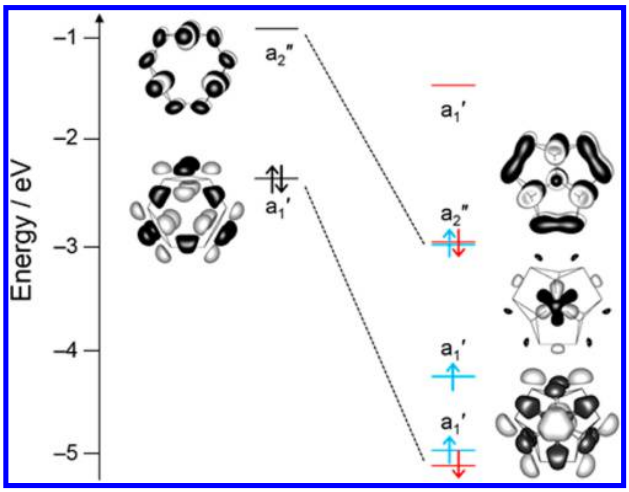

Figure 2. Frontier orbitals of Bi_{12}^{6-} and $[U@Bi_{12}]^{3-}$. Contours are drawn at ±0.025 au. The (singly occupied) open shell orbitals of $[U@Bi_{12}]^{3-}$ are indicated by blue (α) or red (β) color.

orbitals, being antibonding within the Bi_4 rings, but bonding between them. Insertion of a U atom stabilizes this MO by admixture of the f_{z^3} orbital (also a_2'') and its occupation. This results in elongation of bonds within the Bi_4 rings and shortening between them. The unpaired (f) electron occupies an a_1' orbital; a second a_1' orbital is a bonding combination of the HOMO of the Bi_{12}^{6-} unit and the d_{z^2} of U, again being antibonding within the Bi_4 rings and bonding between them. Further f (as well as d and s) contributions occur in the other MOs, leading to a (Mulliken)[16] population of 1.80 electrons and (weak) antiferromagnetic coupling. This is reflected by a surplus of 1.36 α electrons at U and 0.05 β electrons for each of the six Bi atoms closest to U, in line with the magnetic measurements that indicate antiferromagnetic coupling (*vide infra*) and the slight deviation of $\langle S^2\rangle$ from the ideal value of 0.75.

The crucial role of the f electrons becomes even more evident when they are included in the effective core potential, MWB-ECP-81.[15g] This restricts the bonding activity of the U atom to its s and d electrons and its maximum oxidation state to +3. Calculated distances within the Bi_4 rings are then shorter (3.027 Å), while between them they are longer (3.200 Å). Hence, the use of f electrons, formally producing U^{4+}, must be considered for the computed structural trend to agree with the experimental observation.

A similar anion was reported very recently for Ln^{3+}/Sb clusters.[17] However, as f electrons are not involved in the bonding of Ln^{3+} ions, no folding of the main group metal four-membered rings is observed, and the bond lengths within/between the main group metal four-membered rings comply with the trend that was calculated for $[U@Bi_{12}]^{3-}$ when forcing it into a U^{3+} situation. This supports once more the involvement of f electrons in the bonding of **1** and rationalizes its electronic and magnetic peculiarities.

To explore whether the result obtained with $(GaBi_3)^{2-}$ was due to the group 13/15 elemental combination in general or due to the inhomogeneous Ga/Bi combination in particular, we

DOI: 10.1021/jacs.6b04363
J. Am. Chem. Soc. 2016, 138, 9033−9036

further tested the pseudo-homoatomic anion $(TlBi_3)^{2-}$. This afforded **2** in a 65% yield. The cluster anion in **2**, $[U@Tl_2Bi_{11}]^{3-}$, adopts a 13-atom cage structure with a 2:11 ratio of the group 13:15 elements, as confirmed by μ-XFS analysis (see Table S6). The composition is in agreement with quantum chemical studies applying DFT methods[15] along with first-order perturbation theory that also allows for the assignment of atomic positions of atoms of similar nuclear charge.[18] Although the overall topology and formation mechanism of the 13-atom cage is known,[13c] the anion in **2** exhibits some structural peculiarities (Figure 3). A notable folding of the basal face is

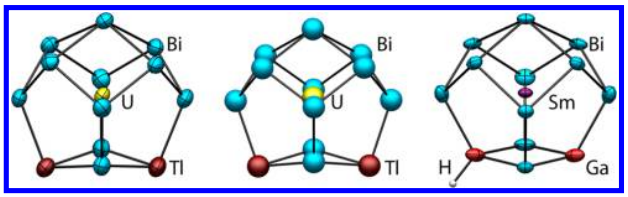

Figure 3. Experimentally determined structures (thermal ellipsoids at 50% probability) of $[U@Tl_2Bi_{11}]^{3-}$ (left, for structural parameters see Table S3) and $[Sm@Ga_2HBi_{11}]^{3-}$ (right)[9d] and the optimized structure of $[U@Tl_2Bi_{11}]^{3-}$, as obtained from DFT calculations (center).

observed, in agreement with DFT calculations for $[U@Tl_2Bi_{11}]^{3-}$. This is probably due to the relatively large (anionic) Tl atoms that do not allow for a planar four-membered Tl_2Bi_2 ring.

The total charge of the cluster is 3−. However, unlike the situation in the Sm^{3+} clusters in $[K(crypt\text{-}222)]_3[Sm@Ga_2HBi_{11}]_{0.9}[Sm@Ga_3H_3Bi_{10}]_{0.1}\cdot en\cdot tol$,[9d] there is no indication for a protonation of the (Lewis-basic) "Tl^{2-}" atoms in the high-resolution mass spectrum (see Figure S18). This, along with the magnetic measurements (*vide infra*), confirms the formal 4+ oxidation state of the U atom. Again, a formation from $[UCp^{\#}_3Cl]$ is successful, in accordance with the given oxidation state.

As another validation of the observed inclusion of U^{4+}, we reacted $[UCp^{\#}_3]$ with the $(Pb_2Bi_2)^{2-}$ anion,[19] from which well-studied Ln^{3+} compounds have been previously derived.[9e] Compound **3** crystallizes from this reaction in ∼28% yield. It is isomorphic with the known Nd^{3+} compound, $[K(crypt\text{-}222)]_3[Nd@Pb_6Bi_8]_{0.545}[Nd@Pb_3Bi_{10}]_{0.455}\cdot 2tol$.[9e] Again, magnetic measurements (*vide infra*) are in agreement with a 4+ oxidation state for the U atom, which agrees with the observation that compound **3** can also be directly obtained from $[UCp^{\#}_3Cl]$. Because the clusters in **3** have overall 3− charges, their formulations differ from those in the Nd^{3+} congener: $[U^{4+}@(Pb_7Bi_7)^{7-}]^{3-}$ and $[U^{4+}@(Pb_4Bi_9)^{7-}]^{3-}$ in agreement with all further analytic data.

As shown in Figure 4, the χT product is about 0.66 cm^3 K/mol for **1** and 1.0 cm^3 K/mol for **2** and **3** at 270 K. The high temperature value for **2** and **3** most likely indicates the presence of a U^{4+} center here, although these data alone cannot exclude 3+ and 5+ oxidation states.[8b] In the case of **1**, the lower χT product at 270 K supports a strong antiferromagnetic coupling between the $S = 1/2$ radical Bi_{12}^{7-} shell and the U^{4+} magnetic center. The almost identical temperature dependence of the magnetic susceptibility, and particularly the low 1.8-K χT values for **2** and **3** (0.09 and 0.11 cm^3 K/mol, respectively), leave no doubt of the 4+ oxidation state of the U site,[8b] in agreement with the above-mentioned compositions and total charges of

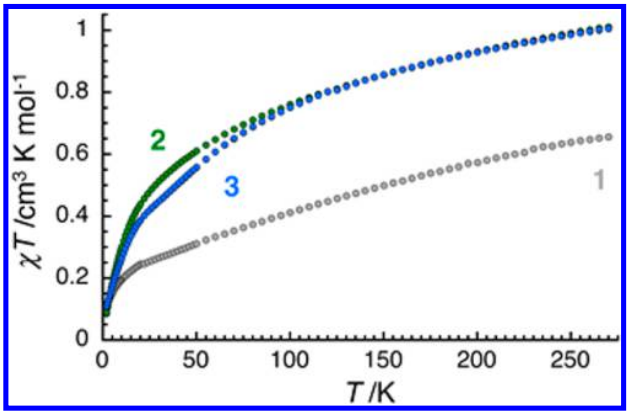

Figure 4. Temperature dependence of χT (magnetic susceptibility $\chi = M/H$ per mole of cluster at 0.1 and 1 T below and above 100 K, respectively) for **1**−**3**.

the anions in **2** and **3**. For **1**, the strong antiferromagnetic coupling between the radical Bi_{12}^{7-} shell and the U^{4+} centers induces a thermal decrease of the χT product that is superposed to the intrinsic magnetic properties of the actinide ion seen in **2** and **3**. The low 1.8 K χT value (0.10 cm^3 K/mol) suggests that the resulting magnetic entity has a singlet or weakly paramagnetic ground state.

■ ASSOCIATED CONTENT

Supporting Information

The Supporting Information is available free of charge on the ACS Publications website at DOI: 10.1021/jacs.6b04363.

Crystallographic data (CIF)
Crystallographic data (CIF)
Crystallographic data (CIF)
Details on syntheses, single-crystal XRD, EDX, μ-XFS, ESI-MS, magnetic measurements, DFT studies (PDF)

■ AUTHOR INFORMATION

Corresponding Author

*dehnen@chemie.uni-marburg.de

Author Contributions

‖These authors contributed equally.

Notes

The authors declare no competing financial interest.

■ ACKNOWLEDGMENTS

Financial support by Deutsche Forschungsgemeinschaft (DFG) within the framework of GRK1782, University of Bordeaux, Conseil Régional d'Aquitaine, CNRS, Marburg University Research Academy (MARA). We thank C. Donsbach for help with μ-XFS and F. Kraus and S. Rudel for provision of UCl_4.

■ REFERENCES

(1) (a) Jena, P. *J. Phys. Chem. Lett.* **2013**, *4*, 1432. (b) Luo, Z. X.; Castleman, A. W. *Acc. Chem. Res.* **2014**, *47*, 2931.
(2) (a) McCoy, R. S.; Choi, S.; Collins, G.; Ackerson, B. J.; Ackerson, C. J. *ACS Nano* **2013**, *7*, 2610. (b) Reveles, J. U.; Clayborne, P. A.; Reber, A. C.; Khanna, S. N.; Pradhan, K.; Sen, P.; Pederson, M. R. *Nat. Chem.* **2009**, *1*, 310.
(3) (a) Medel, V. M.; Reveles, J. U.; Khanna, S. N.; Chauhan, V.; Sen, P.; Castleman, A. W. *Proc. Natl. Acad. Sci. U. S. A.* **2011**, *108*, 10062. (b) Korber, N. *Angew. Chem., Int. Ed.* **2009**, *48*, 3216.

DOI: 10.1021/jacs.6b04363
J. Am. Chem. Soc. 2016, 138, 9033−9036

(4) (a) Sevov, S. C.; Goicoechea, J. M. *Organometallics* **2006**, *25*, 5678. (b) Scharfe, S.; Kraus, F.; Stegmaier, S.; Schier, A.; Fässler, T. F. *Angew. Chem., Int. Ed.* **2011**, *50*, 3630. (c) Fässler, T. F. *Struct. Bonding (Berlin, Ger.)* **2011**, *140*, 91. (d) Weinert, B.; Dehnen, S. *Structure and Bonding (Berlin)*; Springer: Berlin, 2016 10.1007/430_2015_5002.
(5) (a) Cui, L.-F.; Huang, X.; Wang, L.-M.; Li, J.; Wang, L.-S. *Angew. Chem., Int. Ed.* **2007**, *46*, 742. (b) Grubisic, A.; Wang, H. P.; Ko, Y. J.; Bowen, K. H. *J. Chem. Phys.* **2008**, *129*, 054302. (c) Grubisic, A.; Ko, Y. J.; Wang, H. P.; Bowen, K. H. *J. Am. Chem. Soc.* **2009**, *131*, 10783.
(6) (a) Li, T.; Feng, Z.; Jing, C.; Hong, F.; Cao, S.; Zhang, J. *Chem. Phys. Lett.* **2012**, *543*, 106. (b) Goicoechea, J. M.; McGrady, J. E. *Dalton Trans.* **2015**, *44*, 6755.
(7) (a) Singh, A. K.; Kumar, V.; Kawazoe, Y. *J. Phys. Chem. B* **2005**, *109*, 15187. (b) Dognon, J. P.; Clavaguera, C.; Pyykkö, P. *Angew. Chem., Int. Ed.* **2007**, *46*, 1427. (c) Dognon, J.-P.; Clavaguera, C.; Pyykkö, P. *C. R. Chim.* **2010**, *13*, 884. (d) Dognon, J.-P.; Clavaguera, C.; Pyykkö, P. *Chem. Sci.* **2012**, *3*, 2843.
(8) (a) Hayton, T. W. *Chem. Commun.* **2013**, *49*, 2956. (b) Kindra, D. R.; Evans, W. J. *Chem. Rev.* **2014**, *114*, 8865. (c) La Pierre, H. S.; Meyer, K. *Prog. Inorg. Chem.* **2014**, *58*, 303. (d) Liddle, S. T. *Angew. Chem., Int. Ed.* **2015**, *54*, 8604. (e) Meihaus, K. R.; Long, J. R. *Dalton Trans.* **2015**, *44*, 2517.
(9) (a) Lips, F.; Clérac, R.; Dehnen, S. *Angew. Chem., Int. Ed.* **2011**, *50*, 960. (b) Lips, F.; Holynska, M.; Clérac, R.; Linne, U.; Schellenberg, I.; Pöttgen, R.; Weigend, F.; Dehnen, S. *J. Am. Chem. Soc.* **2012**, *134*, 1181. (c) Weinert, B.; Weigend, F.; Dehnen, S. *Chem. - Eur. J.* **2012**, *18*, 13589. (d) Weinert, B.; Müller, F.; Harms, K.; Clérac, R.; Dehnen, S. *Angew. Chem., Int. Ed.* **2014**, *53*, 11979. (e) Ababei, R.; Massa, W.; Weinert, B.; Pollak, P.; Xie, X.; Clérac, R.; Weigend, F.; Dehnen, S. *Chem. - Eur. J.* **2015**, *21*, 386.
(10) crypt-222 = 4,7,13,16,21,24-hexaoxa-1,10-diazabicyclo[8.8.8] hexacosane.
(11) (a) Cloke, F. G. N.; Hawkes, S. A.; Hitchcock, P. B.; Scott, P. *Organometallics* **1994**, *13*, 2895. (b) Parry, J.; Carmona, E.; Coles, S.; Hursthouse, M. *J. Am. Chem. Soc.* **1995**, *117*, 2649. (c) del Mar Conejo, M.; Parry, J. S.; Carmona, E.; Schultz, M.; Brennann, J. G.; Beshouri, S. M.; Andersen, R. A.; Rogers, R. D.; Coles, S.; Hursthouse, M. *Chem. - Eur. J.* **1999**, *5*, 3000. (d) Evans, W. J.; Kozimor, S. A.; Ziller, J. W.; Fagin, A. A.; Bochkarev, M. N. *Inorg. Chem.* **2005**, *44*, 3993.
(12) (a) Lips, F.; Clérac, R.; Dehnen, S. *J. Am. Chem. Soc.* **2011**, *133*, 14168. (b) Withers, N. *Nat. Chem.* **2011**, *3*, 752.
(13) (a) Espinoza-Quintero, G.; Duckworth, J. C.; Myers, W. K.; McGrady, J. E.; Goicoechea, J. M. *J. Am. Chem. Soc.* **2014**, *136*, 1210. (b) Mitzinger, S.; Broeckaert, L.; Massa, W.; Weigend, F.; Dehnen, S. *Chem. Commun.* **2015**, *51*, 3866. (c) Mitzinger, S.; Broeckaert, L.; Massa, W.; Weigend, F.; Dehnen, S. *Nat. Commun.* **2016**, *7*, 10480.
(14) Weinert, B.; Eulenstein, A. R.; Ababei, R.; Dehnen, S. *Angew. Chem., Int. Ed.* **2014**, *53*, 4704.
(15) (a) TURBOMOLE V7.0 2015, a development of University of Karlsruhe and Forschungszentrum Karlsruhe GmbH, 1989–2007,TURBOMOLE GmbH, since 2007; available from http://www.turbomole.com. (b) Lee, C. T.; Yang, W. T.; Parr, R. G. *Phys. Rev. B: Condens. Matter Mater. Phys.* **1988**, *37*, 785. (c) Küchle, W.; Dolg, M.; Stoll, H.; Preuss, H. *Mol. Phys.* **1991**, *74*, 1245. (d) Becke, A. D. *J. Chem. Phys.* **1993**, *98*, 5648. (e) Klamt, A.; Schüürmann, G. *J. Chem. Soc., Perkin Trans. 2* **1993**, 799. (f) Eichkorn, K.; Weigend, F.; Treutler, O.; Ahlrichs, R. *Theor. Chem. Acc.* **1997**, *97*, 119. (g) Moritz, A.; Cao, X. Y.; Dolg, M. *Theor. Chem. Acc.* **2007**, *117*, 473. (h) Moritz, A.; Dolg, M. *Theor. Chem. Acc.* **2008**, *121*, 297.
(16) Mulliken, R. S. *J. Chem. Phys.* **1955**, *23*, 1833.
(17) Min, X.; Popov, I. A.; Pan, F. X.; Li, L. J.; Matito, E.; Sun, Z. M.; Wang, L. S.; Boldyrev, A. I. *Angew. Chem., Int. Ed.* **2016**, *55*, 5531.
(18) (a) Weigend, F.; Schrodt, C. *Chem. - Eur. J.* **2005**, *11*, 3559. (b) Weigend, F.; Schrodt, C.; Ahlrichs, R. *J. Chem. Phys.* **2004**, *121*, 10380.
(19) Ababei, R.; Heine, J.; Holynska, M.; Thiele, G.; Weinert, B.; Xie, X.; Weigend, F.; Dehnen, S. *Chem. Commun.* **2012**, *48*, 11295.

DOI: 10.1021/jacs.6b04363
J. Am. Chem. Soc. 2016, 138, 9033–9036

3.2 Between Localization and Delocalization: $Ru(cod)^{2+}$ Units in the Zintl Clusters $[Bi_9\{Ru(cod)\}_2]^{3-}$ and $[Tl_2Bi_6\{Ru(cod)\}]^{2-}$

Die Publikation erschien in der Zeitschrift *Angewandte Chemie International Edition* und trägt in der deutschen Ausgabe den Titel: „Zwischen Lokalisierung und Delokalisierung: $Ru(cod)^{2+}$-Einheiten in den Zintl-Clustern $[Bi_9\{Ru(cod)\}_2]^{3-}$ und $[Tl_2Bi_6\{Ru(cod)\}]^{2-}$“
Zitat: N. Lichtenberger, N. Spang, A. Eichhöfer, S. Dehnen, *Angew. Chem. Int. Ed.* **2017**, *56*, 13253–13258.
Deutsche Version: N. Lichtenberger, N. Spang, A. Eichhöfer, S. Dehnen, *Angew. Chem.* **2017**, *129*, 13436–13442.

Abstract

Reactions of $[K(crypt{-}222)]_2(TlBi_3)\cdot 0.5en$ (**1b**) with $[Ru(cod)(H_2CC(Me)CH_2)_2]$ (**A**) in 1,2-diaminoethane (en) led to the formation of two compounds with new bismuth-rich cluster anions, $[K(crypt{-}222)]_3[Bi_9\{Ru(cod)\}_2]\cdot 1.5en$ (**2**) and $[K(crypt{-}222)]_2[Tl_2Bi_6\{Ru(cod)\}]\cdot 2tol$ (**3**), alongside the salt of a binary nido cluster, $[K(crypt{-}222)]_3(Tl_4Bi_5)\cdot 2en$ (**4**). The anions in **2** and **3** are two further examples of rare heterometallic clusters containing Ru atoms. As one cod ligand is retained on each Ru atom in both clusters, the anions may be viewed as intermediates on the way towards larger, ligand-free intermetalloid clusters. Quantum-chemical studies provided insight into the bonding situation in these clusters. According to these studies, the anion of **2** features both electron-precise and electron-deficient parts. Electrospray ionization mass spectrometry analysis indicated that the clusters undergo stepwise fragmentation.

Zusammenfassung

Die Veröffentlichung berichtet über die Synthese der ersten heterometallischen Clusteranionen, die aus einer Reaktion eines binären *Zintl*-Anions mit Trielatomen und einem Übergangsmetallkomplex erhalten wurden. Durch Umsetzung des Anions $(TlBi_3)^{2-}$ mit dem heteroleptischen Rutheniumkomplex $[Ru(cod)(Me{-}Allyl)_2]$ wurden die $[K(Krypt{-}222)]^+$-Salze der Clusteranionen $[Bi_9\{Ru(cod)\}_2]^{3-}$ und $[Tl_2Bi_6\{Ru(cod)\}]^{2-}$ dargestellt. Weiterhin wird über die Synthese der [K

(Krypt−222)$]^+$-Salze der Anionen $(TlBi_3)^{2-}$ und $(Tl_4Bi_5)^{3-}$ berichtet. Das tetraedrische Anion $(TlBi_3)^{2-}$ dient als Ausgangsmaterial zur Synthese der heterometallischen Cluster, während $(Tl_4Bi_5)^{3-}$ als weiteres Reaktionsprodukt der Synthese auftritt, wenn die Kristallisationsbedingungen variiert werden. Alle Verbindungen wurden mittels Einkristallstrukturanalyse, ESI-MS, μ-RFA und, außer dem $(TlBi_3)^{2-}$-Anion, quantenchemischen Studien untersucht.

Wird $(TlBi_3)^{2-}$ mit dem Komplex [Ru(cod)(Me−Allyl)$_2$] in en zur Reaktion gebracht und die Lösung anschließend mit THF überschichtet, so kristallisiert zunächst [K(Krypt−222)$]_3$[Bi$_9${Ru(cod)$\}_2$]·1.5en. Nach Isolation der Verbindung kann anschließend [K(Krypt−222)$]_2$[Tl$_2$Bi$_6${Ru(cod)$\}$]·2tol durch Reduzierung des Lösungsmittelvolumens um 50% und Einsatz von Toluol als Antisolvenz kristallisiert werden. Durch Einsatz von Toluol statt THF im ersten Kristallisationsschritt wird ausschließlich [K(Krypt−222)$]_3$(Tl$_4$Bi$_5$)·2en erhalten.

Das Anion $[Bi_9\{Ru(cod)\}_2]^{3-}$ weist eine neuartige Clustergeometrie auf (s. Abb. 3.2), und die Struktur lässt sich weder in einem elektronenpräzisen Bild noch durch Interpretation gemäß der Wade-Mingos-Regeln erklären. Die Zusammensetzung, und somit auch die Abwesenheit von Tl-Atomen in dem Cluster, wurde durch ESI-MS und μ-RFA bestimmt. Zur Aufklärung der Bindungssituation dienten quantenchemische Studien, in denen die lokalisierten Molekülorbitale der Clusterverbindung betrachtet wurden. Die LMOs zeigen, dass innerhalb der Clusterverbindung eine Kombination von lokalisierten und Mehrzentrenbindungen vorhanden ist. In den Massenspektren lässt sich die Fragmentierung des Clustermonoanions durch den sukzessiven Verlust der cod-Liganden beobachten. Dieser Fragmentierungspfad wurde quantenchemisch nachvollzogen, wobei sowohl eine vorausgehende Oxidation zum Monoanion als auch der umgekehrte Fall in Betracht gezogen wurden. Somit konnten ungefähre Bindungsenergien für die Ru-cod-Bindungen ermittelt werden. In beiden Fällen benötigt der Verlust des ersten Liganden etwas mehr als 200 kJ/mol, während der nachfolgende Schritt zum ligandenfreien Cluster exotherm ist. Diese Ergebnisse erklären die Beobachtung, dass das ESI-MS-Signal des ligandenfreien Clusters deutlich intensiver ist als das des Clusters mit einem gebundenen Liganden. Um die Clusterzusammensetzung zusätzlich abzusichern wurden quantenchemische Studien durchgeführt, in denen das einzige symmetrieunabhängige Bi-Atom durch Tl substituiert wurde. Dies führt nach Optimierung zu einer Struktur, die sehr ähnlich zu der optimierten Struktur des Bi-Monoanions ist. Sowohl die Oxidation des Trianions zum Monoanion als auch die Substitution eines Bi-Atoms durch ein Tl-Atom reduziert die VE-Zahl des Clusters um zwei

Elektronen. Die resultierende Struktur ist deutlich symmetrischer als die in der Kristallstruktur ermittelte Clustergeometrie (C_{2v} gegenüber C_2), woraus zusätzlich geschlossen werden kann, dass in der Tat keine Tl-Atome in das Clustergerüst eingebaut sind.

Das zweite Reaktionsprodukt $[Tl_2Bi_6\{Ru(cod)\}]^{2-}$ wurde ebenfalls quantenchemisch untersucht. Obwohl die Gesamtelektronenzahl zu einem *nido*-Wade-Cluster passt, werden deutliche Unterschiede zwischen der dadurch erwarteten Struktur und den Einkristallstrukturdaten gefunden. Die quantenchemischen Studien reproduzieren die experimentell bestimmten Parameter sehr gut und die Analyse der LMOs zeigt, dass die Bindungen zwischen den Bi-Atomen und dem Ru-Atom stark kovalenten Charakter haben. Alle übrigen Bindungen im Clustergerüst sind 2e-3c-Mehrzentrenbindungen, durch die kovalenten Bindungen ist jedoch die differenziertere Beschreibung der elektronischen Verhältnisse wesentlich geeigneter als der einfache Vergleich mit einem *nido*-Wade-Cluster.

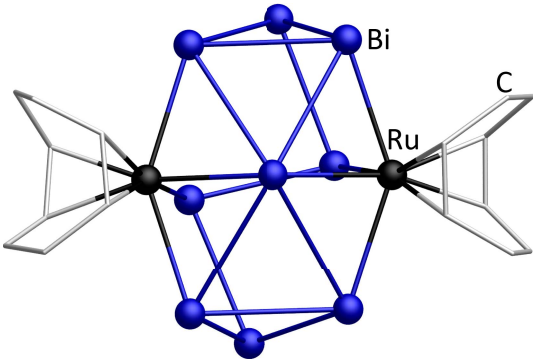

(a) $[Bi_9\{Ru(cod)\}_2]^{3-}$

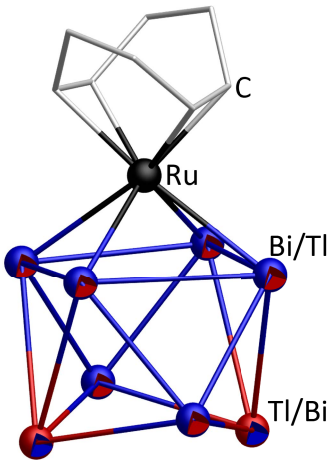

(b) $[Tl_2Bi_6\{Ru(cod)\}]^{2-}$

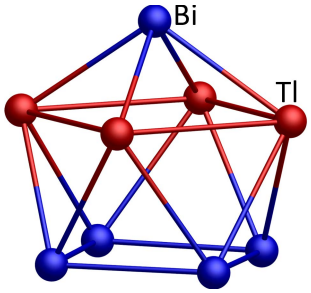

(c) $(Tl_4Bi_5)^{3-}$

Abbildung 3.2: Strukturen der Reaktionsprodukte von $(TlBi_3)^{2-}$ mit $[Ru(cod)(Me-Allyl)_2]$.[21]

Eigener Anteil

Die Verbindungen $[K(Krypt{-}222)]_2(TlBi_3)\cdot 0.5en$ und $[K(Krypt{-}222)]_3(Tl_4Bi_5)\cdot 2en$ wurden von mir bereits im Rahmen meiner Masterarbeit erstmals synthetisiert und sowohl strukturell als auch massenspektrometrisch charakterisiert.[97]

Die Idee für die Umsetzung des $(TlBi_3)^{2-}$-Anions mit $[Ru(cod)(Me{-}Allyl)_2]$ wurde von mir entwickelt und zunächst von dem Vertiefungsstudenten *Michael Dasbach* unter meiner Anleitung experimentell durchgeführt. Ihm gelang es, erste Kristalle der Verbindung $[K(Krypt{-}222)]_3[Bi_9\{Ru(cod)\}_2]\cdot 1.5en$ zu züchten, wobei eine mangelhafte Kristallqualität zunächst keine Rückschlüsse über die an den Ru-Atomen gebundenen Liganden und somit auch nicht über die Bindungssituation im Clusteranion zuließ. *Nils Spang* führte anschließend ein Masterpraktikum unter meiner Anleitung im Labor durch und beschäftigte sich unter anderem mit der Reproduktion dieser Verbindung, was auch gelang. Ihm gelang ebenfalls die Synthese der Verbindung $[K(Krypt{-}222)]_2[Tl_2Bi_6\{Ru(cod)\}]\cdot 2tol$, wobei deren Syntheseweg zunächst von mir als weiterer Ansatz zur möglichen Verbesserung der Kristallqualität der Verbindung $[K(Krypt{-}222)]_3[Bi_9\{Ru(cod)\}_2]\cdot 1.5en$ vorgeschlagen wurde.

Alle analytischen und quantenchemischen Daten (mit Ausnahme der von PD. Dr. *Florian Weigend* durch einen genetischen Algorithmus ermittelten Minimumsstrukturen von $(Ru_2Bi_9)^-$ und $(Ru_2Bi_9)^{3-}$), die in dieser Veröffentlichung diskutiert werden, wurden von mir aufgenommen und ausgewertet, wobei die Aufnahme der Massenspektren durch *Jan Bamberger* erfolgte. Das Einkristall-Röntgenbeugungsexperiment zur Differenzierung von Tl- und Bi-Positionen in der Verbindung $[K(Krypt{-}222)]_3(Tl_4Bi_5)\cdot 2en$ wurde durch *Andreas Eichhöfer* am ANKA-Synchrotron in Karlsruhe durchgeführt, wobei die Auswertung der Daten wiederum mir unterlag. Die Aufnahme von μ-Röntgenfluoreszenzspektren wurde in meinem Beisein durch Dr. *Bastian Weinert* und *Carsten Donsbach* durchgeführt. Das Manuskript wurde von mir in Zusammenarbeit mit Prof. Dr. *Stefanie Dehnen* verfasst, wobei ich in dieser Zeit die Synthesen mehrfach wiederholt habe. *Nils Spang* hat wichtige Beiträge zum synthetischen Teil dieser Arbeit geleistet und war an der Überarbeitung des Manuskripts mit beteiligt.

Zintl Clusters

International Edition: DOI: 10.1002/anie.201707632
German Edition: DOI: 10.1002/ange.201707632

Between Localization and Delocalization: $Ru(cod)^{2+}$ Units in the Zintl Clusters $[Bi_9\{Ru(cod)\}_2]^{3-}$ and $[Tl_2Bi_6\{Ru(cod)\}]^{2-}$

*Niels Lichtenberger, Nils Spang, Andreas Eichhöfer, and Stefanie Dehnen**

Dedicated to Professor Wolfgang Schnick on the occasion of his 60th birthday

Abstract: *Reactions of $[K(crypt\text{-}222)]_2(TlBi_3)\cdot 0.5\,en$ (**1b**) with $[Ru(cod)(H_2CC(Me)CH_2)_2]$ (**A**) in 1,2-diaminoethane (en) led to the formation of two compounds with new bismuth-rich cluster anions, $[K(crypt\text{-}222)]_3[Bi_9\{Ru(cod)\}_2]\cdot 1.5\,en$ (**2**) and $[K(crypt\text{-}222)]_2[Tl_2Bi_6\{Ru(cod)\}]\cdot 2\,tol$ (**3**), alongside the salt of a binary nido cluster, $[K(crypt\text{-}222)]_3(Tl_4Bi_5)\cdot 2\,en$ (**4**). The anions in **2** and **3** are two further examples of rare heterometallic clusters containing Ru atoms. As one cod ligand is retained on each Ru atom in both clusters, the anions may be viewed as intermediates on the way towards larger, ligand-free intermetalloid clusters. Quantum-chemical studies provided insight into the bonding situation in these clusters. According to these studies, the anion of **2** features both electron-precise and electron-deficient parts. Electrospray ionization mass spectrometry analysis indicated that the clusters undergo stepwise fragmentation.*

A large number of intermetalloid clusters have been reported recently that were formed in reactions of homoatomic[1] or heteroatomic[2] Zintl anions with transition-metal complexes.[3] Comprehensive studies on the reactivity of binary tetrahedral Zintl ions $(Tt_2Pn_2)^{2-}$ (Tt = Ge, Sn, or Pb; Pn = As, Sb, or Bi),[2,4] and the use of $(Tt_2Pn_2)^{2-}$ or $(TrBi_3)^{2-}$ (Tr = Ga, In, or Tl)[5] in reactions with f block metal complexes $[M(C_5Me_4H)_3]$ (M = Ln, U), all of which led to the isolation of a variety of ternary intermetalloid clusters, have also been reported.[6] However, the corresponding reactions of $(TrBi_3)^{2-}$ (Tr = Ga, In, or Tl) with d block transition-metal complexes have remained unsuccessful to date. Many attempts have been undertaken in this direction as the inclusion of transition-metal atoms is of particular interest considering the potential catalytic properties of the resulting metal clusters.[6d,7]

All reported reactions indicate the distinct tendency of the $(TrBi_3)^{2-}$ precursor to undergo redox processes that lead to the (partial) release of Tr^0 and the formation of polybismuthide anions.[6d,8] This emphasizes the necessity for an even more careful choice of the transition-metal reactant when using the very sensitive $(TrBi_3)^{2-}$ anions as these comprise formally charged, "Tr^{2-}" pseudo-pnictogen sites. These suffer from a distinct charge overload with regard to the neutral Tr atom. To overcome this problem, we intended to use less reactive transition-metal complexes, in particular avoiding oxidizing metal atoms and/or ligands.

$[K(crypt\text{-}222)]_2(TlBi_3)\cdot solv$ (solv = 0.58 thf/0.42 en: **1a**, monoclinic space group $P2_1$[9] or solv = 0.5 en: **1b**, isostructural, see the Supporting Information; en = 1,2-diaminoethane)[10] was reacted with $[Ni(cod)_2]$ (cod = 1,5-cycloocatadiene) in a first series of test reactions. However, the recrystallized precursor **1b** was obtained as the only crystalline product. Electrospray ionization mass spectrometry (ESI-MS) studies of the reaction solutions provided evidence for the formation of $[Ni@Tl_4Bi_5]^{3-}$, but only besides unreacted precursor (see the Supporting Information). Thus far, this product has not been isolated in crystalline form. We ascribed this phenomenon to the strong Ni–cod interaction, which cannot be effectively attacked by the $(TlBi_3)^{2-}$ anion. Hence, the heteroleptic complex $[Ru(cod)(H_2CC(Me)CH_2)_2]$ (**A**), which has previously been employed in the synthesis of the binary intermetalloid cluster $[Ru@Ge_{12}]^{3-}$,[1d] seemed to be a much more suitable reactant.

Indeed, the reaction of **1b** with **A** in en, followed by filtration and layering with THF, reproducibly afforded crystals of $[K(crypt\text{-}222)]_3[Bi_9\{Ru(cod)\}_2]\cdot 1.5\,en$ (**2**) as thin black platelets in approximately 13% yield. X-ray structure solution and refinement (triclinic space group $P\bar{1}$)[9] revealed the presence of a $[Bi_9\{Ru(cod)\}_2]^{3-}$ anion in **2** (Figure 1), as unambiguously confirmed by ESI-MS (see the Supporting Information, Figures S18–S25).[11]

The atoms adopt a previously unprecedented cluster arrangement, which can either be regarded as being composed of two eclipsed Bi_3 triangles that sandwich a slightly corrugated five-membered Bi_3Ru_2 ring (Figure 1, top) or as a Bi_4 zigzag chain that is capped by seven atoms, which form an elongated Bi_5Ru_2 hexagonal pyramid (Figure 1, bottom).

The anion has almost ideal C_2 symmetry with the rotation axis running through Bi1 and the center of the Bi5–Bi6 bond. While all Ru–Bi distances are within a narrow range of 2.7518(9) to 2.800(1) Å, there are three types of Bi–Bi bonds

[*] N. Lichtenberger, N. Spang, Prof. Dr. S. Dehnen
Fachbereich Chemie und Wissenschaftliches Zentrum für Materialwissenschaften, Philipps-Universität Marburg
Hans-Meerwein-Strasse 4, 35032 Marburg (Germany)
E-mail: dehnen@chemie.uni-marburg.de
Dr. A. Eichhöfer
Institute of Nanotechnology
Karlsruher Institute of Technologie (KIT), Campus North
Hermann-von-Helmholtz-Platz 1
76344 Eggenstein-Leopoldshafen (Germany)
and
Karlsruhe Nano Micro Facility (KNMF)
Hermann-von-Helmholtz-Platz 1
76344 Eggenstein-Leopoldshafen (Germany)
Supporting information and the ORCID identification number(s) for the author(s) of this article can be found under: https://doi.org/10.1002/anie.201707632.

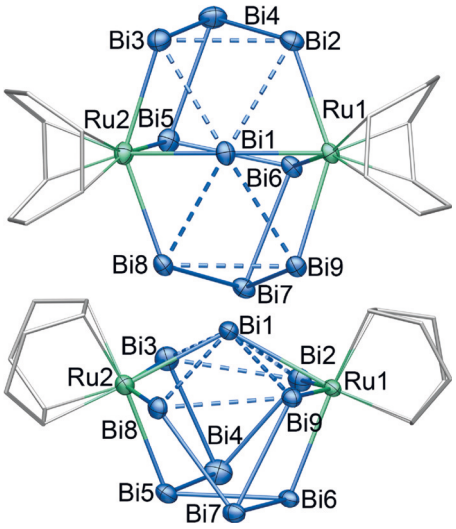

Figure 1. Two perpendicular views of the molecular structure of the $[Bi_9\{Ru(cod)\}_2]^{3-}$ anion in **2** (thermal ellipsoids of heavy atoms set at 50% probability; cod molecules shown in gray wire representation; dashed bonds indicate bond delocalization). Selected distances [Å]: Ru–Bi 2.7518(9)–2.800(1), Bi1–Bi(2,3,8,9) 3.2660(7)–3.3943(8), Bi2–Bi3 3.1293(7), Bi8–Bi9 3.1380(6), Bi(2,3)–Bi4 3.0224(7), 3.0139(9), Bi(8,9)–Bi7 3.0364(7), 3.0056(6), Bi5–Bi6 2.9468(6), Bi4–Bi5 3.0737(9), Bi6–Bi7 3.0583(8). Note that **2** crystallizes as a racemic mixture of two enantiomers, only one of which is shown here.

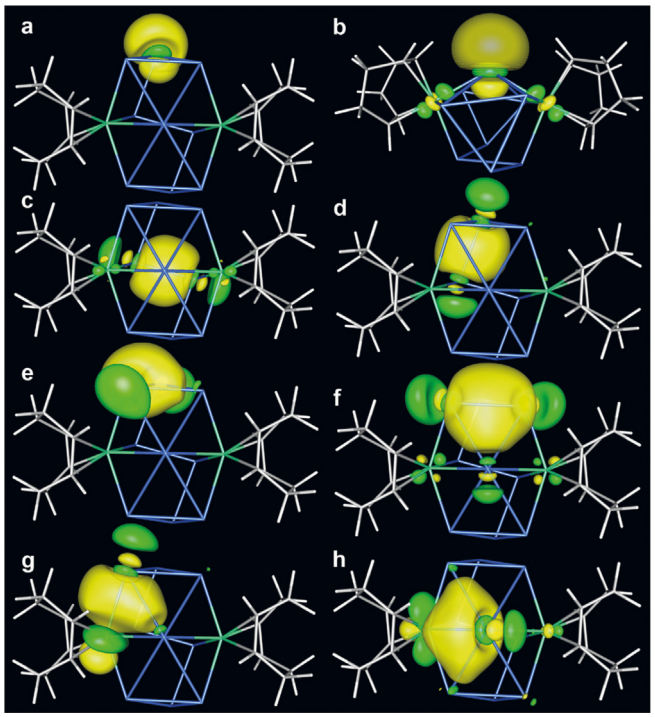

Figure 2. Representative localized molecular orbitals (LMOs) of the $[Bi_9\{Ru(cod)\}_2]^{3-}$ anion in **2**. a, b) Lone pairs on the Bi atoms. c, d) 2e2c Bi–Bi bonds (shown for Bi5–Bi6 (c) and Bi4–Bi5 (d)). e) A 2e2c Bi–Bi bond with a small contribution from a third atom (Bi3–Bi4···Bi2). f) A 2e3c Bi–Bi–Bi bond (Bi1–Bi2–Bi3). g) A 2e2c Bi–Ru bond with a small contribution from a third atom (Bi3–Ru2···Bi1). h) A 2e2c Bi–Ru bond with very small contributions from two further Bi atoms (Bi1–Ru2···Bi3,Bi8). Amplitudes are drawn at ±0.03 a.u.; the color code is the same as in Figure 1.

that differ in length. The shortest bonds involve the atoms of the zigzag chain: Bi5–Bi6 (2.9468(6) Å) and Bi(4/7)–Bi (3.0056(6)–3.0737(9) Å). The bond lengths within the zigzag chain thus adopt the opposite order as compared to those reported for the anionic Bi_4^{6-} chain in $K_6(Bi_4)\cdot 8NH_3$.[12] In that compound, the bonds to the terminal atoms (3.0828(4) Å) are shorter than the central bond (3.2058(3) Å), which is additionally elongated because of close interactions of the highly charged Bi atoms with K^+ cations. Owing to the significantly lower charge per atom in **2**, the average Bi–Bi distance within the zigzag chain is much shorter here (3.026 Å) than in Bi_4^{6-} (3.144 Å). Compound **2** further comprises two slightly longer bonds, Bi2–Bi3 (3.1293(7) Å) and Bi8–Bi9 (3.1380(6) Å). The largest distances between adjacent Bi atoms are found around Bi1 (3.2660(7)–3.3943(8) Å).

The different ranges reflect different bonding situations, as confirmed by quantum-chemical studies using density function theory (DFT) methods.[13] According to these, the anion combines structural motifs that indicate an electron-precise situation, as is typical for non-deltahedral polypnictides,[8,12,14] with deltahedral three-center bonding indicating electron deficiency, which is quite rare in Bi chemistry.[15] Figure 2 shows representative localized molecular orbitals (LMOs) of the anion in **2**.

Inspection of the LMOs indicates the presence of lone pairs at all of the Bi atoms (Figure 2a,b) and mainly 2e2c bonds in the zigzag Bi_4 chain (Figure 2c,d). The Bi–Bi bonds from the zigzag chain towards the two neighboring atoms within the seven-atom "cap" of the anion (Bi7–Bi8, Bi7–Bi9, and equivalents) are also mainly 2e2c bonds, with a very slight polarization towards the third atom (Figure 2e). In contrast, electron delocalization is dominant within the Bi_5Ru_2 capping unit of the anion. Three-center bonding is clearly visible for the Bi_3 units (Bi8-Bi9-Bi1 and Bi2-Bi3-Bi1, Figure 2f). To a smaller extent, it is also found at the Bi–Ru bonds formed by Bi2, Bi3, Bi8, and Bi9, which show a smaller, but notable Bi1 contribution (Figure 2g). The Bi1–Ru bonds are mainly 2e2c bonds, with some polarization towards the neighboring Bi atoms (Figure 2h).

The coexistence of localized and delocalized bonds within one metal cluster is very rare, and has only been observed in metalloid clusters such as $[Ge_{10}\{Fe(CO)_4\}_8]^{6-}$ and $[Sn_{10}\{Si(SiMe_3)_3\}_{6-x}]^{x-}$ $(x=0–2)$,[16] whereas this phenomenon is completely untypical for polybismuthides. Thus far, polyhedral polyanions including Bi atoms have only been described to match one of these concepts. Some polybismuthide anions are electron-precise aggregates, namely Bi_7^{3-},[14b] Bi_{11}^{3-},[8] and all known ternary intermetalloid clusters with Bi[2a,b,4b–d,6] except for $[Ni_2@E^{14}{}_7Bi_5]^{3-}$ and $[Zn@Zn_5E^{14}{}_3Bi_3@Bi_5]^{4-}$[2a,4b,d] $(E^{14}=Sn, Pb)$. The remaining polybismuthide anions are electron-deficient cages that follow the Wade–Mingos rules:[17] $[Bi_xM_y(CO)_z]^{q-}$ $(M/x/y/z/q = Cr/Mo/3/2/6/3$,[18] Ni/3/4/6/3, Ni/3/6/9/3, Ni/4/4/6/2,[19] Fe/4/4/13/2[20]), $[Ni@Bi_6Ni_6(CO)_8]^{4-}$,[19] and $(E^{14}{}_7Bi_2)^{2-}$ $(E^{14}=Sn, Pb)$,[2a,4b] as well as the clusters quoted above.

The bonding within **2** can also be regarded from the Ru^{2+} point of view. Each of the d^6 metal ions forms four bonds with adjacent "Bi^-" atoms, which act as two-electron donors. With another four electrons from the cod ligand, a closed 18 electron shell is thus achieved. However, the "Bi_9^{7-}" fragment itself contains 52 electrons ($9\times5+7$), which neither matches an interpretation according to the Wade–Mingos rules ($52-9\times2=34=2n+16$ skeleton electrons) nor a purely electron-precise interpretation: 34 skeleton electrons would serve to form 17 2e2c bonds while setting apart Bi1 in a way that counting its electrons would no longer be reasonable. This interpretation would neglect the existing contacts from Bi1 to the adjacent Bi atoms and the visible elongation of the Bi2–Bi3 and Bi8–Bi9 bonds. In summary, only the more differentiated interpretation of the bonding situation is appropriate.

The quantum-chemical calculations also served to rationalize the fact that the anion in **2** does not comprise Tl atoms. As indicated below (Figure 3c) and as detailed in Figure S64, an anion with two electrons less (either by replacement of one Bi with one Tl atom or by two-electron oxidation) would adopt a different, more symmetric structure.

Furthermore, the cluster as well as several fragments of it are clearly visible in the negative-ion ESI mass spectrum of fresh solutions of the crystals in DMF (Figure 3a; note that the charge of the Zintl anions identified by mass spectrometry is typically −1 and does not need to correlate with their originally higher anionic charge). The two predominant cluster signals belong to the intact (oxidized) cluster species, $[Bi_9\{Ru_2(cod)\}_2]^-$, and the purely inorganic core of it, $[Bi_9Ru_2]^-$. A species with only one cod ligand, $[Bi_9Ru_2(cod)]^-$, was also detected, but with significantly lower intensity.

We performed DFT studies of the corresponding fragmentation reactions. As the experiments did not allow for a decision as to whether the fragmentations occurred in solution (i.e., prior to partial oxidation of the triply charged anions during the ESI-MS measurement), or whether they occurred on the monoanions, we calculated both scenarios. We obtained qualitatively identical results, but with slightly different structures and reaction energies.

Both $[Bi_9\{Ru(cod)\}_2]^{3-}$ and "$[Bi_9\{Ru(cod)\}_2]^{-}$" release the first cod ligand in an endothermic process (+224 kJ mol^{-1} or +203 kJ mol^{-1}, respectively) with formation of the significantly destabilized clusters "$[Bi_9Ru\{Ru(cod)\}]^{3-}$" or "$[Bi_9Ru\{Ru(cod)\}]^{-}$", respectively, without affecting the overall cluster architecture (see Figure 3b and 3c, top). After release of the second cod ligand, significant rearrangements occur that are obviously needed to stabilize the remaining, naked "$[Bi_9Ru_2]^{3-}$" or "$[Bi_9Ru_2]^{-}$" cluster cores. The global-minimum structures of these hypothetic species, as determined by a DFT genetic algorithm study (Figure 3b and 3c, bottom left),[21] possess completely different structures, with two Ru^{2+} ions sandwiched between a Bi_3 ring, a Bi_4, and a Bi_2 unit (the latter two are connected in a Bi_5 ring).

To date, the actual structures of the species detected by ESI-MS remain unclear. Even though the detachment of cod units including the said cluster rearrangement process would be exoenergetic overall (−92 kJ mol^{-1} or −6 kJ mol^{-1}, respectively), we cannot exclude detection of the unaltered cluster cores after detachment of the second cod ligand (196 kJ mol^{-1} or 243 kJ mol^{-1} above the global-minimum structures, respectively). This assumption is supported by the fact that all singly charged, and thus partially oxidized, anions detected by ESI-MS would equally undergo dramatic structural changes in

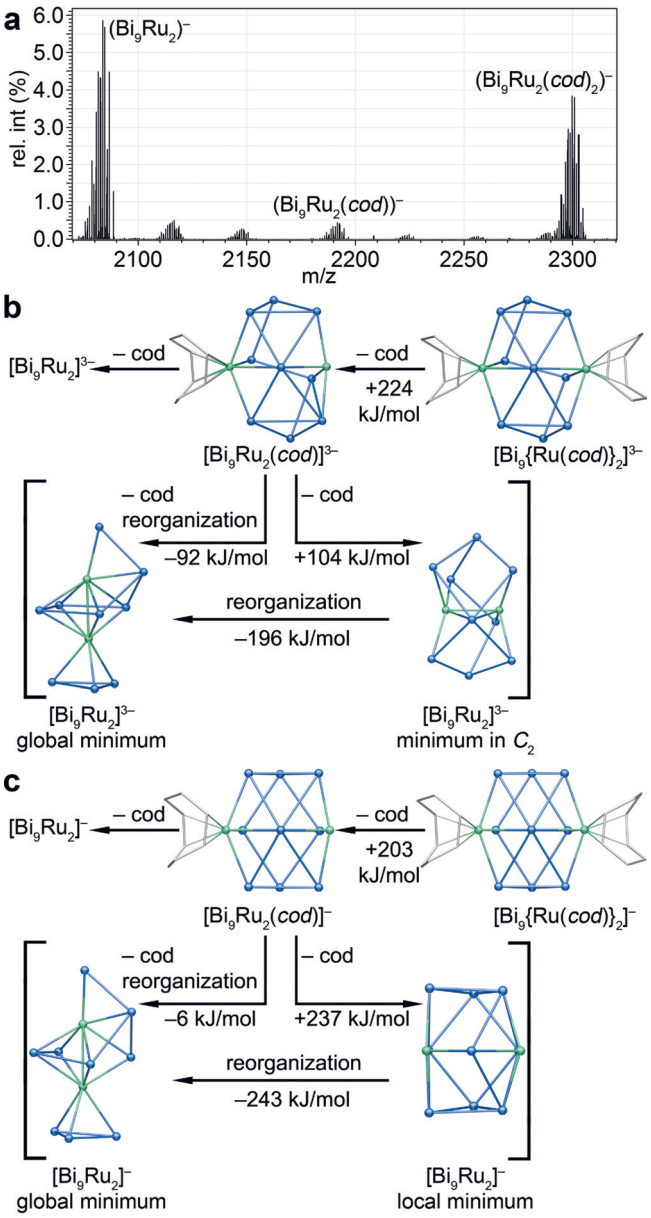

Figure 3. a) ESI(−) mass spectrum of a fresh solution of **2** in DMF in the high *m*/*z* region, indicating the molecular peak and fragments upon release of one or two cod ligands, respectively (for the full spectrum and high-resolution figures of all assignable peaks, see the Supporting Information). Note that intermetalloid cluster anions are typically detected as singly charged species regardless of their original charge. b, c) The corresponding fragmentation pathway was simulated by DFT calculations of the structures, taking into account the original charge of the cluster anion (b) or partially oxidized monoanions with slightly affected cluster structures (c). All species were calculated without symmetry restrictions (C_1), unless denoted otherwise.

solution and ultimately decompose, but are stable on the ESI-MS timescale.

The fragmentations do not provide an explanation for the formation of the anion in **2**. However, it is noteworthy that the cod-free anions feature (partially linked) Bi_2, Bi_3, Bi_4, and Bi_5 units, such as those found in other intermetalloid clusters. In this regard, the anion in **2** may be regarded as an intermediate towards a ligand-free intermetalloid cluster anion upon release of all of the cod molecules.

In contrast to the reaction of **A** with homoatomic Ge_9^{4-} anions,[1d] and in contrast to the reaction of $(TrBi_3)^{2-}$ with lanthanide or actinide complexes of the type $[M(C_5Me_4H)_3]$ (Tr = Ga, In, or Tl; M = Ln, U),[6c,d,f] the cod ligand in **2** is retained on the Ru^{2+} ions, which are therefore not incorporated as naked transition-metal ions into a main-group atom shell. We ascribe this observation to the fact that a) the Ru–Ge interaction is stronger and the Ru–Bi interaction is weaker than the Ru–cod interaction and b) that the interaction between cod and Ru^{2+} is stronger than that between $(C_5Me_4H)^-$ and La^{3+} or U^{3+}. The latter also serves to explain why the reaction led to an isolable compound, while reactions with less stable (more reactive) complexes proceeded to form thermodynamically stable compounds (metals, binary salts).

Similar reactions of homoatomic E_9^{4-} anions (E = Sn, Pb) with $[Ir(cod)Cl]_2$ have been reported, which both yielded the binary *closo* clusters $[E_9\{Ir(cod)\}]^{3-}$.[22] In the case of Sn, a follow-up reaction gave the intermetalloid cluster $[Ir@Sn_{12}]^{3-}$.

Compound **2** is clearly not the only product formed during the described reaction. This is indicated by the moderate yield and the absence of Tl atoms in the cluster anion. Furthermore, ESI mass spectra recorded on a solution of the solid material obtained during the synthesis of **2** pointed to the presence of further cluster compounds that co-precipitated alongside **2**, but not in single-crystalline form (Figures S18–S32). Thus we intended to identify and isolate further reaction products from the mother liquor. After crystallization of **2** from the en/THF mixture, the solution was further concentrated and subsequently layered with toluene. The ternary cluster $[Tl_2Bi_6\{Ru(cod)\}]^{2-}$ was isolated as $[K(crypt\text{-}222)]^+$ salt **3**, which crystallizes in very low yield (several black crystals) with two toluene molecules in the triclinic space group $P\bar{1}$.[9] The molecular structure of the anion in **3** is shown in Figure 4. Its composition was unambiguously confirmed by ESI-MS (Figures S19 and S20) and micro-X-ray fluorescence spectroscopy (μ-XFS, Table S8). Owing to the similar scattering properties of thallium and bismuth in single-crystal X-ray experiments with Mo-K_α radiation, we assigned the two atom types be means of quantum chemistry (see the Supporting Information), as previously done for related compounds.[2b–e,4a,6e,f] The result is highlighted in Figure 4 with a color code; it indicates that the Tl atoms prefer to occupy two opposing positions within the open four-membered ring. This specific atom distribution seems to be a common feature of Tl_2Bi_x cages, and has also been observed in the structure of $[U@Tl_2Bi_{11}]^{3-}$.[6f] In this context, we note that the reliability of quantum-chemical methods for atom assignments in such mixed Tl/Bi Zintl cluster anions was additionally confirmed by a single-crystal X-ray diffraction experiment that made use of the effect of anomalous dispersion on compound **4** (see below).

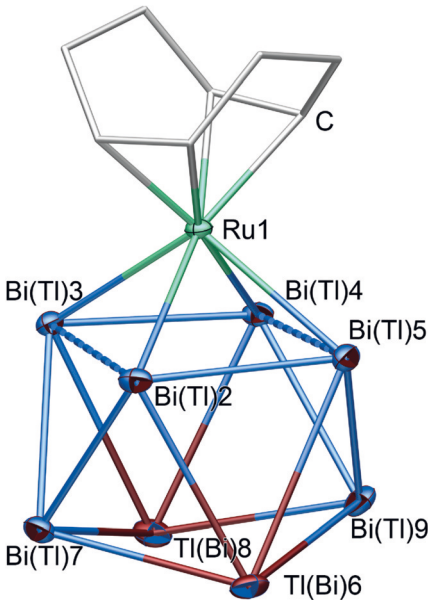

Figure 4. Molecular structure of the $[Tl_2Bi_6\{Ru(cod)\}]^{2-}$ anion in **3** (thermal ellipsoids of heavy atoms set at 50% probability; cod molecules shown as gray wires). Selected distances [Å]: Ru–Bi 2.7915(7)–2.8091(5), Bi–Bi(capped) 2.9677(4), 2.9817(4), 3.4846(6), and 3.5623(6), Bi–Bi(deltahedral) 3.0278(7)–3.1042(6), Tl–Bi(open) 3.0691(3)–3.1397(7), Tl–Bi(deltahedral) 3.2787(6)–3.4257(5). The positions of Tl versus Bi atoms that are indistinguishable with Mo-K_α radiation were determined by means of quantum chemistry (see the Supporting Information). As the X-ray structure is shown, the result is illustrated by an according numbering and coloring scheme: Ellipsoids representing atomic sites with a preference for Bi are shown in blue-red, and a preference for Tl is indicated by red-blue.

With a total number of $(8+4+2\times3+6\times5+2)=50$ valence electrons, or $(50-1\times12-8\times2)=22=2n+4$ skeleton electrons for the bonding within the nine-atom cage, the anion in **3** fulfills the Wade–Mingos rules for a *nido*-type cluster. However, it is worth noting that despite the correct electron count, its structure, and thus the bonding situation, differs slightly from that observed for typical C_{4v}-symmetric *nido*-type clusters, most probably owing to the asymmetric coordination of the apical Ru atom; two of the four Bi–Bi distances in the capped square plane are elongated (3.4846(6), 3.5623(6) Å) while the other two are well within the range of typical Bi–Bi 2e2c bonds (2.9677(4), 2.9817(4) Å). A tendency towards bond length alternation can be found for all other bonds within the cluster, albeit to a lesser extent. Furthermore, the non-capped four-membered ring is also not planar but bent (Figure 4). These observations correlate with the illustration of the bonding interactions by means of LMOs (see the Supporting Information). Hence, a tendency towards the alternative, tricapped trigonal-prismatic cage structure known for electron-deficient nine-atom clusters is recognized.[23]

The anion in **3** is the first ternary *nido*-type cluster combining transition-metal atoms and two types of main-group-element atoms, and the second *nido*-type cluster

combining main-group and transition-metal atoms besides $[Ge_8Fe(CO)_3]^{3-}$.[24] All related clusters in which one transition-metal complex fragment ML_n contributes to a Wade–Mingos-type cluster have been *closo*-type cages thus far, for example, $[E^{14}{}_9\{ML\}]^{3-}$ (E^{14} = Si to Pb, ML = ZnPh;[25] E^{14} = Sn, Pb, ML = CdPh,[26] Ir(cod)[22]).

Another major signal observed in the ESI mass spectra, aside from those of the two described anions and their fragmentation products, can be assigned to the species $(Tl_4Bi_5)^-$ (Figure S27), corresponding to the anion $(Tl_4Bi_5)^{3-}$. Indeed, this cluster can be isolated as its $[K(crypt\text{-}222)]^+$ salt **4** (in low yields of some metallic black blocks) with two en molecules (triclinic space group $P\bar{1}$,[9] see the Supporting Information) by using toluene instead of THF for layering of the mother liquor. Its composition was confirmed by μ-XFS (Figure S54). Its direct synthesis is also possible by using different ternary Zintl phases (see the Supporting Information). It is worth noting that **4** is often observed as an oxidation byproduct of the reactant $(TlBi_3)^{2-}$ after reactions with metal complexes, which has not been previously documented in the literature.

The anionic structure (Figure S50) represents the second known E^{13}/E^{15} binary nine-atom *nido* cluster, the other being $(In_4Bi_5)^{3-}$.[5] Both are isoelectronic to the well-known anions $(E^{14}{}_9)^{4-}$ [27] and $(E^{14}{}_7E^{15}{}_2)^{2-}$ [2a,4b] and the cations $(E^{15}{}_9)^{5+}$.[15a,b] The assignment of the Tl and Bi atoms was again rationalized by means of quantum chemistry (the best isomer is 15.8 kJ mol^{-1} more stable than the second best one; see the Supporting Information), and matches the atomic distribution in $(In_4Bi_5)^{3-}$.[5] To confirm the reliability of the quantum-chemical assignment of metal sites in mixed Tl/Bi Zintl cluster anions, we exemplarily performed an "anomalous dispersion experiment" for **4** at the ANKA synchrotron source. X-ray structure analysis was carried out at a wavelength close to the Tl L_{III} absorption edge (0.97626 Å).[28] As a result of enlarged differences in the atomic form factors of thallium and bismuth, reasonable thermal displacement parameters and better *R* values were obtained exclusively for the atom assignment shown in Figure S50 (for further details, see the Supporting Information).

In summary, we have reported reactions of $(TlBi_3)^{2-}$ with $[Ru(cod)(H_2CC(Me)CH_2)_2]$ to form the cluster anions $[Bi_9\{Ru(cod)\}_2]^{3-}$ and $[Tl_2Bi_6\{Ru(cod)\}]^{2-}$ with unique structures and bonding situations. The latter were analyzed by means of quantum chemistry, revealing that the $[Bi_9\{Ru(cod)\}_2]^{3-}$ anion combines an electron-precise part with a delocalized part, a rarely observed phenomenon and unprecedented for Zintl clusters. We are currently investigating the controlled detachment of the cod ligands, aiming at the identification of the resulting rearrangement products in solution.

Acknowledgements

This work was supported by the Deutsche Forschungsgemeinschaft (DFG). N.L. acknowledges a PhD grant by the Marburg University Research Academy (MARA). We thank PD Dr. F. Weigend for performing the genetic algorithm study on "$[Bi_9Ru_2]^{x-}$". A.E.'s contribution is restricted to the performance of the synchrotron X-ray diffraction experiment and the refinement of the resulting data. We thank Dr. G. Buth (Institut für Beschleunigerphysik und Technologie, Karlsruher Institut für Technologie, KIT) for his help with this experiment.

Conflict of interest

The authors declare no conflict of interest.

Keywords: bismuth · bonding · ruthenium · thallium · Zintl clusters

How to cite: *Angew. Chem. Int. Ed.* **2017**, *56*, 13253–13258
Angew. Chem. **2017**, *129*, 13436–13442

[1] a) M. J. Moses, J. C. Fettinger, B. W. Eichhorn, *Science* **2003**, *300*, 778–780; b) B. Zhou, M. S. Denning, D. L. Kays, J. M. Goicoechea, *J. Am. Chem. Soc.* **2009**, *131*, 2802–2803; c) T. Krämer, J. C. Duckworth, M. D. Ingram, B. Zhou, J. E. McGrady, J. M. Goicoechea, *Dalton Trans.* **2013**, *42*, 12120–12129; d) G. Espinoza-Quintero, J. C. Duckworth, W. K. Myers, J. E. McGrady, J. M. Goicoechea, *J. Am. Chem. Soc.* **2014**, *136*, 1210–1213; e) C. B. Benda, M. Waibel, T. F. Fässler, *Angew. Chem. Int. Ed.* **2015**, *54*, 522–526; *Angew. Chem.* **2015**, *127*, 532–536; f) Y. Wang, M. Moses-DeBusk, L. Stevens, J. Hu, P. Zavalij, K. Bowen, B. I. Dunlap, E. R. Glaser, B. Eichhorn, *J. Am. Chem. Soc.* **2017**, *139*, 619–622; g) L. G. Perla, S. C. Sevov, *Angew. Chem. Int. Ed.* **2016**, *55*, 6721–6724; *Angew. Chem.* **2016**, *128*, 6833–6836.

[2] a) R. Ababei, J. Heine, M. Holynska, G. Thiele, B. Weinert, X. Xie, F. Weigend, S. Dehnen, *Chem. Commun.* **2012**, *48*, 11295–11297; b) R. Ababei, W. Massa, K. Harms, X. Xie, F. Weigend, S. Dehnen, *Angew. Chem. Int. Ed.* **2013**, *52*, 13544–13548; *Angew. Chem.* **2013**, *125*, 13786–13790; c) S. Mitzinger, L. Broeckaert, W. Massa, F. Weigend, S. Dehnen, *Chem. Commun.* **2015**, *51*, 3866–3869; d) S. Mitzinger, L. Broeckaert, W. Massa, F. Weigend, S. Dehnen, *Nat. Commun.* **2016**, *7*, 10480; e) R. J. Wilson, L. Broeckaert, F. Spitzer, F. Weigend, S. Dehnen, *Angew. Chem. Int. Ed.* **2016**, *55*, 11775–11780; *Angew. Chem.* **2016**, *128*, 11950–11955.

[3] a) S. C. Sevov, J. M. Goicoechea, *Organometallics* **2006**, *25*, 5678–5692; b) S. Scharfe, T. F. Fässler, *Philos. Trans. R. Soc. A* **2010**, *368*, 1265–1284; c) S. Scharfe, F. Kraus, S. Stegmaier, A. Schier, T. F. Fässler, *Angew. Chem. Int. Ed.* **2011**, *50*, 3630–3670; *Angew. Chem.* **2011**, *123*, 3712–3754; d) B. Weinert, S. Dehnen, in *Clusters—Contemporary Insight in Structure and Bonding* (Ed.: S. Dehnen), Springer International Publishing, Berlin, **2017**, pp. 99–134.

[4] a) F. Lips, I. Schellenberg, R. Pöttgen, S. Dehnen, *Chem. Eur. J.* **2009**, *15*, 12968–12973; b) F. Lips, S. Dehnen, *Angew. Chem. Int. Ed.* **2009**, *48*, 6435–6438; *Angew. Chem.* **2009**, *121*, 6557–6560; c) F. Lips, R. Clérac, S. Dehnen, *J. Am. Chem. Soc.* **2011**, *133*, 14168–14171; d) F. Lips, S. Dehnen, *Angew. Chem. Int. Ed.* **2011**, *50*, 955–959; *Angew. Chem.* **2011**, *123*, 986–990.

[5] L. Xu, S. C. Sevov, *Inorg. Chem.* **2000**, *39*, 5383–5389.

[6] a) F. Lips, R. Clérac, S. Dehnen, *Angew. Chem. Int. Ed.* **2011**, *50*, 960–964; *Angew. Chem.* **2011**, *123*, 991–995; b) F. Lips, M. Holynska, R. Clérac, U. Linne, I. Schellenberg, R. Pöttgen, F. Weigend, S. Dehnen, *J. Am. Chem. Soc.* **2012**, *134*, 1181–1191; c) B. Weinert, F. Weigend, S. Dehnen, *Chem. Eur. J.* **2012**, *18*, 13589–13595; d) B. Weinert, F. Müller, K. Harms, R. Clérac, S. Dehnen, *Angew. Chem. Int. Ed.* **2014**, *53*, 11979–11983; *Angew. Chem.* **2014**, *126*, 12173–12177; e) R. Ababei, W. Massa, B.

Weinert, P. Pollak, X. Xie, R. Clérac, F. Weigend, S. Dehnen, *Chem. Eur. J.* **2015**, *21*, 386 – 394; f) N. Lichtenberger, R. J. Wilson, A. R. Eulenstein, W. Massa, R. Clérac, F. Weigend, S. Dehnen, *J. Am. Chem. Soc.* **2016**, *138*, 9033 – 9036.

[7] N. Korber, *Angew. Chem. Int. Ed.* **2009**, *48*, 3216 – 3217; *Angew. Chem.* **2009**, *121*, 3262 – 3264.

[8] B. Weinert, A. R. Eulenstein, R. Ababei, S. Dehnen, *Angew. Chem. Int. Ed.* **2014**, *53*, 4704 – 4708; *Angew. Chem.* **2014**, *126*, 4792 – 4797.

[9] CCDC 1548729 (**1**), 1548730 (**4**), 1548731 (**3**), and 1548732 (**2**) contain the supplementary crystallographic data for this paper. These data can be obtained free of charge from The Cambridge Crystallographic Data Centre.

[10] Crypt-222: 4,7,13,16,21,24-hexaoxa-1,10-diazabicyclo-[8.8.8]hexacosane.

[11] Micro-X-ray fluorescence spectroscopy (μ-XFS) indicated the presence of Tl in the sample (Table S8), but in varying, small amounts below Tl/Bi = 1:8, which hence most probably stems from adhesive impurities. As outlined in the discussion, the structure can only be rationalized with the electron number realized in the given composition.

[12] C. B. Benda, T. F. Fässler, *Z. Anorg. Allg. Chem.* **2014**, *640*, 40 – 45.

[13] a) TURBOMOLE V6.6 2015, a development of the University of Karlsruhe and Forschungszentrum Karlsruhe GmbH, 1989 – 2007, TURBOMOLE GmbH, since 2007; available from http://www.turbomole.com; b) A. D. Becke, *J. Chem. Phys.* **1993**, *98*, 5648 – 5652; c) P. A. M. Dirac, *Proc. R. Soc. London Ser. A* **1929**, *123*, 714 – 733; d) J. P. Perdew, *Phys. Rev. B* **1986**, *33*, 8822 – 8824; e) J. C. Slater, *Phys. Rev.* **1951**, *81*, 385 – 390; f) S. H. Vosko, L. Wilk, M. Nusair, *Can. J. Phys.* **1980**, *58*, 1200 – 1211; g) F. Weigend, R. Ahlrichs, *Phys. Chem. Chem. Phys.* **2005**, *7*, 3297 – 3305; h) F. Weigend, *Phys. Chem. Chem. Phys.* **2006**, *8*, 1057 – 1065; i) D. Andrae, U. Häußermann, M. Dolg, H. Stoll, H. Preuß, *Theor. Chim. Acta* **1990**, *77*, 123 – 141; j) B. Metz, H. Stoll, M. Dolg, *J. Chem. Phys.* **2000**, *113*, 2563 – 2569; k) A. Klamt, G. Schüürmann, *J. Chem. Soc. Perkin Trans. 2* **1993**, 799 – 805; l) S. F. Boys, *Rev. Mod. Phys.* **1960**, *32*, 296 – 299; m) J. M. Foster, S. F. Boys, *Rev. Mod. Phys.* **1960**, *32*, 300 – 302; n) D. L. Bergman, L. Laaksonen, A. Laaksonen, *J. Mol. Graphics Modell.* **1997**, *15*, 301 – 306.

[14] a) R. S. P. Turbervill, J. M. Goicoechea, *Chem. Rev.* **2014**, *114*, 10807 – 10828; b) L. G. Perla, A. G. Oliver, S. C. Sevov, *Inorg. Chem.* **2015**, *54*, 872 – 875.

[15] a) A. Hershaft, J. D. Corbett, *Inorg. Chem.* **1963**, *2*, 979 – 985; b) J. Beck, T. Hilbert, *Eur. J. Inorg. Chem.* **2004**, 2019 – 2026; c) M. F. Groh, A. Isaeva, C. Frey, M. Ruck, *Z. Anorg. Allg. Chem.* **2013**, *639*, 2401 – 2405; d) U. Müller, A. Isaeva, J. Richter, M. Knies, M. Ruck, *Eur. J. Inorg. Chem.* **2016**, 3580 – 3584; e) M. F. Groh, A. Wolff, B. Wahl, B. Rasche, P. Gebauer, M. Ruck, *Z. Anorg. Allg. Chem.* **2017**, *643*, 69 – 80.

[16] a) A. Schnepf, C. Schenk, *Angew. Chem. Int. Ed.* **2006**, *45*, 5373 – 5376; *Angew. Chem.* **2006**, *118*, 5499 – 5502; b) C. Schrenk, F. Winter, R. Pöttgen, A. Schnepf, *Chem. Eur. J.* **2015**, *21*, 2992 – 2997; c) C. Schrenk, J. Helmlinger, A. Schnepf, *Z. Anorg. Allg. Chem.* **2012**, *638*, 589 – 593; d) C. Schrenk, I. Schellenberg, R. Pöttgen, A. Schnepf, *Dalton Trans.* **2010**, *39*, 1872 – 1876.

[17] a) K. Wade, *Inorg. Nucl. Chem. Lett.* **1972**, *8*, 559 – 562; b) K. Wade in *Adv. Inorg. Chem. Radiochem., Vol. 18* (Eds.: H. J. Emeléus, A. G. Sharpe), Academic Press, San Diego, **1976**, pp. 1 – 66; c) D. M. P. Mingos, T. Slee, Z. Y. Lin, *Chem. Rev.* **1990**, *90*, 383 – 402.

[18] L. Xu, A. Ugrinov, S. C. Sevov, *J. Am. Chem. Soc.* **2001**, *123*, 4091 – 4092.

[19] J. M. Goicoechea, M. W. Hull, S. C. Sevov, *J. Am. Chem. Soc.* **2007**, *129*, 7885 – 7893.

[20] K. H. Whitmire, M. R. Churchill, J. C. Fettinger, *J. Am. Chem. Soc.* **1985**, *107*, 1056 – 1057.

[21] a) D. M. Deaven, K. M. Ho, *Phys. Rev. Lett.* **1995**, *75*, 288 – 291; b) M. Sierka, J. Dobler, J. Sauer, G. Santambrogio, M. Brummer, L. Woste, E. Janssens, G. Meijer, K. R. Asmis, *Angew. Chem. Int. Ed.* **2007**, *46*, 3372 – 3375; *Angew. Chem.* **2007**, *119*, 3437 – 3440.

[22] a) D. O. Downing, P. Zavalij, B. W. Eichhorn, *Eur. J. Inorg. Chem.* **2010**, 890 – 894; b) J. Q. Wang, S. Stegmaier, B. Wahl, T. F. Fässler, *Chem. Eur. J.* **2010**, *16*, 1793 – 1798.

[23] a) L. J. Guggenberger, E. L. Muetterties, *J. Am. Chem. Soc.* **1976**, *98*, 7221 – 7225; b) V. Queneau, S. C. Sevov, *Inorg. Chem.* **1998**, *37*, 1358 – 1360.

[24] B. Zhou, J. M. Goicoechea, *Chem. Eur. J.* **2010**, *16*, 11145 – 11150.

[25] J. M. Goicoechea, S. C. Sevov, *Organometallics* **2006**, *25*, 4530 – 4536.

[26] B. Zhou, M. S. Denning, T. A. D. Chapman, J. M. Goicoechea, *Inorg. Chem.* **2009**, *48*, 2899 – 2907.

[27] a) D. Kummer, L. Diehl, *Angew. Chem. Int. Ed. Engl.* **1970**, *9*, 895; *Angew. Chem.* **1970**, *82*, 881 – 882; b) L. Diehl, K. Khodadadeh, D. Kummer, J. Strähle, *Chem. Ber.* **1976**, *109*, 3404 – 3418; c) J. Campbell, D. A. Dixon, H. P. A. Mercier, G. J. Schrobilgen, *Inorg. Chem.* **1995**, *34*, 5798 – 5809; d) H. G. von Schnering, M. Somer, M. Kaupp, W. Carrillo-Cabrera, M. Baitinger, A. Schmeding, Y. Grin, *Angew. Chem. Int. Ed.* **1998**, *37*, 2359 – 2361; *Angew. Chem.* **1998**, *110*, 2507 – 2509; e) C. B. Benda, T. Henneberger, W. Klein, T. F. Fässler, *Z. Anorg. Allg. Chem.* **2017**, *643*, 146 – 148.

[28] D. R. Lide, *CRC Handbook of Chemistry and Physics*, 90th ed., CRC Press, Taylor & Francis Group, Boca Raton, FL, **2009 – 2010**.

Manuscript received: July 26, 2017
Accepted manuscript online: August 21, 2017
Version of record online: September 13, 2017

3.3 The Identity of Ternary A/Tl/Pb or K/Tl/Bi Solid Mixtures and Binary Zintl Anions Isolated From Their Solutions

Zitat: N. Lichtenberger, Y. J. Franzke, W. Massa, F. Weigend, S. Dehnen, *Chem. Eur. J.* **2018**, *24*, 12022–12030.

Abstract

Investigations of solid mixtures of the elemental combinations A/Tl/Pb (A=Na, K) and K/Tl/Bi indicate the presence of multiple binary and ternary Zintl phases, among them new ones containing Tl and Pb or Bi, respectively. Extractions with en/crypt-222 afford single crystals of several novel binary anions, including $[Tl@Tl_4Pb_8]^{4-}$ and $(Tl_4Bi_3)^{3-}$. $[Tl@Tl_4Pb_8]^{4-}$ adopts a *closo*-type cage structure despite possessing one additional electron; it is therefore isostructural, yet not isoelectronic, with homoatomic $[Tl@Tl_{12}]^{11-}$ obtained by solid state reactions. $(Tl_4Bi_3)^{3-}$is a rare case of a pentagonal bipyramidal Zintl anion, yet the first binary one, and (unlike Tl_7^{7-}) the first one with a proper closo-type electron count. Assignment of the numbers and positions of the Tl/Pb or Tl/Bi atoms within the anionic clusters, indistinguishable in classical X-ray diffraction experiments, was achieved by means of quantum chemistry. The studies shed light on the complex situation in solid heavy element mixtures and their substantial differences from the composition of the Zintl anions obtained from them by extraction.

Zusammenfassung

In dieser Veröffentlichung werden ternäre Verbindungen der Elementkombinationen A/Tl/Pb und K/Tl/Bi und deren Extraktionsprodukte durch Auflösung der Verbindungen in en in Gegenwart des Kryptanden Krypt-222 betrachtet. Die Ergebnisse dieser Studien stellen die Basis für die Untersuchungen binärer *Zintl*-Anionen der Elementkombinationen Tl/Pb und Tl/Bi dar. Ziel war es, einen Zugang zu löslichen *Zintl*-Anionen dieser Elemente zu finden, um anschließend deren Reaktionsverhalten studieren zu können. Hierzu mussten zunächst Ausgangsmaterialen für die Synthese gefunden werden, da diese bisher noch nicht bekannt waren. Es wurden, auf Basis der bereits publizierten Festkörperstruktur Na_5TlSn_3 mit isolierten $(TlSn_3)^{5-}$-Anionen, die Zusammensetzungen „A_5TlPb_3“

(A = Na, K) untersucht.[99] Im System K/Tl/Bi diente die Zusammensetzung „$K_5Tl_2Bi_4$“, ebenfalls basierend auf der bereits publizierten Synthese der binären Anionen $(GaBi_3)^{2-}$, $(InBi_3)^{2-}$ und $(In_4Bi_5)^{3-}$ aus „$K_5Tr_2Bi_4$“ (Tr = Ga, In), als Ausgangspunkt für die Untersuchungen.[58] Durch eine Kombination von Röntgen-Einkristall- und Pulverdiffraktometrie konnten die Hauptkomponenten der festen Mischungen „Na_5TlPb_3“ und „$K_5Tl_2Bi_4$“ strukturell charaktierisiert werden. Im Fall von „Na_5TlPb_3“ stellte sich heraus, dass die Verbindung $Na_{17}Tl_5Pb_7$ mit darin vorliegenden, isolierten $Na_4[Na@Tl_5Pb_7]^{12-}$-Clustern, die ternäre Hauptkomponente der festen Mischung, zusammen mit dem binären NaPb, ist. Auch in „K_5TlPb_3“ sind mindestens zwei kristalline Verbindungen vorhanden, wovon eine wiederum das binäre KPb ist. Das Pulverdiffraktogramm zeigt einen zweiten Satz an Reflexen, die jedoch mit sehr geringer Intensität auftreten und nicht mit einer entsprechenden Verbindung „$K_{17}Tl_5Pb_7$“ zu vereinbaren sind. Eine Identifikation der entsprechenden Verbindung ist bis heute nicht gelungen.

Durch die eingehende Analyse von „$K_5Tl_2Bi_4$“ wurde K_2TlBi, die erste strukturell charakterisierte K/Tl/Bi-Verbindung, als die Hauptkomponente der festen Mischung identifiziert, während weitere Komponenten bis heute unbekannt bleiben. Der Versuch K_2TlBi direkt durch entsprechendes Zusammenschmelzen der Elemente in einer 2:1:1-Stöchiometrie zu synthetisieren führte zu einer neuen festen Mischung „K_2TlBi“, die kein K_2TlBi enthielt. Statttdessen konnte $K_6Tl_2Bi_3$ charakterisiert werden, wobei die weitere(n) Komponente(n) unidentifiziert blieben. Die Verbindung ist isostrukturell zu der bereits in der Literatur beschriebenen Verbindung $K_6Tl_2Sb_3$ und enthält unendliche, eindimensionale Ketten eines $^1_\infty[Tl_4Bi_6]^{12-}$-Käfigs.[100]

Ziel der Untersuchungen im Phasensystem K/Tl/Bi war es, einen synthetischen Zugang zu der Verbindung $[K(Krypt{-}222)]_2(TlBi_3)$ in guter Reinheit und hoher Ausbeute zu finden. Für die entsprechenden Ga- und In-Homologen ist dies durch die Verbindungen „$K_5Tr_2Bi_4$“ möglich. Die Extraktion der entsprechenden Tl-Verbindung liefert zwar das Salz des Anions $(TlBi_3)^{2-}$, aber in einem ungefähren 1:1-Verhältnis mit dem entsprechenden $(Tl_4Bi_5)^{3-}$-Salz. Dies verhindert, dass das nach Extraktion der festen Mischung erhaltene Produktgemisch sinnvoll in weiteren Reaktionen eingesetzt werden kann. Als alternative Syntheseroute wurde die 2:1:3 (K:Tl:Bi)-Zusammensetzung der Zielverbindung bereits in der Festkörpersynthese vorgegeben. Die so erhaltene feste Mischung „K_2TlBi_3“ wurde auf ihre einzelnen Komponenten hin untersucht. Hierbei stellte sich heraus, dass es sich um eine 1:1-Mischung der bereits bekannten Verbindung KBi_2 und der neuen ternären

Verbindung KTlBi handelt. Diese ist isostrukturell zu der bereits bekannten hexagonalen *Laves*-Phase KPb_2. Alle beschriebenen festen Mischungen wurden im Anschluss an die Untersuchungen ihrer Natur auf ihr Potential zur Bildung binärer *Zintl*-Anionen hin untersucht, indem sie unter Zusatz von Krypt-222 in en aufgelöst wurden.

Die Extraktion der eingangs erwähnten Verbindung Na_5TlSn_3 führt zur Bildung der bereits bekannten Anionen $(TlSn_9)^{3-}$ und $(TlSn_8)^{3-}$.[101] Wird „Na_5TlPb_3“ extrahiert, so kann ein Mischsalz $[Na(Krypt{-}222)]_3(TlPb_9)_{0.94}(TlPb_{11})_{0.06}$ kristallisiert werden. Beide Anionen sind typische Wade-Cluster und dieses Ergebnis entsprach den Erwartungen. Wird hingegen „K_5TlPb_3“ auf die gleiche Art extrahiert, die Lösung anschließend lediglich aufkonzentriert und für einige Tage bei niedrigen Temperaturen gelagert, so kristallisiert zunächst $[K(Krypt{-}222)]_2(Pb_5)$, welches sich anschließend teils wieder auflöst und parallel die Verbindung$[K(Krypt{-}222)]_4$ $[Tl@Tl_4Pb_8]_{0.51}(Tl_2Pb_{10})_{0.11}(Pb_9)_{0.38}$ entsteht. Diese enthält zwei neue Anionen, $[Tl@Tl_4Pb_8]^{4-}$ und $(Tl_2Pb_{10})^{4-}$. Letzteres ist ein klassischer Wade-Cluster, während die Bildung des ersteren ungewöhnlich ist. Die Zusammensetzung wurde mittels ESI-MS und μ-RFA bestimmt und weicht von der durch die Wade-Mingos-Regeln zu erwartenden Zusammensetzung $[Tl@Tl_5Pb_7]^{4-}$ ab. Insbesondere die Tatsache, dass die Zusammensetzung $[Tl@Tl_4Pb_8]^{4-}$ ein zusätzliches Elektron im Vergleich zu den 50 Valenzelektronen, die für einen 12-Atom *closo* Wade-Cluster ist bemerkenswert. Mittels ausgiebiger quantenchemischer Studien aller Isomere für 50 VE, 51 VE und 52 VE konnten wir zeigen, dass die Bildung des 51 VE Clusters gegenüber dem 50 VE Cluster energetisch leicht bevorzugt ist und, dass die strukturellen Parameter im 51 VE-Fall innerhalb des zu erwartenden Fehlerbereichs besser zu den experimentellen Daten passen, als im 50 VE Fall.

Wird die feste Mischung „$K_5Tl_2Bi_4$“ extrahiert, so wird ein Gemisch der Verbindungen $[K(Krypt{-}222)]_2(TlBi_3)\cdot 0.5en$ und $[K(Krypt{-}222)]_3(Tl_4Bi_5)\cdot 2en$ in einem ungefähren 1:1-Verhältnis erhalten. Der Anteil an $[K(Krypt{-}222)]_3(Tl_4Bi_5)$ $\cdot 2en$ kann auf nahezu null reduziert werden, wenn die feste Mischung „K_2TlBi_3“ (KTlBi + KBi_2) extrahiert wird. Über diese Synthesen wurde bereits zuvor berichtet.[21] Durch den Einsatz von „K_2TlBi“ kann eine Verbindung mit einem neuartigen *Zintl*-Anion erhalten werden. So kristallisiert nach der Extraktion und anschließendem Überschichten der Lösung mit einem geeigneten Antisolvenz oder einfacher Aufkonzentration die Verbindung $[K(Krypt{-}222]_3(Tl_4Bi_3)$. In dieser liegt das pentagonal bipyramidale Anion $(Tl_4Bi_3)^{3-}$ vor, welches das erste binäre *Zintl*-Anion mit diesem Strukturmotiv ist. Zuvor wurde zwar über das Anion

Tl_7^{7-} berichtet, dieses liegt aufgrund seiner hohen Ladung aber nur im binären Festkörper $K_{10}Tl_7$ vor.[19] Die Zusammensetzung wurde mittels ESI-MS und μ-RFA bestätigt und alle möglichen Isomere mit quantenchemischen Rechnungen analysiert. Der Cluster erfüllt mit 30 VE die Voraussetzungen für einen 7-Atom *closo*-Wade-Cluster und stellt damit auch das erste *Zintl*-Anion dieser Clusterklasse in Lösung dar.

Insgesamt zeigen die Ergebnisse in dieser Veröffentlichung, dass eine nähere Betrachtung der ternären Phasendiagramme für die Synthese binärer *Zintl*-Anionen lohnenswert ist und neuartige, interessante Clusterverbindungen zugänglich sind. Bisher wurde die Beziehung zwischen den Ausgangsmaterialen zur Synthese dieser Anionen nur spärlich untersucht aber, wie sich insbesondere im Phasensystem K/Tl/Bi zeigt, ist sie essenziell um die Chemie der Anionen besser zu verstehen. Alle in dieser Publikation behandelten festen Mischungen mit ihren nominellen und realen Zusammensetzungen sowie deren Extraktionsprodukte sind in Tabelle 3.1 zusammengefasst. Die Strukturen der diskutierten intermetallischen Verbindungen sind in Abbildung 3.3 dargestellt. Abbildung 3.4 zeigt die Strukturen der vorgestellten *Zintl*-Anionen.

Tabelle 3.1: Nominelle und reale Zusammensetzungen der untersuchten ternären festen Mischungen in den Phasensystemen A/Tl/Pb und K/Tl/Bi und deren anionische Extraktionsprodukte durch Auflösen der Verbindungen in einer en/Krypt-222-Mischung. Die Gegenionen sind die entsprechenden $[A(Krypt{-}222)]^+$-Komplexe.

Zusammensetzungen		**Extraktionsprodukt(e)**		
Nominell	**Real**			
Na_5TlSn_3	Na_5TlSn_3	$(TlSn_9)^{3-}$	$(TlSn_8)^{3-}$	
„Na_5TlPb_3“	$Na_{17}Tl_5Pb_7$ + NaPb	$(TlPb_9)^{3-}$	$(TlPb_{11})^{3-}$	
„K_5TlPb_3“	KPb + ?	$[Tl@Tl_4Pb_8]^{4-}$	$(Tl_2Pb_{10})^{4-}$	Pb_9^{4-}
„$K_5Tl_2Bi_4$“	K_2TlBi + ?	$(TlBi_3)^{2-}$	$(Tl_4Bi_5)^{3-}$	
„K_2TlBi_3“	KTlBi + KBi_2	$(TlBi_3)^{2-}$		
„K_2TlBi“	$K_6Tl_2Bi_3$ + ?	$(Tl_4Bi_3)^{3-}$		

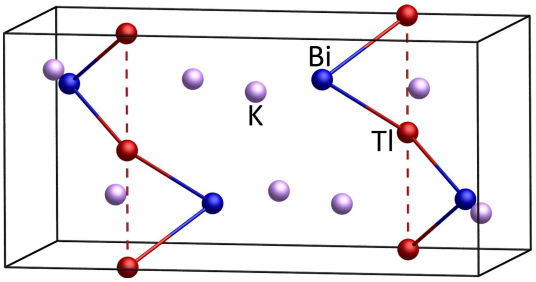

(a) K_2TlBi

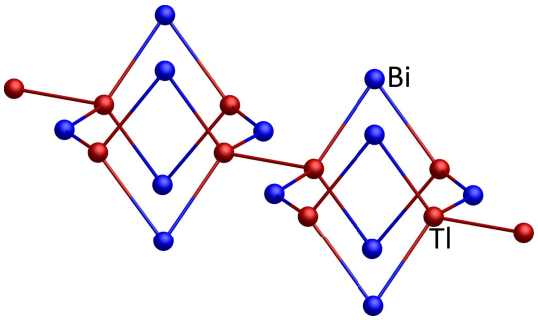

(b) ${}^{1}_{\infty}[Tl_4Bi_6]^{12-}$-Stränge in $K_6Tl_2Bi_3$

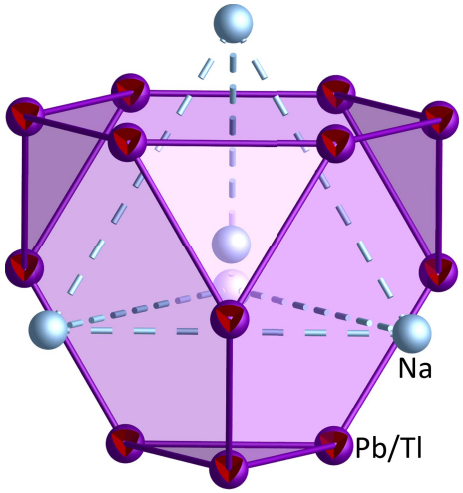

(c) $Na_4[Na@Tl_5Pb_7]^{12-}$-Cluster in $Na_{17}Tl_5Pb_7$

Abbildung 3.3: Ausschnitte aus den Strukturen der charakterisierten ternären Festkörper. KTlBi ist isostrukturell zur hexagonalen *Laves*-Phase KPb_2 und nicht dargestellt.[20]

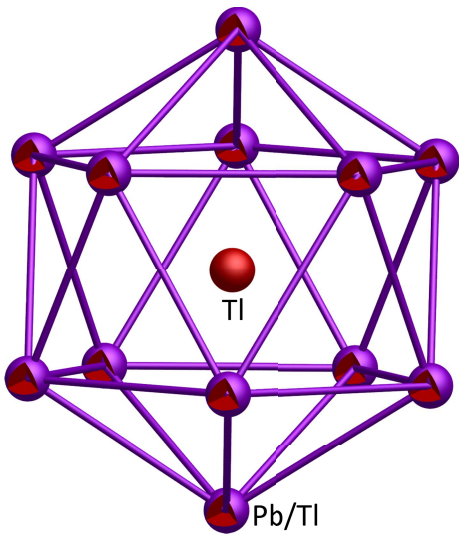

(a) $[Tl@Tl_4Pb_8]^{4-}$

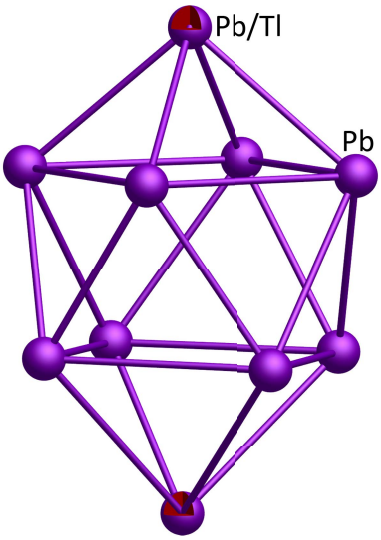

(b) $(TlPb_9)^{3-}$

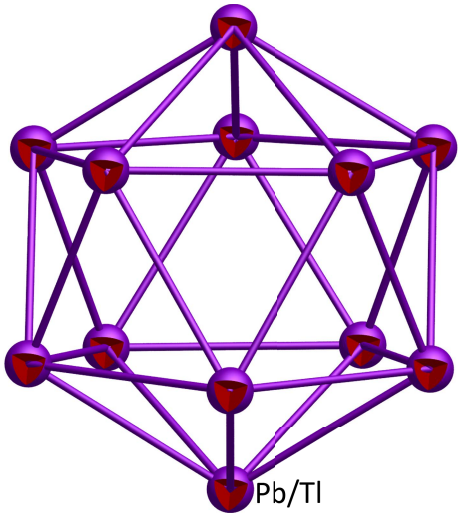

(c) $(TlPb_{11})^{3-}$

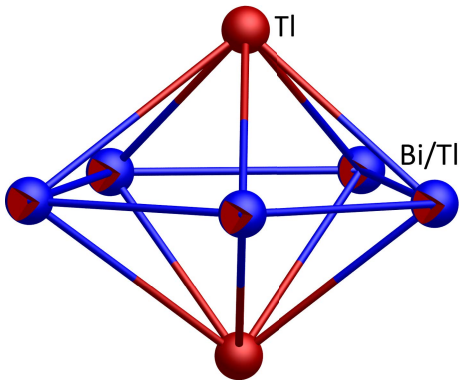

(d) $(Tl_4Bi_3)^{3-}$

Abbildung 3.4: Strukturen der aus den dargestellten intermetallischen Verbindungen synthetisierbaren binären *Zintl*-Anionen und des intermetalloiden Clusters.[20]

Eigener Anteil

Alle Experimente wurden von mir konzipiert und ein Großteil der Synthesen selbst durchgeführt. Alle Festkörpersynthesen habe ich zunächst selber durchgeführt, ebenso wie die Extraktionen der allermeisten dieser Verbindungen. Lediglich die Extraktionen der Verbindungen „Na_5TlPb_3“ und „K_5TlPb_3“ erfolgten dann durch *Sebastian Ullrich* im Rahmen eines Masterpraktikums unter meiner Anleitung. Zudem habe ich alle Röntgenbeugungsdaten aufgenommen und alle Sturkturlösungen und -verfeinerungen selbst durchgeführt. Aufgrund massiver Fehlordnungsprobleme in den Verbindungen $[K(Krypt{-}222)]_3(Tl_4Bi_3)$ und $[K(Krypt{-}222)]_4[Tl@Tl_4Pb_8]_{0.51}(Tl_2Pb_{10})_{0.11}(Pb_9)_{0.38}$ sowie einer pseudo-merohedrischen Verzwilligung in Kombination mit einer Überstruktur in der Verbindung $[K(Krypt{-}222)]_3(Tl_4Bi_3)$ hat Prof. Dr. *Werner Massa* die finale Bearbeitung und Aufbereitung der Datensätze dieser Verbindungen übernommen. Alle massenspektrometrischen Daten wurden an von mir präparierten Proben in meinem Beisein durch *Jan Bamberger* aufgenommen. Zur Aufnahme der μ-RFA-Spektren habe ich mit *Carsten Donsbach* und Dr. *Bastian Weinert* zusammengearbeitet. Die quantenchemischen Studien aller untersuchten Verbindungen wurden durch *Yannik J. Franzke* und PD. Dr. *Florian Weigend* durchgeführt. Die Verfassung des Manuskripts erfolgte durch mich und Prof. Dr. *Stefanie Dehnen* im Dialog, wobei der Abschnitt über die quantenchemischen Analysen durch die Kooperationspartner verfasst und durch alle Autoren überarbeitet wurde.

ChemPubSoc Europe

DOI: 10.1002/chem.201802382

CHEMISTRY A European Journal Full Paper

Intermetallic Compounds

The Identity of "Ternary" A/Tl/Pb or K/Tl/Bi Solid Mixtures and Binary Zintl Anions Isolated From Their Solutions

Niels Lichtenberger,[a] Yannick J. Franzke,[b] Werner Massa,[a] Florian Weigend,[c] and Stefanie Dehnen*[a]

Dedicated to Professor Wolfgang Bensch on the occasion of his 65th birthday

Abstract: Investigations of solid mixtures of the elemental combinations A/Tl/Pb (A = Na, K) and K/Tl/Bi indicate the presence of multiple binary and ternary Zintl phases, among them new ones containing Tl and Pb or Bi, respectively. Extractions with en/crypt-222 afford single crystals of several novel binary anions, including $[Tl@Tl_4Pb_8]^{4-}$ and $(Tl_4Bi_3)^{3-}$. $[Tl@Tl_4Pb_8]^{4-}$ adopts a *closo*-type cage structure despite possessing one additional electron; it is therefore isostructural, yet not isoelectronic, with homoatomic $[Tl@Tl_{12}]^{11-}$ obtained by solid state reactions. $(Tl_4Bi_3)^{3-}$ is a rare case of a pentagonal bipyramidal Zintl anion, yet the first binary one, and (unlike Tl_7^{7-}) the first one with a proper *closo*-type electron count. Assignment of the numbers and positions of the Tl/Pb or Tl/Bi atoms within the anionic clusters, indistinguishable in classical X-ray diffraction experiments, was achieved by means of quantum chemistry. The studies shed light on the complex situation in solid heavy element mixtures and their substantial differences from the composition of the Zintl anions obtained from them by extraction.

Introduction

The solution chemistry of Zintl anions comprising group 13–15 elements has been studied extensively over the last two decades.[1] Reactions with transition metal complexes led to the formation of intermetalloid clusters, in which the metal atoms are incorporated into main-group element cluster shells of different sizes and geometries.[2] These represent defined superatom-like, all-metal clusters, which are considered promising for homogeneous catalysis.[3]

Most of the intermetalloid cluster syntheses start out from soluble Zintl anions. This is a strong motivation for the use of binary Zintl anions, which are significantly better soluble if the mixture leads to a reduction of the charge, like upon introduction of group 15 elements to group 14 or (especially) group 13 elements. According anions were recently proven versatile starting materials.[4] Furthermore, they enhance the structural variety of the products and create uncommon bonding situations.

While this chemistry is fascinating and fruitful in itself, one very important aspect is usually neglected that gives most of the studies so far a taste of serendipity: the reactive anions are isolated as their $[A(crypt\text{-}222)]^+$ salts (A = Na–Rb) or formed in situ by dissolving a parent solid in an en/crypt-222 solution (en = ethane-1,2-diamine). Although the underlying solids are the key component that determine which anions are formed in solution, they are rarely looked at in detail. Typically, the structures of these compounds remain unknown and it is even unclear how many components are present in the solid mixtures.

Whereas the synthesis of most homoatomic cluster anions is straight-forward, involving the dissolution of one well-defined, solid binary phase that comprises pre-formed cluster anions, this is more complicated for binary anions. For element combinations A/E′/E″ the ternary phase-diagrams are widely unknown. Most of the tetrahedral anions $(E^{14}_2E^{15}_2)^{2-}$ can be accessed upon use of the according $K/E^{14}/E^{15}$ (1:1:1) solids.[5] Of these systems, only KPb_xBi_{2-x} $(0 < x \leq 1)$ was studied, but a

[a] N. Lichtenberger, Prof. Dr. W. Massa, Prof. Dr. S. Dehnen
Fachbereich Chemie und
Wissenschaftliches Zentrum für Materialwissenschaften
Philipps-Universität Marburg,
Hans-Meerwein-Straße 4
35043 Marburg (Germany)
E-mail: dehnen@chemie.uni-marburg.de

[b] Y. J. Franzke
Karlsruhe Institute of Technology (KIT)
Institute of Physical Chemistry
Kaiserstraße 12
76131 Karlsruhe (Germany)

[c] Dr. F. Weigend
Karlsruhe Institute of Technology (KIT)
Institute of Nanotechnology
Hermann-von-Helmholtz-Platz 1
76344 Eggenstein-Leopoldshafen (Germany)

Supporting information and the ORCID identification number(s) for the author(s) of this article can be found under: https://doi.org/10.1002/chem.201802382.

Part of the Special Issue for the 7th EuCheMS Chemistry Congress consisting of contributions from selected speakers and conveners. To view the complete issue, visit Issue 46.

direct synthesis of KPbBi failed, and no single crystal structure was obtained.[6] There is only one case, in which the crystal structure of the parent phase for a binary anion synthesis was determined, however indicating no structural relationship.[7]

The introduction of group 13 elements into the binary cluster anions alters the electronic situations of the resulting products due to their high charge, usually −2, in Zintl anions. Homoatomic Zintl anions of group 13 elements in solution will thus remain elusive in classical solvents, maybe with the exception of liquid NH_3.[8] A few examples of binary Zintl anions containing Tl atoms and group 14 atoms have been reported in the literature. These were first characterized solely by NMR-spectroscopy and later also crystallographically.[9] Our goal was to find a synthetic access to new binary Zintl anions with group 13 elements, aiming for their further use as synthetic building blocks for ternary intermetalloid clusters, as previously shown for $(E^{13}Bi_3)^{2-}$ (E^{13} = Ga, In, Tl). In these anions, the high charge of the E^{13} atoms is "diluted" by formally neutral Bi atoms.[4f,10] Even though the synthesis of new phases sounds easy in theory, it is a very challenging task, as there are hardly any reports on Zintl anions with group 13 elements and also only few ternary phases that could serve as a starting point.

Here, we present our results obtained for three different ternary systems, A/Tl/Pb (A = Na, K), and K/Tl/Bi. These were chosen due to the *pseudo*-homoatomic nature of the involved heavy metal atoms, a fact that greatly enhances the solubility of the anions obtained from such phases.[11] Hence, the solution chemistry of these materials is discussed with respect to their use as starting materials for the synthesis of binary Zintl anions. An overview over all studies reported in this paper is given in Scheme 1. Throughout this paper, the following numbering scheme is used: Roman letters are used to denote compounds that have previously been described in the literature and that are repetitively mentioned in the discussion. Roman numerals indicate nominal compositions of solid material as determined through initial stoichiometry. Arabic numerals are assigned to all new compounds presented herein. We further note that due to the fact that Tl, Pb, and Bi atoms are virtually indistinguishable for $Mo_{K\alpha}$ X-rays, the solid-state compositions are formally hypothetical, but reasonable pursuant to the Zintl–Klemm pseudo element concept.

Results and Discussion

Solid State Chemistry

Ternary Solids of $A_xTl_yPb_z$ (A = Na, K)

In order to work with the mentioned pseudo-homoatomic system, the first step was to find a suitable initial stoichiometry for the fusion of the elements such that a defined binary anion would form in the solid state. Though this might not be necessarily a strict requirement for a successful preparation of cluster anions in solution, it should strongly assist herein. The known compound Na_5TlSn_3 contains isolated $(TlSn_3)^{5-}$ tetrahedra.[12] As these anions cannot be dissolved/stabilized by conventional solvents due to their high negative charge, they are

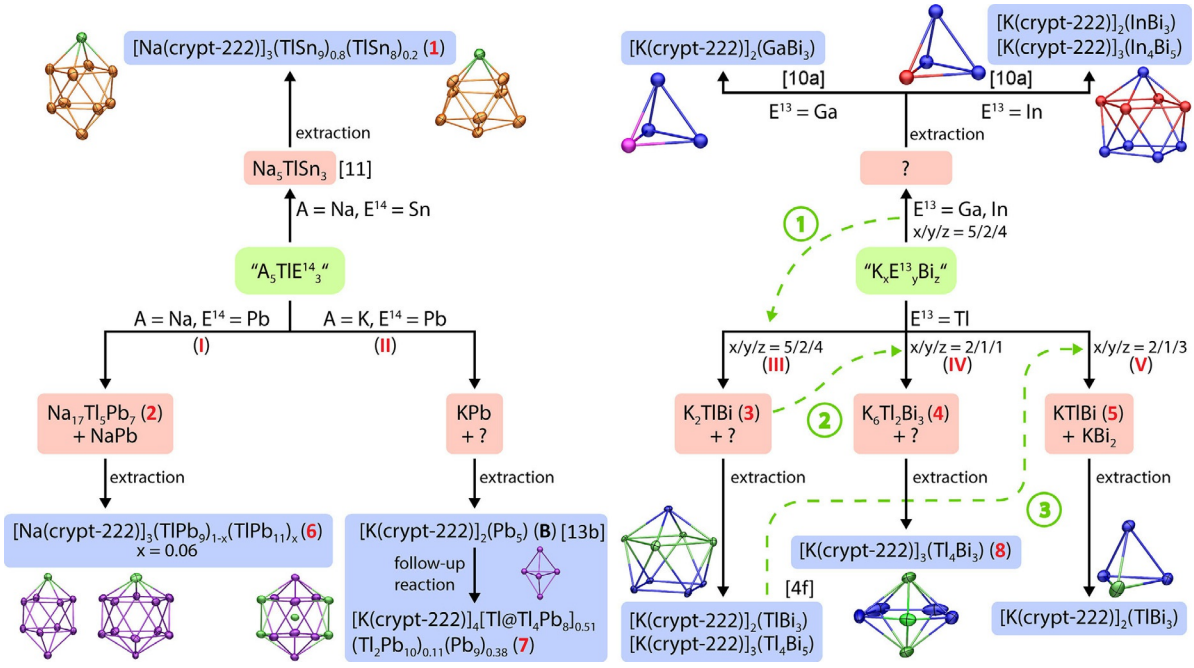

Scheme 1. Overview of the solid-state syntheses (red boxes) and extraction procedures (blue boxes) reported in this paper. All extraction experiments were carried out with crypt-222 in ethane-1,2-diamine (en). Left: the systems A/Tl/Pb (A = Na, K; bottom) in comparison to Na/Tl/Sn (top). Right: the system K/Tl/Bi (bottom) in comparison to K/Ga/Bi and K/In/Bi (top) reported in the literature.[10a] Green dashed lines indicate the course of our experiments in the K/E^{13}/Bi system: 1, transfer of previous findings to the element combination K/Tl/Bi; 2, attempt to synthesize K_2TlBi based on the first result; 3: selective synthesis of $[K(crypt\text{-}222)]_2(TlBi_3)$. For further details, see the text.

likely to undergo rearrangement and redox reactions to form lower-charged cluster anions in solution. Indeed, extraction of Na_5TlSn_3 with en/crypt-222 yielded the salt $[Na(crypt\text{-}222)]_3(TlSn_8)_{0.2}(TlSn_9)_{0.8}\cdot 0.55en\cdot 0.45thf$ (**1**, see Supporting Information). The Zintl anions in **1**, $(TlSn_9)^{3-}$ and $(TlSn_8)^{3-}$, are two of the few binary ones comprising group 13 atoms that were already described in the literature, yet being previously obtained as their $[K(crypt\text{-}222)]^+$ salts.[9b] In **1**, they again do co-crystallize, but with a different type of disorder.

Encouraged by these findings and the fact that the atomic radii for Sn and Pb are similar, we prepared two solids with the analogous nominal compositions "A_5TlPb_3" [A = Na (**I**), K (**II**)] by fusion of the elements in the desired ratio in sealed Nb-tubes. The resulting substances were characterized by powder X-ray diffraction (PXRD) and single-crystal X-ray diffraction (SCXRD). In these studies, it became immediately evident that the nominal compositions are to be handled with great caution. Both **I** and **II** turned out to be mixtures of binary APb[13] and at least one further, previously unknown crystalline phase. It is noteworthy that none of the products contained a crystalline substance that yields reflections which would account for an according 5:1:3 phase. In the case of **I**, we were able to isolate single crystals of the second component, which turned out to be $Na_{17}Tl_5Pb_7$ (**2**) according to SCXRD, and under consideration of the Zintl–Klemm–Busmann pseudo element concept. **2** crystallizes in the cubic space group $I\bar{4}3m$, with $a = 11.811(2)$ Å, $V = 1647.7(5)$ Å^3, and $Z = 2$. The structure is quite complex and is described in more detail in the Supporting Information. It can be interpreted as $(Na_4)_3[Na@Na_4Tl_5Pb_7]$, featuring a network of corner-sharing (Na_4) tetrahedra (Na3···Na3′ = 3.4812(1), 3.6331(1) Å) that form closely packed β-cages. The network embeds clusters of the composition $[Na@Na_4Tl_5Pb_7]^{12-}$, which represent Na-centered 16-atom Frank–Kasper polyhedra, isostructural to the coordination polyhedra embedding Mg atoms in the cubic Laves phase $MgCu_2$.[14] Hence, the Tl/Pb atoms form a truncated tetrahedron (Tl/Pb···Tl/Pb 3.1348(1), 3.1788(1) Å) around one central Na atom (Tl/Pb···Na1 3.7040(1)) Å), and all four hexagonal faces are capped by another Na atom (Tl/Pb···Na2 3.4776(1) Å). The crystal structure of **2** is illustrated in Figure 1. Both the composition and structure of **2** accord with the classic Zintl–Klemm–Busmann pseudo-element concept: each heavy metal atom is three-bonded, thus mimicking a group 15 element, formally Tl^{2-} or Pb^-. The 17 Na atoms per formula unit are to be considered as Na^+ cations for an overall charge compensation of the $[(Tl_5)^{10-}(Pb_7)^{7-}]^{17-}$ clusters. The structure of **2** can further be derived from the elemental structure of α-Mn (*cI*58) and the intermetallic phase $Mg_{17}Al_{12}$ (see Table S4 and Figure S30 in the Supporting Information).[15] Thus, **2** is also highly related to the previously reported compounds $(M^{2+})Na_{10}Sn_{12}$ (M^{2+} = Ca, Sr, Eu, Yb) that feature the same heavy metal clusters within a similar environment of cations,[16] however differing in the total number of cations due to different anionic charges as compared with **2**.

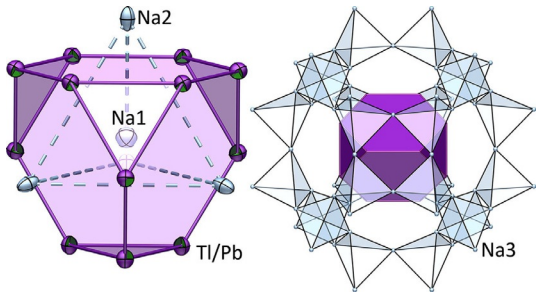

Figure 1. Cut-out from the crystal structure of **2**. Left: $[Na@Na_4Tl_5Pb_7]^{12-}$ clusters. Right: one of the β-cages formed by the Na3 atoms within the framework surrounding the clusters. Thermal displacement ellipsoids are drawn at 50% probability. Further illustrations and a full structure description are provided in the Supporting Information.

According to the PXRD results, **I** contains both NaPb and **2** (Figure 2, top).[13a] Although a quantitative analysis of the powder pattern was unsuccessful due to the relatively poor data quality caused by high absorption coefficients, it is worth noting that in a 1:8 ratio of the two compounds, the mixture represents the nominal composition of the parent solid: $Na_{17}Tl_5Pb_7 + 8\,NaPb = "Na_{25}Tl_5Pb_{15}" = 5\ "Na_5TlPb_3"$. A subsequent experiment indicated that **2** can also be prepared directly by fusion of the elements in the according 17:5:7 ratio.

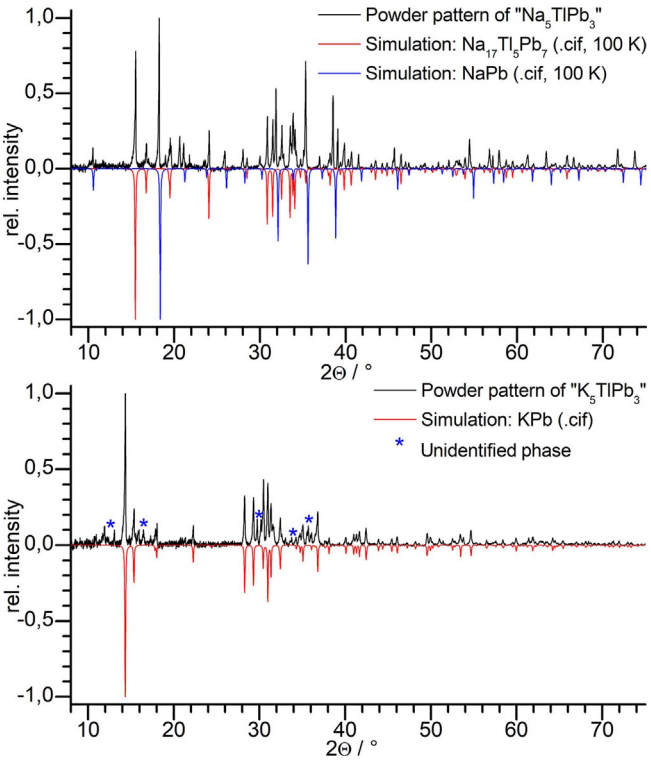

Figure 2. Comparison of measured and simulated powder patterns for "A_5TlPb_3". Top: A = Na, identified phases: $Na_{17}Tl_5Pb_7$ (**2**) and NaPb. Bottom: A = K, identified phase: KPb.

In the case of **II**, PXRD shows that KPb is the main component as well, but the according K^+ salt of **2** is not formed (Figure 2, bottom).[13b] A closer inspection and comparison of the two PXRD patterns of **I** and **II** reveals that the fractional contribution of the second component in **II** is very small. As the different components in the solid mixtures cannot be

distinguished optically we tried to mount numerous crystals on a single-crystal diffractometer but never succeeded in picking one of the unknown compound.

The extraction chemistry of both solid mixtures, **I** and **II**, is discussed below.

Ternary Solids of $K_xTl_yBi_z$

The first solid material we studied in the K/Tl/Bi system was a solid with the nominal composition "$K_5Tl_2Bi_4$" (**III**), thus a homologue of the known solids "$K_5Tr_2Bi_4$" (Tr = Ga, In).[10a] Our findings once more confirmed that the nominal composition can deviate strongly from the true composition. **III** was prepared by fusion of the elements in a 5:2:4 ratio, with the original goal to produce a starting material for salts that comprise $(TlBi_3)^{2-}$ anions—in analogy to the chemical behavior of the lighter homologues. Even though the latter were not structurally characterized, several others with slightly different compositions were.[17] All of them feature indium-centered $[InBi_4]$ tetrahedra, which are connected into extended network structures, as a common structural motif.

Prior to the extraction experiments, we analyzed the as-prepared solid product with PXRD (Figure S56). We were able to isolate single crystals of the main component, which was shown to be the novel compound K_2TlBi (**3**; approx. 80%) by means of SCXRD. **3** crystallizes in the orthorhombic space group *Pbcm*, with the unit cell parameters $a = 6.8048(5)$ Å, $b = 13.4464(9)$ Å, $c = 6.5212(6)$ Å, $V = 596.69(8)$ Å^3, and $Z = 4$, and it is isostructural to the known phase K_2SnBi,[18] despite a one-electron deficit arising from the formal exchange of Sn for Tl. The crystal structure is depicted in Figure 3. Its central motif is

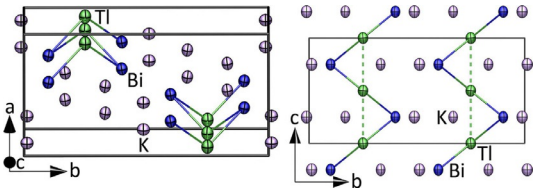

Figure 3. Extended unit cell representations of 3. Infinite Tl–Bi chains parallel to c. Views approx. along [001] (left) and [$\bar{1}$00] (right). Thermal displacement ellipsoids are drawn at 50% probability. Selected interatomic distances and angles [Å, °]: Tl–Tl: 3.2606(3), Tl–Bi: 3.160(1), Bi···K: 3.569(7)–3.788(3), Tl···K: 3.818(6)–4.043(6); Bi–Tl–Bi: 110.478(2), Tl–Bi–Tl: 62.11(2); Bi–Tl–Tl–Bi: 96.55(3).

an infinite zig-zag chain with a strand of thallium atoms generating the backbone, and the bismuth atoms bridging between two Tl atoms in an alternating fashion. The opposing, triangular Tl-Bi-Tl planes enclose an angle of 96.55(3)°. For a full structural description, see the Supporting Information.

The subsequently attempted, direct synthesis of **3** by fusion of the elements in a 2:1:1 ratio yielded the crude phase "K_2TlBi" (**IV**). Upon close inspection, **IV** turned out not to be the targeted compound **3**, but instead contains a new phase with a near 2:1:1 stoichiometry, $K_6Tl_2Bi_3$ (**4**), according to PXRD and SCXRD (see Figure S57). Although unprecedented, this result is not completely surprising in retrospect. The ternary system K/Tl/Bi has not been explored up to date, and our findings indicate that a variety of compounds with similar composition exist, which seem to possess similar stabilities. Compound **4** crystallizes in the monoclinic space group *C*2/*c*, with the unit cell parameters $a = 10.0799(7)$ Å, $b = 17.2809(7)$ Å, $c = 20.002(1)$ Å, $\beta = 103.711(5)°$, $V = 3384.9(4)$ Å^3, and $Z = 8$. The intermetallic phase is isostructural to its lighter homologue $K_6Tl_2Sb_3$,[19] and represents the second example of this structure type. The structure features infinite chains of $(Tl_4Bi_6)^{12-}$ cages that are linked via Tl–Tl bonds. A section of one of these chains is shown in Figure 4.

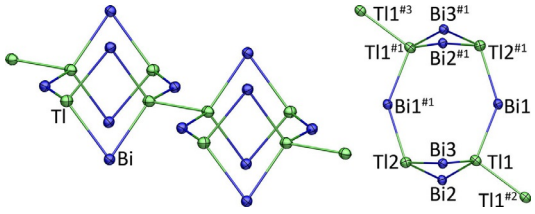

Figure 4. Cut-outs from the crystal structure of **4**, showing a fragment of one infinite $^1_\infty[Tl_4Bi_6]^{12-}$ chain (left) and one $(Tl_4Bi_6)^{12-}$ cage (right). Thermal displacement ellipsoids are drawn at 50% probability. Counter ions are omitted for clarity. Selected bond lengths and angles [Å, °]: Tl1–Bi 3.163(1)–3.258(1), Tl2–Bi: 3.254(1)–3.268(1), Tl1–Tl1: 3.289(2); Bi–Tl–Bi: 104.03(3), 108.03(3), 108.91(3), 108.76(3); Bi–Tl–Tl: 105.56(4), 108.67(3), 109.70(3), Tl–Bi–Tl: 70.10(3), 70.58(3) 141.46(4); #1: 2−*x*, *y*, $^1/_2-z$; #2: 1−*x*, *y*, $^1/_2-z$; #3: 1+*x*, *y*, *z*.

The assignment of atomic positions was done in analogy to $K_6Tl_2Sb_3$ and can also be rationalized with the pseudo-element concept:[20] all Bi atoms and the four-coordinate Tl1 atom can formally be assigned a 1− charge in accordance with their role as pseudo-chalcogen and pseudo-tetrel atoms, respectively. The three-coordinate Tl2 atom behaves like a pseudo-pentel atom, thus carrying a formal 2− charge. Together, these atoms form a double-decker-like, near D_{2h}-symmetric cage structure (crystallographic C_2 symmetry) with two parallel (Tl_2Bi_2) rings being linked via two μ-Bi bridges. Each cage is connected to two adjacent ones through Tl1–Tl1′ bonds. For a full structure description, see the Supporting Information.

Another key composition for a ternary mixture in this phase system is "K_2TlBi_3" (**V**), as this solid has proven suitable as starting material for the solution chemistry of the $(TlBi_3)^{2-}$ anion (see also below).[4f] Fusion of the elements in the 2:1:3 ratio yields a brittle, dark metallic solid that was analyzed by combined PXRD and SCXRD studies. PXRD indicates the presence of two different phases, one of which is easily identifiable as KBi_2. A closer inspection of the crude material obtained from the synthesis with SCXRD finally helped to identify the second component. It forms single crystals with the hexagonal unit cell parameters of $a = 6.8037(3)$ Å, $c = 10.491(1)$ Å, $V = 420.59(5)$ Å^3. These values are very close to the unit cell parameters of KPb_2, and the initial structure solution led to an isostructural atom arrangement.[21] As no Pb was used during the synthesis, the isoelectronic composition in this case is KTlBi (**5**), which can again be explained in terms of the *pseudo*-element

concept. Its structure adopts the architecture of a hexagonal Laves phase, thus according to the $MgZn_2$ prototype. Noteworthy, the 1:1 combination of KBi_2 and **5** adds up to a nominal composition of "K_2TlBi_3", and also fully accounts for all reflections found in the PXRD of the solid (see Figure S58), thus unravelling its true identity. However, a targeted synthesis of pure **5** in a separate form has not yet been successful to date.

In stark contrast to all known A/In/Bi phases, none of the reported compounds contains Tl-centered [$TlBi_4$] tetrahedra.[17] Our results indicate that the ternary phase system K/Tl/Bi is very complex and deserves further studies. As the direct synthesis of already identified compounds remains challenging, this will be the focus of future investigations, along with their behavior in solution.

Solution Chemistry: Binary Zintl Anions

Extraction of "A_5TlPb_3" (A = Na, K)

Extraction of phases with the nominal composition "A_5TlPb_3", A = Na (**I**) or K (**II**), indicated a distinct dependency of the product formation on the choice of the counter ion. The extraction of **I** with en/crypt-222 yields black blocks of [Na(crypt-222)]$_3$($TlPb_9$)$_{0.94}$($TlPb_{11}$)$_{0.06}$·0.9*thf* (**6**) besides red needles of [Na(crypt-222)]$_2$(Pb_5) (**A**) upon layering with THF at 5 °C. This very same procedure applied to **II** afforded exclusively red needles of the known salt [K(crypt-222)]$_2$(Pb_5) (**B**).[22] Storage of a concentrated extraction solution of **II** in en/crypt-222 at 5 °C again afforded red needles of **B** within 12 hours. However, these needles partly re-dissolved within days, whereupon [K(crypt-222)]$_4$[Tl@Tl_4Pb_8]$_{0.51}$(Tl_2Pb_{10})$_{0.11}$(Pb_9)$_{0.38}$·2*en* (**7**) crystallized as black blocks. This hints towards the co-existence and involvement of more than one species, with different solubilities, in the formation of **7**. This is supported by the fact that the formation of **7** is furthermore dependent on the extraction time t_{ext}, and only forms for $t_{ext} > 24$ h. For $t_{ext} < 24$ h, we only observed the formation of **B**. Nevertheless, as the yields are far from being quantitative, we cannot fully exclude that all of the said anions are formed from both **I** and **II**, but do not crystallize under the given conditions. **6** and **7** were structurally characterized by means of SCXRD. Their A:Tl:Pb compositions were confirmed semi-quantitatively by micro X-ray fluorescence (μ-XRF) spectroscopy (see Table S12), and also by quantum chemical investigations, as will be detailed below.

Compound **6** crystallizes in the monoclinic space group $P2_1/c$, with the unit cell parameters $a = 14.3233(3)$ Å, $b = 21.8968(5)$ Å, $c = 28.7725(6)$ Å, $\beta = 102.798(2)°$, $V = 8799.9(3)$ Å^3, and $Z = 4$. Three [Na(crypt-222)]$^+$ cations surround the heavy atom cluster anions ($TlPb_9$)$^{3-}$ and ($TlPb_{11}$)$^{3-}$, both of which are disordered on one position. As observed in the case of Na_5TlSn_3, a redox reaction occurs in solution, causing the product compositions to deviate from NaPb and $Na_{17}Tl_5Pb_7$ observed within the solid **I**, thereby affording the deltahedral polyanions. We attribute this finding to the high stability of the respective *closo*-type anions with 10 and 12 atoms (for structural details see Supporting Information).[23] As Tl and Pb atoms cannot be distinguished by classical X-ray experiments, we confirmed the actual composition and individual atom positions with electrospray ionization mass spectrometry (ESI-MS), μ-XRF and quantum chemical studies employing density functional theory (DFT) methods (see below). The latter showed a distinct preference (by 17 kJ mol^{-1}) for the Tl atom to be positioned in a capping position. Furthermore, these studies served to estimate the errors of the employed quantum chemical method for Pb–Pb distances, up to +0.03 Å, and for Tl-Pb distances, +0.05 Å (see section 6.2. in the Supporting Information), as there were no binary experimental reference systems reported so far.

Compound **7** crystallizes in the triclinic space group $P\bar{1}$, with the unit cell parameters $a = 14.4510(6)$ Å, $b = 15.3339(6)$ Å, $c = 16.2360(8)$ Å, $\alpha = 62.643(3)°$, $\beta = 63.955(3)°$, $\gamma = 86.421(3)°$, $V = 2826.4(2)$ Å^3, and $Z/Z' = 1/0.5$. The structure is very similar to that of [K(crypt-222)]$_2$[Ni@Pb_{12}]·*en* that was previously reported by Eichhorn,[1c] albeit differing in the cluster charge and thus the number of cation complexes. Yet, the [Tl@Tl_4Pb_8]$^{4-}$ anion in **7** features the second known heteroatomic icosahedron besides [Pd@$Pd_2Pb_{10}Bi_6$]$^{4-}$ and the first one that embeds a main group atom as 13th atom, as depicted in Figure 5.[24] The cluster composition was investigated with ESI-MS, which helped to confirm the element ratio and also indicated a stepwise cluster fragmentation (see Supporting Information for details).

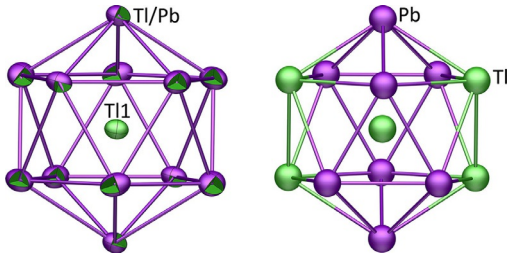

Figure 5. Left: structure of the [Tl@Tl_4Pb_8]$^{4-}$ anion in **7**, indicating the consideration of the 12 outer atoms as mixed Tl/Pb sites; the central atom was treated as pure Tl atom upon the clear preference for it according to DFT calculations (see text). Thermal displacement ellipsoids are drawn at 50% probability. Right: Optimized geometry of the lowest energy isomer (DFT). Selected bond lengths [Å]: Tl1–Tl/Pb (center···shell) 3.0667(2)–3.1934(2), Tl/Pb–Tl/Pb (icosahedral shell) 3.2543(2)–3.3970(1).

The found Tl:Pb = 5:8 ratio in the [Tl@Tl_4Pb_8]$^{4-}$ anion in **7**, which was reliably determined by mass spectrometry and μ-XRF measurements, together with the charge of −4, as unambiguously determined from the number of counter ions, exceeds the prediction of Wade–Mingos rules for a *closo* cluster by one electron. Given that the electrons of the inner Tl atom contribute to the charge of the 12-atom shell (as [(Tl^{3+})@(Tl_4Pb_8)$^{7-}$]$^{4-}$, analogous to the reported interpretation of [(Tl^{3+})@(Tl_{12})$^{14-}$]$^{11-}$)[25] we calculate $5\times3+8\times4+4\times1=51$ valence electrons (VE) and thus $51-12\times2=27$ skeleton electrons (SE). This corresponds with a 2n+3 electron count ($n = 12$), featuring one additional electron in comparison to a normal *closo* cluster (50 VE, 2n+2 SE). However, despite the additional electron and the heteroatomic nature of the anion, there are only slight deviations from a perfect I_h symmetry in the crystal structure, with bond lengths of 3.2543(2)–

3.3970(1) Å (3.299 Å on average) on the icosahedral shell and 3.0667(2)–3.1934(2) Å (3.137 Å on average) between the interstitial atom and the cluster shell.

The anion in **7** represents a link between a series of icosahedral intermetalloid clusters with interstitial transition-metal atoms, $[M@E_{12}]^{q-}$ (M/E/q = Ir/Sn/3[26] or Ni/Pb/2, Pd/Pb/2, Pt/Pb/2),[1b,c] and the solid phases $Na_4A_6Tl_{13}$ (A = K-Cs) and $Na_3K_8Tl_{13}$ with $[Tl@Tl_{12}]^{10/11-}$ clusters.[25] While the $[M@E_{12}]^{q-}$ clusters all crystallized from solutions with a respective number of $[K(crypt\text{-}222)]^+$ counterions, the neat solids contain exclusively un-sequestered cations. The strong Coulomb forces that occur in those phases prohibit the solids from being soluble in common solvents. Additionally, they drastically affect the cluster structures. The closed-shell $[Tl@Tl_{12}]^{11-}$ anion, for example, shows much larger deviations from I_h symmetry than the anion in **7**, even though its skeleton electron count of 26 (= 2n + 2) accords with the expectations for a *closo* cluster. It further exhibits considerably longer bonds (3.216–3.578 Å in the Tl_{12} shell, 3.404 Å on average; 3.204 and 3.273 Å towards the inner atom, 3.284 Å on average), as a consequence of a relatively inhomogeneous counterion environment (Tl···Na: 3.145 and 3.309 Å, Tl···K: 3.548–3.818 Å). There have been several examples of main group element atoms serving as endohedral atoms in the case of metalloid clusters.[27] However, in the case of intermetalloid clusters, comprising both main group and transition metal atoms, only one cluster type has been published to date, in which a main group element atom takes this role. Of the four known variants of $[MG@TM_{12}@MG_{20}]^{q-}$ (MG/TM/q = As/Ni/3,[1a] Sn/Cu/12,[28] Sb/(Ni/Pd)/(3/4)[1j]).[29] three were obtained by classical solution reactions of Zintl anions while the fourth occurs in a neat solid. All of these anions feature the same onion-type structure.

Still, the $(Tl_5Pb_8)^{4-}$ composition with its 51 VE is rather unexpected, as heavy-element Zintl clusters usually do not show partially filled electronic shells—with some known exceptions of clusters exhibiting open-shell main group (semi-)metal clusters, for example, $[Ru@Ge_{12}]^{3-}$ [1f] and $[U@Bi_{12}]^{3-}$.[4e] Usually, such clusters prefer energetically well separated fully occupied and fully unoccupied orbitals, which in the present case would correspond to $(Tl_4Pb_9)^{4-}$ (52 VE) or to $(Tl_6Pb_7)^{4-}$ (50 VE). In particular the latter was considered plausible at first, as it would be isoelectronic to the known anions $[M@Pb_{12}]^{2-}$ (M = Ni, Pd, Pt) mentioned above.[1b,c] As the reaction mixture comprised a binary Tl/Pb source, it is surprising that the system did not take the freedom to choose another elemental combination for tuning the total electron count to form a Wade–Mingos *closo* cluster (under preservation of the apparently preferential total charge), such as "$[Tl@Tl_5Pb_7]^{4-}$", which we can rule out with certainty. A final experimental proof of the unpaired electron was so far hampered by contaminations with metallic co-precipitate that typically occur along with single-crystals of such heavy metal cluster salts.

Hence, in order to check whether and to rationalize why the 51 VE system in the present case is realistic, quantum chemical calculations were done with a pre-version of TURBOMOLE V7.3.[30] The two-component relativistic all-electron method X2C[31] was applied, which accounts for spin-orbit interaction in a self-consistent manner. We employed the density functional TPSS,[32] optimized basis sets of type x2c-TZVPall-2c[33] and corresponding auxiliary basis sets.[33] The diagonal local approximation to the unitary decoupling transformation (DLU)[34] was applied both for the calculation of energies[35] and gradients.[36] The finite nucleus model based on a Gaussian charge distribution was applied.[36,37] For compensation of the negative charge the conductor-like screening model (COSMO)[38] was employed. In this way, full structure optimizations for all symmetry-non-redundant isomers of $(Tl_4Pb_9)^{4-}$, $(Tl_5Pb_8)^{4-}$ and $(Tl_6Pb_7)^{4-}$ were carried out. Each isomer may be characterized by its average distance from the central atom to the atoms of the icosahedral shell (d_{c-s}) and the average distance within the icosahedral shell (d_{s-s}) together with the corresponding standard deviations σ_{c-s} and σ_{s-s}; these values have to be compared to the experimental values of 3.137 ± 0.04 Å and 3.298 ± 0.04 Å (see also below). Furthermore, each isomer can be characterized by its energy relative to the most stable one within each composition. These data are visualized in Figure 6 and additionally available in the Supporting Information together with the molecular Cartesian coordinates.

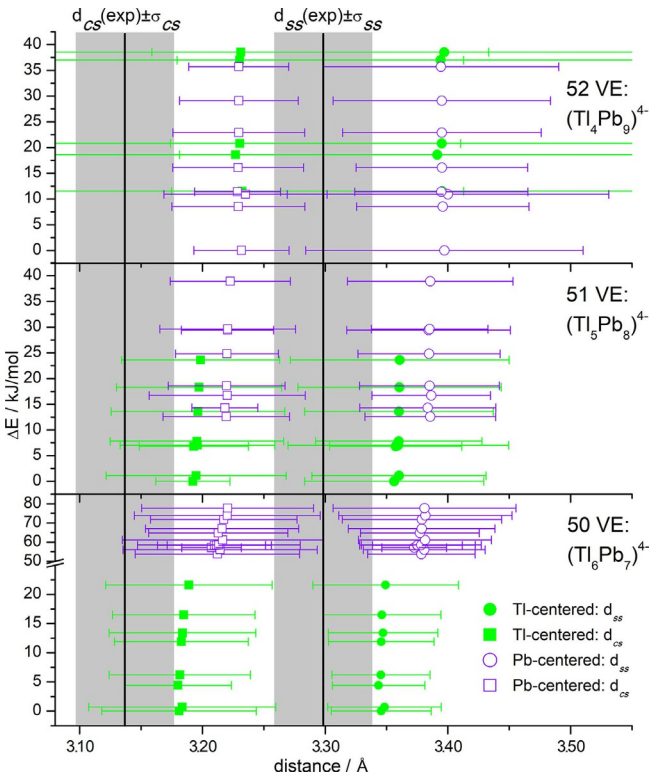

Figure 6. Relative energies (abscissa) and mean values ± standard deviations of core–shell and shell-shell interatomic distances for all symmetry-non-redundant isomers of the centered icosahedral cluster anion for different valence electron (VE) numbers. The experimental distances and their variations (standard deviation) are represented by vertical lines and grey areas. For a full discussion see also the main text.

The following picture is revealed: Pb-centered systems with 50 or 51 VE, or systems with 52 VE in general show comparably large deviations to measured data for average distances,

typically +0.10 Å, which is more than is observed for $(TlPb_9)^{3-}$, see above. Further, for the 50 VE and the 51 VE systems, Pb-centered species are energetically disfavored over Tl-centered ones; for the 52 VE systems, the energetically best isomer, which is favored over the second by around 10 kJ mol^{-1}, shows a large scatter in the interatomic distances within the icosahedral shell (+0.11 Å), which does not fit to the experiment. We thus may rule out Pb-centered systems with 50 or 51 VE, and systems with 52 VE in general. For the Tl-centered 50 and 51 VE species in contrast, calculated average distances are significantly closer to the experimental data. The differences amount to ca. 0.05 Å, which is very similar to the deviations observed for $(TlPb_9)^{3-}$, see above. Also the standard deviations σ_{c-s} (σ_{s-s}) are reasonably in line with the measured data. For the energetically favored isomers (relative energies up to 10 kJ mol^{-1}), which are shown in Figure 7, they amount to

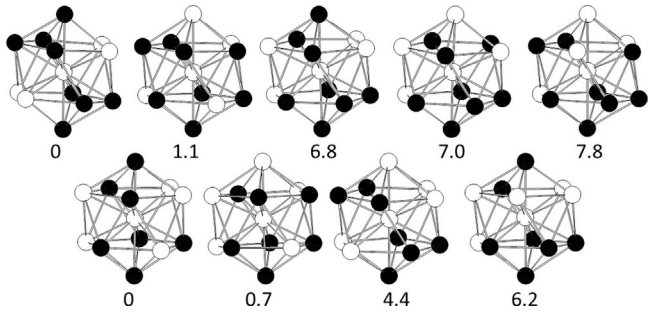

Figure 7. Most stable 51 VE (upper row) and 50 VE (lower row) isomers. Relative energies are given in kJ mol^{-1}.

0.04–0.08 (0.04–0.05) Å for the 50 VE systems, and to 0.03–0.07 (0.05–0.09) Å for the 51 VE systems. For both cases, the third-most-stable isomer almost exactly meets the experimental scattering (0.04 Å), and in both cases, it is disfavored over the respective minimum by only a very few kJ mol^{-1}.

Thus, from structure parameters, no preference for either the 50 or the 51 VE cluster is evident. The energetic preference may be estimated best by the energy of an exchange reaction [Eq. (1)], which very slightly favors the right-hand side, hence the 51 VE species, by 3.8 kJ mol^{-1} (calculated for the most favorable isomer of each composition). The 4–5 most stable isomers of the 50 and 51 VE clusters are depicted in Figure 7.

$$(Tl_6Pb_7)^{4-} + Pb \rightarrow (Tl_5Pb_8)^{4-} + Tl \quad (1)$$

In summary, although we cannot give a final answer of why the 51 VE cluster was selectively formed, we may state that the 51 VE species is at least as realistic as the 50 VE species. The reason for this is evident from the electronic structure of the 50 VE species, for which the LUMO (an s-type cluster orbital) is energetically close to the HOMO: the energy gap amounts to only 0.9 eV. This is very different from related systems like $[Pt@Pb_{12}]^{2-}$: there, the s-type cluster orbital is much higher in energy (3.3 eV above the HOMO), and also the LUMO is separated from the HOMO by 2.0 eV, which makes this anion a clear 50 VE case.

Extractions of "$K_xTl_yBi_z$" (III, IV, and V)

As recently reported, the extraction of "K_2TlBi_3" (**V**, comprising KBi_2 + KTlBi, see above) with en/crypt-222 is a very efficient way for the synthesis of $[K(crypt\text{-}222)]_2(TlBi_3)\cdot 0.5en$, while the extraction of "$K_5Tl_2Bi_4$" (**III**, comprising K_2TlBi + an unknown compound, see above) always yields a mixture of $[K(crypt\text{-}222)]_2(TlBi_3)$ and $[K(crypt\text{-}222)]_3(Tl_4Bi_5)$.[4f] As the yields in the synthesis of $[K(crypt\text{-}222)]_2(TlBi_3)$ from **V** are usually greater than 80%, both KBi_2 and KTlBi (**5**) must directly be involved in the formation of the anion. This is in line with the previous report on the formation of $(Sn_2Bi_2)^{2-}$ from KSn_2 and K_3Bi_2, and only the second example in which the formation of a binary anion from two different binary parent phases has been reliably observed.[5a]

Upon extraction of "K_2TlBi" (**IV**, comprising $K_6Tl_2Bi_3$ plus an unknown compound, see above) with en/crypt-222, we obtained $[K(crypt\text{-}222)]_3(Tl_4Bi_3)$ (**8**, approx. 50%) as large black blocks upon layering of the solution with toluene or THF, or simply upon storing a concentrated solution ($^1/_4$ volume) at 5 °C. Compound **8** crystallizes in the monoclinic space group $P2_1/n$, with the unit cell parameters $a = 21.2179(5)$ Å, $b = 33.375(1)$ Å, $c = 24.2254(6)$ Å, $\beta = 90.216(2)$, $V = 17155.2(8)$ Å^3, and $Z = 8$ (with 2 formula units in the asymmetric unit). The compound shows an intrinsic tendency to crystallize as *pseudo*-merohedral twin, with a fourfold superstructure along the *b* axis and severe disorder of the anions, which strongly affects the data set quality (see the Supporting Information). Therefore, we present a structural model only, which is corroborated by PXRD results and quantum chemical investigations. Furthermore, the composition of **8** was confirmed by μ-XRF, ESI-MS, and quantum chemical studies (see Supporting Information). The $(Tl_4Bi_3)^{3-}$ anion adopts a distorted pentagonal bipyramidal shape and accords with a 2n + 2 = 16 skeleton electron Wade–Mingos *closo* cluster (Figure 8). Only a few years ago, the corresponding parent borate cluster anion $(B_7H_7)^{2-}$ was structurally characterized.[39]

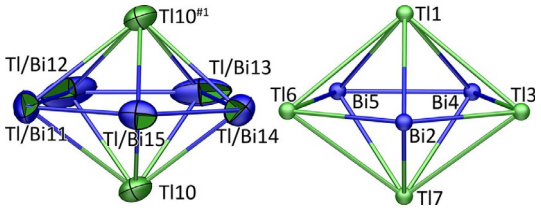

Figure 8. Left: Molecular structure of one of the disordered positions of the $(Tl_4Bi_3)^{3-}$ anion in **8** (for the whole model, see the Supporting Information); the picture indicates the consideration of the five atoms placed on the equatorial ring as mixed Tl/Bi sites; the apical atoms were treated as pure Tl atoms, in line with their clear preference on this site according to DFT calculations. Thermal displacement ellipsoids are drawn at 50% probability. Right: Optimized geometry of the lowest energy isomer (DFT; by 39 kJ mol^{-1} lower in energy than the second best one). The location of Tl atoms in the two apical positions is preferred by 39 (90) kJ mol^{-1} over the most stable isomer(s) with one (two) Bi atom(s) on the apex (apices). Selected bond lengths and interatomic distances [Å]: *SC-XRD*: Tl10/Tl10$^{\#1}$—Tl/Bi 3.07–3.55, ring Tl/Bi—Tl/Bi 2.99–3.14, Tl10···Tl10$^{\#1}$ 4.086(3). *DFT*: Tl1/7—Bi 3.23–3.26, Tl1/7—Tl 3.39, ring: Tl—Bi: 3.10, Bi4—Bi5 3.09, Tl1···Tl7 3.99. Symmetry operation #1: $-x$, $2-y$, $1-z$.

A very similar, yet not isoelectronic, structure was previously observed for the $(Tl_7)^{7-}$ unit within the solid phase $K_{10}Tl_7$.[40] With a skeletal electron number of 2n = 14, the quoted anion lacks two skeletal electrons and was therefore described as *pre-closo* cluster (additionally indicating the apparently high tolerance for different total electron counts in these heavy metal cluster anions). Therefore, the anion in **8** represents the first 7-atom *closo* cluster within the Zintl anion family. The most striking consequence of the two additional electrons for the structure is a significant elongation of the apical···apical interatomic distance from 3.4622(9) Å in $(Tl_7)^{7-}$ (in $K_{10}Tl_7$) to 4.10 Å on average in $(Tl_4Bi_3)^{3-}$ (4.08 and 4.11 Å in the two symmetry-independent anions in **8**).

Regarding discrete molecular compounds based on pentagonal bipyramidal main group metal clusters, only three examples have been published so far, $[Li(thf)_4](Ga_7R_4(GaR)_2)$, $Sn_5(SnR')_2$, and $[Sn_7\{GaCl(ddp)\}_2]$ [R = $Si(SiMe_3)_3$, R′ = terphenyl, dpp = $HC(CMeNC_6H_3\text{-}2,6\text{-}iPr_2)_2$].[41] However, each of these clusters carries at least two ligands (one per apical atom). Despite their different compositions and the nature of the ligands, all of the quoted molecules represent *closo* clusters with very similar apical···apical values of 3.295(2)–3.370(1) Å.

Due to the binary nature of the $(Tl_4Bi_3)^{3-}$ anion, five different isomers can be formed in theory. Their geometric and electronic structures were investigated by means of DFT methods to identify the energetically most favorable one (for details, see the Supporting Information). The experimentally determined structure and the lowest-energy isomer are depicted in Figure 8. As the SCXRD data do not allow for an identification of the atomic positions in the equatorial ring due to rotational disorder, only average values are given and discussed here. The best isomer is favored over the second best one by 39 kJ mol^{-1}, and this is the only one that reproduces the observed (non-bonding) apical···apical interatomic distance best, with 3.99 Å. Also the other two structural parameters are reproduced well: the distance within the equatorial ring (SCXRD: 2.98–3.14 Å, 3.04 Å on average; DFT 3.09–3.10 Å, 3.09 Å on average) and the distance within the hemispheres (SCXRD: 3.07–3.60 Å, 3.30 Å on average; DFT: 3.23–3.40 Å, 3.30 Å on average).

Future experiments will serve to investigate the reactivity of this new anion as Tl/Bi source for the synthesis of intermetalloid clusters.

Conclusions

The close inspection of a set of nominally ternary A/Tl/Pb (A = Na, K) and K/Tl/Bi solids and their subsequent extraction has shown the striking difference between the stoichiometric reaction mixture and the identity of the actually formed solids on one hand, and their difference to the nature and structure of the soluble anions obtained from such phases on the other hand. We therefore wish to emphasize that it is crucial to analyze the whole reaction space as completely as possible prior to discussing and understanding any cluster formation reactions. This is a very basic principle in chemistry but has remained fragmentary or even undone so far in the field of Zintl chemistry.

In summary, we have reported on the synthesis of several solid mixtures of the elemental combinations A/Tl/Pb (A = Na, K) and K/Tl/Bi, which turned out to be mixtures of various defined binary and ternary intermetallic compounds. By extraction in en/crypt-222, we prepared the soluble salts of binary Zintl anions, among them an electron-rich Tl-centered icosahedral cluster anion, $[Tl@Tl_4Pb_8]^{4-}$, and the first 7-atom *closo*-type Zintl anion, $(Tl_4Bi_3)^{3-}$. Future investigations will focus on an even closer inspection of the respective phase diagrams and an expansion onto further element combinations, as well as on the reactivity of the novel binary $(Tl_4Bi_3)^{3-}$ anion.

Experimental Section

Details for all described reactions, characterization methods, and analyses are provided comprehensively in the Supporting Information. Further details of the crystal structure investigations of the binary and ternary solids (compounds **2**, **3**, **4**, and **5**) may be obtained from FIZ Karlsruhe, 76344 Eggenstein-Leopoldshafen, Germany (fax: (+49)7247-808-666; e-mail: crysdata@fiz-karlsruhe.de, on quoting the deposition number numbers CSD-434528, −434529, −434520, and −434531. CCDC 1841189 (**1**), 1841188, (**6**), 1841187 (**7**), and 1841190 (**8**) contain the supplementary crystallographic data for this paper. These data can be obtained free of charge from The Cambridge Crystallographic Data Centre.

Acknowledgements

This work was supported by Deutsche Forschungsgemeinschaft (DFG). N.L. acknowledges a Ph.D. fellowship by Marburg University Research Academy (MARA). Y.J.F. acknowledges support by Fonds der Chemischen Industrie (Kekulé scholarship). The authors thank Jakob Hauns for exploratory calculations.

Conflict of interest

The authors declare no conflict of interest.

Keywords: binary Zintl anions · bismuth · intermetallic compounds · lead · thallium

[1] a) M. J. Moses, J. C. Fettinger, B. W. Eichhorn, *Science* **2003**, *300*, 778–780; b) E. N. Esenturk, J. Fettinger, Y. F. Lam, B. Eichhorn, *Angew. Chem. Int. Ed.* **2004**, *43*, 2132–2134; *Angew. Chem.* **2004**, *116*, 2184–2186; c) E. N. Esenturk, J. Fettinger, B. Eichhorn, *J. Am. Chem. Soc.* **2006**, *128*, 9178–9186; d) B. Zhou, M. S. Denning, D. L. Kays, J. M. Goicoechea, *J. Am. Chem. Soc.* **2009**, *131*, 2802–2803; e) J. Q. Wang, S. Stegmaier, T. F. Fässler, *Angew. Chem. Int. Ed.* **2009**, *48*, 1998–2002; *Angew. Chem.* **2009**, *121*, 2032–2036; f) G. Espinoza-Quintero, J. C. Duckworth, W. K. Myers, J. E. McGrady, J. M. Goicoechea, *J. Am. Chem. Soc.* **2014**, *136*, 1210–1213; g) O. Kysliak, C. Schrenk, A. Schnepf, *Angew. Chem. Int. Ed.* **2016**, *55*, 3216–3219; *Angew. Chem.* **2016**, *128*, 3270–3274; h) F.-X. Pan, L.-J. Li, Y.-J. Wang, J.-C. Guo, H.-J. Zhai, L. Xu, Z.-M. Sun, *J. Am. Chem. Soc.* **2015**, *137*, 10954–10957; i) L. G. Perla, S. C. Sevov, *J. Am. Chem. Soc.* **2016**, *138*, 9795–9798; j) Y. Wang, M. Moses-DeBusk, L. Stevens, J. Hu, P. Zavalij, K. Bowen, B. I. Dunlap, E. R. Glaser, B. Eichhorn, *J. Am. Chem. Soc.* **2017**, *139*, 619–622.

[2] a) S. C. Sevov, J. M. Goicoechea, *Organometallics* **2006**, *25*, 5678 – 5692; b) S. Scharfe, F. Kraus, S. Stegmaier, A. Schier, T. F. Fässler, *Angew. Chem. Int. Ed.* **2011**, *50*, 3630 – 3670; *Angew. Chem.* **2011**, *123*, 3712 – 3754; c) R. S. P. Turbervill, J. M. Goicoechea, *Chem. Rev.* **2014**, *114*, 10807 – 10828.

[3] a) N. Korber, *Angew. Chem. Int. Ed.* **2009**, *48*, 3216 – 3217; *Angew. Chem.* **2009**, *121*, 3262 – 3264; b) A. W. Castleman, Jr., S. N. Khanna, *J. Phys. Chem. C* **2009**, *113*, 2664 – 2675; c) A. W. Castleman, Jr., *J. Phys. Chem. Lett.* **2011**, *2*, 1062 – 1069; d) P. Jena, *J. Phys. Chem. Lett.* **2013**, *4*, 1432 – 1442; e) E. S. Smirnova, A. M. Echavarren, *Angew. Chem. Int. Ed.* **2013**, *52*, 9023 – 9026; *Angew. Chem.* **2013**, *125*, 9193 – 9196; f) Z. Luo, A. W. Castleman, Jr., *Acc. Chem. Res.* **2014**, *47*, 2931 – 2940; g) S. S. Wang, G. Y. Yang, *Chem. Rev.* **2015**, *115*, 4893 – 4962; h) Z. Luo, A. W. Castleman, Jr., S. N. Khanna, *Chem. Rev.* **2016**, *116*, 14456 – 14492.

[4] a) F. Lips, S. Dehnen, *Angew. Chem. Int. Ed.* **2009**, *48*, 6435 – 6438; *Angew. Chem.* **2009**, *121*, 6557 – 6560; b) B. Weinert, A. R. Eulenstein, R. Ababei, S. Dehnen, *Angew. Chem. Int. Ed.* **2014**, *53*, 4704 – 4708; *Angew. Chem.* **2014**, *126*, 4792 – 4797; c) R. J. Wilson, L. Broeckaert, F. Spitzer, F. Weigend, S. Dehnen, *Angew. Chem. Int. Ed.* **2016**, *55*, 11775 – 11780; *Angew. Chem.* **2016**, *128*, 11950 – 11955; d) S. Mitzinger, L. Broeckaert, W. Massa, F. Weigend, S. Dehnen, *Nat. Commun.* **2016**, *7*, 10480; e) N. Lichtenberger, R. J. Wilson, A. R. Eulenstein, W. Massa, R. Clérac, F. Weigend, S. Dehnen, *J. Am. Chem. Soc.* **2016**, *138*, 9033 – 9036; f) N. Lichtenberger, N. Spang, A. Eichhöfer, S. Dehnen, *Angew. Chem. Int. Ed.* **2017**, *56*, 13253 – 13258; *Angew. Chem.* **2017**, *129*, 13436 – 13442.

[5] a) S. C. Critchlow, J. D. Corbett, *Inorg. Chem.* **1982**, *21*, 3286 – 3290; b) S. C. Critchlow, J. D. Corbett, *Inorg. Chem.* **1985**, *24*, 979 – 981.

[6] S. Ponou, N. Müller, T. F. Fässler, U. Häussermann, *Inorg. Chem.* **2005**, *44*, 7423 – 7430.

[7] F. Lips, I. Schellenberg, R. Pöttgen, S. Dehnen, *Chem. Eur. J.* **2009**, *15*, 12968 – 12973.

[8] J. D. Corbett, *Angew. Chem. Int. Ed.* **2000**, *39*, 670 – 690; *Angew. Chem.* **2000**, *112*, 682 – 704.

[9] a) R. W. Rudolph, W. L. Wilson, R. C. Taylor, *J. Am. Chem. Soc.* **1981**, *103*, 2480 – 2481; b) R. C. Burns, J. D. Corbett, *J. Am. Chem. Soc.* **1982**, *104*, 2804 – 2810; c) W. L. Wilson, R. W. Rudolph, L. L. Lohr, R. C. Taylor, P. Pyykkö, *Inorg. Chem.* **1986**, *25*, 1535 – 1541; d) D. Rios, M. M. Gillett-Kunnath, J. D. Taylor, A. G. Oliver, S. C. Sevov, *Inorg. Chem.* **2011**, *50*, 2373 – 2377.

[10] a) L. Xu, S. C. Sevov, *Inorg. Chem.* **2000**, *39*, 5383 – 5389; b) B. Weinert, F. Weigend, S. Dehnen, *Chem. Eur. J.* **2012**, *18*, 13589 – 13595; c) B. Weinert, F. Müller, K. Harms, R. Clérac, S. Dehnen, *Angew. Chem. Int. Ed.* **2014**, *53*, 11979 – 11983; *Angew. Chem.* **2014**, *126*, 12173 – 12177.

[11] R. Ababei, J. Heine, M. Holynska, G. Thiele, B. Weinert, X. Xie, F. Weigend, S. Dehnen, *Chem. Commun.* **2012**, *48*, 11295 – 11297.

[12] a) W. Blase, G. Cordier, *Z. Kristallogr.* **1990**, *193*, 319 – 320; b) W. Blase, G. Cordier, *Z. Kristallogr.* **1991**, *196*, 207 – 211.

[13] a) R. E. Marsh, D. P. Shoemaker, *Acta Crystallogr.* **1953**, *6*, 197 – 205; b) I. F. Hewaidy, E. Busmann, W. Klemm, *Z. Anorg. Allg. Chem.* **1964**, *328*, 283 – 293.

[14] J. B. Friauf, *J. Am. Chem. Soc.* **1927**, *49*, 3107 – 3114.

[15] a) P. Schobinger-Papamantellos, P. Fischer, *Naturwissenschaften* **1970**, *57*, 128 – 129; b) J. A. Oberteuffer, J. A. Ibers, *Acta Crystallogr. Sect. B* **1970**, *26*, 1499 – 1504.

[16] a) S. Bobev, S. C. Sevov, *Inorg. Chem.* **2001**, *40*, 5361 – 5364; b) I. Todorov, S. C. Sevov, *Inorg. Chem.* **2006**, *45*, 4478 – 4483.

[17] a) S. Bobev, S. C. Sevov, *Inorg. Chem.* **1999**, *38*, 2672 – 2675; b) S. Bobev, S. C. Sevov, *J. Solid State Chem.* **2002**, *163*, 436 – 448.

[18] M. Asbrand, B. Eisenmann, *Z. Kristallogr.* **1992**, *198*, 283 – 284.

[19] L. Chi, J. D. Corbett, *Inorg. Chem.* **2001**, *40*, 2705 – 2708.

[20] W. Klemm, E. Busmann, *Z. Anorg. Allg. Chem.* **1963**, *319*, 297 – 311.

[21] D. Gilde, *Z. Anorg. Allg. Chem.* **1956**, *284*, 142 – 143.

[22] P. A. Edwards, J. D. Corbett, *Inorg. Chem.* **1977**, *16*, 903 – 907.

[23] a) K. Wade, *Inorg. Nucl. Chem. Lett.* **1972**, *8*, 559 – 562; b) D. M. P. Mingos, *Nat. Phys. Sci.* **1972**, *236*, 99 – 102; c) K. Wade in *Adv. Inorg. Chem. Radiochem., Vol. 18* (Eds.: H. J. Emeléus, A. G. Sharpe), Academic Press, **1976**, pp. 1 – 66; d) D. M. P. Mingos, T. Slee, Z. Y. Lin, *Chem. Rev.* **1990**, *90*, 383 – 402.

[24] R. Ababei, W. Massa, K. Harms, X. Xie, F. Weigend, S. Dehnen, *Angew. Chem. Int. Ed.* **2013**, *52*, 13544 – 13548; *Angew. Chem.* **2013**, *125*, 13786 – 13790.

[25] Z. C. Dong, J. D. Corbett, *J. Am. Chem. Soc.* **1995**, *117*, 6447 – 6455.

[26] J. Q. Wang, S. Stegmaier, B. Wahl, T. F. Fässler, *Chem. Eur. J.* **2010**, *16*, 1793 – 1798.

[27] a) M. Brynda, R. Herber, P. B. Hitchcock, M. F. Lappert, I. Nowik, P. P. Power, A. V. Protchenko, A. Ruzicka, J. Steiner, *Angew. Chem. Int. Ed.* **2006**, *45*, 4333 – 4337; *Angew. Chem.* **2006**, *118*, 4439 – 4443; b) H. Schnöckel, *Dalton Trans.* **2008**, 4344 – 4362.

[28] S. Stegmaier, T. F. Fässler, *J. Am. Chem. Soc.* **2011**, *133*, 19758 – 19768.

[29] D. M. Carey, C. Morales-Verdejo, A. Muñoz-Castro, *Chem. Phys. Lett.* **2015**, *638*, 99 – 102.

[30] TURBOMOLE V7.3 2018, a development of University of Karlsruhe and Forschungszentrum Karlsruhe GmbH, 1989–2007, TURBOMOLE GmbH, since 2007; available from http://www.turbomole.com.

[31] W. Kutzelnigg, W. Liu, *J. Chem. Phys.* **2005**, *123*, 241102.

[32] J. M. Tao, J. P. Perdew, V. N. Staroverov, G. E. Scuseria, *Phys. Rev. Lett.* **2003**, *91*, 146401.

[33] P. Pollak, F. Weigend, *J. Chem. Theory Comput.* **2017**, *13*, 3696 – 3705.

[34] D. Peng, M. Reiher, *J. Chem. Phys.* **2012**, *136*, 244108.

[35] D. Peng, N. Middendorf, F. Weigend, M. Reiher, *J. Chem. Phys.* **2013**, *138*, 184105.

[36] Y. J. Franzke, N. Middendorf, F. Weigend, *J. Chem. Phys.* **2018**, *148*, 104110.

[37] L. Visscher, K. G. Dyall, *At. Data Nucl. Data Tables* **1997**, *67*, 207 – 224.

[38] A. Klamt, G. Schüürmann, *J. Chem. Soc. Perkin Trans. 2* **1993**, 799 – 805.

[39] F. Schlüter, E. Bernhardt, *Inorg. Chem.* **2011**, *50*, 2580 – 2589.

[40] S. Kaskel, J. D. Corbett, *Inorg. Chem.* **2000**, *39*, 778 – 782.

[41] a) W. Köstler, G. Linti, *Angew. Chem. Int. Ed. Engl.* **1997**, *36*, 2644 – 2646; *Angew. Chem.* **1997**, *109*, 2758 – 2760; b) E. Rivard, J. Steiner, J. C. Fettinger, J. R. Giuliani, M. P. Augustine, P. P. Power, *Chem. Commun.* **2007**, 4919 – 4921; c) G. Prabusankar, A. Kempter, C. Gemel, M.-K. Schröter, R. A. Fischer, *Angew. Chem. Int. Ed.* **2008**, *47*, 7234 – 7237; *Angew. Chem.* **2008**, *120*, 7344 – 7347.

Manuscript received: May 12, 2018
Revised manuscript received: June 26, 2018
Accepted manuscript online: June 28, 2018
Version of record online: July 23, 2018

3.4 Polybismuthide Anions as Ligands: The Homoleptic Complex $[(Bi_7)Cd(Bi_7)]^{4-}$ and the Ternary Cluster $[(Bi_6)Zn_3(TlBi_5)]^{4-}$

Zitat: N. Lichtenberger, W. Massa, S. Dehnen, *Angew. Chem. Int. Ed.* **2019**, DOI 10.1002/anie.201812473.

Abstract

We present the results from a reactivity study of the binary anion $(TlBi_3)^{2-}$ towards Group 12 metal compounds MPh_2 (M = Zn, Cd, Hg) in order to get access to coordination compounds of polycyclic polypnictide molecules like Bi_7^{3-} or Bi_{11}^{3-}. The coordination chemistry of these polybismuthide cages has been unprecedented to date, while it has been known for a long time for the lighter Group 15 anions Pn_7^{3-} (Pn = P, As, Sb). The use of $(TlBi_3)^{2-}$, previously shown to release Tl under certain conditions in-situ, resulted in the formation of the first heterometallic polyanion in which a nortricyclane-type polybismuthide coordinates a transition metal atom, $[(Bi_7)Cd(Bi_7)]^{4-}$. Reactions with the lighter group 12 metal precursor yielded the uncommon ternary cluster $[(Bi_6)Zn_3(TlBi_5)]^{4-}$, most likely representing a reaction intermediate, and at the same time hinting at the formation of the nortricyclane-shaped cage. Quantum chemical studies provide a deeper insight into stability trends of the $[(E_7)M(E_7)]^{4-}$ anion family and reveal a complex bonding situation in $[(Bi_6)Zn_3(TlBi_5)]^{4-}$, which features both localized and multicenter bonding.

Zusammenfassung

Die Veröffentlichung berichtet über eine Reaktivitätsstudie des binären *Zintl*-Anions $(TlBi_3)^{2-}$ gegenüber den Gruppe 12-Organometallverbindungen MPh_2 (M = Zn, Cd, Hg). Für die leichteren Homologen des Elementes Bismut sind die Polyanionen Pn_7^{3-} leicht aus entsprechenden A_3Pn_7-Verbindungen zugänglich und die Reaktivität dieser Käfige ist gut untersucht. Eine entsprechende Ausgangsverbindung ist bisher nicht für Bismut bekannt, so dass das entsprechende Bi_7^{3-}-Anion erst vor einigen Jahren auf einem Umweg durch Oxidation von Bi_4^{2-} mit einem Übergangsmetallkomplex synthetisiert wurde.[26b] Dieser Umweg erschwert Studien der Reaktivität dieses Anions, weshalb bisher nicht geklärt werden konnte, ob

der Käfig zu instabil für Folgechemie ist oder ob lediglich aufgrund mangelnder Synthesewege für das Edukt keine entsprechenden Untersuchungen durchgeführt wurden.

In früheren Studien hat sich gezeigt, dass das Anion $(TlBi_3)^{2-}$ unter geeigneten Bedingungen in Lösung als Quelle für Bi-Polyanionen fungieren kann.[21] Um zu testen, ob ein Zugang zu Verbindungen des Bi_7^{3-} auf diesem Weg möglich ist, wurden Umsetzungen mit den Gruppe 12-Diphenylverbindungen durchgeführt, welche häufig zur Synthese der entsprechenden $[(Pn_7)M(Pn_7)]^{4-}$-Cluster eingesetzt werden. Die Umsetzung von $(TlBi_3)^{2-}$ mit $CdPh_2$ führte zur Bildung des $[(Bi_7)Cd(Bi_7)]^{4-}$, der ersten Koordinationsverbindung eines Bismut-Polyanions. Als weiteres Reaktionsprodukt wurde $[K(Krypt{-}222)]_3(Tl_4Bi_5)$ erhalten, welches immer neben dem $[K(Krypt{-}222)]_4[(Bi_7)Cd(Bi_7)]$ kristallisiert. Eine Strukturaufklärung mittels Einkristall-Röntgenstrukturanalyse belegte, dass das Clusteranion isostrukturell zu den bereits bekannten Verbindungen dieser Art ist. Mittels quantenchemischer Studien wurde die relative Stabilität aller $[(Pn_7)M(Pn_7)]^{4-}$-Käfige (M = Zn - Hg, HgHg; Pn = P - Bi) untersucht. Hierzu wurden Austauschreaktionen der Käfige bzw. der Übergangsmetallatome betrachtet.

Die Umsetzung von $(TlBi_3)^{2-}$ mit $HgPh_2$ führte ausschließlich zur Bildung von $[K(Krypt{-}222)]_3(Tl_4Bi_5)$, welches ebefalls das Hauptprodukt der Reaktion mit $ZnPh_2$ war. Aus dieser Reaktionslösung konnte allerdings zusätzlich ein Reaktionsintermediat kristallisiert werden. Die asymmetrische Einheit der Verbindung $[K(Krypt{-}222)]_7[(Bi_6)Zn_3(TlBi_5)](Tl_4Bi_5)_{0.93}(Bi_7)_{0.07}$ enthält zwei separate Hälften des $(Tl_4Bi_5)^{3-}$-Anions, von denen eines eine Fehlordnung mit einem Bi_7^{3-}-Anion zeigt, sowie das ternäre Clusteranion $[(Bi_6)Zn_3(TlBi_5)]^{4-}$. Aufgrund einer schlechten Kristallqualität konnte nur ein Strukturmodell aufgestellt werden, welches durch quantenchemische Studien gestützt wird. Insbesondere die Zusammensetzung des Clusteranions lies sich nur auf diese Weise ermitteln, da die Kristallgröße und das Vorhandensein mehrerer Anionen in der asymmetrischen Einheit eine eindeutige Aussage über deren Natur nicht ermöglichten. Das Anion besteht aus einem Bi_6-Fragment, welches sich vom Bi_7-Nortricyclankäfig durch Entfernung des apikalen Atoms ableitet, drei Zinkatomen und einem $(TlBi_5)$-Fragment, in dem ein Bi_5-Ring in einer Briefumschlagskonformation vorliegt und an dessen „Lasche“ ein exponiertes Tl-Atom gebunden ist. Zunächst wurde die Zusammensetzung des Anions sowie die Atompositionen mittels quantenchemischer Studien bestätigt, bevor im Anschluss daran die Bindungsverhältnisse analysiert wurden. Hierbei zeigte sich, dass in diesem Anion eine Kombination von lokalisierten 2e-

2c-Bindungen und 2e-3c-Mehrzentrenbindungen vorliegt. Die Strukturen der vorgestellten Clusteranionen sind in Abbildung 3.5 dargestellt.

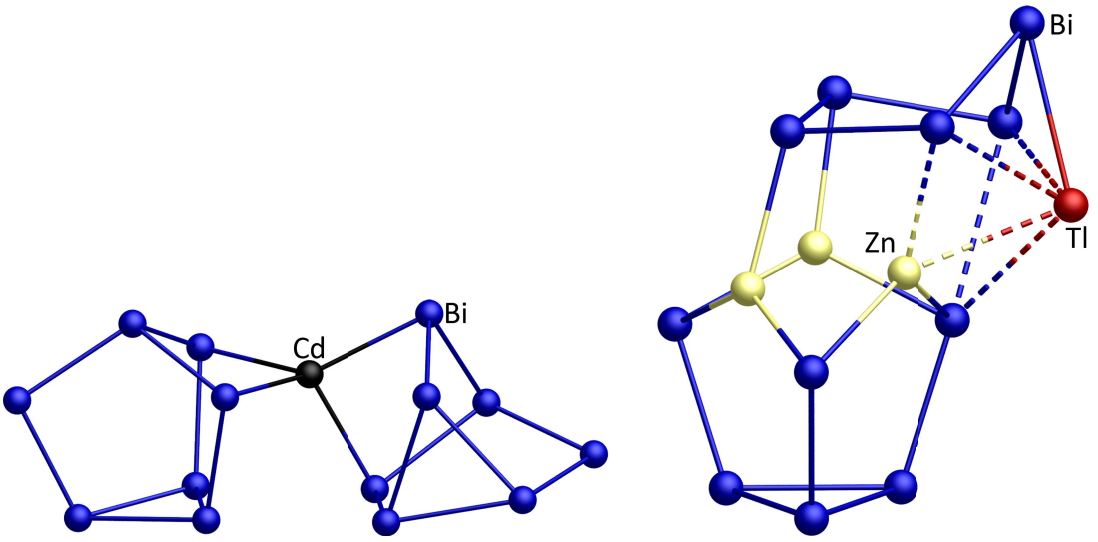

(a) $[(Bi_7)Cd(Bi_7)]^{4-}$ **(b)** $[(Bi_6)Zn_3(TlBi_5)]^{4-}$

Abbildung 3.5: Strukturen der ersten Koordinationsverbindung mit Bi_7^{3-}-Liganden und des Reaktionsintermediats der Umsetzung von $(TlBi_3)^{2-}$ mit $ZnPh_2$.

Eigenanteil

Alle Experimente, über die in der Veröffentlichung berichtet werden, wurden von mir geplant und zunächst von den Vertiefungsstudenten *Sebastian Ullrich* und *Nils Spang* unter meiner Anleitung durchgeführt. Alle Reproduktionen zu Charakterisierungszwecken wurden von mir persönlich durchgeführt, ebenso wie die Einkristallstrukturanalysen und ein Großteil der quantenchemischen Untersuchungen. Prof. Dr. *Werner Massa* übernahm die finale Verfeinerung der Kristallstruktur von $[K(Krypt{-}222)]_7[(Bi_6)Zn_3(TlBi_5)](Tl_4Bi_5)_{0.93}(Bi_7)_{0.07}$. Die ersten quantenchemischen Untersuchungen am Anion zur Bestimmung der Zusammensetzung sowie der Atompositionen wurden in einer Bachelorarbeit durch *Christian Schmidt* unter Anleitung von PD. Dr. *Florian Weigend* am KIT in einer Kooperation durchgeführt. Alle massenspektrometrischen Daten wurden an von mir präparierten Proben in meinem Beisein durch *Jan Bamberger* aufgenommen. Zur Aufnahme der μ-RFA-Spektren habe ich mit *Carsten Donsbach* und *Bertram Peters* zusammengearbeitet.

A Journal of the Gesellschaft Deutscher Chemiker

Angewandte International Edition

GDCh

Chemie

www.angewandte.org

Accepted Article

Title: Polybismuthide Anions as Ligands: The Homoleptic Complex [(Bi7)Cd(Bi7)]4− and the Ternary Cluster [(Bi6)Zn3(TlBi5)]4−

Authors: Stefanie Dehnen, Niels Lichtenberger, and Werner Massa

To be cited as: *Angew. Chem. Int. Ed.* 10.1002/anie.201812473
Angew. Chem. 10.1002/ange.201812473

Link to VoR: http://dx.doi.org/10.1002/anie.201812473
http://dx.doi.org/10.1002/ange.201812473

WILEY-VCH

10.1002/anie.201812473

WILEY-VCH

COMMUNICATION

Polybismuthide Anions as Ligands: The Homoleptic Complex $[(Bi_7)Cd(Bi_7)]^{4-}$ and the Ternary Cluster $[(Bi_6)Zn_3(TlBi_5)]^{4-}$

Niels Lichtenberger, Werner Massa, Stefanie Dehnen*

Abstract: We present the results from a reactivity study of the binary anion $(TlBi_3)^{2-}$ towards Group 12 metal compounds MPh_2 (M = Zn, Cd, Hg) in order to get access to coordination compounds of polycyclic polypnictide molecules like Bi_7^{3-} or Bi_{11}^{3-}. The coordination chemistry of these polybismuthide cages has been unprecedented to date, while it has been known for a long time for the lighter Group 15 anions Pn_7^{3-} (Pn = P, As, Sb). The use of $(TlBi_3)^{2-}$, previously shown to release Tl under certain conditions in-situ, resulted in the formation of the first heterometallic polyanion in which a nortricyclane-type polybismuthide coordinates a transition metal atom, $[(Bi_7)Cd(Bi_7)]^{4-}$. Reactions with the lighter group 12 metal precursor yielded the uncommon ternary cluster $[(Bi_6)Zn_3(TlBi_5)]^{4-}$, most likely representing a reaction intermediate, and at the same time hinting at the formation of the nortricyclane-shaped cage. Quantum chemical studies provide a deeper insight into stability trends of the $[(E_7)M(E_7)]^{4-}$ anion family and reveal a complex bonding situation in $[(Bi_6)Zn_3(TlBi_5)]^{4-}$, which features both localized and multi-center bonding.

Polypnictides belong to the most prominent representatives of the Zintl anion family and have found their way into many inorganic and general chemistry textbooks.[1] The nortricyclane-like anions E_7^{3-} (E = P, As, Sb) are particularly well known, and have been studied extensively since their discovery and first isolation.[2] They show a wide variety of reactivity patterns and open up interesting follow-up chemistry, for example through carbonylation of P_7^{3-} with CO to form PCO^- or by formation of novel types of ligands for transition metals.[3] Especially P_7^{3-} is a commonly used reagent as it is readily available and its reactions can easily be monitored by means of NMR studies.[4] Polyarsenides have also been applied in transition metal chemistry as a surprisingly versatile class of ligands. This class of compounds can be prepared either from (functionalized) (poly)arsenides or, as recently demonstrated, upon use of an As_4 source and subsequent *in-situ* formation.[5-8] However, it was only recently that the first two polycyclic polyanions of bismuth, Bi_7^{3-} and Bi_{11}^{3-}, long believed to be non-existent or non-isolable, were finally synthesized and characterized as their $[K(crypt\text{-}222)]^+$ salts.[9] Besides these two homoatomic polybismuthides, one binary $(Ge_4Bi_{14})^{4-}$ anion has been reported in which two Bi_7 fragments are present that are bonded to a Ge_4 chain.[10] Despite these proven syntheses, the availability of the polycyclic polybismuthides for subsequent chemistry is limited due to the synthetic procedure involving the oxidation of a smaller bismuth polyanion with a transition metal complex and due to poor yields. In contrast to all other Pn_7^{3-} cages, none of the reported synthetic procedures allows the polybismuthide anions' direct extraction from a binary solid.[2b] This leaves the question unanswered whether they might show a similar reactivity as their lighter congeners in terms of coordination chemistry.

We recently studied reactions of the binary Zintl anion $(TlBi_3)^{2-}$ towards transition metal compounds, in particular [Ru(cod)(Me-allyl)$_2$], and observed the formation of the cluster anion $[Bi_9\{Ru(cod)\}_2]^{3-}$ upon release of Tl.[11] This cluster anion can be viewed as being comprised of a non-classical Bi_9^{7-} polybismuthide unit and two stabilizing $\{Ru(cod)\}^{2+}$ fragments.

We were eager to investigate whether the $(TlBi_3)^{2-}$ anion may also serve as a source for polybismuthides in reactions with other transition metal complexes, and whether we could get hold of typical polypnictide-shaped anionic ligands this way. Our idea was to stabilize eventually forming polybismuthides through provision of a suitable metal complex (fragment). The most commonly used metals to coordinate E_7^{3-} anions are group 12 metals, typically introduced as MPh_2 (M = Zn, Cd, Hg). A whole variety of homoleptic complexes of the type $[(Pn_7)M(Pn_7)]^{4-}$ was previously prepared this way with polyphosphides, polyarsenides and polyantimonides, respectively (Pn = P, M = Zn, Cd[4]; Pn = As, M = Zn[12], Cd[12b], HgHg[12b], Pn = Sb, M = Zn[2e]). One alternative approach for the introduction of a group 12 metal atom into a polyanionic cage was realized through the extraction of a ternary intermetallic compound "K_6ZnSb_5" which resulted in the formation of $[(Sb_6Zn)_2]^{4-}$.[13] In this compound the Zn atoms become part of the nortricyclane cages instead of being coordinated by them.

We therefore explored the potential of $(TlBi_3)^{2-}$ for the *in-situ* formation of a corresponding $[(Bi_7)M(Bi_7)]^{4-}$ anion. This was successful upon reaction of $[K(crypt\text{-}222)](TlBi_3)\cdot 0.5en$ (**A**) with $CdPh_2$ in *en* and subsequent layering of the reaction solution with THF. After several days, black needle-shaped crystals of the first coordination compound of a nortricyclane-type polybismuthide anion, $[K(crypt\text{-}222)]_4[(Bi_7)Cd(Bi_7)]\cdot en$ (**1**)[14] grew besides black block-shaped crystals of $[K(crypt\text{-}222)]_3(Tl_4Bi_5)\cdot 2en$ (**B**).[11] **1** crystallizes in the triclinic space group $P\bar{1}$ with unit cell parameters a = 14.1287(3), b = 18.1174(4), c = 23.9198(4), α = 86.423(2), β = 88.658(2), γ = 79.936(2), V = 6016.4(2) and Z = 2. The complex anion is shown in Figure 1.

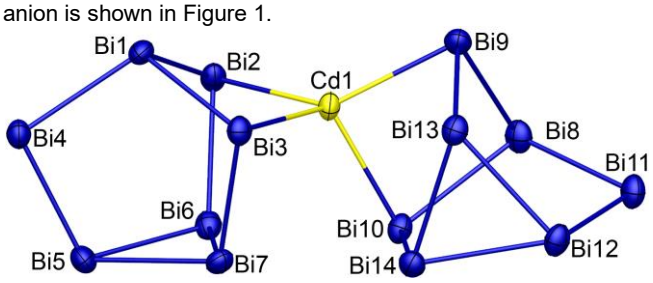

Figure 1. Molecular structure of the cluster anion $[(Bi_7)Cd(Bi_7)]^{4-}$ in **1**. Thermal displacement ellipsoids are drawn at 50% probability. Selected structural parameters [Å/°]: Bi–Bi(triangular): 3.029(1) – 3.0723(9); Bi1,8–Bi: 2.954(1) – 3.009(1); Bi_{triang}–Bi: 2.923(1) – 2.9497(9); Bi–Cd–Bi: 91.35(4), 92.44(4). The two polyanionic cages are rotated against each other by 79.43(2)° regarding the planes including Bi2–Cd1–Bi3 and Bi9–Cd1–Bi10, respectively.

[*] N. Lichtenberger, Prof. Dr. W. Massa, Prof. Dr. S. Dehnen
Fachbereich Chemie und Wissenschaftliches Zentrum für Materialwissenschaften
Philipps-Universität Marburg
Hans-Meerwein-Straße 4, 35043 Marburg (Germany)
E-mail: dehnen@chemie.uni-marburg.de

Supporting information for this article is given via a link at the end of the document.

10.1002/anie.201812473

As for the homologous compounds with P_7^{3-}, As_7^{3-}, or Sb_7^{3-} ligands, the anion's structure can best be described as two Bi_7^{3-} nortricyclane cages coordinating a central Cd^{2+} ion through two of the former two-bonded Bi-atoms of each cage. The cages are rotated against each other by 79.43(2)° (Bi–Cd–Bi planes) so that a *pseudo*-tetrahedral coordination environment around the Cd^{2+} ion results, however with almost rectangular Bi–Cd–Bi angles (91,35(4)°, 92.44(4)°) owing to the restrictions by the cages' bite angle and the Cd–Bi bond lengths. The observed structural parameters agree well with the expectations upon extrapolation of the values of other clusters of this type. Hence, the metrics of the Bi_7^{3-} units in the complex anion deviate only slightly from those of the free polybismuthide anion, although the Bi–Bi bonds involving the coordinating Bi atoms are slightly elongated (for full structural parameters see SI, Table S2).[9a]

To learn more about this type of unusual homoleptic complexes, and potentially see, why there is a relative shortage of Sb clusters, too, we investigated the stability of the whole series of $[(Pn_7)M(Pn_7)]^{4-}$ species by means of quantum chemical methods. For this, two exchange reactions [eqs. (1) and (2)] were taken into account for all possible elemental combinations of E, E' = P, As, Sb, Bi and M, M' = Zn, Cd, Hg, Hg_2. These two reactions allow for an insight into stability trends (Figure 2).

$$[(E_7)M(E_7)]^{4-} + 2\ (E'_7)^{3-} \rightarrow [(E_7')M(E_7')]^{4-} + 2\ (E_7)^{3-} \quad (1)$$

$$[(E_7)M(E_7)]^{4-} + M'^{2+} \rightarrow [(E_7)M'(E_7)]^{4-} + M^{2+} \quad (2)$$

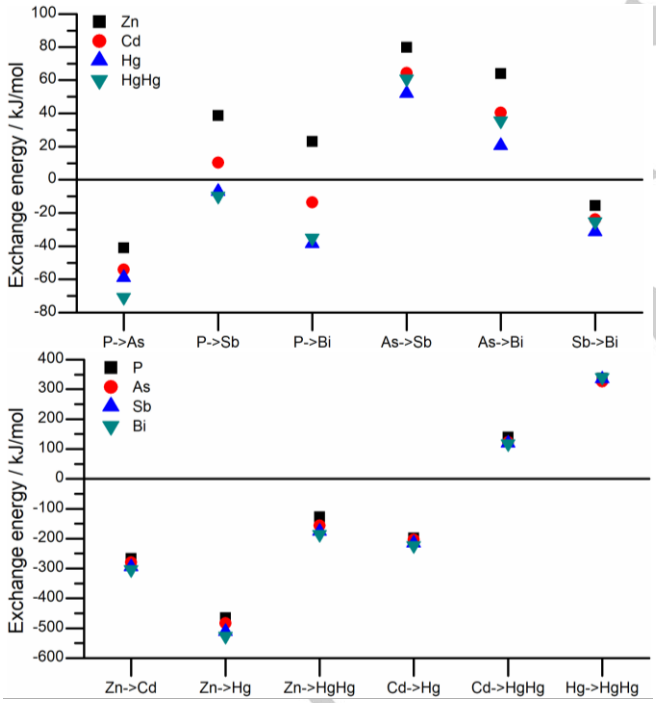

Figure 2. Reaction energies (given in kJ/mol) calculated for the reactions indicated in equations (1), top, and (2), bottom. E = P, As, Sb, Bi; M = Zn, Cd, Hg, and Hg_2. The involved atom types E and M are denoted by colored symbols and at the horizontal axes.

These two reactions allow for an insight into stability trends, which show a consistent picture (Figure 2). The exchange reaction energies calculated for the different sets of elements [equation (1)] may be in a very narrow range, <16 kJ/mol (replacement of Sb with Bi on $Zn^{2+}\cdots Hg_2^{2+}$), or may vary widely, >60 kJ/mol (replacement of P_7^{3-} with Bi_7^{3-} on $Zn^{2+}\cdots Hg_2^{2+}$). The exchange of metal ions [equation (2)] generally comes along with similar ranges of reaction energies along the series, being broadest (61 or 58 kJ/mol) for the replacement of Zn^{2+} with Hg^{2+} or Hg_2^{2+} between the given E_7^{3-} ligands.

As illustrated in Figure 2 (top), the complexes with As_7^{3-} are more stable than their P and Sb analogues, and the complexes with Bi_7^{3-} are more stable than the Sb congeners, which we ascribe to the inert pair effect of the Bi atoms. This increases the s character of the lone pair and correspondingly increases the p contribution to the Bi–Cd bond as compared to the Sb–Cd bond. This obviously serves to over-compensate the typical decrease in bond energy as going down group 15. The graphic further illustrates that only for a replacement of P_7^{3-} with Sb_7^{3-} or Bi_7^{3-}, the nature of the central metal cation would determine the sign of the respective exchange reaction energy. Here, the replacement of the ligand is endoenergetic for cations with small ionic radii (especially Zn^{2+}; yet, in the P→Sb scenario also for Cd^{2+}), while for Cd^{2+} (P→Bi scenario), Hg^{2+} or Hg_2^{2+}, the replacement of the P_7^{3-} cage with its heavier homologs would lead to a more stable complex. This indicates the good match of P_7^{3-} with harder ions, but also emphasizes the general possibility to form stable complexes of other elemental combinations.

The graphic shown in Figure 2 (bottom) addresses the exchange of cations in a complex of a given type of 7-atom cage ligands. Interestingly, although the insertion of an Hg^{2+} ion into a tetrahedral coordination environment would result in the most stable complexes throughout, this has not been observed experimentally so far. The only isolated mercury compound of this type until today, $[(As_7)Hg\text{-}Hg(As_7)]^{4-}$,[12b] featured a bridging Hg_2^{2+} unit instead, although this complex should be significantly less stable than a simple (yet unknown) Hg^{2+} complex according to the calculations. The results further suggest that a Zn^{2+} complex is disadvantaged with respect to all other central metal ions, including the Hg_2^{2+} unit. It is important to note that these results do not suggest that coordination complexes of the anions with Zn^{2+} would not form (which they actually do, see above[2e,4,12]), but only that an exchange of Zn^{2+} for softer metal cations would result in an energy gain. This is in line with predictions from the HSAB concept.[15]

We would like to note that the experimental non-existence of polycyclic polybismuthides has long been taken as a proof for the impossibility of isolating them, which was finally disproven upon discovery of suitable formation and crystallization conditions.[9] Hence, we assume that at least all of the complexes that are more stable than already known ones should be obtainable in theory.

In order to experimentally probe the formation of related compounds with Zn^{2+} and Hg^{2+}, we repeated the reaction affording **1** with $ZnPh_2$ and $HgPh_2$ instead of $CdPh_2$. The reaction of **A** with $HgPh_2$ only yielded black crystals of **B**. The latter was also obtained upon reactions with $ZnPh_2$, but here were also able to crystallize the salt of a species that contains an unprecedented intermetalloid cluster anion. A few tiny hexagonal plates of the triple salt $[K(crypt\text{-}222)]_7[(Bi_6)Zn_3(TlBi_5)][(Tl_4Bi_5)_{0.93}(Bi_7)_{0.07}$ (**2**)[14] crystallized besides large black blocks of **B**. Although the overall crystal quality was very poor, we managed to obtain enough SC-XRD data to determine the cluster structure and the number

10.1002/anie.201812473

of $[K(crypt\text{-}222)]^+$ counterions that informed about the anion's total charge. This helped to further study the cluster by means of quantum chemistry.

2 crystallizes in the monoclinic space group $P2_1/m$ with the unit cell parameters of a = 21.1602(6), b = 41.969(1), c = 23.4269(6), β = 93.737(2), and Z = 4. One $[(Bi_6)Zn_3(TlBi_5)]^{4-}$ anion and two halves of co-crystallizing $(Tl_4Bi_5)^{3-}$ anions, one of which is partially disordered with a Bi_7^{3-} cage, form the asymmetric unit along with (6 + 2×0.5) = 7 $[K(crypt\text{-}222)]^+$ cation complexes. These compensate the charge of the $[(Bi_6)Zn_3(TlBi_5)]^{4-}$ cluster anion and that of one $(Tl_4Bi_5)^{3-}/Bi_7^{3-}$ anion per formula unit. The molecular structure of the ternary anion is depicted in Figure 3. Its structure can be described as a truncated Bi_7 fragment, in which the capping atom was replaced by three Zn^{2+} atoms, each sitting between two Bi atoms to form a crown-shaped Bi_3Zn_3 substructure. The Zn^{2+} ions are further bonded to three Bi atoms of a $TlBi_5$ fragment. The five Bi atoms of the latter form a five-membered ring in an envelope conformation, while the Tl atom binds to the folded-up part of the ring and also to one of the Bi atoms of the Bi_6 unit below.

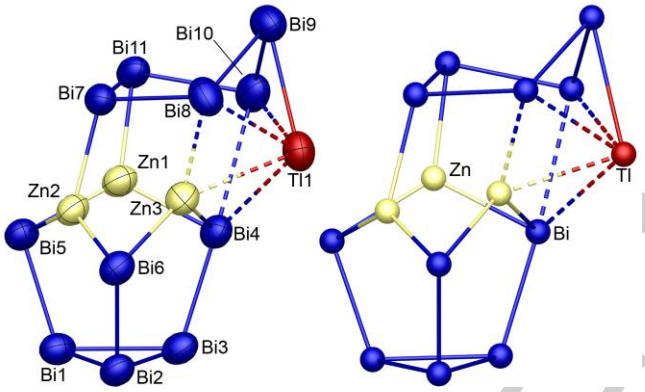

Figure 3. Molecular structure of the cluster anion $[(Bi_6)Zn_3(TlBi_5)]^{4-}$ in **2** (left), and as calculated with DFT methods (right). Selected interatomic distances (SC-XRD/*DFT*) [Å]: Bi–Bi: 2.955(2) – 3.056(2)/*2.97* – *3.08*; Tl1–Bi8,9,10: 3.199(2)/*3.28*, 3.236(2)/3.33, 3.139(2)/3.25*;* Tl1–Bi4: 3.410(2)/*3.39*; Zn1–2,2-3,1-3: 2.784(5)/2.73, 2.762(5)/2.70, 3.317(5)/*3.09*; Zn–Bi4-6: 2.666(4) – 2.798(4)/*2.68* – *2.83*; Zn–Bi7,8,11: 2.717(4) – 3.272(4)/*2.78* – *3.13*. Thermal displacement ellipsoids are drawn at 50% probability. Tl and Bi positions in the experimental structure were assigned in agreement with the unambiguous quantum chemical results. Solid lines indicate 2e-2c bonds, while dashed lines represent 2e-3c contacts. Note that in its salt, the anion occurs as racemic mixture, of which only one enantiomer is shown here.

Most probably, the ternary anion in **2** represents an intermediate on the way towards other, more symmetric clusters. $[(Bi_6)Zn_3(TlBi_5)]^{4-}$ contains a partially formed Bi_7^{3-} anion, hence it may even be viewed as a snapshot of the formation of this 7-atom cage anion. In this scenario, Zn^{2+} would serve as sacrificial ions that help in the construction of the cage and are released thereupon. This would also explain the complicated reaction conditions that have so far been necessary to synthesize this nortricyclane-type polyanion[9a] – which actually co-crystallizes in the triple salt **2**. Additionally, the second cluster half of the ternary anion in **2** reminds of deltahedral clusters, like the co-crystallizing 9-atomic anion $(Tl_4Bi_5)^{3-}$ (within **2**, and as the main product of the reaction). In summary, the ternary cluster can be viewed as a reactive intermediate of both, the 7-atom and the binary 9-atom cage. It is well possible that slight variations of the reaction conditions might in fact allow for the successful synthesis of a homoleptic complex $[(Bi_7)Zn(Bi_7)]^{4-}$ from these starting materials, upon only partial release of the Zn^{2+} ions involved in the initial cage formation.

Regarding the cluster's composition, neither electrospray ionization mass spectrometry (ESI-MS) nor energy-dispersive X-ray (EDX) spectroscopy helped. The cluster anion was not detectable in the ESI mass spectrum, and the isolated crystals were too small to yield reliable EDX data, especially with two other (albeit known) anions being present in the crystal structure. Furthermore, Tl and Bi atoms cannot be distinguished in classical SC-XRD experiments using Mo-K_α radiation. Therefore, the composition was determined with the help of quantum chemical studies employing density functional theory (DFT) methods[16,17] and perturbation theory in the nuclear charge;[18] details on the quantum chemical studies, including the procedure used to identify the cluster anion's composition, are given in the ESI. The results clearly indicate that only one Tl atom is present in the cluster, so that the overall composition must be $[Zn_3Tl_1Bi_{11}]^{4-}$. Its favored position was unambiguously determined to be in the exposed position within the $TlBi_5$ unit (see Figure 3).

In order to understand the bonding situation in the cluster, we inspected the electronic structure and analyzed the molecular orbitals. Localized molecular orbitals (LMOs) were gained by employing Boy's methods.[17] Examples for relevant LMOs are depicted in Figure 4.

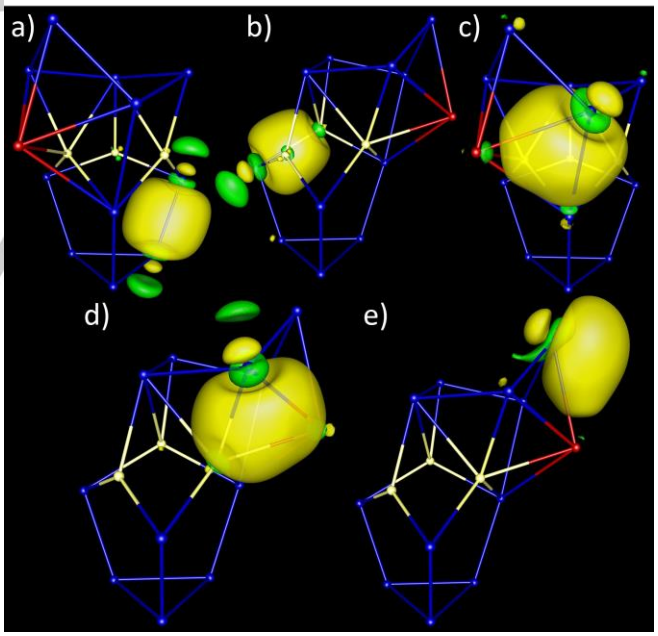

Figure 4. Representative localized molecular orbitals (LMOs) of the $[(Bi_6)Zn_3(TlBi_5)]^{4-}$ anion. a) Bi–Bi bond b) Bi–Zn bond; c) 2e-3c Tl–Bi–Bi bond; d) 2e-3c Tl–Bi–Zn bond; e) polar interaction between the Tl1 and Bi9 atoms. Element color code as used in Figure 3. Contours are drawn at ±0.04 a.u..

The cluster anion comprises 11×5 (Bi) + 1×3 (Tl) + 3×2 (Zn) + 4 (charge) = 68 valence electrons (VEs). According to the DFT investigations, these are distributed over the cluster as follows: each Bi atom and the Tl atom have one lone pair (24 VEs). The

10.1002/anie.201812473

Bi atoms form eleven regular 2e-2c bonds to neighboring Bi atoms (22 VEs) and eight 2e-2c bonds to Zn neighbors (16 VEs). The way, in which the Tl atom is incorporated into the framework is not trivial. Tl1 forms two 2e-3c bonds (Tl1–Zn3–Bi8, Tl1–Bi4–Bi10; 4 VEs) and one highly polar interaction with Bi9 (2 VEs). This way, the cluster anion combines localized and multi-center bonding, similar to the situation described for $[Bi_9\{Ru(cod)\}_2]^{3-}$,[11] yet even more complex.

The results presented in this paper emphasize once more the potential of binary Bi-containing Zintl anions to form polybismuthide anions, which may serve for the *in-situ* formation of metal complexes with these anions as ligands. This way, we proved that the Bi_7^{3-} anion possesses a reactivity similar to that of its lighter congeners, even though a direct way to target its reactivity is still lacking. However, in reactions of $(TlBi_3)^{2-}$ with MPh_2 (M = Zn, Cd, Hg), we observed a distinct preference for the formation of the Cd complex, $[(Bi_7)Cd(Bi_7]^{4-}$, while corresponding reactions with $ZnPh_2$ and $HgPh_2$ tend to yield a salt of the known binary anion $(Tl_4Bi_5)^{3-}$. Besides this, the reactions with $ZnPh_2$ also afforded a triple salt with a very uncommon ternary cluster anion $[(Bi_6)Zn_3(TlBi_5)]^{4-}$ that combines localized and multi-center bonding, and may be viewed as an intermediate on the way towards other anions, maybe even towards complexes such as the homoleptic one gained with $CdPh_2$. The presented synthetic concept will be subject to future studies with further transition metal complexes.

Experimental Section

Experimental details on the syntheses, employed characterization methods and quantum chemical studies are given in the SI.

Acknowledgements

This work was supported by Deutsche Forschungsgemeinschaft (DFG). N.L. acknowledges a Ph.D. scholarship from the Marburg University Research Academy (MARA). We thank C. Schmidt for exploratory quantum chemical calculations on $[(Bi_6)Zn_3(TlBi_5)]^{4-}$ as a part of his B.Sc. work, and PD Dr. F. Weigend for fruitful discussions on the theoretical studies.

Conflict of interest

The authors declare no conflict of interest.

Keywords: Polybismuthides • Thallium • Heterometallic Anions • X-Ray Diffraction • DFT Calculations

[1] a) J. E. Huuhey, E. A. Keiter, R. L. Keiter, *Inorganic Chemistry - Principley of Structure and Reactivity*, 4th ed., Addison Wesley, **1993**; b) T. F. Fässler, *Zintl Phases - Principles and Recent Developments*, Springer, **2011**; c) A. F. Holleman, N. Wiberg, *Lehrbuch der Anorganischen Chemie*, 102nd ed., Walter de Gruyter, **2007**; d) C. E. Housecroft, A. G. Sharpe, *Inorganic Chemistry*, 4th ed., Pearson, **2012**.

[2] a) S. Scharfe, F. Kraus, S. Stegmaier, A. Schier, T. F. Fässler, *Angew. Chem.* **2011**, *123*, 3712-3754; *Angew. Chem. Int. Ed.* **2011**, *50*, 3630-3670; b) R. S. P. Turbervill, J. M. Goicoechea, *Chem. Rev.* **2014**, *114*, 10807-10828; Early and most recent examples for this As and Sb chemistry: c) D. G. Adolphson, J. D. Corbett, D. J. Merryman, *J. Am. Chem. Soc.* **1976**, *98*, 7234-7239; d) H.-G. v. Schnering, D. Fenske, W. Hönle, M. Binnewies, K. Peters, *Angew. Chem.* **1979**, *91*, 755; *Angew. Chem. Int. Ed. Engl.* **1979**, *18*, 679-680; e) M. Kaas, N. Korber, *Z. Anorg. Allg. Chem.* **2017**, *643*, 1331-1334; f) A. E. Seitz, M. Eckhardt, S. S. Sen, A. Erlebach, E. V. Peresypkina, H. W. Roesky, M. Sierka, M. Scheer, *Angew. Chem.* **2017**, *129*, 6755-6759; *Angew. Chem. Int. Ed.* **2017**, *56*, 6655-6659.

[3] a) R. S. P. Turbervill, J. M. Goicoechea, *Chem. Commun.* **2012**, *48*, 6100-6102; b) A. R. Jupp, J. M. Goicoechea, *Angew. Chem.* **2013**, *125*, 10248-10251; *Angew. Chem. Int. Ed.* **2013**, *52*, 10064-10067; c) R. S. P. Turbervill, J. M. Goicoechea, *Inorg. Chem.* **2013**, *52*, 5527-5534; d) R. S. P. Turbervill, A. R. Jupp, P. S. B. McCullough, D. Ergöçmen, J. M. Goicoechea, *Organometallics* **2013**, *32*, 2234-2244.

[4] C. Knapp, B. B. Zhou, M. S. Denning, N. H. Rees, J. M. Goicoechea, *Dalton Trans.* **2010**, *39*, 426-436.

[5] a) O. J. Scherer, *Angew. Chem. Int. Ed. Engl.* **1990**, *29*, 1104-1122; b) O. J. Scherer, C. Blath, G. Wolmershäuser, *J. Organomet. Chem.* **1990**, *387*, C21-C24; c) O. J. Scherer, *Acc. Chem. Res.* **1999**, *32*, 751-762; d) H. Krauss, G. Balázs, M. Bodensteiner, M. Scheer, *Chem. Sci.* **2010**, *1*, 337-342.

[6] C. M. Knapp, B. H. Westcott, M. A. C. Raybould, J. E. McGrady, J. M. Goicoechea, *Chem. Commun.* **2012**, *48*, 12183-12185.

[7] a) C. Schwarzmaier, S. Heinl, G. Balázs, M. Scheer, *Angew. Chem.* **2015**, *127*, 13309-13314; *Angew. Chem. Int. Ed.* **2015**, *54*, 13116-13121; b) N. Arleth, M. T. Gamer, R. Köppe, S. N. Konchenko, M. Fleischmann, M. Scheer, P. W. Roesky, *Angew. Chem.* **2016**, *128*, 1583-1586; *Angew. Chem. Int. Ed.* **2016**, *55*, 1557-1560; c) C. Schoo, S. Bestgen, M. Schmidt, S. N. Konchenko, M. Scheer, P. W. Roesky, *Chem. Commun.* **2016**, *52*, 13217-13220; d) M. Schmidt, D. Konieczny, E. V. Peresypkina, A. V. Virovets, G. Balázs, M. Bodensteiner, F. Riedlberger, H. Krauss, M. Scheer, *Angew. Chem.* **2017**, *129*, 7413-7417; *Angew. Chem. Int. Ed.* **2017**, *56*, 7307-7311; e) C. Schoo, R. Köppe, M. Piesch, M. T. Gamer, S. N. Konchenko, M. Scheer, P. W. Roesky, *Chem. Eur. J.* **2018**, *24*, 7890-7895.

[8] a) R. Ahlrichs, D. Fenske, K. Fromm, H. Krautscheid, U. Krautscheid, O. Treutler, *Chem. Eur. J.* **1996**, *2*, 238-244; b) C. v. Hänisch, D. Fenske, F. Weigend, *Chem. Eur. J.* **1997**, *3*, 1494-1498; c) C. v. Hänisch, D. Fenske, *Z. Anorg. Allg. Chem.* **1998**, *624*, 367-369.

[9] a) L. G. Perla, A. G. Oliver, S. C. Sevov, *Inorg. Chem.* **2015**, *54*, 872-875; b) B. Weinert, A. R. Eulenstein, R. Ababei, S. Dehnen, *Angew. Chem.* **2014**, *126*, 4792-4797; *Angew. Chem. Int. Ed.* **2014**, *53*, 4704-4708.

[10] R. J. Wilson, S. Dehnen, *Angew. Chem.* **2017**, *129*, 3144-3149; *Angew. Chem. Int. Ed.* **2017**, *56*, 3098-3102.

[11] N. Lichtenberger, N. Spang, A. Eichhöfer, S. Dehnen, *Angew. Chem.* **2017**, *129*, 13436-13442; *Angew. Chem. Int. Ed.* **2017**, *56*, 13253-13258.

[12] a) M. C. Qian, A. C. Reber, A. Ugrinov, N. K. Chaki, S. Mandal, H. M. Saavedra, S. N. Khanna, A. Sen, P. S. Weiss, *ACS Nano* **2010**, *4*, 235-240; b) S. Mandal, A. C. Reber, M. Qian, R. Liu, H. M. Saavedra, S. Sen, P. S. Weiss, S. N. Khanna, A. Sen, *Dalton Trans.* **2012**, *41*, 12365-12377.

[13] Y. Wang, P. Zavalij, B. Eichhorn, *Chem. Commun.* **2017**, *53*, 11600-11602.

[14] CCDC 1875914 (**1**), and 1875516 (**2**) contain the supplementary crystallographic data for the compounds **1**, and **2** in this paper. The data can be obtained free of charge via www.ccdc.cam.ac.uk/data_request/cif.

[15] R. G. Pearson, *J. Am. Chem. Soc.* **1963**, *85*, 3533-3539.

[16] a) TURBOMOLE V7.2 2017, a development of University of Karlsruhe and Forschungszentrum Karlsruhe GmbH, 1989-2007, TURBOMOLE GmbH, since 2007; available from http://www.turbomole.com; References for the used methods and tools: b) F. Weigend, R. Ahlrichs, *Phys. Chem. Chem. Phys.* **2005**, *7*, 3297-3305; c) F. Weigend, *Phys.*

10.1002/anie.201812473

Chem. Chem. Phys. **2006**, *8*, 1057-1065; d) D. Andrae, U. Häußermann, M. Dolg, H. Stoll, H. Preuß, *Theor. Chim. Acta* **1990**, *77*, 123-141; e) B. Metz, H. Stoll, M. Dolg, *J. Chem. Phys.* **2000**, *113*, 2563-2569; f) P. A. M. Dirac, *Proc. R. Soc. A* **1929**, *123*, 714-733; g) J. C. Slater, *Phys. Rev.* **1951**, *81*, 385-390; h) J. P. Perdew, *Phys. Rev. B* **1986**, *33*, 8822-8824; i) J. M. Tao, J. P. Perdew, V. N. Staroverov, G. E. Scuseria, *Phys. Rev. Lett.* **2003**, *91*, 146401; j) A. Klamt, G. Schüürmann, *J. Chem. Soc., Perkin Trans. 2* **1993**, 799-805; k) R. S. Mulliken, *J. Chem. Phys.* **1955**, *23*, 1833-1840; l) D. L. Bergman, L. Laaksonen, A. Laaksonen, *J. Mol. Graph. Model.* **1997**, *15*, 301-306.

[17] a) S. F. Boys, *Rev. Mod. Phys.* **1960**, *32*, 296-299; b) J. M. Foster, S. F. Boys, *Rev. Mod. Phys.* **1960**, *32*, 300-302.

[18] a) F. Weigend, C. Schrodt, R. Ahlrichs, *J. Chem. Phys.* **2004**, *121*, 10380-10384; b) F. Weigend, C. Schrodt, *Chem. Eur. J.* **2005**, *11*, 3559-3564; c) F. Weigend, *J. Chem. Phys.* **2014**, *141*, 134103.

10.1002/anie.201812473

WILEY-VCH

Entry for the Table of Contents

COMMUNICATION

The first coordination compound with intact Bi_7^{3-} ligands, the homoleptic complex $[(Bi_7)Cd(Bi_7)]^{4-}$, and the ternary cluster $[(Bi_6)Zn_3(TlBi_5)]^{4-}$, were prepared through in-situ degradation of the binary Zintl anion $(TlBi_3)^{2-}$. The compounds provide a glimpse into a possible formation pathway of the polycyclic polybismuthide, the follow-up chemistry of which has been unprecedented to date. Both title compounds were further studied by means of DFT methods.

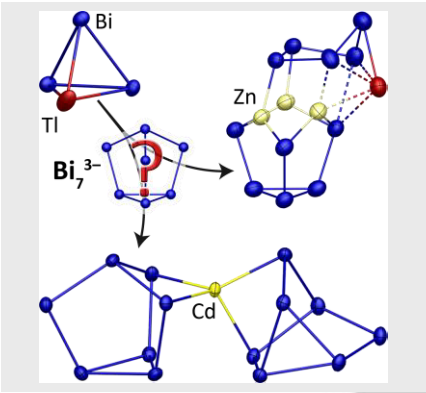

*N. Lichtenberger, W. Massa, S. Dehnen**

Page No. – Page No.

Polybismuthide Anions as Ligands: The Homoleptic Complex $[(Bi_7)Cd(Bi_7)]^{4-}$ and the Ternary Cluster $[(Bi_6)Zn_3(TlBi_5)]^{4-}$

3.5 Intermetalloid and Heterometallic Clusters Combining p-Block (Semi)Metals with d- or f-Block Metals

Bei dieser Publikation handelt es sich um einen eingeladenen Übersichtsartikel des Fachjournals *Chemical Reviews* der *American Chemical Society* zu dem Themengebiet der intermetalloiden und heterometallischen Cluster, der sich derzeit im Begutachtungsprozess befindet. Um einen Überblick über die darin abgedeckten Themengebiete zu geben sind im Folgenden der Abstract und das Inhaltsverzeichnis des Artikels abgedruckt. Dr. *Robert J. Wilson* und ich teilen uns die Erstautorenschaft dieses Artikels.

Zitat: R. J. Wilson, N. Lichtenberger, B. Weinert, S. Dehnen, *Manuskript eingereicht.*

Abstract

Clusters have been the subject of intense investigations since their famous definition launched by Cotton in 1963, and the area has expanded ever since. One obvious development addresses the widening of the definition of what to call a cluster: from purely (transition) metal-metal linked assemblies, as per Cotton's early denomination, to non-metal-bridged molecules or purely non-metal cages, like fullerenes, and even van-der-Waals aggregates such as water clusters. The other extension concerns the broadened spectrum of compositions within the named families and the corresponding cluster structures that reach from trinuclear and hence triangular motifs to clusters with sizes in the range of the hemoglobin unit. This review article reports on one cluster family that has its origins in traditional Zintl anion chemistry, but has undergone rapid development in recent years, namely ligand-free clusters that combine main group and transition metal atoms. Depending on the position of the transition metal atom(s), one refers to such clusters as intermetalloid (endohedral) clusters or as a special type of heterometallic clusters. The predominant synthetic access makes use of soluble Zintl anions. Other pathways for their preparation include traditional solid state reactions of according elemental combinations or the bottom-up synthesis employing low valent organo-main group element sources. This survey will shed light on all of these approaches, with an emphasis on the syntheses that employ soluble Zintl

anion compounds. The article will give a comprehensive overview of the currently known compounds, their different syntheses protocols and analytic techniques for determination of their compositions, structures and further properties. Additionally, this survey will report peculiarities of the bonding situation found within some of the cluster molecules, which were studied by means of sophisticated quantum chemical investigations.

Intermetalloid and Heterometallic Clusters Combining p-Block (Semi)Metals with d- or f-Block Metals

Journal:	*Chemical Reviews*
Manuscript ID	Draft
Manuscript Type:	Thematic Review
Date Submitted by the Author:	n/a
Complete List of Authors:	Dehnen, Stefanie; Philipps-University Marburg, Chemistry Wilson, Robert; Philipps-Universitat Marburg, Chemistry Lichtenberger, Niels; Philipps-Universitat Marburg, Weinert, Bastian; Philipps-University Marburg, Chemistry

Intermetalloid and Heterometallic Clusters Combining p-Block (Semi)Metals with d- or f-Block Metals

Robert J. Wilson,[†,‡] Niels Lichtenberger,[†,‡] Bastian Weinert,[†] and Stefanie Dehnen[†]*

Fachbereich Chemie und Wissenschaftliches Zentrum für Materialwissenschaften, Philipps Universität Marburg, Hans-Meerwein-Straße 4, 35043 Marburg, Germany.

KEYWORDS (Word Style "BG_Keywords"). If you are submitting your paper to a journal that requires keywords, provide significant keywords to aid the reader in literature retrieval.

ABSTRACT: Clusters have been the subject of intense investigations since their famous definition launched by Cotton in 1963, and the area has expanded ever since. One obvious development addresses the widening of the definition of what to call a cluster: from purely (transition) metal–metal linked assemblies, as per Cotton's early denomination, to non-metal-bridged molecules or purely non-metal cages, like fullerenes, and even van-der-Waals aggregates such as water clusters. The other extension concerns the broadened spectrum of compositions within the named families and the corresponding cluster structures that reach from trinuclear and hence triangular motifs to clusters with sizes in the range of the hemoglobin unit. This review article reports on one cluster family that has its origins in traditional Zintl anion chemistry, but has undergone rapid development in recent years, namely ligand-free clusters that combine main group and transition metal atoms. Depending on the position of the transition metal atom(s), one refers to such clusters as intermetalloid (endohedral) clusters or as a special type of heterometallic clusters. The predominant synthetic access makes use of soluble Zintl anions. Other pathways for their preparation include traditional solid state reactions of according elemental combinations or the bottom-up synthesis employing low valent organo-main group element sources. This survey will shed light on all of these approaches, with an emphasis on the syntheses that employ soluble Zintl anion compounds. The article will give a comprehensive overview of the currently known compounds, their different syntheses protocols and analytic techniques for determination of their compositions, structures and further properties. Additionally, this survey will report peculiarities of the bonding situation found within some of the cluster molecules, which were studied by means of sophisticated quantum chemical investigations.

CONTENTS

1. INTRODUCTION

1.1. Intermetalloid and Heterometallic Clusters

In 2002, Schnöckel introduced the term "metalloid cluster" to describe subvalent (main group metal) clusters, which comprise "metallic" inner parts with formally uncharged metal atoms within outer shells of formally positively charged atoms.[1] Similar to this classification, yet concentrating on structural features, Fässler derived the term "intermetalloid cluster" in 2004. It denominates heteroatomic endohedral clusters with inner (usually transition) metal atoms, which are surrounded by a significantly larger number of (mainly main group) metal or semi-metal atoms.[2] They are thus reminiscent of the structural situation in intermetallic phases, such as the Laves phases with their typical high coordination numbers.

Another definition of "intermetalloid clusters" was introduced by Kempe in 2010. In this case, they were defined as polyatomic, metal–metal bonded assemblies combining d-block and f-block metal atoms, regardless of structural features or coordination numbers.[3] In this article the term will be used according to Fässler's definition, hence classifying them as endohedral clusters only. Such intermetalloid clusters can be represented by the general formula $[M_x@E_y]^{q-}$ or $[M_x@E_yM_z]^{q-}$, with M being a transition metal, lanthanide, or actinide atom, and E a p-block (semi)metal atom or different types of main group atoms. The charge depends on many factors, including the cluster size, the identity of E, and the charge of the interstitial atom(s). In such $[M_x@E_y]^{q-}$ clusters, x is typically much smaller than y. All other combinations of main group and transition metal atoms $[M_xE_y]^{q-/+}$, which lack an inner atom or an inner group of atoms, will be referred in this article as "heterometallic clusters".

Since the seminal characterization of $[Pt@Pb_{12}]^{2-}$ in 2004,[4] dozens of such transition metal-centered p-block element clusters have been reported. These have been astonishingly varied in terms of both their physical and electronic structures. Additionally, investigations into intermetalloid cluster syntheses have afforded many related heterometallic clusters. The vast majority of intermetalloid and p-block-atom-rich heterometallic clusters are synthesized using Zintl anion precursors. The field of Zintl anion chemistry has matured beyond exploratory synthesis and could be said to be in a "pre-application" phase, with their modification and controlled decomposition becoming routine. In contrast, the field of intermetalloid cluster research is still primarily one of exploratory synthesis and computational investigation. However, an impressive foundation of knowledge has been assembled, upon which future innovative research can build. One of the goals of this review is to stimulate such research by assembling all of the evidence available regarding the reactivity of these clusters, as well as the relationship between their electronic and physical structures.

Many intermetalloid clusters are ligand free and can, due to their mixed-metallic nature, be viewed as molecular models of doped metals, intermetallic phases, or alloys in general.[2,5] Furthermore, as soluble, monodisperse, and redox active metal clusters, they are potentially interesting candidates for a variety of applications. One near-term possibility is the use of intermetalloid cluster compounds as precursors to new intermetallic phases. Such an application would be analogous to the oxidative formation of the clathrate-like germanium modification Ge(cF136) from the ubiquitous homoatomic Zintl anion Ge_9^{4-}.[6] Other potential applications could be facilitated by the post-synthetic modification of intermetalloid clusters. While Zintl anions have been extensively modified via the attachment of organic, organometallic, and element-organic ligands, success in this arena is conspicuously absent for intermetalloid clusters. However, such an advancement would critically allow for the control of cluster solubility, the addition of functional moieties, or even the linking of clusters into a hybrid network. Progress on these and other fronts is currently hindered by experimental difficulties, such as low yields and the generation of unwanted byproducts. Therefore, fundamental research into the scalable synthesis of pure intermetalloid cluster compounds is still needed for the evolution of this field.

As a note to the reader, this review will cover clusters in which d- and f-block metals are combined with metals and semimetals of groups 13-15 (Al-Tl, Si-Pb, As-Bi). In particular, we will focus on clusters that are majority p-block elements (i.e., y > x) and are most often derived from Zintl anions. Thus the class of transition metal carbonyl clusters comprising endohedral main group atoms falls outside the scope of this review.[7] Furthermore, only selected examples of pnictogen-transition metal compounds will be covered, as much of this extensive field has been reviewed elsewhere. One recent review covers the chemistry of Pn_7^{3-} (P – Sb),[5d] while another gives a survey of transition metal complexes of the pnictides.[8] Furthermore, reactions of P_4 with d-block metal compounds have also been reviewed.[9]

4 Zusammenfassungen

4.1 Zusammenfassung in deutscher Sprache

Im Rahmen der Doktorarbeit wurde die Chemie binärer *Zintl*-Anionen mit Trielelementen untersucht. Hierzu wurden sowohl neue Edukte zur Darstellung der Anionen als auch deren Folgechemie mit Übergangsmetallkomplexen näher betrachtet. Die Synthese des bereits in meiner Masterarbeit erstmals dargestellten Anions $(TlBi_3)^{2-}$ konnte durch Entwicklung einer neuen Syntheseroute soweit optimiert werden, dass Umsetzungen dessen möglich wurden.

Zu diesem Zweck wurde erstmals ein genauerer Blick auf die zur Synthese der Anionen verwendeten intermetallischen Verbindungen geworfen. Es zeigte sich, dass komplexe Zusammenhänge zwischen der eingangs vorgegebenen Zusammensetzung des Reaktionsgemisches, den tatsächlich erhaltenen Produkten und den daraus darstellbaren *Zintl*-Anionen bestehen. Aus diesem Anlass wurde eine Reihe formal ternärer intermetallischer Verbindungen dargestellt und auf ihre Bestandteile hin untersucht. Dies gelang durch die Kombination von Röntgenpulver- und Einkristalldiffraktometrie. Im Rahmen der Studien wurden Einflüsse des gewählten Alkalimetalls und die Rolle der initialen Stöchiometrie auf die Produktbildung studiert. Durch Extraktion der erhaltenen intermetallischen Verbindungen wurde eine Reihe neuer binärer *Zintl*-Anionen dargestellt und charakterisiert. Die Ergebnisse zeigten, dass das Anion $(TlBi_3)^{2-}$ aus „K_2TlBi_3“, eigentlich einer Mischung aus KTlBi und KBi_2, in hohen Ausbeuten und sehr guter Reinheit dargestellt werden kann. Die Reaktivität dessen wurde in einer Reihe von Umsetzungen mit Metallkomplexen studiert.

In Reaktionen mit Lanthanoidkomplexen $[Ln(cpMe_4H)_3]$ entstehen, wie im Fall der leichteren Homologen Ga und In, intermetalloide 13-Atomkäfige $[Ln@Tl_2Bi_{11}]^{4-}$ (Ln = La, Ce, Nd, Sm).[61, 88c, 88d] Werden stattdessen Actinoidkomplexe $[U(cpMe_4H)_3]$ oder $[An(cpMe_4H)_3Cl]$ (An = U, Th) eingesetzt, entstehen wiederum 13-Atomkäfige $[An@Tl_2Bi_{11}]^{3-}$ (An = U, Th), die jedoch statt eines M^{3+}-Ions ein M^{4+} enthalten.[61, 88f] Diese Oxidation wurde für eine Reihe unterschiedlicher Edukte

$(GaBi_3)^{2-}$ und $(Pb_2Bi_2)^{2-}$ in Zusammenarbeit mit meinen Kollegen *Armin Eulenstein* und Dr. *Robert J. Wilson* beobachtet, woraus weitere intermetalloide Cluster $[An@Bi_{12}]^{q-}$ (An/q = U/3, Th/4), $[U@Pb_7Bi_7]^{3-}$ und $[An@Pb_4Bi_9]^{3-}$ (An = U, Th) resultierten.[104] Quantenchemische Studien deuten auf eine starke Interaktion zwischen der Clusterschale und dem Zentralatom in $[An@Bi_{12}]^{q-}$ (An/q = U/3, Th/4) hin. Erstmalig wurden durch diese Synthesen intermetalloide Clusteranionen mit endohedralen Actinoidionen dargestellt und charakterisiert.

In einer Reaktion von $(TlBi_3)^{2-}$ mit [Ru(cod)(Me−Allyl)$_2$] entstehen die Clusteranionen $[Bi_9\{Ru(cod)\}_2]^{3-}$ und $[Tl_2Bi_6\{Ru(cod)\}]^{2-}$.[21] Das Clusteranion $[Bi_9\{Ru(cod)\}_2]^{3-}$ enthält das neuartige Polybismuthidfragment Bi_9^{7-} und weist eine elektronische Struktur auf, in der lokalisierte und Mehrzentrenbindungen nebeneinander vorliegen. Das Anion $[Tl_2Bi_6\{Ru(cod)\}]^{2-}$ war das erste ternäre Clusteranion mit Atomen der Gruppe 13, das ein d-Block-Übergangsmetallatom enthielt. Obwohl der Cluster formal die Wade-Mingos-Regeln für einen *nido*-Cluster erfüllt zeigen die strukturellen Parameter Auffälligkeiten, die eine nähere Betrachtung der Bindungssituation mit quantenchemischen Methoden erforderten. So zeigte sich, dass in dem (Tl_2Bi_6)-Fragment 2e-3c-Mehrzentrenbindungen und zu dem Ru-Atom hauptsächlich kovalente Bindungen vorliegen.

Das Potential des $(TlBi_3)^{2-}$-Anions zur Bildung von Polybismuthiden wurde in einer Reaktionsserie mit MPh_2-Komplexen (M = Zn, Cd, Hg) untersucht. Aus der Umsetzung mit $CdPh_2$ ging die Koordinationsverbindung $[(Bi_7)Cd(Bi_7)]^{4-}$ hervor, in der zum ersten Mal das Anion Bi_7^{3-} als Ligand für ein Metallatom fungiert. Die Stabilität der $[(Pn_7)M(Pn_7)]^{4-}$-Verbindungen (Pn = P - Bi, M = Zn - Hg, Hg_2^{2+}) wurde mit quantenchemischen Methoden untersucht. Analoge Umsetzungen von $(TlBi_3)^{2-}$ mit $ZnPh_2$ und $HgPh_2$ liefern $(Tl_4Bi_5)^{3-}$ als Hauptprodukt, im Fall von $ZnPh_2$ gelang jedoch zusätzlich die Kristallisation eines Reaktiosintermediates. In diesem ist das Anion $[(Bi_6)Zn_3(TlBi_5)]^{4-}$ zu finden, dessen elektronische Struktur mit quantenchemischen Untersuchungen näher betrachtet wurde. Diese ist, ähnlich wie im Fall von $[Bi_9\{Ru(cod)\}_2]^{3-}$, komplex und es liegt wieder eine Kombination von lokalisierten und Mehrzentrenbindungen vor. Da das Anion ein fast vollständiges Bi_7-Nortricyclanfragment enthält, kann es als Intermediat auf dem Weg zu dessen Bildung verstanden werden.

Sowohl im Bereich der zur Synthese der binären *Zintl*-Anionen verwendeten Edukte als auch in den Reaktivitätsstudien wurde erst ein kleiner Einblick gewonnen. Diese Arbeit soll hierbei als Grundlage für weitere Untersuchungen in diesen Feldern dienen.

4.2 English Summary

The main focus of this doctoral thesis was on the chemistry of binary *Zintl* anions comprising group 13 elements. During the course of these studies both new starting materials for their syntheses as well as their reactivity towards transition metal complexes were investigated. Initially the synthesis of the $(TlBi_3)^{2-}$ anion, previously characterized in my master thesis, was optimized to an extent that allowed for its subsequent use in reactions. This was achieved by detailed investigations of the intermetallic compounds used for the preparation. Herein I observed complex relationships between the initial stoichiometry, the resulting products and the *Zintl* anions prepared from them. A series of formally ternary intermetallic compounds was analyzed for their true components with a combination of powder and single crystal X-ray diffraction measurements. Two influences on the product formation were taken into account: the choice of alkaline metal and the initial stoichiometry. The extraction of all obtained materials led to the formation of a series of novel binary *Zintl* anions that were subsequently crystallized and characterized. "K_2TlBi_3" was shown to be a very good starting material for the synthesis of $(TlBi_3)^{2-}$, affording the product in high yield and purity. However, it was shown to actually be a mixture of two intermetallic compounds, KTlBi and KBi_2. The reactivity of $(TlBi_3)^{2-}$ was studied in a series of reactions with transition metal complexes.

Reactions with lanthanide complexes $[Ln(cpMe_4H)_3]$ afford intermetalloid 13 atom cages $[Ln@Tl_2Bi_{11}]^{4-}$ (Ln = La, Ce, Nd, Sm), as observed for the lighter homologues Ga and In.[61, 88c, 88d] Utilization of actinide complexes $[U(cpMe_4H)_3]$ or $[An(cpMe_4H)_3Cl]$ (An = U, Th) again affords intermetalloid 13 atom cages, this time however containing M^{4+} ions instead of M^{3+} ions.[61, 88f] This oxidation was observed for a series of different starting materials $(GaBi_3)^{2-}$ and $(Pb_2Bi_2)^{2-}$ in cooperation with my colleagues *Armin Eulenstein* und Dr. *Robert J. Wilson*, leading to the formation of further intermetalloid clusters $[An@Bi_{12}]^{q-}$ (An/q = U/3, Th/4), $[U@Pb_7Bi_7]^{3-}$ and $[An@Pb_4Bi_9]^{3-}$ (An = U, Th).[88f, 104] Quantum chemical investigations hint towards a strong interaction between the cluster shell and the central atoms in $[An@Bi_{12}]^{q-}$ (An/q = U/3, Th/4). These studies are the first reports of intermetalloid clusters containing endohedral actinide ions.

Reactions of $(TlBi_3)^{2-}$ with $[Ru(cod)(Me{-}Allyl)_2]$ afford the cluster anions $[Bi_9\{Ru(cod)\}_2]^{3-}$ and $[Tl_2Bi_6\{Ru(cod)\}]^{2-}$.[21] The cluster $[Bi_9\{Ru(cod)\}_2]^{3-}$ comprises the novel polybismuthide fragment Bi_9^{7-} and its electronic structure combines localized and multi-center bonding. The anion $[Tl_2Bi_6\{Ru(cod)\}]^{2-}$ was the first

ternary cluster anion with group 13 atoms that also contains a d-block transition metal atom. Even though the cluster is formally in accordance with the Wade-Mingos rules for a *nido* cluster the structural parameters show abnormalities that required a more detailed investigation with quantum chemical methods. These showed that 2e-3c multi-center bonds exist within the (Tl_2Bi_6)-fragment while all bonds to the Ru atom are mainly covalent.

The potential of the $(TlBi_3)^{2-}$ anion to form novel polybismuthide ions was tested in a reaction series with MPh_2 complexes (M = Zn, Cd, Hg). Reactions with $CdPh_2$ afford the coordination compound $[(Bi_7)Cd(Bi_7)]^{4-}$, which is the first report of the Bi_7^{3-} anion acting as a ligand. The stabilities of $[(Pn_7)M(Pn_7)]^{4-}$ compounds (Pn = P - Bi, M = Zn - Hg, Hg_2^{2+}) were investigated with quantum chemical methods. Equivalent reactions of $(TlBi_3)^{2-}$ with $ZnPh_2$ and $HgPh_2$ afford $(Tl_4Bi_5)^{3-}$ as the main product. However, in the case of $ZnPh_2$ a reaction intermediate could be crystallized. This salt contains the anion $[(Bi_6)Zn_3(TlBi_5)]^{4-}$, which was again studied with quantum chemical methods. Its electronic structure is comparable to that of $[Bi_9\{Ru(cod)\}_2]^{3-}$ in terms of bonding, as it again combines localized with multi-center bonds. The anion comprises an almost complete Bi_7 nortricyclane fragment in which only the apical atom was replaced by three Zn^{2+} ions and can, in that aspect, be regarded as an intermediate of the Bi_7^{3-} formation.

The presented studies only provide a glimpse into the large research topics of intermetallic compounds for the syntheses of binary *Zintl* anions as well as their reactivities. This work will hopefully spark further research and serve as a foundation for these studies.

5 Literatur

[1] (a) A. F. Holleman, N. Wiberg, *Lehrbuch der Anorganischen Chemie*, 102. Ausgabe, Walter de Gruyter, **2007**; (b) A. Lennartson, *Nat. Chem.* **2015**, *7*, 610.

[2] (a) J. F. Hinton, K. R. Metz, R. W. Briggs, *Prog. Nucl. Magn. Reson. Spectrosc.* **1988**, *20*, 423–513; (b) J. F. Hinton, R. W. Briggs, *J. Magn. Reson.* **1975**, *19*, 393–397.

[3] A. V. Protchenko, D. Dange, J. R. Harmer, C. Y. Tang, A. D. Schwarz, M. J. Kelly, N. Phillips, R. Tirfoin, K. H. Birjkumar, C. Jones, N. Kaltsoyannis, P. Mountford, S. Aldridge, *Nat. Chem.* **2014**, *6*, 315–319.

[4] J. D. Corbett, *Angew. Chem. Int. Ed.* **2000**, *39*, 670–690.

[5] S. Acharya, *Nat. Chem.* **2013**, *5*, 894.

[6] P. Pyykkö, J. P. Desclaux, *Acc. Chem. Res.* **1979**, *12*, 276–281.

[7] (a) M. Joannis, *Hebd. Seances Acad. Sci.* **1891**, *113*, 795–798; (b) M. Joannis, *Hebd. Seances Acad. Sci.* **1892**, *114*, 585–587.

[8] R. Mohan, *Nat. Chem.* **2010**, *2*, 336.

[9] P. de Marcillac, N. Coron, G. Dambier, J. Leblanc, J.-P. Moalic, *Nature* **2003**, *422*, 876.

[10] (a) N. Tokitoh, Y. Arai, R. Okazaki, S. Nagase, *Science* **1997**, *277*, 78–80; (b) B. Twamley, C. D. Sofield, M. M. Olmstead, P. P. Power, *J. Am. Chem. Soc.* **1999**, *121*, 3357–3367; (c) R. Wolf, J. Fischer, R. C. Fischer, J. C. Fettinger, P. P. Power, *Eur. J. Inorg. Chem.* **2008**, *2008*, 2515–2521.

[11] (a) A. Hershaft, J. D. Corbett, *Inorg. Chem.* **1963**, *2*, 979–985; (b) R. M. Friedman, J. D. Corbett, *Inorg. Chem.* **1973**, *12*, 1134–1139; (c) M. Ruck, V. Dubenskyy, T. Söhnel, *Angew. Chem. Int. Ed.* **2003**, *42*, 2978–2982; (d) B. Wahl, L. Kloo, M. Ruck, *Angew. Chem. Int. Ed.* **2008**, *47*, 3932–3935; (e) B. Wahl, M. Erbe, A. Gerisch, L. Kloo, M. Ruck, *Z. Anorg. Allg. Chem.* **2009**, *635*, 743–752; (f) M. F. Groh, A. Isaeva, C. Frey, M. Ruck,

Z. Anorg. Allg. Chem. **2013**, *639*, 2401–2405; (g) M. Knies, M. Kaiser, A. Isaeva, U. Müller, T. Doert, M. Ruck, *Chem. Eur. J.* **2018**, *24*, 127–132.

[12] F. Laves in *Die Naturwissenschaften*, (Hrsg.: F. Süffert), Springer Berlin Heidelberg, **1941**, Kap. 26, 244–256.

[13] T. F. Fässler, S. D. Hoffmann, *Angew. Chem. Int. Ed.* **2004**, *43*, 6242–6247.

[14] (a) E. Zintl, H. Kaiser, *Z. Anorg. Allg. Chem.* **1933**, *211*, 113–131; (b) E. Zintl, *Angew. Chem.* **1939**, *52*, 1–6.

[15] (a) J. D. Corbett, D. G. Adolphson, D. J. Merryman, P. A. Edwards, F. J. Armatis, *J. Am. Chem. Soc.* **1975**, *97*, 6267–6268; (b) J. D. Corbett, P. A. Edwards, *J. Chem Soc. Chem. Commun.* **1975**, 984.

[16] (a) A. M. Guloy, R. Ramlau, Z. Tang, W. Schnelle, M. Baitinger, Y. Grin, *Nature* **2006**, *443*, 320–323; (b) T. F. Fässler, *Angew. Chem. Int. Ed.* **2007**, *46*, 2572.

[17] (a) S. C. Sevov, J. M. Goicoechea, *Organometallics* **2006**, *25*, 5678–5692; (b) S. Scharfe, F. Kraus, S. Stegmaier, A. Schier, T. F. Fässler, *Angew. Chem. Int. Ed.* **2011**, *50*, 3630–3670; (c) R. S. P. Turbervill, J. M. Goicoechea, *Chem. Rev.* **2014**, *114*, 10807–10828; (d) B. Weinert, S. Dehnen in *Clusters – Contemporary Insight in Structure and Bonding*, (Hrsg.: S. Dehnen), Springer International Publishing, **2017**, 99–134; (e) R. J. Wilson, B. Weinert, S. Dehnen, *Dalton Trans.* **2018**, *47*, 14861–14869.

[18] (a) K. Wade, *Inorg. Nucl. Chem. Lett.* **1972**, *8*, 559–562; (b) D. M. P. Mingos, *Nature - Phys. Sci.* **1972**, *236*, 99–102; (c) D. M. P. Mingos, *Acc. Chem. Res.* **1984**, *17*, 311–319; (d) D. M. P. Mingos, T. Slee, Z. Y. Lin, *Chem. Rev.* **1990**, *90*, 383–402.

[19] S. Kaskel, J. D. Corbett, *Inorg. Chem.* **2000**, *39*, 778–782.

[20] N. Lichtenberger, Y. J. Franzke, W. Massa, F. Weigend, S. Dehnen, *Chem. Eur. J.* **2018**, *24*, 12022–12030.

[21] N. Lichtenberger, N. Spang, A. Eichhöfer, S. Dehnen, *Angew. Chem. Int. Ed.* **2017**, *56*, 13253–13258.

[22] B. Krebs, M. Hucke, C. J. Brendel, *Angew. Chem. Int. Ed.* **1982**, *21*, 445–446.

[23] U. Friedrich, N. Korber, *ChemistryOpen* **2016**, *5*, 306–310.

[24] W. Klemm, E. Busmann, *Z. Anorg. Allg. Chem.* **1963**, *319*, 297–311.

[25] (a) T. K. Chattopadhyay, W. May, H. G. von Schnering, G. S. Pawley, *Z. Kristallogr. - Cryst. Mater.* **1983**, *165*, 47–64; (b) I. Raabe, S. Antonijevic, I. Krossing, *Chem. Eur. J.* **2007**, *13*, 7510–7522.

[26] (a) W. Hönle, H. G. von Schnering, A. Schmidpeter, G. Burget, *Angew. Chem. Int. Ed.* **1984**, *23*, 817–818; (b) L. G. Perla, A. G. Oliver, S. C. Sevov, *Inorg. Chem.* **2015**, *54*, 872–875.

[27] (a) S. F. Boys, *Rev. Mod. Phys.* **1960**, *32*, 296–299; (b) J. M. Foster, S. F. Boys, *Rev. Mod. Phys.* **1960**, *32*, 300–302.

[28] (a) A. E. Reed, R. B. Weinstock, F. Weinhold, *J. Chem. Phys.* **1985**, *83*, 735–746; (b) R. S. Mulliken, *J. Chem. Phys.* **1955**, *23*, 1833–1840; (c) C. Ehrhardt, R. Ahlrichs, *Theor. Chim. Acta* **1985**, *68*, 231–245.

[29] (a) W. Massa, *Kristallstrukturbestimmung*, 7. Ausgabe, Vieweg + Teubner, **2011**; (b) D. W. Bennett, *Understanding Single-Crystal X-Ray Crystallography*, Wiley-VCH, **2010**.

[30] (a) F. Weigend, C. Schrodt, R. Ahlrichs, *J. Chem. Phys.* **2004**, *121*, 10380–10384; (b) F. Weigend, C. Schrodt, *Chem. Eur. J.* **2005**, *11*, 3559–3564.

[31] F. Weigend, *J. Chem. Phys.* **2014**, *141*, 134103.

[32] (a) R. E. Marsh, D. P. Shoemaker, *Acta Cryst.* **1953**, *6*, 197–205; (b) I. F. Hewaidy, E. Busmann, W. Klemm, *Z. Anorg. Allg. Chem.* **1964**, *328*, 283–293; (c) C. Röhr, *Z. Naturforsch. B: Chem. Sci.* **1995**, *50*, 802–808.

[33] (a) V. Quéneau, E. Todorov, S. C. Sevov, *J. Am. Chem. Soc.* **1998**, *120*, 3263–3264; (b) G. Siddiqi, V. Mougel, C. Coperet, *Dalton Transactions* **2015**, *44*, 14349–14353; (c) C. Hoch, M. Wendorff, C. Röhr, *J. Alloys Compd.* **2003**, *361*, 206–221.

[34] (a) W. Carrillo-Cabrera, R. Cardoso Gil, M. Somer, Ö. Persil, H. G. von Schnering, *Z. Anorg. Allg. Chem.* **2003**, *629*, 601–608.

[35] J. M. Goicoechea, S. C. Sevov, *Organometallics* **2006**, *25*, 4530–4536.

[36] M. Waibel, F. Kraus, S. Scharfe, B. Wahl, T. F. Fässler, *Angew. Chem. Int. Ed.* **2010**, *49*, 6611–6615.

[37] (a) G. Gnutzmann, F. Wilhelm Dorn, W. Klemm, *Z. Anorg. Allg. Chem.* **1961**, *309*, 210–225; (b) G. Brauer, E. Zintl, *Z. Phys. Chem. Abt. B* **1937**, *37*, 323–352; (c) D. E. Sands, D. H. Woods, W. J. Ramsey, *Acta Cryst.* **1963**, *16*, 316.

[38] Y. Wang, P. Zavalij, B. Eichhorn, *Chem. Commun.* **2018**, *54*, 11917–11920.

[39] (a) E. Amberger, R. W. Salazar G, *J. Organomet. Chem.* **1967**, *8*, 111–114; (b) J. Bruckmann, C. Kruger, *Acta Cryst.* **1995**, *C51*, 1152–1155; (c) K. Merz, R. Bieda, *Z. Kristallogr. - Cryst. Mater.* **2014**, *229*, 635; (d) H. J. Breunig, M. Jönsson, R. Rösler, E. Lork, *J. Organomet. Chem.* **2000**, *608*, 60–62; (e) G. Becker, M. Rößler, *Z. Naturforsch. B.* **1982**, *37*, 91.

[40] F. Gascoin, S. C. Sevov, *J. Am. Chem. Soc.* **2000**, *122*, 10251–10252.

[41] (a) M. Somer, M. Hartweg, K. Peters, H. G. von Schnering, *Z. Kristallogr. - Cryst. Mater.* **1991**, *195*, 103; (b) F. Gascoin, S. C. Sevov, *Inorg. Chem.* **2001**, *40*, 5177–5181.

[42] L. Xu, S. Bobev, J. El-Bahraoui, S. C. Sevov, *J. Am. Chem. Soc.* **2000**, *122*, 1838–1839.

[43] (a) S. C. Critchlow, J. D. Corbett, *Inorg. Chem.* **1984**, *23*, 770–774; (b) A. Cisar, J. D. Corbett, *Inorg. Chem.* **1977**, *16*, 2482–2487.

[44] (a) H. G. von Schnering, W. Hönle, *Z. Anorg. Allg. Chem.* **1979**, *456*, 194–206; (b) F. Emmerling, C. Röhr, *Z. Naturforsch. B.* **2002**, *57*, 963; (c) E. Busmann, S. Lohmeyer, *Z. Anorg. Allg. Chem.* **1961**, *312*, 53–59; (d) F. Emmerling, N. Längin, D. Petri, M. Kroeker, C. Röhr, *Z. Anorg. Allg. Chem.* **2004**, *630*, 171–178.

[45] S. Ponou, N. Müller, T. F. Fässler, U. Häussermann, *Inorg. Chem.* **2005**, *44*, 7423–7430.

[46] H. G. von Schnering, M. Somer, G. Kliche, W. Hönle, T. Meyer, J. Wolf, L. Ohse, P. B. Kempa, *Z. Anorg. Allg. Chem.* **1991**, *601*, 13–30.

[47] (a) V. Manriquez, W. Hönle, H. G. von Schnering, *Z. Anorg. Allg. Chem.* **1986**, *539*, 95–109; (b) C. Hirschle, C. Röhr, *Z. Anorg. Allg. Chem.* **2000**, *626*, 1992–1998.

[48] (a) L. Xu, A. Ugrinov, S. C. Sevov, *J. Am. Chem. Soc.* **2001**, *123*, 4091–4092; (b) J. M. Goicoechea, M. W. Hull, S. C. Sevov, *J. Am. Chem. Soc.* **2007**, *129*, 7885–7893; (c) L. G. Perla, S. C. Sevov, *Inorg. Chem.* **2015**, *54*, 8401–8405.

[49] (a) K. Wiesler, K. Brandl, A. Fleischmann, N. Korber, *Z. Anorg. Allg. Chem.* **2009**, *635*, 508–512; (b) M. Neumeier, F. Fendt, S. Gartner, C. Koch, T. Gartner, N. Korber, R. M. Gschwind, *Angew. Chem. Int. Ed.* **2013**, *52*, 4483–4486; (c) C. B. Benda, T. Henneberger, W. Klein, T. F. Fässler, *Z. Anorg. Allg. Chem.* **2017**, *643*, 146–148; (d) C. Lorenz, S. Gärtner, N. Korber, *Z. Anorg. Allg. Chem.* **2017**, *643*, 141–145; (e) M. Waibel, T. Henneberger, L.-A. Jantke, T. F. Fässler, *Chem. Commun.* **2012**, *48*, 8676–8678.

[50] (a) J. M. Goicoechea, S. C. Sevov, *J. Am. Chem. Soc.* **2004**, *126*, 6860–6861; (b) C. H. E. Belin, J. D. Corbett, A. Cisar, *J. Am. Chem. Soc.* **1977**, *99*, 7163–7169; (c) C. Downie, J.-G. Mao, A. M. Guloy, *Inorg. Chem.* **2001**, *40*, 4721–4725; (d) R. C. Burns, J. D. Corbett, *Inorg. Chem.* **1985**, *24*, 1489–1492; (e) J. Campbell, D. A. Dixon, H. P. A. Mercier, G. J. Schrobilgen, *Inorg. Chem.* **1995**, *34*, 5798–5809.

[51] (a) C. Suchentrunk, N. Korber, *New J. Chem.* **2006**, *30*, 1737–1739; (b) P. A. Edwards, J. D. Corbett, *Inorg. Chem.* **1977**, *16*, 903–907.

[52] L. Schiegerl, A. Karttunen, W. Klein, T. F. Fässler, *Chem. Eur. J.* **2018**, *24*, 19171–19174.

[53] (a) F. Kraus, N. Korber, *Chem. Eur. J.* **2005**, *11*, 5945–5959; (b) T. Hanauer, M. Grothe, M. Reil, N. Korber, *Helv. Chim. Acta* **2005**, *88*, 950–961; (c) M. Somer, W. Hönle, H. G. von Schnering, *Z. Naturforsch. B.* **1989**, *44*, 296; (d) F. Mutzbauer, N. Korber, *Acta Cryst.* **2011**, *E67*, 1551.

[54] T. Hanauer, F. Kraus, M. Reil, N. Korber, *Monatsh. Chem.* **2006**, *137*, 147–156.

[55] (a) D. Knettel, M. Reil, N. Korber, *Z. Naturforsch. B.* **2001**, *56*, 965–969; (b) C. H. E. Belin, *J. Am. Chem. Soc.* **1980**, *102*, 6036–6040; (c) U. Bolle, W. Tremel, *J. Chem. Soc. Chem. Commun.* **1992**, 91–93; (d) B. Weinert, A. R. Eulenstein, R. Ababei, S. Dehnen, *Angew. Chem. Int. Ed.* **2014**, *53*, 4704–4708.

[56] F. Lips, I. Schellenberg, R. Pöttgen, S. Dehnen, *Chem. Eur. J.* **2009**, *15*, 12968–12973.

[57] S. C. Critchlow, J. D. Corbett, *Inorg. Chem.* **1982**, *21*, 3286–3290.

[58] L. Xu, S. C. Sevov, *Inorg. Chem.* **2000**, *39*, 5383–5389.

[59] R. Ababei, J. Heine, M. Holynska, G. Thiele, B. Weinert, X. Xie, F. Weigend, S. Dehnen, *Chem. Commun.* **2012**, *48*, 11295–11297.

[60] (a) R. J. Wilson, L. Broeckaert, F. Spitzer, F. Weigend, S. Dehnen, *Angew. Chem. Int. Ed.* **2016**, *55*, 11775–11780; (b) R. J. Wilson, S. Dehnen, *Unveröffentlichte Ergebnisse*; (c) A. R. Eulenstein, S. Mitzinger, S. Dehnen, *Unveröffentlichte Ergebnisse.*

[61] N. Lichtenberger, S. Dehnen, *Unveröffentlichte Ergebnisse.*

[62] S. S. Dehnen, S. Mitzinger, J. Bandemehr, J. F. Corrigan, F. Weigend, K. Reiter, J. S. McIndoe, X. Xie, *Chem. Commun.* **2017**, *54*, 1421–1424.

[63] S. Mitzinger, L. Broeckaert, W. Massa, F. Weigend, S. Dehnen, *Nat. Commun.* **2016**, *7*, 10480.

[64] M. M. Gillett-Kunnath, A. G. Oliver, S. C. Sevov, *J. Am. Chem. Soc.* **2011**, *133*, 6560–6562.

[65] R. J. Wilson, S. Dehnen, *Angew. Chem. Int. Ed.* **2017**, *56*, 3098–3102.

[66] R. C. Haushalter, B. W. Eichhorn, A. L. Rheingold, S. J. Geib, *J. Chem. Soc. Chem. Commun.* **1988**, 1027–1028.

[67] U. Friedrich, M. Neumeier, C. Koch, N. Korber, *Chem. Commun.* **2012**, *48*, 10544–10546.

[68] (a) A. Purath, R. Köppe, H. Schnöckel, *Angew. Chem. Int. Ed.* **1999**, *38*, 2926–2928; (b) A. Schnepf, G. Stosser, H. Schnöckel, *J. Am. Chem. Soc.* **2000**, *122*, 9178–9181; (c) A. Schnepf, H. Schnöckel, *Angew. Chem. Int. Ed.* **2002**, *41*, 3532–3554.

[69] E. N. Esenturk, J. Fettinger, Y. F. Lam, B. Eichhorn, *Angew. Chem. Int. Ed.* **2004**, *43*, 2132–2134.

[70] C. Döring, A.-M. Dietel, M. V. Butovskii, V. Bezugly, F. R. Wagner, R. Kempe, *Chem. Eur. J.* **2010**, *16*, 10679–10683.

[71] J. A. Bertrand, W. A. Dollase, F. A. Cotton, *Inorg. Chem.* **1963**, *2*, 1166–1171.

[72] (a) S. Scharfe, T. F. Fässler, S. Stegmaier, S. D. Hoffmann, K. Ruhland, *Chem. Eur. J.* **2008**, *14*, 4479–4483; (b) E. N. Esenturk, J. Fettinger, B. Eichhorn, *J. Am. Chem. Soc.* **2006**, *128*, 9178–9186.

[73] J. Q. Wang, S. Stegmaier, B. Wahl, T. F. Fässler, *Chem. Eur. J.* **2010**, *16*, 1793–1798.

[74] (a) E. N. Esenturk, J. Fettinger, B. Eichhorn, *Chem. Commun.* **2005**, 247–249; (b) A. Spiekermann, S. D. Hoffmann, T. F. Fässler, *Angew. Chem. Int. Ed.* **2006**, *45*, 3459–3462; (c) M. M. Bentlohner, C. Fischer, T. F. Fässler, *Chem. Commun.* **2016**, *52*, 9841–9843.

[75] (a) J. M. Goicoechea, S. C. Sevov, *J. Am. Chem. Soc.* **2005**, *127*, 7676–7677; (b) E. N. Esenturk, J. C. Fettinger, B. W. Eichhorn, *J. Am. Chem. Soc.* **2006**, *128*, 12–13; (c) Z. M. Sun, H. Xiao, J. Li, L. S. Wang, *J. Am. Chem. Soc.* **2007**, *129*, 9560–9561; (d) F. S. Kocak, P. Zavalij, Y. F. Lam, B. W. Eichhorn, *Inorg. Chem.* **2008**, *47*, 3515–3520; (e) X. Jin, G. Espinoza-Quintero, B. Below, V. Arcisauskaite, J. M. Goicoechea, J. E. McGrady, *J. Organomet. Chem.* **2015**, *792*, 149–153; (f) C. Liu, I. A. Popov, L.-J. Li, N. Li, A. I. Boldyrev, Z.-M. Sun, *Chem. Eur. J.* **2018**, *24*, 699–705.

[76] (a) B. Zhou, M. S. Denning, D. L. Kays, J. M. Goicoechea, *J. Am. Chem. Soc.* **2009**, *131*, 2802–2803; (b) J. Q. Wang, S. Stegmaier, T. F. Fässler, *Angew. Chem. Int. Ed.* **2009**, *48*, 1998–2002; (c) G. Espinoza-Quintero, J. C. Duckworth, W. K. Myers, J. E. McGrady, J. M. Goicoechea, *J. Am. Chem. Soc.* **2014**, *136*, 1210–1213.

[77] (a) M. J. Moses, J. C. Fettinger, B. W. Eichhorn, *Science* **2003**, *300*, 778–780; (b) Y. Wang, M. Moses-DeBusk, L. Stevens, J. Hu, P. Zavalij, K. Bowen, B. I. Dunlap, E. R. Glaser, B. Eichhorn, *J. Am. Chem. Soc.* **2017**, *139*, 619–622.

[78] (a) J. M. Goicoechea, S. C. Sevov, *Angew. Chem. Int. Ed.* **2006**, *45*, 5147–5150; (b) X. Min, I. A. Popov, F. X. Pan, L. J. Li, E. Matito, Z. M. Sun, L. S. Wang, A. I. Boldyrev, *Angew. Chem. Int. Ed.* **2016**, *55*, 5531–5535.

[79] (a) F.-X. Pan, L.-J. Li, Y.-J. Wang, J.-C. Guo, H.-J. Zhai, L. Xu, Z.-M. Sun, *J. Am. Chem. Soc.* **2015**, *137*, 10954–10957; (b) I. A. Popov, F.-X. Pan, X.-R. You, L.-J. Li, E. Matito, C. Liu, H.-J. Zhai, Z.-M. Sun, A. I. Boldyrev, *Angew. Chem. Int. Ed.* **2016**, *55*, 15344–15346.

[80] J. M. Goicoechea, S. C. Sevov, *Angew. Chem. Int. Ed.* **2005**, *44*, 4026–4028.

[81] (a) B. Kesanli, J. Fettinger, B. Eichhorn, *Angew. Chem. Int. Ed.* **2001**, *40*, 2300–2302.

[82] K. H. Whitmire, *Coord. Chem. Rev.* **2018**, *376*, 114–195.

[83] M. J. Moses, J. Fettinger, B. Eichhorn, *J. Am. Chem. Soc.* **2002**, *124*, 5944–5945.

[84] B. Zhou, J. M. Goicoechea, *Chem. Eur. J.* **2010**, *16*, 11145–50.

[85] L. G. Perla, S. C. Sevov, *Angew. Chem. Int. Ed.* **2016**, *55*, 6721–6724.

[86] Y. Wang, P. Zavalij, B. Eichhorn, *Chem. Commun.* **2017**, *53*, 11600–11602.

[87] (a) F. Lips, S. Dehnen, *Angew. Chem. Int. Ed.* **2009**, *48*, 6435–6438; (b) F. Lips, S. Dehnen, *Angew. Chem. Int. Ed.* **2011**, *50*, 955–959; (c) R. J. Wilson, F. Hastreiter, K. Reiter, P. Buschelberger, R. Wolf, R. M. Gschwind, F. Weigend, S. Dehnen, *Angew. Chem. Int. Ed.* **2018**, *57*, 15359–15363.

[88] (a) F. Lips, R. Clérac, S. Dehnen, *Angew. Chem. Int. Ed.* **2011**, *50*, 960–964; (b) F. Lips, M. Holynska, R. Clérac, U. Linne, I. Schellenberg, R. Pöttgen, F. Weigend, S. Dehnen, *J. Am. Chem. Soc.* **2012**, *134*, 1181–1191; (c) B. Weinert, F. Weigend, S. Dehnen, *Chem. Eur. J.* **2012**, *18*, 13589–13595; (d) B. Weinert, F. Müller, K. Harms, R. Clérac, S. Dehnen, *Angew. Chem. Int. Ed.* **2014**, *53*, 11979–11983; (e) R. Ababei, W. Massa, B. Weinert, P. Pollak, X. Xie, R. Clérac, F. Weigend, S. Dehnen, *Chem. Eur. J.* **2015**, *21*, 386–394; (f) N. Lichtenberger, R. J. Wilson, A. R. Eulenstein, W. Massa, R. Clérac, F. Weigend, S. Dehnen, *J. Am. Chem. Soc.* **2016**, *138*, 9033–9036.

[89] (a) F. X. Pan, L. J. Li, Z. M. Sun, *Chin. J. Struct. Chem.* **2016**, *35*, 1099–1106; (b) D. P. Huang, J. D. Corbett, *Inorg. Chem.* **1998**, *37*, 5007–5010; (c) L. J. Li, F. X. Pan, F. Y. Li, Z. F. Chen, Z. M. Sun, *Inorg. Chem. Front.* **2017**, *4*, 1393–1396.

[90] F. Lips, R. Clérac, S. Dehnen, *J. Am. Chem. Soc.* **2011**, *133*, 14168–14171.

[91] F. X. Pan, C. Q. Xu, L. J. Li, X. Min, J. Q. Wang, J. Li, H. J. Zhai, Z. M. Sun, *Dalton Trans.* **2016**, *45*, 3874–3879.

[92] C. Liu, L. Li, I. A. Popov, R. J. Wilson, C. Xu, J. Li, A. I. Boldyrev, Z. Sun, *Chin. J. Chem.* **2018**, DOI `10.1002/cjoc.201800434`.

[93] (a) T. Kramer, J. C. Duckworth, M. D. Ingram, B. Zhou, J. E. McGrady, J. M. Goicoechea, *Dalton Trans.* **2013**, *42*, 12120–12129; (b) J. M. Goicoechea, J. E. McGrady, *Dalton Trans.* **2015**, *44*, 6755–6766; (c) X. Jin, V. Arcisauskaite, J. E. McGrady, *Dalton Trans.* **2017**, *46*, 11636–11644.

[94] (a) A. Schnepf, *Angew. Chem. Int. Ed.* **2003**, *42*, 2624–2625; (b) F. Li, S. C. Sevov, *J. Am. Chem. Soc.* **2014**, *136*, 12056–12063; (c) F. Li, S. C. Sevov, *Inorg. Chem.* **2015**, *54*, 8121–8125; (d) O. Kysliak, C. Schrenk, A. Schnepf, *Chem. Eur. J.* **2016**, *22*, 18787–18793; (e) L. G. Perla, S. C. Sevov, *J. Am. Chem. Soc.* **2016**, *138*, 9795–9798; (f) M. Binder, C. Schrenk, T. Block, R. Pöttgen, A. Schnepf, *Chem. Commun.* **2017**, *53*, 11314–11317; (g) L. G. Perla, A. Munoz-Castro, S. C. Sevov, *J. Am. Chem. Soc.* **2017**, *139*, 15176–15181.

[95] M. M. Bentlohner, L. A. Jantke, T. Henneberger, C. Fischer, K. Mayer, W. Klein, T. F. Fässler, *Chem. Eur. J.* **2016**, *22*, 13946–13952.

[96] J. Q. Wang, B. Wahl, T. F. Fässler, *Angew. Chem. Int. Ed.* **2010**, *49*, 6592–6595.

[97] N. Lichtenberger, Masterarbeit, Philipps-Universität Marburg, **2013**.

[98] N. Lichtenberger, N. Spang, A. Eichhöfer, S. Dehnen, *Angew. Chem.* **2017**, *129*, 13436–13442.

[99] (a) W. Blase, G. Cordier, *Z. Kristallogr.* **1990**, *193*, 319–320; (b) W. Blase, G. Cordier, *Z. Kristallogr.* **1991**, *196*, 207–211.

[100] L. Chi, J. D. Corbett, *Inorg. Chem.* **2001**, *40*, 2705–2708.

[101] R. C. Burns, J. D. Corbett, *J. Am. Chem. Soc.* **1982**, *104*, 2804–2810.

[102] N. Lichtenberger, W. Massa, S. Dehnen, *Angew. Chem. Int. Ed.* **2019**, DOI `10.1002/anie.201812473`.

[103] R. J. Wilson, N. Lichtenberger, B. Weinert, S. Dehnen, *Manuskript eingereicht.*

[104] N. Lichtenberger, A. R. Eulenstein, R. J. Wilson, S. Dehnen, *Manuskript in Vorbereitung.*

[105] G. Thiele, N. Lichtenberger, R. Tonner, S. Dehnen, *Z. Anorg. Allg. Chem.* **2013**, *639*, 2809–2815.

A Publikationsliste

Publikationen in Fachjournalen

7. N. Lichtenberger, A. R. Eulenstein, R. J. Wilson, S. Dehnen, *Manuskript in Vorbereitung.*

6. R. J. Wilson, N. Lichtenberger, B. Weinert, S. Dehnen, *Manuskript eingereicht.**

5. N. Lichtenberger, W. Massa, S. Dehnen, *Angew. Chem. Int. Ed.* **2019**, DOI 10.1002/anie.201812473.*

4. N. Lichtenberger, Y. J. Franzke, W. Massa, F. Weigend, S. Dehnen, *Chem. Eur. J.* **2018**, *24*, 12022–12030.*

3. N. Lichtenberger, N. Spang, A. Eichhöfer, S. Dehnen, *Angew. Chem. Int. Ed.* **2017**, *56*, 13253–13258.*

2. N. Lichtenberger, R. J. Wilson, A. R. Eulenstein, W. Massa, R. Clérac, F. Weigend, S. Dehnen, *J. Am. Chem. Soc.* **2016**, *138*, 9033–9036.*

1. G. Thiele, N. Lichtenberger, R. Tonner, S. Dehnen, *Z. Anorg. Allg. Chem.* **2013**, *639*, 2809–2815.

Mit * gekennzeichnete Publikationen sind Gegenstand dieser Dissertationsschrift.

B Lebenslauf

Zum Schutz personenbezogener Daten wurde der Lebenslauf aus der öffentlich zugänglichen Version dieser Dissertationsschrift entfernt.

The CV has been removed from the publically available version of this document for the protection of personal data.

C Elektronische Zusatzinformationen der Publikationen

Inhalt

C.1 Main Group Metal-Actinide Magnetic Coupling and Structural Response Upon U^{4+} Inclusion Into Bi, Tl/Bi, or Pb/Bi Cages

Supporting Information

Main Group Metal–Actinide Magnetic Coupling and Structural Response Upon U^{4+} Inclusion Into Bi, Tl/Bi, or Pb/Bi Cages

Niels Lichtenberger,[†] Robert J. Wilson,[†] Armin R. Eulenstein,[†] Werner Massa,[†] Rodolphe Clérac,[◊,∅] Florian Weigend,[‡,§] and Stefanie Dehnen*[,†]

[†] *Fachbereich Chemie und Wissenschaftliches Zentrum für Materialwissenschaften (WZMW), Philipps-Universität Marburg, Hans-Meerwein-Straße, 35043 Marburg, Germany.*

[‡] *Institut für Physikalische Chemie, Karlsruher Institut für Technologie (KIT), Fritz-Haber-Weg 2, 76131 Karlsruhe, Germany.*

[§] *Institut für Nanotechnologie, Karlsruher Institut für Technologie, Hermann-von-Helmholtz Platz 1, D-76344 Eggenstein-Leopoldshafen, Germany.*

[◊] *CNRS, CRPP, UPR 8641, F-33600 Pessac, France.*

[∅] *Univ. Bordeaux, CRPP, UPR 8641, F-33600 Pessac, France.*

Contents

1. Synthesis Details

1.1. General

All manipulations and reactions were performed under dry Ar atmosphere using standard Schlenk or glovebox techniques. All solvents were dried and freshly distilled prior to use. Crypt-222[1] (Merck) was dried *in vacuo* for at least 18 hours. $[K(crypt\text{-}222)]_2(GaBi_3)\cdot en$[2] and KPbBi[3] were prepared according to the literature procedures. $[U(C_5Me_4H)_3]$[4] (**A**, C_5Me_4H is denoted as $Cp^{\#}$ in the following)[5] was prepared according to a modified literature procedure wherein $[UCp^{\#}_3Cl]$[6] was synthesized from UCl_4 by metathesis with $KCp^{\#}$, followed by reduction with sodium naphthalenide. Purity of the highly crystalline $[UCp^{\#}_3]$ and $[UCp^{\#}_3Cl]$ was confirmed by powder X-ray diffraction (Section 1.2). A phase with a nominal composition "$K_2Tl_1Bi_3$" was synthesized by combining K, Tl, and Bi in stoichiometric amounts in a niobium ampoule. The ampoule was then sealed by arc-welding and was placed in an oven. Upon extraction of the resultant phase with en/crypt-222, $[K(crypt\text{-}222)]_2(TlBi_3)\cdot 0.5en$ was obtained in crystalline form after removal of the solvent.[7] Samples were shielded from ambient light throughout cluster syntheses.

1.2. Characterization of the used Precursors $[UCp^{\#}_3]$ and $[UCp^{\#}_3Cl]$

Powder X-ray diffraction patterns of $[UCp^{\#}_3]$ and $[UCp^{\#}_3Cl]$ were measured on a Stoe StadiMP diffractometer system equipped with a Mythen 1K silicon strip detector and a Cu-K_α (λ = 1.54056 Å) radiation source. The small dark red ($[UCp^{\#}_3]$) or bright red ($[UCp^{\#}_3Cl]$) crystals were filled into a 0.6 mm mark tube which was then sealed air-tight with soft wax. The tube was then mounted onto the goniometer head using wax (horizontal setup) and rotated throughout the measurement. Figures S1 and S2 show the measured diffraction patterns in comparison with the simulated ones for both starting compounds.

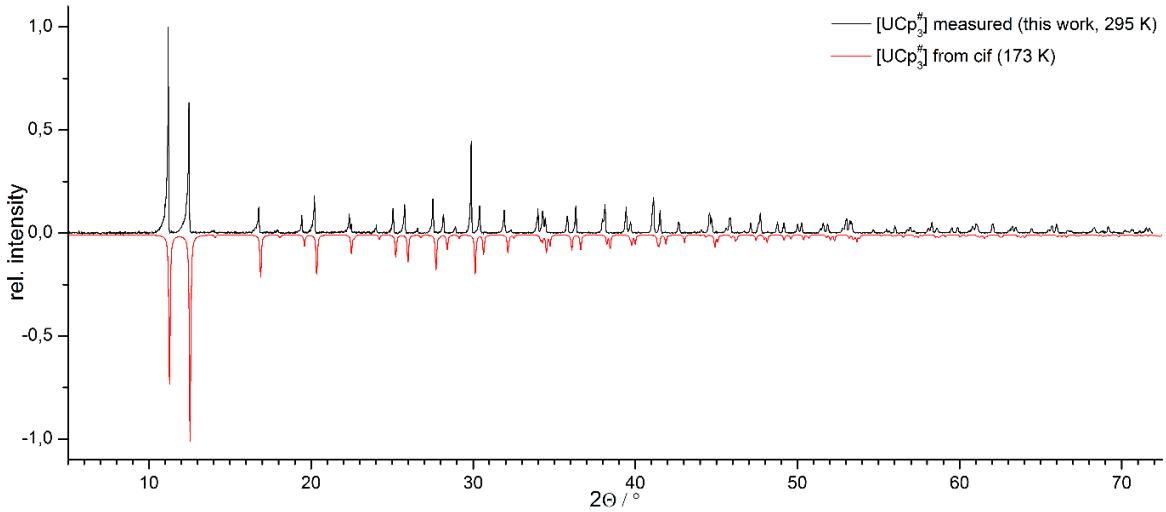

Figure S1. Comparison of the measured (black line) and simulated (red line) diffraction pattern of the prepared [UCp$^{\#}_3$]. The increasing shift of reflection position with higher angles is due to the change of the lattice parameters caused by different temperatures used for the single-crystal and powder X-ray diffraction measurements. The pronounced peak asymmetry is caused by the used slit collimator as well as by the detector system.

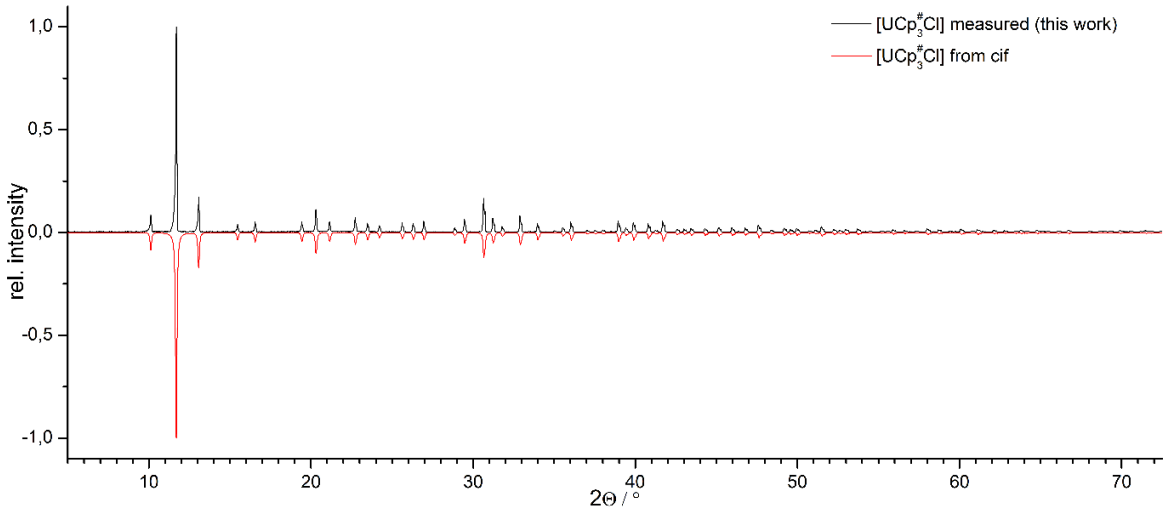

Figure S2. Comparison of the measured (black line) and simulated (red line) diffraction pattern of the prepared [UCp$^{\#}_3$Cl]. The pronounced peak asymmetry is caused by the used slit collimator as well as by the detector system.

1.3. Syntheses

1.3.1. Synthesis of [K(crypt-222)]$_3$[U@Bi$_{12}$]·tol·1.5en (1)

90 mg (0.060 mmol) of [K(crypt-222)]$_2$[GaBi$_3$]·en and 18 mg (0.030 mmol) of [UCp$^{\#}{}_3$] or 19 mg (0.030 mmol) of [UCp$^{\#}{}_3$Cl], respectively, were combined in a Schlenk tube and dissolved in en (5 mL). The initially dark green solution slowly changed to dark brown. The reaction mixture was allowed to stir for 3 hours. The resulting dark brown solution was filtered through a standard glass frit, carefully layered with toluene (5 mL), and stored for crystallization at 5 °C. After 10 days, block-like crystals of compound **1** formed at the wall of the Schlenk tube in appr. 13% yield.

1.3.2. Synthesis of [K(crypt-222)]$_2$[K(crypt-222)(en)][U@Tl$_2$Bi$_{11}$]·tol (2)

100 mg (0.059 mmol) of [K(crypt-222)]$_2$(TlBi$_3$)·0.5en and 18 mg (0.030 mmol) of [UCp$^{\#}{}_3$] or 19 mg (0.030 mmol) of [UCp$^{\#}{}_3$Cl], respectively, were combined in a Schlenk tube and dissolved in 5 mL of en, initially forming a greenish brown solution. The reaction was filtered through a standard glass frit after stirring for 3 hours, yielding a goldish brown solution. The solution was then layered with 5 mL of toluene and stored at 5 °C, affording 42 mg (65 %) of **2** as thin black plates after 4 weeks.

1.3.3. Synthesis of [K(crypt-222)]$_3$[U@Pb$_7$Bi$_7$]$_{0.660}$[U@Pb$_4$Bi$_9$]$_{0.340}$·2tol (3)

A phase of the nominal composition "KPbBi" (105 mg, 0.231 mmol), crypt-222 (93 mg, 0.25 mmol), and [UCp$^{\#}{}_3$] (40 mg, 0.066 mmol) or [UCp$^{\#}{}_3$Cl] (35 mg, 0.055 mmol), respectively, were combined in a single Schlenk tube and dissolved in 3 mL of en. The mixture was stirred for 3 hours before being filtered through a standard glass frit. The resulting dark red/brown solution was carefully layered with 4 mL of toluene and allowed to stand at 5 °C. After 32 days, the solvent was removed and the sample was dried, affording 38 mg (28%) of **3** as black crystalline material.

All yields are given as minimum numbers that were obtained in reactions with [UCp$^{\#}{}_3$]. The use of [UCp$^{\#}{}_3$Cl] led to a slight increase of the crystalline yield in all cases. Scheme S1 summarizes the described syntheses.

Scheme S1. General synthesis of compounds 1, 2, and 3.

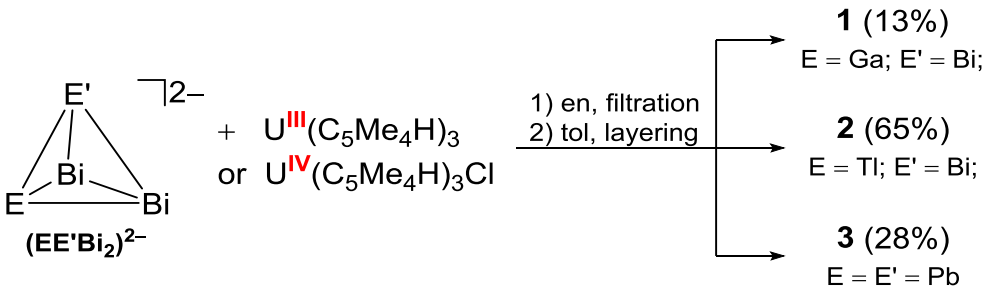

2. Single Crystal X-ray Diffraction

2.1. General

The data for the X-ray structural analyses were collected at T = 100(2) K with Mo-K_α-radiation (λ = 0.71073 Å) on area detector systems Stoe IPDS2 for **1** and Stoe IPDS/2T for **2** and **3**. Structure **1** was solved by direct methods (SHELXS-2013).[8] For **2** and **3** the models were developed from isostructural compounds. The refinement was done by full-matrix-least-squares methods against F^2 with the program SHELXL-2013.[9] All hydrogen atoms were kept riding on calculated positions with isotropic displacement parameters U = 1.2 U_{eq} (or 1.5 U_{eq} for methyl groups) of the bonding partners. Crystallographic data for the three structures reported in this paper have been deposited with the Cambridge Crystallographic Data Center as supplementary publications nos. CCDC-147446 (**1**), CCDC-147447 (**2**), and CCDC-147448 (**3**). The crystal data and experimental parameters of the structure determinations are collected in Table S1.

Table S1. Crystal data and details of the structure determinations of 1 - 3.

Compound	**1**	**2**	**3**
empirical formula	$C_{64}H_{84}Bi_{12}K_3N_9O_{18}U$	$C_{63}H_{124}Bi_{11}K_3N_8O_{18}Tl_2U$	$C_{68}H_{124}Bi_{7.68}K_3N_6O_{18}Pb_{5.98}U$
formula weight [g mol^{-1}]	4130.49	4344.54	4512.92
crystal color, shape	black, block	black, platelet	black, block
crystal size [mm^3]	0.22×0.15×0.13	0.18×0.12×0.06	0.13×0.10×0.098
crystal system	orthorhombic	monoclinic	monoclinic
space group	*Pba*2	$P2_1/m$	$P2_1/n$
a [Å]	31.7268(6)	14.6092(4)	15.1698(3)
b [Å]	39.3976(12)	21.8659(5)	23.0713(5)
c [Å]	16.6980(3)	16.3877(5)	30.3293(7)
β [°]		106.917(2)	96.032(2)
V [Å^3]	20871.8(8)	5008.4(2)	10556.1(4)
Z, ρ_{calc} [g cm^{-3}]	8, 2.629	2, 2.899	4, 2.840
μ ($Mo_{K\alpha}$) [mm^{-1}]	21.871	24.239	23.946
absorption correction type	numerical	numerical	numerical
2θ range [°]	2.76 – 50.00	3.29 - 50.00	4.95 - 53.62
total reflns	115730	39094	93332
unique reflns [R_{int}]	35066	9084	22367
obs. Reflns [$I > 2\sigma(I)$]	15911	6799	13792
Parameters	710	585	1027
wR_2 (all data)/ R_1 [$I > 2\sigma(I)$]	0.0935/ 0.0585	0.1275/ 0.0560	0.0653/ 0.0450
GooF (all data)	0.979	1.178	1.151
max peak/hole [e Å^{-3}]	1.38/ –1.06	2.51/ –3.10	1.92/ –2.23

2.2. Details of the Structure Determinations

2.2.1. Structure Determination of [K(crypt-222)]$_3$[U@Bi$_{12}$]·tol·1.5en (1)

The structure of **1** could be solved using direct methods (SHELXS-2013) in the non-centrosymmetric orthorhombic space group *Pba*2. It revealed two independent $[U@Bi_{12}]^{3-}$ anions (Fig. S3) with pseudo-symmetry D_{3h}. The symmetry of the possible centrosymmetric supergroup *Pbam* is clearly broken by the cations. The structure of the quite similar 12-atom cluster anions can be described as assembly of three butterfly-like Bi_4 rings (folding angles 136.6 – 143.7°) connected by short Bi–Bi bonds in the "equatorial" plane (approx.. plane of projection in Fig. S3). The Bi–Bi distances split into three classes: shortest are the bridging bonds between two "equatorial" Bi_A (see Figure 1 in the main document) atoms with 3.030 Å (average over analogous bonds of both anions). Slightly longer are the Bi–Bi bonds within the Bi_4 rings with 3.075 Å. Much longer are the contacts between the "non-equatorial" Bi_B atoms (yellow in Fig S3) with 3.811 Å in average. There are 7 independent cation sites in the structure, two of them (no. 1 and 2) on a 2-fold axis, one of them strongly disordered. From the remaining 5 cations on general positions three could be refined with restraints in bond lengths and 1–3 distances (SAME option in SHELXL) and isotropic displacement parameters, while the other two are strongly disordered. As for the disordered crypt ligands (no. 2, 3, 6) no sensible disorder model could be established. Its contribution to the data set was subtracted by back Fourier transform (PLATON SQUEEZE).[10] Figure S4 shows the four refined $[K(crypt\text{-}222)]^+$ cations. Figure S5 shows the packing in the structure. The arrangement of anion clusters may be derived from a cubic I-centered sphere packing.

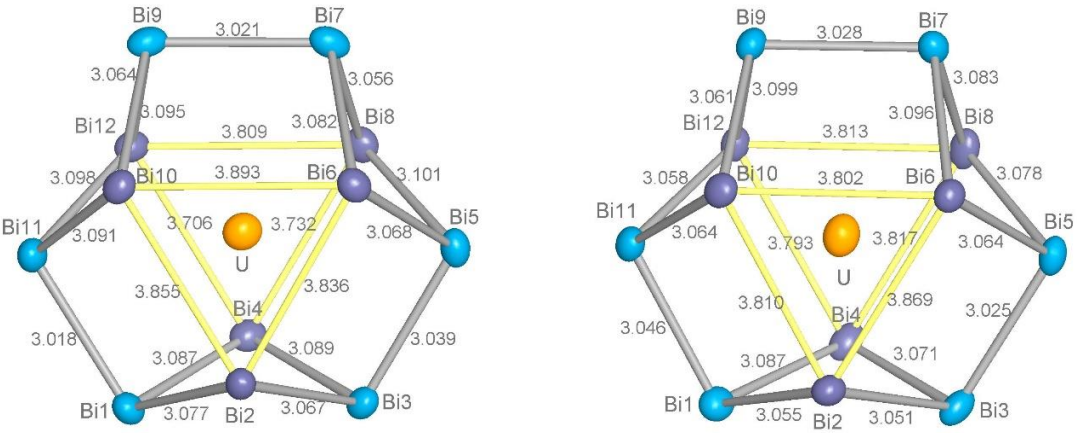

Figure S3. Structure of the anions in 1. Displacement ellipsoids at the 50% probability level. "Equatorial" Bi_A atoms light blue. Bond lengths in Å, esd 0.003 - 0.004 Å. The U–Bi distances are collected in table S2.

Table S2. U–Bi distances (in Å) in the both anions of 1.

	Anion 1	Anion 2		Anion 1	Anion 2
U–Bi1	3.531(3)	3.538(2)	U–Bi7	3.533(2)	3.486(3)
U–Bi2	3.119(3)	3.135(3)	U–Bi8	3.134(3)	3.140(3)
U–Bi3	3.495(3)	3.463(3)	U–Bi9	3.545(3)	3.539(3)
U–Bi4	3.131(3)	3.131(3)	U–Bi10	3.150(3)	3.151(4)
U–Bi5	3.537(3)	3.528(3)	U–Bi11	3.514(3)	3.506(3)
U–Bi6	3.167(4)	3.139(3)	U–Bi12	3.127(3)	3.130(3)
average $U–Bi_A$		3.518	average $U–Bi_B$		3.138

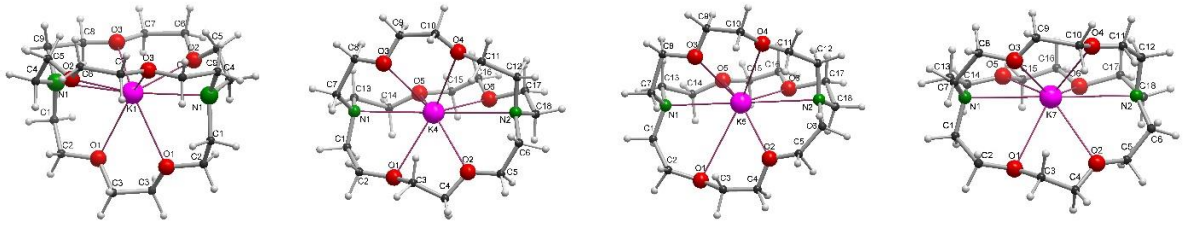

cation 1 (m) cation 4 cation 5 cation 7

Figure S4. Structure of the cations 1, 4, 5, and 7 in 1 as ball and stick models.

In the voids between the anion and cation "spheres" two independent toluene molecules are located. One of them shows disorder of the methyl group that could not be located. Both phenyl rings were refined as idealized rigid groups. In addition, two independent en molecules are found, one of them disordered on a 2-fold axis. It had to be refined using geometrical restraints.

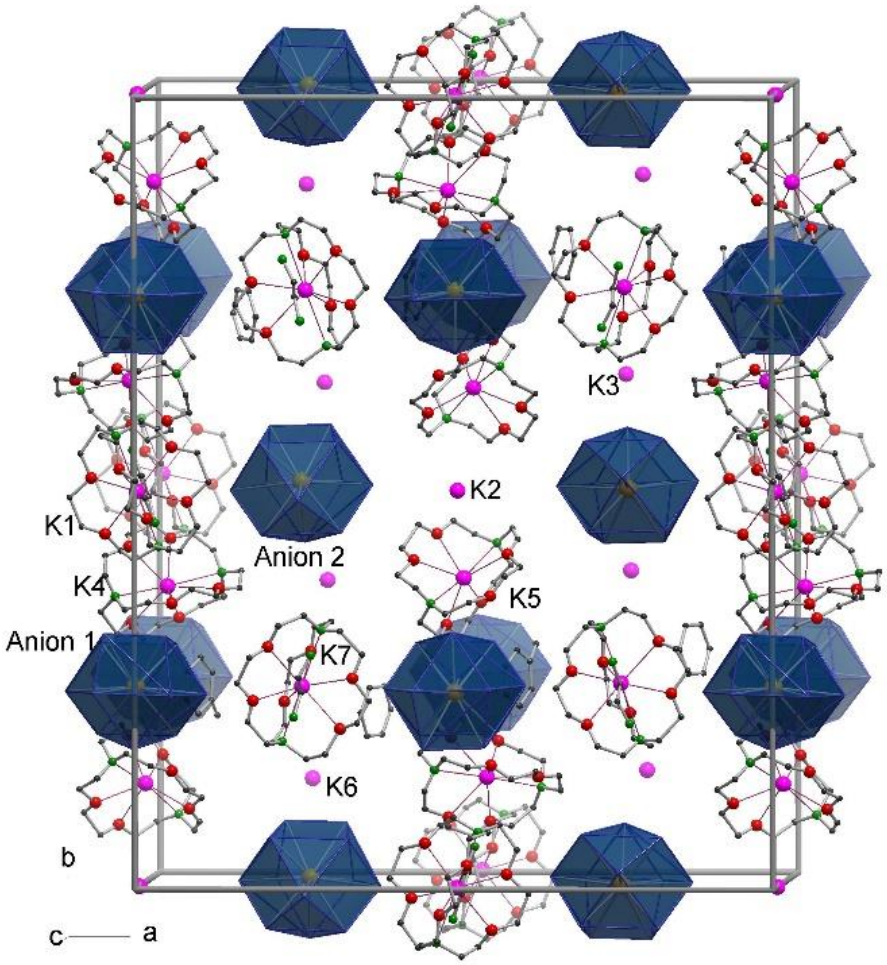

Figure S5. Unit cell of structure 1. Anion clusters as polyhedra, H atoms omitted. Note missing disordered crypt-222 ligands at K2, 3, and 6.

2.2.2. Structure Determination of [K(crypt-222)]$_2$[K(crypt-222)(en)][U@Tl$_2$Bi$_{11}$]·tol (2)

The structure model for **2** could be derived from the quasi-isostructural La compound [K(crypt-222)]$_2$[K(crypt-222)(en)][La@Pb$_6$Bi$_8$]$_{0.038}$[La@Pb$_3$Bi$_{10}$]$_{0.962}$·tol[11] in space group $P2_1/m$. In contrast to that structure, no contribution of a 14-atom cluster was found. The assignment of Tl and Bi is clear due the different distances to the U atom (Table S3). According to the electron density maps, the cluster is disordered with an alternative orientation (11.6(4) %) generated by a 90° rotation around an axis through U and the center of the Tl...Tl line (Fig. S6). The bond lengths are compiled in Table S3. One of the two independent cations, [K(crypt-222)]$^+$, is well ordered on a general position (Fig. S7). A second cation [K(crypt-222)(en)]$^+$ with additional en ligand shows 1:1 disorder by its position on a mirror plane (Fig. S7). The cryptate ligands were refined with geometrical restraints of the bond lengths and 1,3-distances but leaving conformational freedom (SAME option of SHELXL). Even anisotropic displacement parameters could be refined, which indicate high dynamics or disorder of the cryptate ligands. The cluster anions are arranged together with the disordered cations of type 2 and the toluene molecules on the mirror planes parallel to the *a,b* plane (y = 0.25 and 0.75). Cations of type 1 form parallel layers at y = 0 and y = 0.5 (Fig. S8).

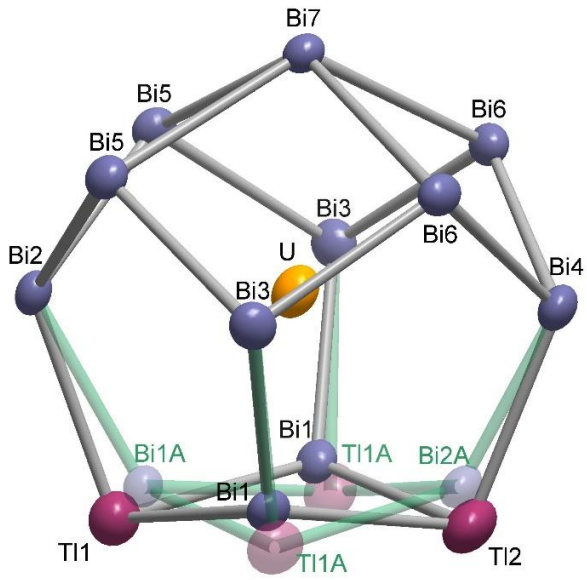

Figure S6. Disordered C_s-symmetric [U@Tl$_2$Bi$_{11}$]$^{3-}$ anion in 2. Displacement ellipsoids at the 50% probability level. Mirror plane through Bi2, Bi4, Bi7. Second orientation (11.4%) transparent, green labels.

Table S3. Interatomic distances [Å] in the anion of 2.

Bi1–Tl1	3.103(1)	Bi3–Bi6	2.9950(9)
Bi1–Tl2	3.093(1)	Bi4–Tl2	3.049(2)
Bi1–Bi3	2.947(1)	Bi4–Bi6	2.9885(9)
Bi2–Tl1	3.060(2)	Bi5–Bi7	3.2944(9)*
Bi2–Bi5	3.0002(8)	Bi6–Bi7	3.2842(9)*
Bi3–Bi5	3.0175(9)		*four-bonded Bi7
U–Tl1	3.774(2)	U–Bi4	3.374(1)
U–Tl2	3.714(2)	U–Bi5	3.4074(9)
U–Bi1	3.229(2)	U–Bi6	3.4289(8)
U–Bi2	3.366(1)	U–Bi7	3.068(1)
U–Bi3	3.4515(6)	U–Tl1a	3.750(9)
U–Bi1a	3.215(1)	U–Bi2a	3.250(1)
average U–Tl	**3.746**	average U–Bi	**3.310**

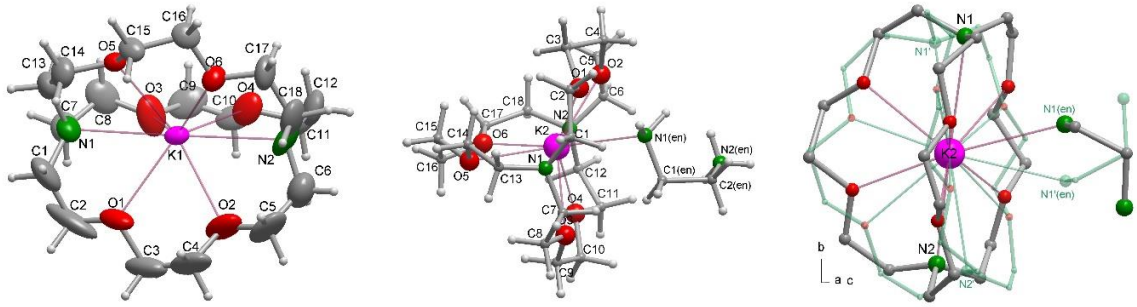

(a) (b) (c)

Figure S7. a) [K(crypt-222)]$^+$ cation 1 of 2. Displacement ellipsoids at the 30% probability level. b) [K(crypt-222)(en)]$^+$ cation 2, ball and stick model, orientation 1. c) Disorder of cation 2 over a mirror plane. Second orientation in transparent green, H atoms omitted. View appr. along the horizontal mirror plane.

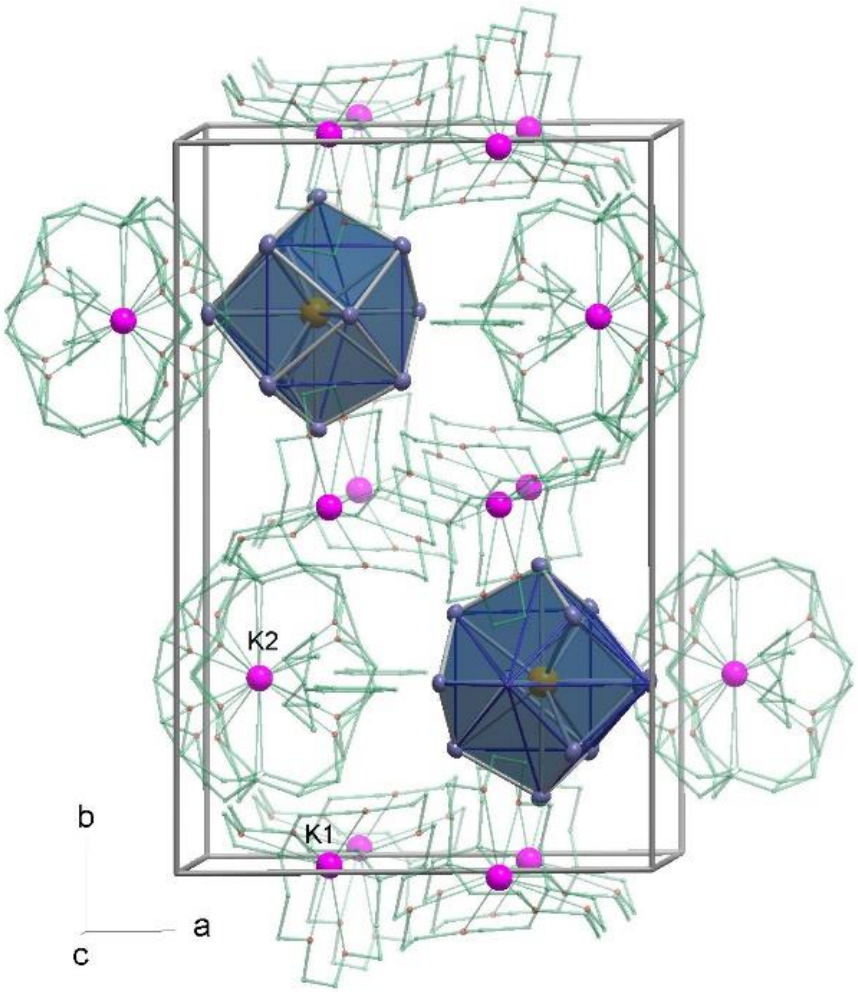

Figure S8. Packing of anions (polyhedra) and cations (wire model) in 2.

2.2.3. Structure Determination of $[K(crypt\text{-}222)]_3[U@Pb_7Bi_7]_{0.66}[U@Pb_4Bi_9]_{0.34}\cdot 2tol$ (3)

For structure **3**, a structure model could be derived from the quasi-isostructural Nd compound $[K(crypt\text{-}222)]_3[Nd@Pb_6Bi_8]_{0.545}[Nd@Pb_3Bi_{10}]_{0.455}\cdot 2tol$[11] in space group $P2_1/n$. Similar to this Nd compound, the cluster region has to be described by superposition of a 14-atom cluster (66.0 %) (Fig. S9) and a 13-atom cluster in three different orientations (1: 23.4 %, 2: 4.5 %, 3: 6.2 %) (Fig. S10). As Bi and Pb are not distinguishable by refinement using data measured with Mo radiation, all heavy metal positions were first half occupied with both elements, and the occupations of the four different cluster types were refined. For the final runs, the distribution of Bi and Pb atoms was calculated assuming the most probable configurations of a $[Pb_7Bi_7]$ 14-atom cluster and a $[Pb_4Bi_9]$ 13-atom cluster in three orientations, as derived from DFT calculations. The occupation numbers are provided in Table S4. Split atoms in the disordered anion closer than 0.5 Å were refined with equal displacement parameters and some bond lengths were restrained. Interatomic distances for the $[U@Pb_7Bi_7]^{3-}$ anion and for the main orientation of the overlaid $[U@Pb_4Bi_9]^{3-}$ anion are given in Table S5. All three independent $[K(crypt\text{-}222)]^+$ cations could be refined using anisotropic displacement parameters (Fig. S11) as well as the two toluene solvent molecules. The packing of structure **3** is shown in Fig. S12. The cations are arranged mainly in layers parallel to the *a,c*-plane at y=0 and 0.5, the anions in parallel layers at y = 0.25 and 0.75.

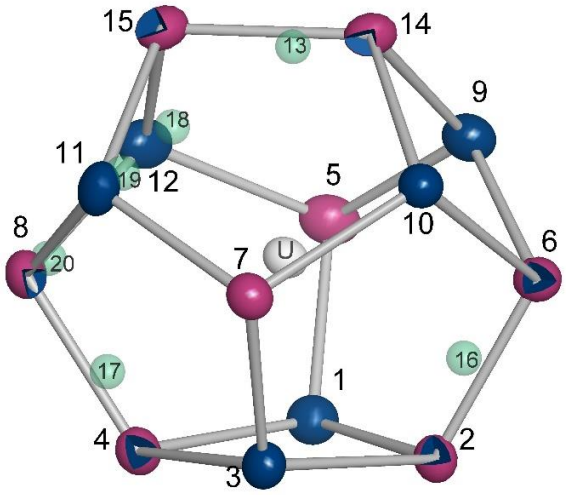

Figure S9. Main component: 14-atom cluster anion $[U@Pb_7Bi_7]^{3-}$ (66.0 %) in 3 and additional disordered Pb/Bi positions (green transparent) interpreted by overlay of a $[U@Pb_4Bi_9]^{3-}$ cluster in three orientations (Fig. S10). Displacement ellipsoids at the 50% probability level. Blue: Bi, red: Pb; red with blue octant: mixed Pb/Bi occupation, see Table S4.

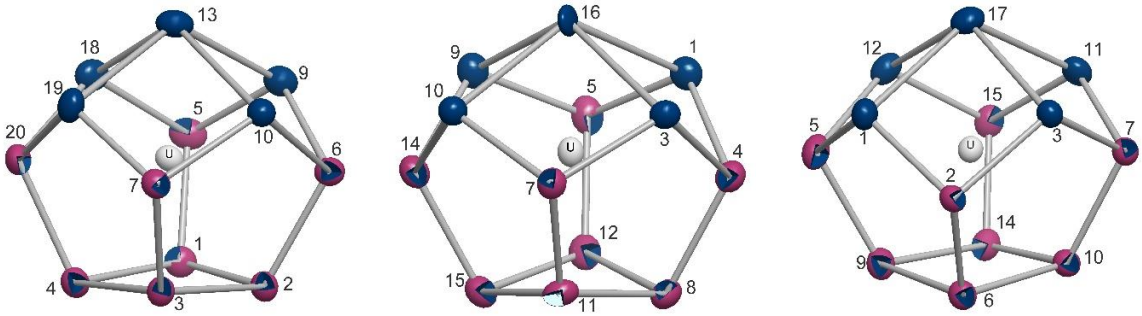

13-Cluster 1, 23.4 % 13-Cluster 2, 4.5 % 13-Cluster 3, 6.2 %

Figure S10. The three overlaid 13-atom cluster anions in 3 in comparable orientations. Atom numbering like in Fig. S9. Displacement ellipsoids at the 50% probability level. Blue: Bi, red with blue octant: mixed Pb/Bi site, see Table S4.

Table S4. Occupations by Bi and Pb for the atom sites in the disordered anions of 3, see Figs. S9, S10.

No.	1	2	3	4	5	6	7	8	9
Bi	0.8829	0.2578	0.8829	0.2493	0.1702	0.2578	0.1702	0.1322	0.9691
Pb	0.1171	0.6975	0.1171	0.6890	0.8298	0.6975	0.8298	0.5719	0.0308

No.	10	11	12	13	14	15	16	17	18
Bi	0.9691	0.7435	0.7435	0.2342	0.1631	0.1631	0.0616	0.0778	0.2342
Pb	0.0308	0.0223	0.0223	0	0.6028	0.6028	0	0	0

No.	19	20
Bi	0.2342	0.1171
Pb	0	0.1171

Table S5. Selected interatomic distances [Å] in the anions of 3. For attribution of Pb and Bi see Table S4. The values may appear adulterated, as several refined positions of atoms are common to different cluster types.

atom numbers		atom numbers		atom numbers	
1–2	2.9942(7)			9–14	2.9886(8)
1–4	3.0313(7)	5–9	2.9848(7)	10–13	3.403(2)
1–5	3.0006(7)	5–12	3.030(1)	10–14	2.9771(8)
1–16	3.556(11)	5–18	2.897(5)	10–16	3.457(11)
1–17	3.486(9)	6–9	3.0051(7)	11–15	3.023(2)
2–3	2.9948(7)	6–10	2.9984(7)	11–17	3.659(9)
2–6	2.9548(7)	7–10	2.9813(6)	12–15	2.9943(12)
3–4	3.0075(7)	7–11	3.005(2)	13–18	3.338(4)
3–7	2.9822(7)	4–20	2.991(7)	13–19	3.312(6)
3–16	3.499(10)	5–9	2.9848(7)	14–15	2.9663(10)
3–17	3.454(8)	8–11	3.013(3)	18–20	2.939(7)
4–8	2.944(2)	8–12	3.028(2)	19–20	3.029(10)
U–1	3.3805(6)	U–8	3.6885(12)	U–15	3.6642(8)
U–2	3.5263(7)	U–9	3.4354(7)	U–16	2.885(9)
U–3	3.3987(7)	U–10	3.4083(8)	U–17	3.029(9)
U–4	3.4913(8)	U–11	3.425(2)	U–18	3.226(5)
U–5	3.5705(6)	U–12	3.4345(13)	U–19	3.234(7)
U–6	3.5778(8)	U–13	3.013(2)	U–20	3.380(5)
U–7	3.5756(6)	U–14	3.4209(8)	Average	3.388

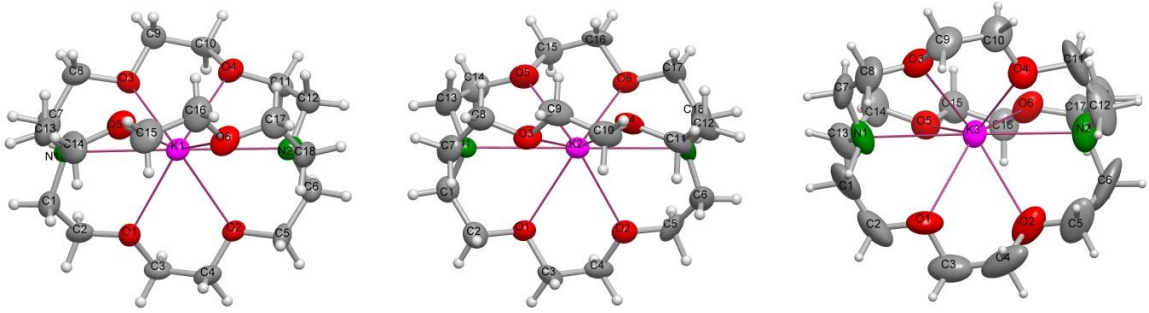

Figure S11. The three [K(crypt-222)]$^+$ cations in 3. Displacement ellipsoids at the 50% probability level.

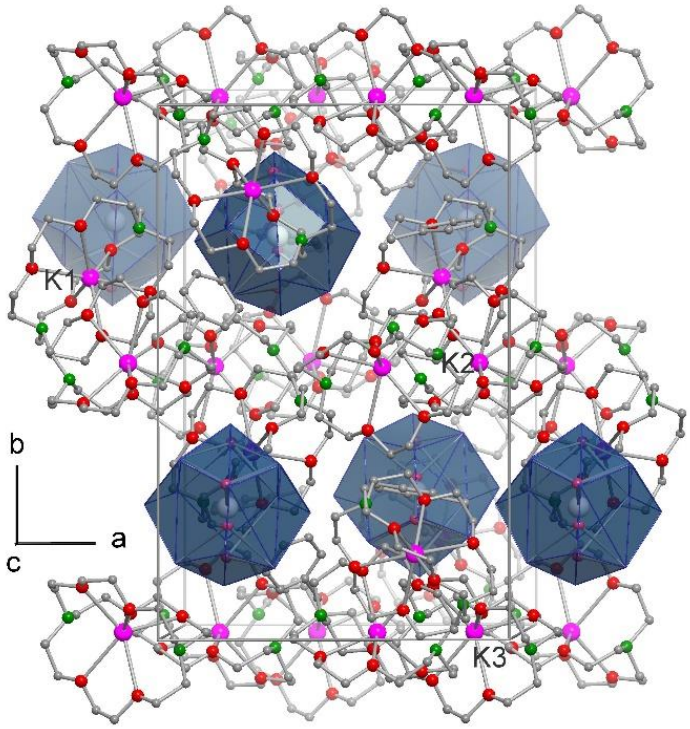

Figure S12. Unit cell of 3. Anion clusters as polyhedra, H atoms omitted.

2.2.4 Comparison of the Anion in 1 with Clusters Comprising Related Shell Topologies with 14 Atoms

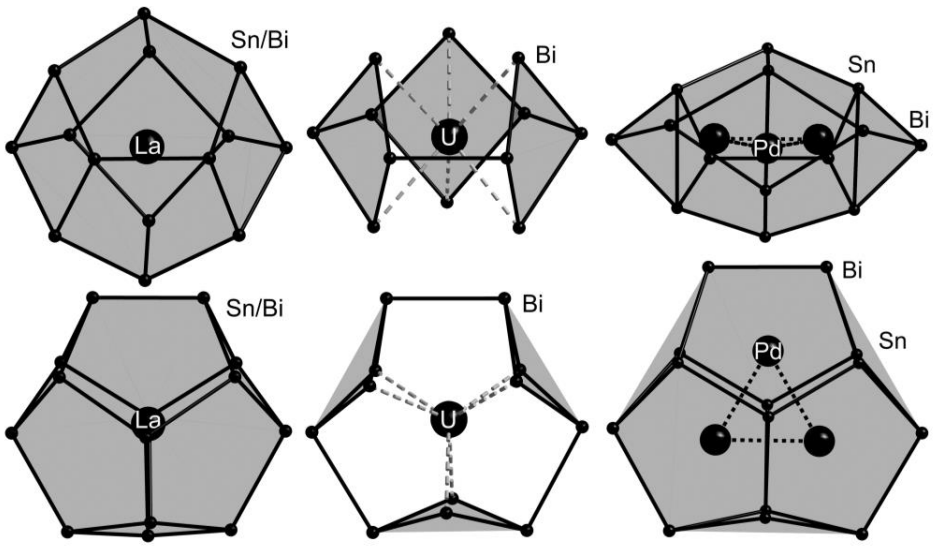

Figure S13. Side view (top) and top view (bottom) of the cluster architectures observed in $[La@Sn_7Bi_7]^{4-}$ (left),[12] the anion in 1 (center), and $[Pd_3@Sn_8Bi_6]^{4-}$ (right).[13]

3. Micro-X-ray Fluorescence Spectroscopy (μ-XFS) and Energy Dispersive X-ray Spectroscopy (EDX) Analysis

3.1. Micro-X-ray Fluorescence Spectroscopy (μ-XFS)

All μ-XFS measurements were performed with a Bruker M4 Tornado, equipped with an Rh-target X-ray tube and a Si drift detector. The emitted fluorescence photons are detected with an acquisition time of 100 s. Quantification of the elements is achieved through deconvolution of the spectra. Results are summarized in Table S6. Figures S14-S16 present the spectra for **1** - **3** along with the results of the deconvolution algorithm. The data for **1** and **2** were collected on freshly mounted crystals that were immersed in a thin protective coating of non-drying high viscosity oil (21 cSt). The data for **3** was collected on the same crystal from which single crystal X-ray diffraction data was collected. Several measurements produced unreasonably large values for the % K. Removal of K from the calculations afforded excellent agreement with the expected atomic ratio of $U_1Pb_{5.98}Bi_{7.68}$ in **3**. We believe that accumulation of K at the crystal surface upon exposure to air is responsible for the anomalous results. This has been observed regularly for very sensitive compounds. For confirmation, energy dispersive X-ray (EDX) spectroscopy was performed on crystals which were protected from air until immediately before being mounted in the instrument (see section 3.2).

Table S6. μ-XFS analysis of 1 - 3 (K, Ga, Tl, Pb, Bi, U).

$[K(crypt\text{-}222)]_3[U@Bi_{12}]\cdot tol\cdot 1.5en$ (**1**)					
Element	Element wt %	Weight % err. (1 sigma)	Atom %	Element ratio observed	Element ratio calc
K-K	4.09	0.00	18.68	2.99	3.00
Ga-K	0.13	0.00	0.32	0.05	0.00
Bi-L	87.49	0.11	74.77	11.96	12.00
U-L	8.30	0.00	6.22	1.00	1.00
Total	100.01		99.99	16.00	16.00
$[K(crypt\text{-}222)]_2[K(crypt\text{-}222)(en)][U@Tl_2Bi_{11}]\cdot tol$ (**2**)					
Element	Element wt %	Weight % err. (1 sigma)	Atom %	Element ratio observed	Element ratio calc
K-K	3.91	0.00	17.97	3.05	3.00
Tl-L	14.53	0.00	12.77	2.17	2.00
Bi-L	73.99	0.07	63.57	10.81	11.00
U-L	7.56	0.00	5.70	0.97	1.00
Total	99.99		100.01	17.00	17.00
$[K(crypt\text{-}222)]_3[U@Pb_7Bi_7]_{0.660}[U@Pb_4Bi_9]_{0.340}\cdot 2tol$ (**3**)					
Element	Element wt %	Weight % err. (1 sigma)	Atom %	Element ratio observed	Element ratio calc
Pb-L	40.53	0.04	41.12	6.03	5.98
Bi-L	51.76	0.06	52.07	7.63	7.68
U-L	7.71	0.00	6.81	1.00	1.00
Total	100.00		100.00	14.66	14.66

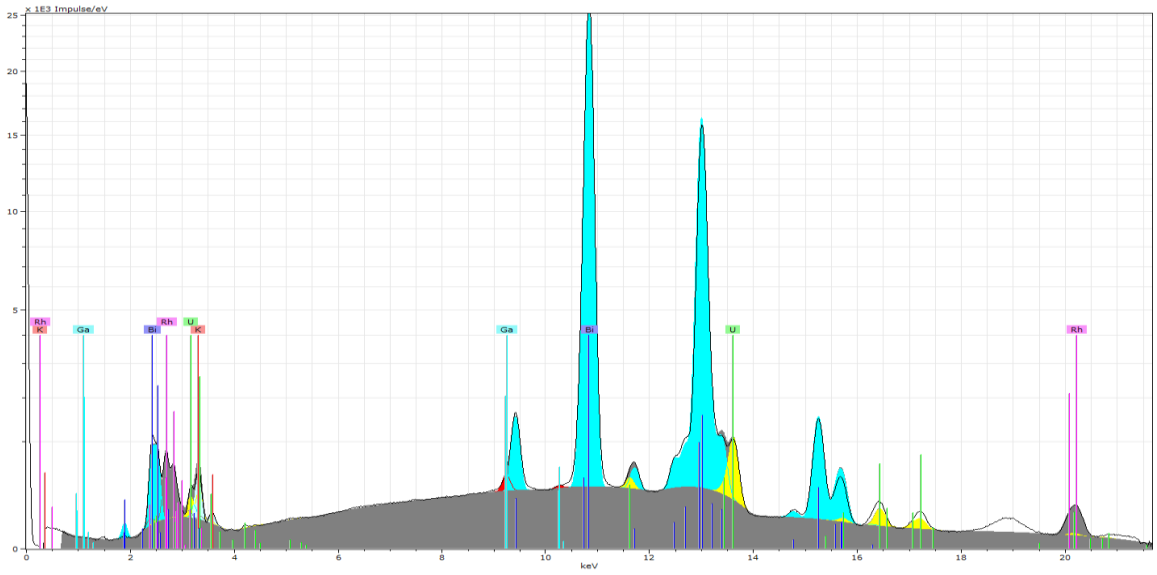

Figure S14. *μ*-XF spectrum of 1 (line) with the results of the deconvolution algorithm (solid, colored). Colors are used as follows: K (faint blue), Ga (red), Bi (blue), U (yellow). Note, that the intensity is displayed on a square root scale to allow for a better visibility of small features in the spectrum.

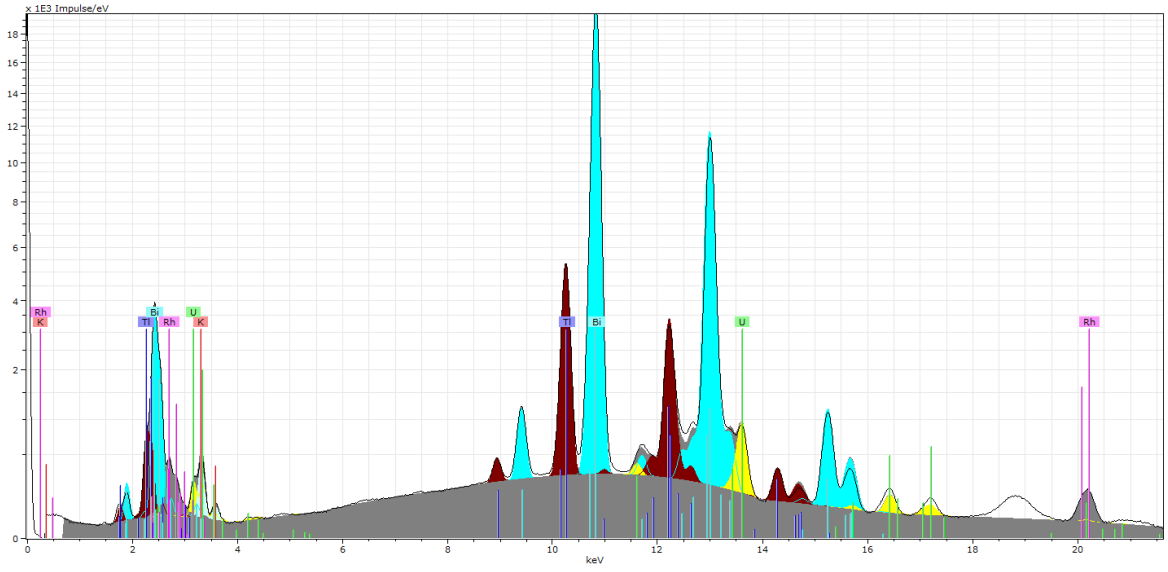

Figure S15. *μ*-XF spectrum of 2 (line) with the results of the deconvolution algorithm (solid, colored). Colors are used as follows: K (faint blue), Tl (dark red), Bi (blue), U (yellow). Note, that the intensity is displayed on a square root scale to allow for a better visibility of small features in the spectrum.

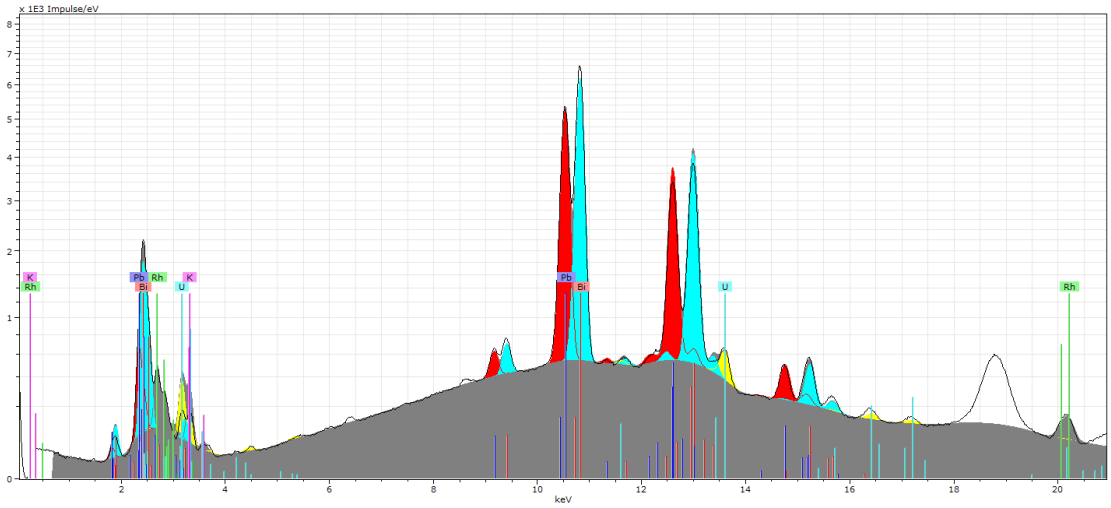

Figure S16. μ-XF spectrum of 3 (line) with the results of the deconvolution algorithm (solid, colored). Colors are used as follows: Pb (red), Bi (blue), U (yellow). Note, that the intensity is displayed on a square root scale to allow for a better visibility of small features in the spectrum.

3.2. Energy Dispersive X-ray Spectroscopy (EDX) of 3

EDX analysis of the most complex compound **3** was performed to support the elemental composition that was suggested based on the μ-XFS experiments. This was carried out using an EDX-device Voyager 4.0 of Noran Instruments coupled with an electron microscope CamScan CS 4DV. Data acquisition was performed with an acceleration voltage of 25 kV and 100 s accumulation time. Results are summarized in Table S7.

Table S7. EDX analysis of 3 (K, Pb, Bi, U)

$[K(crypt\text{-}222)]_3[U@Pb_7Bi_7]_{0.660}[U@Pb_4Bi_9]_{0.340}\cdot 2tol$ (**3**)							
Element	k-ratio	ZAF	Atom %	Element wt %	wt % Err. (1-sigma)	Observed atomic ratio	Expected atomic ratio
K – K	0.0200	1.967	18.05	3.93	± 0.14	3.19	3.00
Pb – L	0.3774	1.017	33.24	38.39	± 1.69	5.87	5.98
Bi – L	0.4950	1.011	42.97	50.05	± 1.94	7.58	7.68
U – M	0.0423	1.805	5.75	7.63	± 0.57	1.02	1.00
Total			100	100		17.66	17.66

4. Electrospray Ionization Mass Spectrometry

4.1. Methods

All mass spectra were recorded with a Thermo Fischer Scientific Finnigan LTQ-FT spectrometer in negative ion mode. Single crystals of the compounds **1** – **3** were dissolved in freshly distilled DMF inside a glovebox. The solutions were injected into the spectrometer with gastight 250 µL Hamilton syringes by syringe pump infusion. All capillaries within the system were washed with dry DMF for 2 hours before and at least 10 minutes in between measurements to avoid decomposition reactions and consequent clogging.

The following ESI parameters were used:

- Spray Voltage: 3.6 kV
- Capillary Temp: 290 °C
- Capillary Voltage: -20
- Tube lens Voltage: -121.75
- Sheath Gas: 45
- Sweep Gas: 0
- Auxiliary Gas: 40

4.2. Mass spectrum of $[K(crypt\text{-}222)]_3[U@Bi_{12}]\cdot tol\cdot 1.5en$ (1)

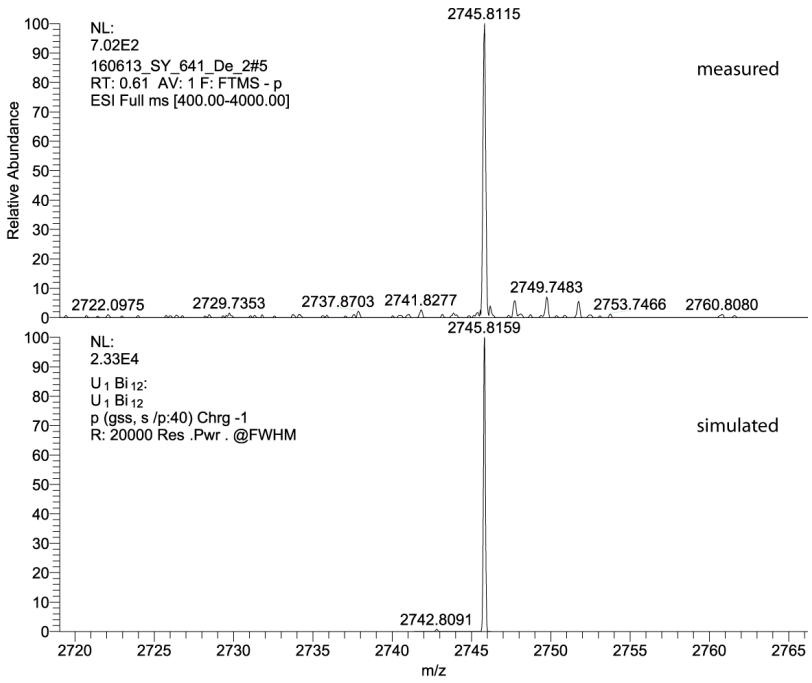

Figure S17. High resolution ESI mass spectrum in negative ion mode of $[U@Bi_{12}]^-$, recorded immediately upon injection of a fresh solution of 1 in DMF.

4.3. Mass spectra of $[K(crypt\text{-}222)]_2[K(crypt\text{-}222)(en)][U@Tl_2Bi_{11}]\cdot tol$ (2)

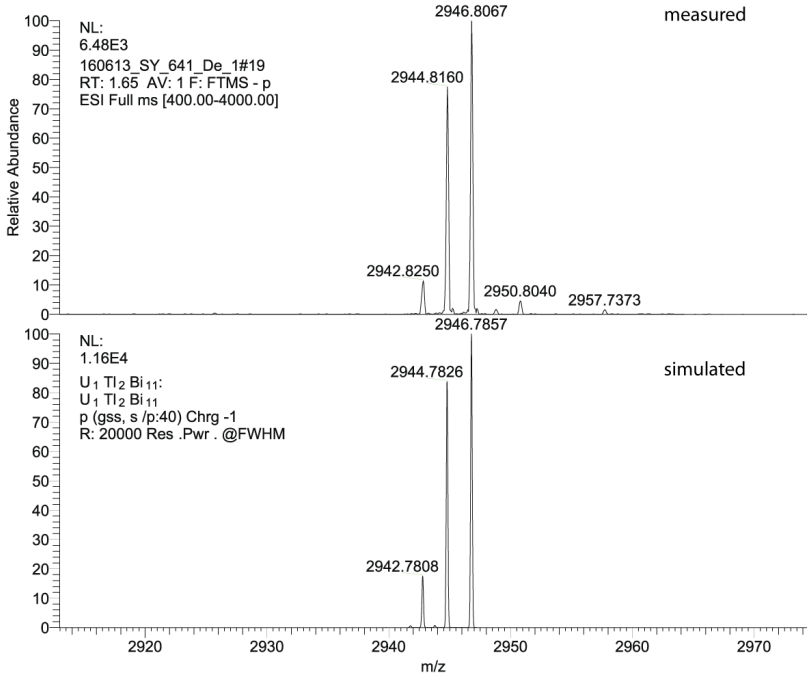

Figure S18. High resolution ESI mass spectrum in negative ion mode of $[U@Tl_2Bi_{11}]^-$, recorded immediately upon injection of a fresh solution of 2 in DMF.

4.4. Mass spectra of $[K(crypt\text{-}222)]_3[U@Pb_7Bi_7]_{0.66}[U@Pb_4Bi_9]_{0.34}\cdot 2tol$ (3)

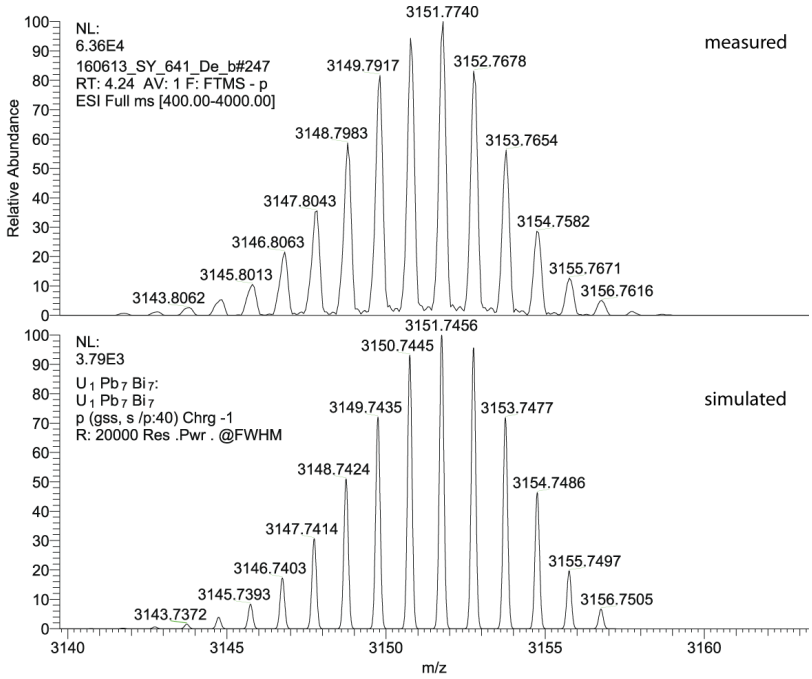

Figure S19. High resolution ESI mass spectrum in negative ion mode of $[U@Pb_7Bi_7]^-$, recorded immediately upon injection of a fresh solution of 3 in DMF.

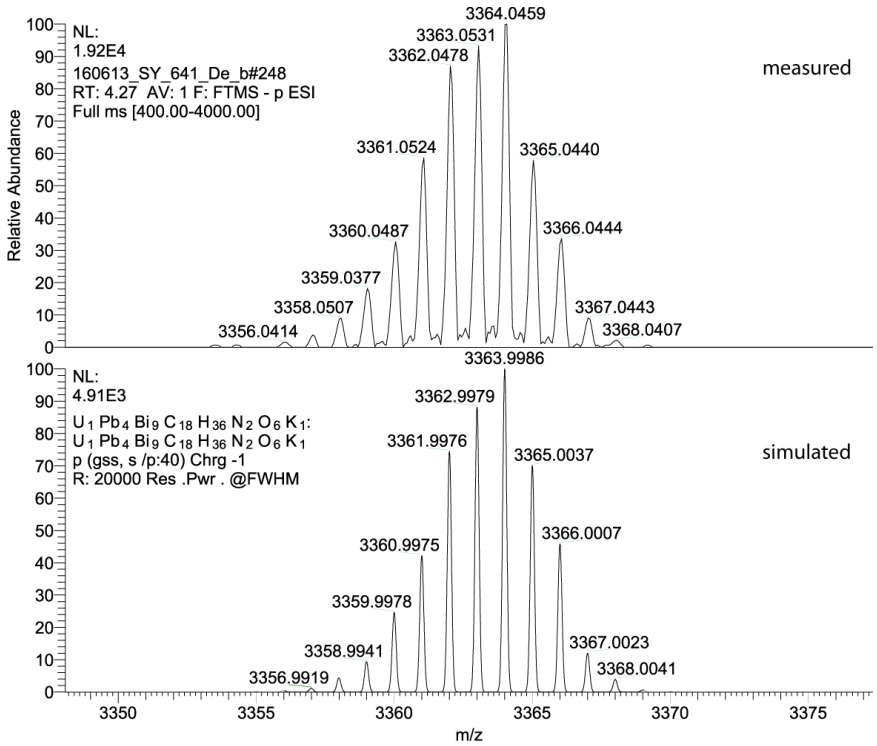

Figure S20. High resolution ESI mass spectrum in negative ion mode of [K(crypt-222)][U@Pb$_4$Bi$_9$]$^-$, recorded immediately upon injection of a fresh solution of 3 in DMF.

5. Electron Paramagnetic Resonance Spectroscopy

Single crystals of compounds **1** - **3** were collected, washed with dry petrol ether and dried under vacuum. The substances were ground to fine powders in a glovebox, filled into EPR tubes and then sealed under vacuum. X-band spectra were recorded at 298 K and 4K .
In all three cases, no signal was observed, indicating EPR silence. Similar observations have been reported for other U(IV) compounds, see for example ref. [14].

6. Magnetic Measurements

6.1. Methods

The magnetic measurements were carried out with the use of a Quantum Design MPMS-XL SQUID magnetometer and a PPMS-9 susceptometer. These instruments work between 1.8 and 400 K with applied dc fields ranging from –7 to 7 T (MPMS). Measurements were performed on polycrystalline samples of **1**, **2** and **3** (5.4, 15.6/18.0 and 17.9 mg) sealed in a polyethylene bag (3×0.5×0.02 cm; typically 20 to 40 mg) and prepared under nitrogen atmosphere. Prior to the experiments, the field-dependent magnetization was measured at 100 K in order to confirm the absence of any bulk ferromagnetic impurities. Ac susceptibility measurements were made with an oscillating field of 1 to 6 Oe with a frequency from 10 to 10000 Hz (PPMS). Above 1.8 K, the out-

of-phase component of the ac susceptibility was systematically found to be zero even under dc field up to 1 T. The magnetic data were corrected for the sample holder and the intrinsic diamagnetic contributions.

7. Quantum Chemical Investigations

7.1. Methods

The DFT calculations were performed with the program system Turbomole.[15] The hybrid functional B3-LYP[16] was applied. For Bi, the basis sets def-TZVPP was used,[17] with an effective core potential ECP-78.[18] For U, ECP-78 and a corresponding AVTZ basis set was used.[19] The influence of the basis set of U on the electronic structure was studied with a smaller AVTZ basis set along with a larger effective core potential, ECP-81.[20] Modelling of counter charges for the anionic compounds was achieved with the COSMO[21] model using the default parameters. Mulliken charges were calculated at the same level of theory.[22] Amplitudes in Figures 3 in the main document are drawn at ±0.025 a.u. by using gOpenMol.[23]

Compositions and atomic positions of atoms of elements that are neighboring in the periodic table were assigned by application of first-order perturbation theory, as outlined in ref [[24]]. This way, the number of atoms of each of the neighboring atom types as well as their preferred positions within the given cluster structure can be determined for a given total charge. In the present cases, latter is given by the number of $[K(crypt\text{-}222)]^+$ counterions, which is determined by single-crystal X-ray diffraction analysis (see section 2).

Geometric and electronic structures were optimized simultaneously and checked for being minimum structures on the energy hypersurface in all cases.

8. References for the Supporting Information

(1) crypt-222: 4,7,13,16,21,24-Hexaoxa-1,10-diazabicyclo[8.8.8]hexacosane

(2) Xu, L.; Sevov, S. C. *Inorg. Chem.* **2000**, *39*, 5383.

(3) Ababei, R.; Heine, J.; Holynska, M.; Thiele, G.; Weinert, B.; Xie, X.; Weigend, F.; Dehnen, S. *Chem. Commun.* **2012**, *48*, 11295.

(4) (a) Parry, J.; Carmona, E.; Coles, S.; Hursthouse, M. *J. Am. Chem. Soc.* **1995**, *117*, 2649. (b) Conejo, M. D.; Parry, J. S.; Carmona, E.; Schultz, M.; Brennann, J. G.; Beshouri, S. M.; Andersen, R. A.; Rogers, R. D.; Coles, S.; Hursthouse, M. *Chem. Eur. J.* **1999**, *5*, 3000. (c) Evans, W. J.; Kozimor, S. A.; Ziller, J. W.; Fagin, A. A.; Bochkarev, M. N. *Inorg. Chem.* **2005**, *44*, 3993.

(5) $Cp^{\#}$: 2,3,4,5-tetramethyl cyclopentadienyl

(6) Cloke, F. G. N.; Hawkes, S. A.; Hitchcock, P. B.; Scott, P. *Organometallics* **1994**, *13*, 2895.

(7) Lichtenberger, N. *Masters Thesis*, Philipps-Universität Marburg, **2013**.

(8) Sheldrick, G. M. *Acta Crystallogr. A* **2008**, *64*, 112.

(9) Sheldrick, G. M. *Acta Crystallogr. C* **2015**, *71*, 3.

(10) (a) Spek, A. *Acta Crystallogr. D* **2009**, *65*, 148. (b) van der Sluis, P.; Spek, A. L. *Acta Crystallogr. A* **1990**, *46*, 194.

(11) Ababei, R.; Massa, W.; Weinert, B.; Pollak, P.; Xie, X.; Clérac, R.; Weigend, F.; Dehnen, S. *Chem. Eur. J.* **2015**, *21*, 386.

(12) Lips, F.; Holynska, M.; Clérac, R.; Linne, U.; Schellenberg, I.; Pöttgen, R.; Weigend, F.; Dehnen, S. *J. Am. Chem. Soc.* **2012**, *134*, 1181.

(13) Lips, F.; Clérac, R.; Dehnen, S. *J. Am. Chem. Soc.* **2011**, *133*, 14168.

(14) Rosenzweig, M. W.; Scheurer, A.; Lamsfus, C. A.; Heinemann, F. W.; Maron, L.; Andrez, J.; Mazzanti, M.; Meyer, K. *Chem. Sci.* **2016**.

(15) TURBOMOLE V7.0 2015, a development of University of Karlsruhe and Forschungszentrum Karlsruhe GmbH, 1989-2007,TURBOMOLE GmbH, since 2007; available from http://www.turbomole.com.

(16) (a) Lee, C. T.; Yang, W. T.; Parr, R. G. *Phys. Rev. B* **1988**, *37*, 785. (b) Becke, A. D. *J. Chem. Phys.* **1993**, *98*, 5648.

(17) Eichkorn, K.; Weigend, F.; Treutler, O.; Ahlrichs, R. *Theor. Chem. Acc.* **1997**, *97*, 119.

(18) Küchle, W.; Dolg, M.; Stoll, H.; Preuss, H. *Mol. Phys.* **1991**, *74*, 1245.

(19) Moritz, A.; Dolg, M. *Theor. Chem. Acc.* **2008**, *121*, 297.

(20) Moritz, A.; Cao, X. Y.; Dolg, M. *Theor. Chem. Acc.* **2007**, *117*, 473.

(21) Klamt, A.; Schüürmann, G. *J. Chem. Soc., Perkin Trans. 2* **1993**, 799.

(22) Mulliken, R. S. *J. Chem. Phys.* **1955**, *23*, 1833.

(23) Bergman, D. L.; Laaksonen, L.; Laaksonen, A. *J. Mol. Graph. Model.* **1997**, *15*, 301.

(24) (a) Weigend, F.; Schrodt, C.; Ahlrichs, R. *J. Chem. Phys.* **2004**, *121*, 10380. (b) Weigend, F.; Schrodt, C. *Chem. Eur. J.* **2005**, *11*, 3559.

C.2 Between Localization and Delocalization: $Ru(cod)^{2+}$ Units in the Zintl Clusters $[Bi_9\{Ru(cod)\}_2]^{3-}$ and $[Tl_2Bi_6Ru(cod)]^{2-}$

Angewandte Chemie
Eine Zeitschrift der Gesellschaft Deutscher Chemiker

Supporting Information

Between Localization and Delocalization: $Ru(cod)^{2+}$ Units in the Zintl Clusters $[Bi_9\{Ru(cod)\}_2]^{3-}$ and $[Tl_2Bi_6\{Ru(cod)\}]^{2-}$

*Niels Lichtenberger, Nils Spang, Andreas Eichhöfer, and Stefanie Dehnen**

anie_201707632_sm_miscellaneous_information.pdf

Contents

1. Syntheses Details

1.1. General

All manipulations and reactions were performed in a dry Ar atmosphere using standard Schlenk or glovebox techniques. All solvents were dried and freshly distilled prior to use. Crypt-222[1] (Merck) was dried *in vacuo* for at least 18 hours. Samples were shielded from ambient light throughout all solution-based syntheses.

1.2. Solid-state Syntheses

1.2.1. General Procedure

All solid state syntheses were carried out according to a standardized procedure. Niobium tubes were cut to size and sealed on one side by arc-welding inside a glovebox. The elements were weighed into beakers, mixed, and afterwards transferred into the Nb containers. These were sealed tight by arc-welding and transferred into quartz tubes. After evacuation and subsequent sealing, they were then placed in a chamber furnace and treated with the desired temperature program.

1.2.2. Synthesis of "$K_2Tl_1Bi_3$" (I)

Samples were heated to 550 °C with 20 K/h, annealed for 7 d and cooled down to room temperature with 5 K/h.

Element	m / g	n / mmol	Eq
K	1.719	44	2
Tl	4.494	22	1
Bi	13.786	66	3

1.2.3. Synthesis of "$K_3Tl_4Bi_5$" (II)

Samples were heated to 550 °C with 20 K/h, annealed for 7 d and cooled down to room temperature with 5 K/h.

Element	m / g	n / mmol	Eq
K	0.119	3	3
Tl	0.826	4	4
Bi	1.056	5	5

1.3. Solution-based Syntheses

1.3.1. Synthesis of [K(crypt-222)]$_2$(TlBi$_3$)·0.5*en* (1b)

Compound **1b** can be prepared by extraction of 1 eq of "K_2TlBi_3" (**I**) with 2.05 eq of crypt-222 in *en* (10+ mL/100 mg of **I**). This procedure is well suited for a large scale synthesis of **1b** (>5 g) and was tested for up to 4 g of **I**.

All solids are weighed into a round-bottom flask of according size and the *en* is added. The solution rapidly turns dark-green. After stirring for 3 days, all remaining solid residues are allowed to settle for several hours. The supernatant solution is then carefully canula-transferred into a second round bottom flask. Slow removal of the solvent under reduced pressure (no stirring!) over the course of hours/days (depending on the amount of solvent) yields large dark metallic blocks of [K(crypt-222)]$_2$(TlBi$_3$)·0.5*en* (**1b**) in 80 – 90% yield.

Note: If the solvent is removed over several days, the concentrated solution is best stored at 5 °C overnight.

Crystals of better quality for SC-XRD were obtained after layering of the extraction solution (5 mL) with THF or toluene respectively (5 mL). This way, we obtained the isostructural compound [K(crypt-222)]$_2$(TlBi$_3$)·0.58*thf*·0.42 *en* (**1a**) that only differs in the crystal solvent content. However, its better scattering properties allowed for the collection of a higher quality dataset, which was deposited with CCDC as indicated.

1.3.2. Synthesis of [K(crypt-222)]$_3$[Bi$_9${Ru(*cod*)}$_2$]·1.5*en* (2)

200 mg (118 µmol) of **1b** and 26 mg (83 µmol, 0.7 eq) of [Ru(*cod*)(CH$_2$C(Me)CH$_2$)$_2$] (**A**) were combined in a Schlenk tube and dissolved in 5 mL of en. The initially dark brown solution slowly changed to dark red brown. The reaction mixture was allowed to stir for 3 hours. The resulting dark brown solution was filtered through a standard glass frit, carefully layered with 5 mL of THF, and stored for crystallization at 5 °C. After 2 days, thin, brittle plates of compound **2** formed at the wall of the Schlenk tube in appr. 13% yield alongside co-precipitates of compound **4** and traces of **3**, as confirmed by mass spectrometry.

1.3.3. Synthesis of [K(crypt-222)]$_2$[{Ru(*cod*)}Tl$_2$Bi$_6$]·2*tol* (3)

The synthesis of **3** was performed as described in 1.3.2. After the crystallization of **2** was completed the remaining solution was transferred into a new Schlenk tube and concentrated to approximately 3 mL. Subsequent layering with 10 mL of toluene led to the formation of few black blocks of **3** after 7 days.

1.3.4. Synthesis of [K(crypt-222)]$_3$(Tl$_4$Bi$_5$)·2*en* (4)

200 mg (101 µmol) of "$K_3Tl_4Bi_5$" (**II**) and 116 mg (305 µmol, 3.05 eq) of crypt-222 were combined in a Schlenk tube and dissolved in 5 mL of *en*. The solution rapidly turns dark brown and is stirred for 3 days. After filtration, 10 mL of the solution are divided equally between two Schlenk tubes and layered with 5 mL of toluene or THF respectively. The remaining 10 mL were concentrated by slow evaporation of the solvent and then stored at 5 °C. All three methods are suitable to afford crystals of **4** in the form of black metallic blocks.

*Crystals of **4** were also obtained after layering of the reaction solution of **1b** with **A**, as described in 1.3.2, with toluene instead of THF.*

2. Mass Spectrometry

2.1. General Procedure

All mass spectra were recorded with a Thermo Fischer Scientific Finnigan LTQ-FT spectrometer in negative ion mode. The solid sample was dissolved in freshly distilled DMF inside a glovebox and filtered with PTFE syringe filters. The solutions were ingested into the spectrometer with gastight 250 µL Hamilton syringes by syringe pump infusion. All capillaries within the system were washed with dry DMF for 2 hours before and at least 10 minutes in between measurements to avoid decomposition reactions and consequent clogging. All simulations and figures were created using the *mMass*[2] software suite.

2.2. Mass Spectrometry of $[K(crypt\text{-}222)]_2(TlBi_3)$ (1b) in en, and the Reaction Mixture of $[K(crypt\text{-}222)]_2(TlBi_3)$ (1b) + $[Ni(cod)_2]$ in *en*

Two samples were prepared in the glovebox. In both cases, 100 mg of **1b** were weighed into a vial. One served as a reference sample while 0.7 equivalents of $[Ni(cod)_2]$ were added to the other one. 2.5 mL of *en* were added to each sample and both were stirred for 3h. Both solutions were of a deep green color after the reaction time. Subsequent filtration through PTFE-syringe filters yielded dark green solutions that were diluted with another 5 mL of *en* to afford solutions with concentrations suitable for syringe-pump infusion ESI-MS. A comparison of the two recorded mass spectra is provided in Figure S1. Figures S2 – S17 represent high-resolution spectra of individual signals along with the corresponding simulations.

The mass spectrum recorded from the reference sample shows signals of $(TlBi_3)^-$, $(Tl_4Bi_5)^-$, as well as their fragmentation products. While the signal of $(Tl_4Bi_5)^-$ has a very low intensity, other species that formed by other fragmentation and re-arrangement processes occur with a much higher intensity.

The mass spectrum recorded from the reaction solution shows that a partial reaction of the $(TlBi_3)^{2-}$ anion with the $[Ni(cod)_2]$ takes place, affording a species $[Ni@Tl_4Bi_5]^-$ cluster as main ternary product. The signal of the starting material (observed here as $(TlBi_3)^-$, as usual) is still clearly visible, and also those of the species $(Tl_4Bi_5)^-$.

Most species co-exist with lighter homologs with a $Tl_{n-1}Bi_{n+1}$ composition. This is markedly different from the observation made at the reaction with the Ru complex (see below). This might be the reason for the fact that the only crystalline product obtained from reactions with $[Ni(cod)_2]$ is the starting material **1b**.

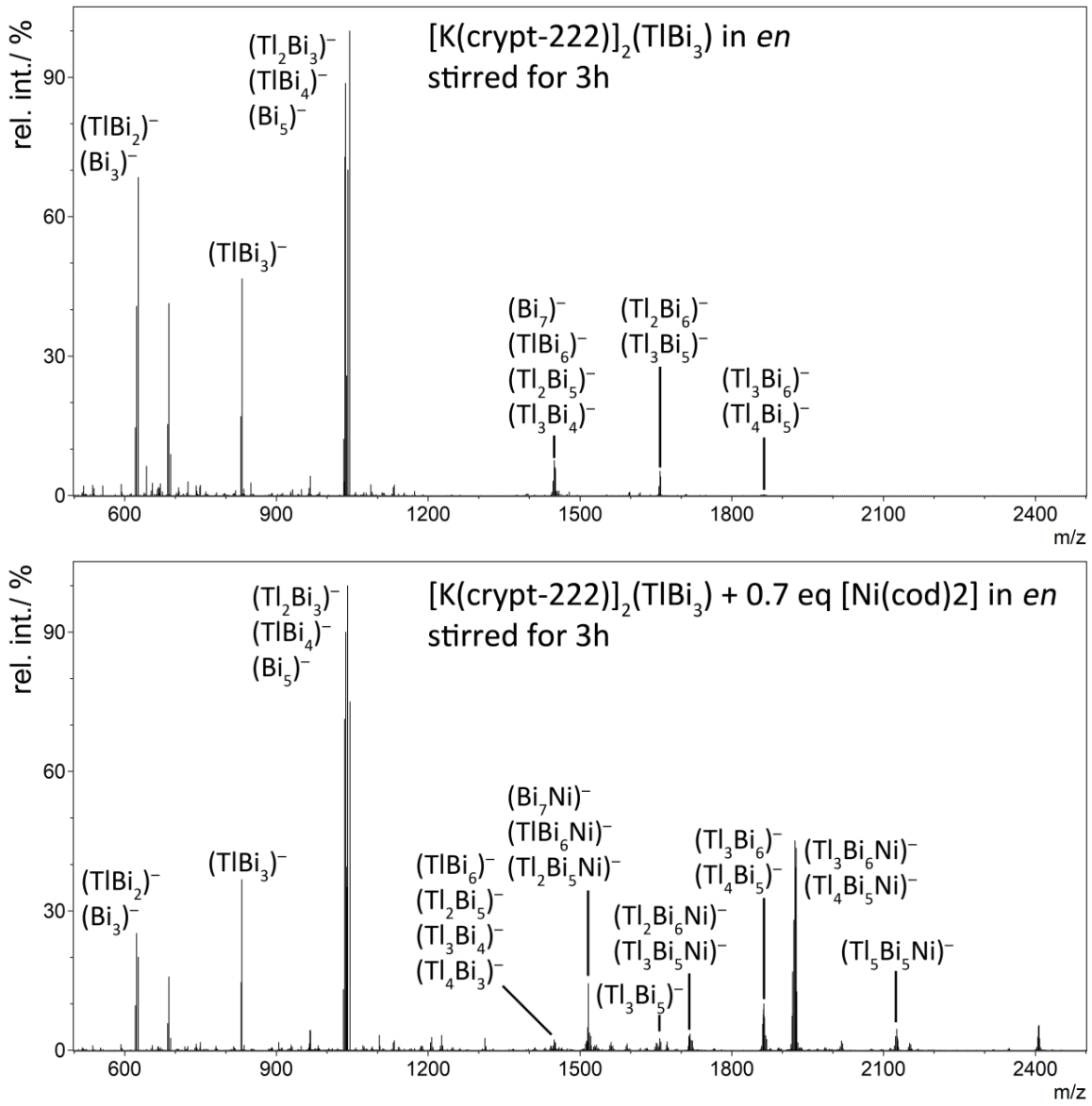

Figure S1. Comparison of the ESI mass spectra of [K(crypt-222)]$_2$(TlBi$_3$) (1b), and [K(crypt-222)]$_2$(TlBi$_3$) (1b) + [Ni(*cod*)$_2$] in *en*.

2.2.1. Mass Spectra Recorded from the Reference Sample $[K(crypt\text{-}222)]_2(TlBi_3)$ (1b) in *en*

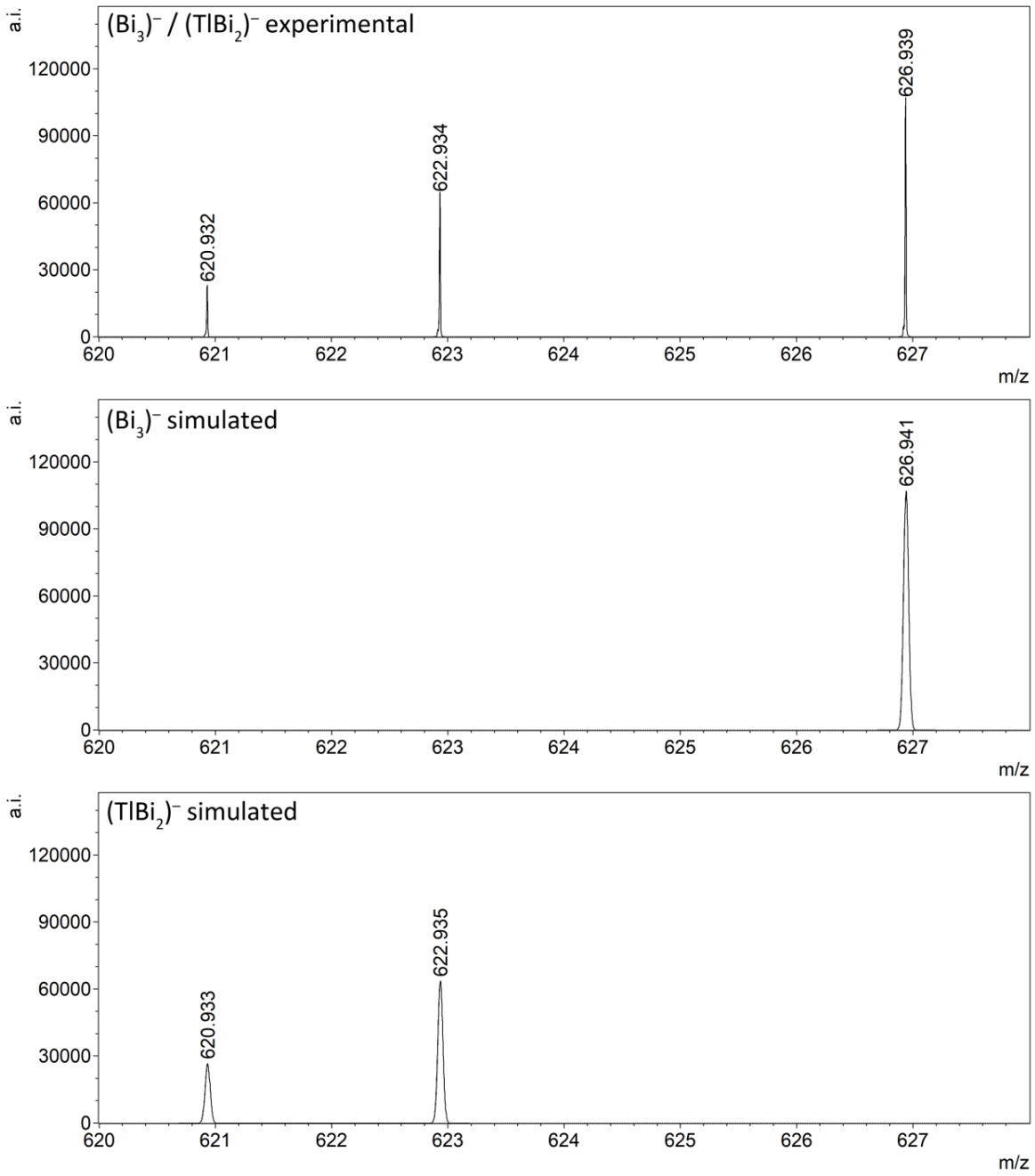

Figure S2. Comparison of experimental (top) and simulated mass spectra of $(Bi_3)^-$ (center) and $(TlBi_2)^-$ (bottom) ions.

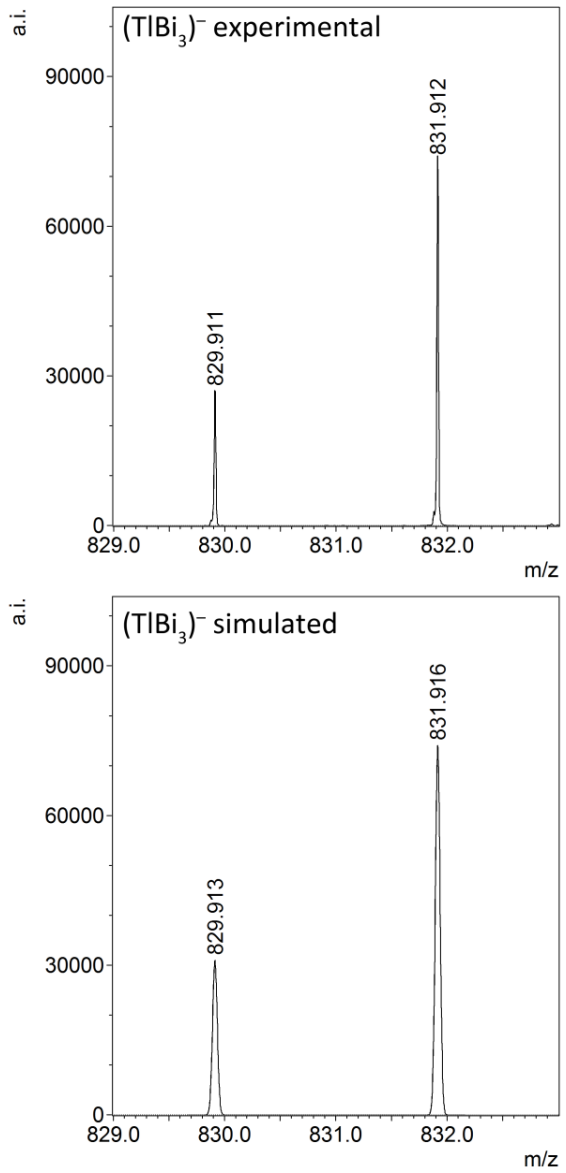

Figure S3. Comparison of experimental (top) and simulated mass spectra of $(TlBi_3)^-$ (bottom) ions.

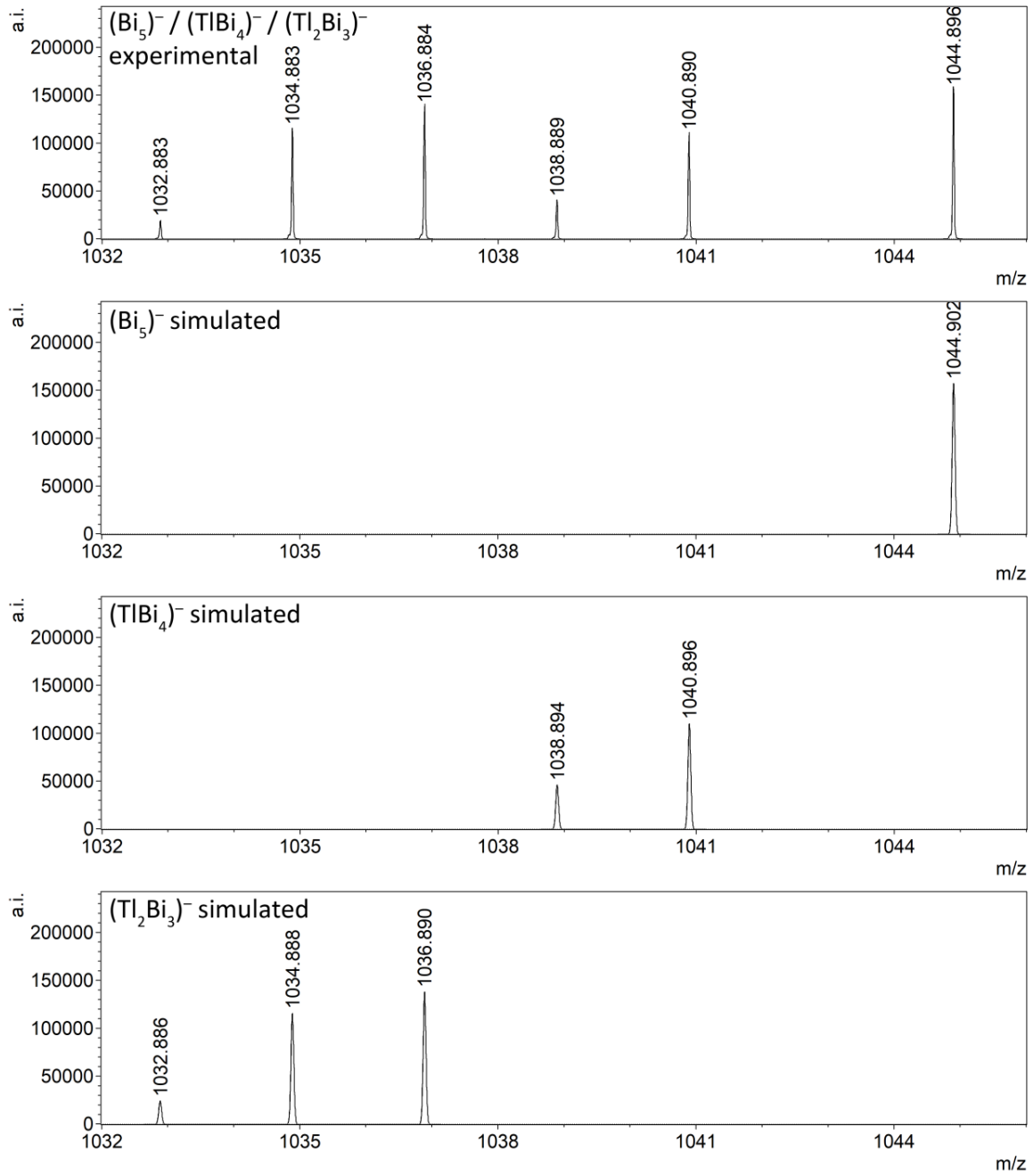

Figure S4. Comparison of experimental (top) and simulated mass spectra of $(Bi_5)^-$, $(TlBi_4)^-$, and $(Tl_2Bi_3)^-$ ions (from top).

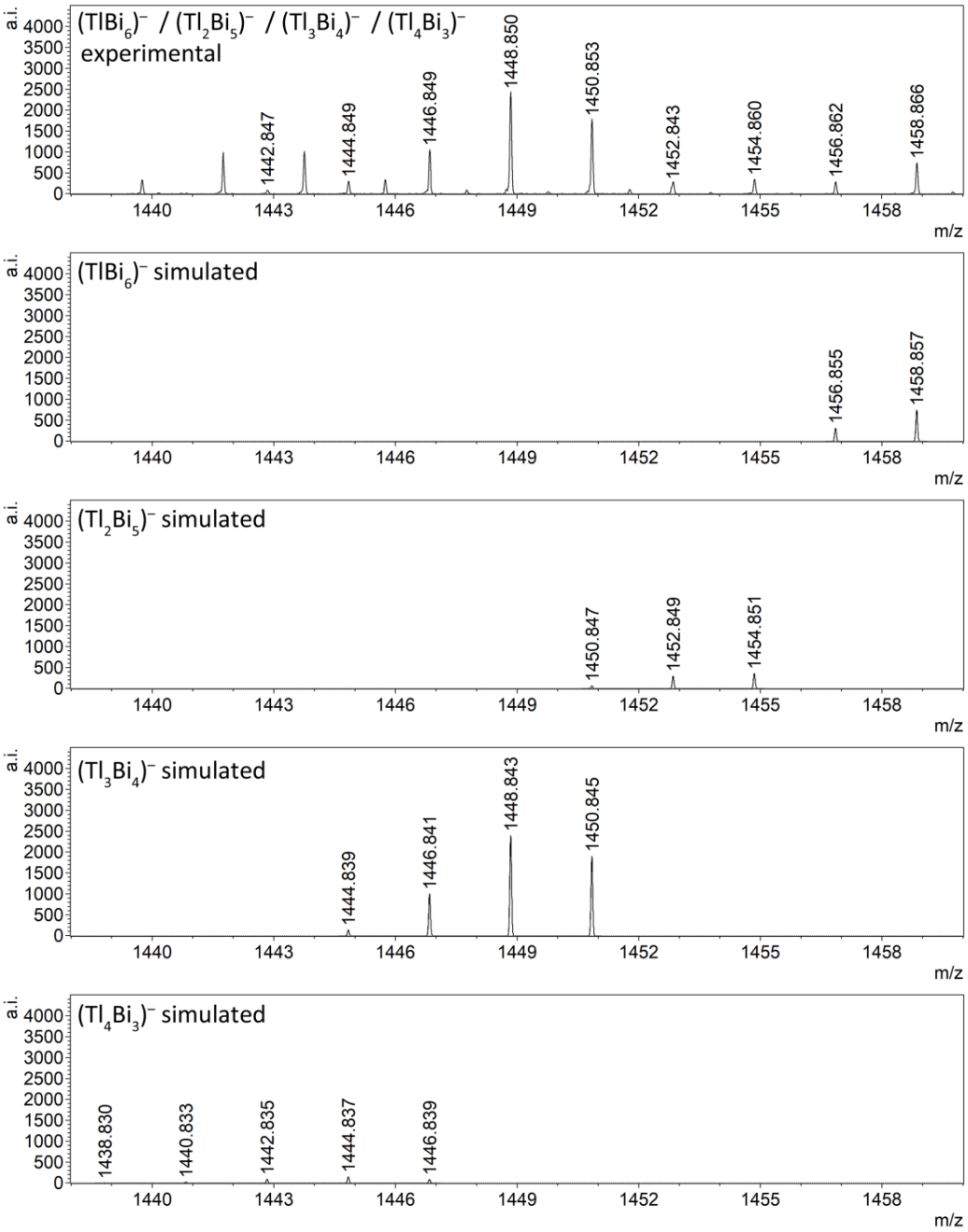

Figure S5. Comparison of experimental (top) and simulated mass spectra of $(TlBi_6)^-$, $(Tl_2Bi_5)^-$, $(Tl_3Bi_4)^-$, and $(Tl_4Bi_3)^-$ ions (from top).

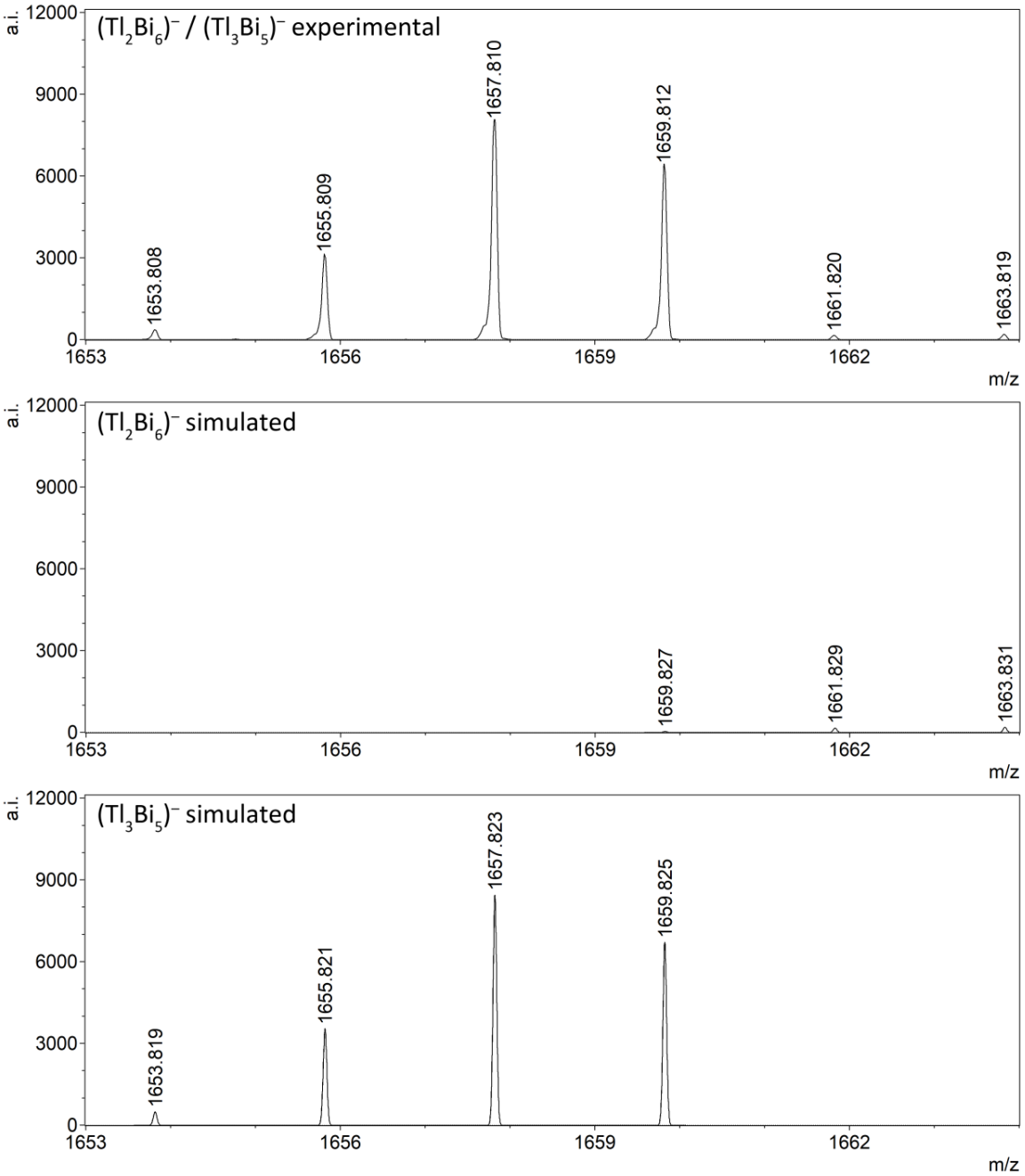

Figure S6. Comparison of experimental (top) and simulated mass spectra of $(Tl_2Bi_6)^-$ (center) and $(Tl_3Bi_5)^-$ (bottom) ions.

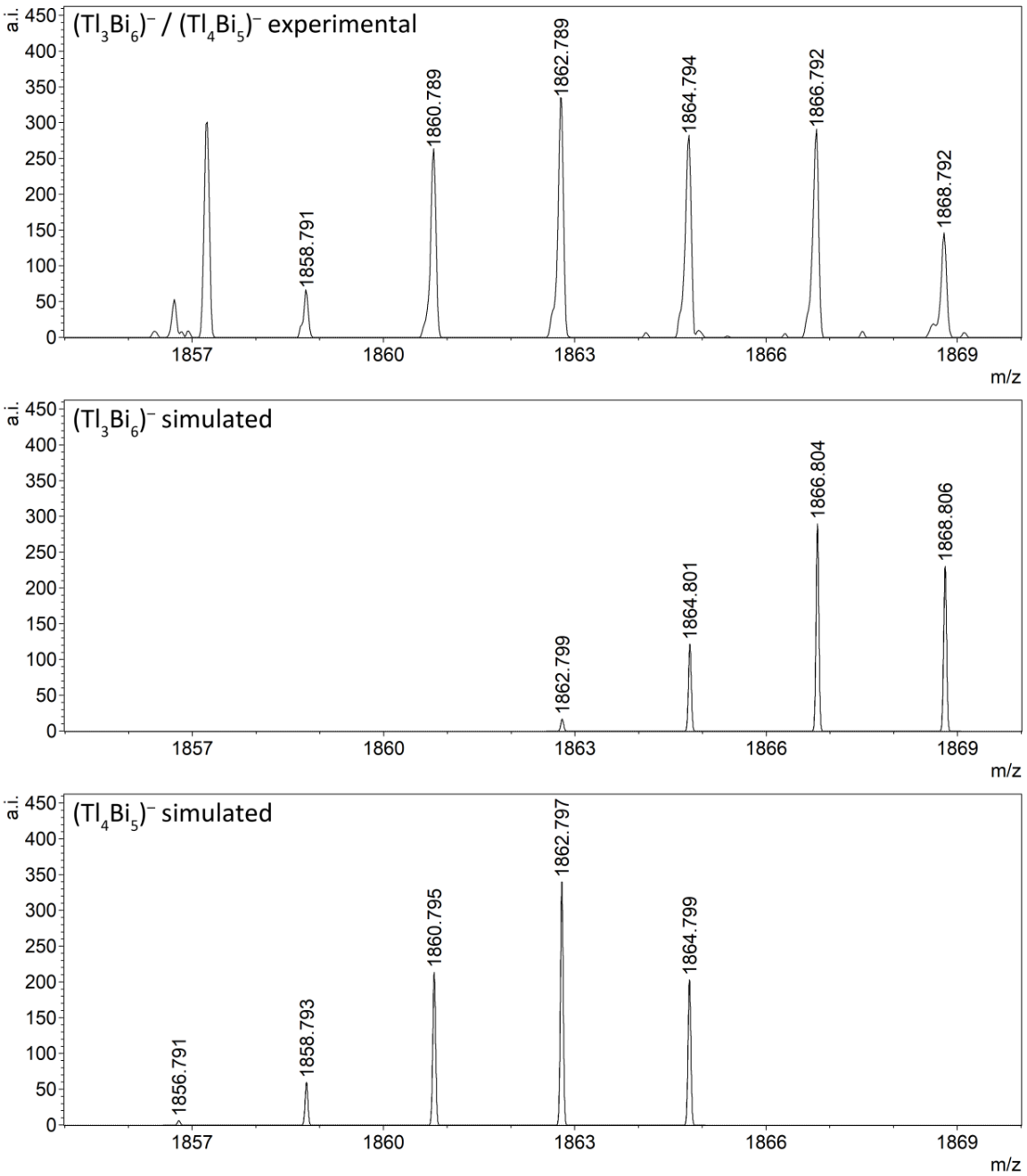

Figure S7. Comparison of experimental (top) and simulated mass spectra of $(Tl_3Bi_6)^-$ (center) and $(Tl_4Bi_5)^-$ (bottom) ions.

2.2.2. Mass Spectra Recorded from the Reaction Solution of [K(crypt-222)]$_2$(TlBi$_3$) (1b) + [Ni(*cod*)$_2$] in *en*

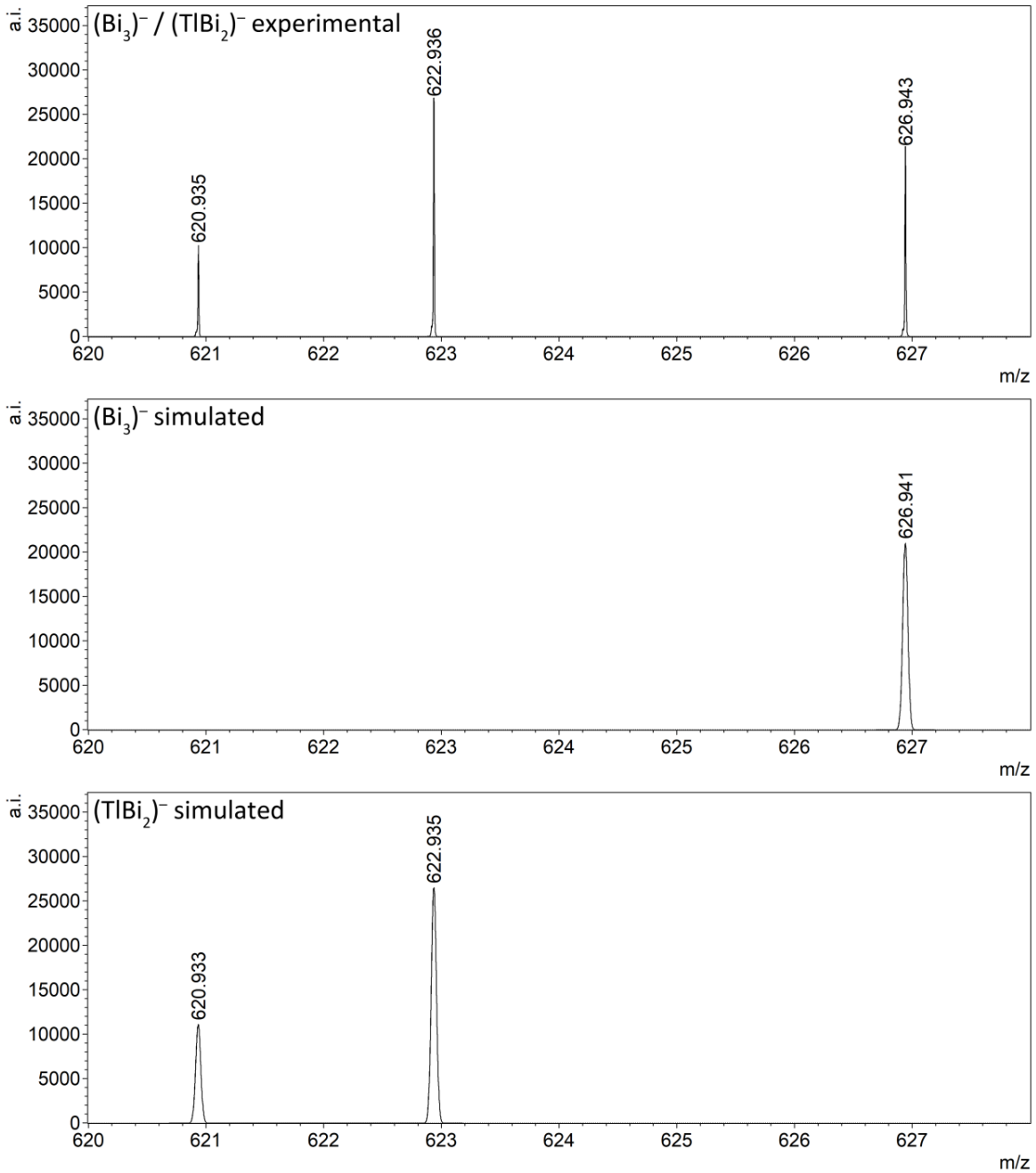

Figure S8. Comparison of experimental (top) and simulated mass spectra of (Bi$_3$)$^-$ (center) and (TlBi$_2$)$^-$ (bottom) ions.

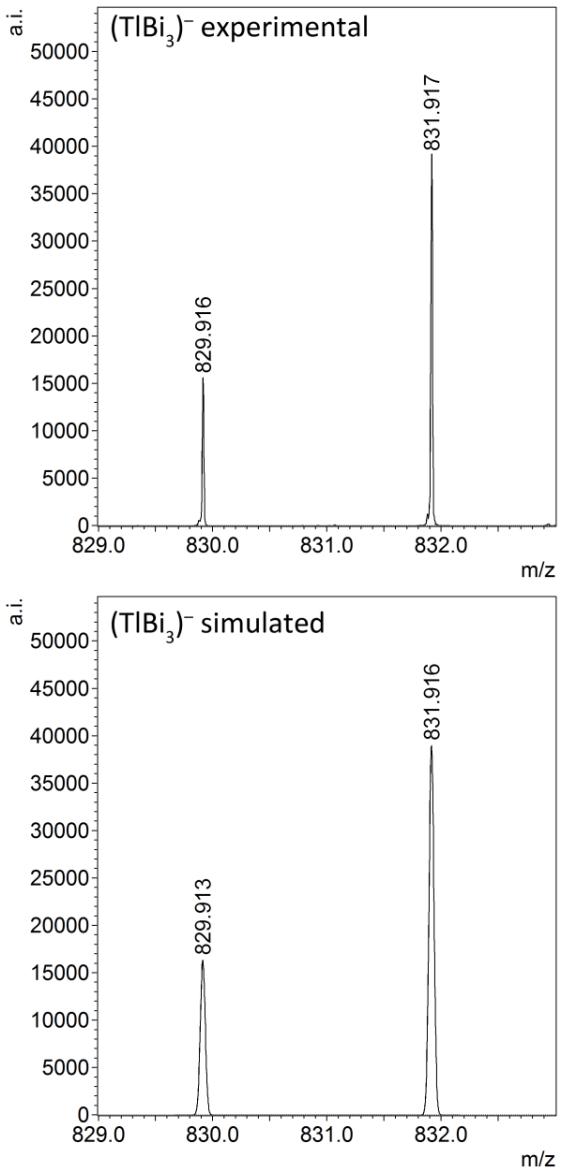

Figure S9. Comparison of experimental (top) and simulated mass spectra of $(TlBi_3)^-$ (bottom) ions.

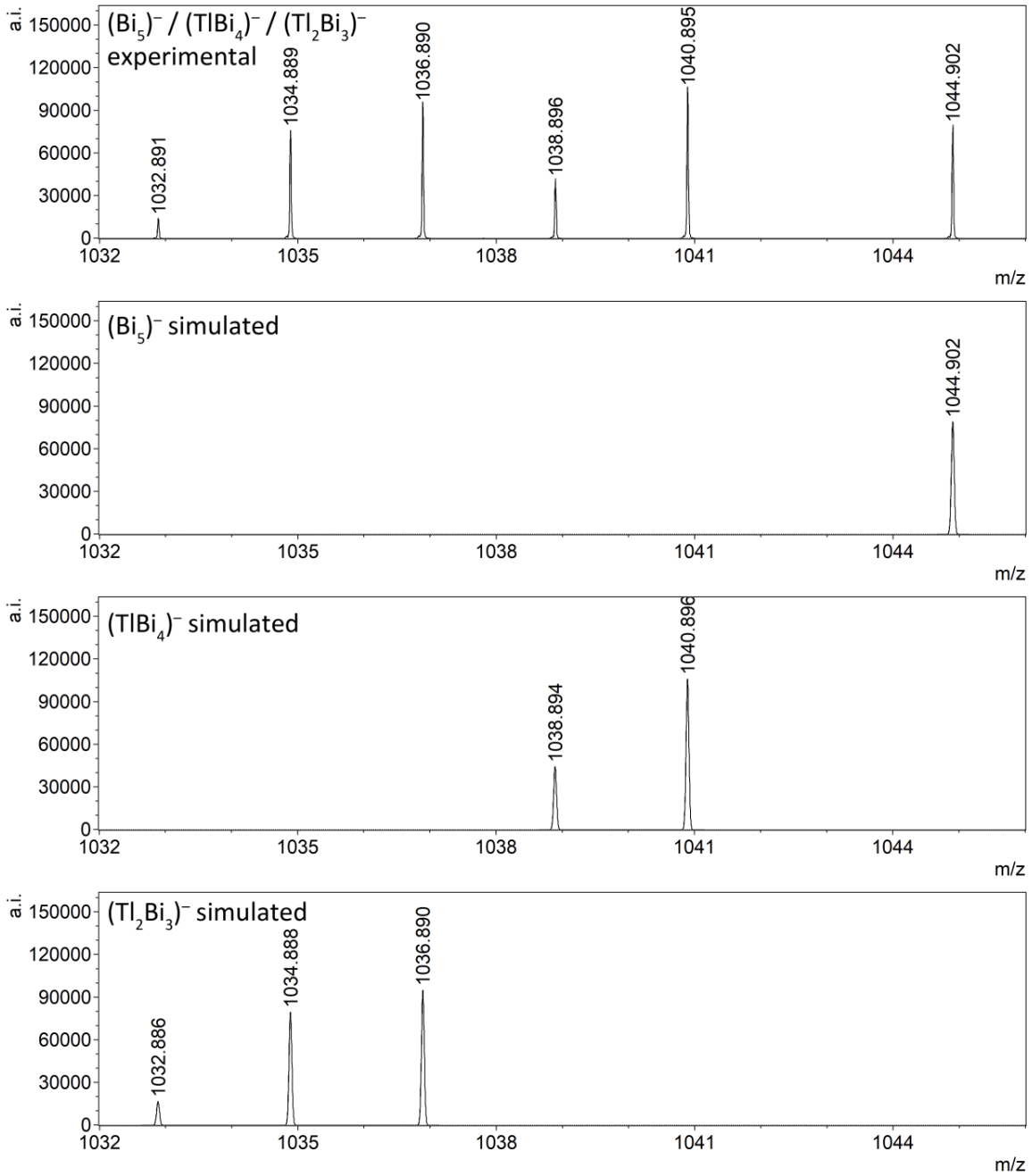

Figure S10. Comparison of experimental (top) and simulated spectra of $(Bi_5)^-$, $(TlBi_4)^-$, and $(Tl_2Bi_3)^-$ ions (from top).

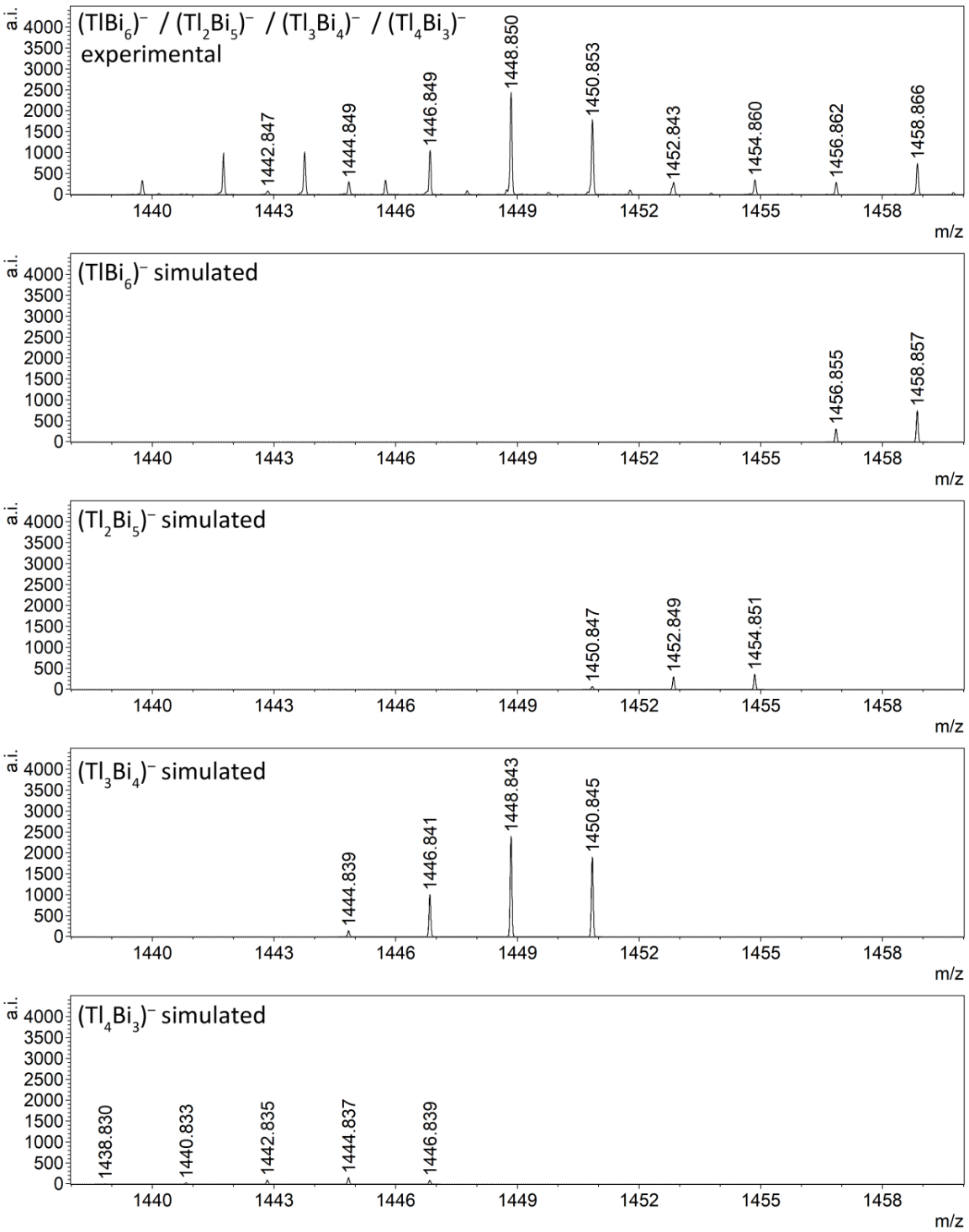

Figure S11. Comparison of experimental (top) and simulated mass spectra of $(TlBi_6)^-$, (Tl_2Bi_5), $(Tl_3Bi_4)^-$, and $(Tl_4Bi_3)^-$ ions (from top).

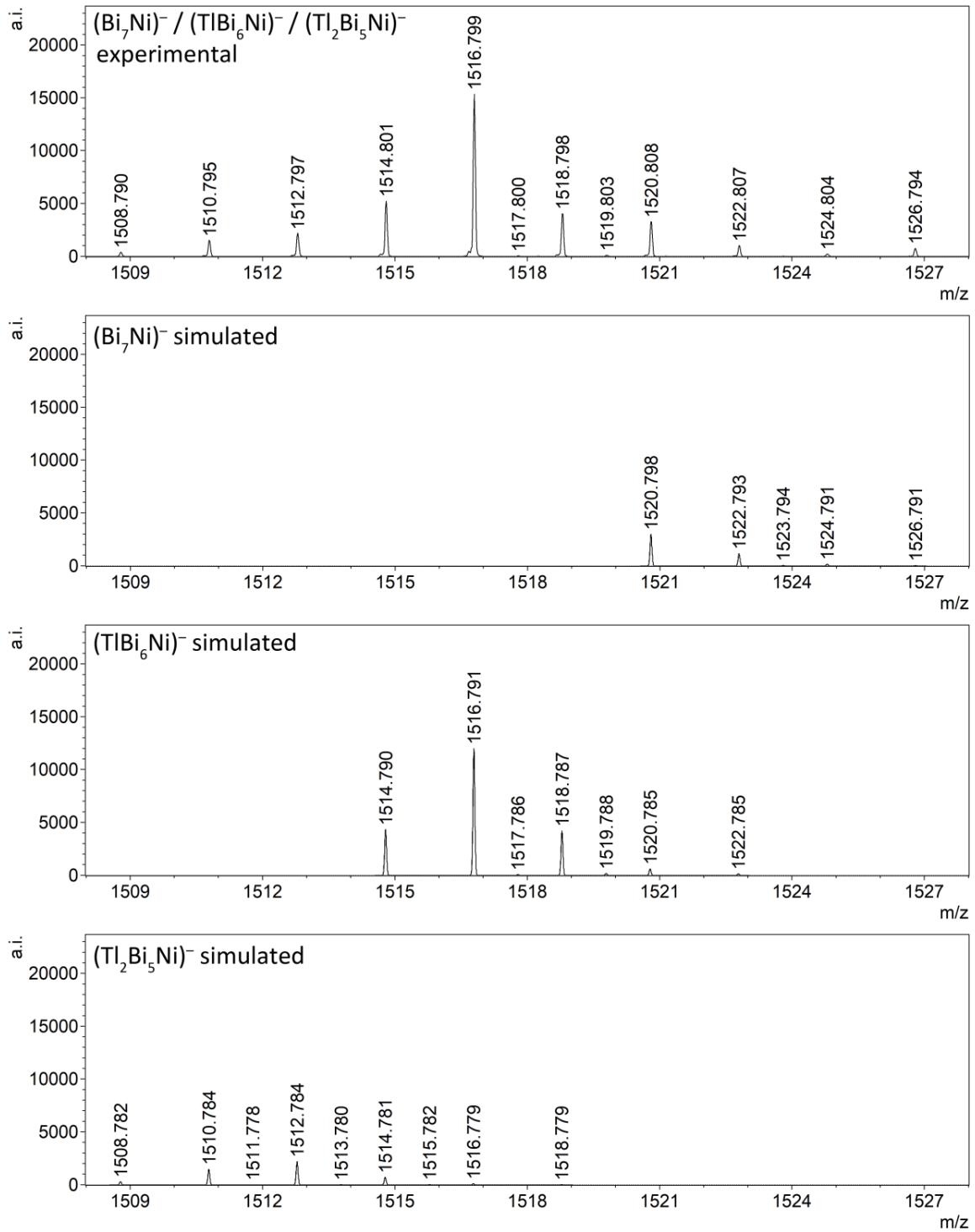

Figure S12. Comparison of experimental (top) and simulated mass spectra of $(Bi_7Ni)^-$, $(TlBi_6Ni)^-$, and $(Tl_2Bi_5Ni)^-$ ions (from top).

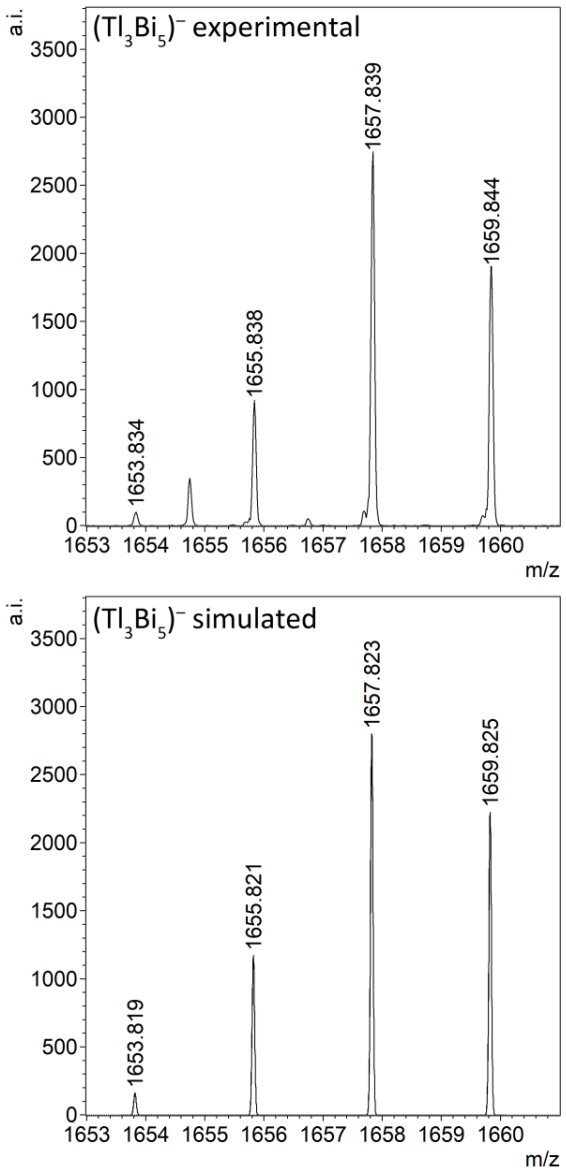

Figure S13. Comparison of experimental (top) and simulated mass spectra of $(Tl_3Bi_5)^-$ (bottom) ions.

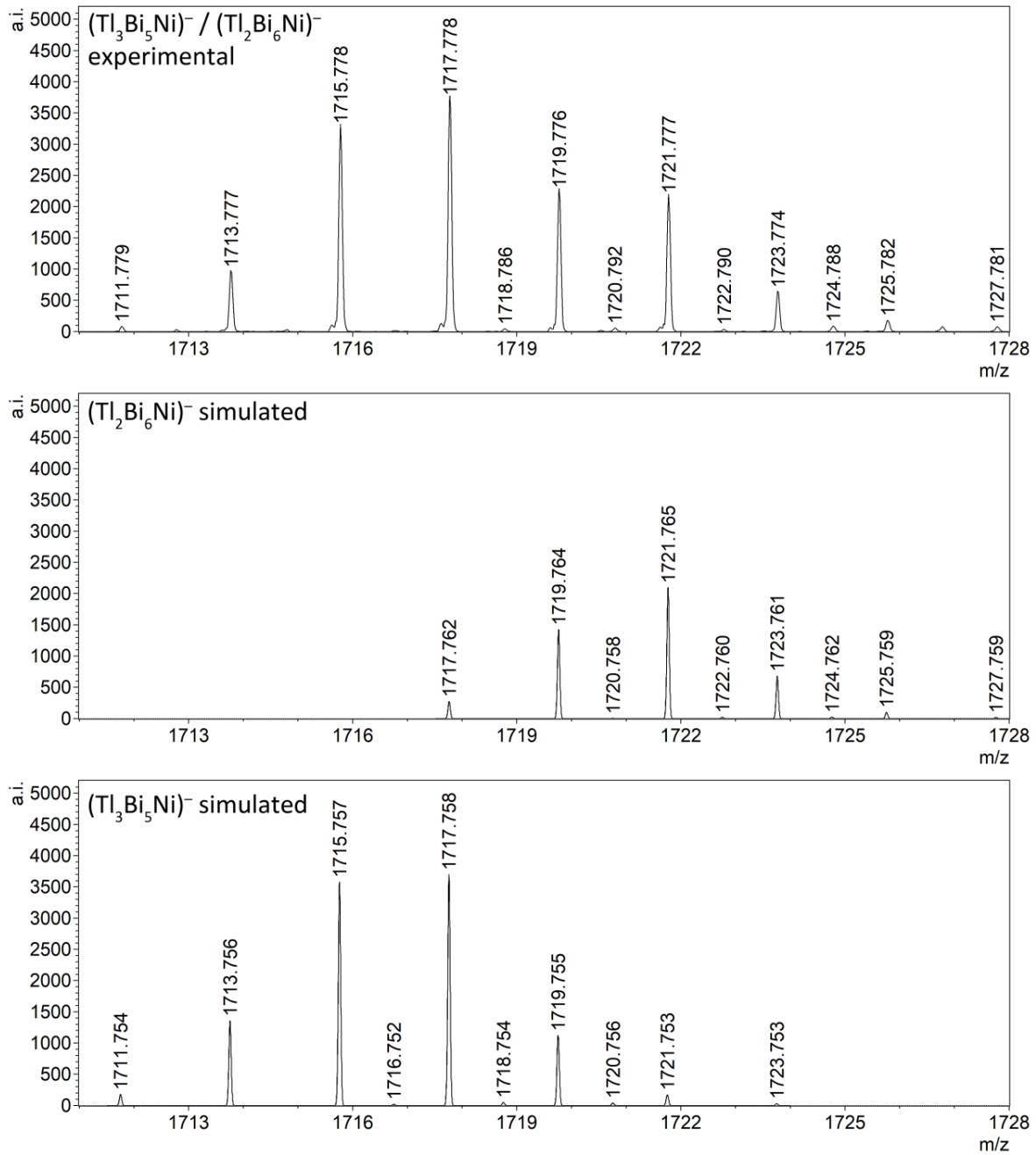

Figure S14. Comparison of experimental (top) and simulated mass spectra of $(Tl_2Bi_6Ni)^-$ (center), and $(Tl_3Bi_5Ni)^-$ (bottom) ions.

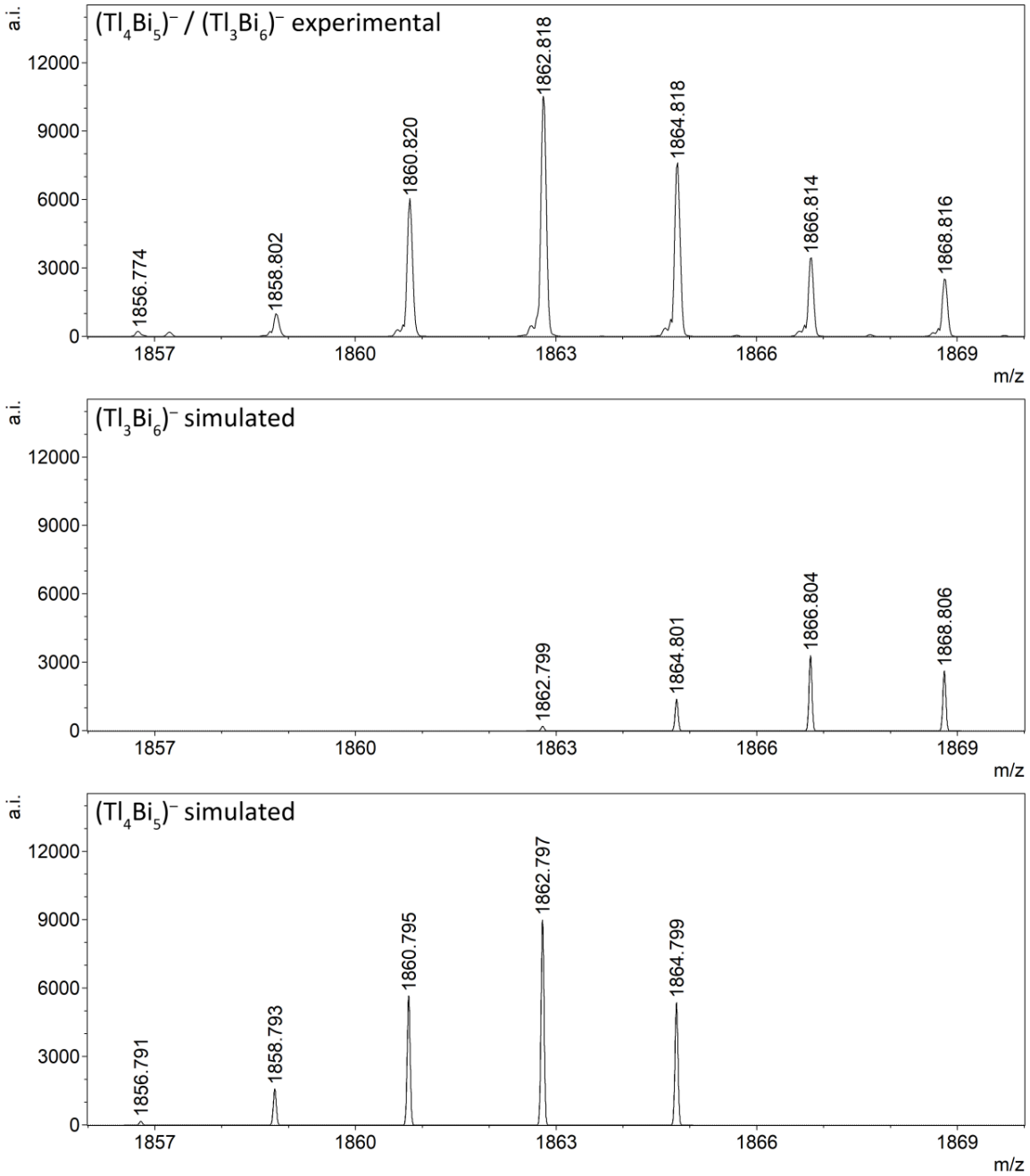

Figure S15. Comparison of experimental (top) and simulated mass spectra of $(Tl_3Bi_6)^-$ (center), and $(Tl_4Bi_5)^-$ (bottom) ions.

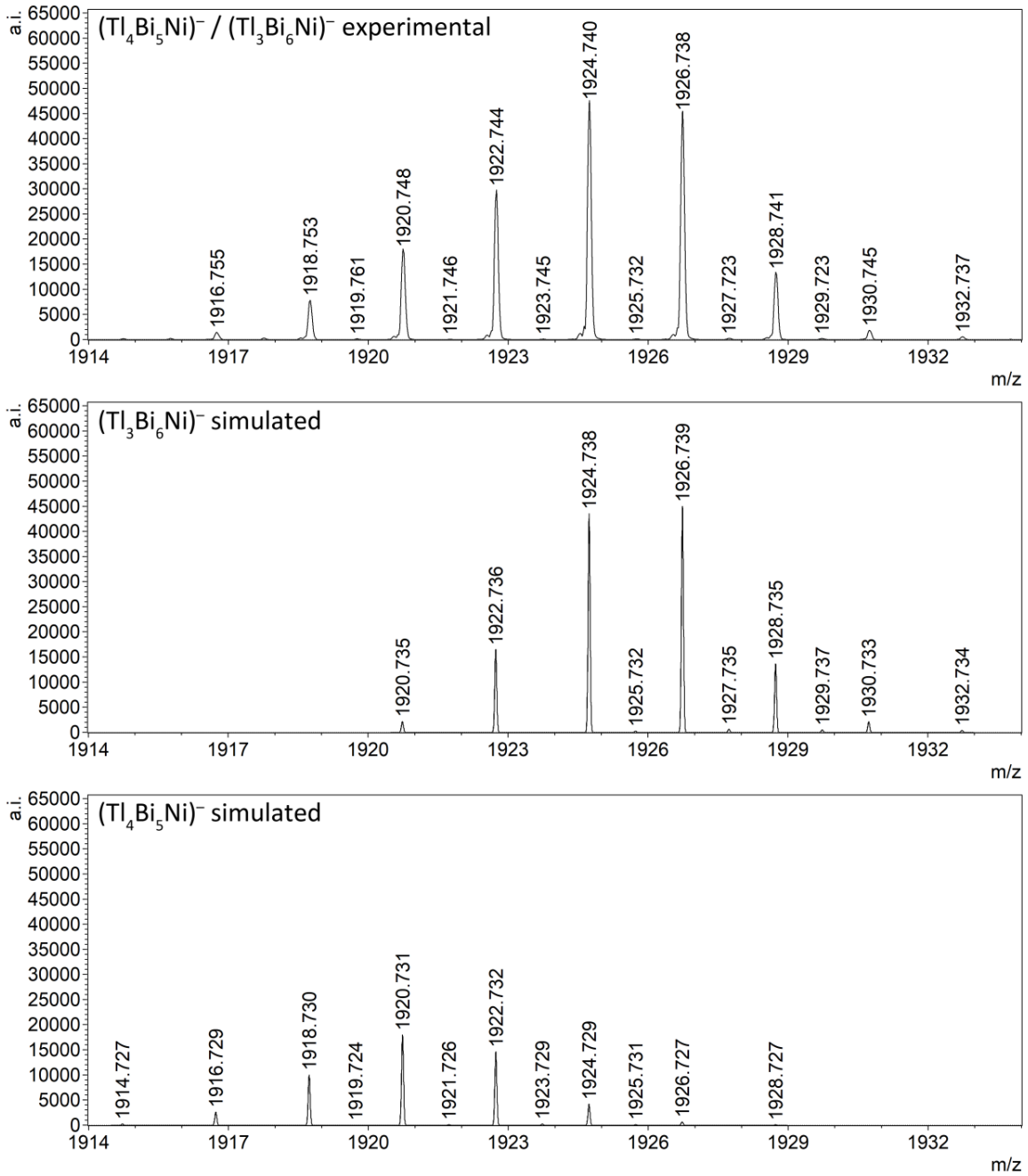

Figure S16. Comparison of experimental (top) and simulated mass spectra of $(Tl_3Bi_6Ni)^-$ (center), and $(Tl_4Bi_5Ni)^-$ (bottom) ions.

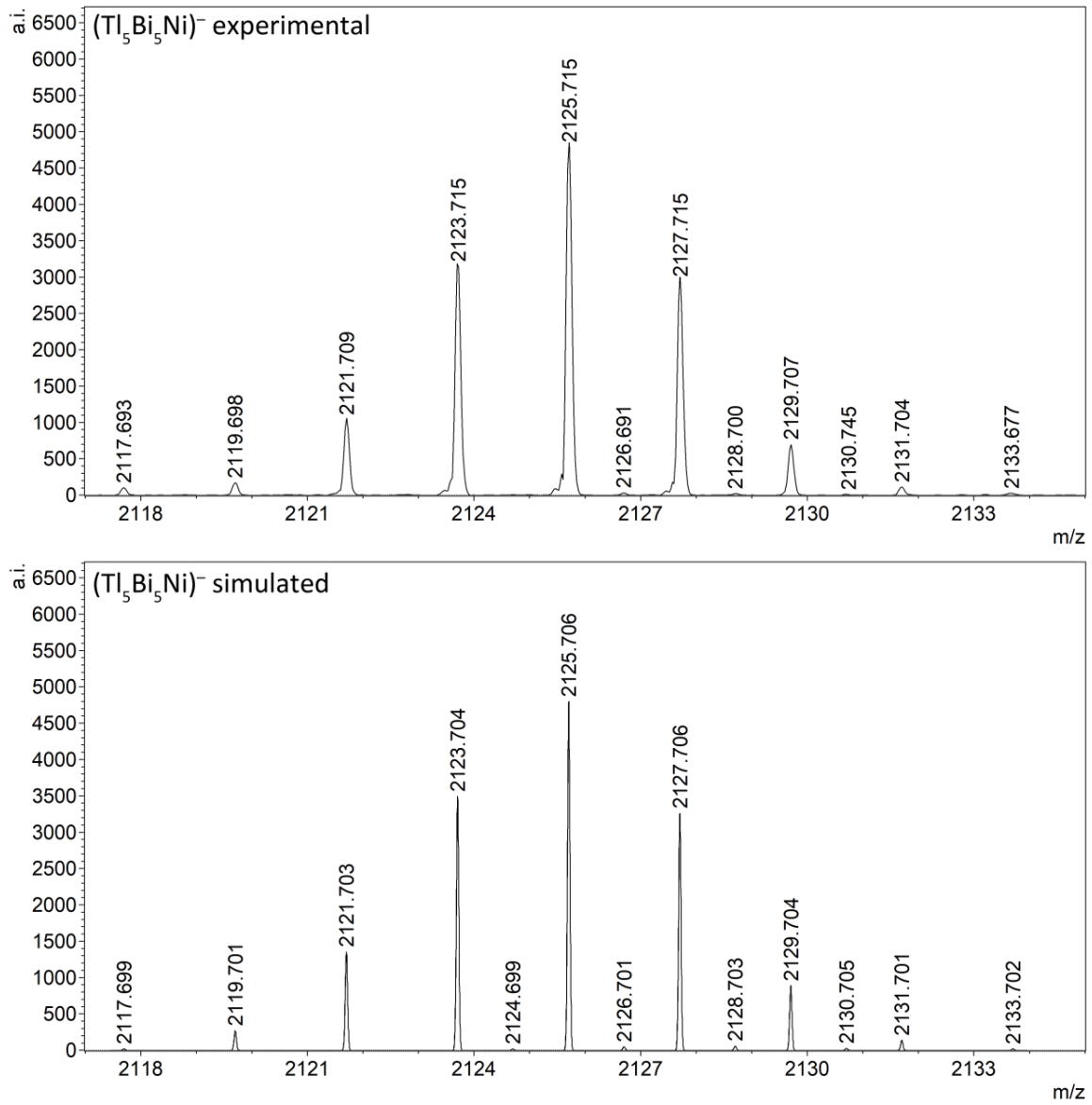

Figure S17. Comparison of experimental (top) and simulated mass spectra of $(Tl_5Bi_5Ni)^-$ (bottom) ions.

2.3. Mass Spectrometry of Fresh Solutions of Single-Crystals of K(crypt-222)]$_3$[Bi$_9${Ru(*cod*)}$_2$] (2) and Co-Precipitates of K(crypt-222)]$_2$[Tl$_2$Bi$_6${Ru(*cod*)}] (3), and K(crypt-222)]$_3$(Tl$_4$Bi$_5$) (4)

Crystals of **2** were obtained from diffusion controlled crystallization experiments. After prolonged crystallization times of several weeks the solution was removed with a syringe. The crystals were washed with 10 mL of dry toluene and then dried *in vacuo* for 30 minutes. Even though the crystals were carefully removed from the Schlenk tube, a contamination with co-precipitates of **3** and **4** could not be avoided, hence signals from all three cluster anions are detectable in the mass spectrum. Figure S18 provides an overview of the obtained mass spectrum. High resolution views of the individual signals are provided in the Figures S19 – S32 along with the corresponding simulations.

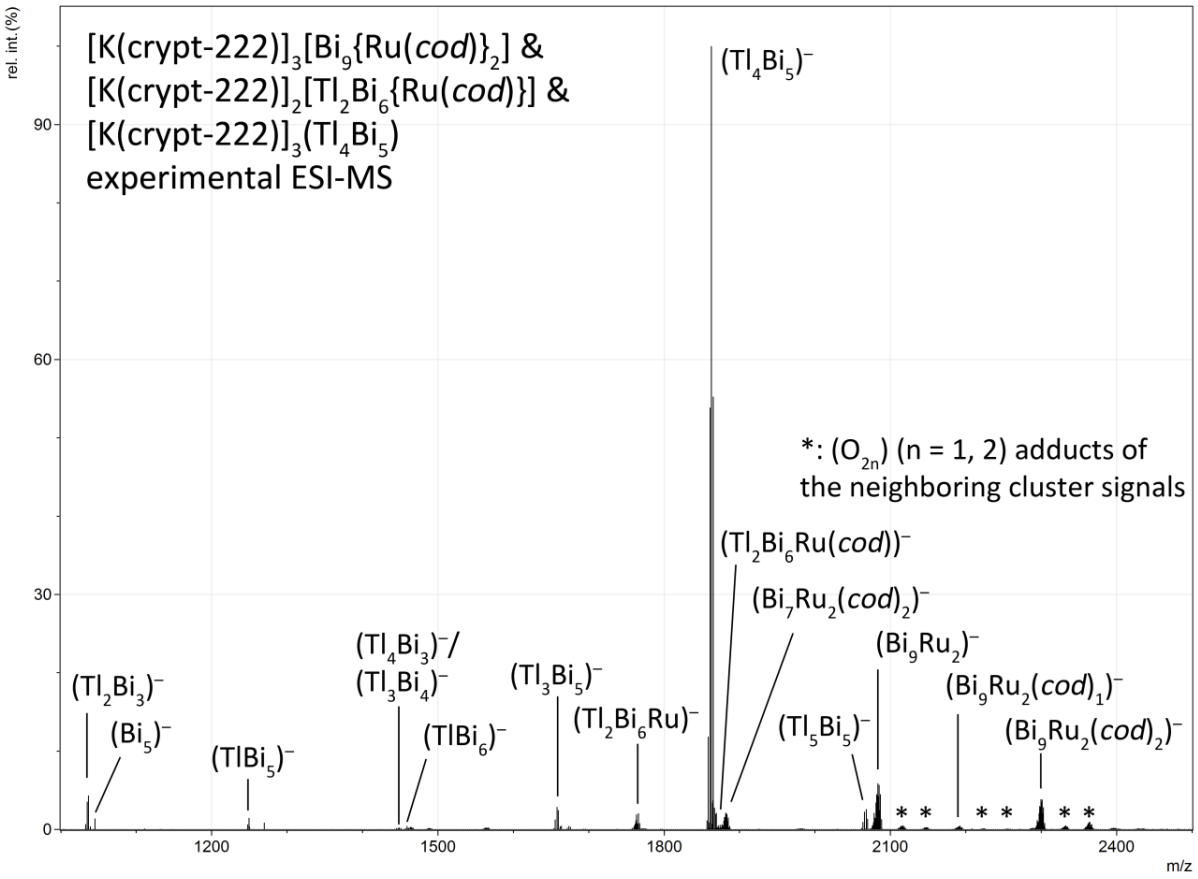

Figure S18. Overview of the ESI mass spectrum recorded from a fresh solution of single-crystals of [K(crypt-222)]$_3$[Bi$_9${Ru(*cod*)}$_2$] (2) alongside co-precipitates of [K(crypt-222)]$_2$[Tl$_2$Bi$_6${Ru(*cod*)}] (3), and [K(crypt-222)]$_3$(Tl$_4$Bi$_5$) (4) in DMF.

2.3.1. Signals of $[Bi_9\{Ru(cod)\}_2]^-$ and Corresponding Fragments

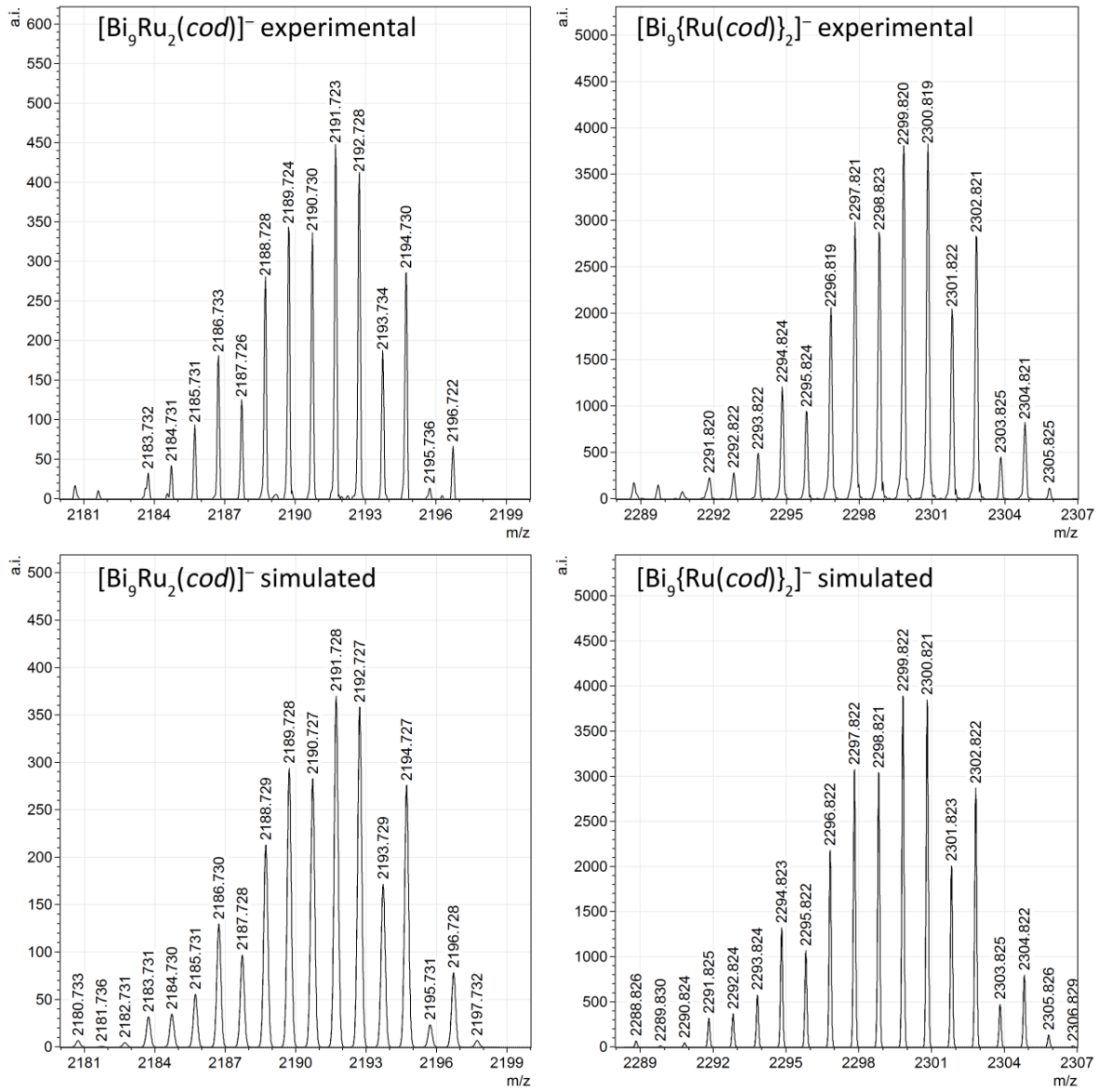

Figure S19. Comparison of experimental (top) and simulated (bottom) mass spectrum of $[Bi_9\{Ru(cod)\}_2]^-$ (right) and $[Bi_9Ru_2(cod)]^-$ (left) ions.

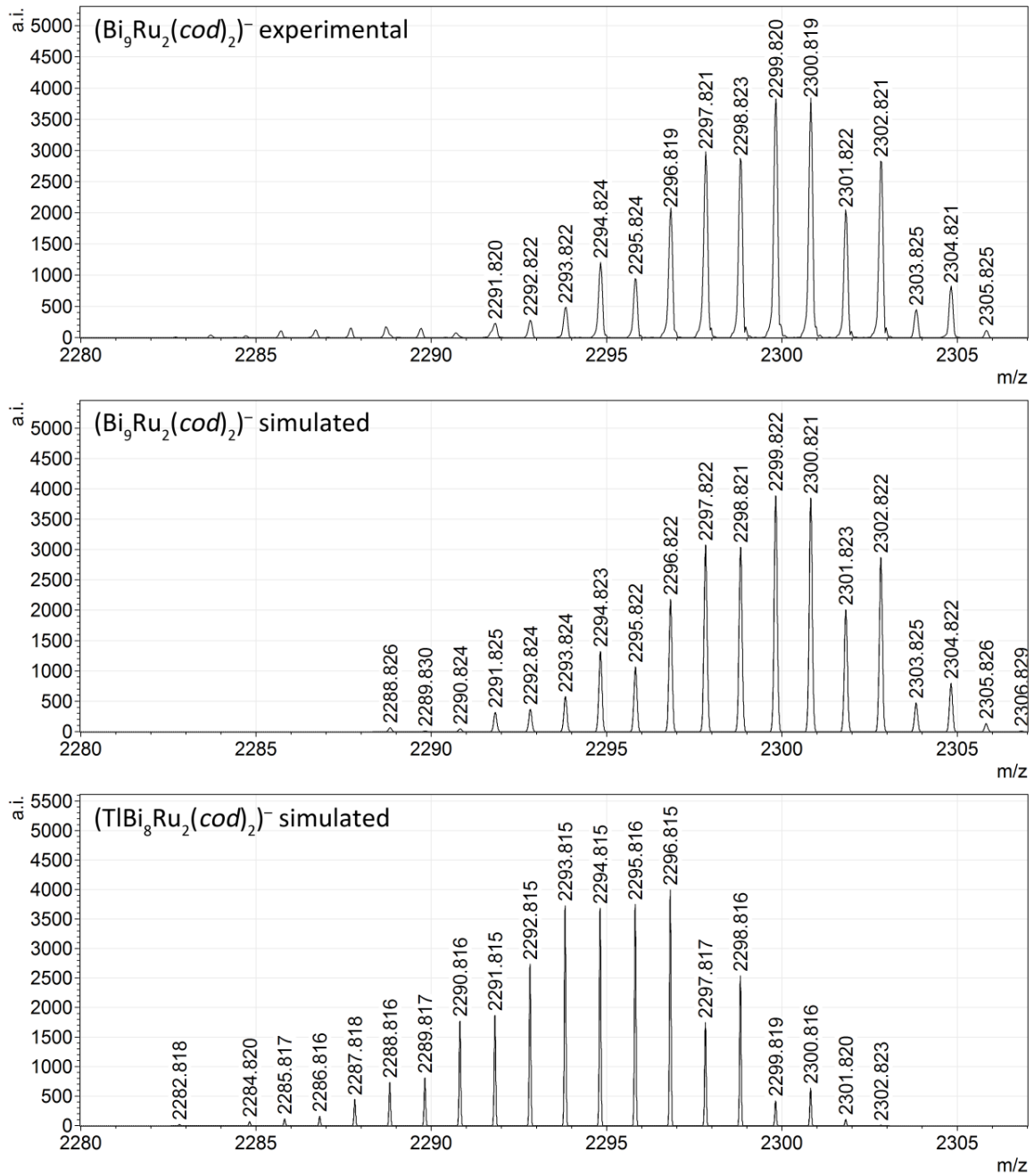

Figure S20. Comparison of experimental (top) and simulated mass spectra of $[Bi_9\{Ru(cod)\}_2]^-$ (center) and the hypothetical $[TlBi_8\{Ru(cod)\}_2]^-$ (bottom) ions.

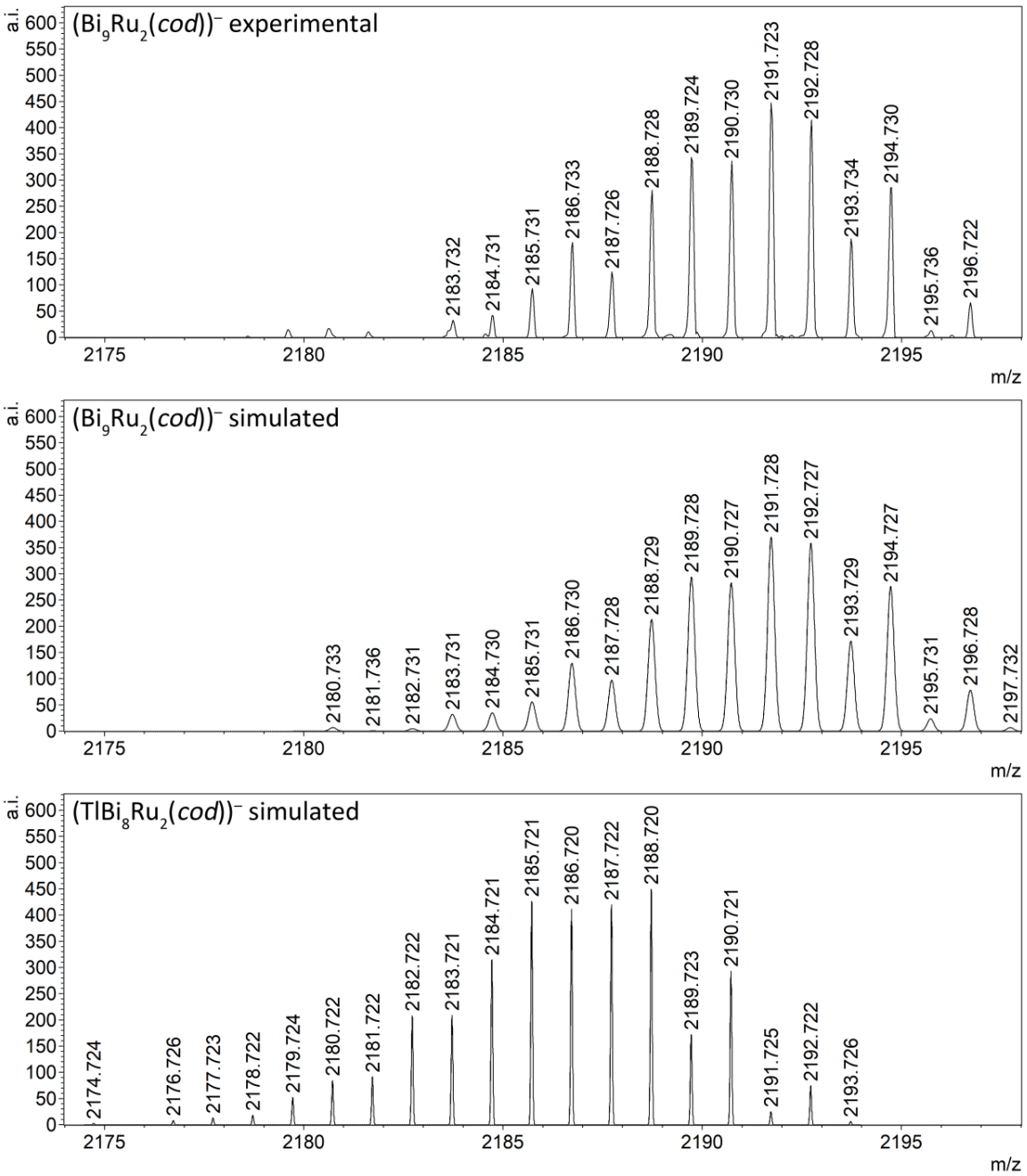

Figure S21. Comparison of experimental (top) and simulated mass spectra of $[Bi_9Ru_2(cod)]^-$ (center) and the hypothetical $[TlBi_8Ru_2(cod)]^-$ (bottom) ions.

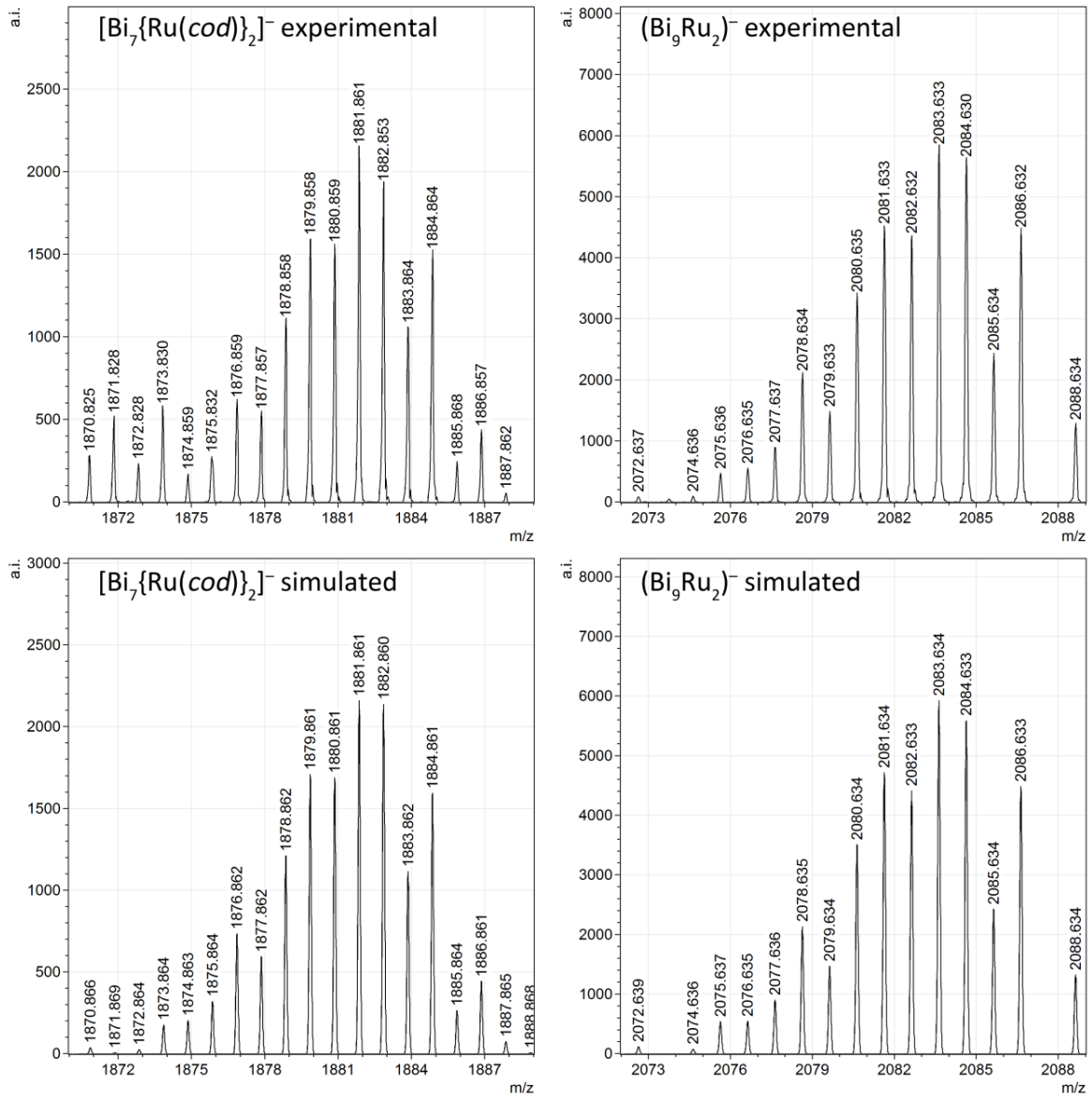

Figure S22. Comparison of experimental (top) and simulated (bottom) mass spectra of $[Bi_9Ru_2]^-$ (right) and $[Bi_7\{Ru(cod)\}_2]^-$ (left) ions.

2.3.2. Signals of Oxygen-Adducts of $[Bi_9\{Ru(cod)\}_2]^-$, and Corresponding Fragments

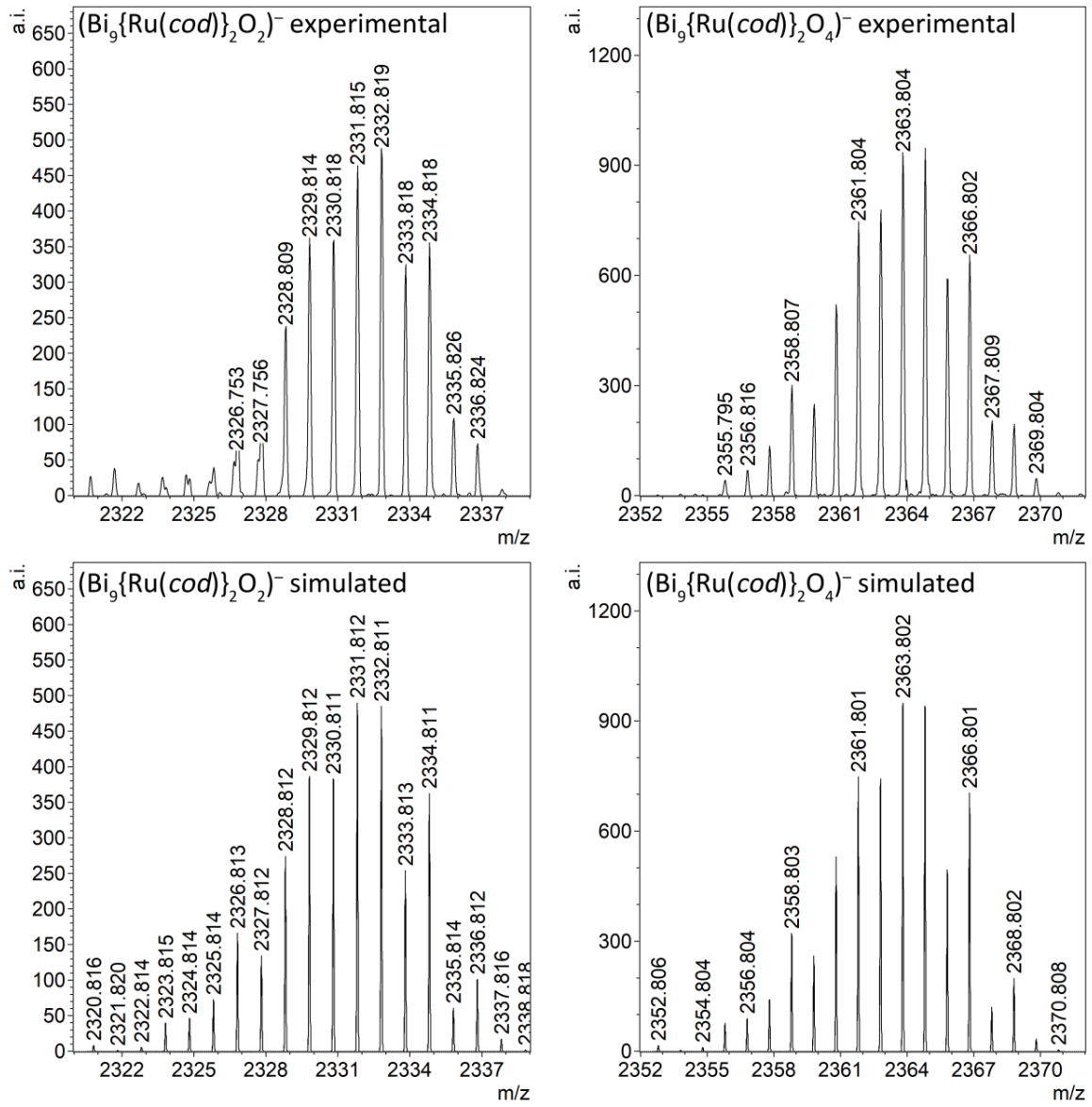

Figure S23. Comparison of experimental (top) and simulated (bottom) mass spectra of $[Bi_9\{Ru(cod)\}_2O_2]^-$ (left) and $[Bi_9\{Ru(cod)\}_2O_4]^-$ (right) ions.

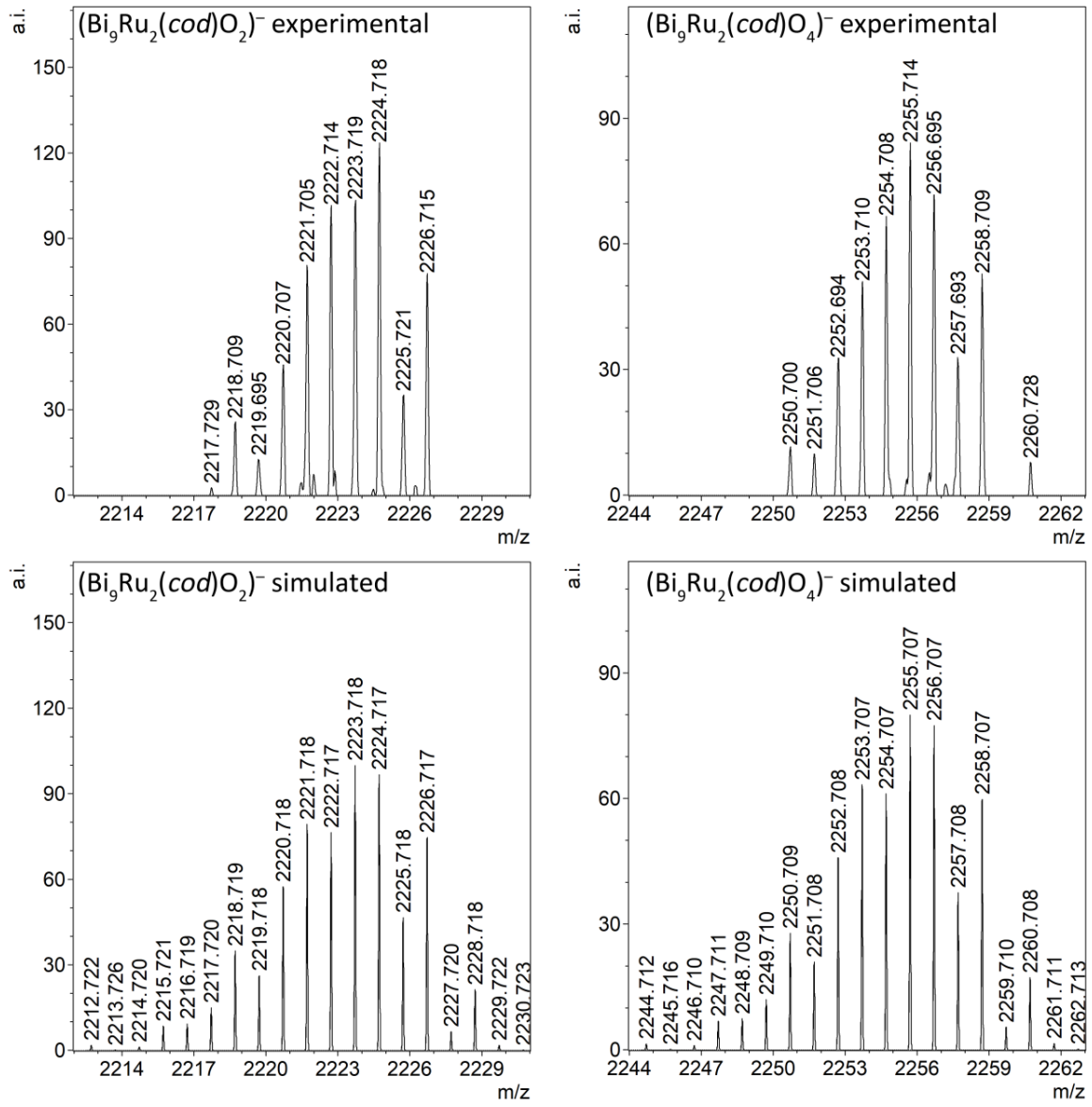

Figure S24. Comparison of experimental (top) and simulated (bottom) mass spectra of $[Bi_9Ru_2(cod)O_2]^-$ (left) and $[Bi_9Ru_2(cod)O_4]^-$ (right) ions.

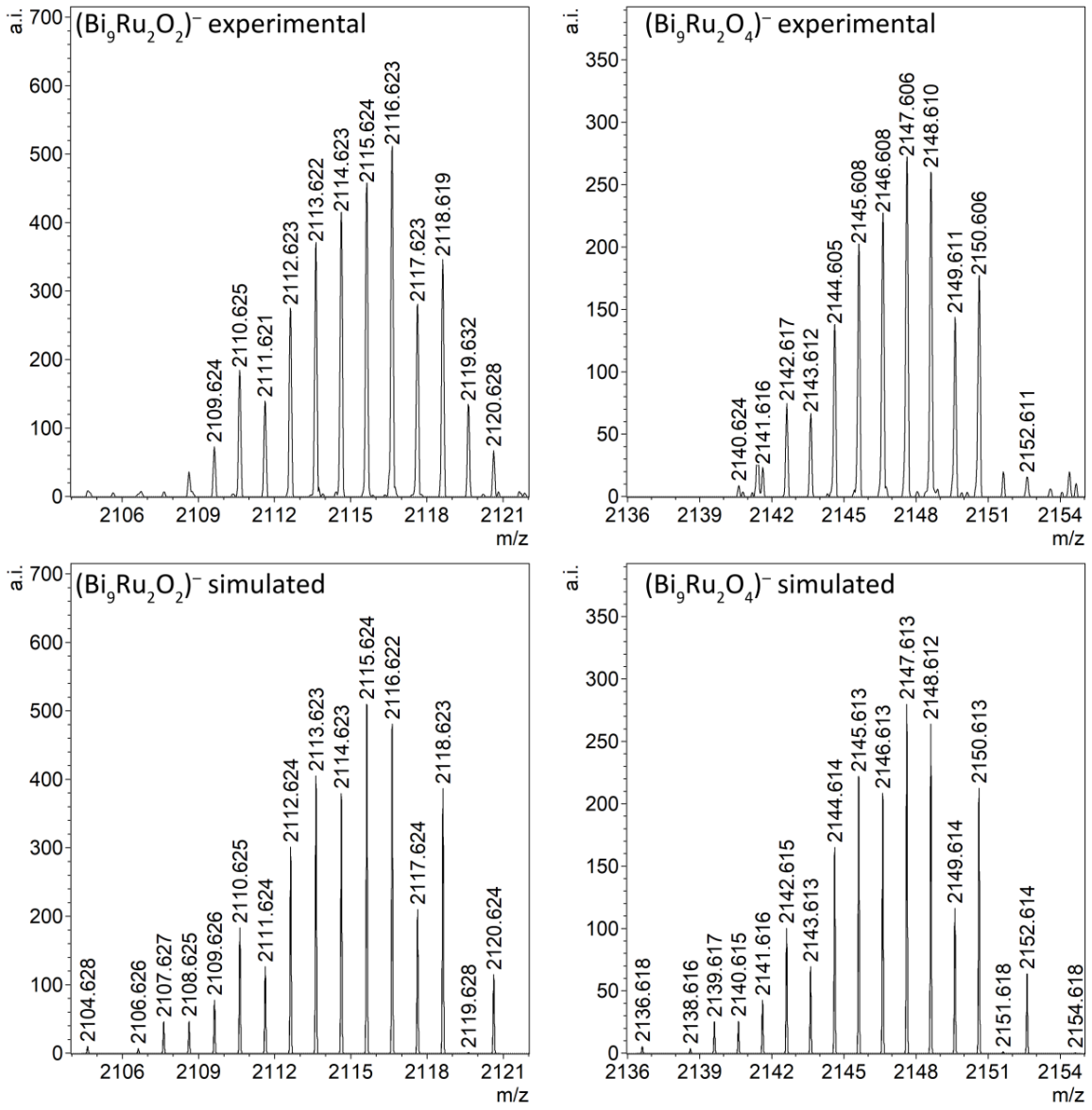

Figure S25. Comparison of experimental (top) and simulated (bottom) mass spectra of $[Bi_9Ru_2O_2]^-$ (left) and $[Bi_9Ru_2O_4]^-$ (right) ions.

2.3.3. Mass Spectra of $[Tl_2Bi_6Ru(cod)]^-$ and Corresponding Fragments

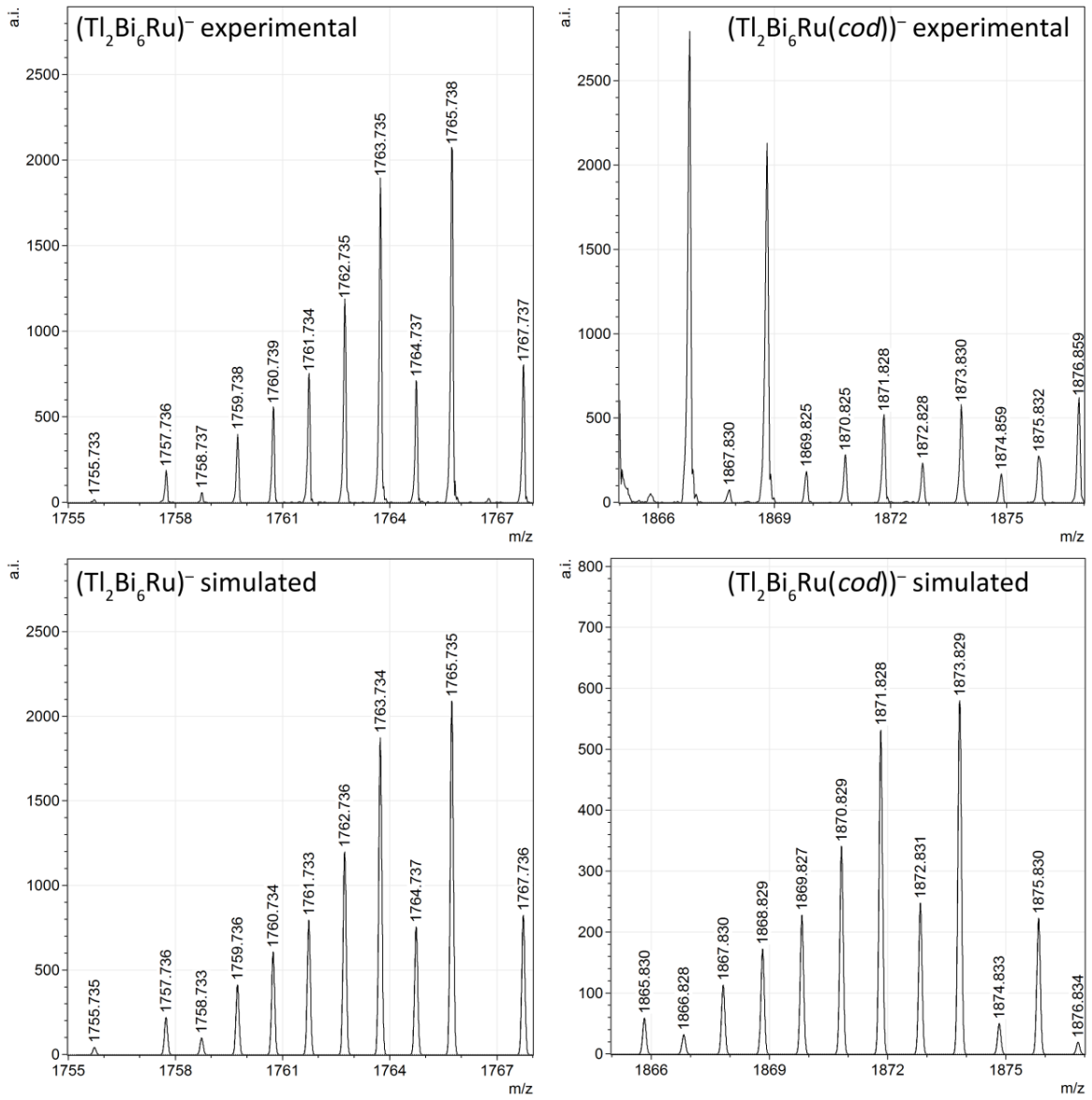

Figure S26. Comparison of experimental (top) and simulated (bottom) mass spectra of $[RuTl_2Bi_6]^-$ (left) and $[Tl_2Bi_6\{Ru(cod)\}]^-$ (right) ions.

2.3.4. Mass Spectra of $(Tl_4Bi_5)^-$ and Corresponding Fragments

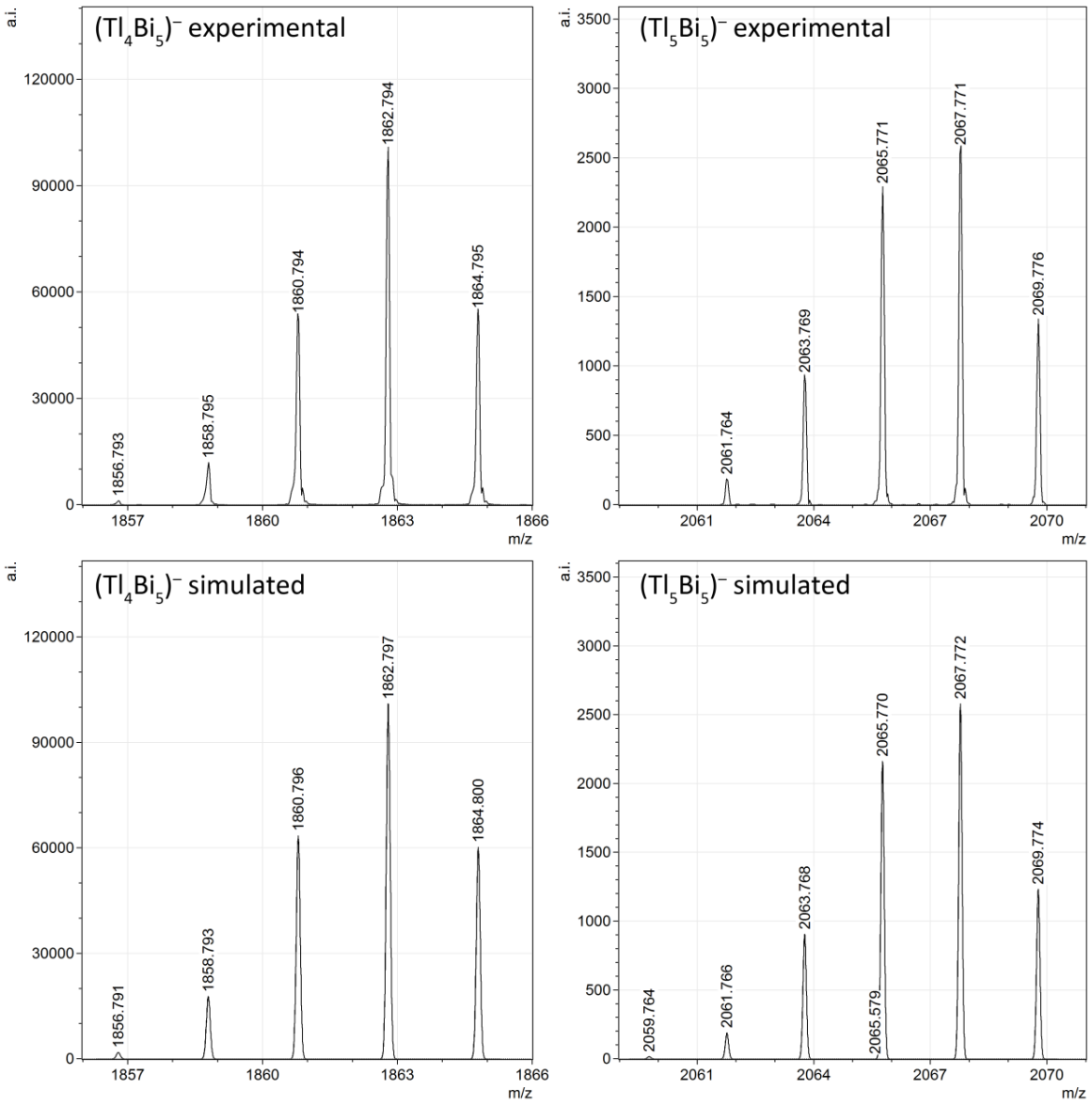

Figure S27. Comparison of experimental (top) and simulated (bottom) mass spectra of $(Tl_4Bi_5)^-$ (left) and $(Tl_5Bi_5)^-$ (right) ions.

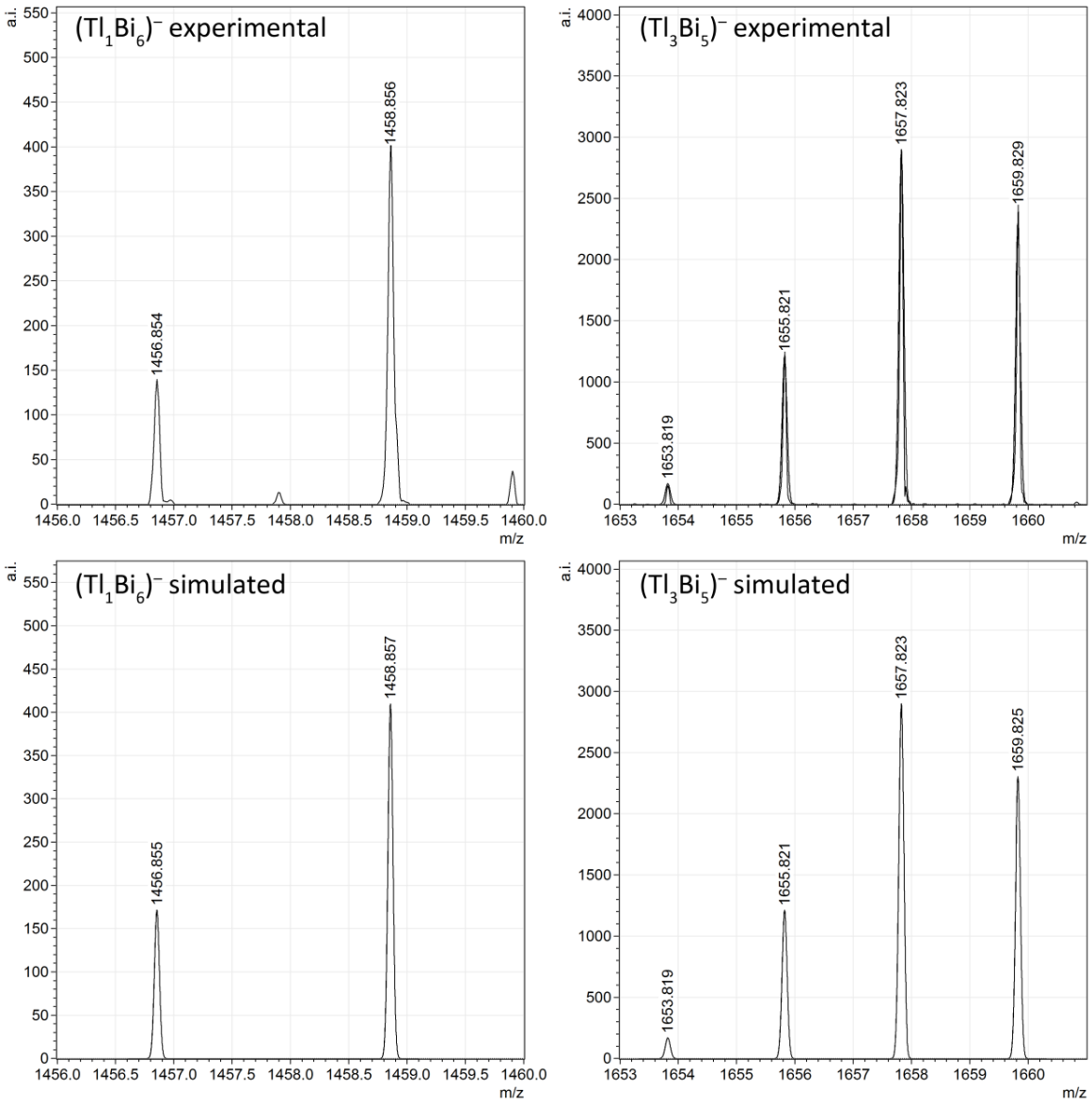

Figure S28. Comparison of experimental (top) and simulated (bottom) mass spectra of $(Tl_1Bi_6)^-$ (left) and $(Tl_3Bi_5)^-$ (right) ions.

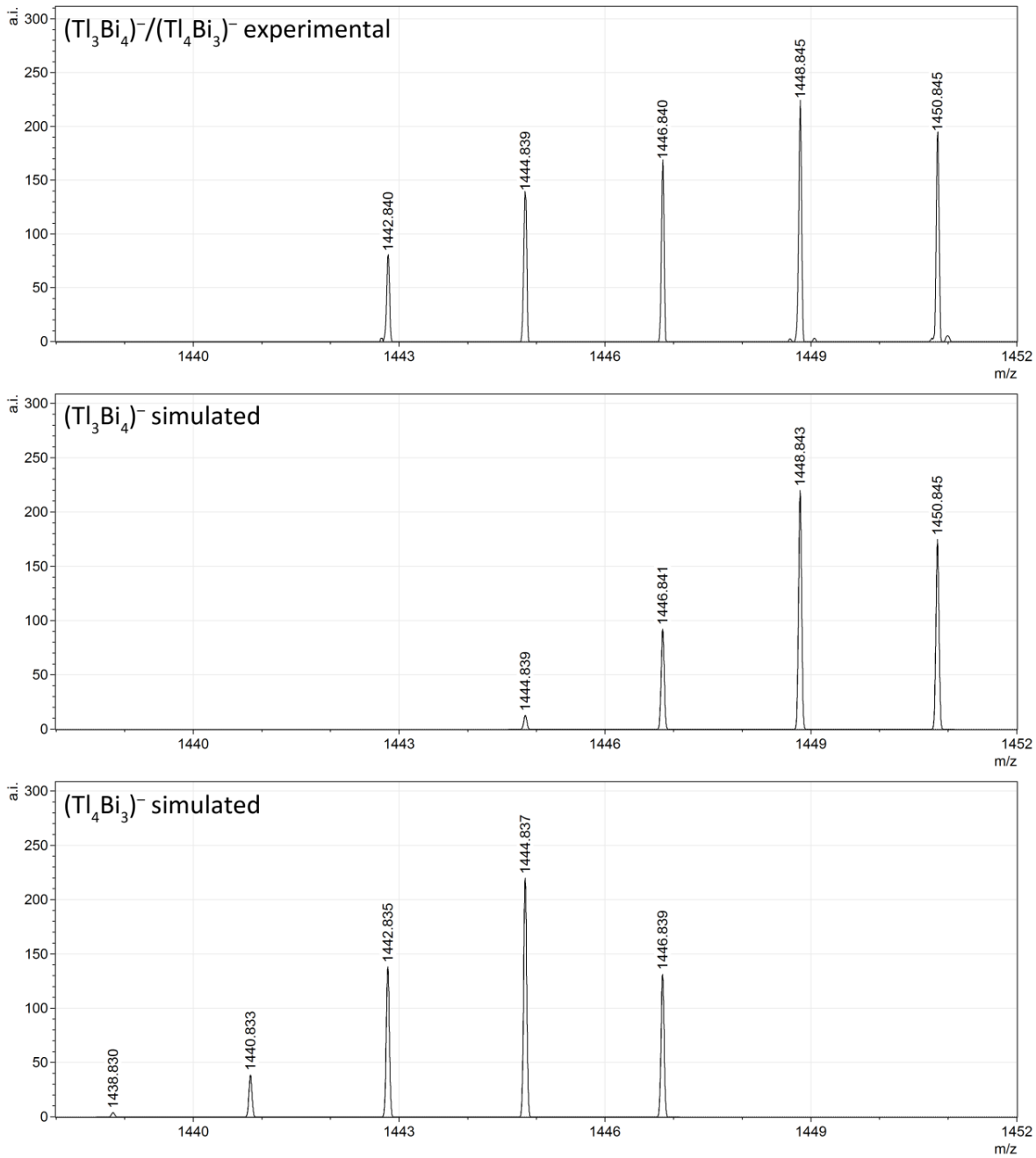

Figure S29. Comparison of experimental (top) and simulated mass spectra of $(Tl_3Bi_4)^-$ (center) and $(Tl_4Bi_3)^-$ (bottom) ions.

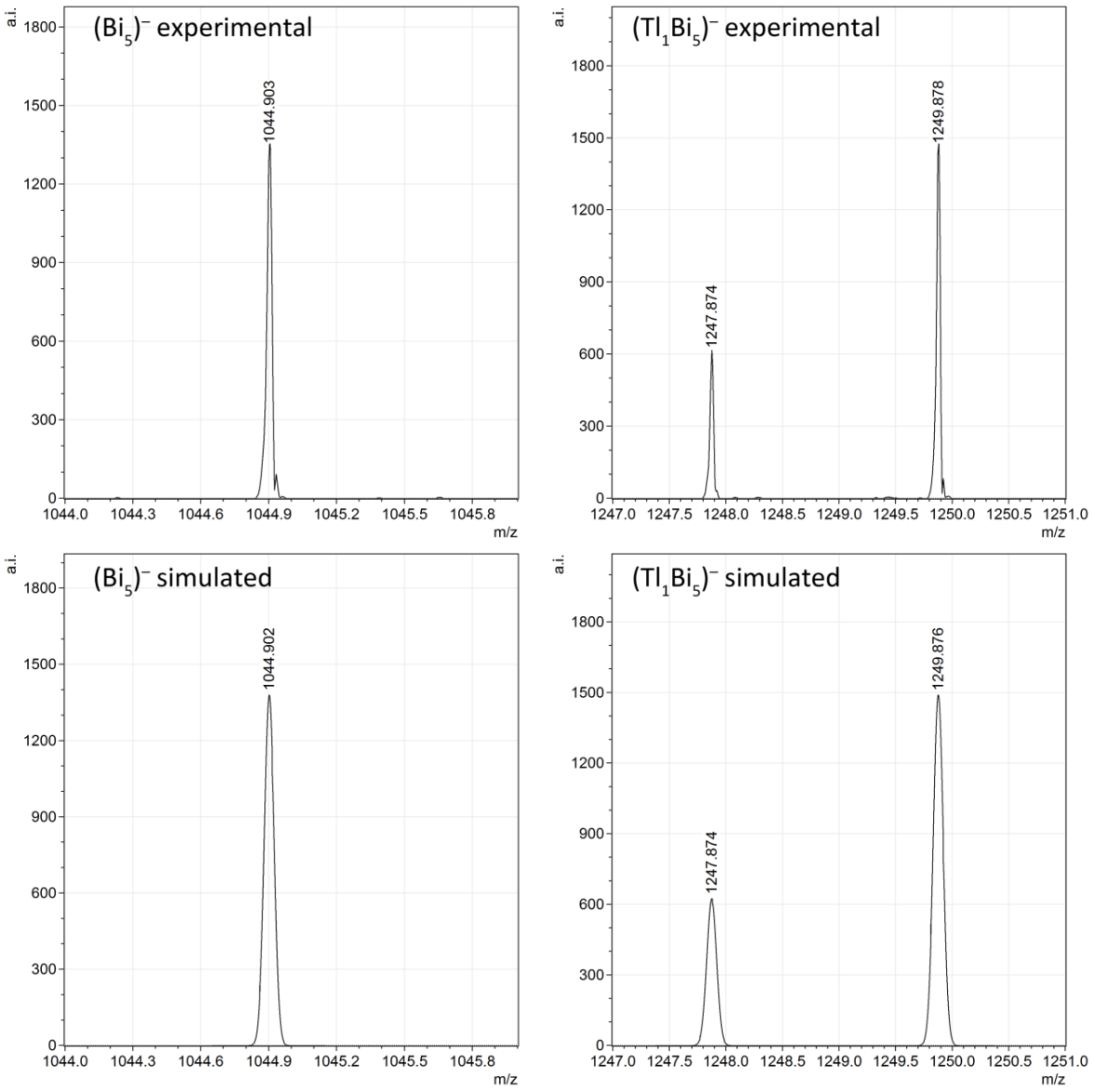

Figure S30. Comparison of experimental (top) and simulated (bottom) mass spectra of $(Bi_5)^-$ (left) and $(Tl_1Bi_5)^-$ (right) ions.

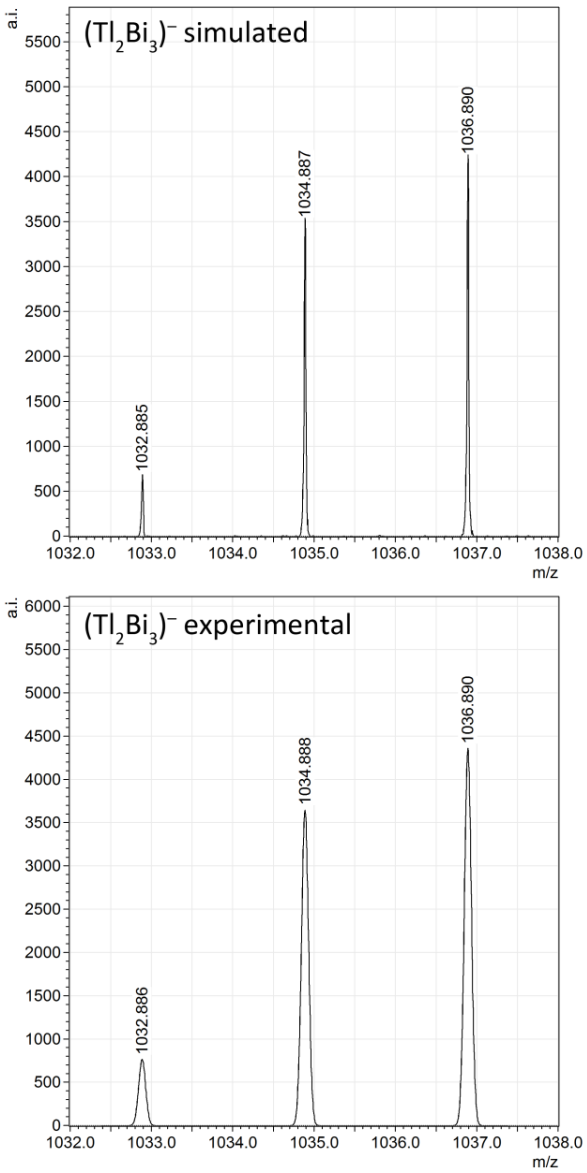

Figure S31. Comparison of experimental (top) and simulated (bottom) mass spectra of $(Tl_2Bi_3)^-$.

2.3.5. High Resolution of the Mass Spectrum at m/z = 1855 – 1890 with Simulations

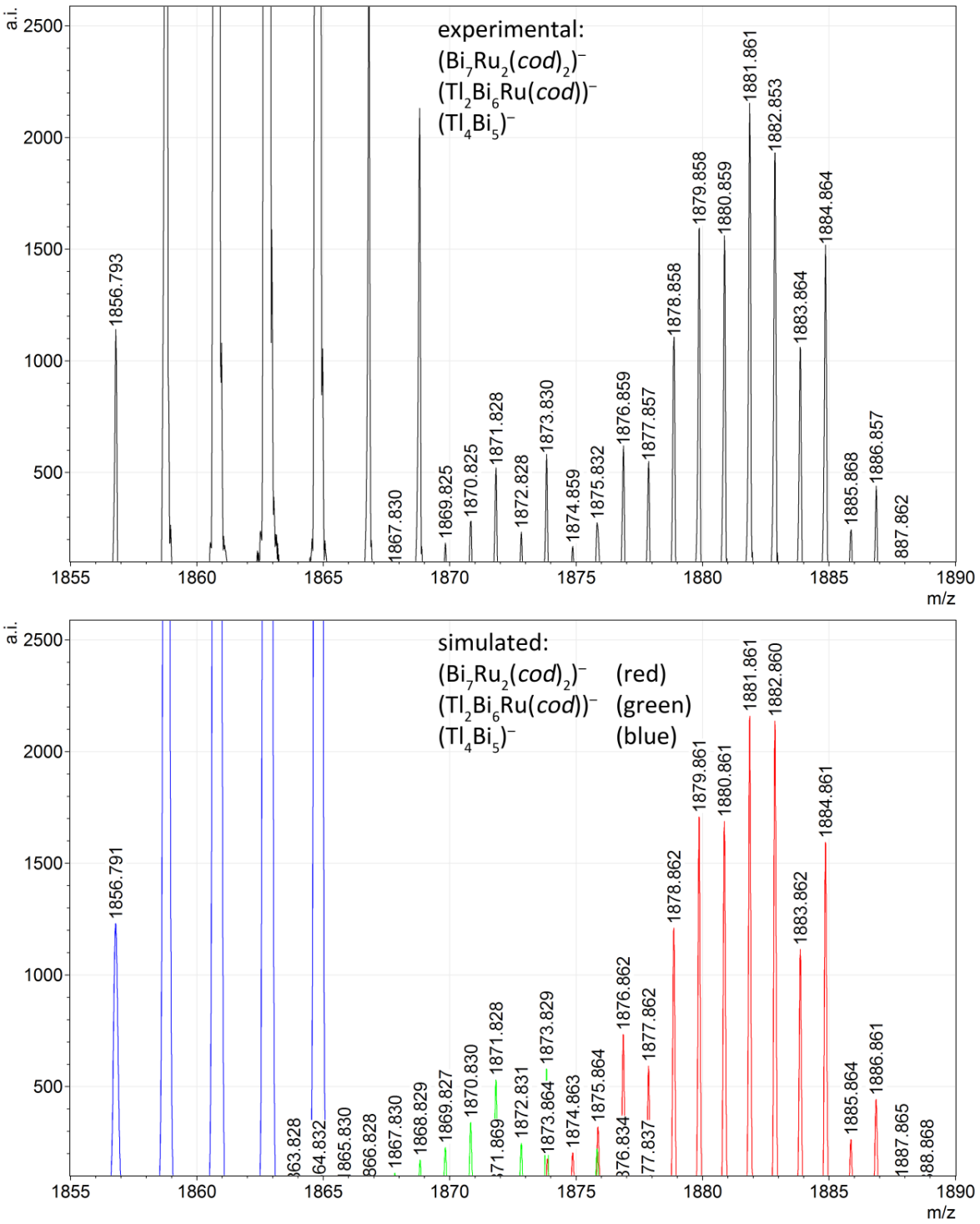

Figure S32. High resolution of the mass spectrum at m/z = 1855 – 1890 with simulations of $(Tl_4Bi_5)^-$ (blue), $[Tl_2Bi_6Ru(cod)]^-$ (green), and $[Bi_7Ru_2(cod)_2]^-$ (red).

2.4. Mass Spectrometry of K(crypt-222)]$_2$[Tl_2Bi_6{Ru(*cod*)}] (3)

Crystals of **3** were obtained from diffusion controlled crystallization experiments. After prolonged crystallization times of several weeks the solution was removed with a syringe. The crystals were washed with 10 mL of dry toluene and then dried *in vacuo* for 30 minutes. Figure S33 provides an overview of the obtained mass spectrum. High resolution views of the individual signals are provided in the Figures S34 and S35 along with the corresponding simulations.

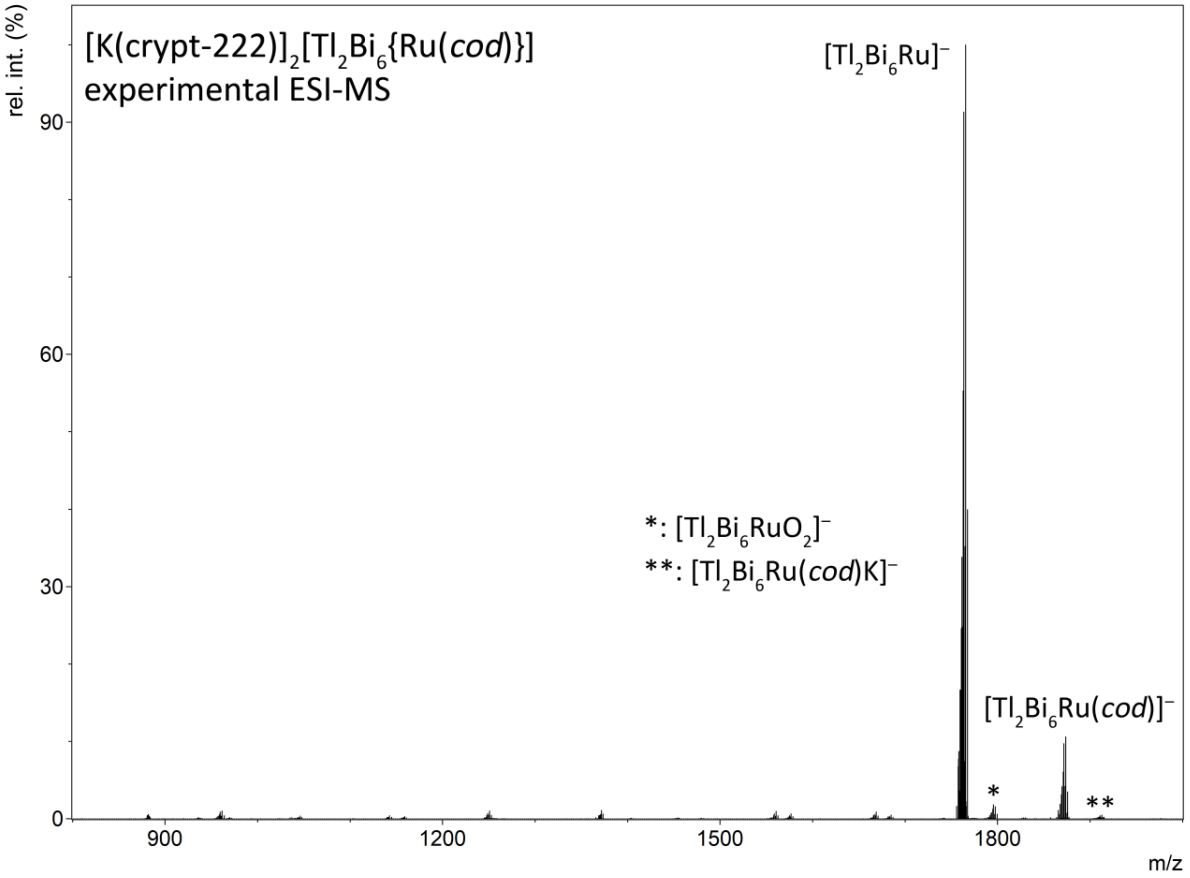

Figure S33. Overview of the ESI mass spectrum of a fresh solution of single-crystals of [K(crypt-222)]$_2$[Tl_2Bi_6{Ru(*cod*)}] (3) in DMF.

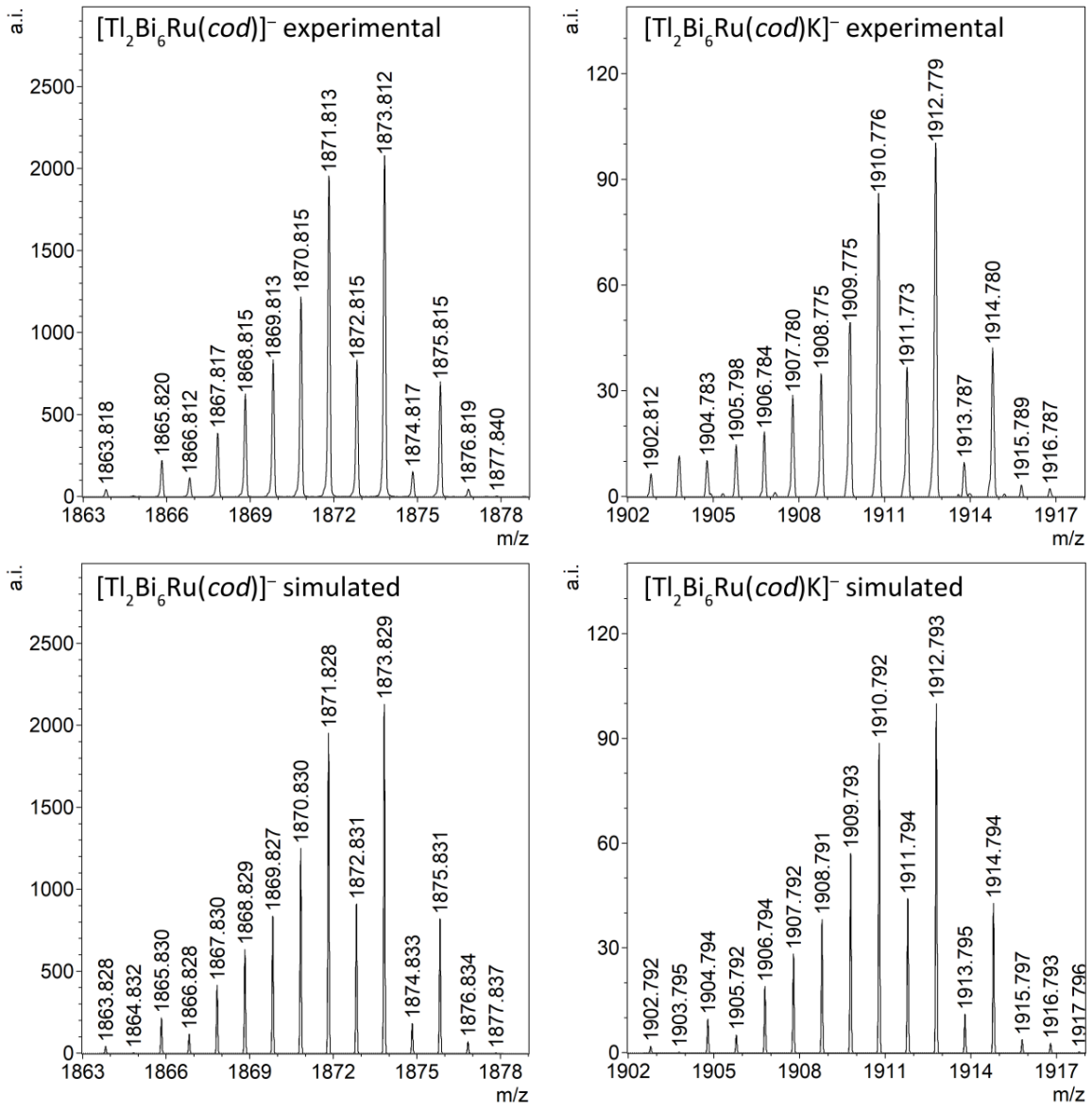

Figure S34. Comparison of experimental (top) and simulated (bottom) mass spectra of $[Tl_2Bi_6Ru(cod)]^-$ (left) and $[Tl_2Bi_6Ru(cod)K]^-$ (right) ions.

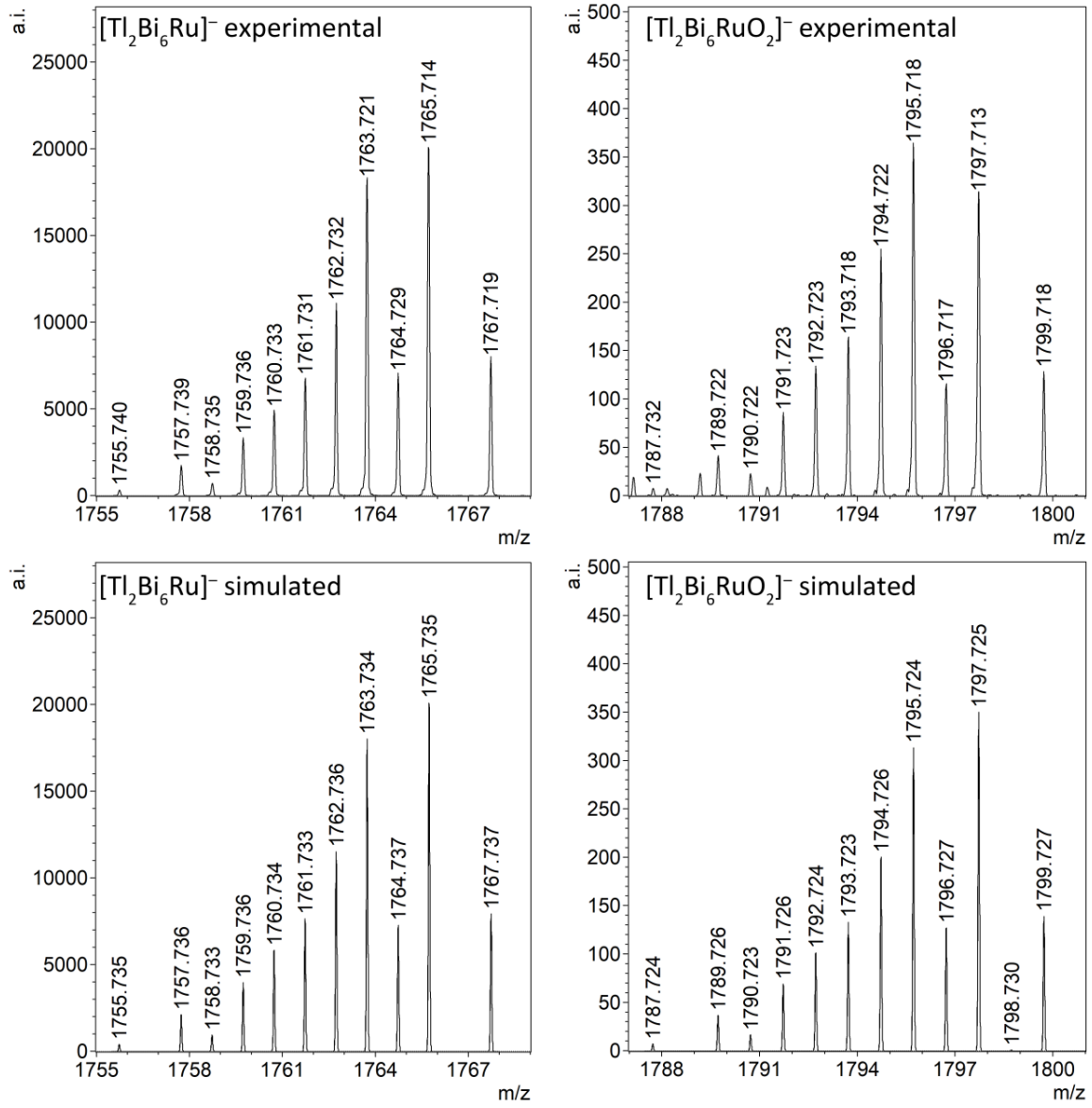

Figure S35. Comparison of experimental (top) and simulated (bottom) mass spectra of $[Tl_2Bi_6Ru]^-$ (left) and $[Tl_2Bi_6RuO_2]^-$ (right) ions.

2.5. Mass Spectrometry of K(crypt-222)]$_3$(Tl$_4$Bi$_5$) (4)

Crystals of **4** were obtained from diffusion controlled crystallization experiments. After prolonged crystallization times of several weeks the solution was removed with a syringe. The crystals were washed with 10 mL of dry toluene and then dried *in vacuo* for 30 minutes. Figure S36 provides an overview of the obtained mass spectrum. High resolution views of the individual signals are provided in the Figures S37 – S40 along with the corresponding simulations.

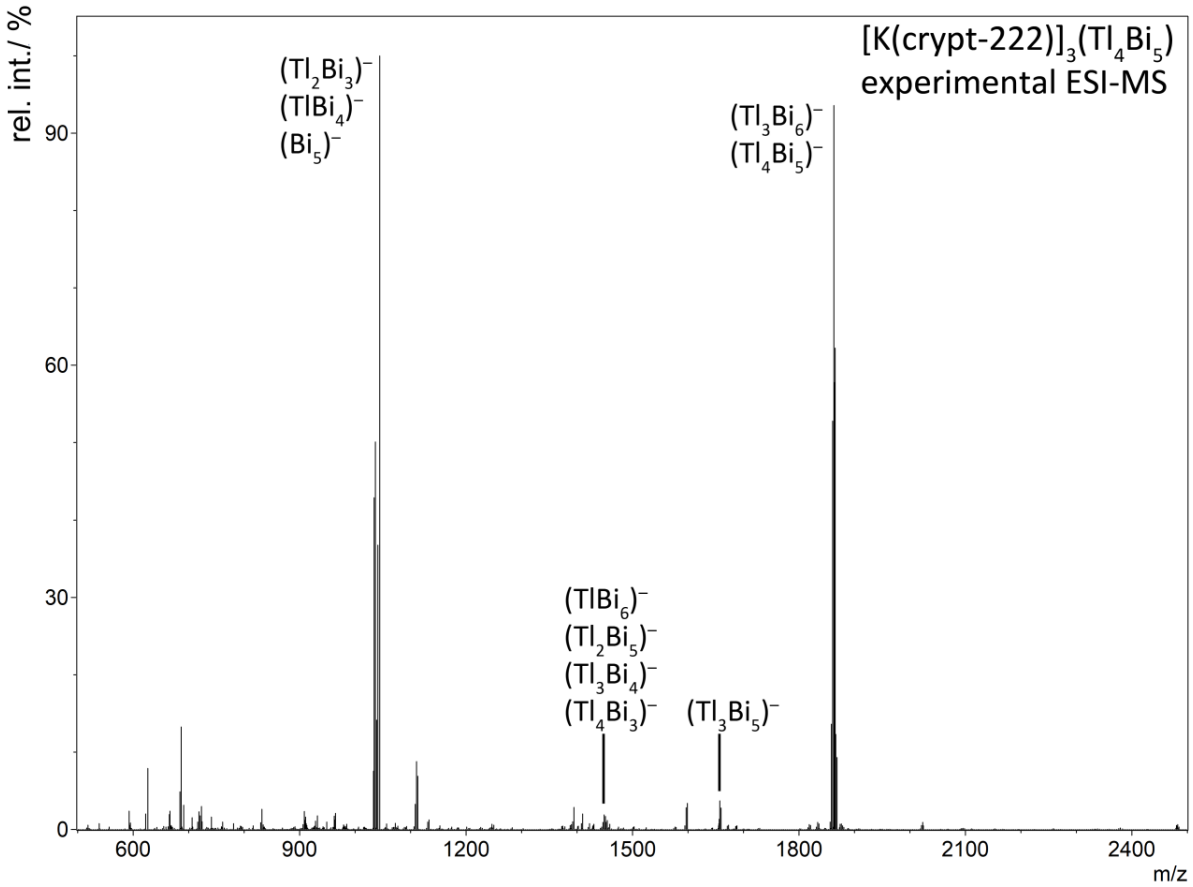

Figure S36. Overview of the ESI mass spectrum of a fresh solution of single-crystals of [K(crypt-222)]$_3$(Tl$_4$Bi$_5$) (4) in DMF.

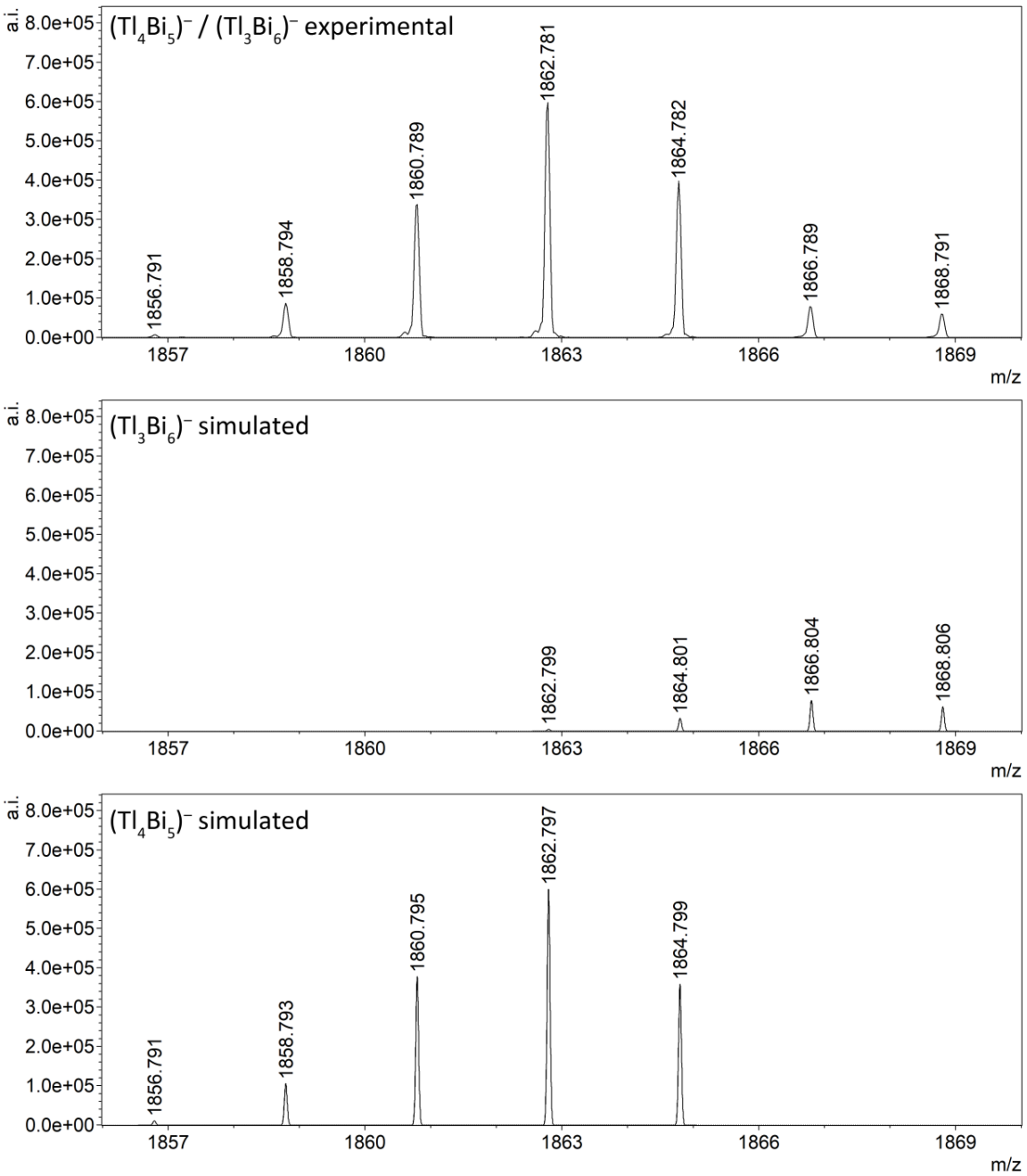

Figure S37. Comparison of experimental (top) and simulated mass spectra of $(Tl_3Bi_6)^-$ (center), and $(Tl_4Bi_5)^-$ (bottom) ions.

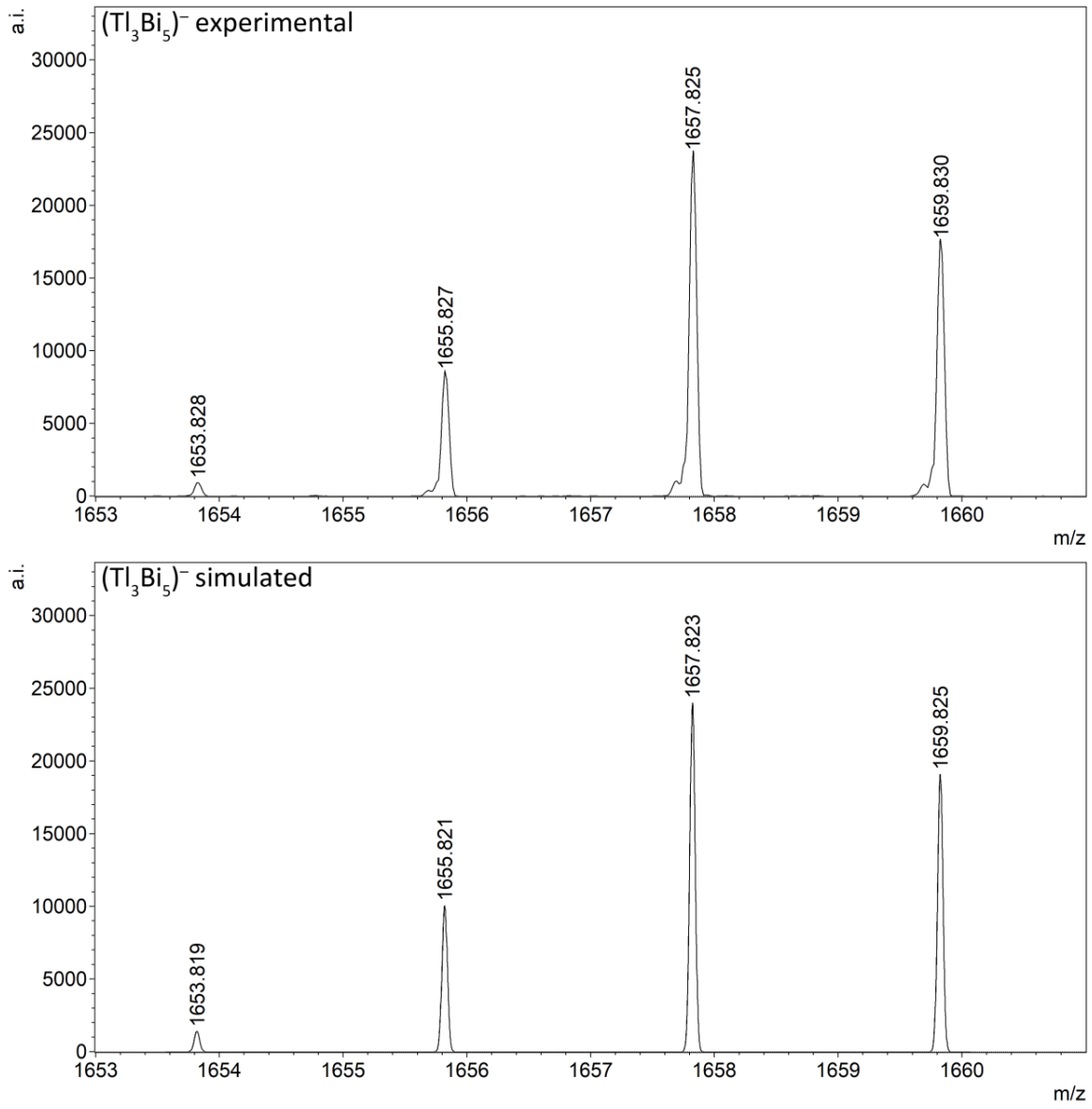

Figure S38. Comparison of experimental (top) and simulated (bottom) mass spectra of $(Tl_3Bi_5)^-$ ions.

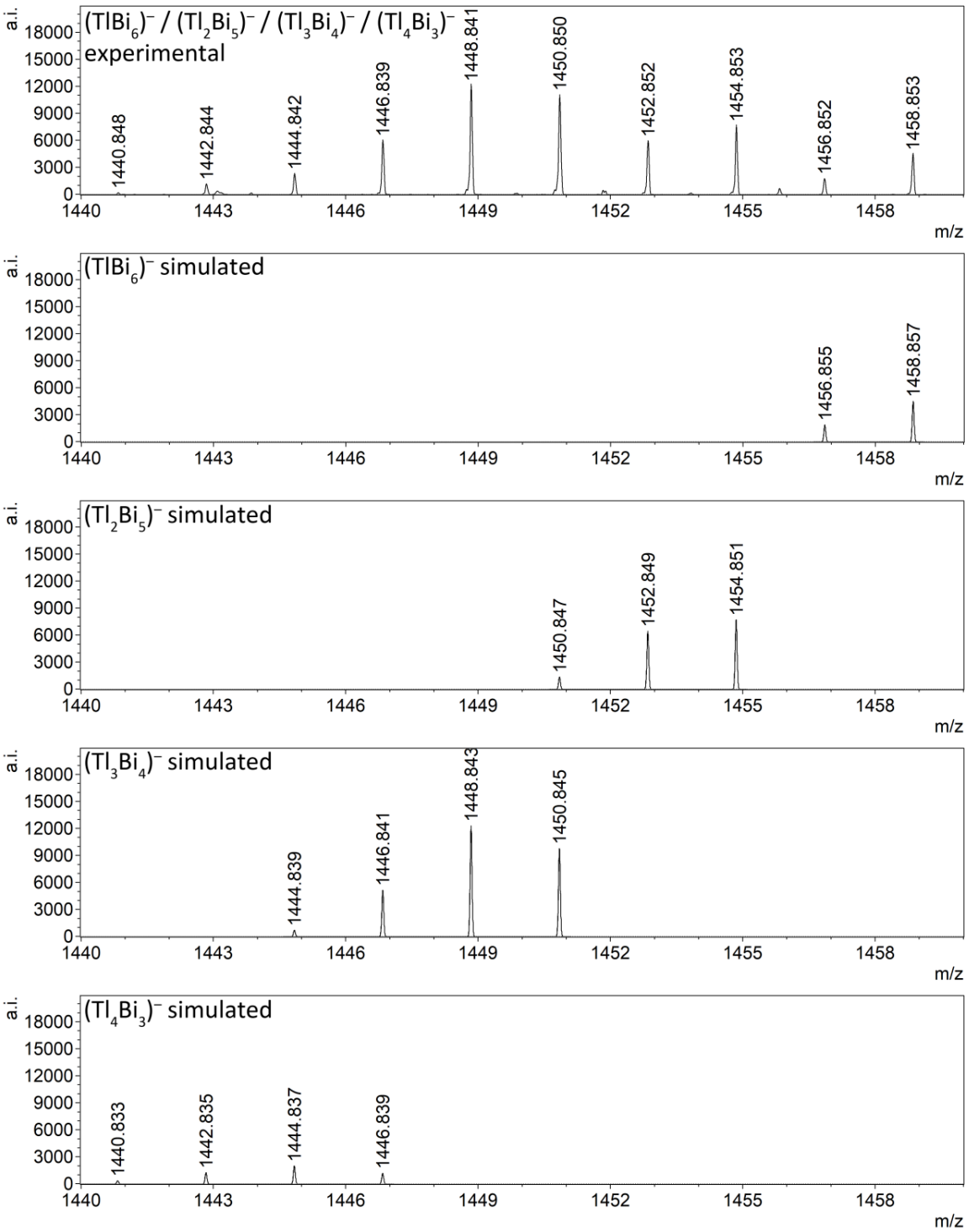

Figure S39. Comparison of experimental (top) and simulated mass spectra of $(TlBi_6)^-$, (Tl_2Bi_5), $(Tl_3Bi_4)^-$, and $(Tl_4Bi_3)^-$ ions (from top).

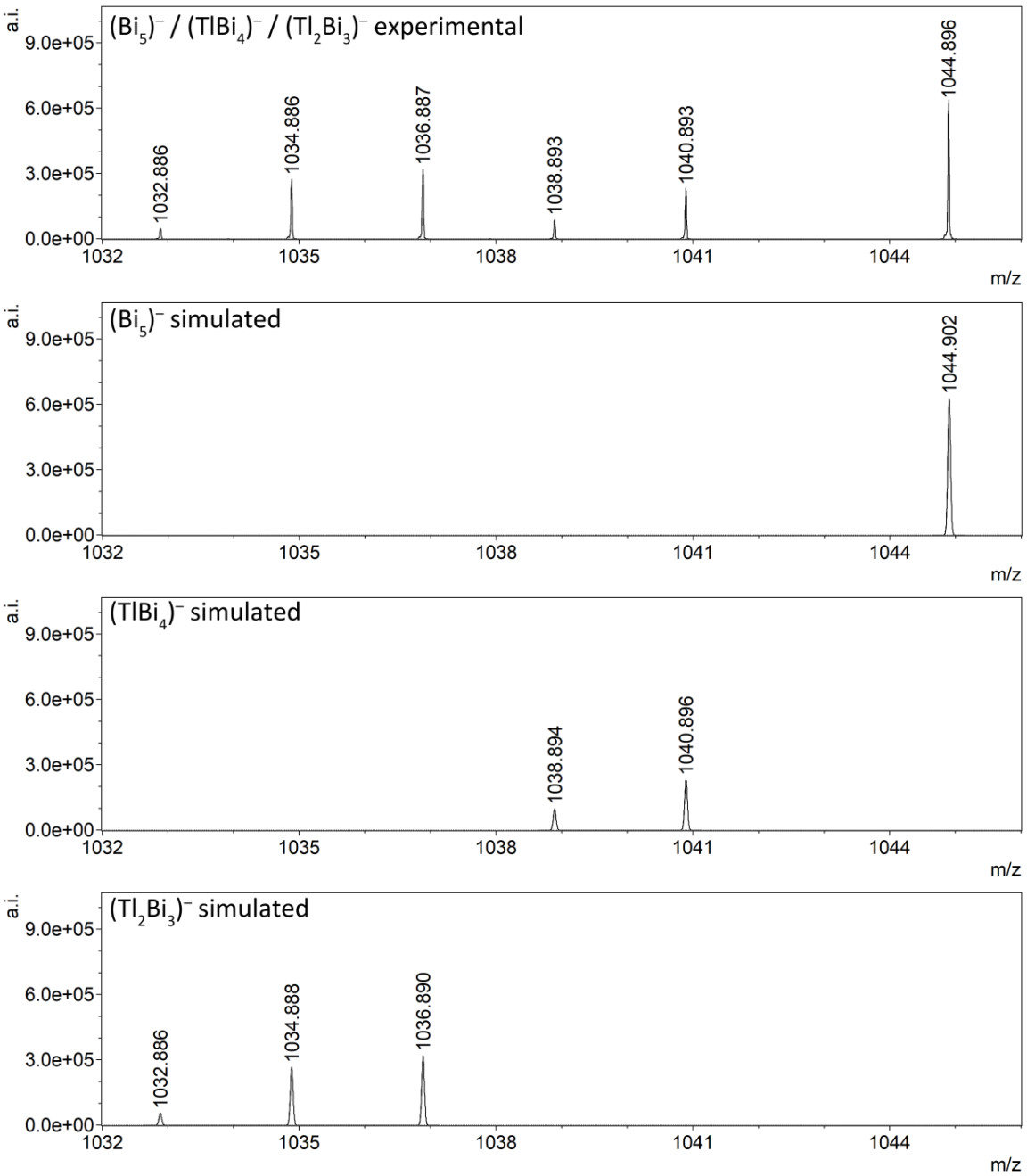

Figure S40. Comparison of experimental (top) and simulated mass spectra of $(Bi_5)^-$, $(TlBi_4)^-$, and $(Tl_2Bi_3)^-$ ions (from top).

3. Single Crystal X-ray Diffraction

3.1. General

The data for the X-ray structural analyses were collected at T = 100(2) K with Mo-K_α-radiation (λ = 0.71073 Å) on area detector systems Stoe IPDS2 for **1,** and **4**, Stoe IPDS/2T for **3** and Bruker D8 Quest for **2**. All structures were solved by intrinsic phasing (SHELXT-2015).[3] The refinement was done by full-matrix-least-squares methods against F^2 with the program SHELXL-2013.[4] The structure solution and subsequent refinement were done in the Olex2 software suite.[5] All hydrogen atoms were kept riding on calculated positions with isotropic displacement parameters U = 1.2 U_{eq} (or 1.5 U_{eq} for methyl groups) of the bonding partners. Crystallographic data for the four structures reported in this paper have been deposited with the Cambridge Crystallographic Data Center as supplementary publications nos. CCDC-1548729 (**1a**), CCDC-1548732 (**2**), CCDC-1548731 (**3**), and CCDC-1548730 (**4**). The crystal data and experimental parameters of the structure determinations are collected in Tables S1 and S2. Figures were created with Diamond4[6] and PovRay.[7]

Table S1. Crystal data and details of the structure determinations of 1a and 2.

Compound	[K(crypt-222)]$_2$ ($TlBi_3$)·0.58*thf*·0.42*en* **(1a)**	[K(crypt-222)]$_3$ [Bi_9{Ru(*cod*)}$_2$]·1.5*en* **(2)**
empirical formula	$C_{39.17}H_{78.33}N_{4.84}O_{12.59}K_2Tl_1Bi_3$	$C_{71.50}H_{132}N_{7.50}O_{18}K_3Ru_2Bi_9$
formula weight [g mol^{-1}]	1727.93	3585.10
crystal color, shape	black block	black plate
crystal size [mm^3]	0.55 x 0.55 x 0.17	0.10 x 0.34 x 0.70
crystal system	monoclinic primitive	triclinic
space group (No.)	$P2_1$ (4)	$P\bar{1}$ (2)
a [Å]	12.1368(4)	14.943(1)
b [Å]	20.5383(4)	15.940(1)
c [Å]	12.6345(4)	24.005(2)
α [°]		83.743(2)
β [°]	118.560(2)	72.831(2)
γ [°]		69.291(2)
V [Å^3]	2766.16(14)	5110.6(6)
Z, ρ_{calc} [g cm^{-3}]	2, 2.075	2, 2.330
μ ($Mo_{K\alpha}$) [mm^{-1}]	12.624	15.899
absorption correction type	numerical	multi-scan
2*θ* range [°]	3.67 – 53.56	4.198 – 52.968
total reflns	23697	212952
unique reflns [R_{int}]	11659	21031
obs. Reflns [$I > 2\sigma(I)$]	10422	17765
R_{int}	0.0591	0.0576
parameters	560	1002
wR_2 (all data)/ R_1 [$I > 2\sigma(I)$]	0.0847, 0.0331	0.1642, 0.0487
GooF (all data)	0.987	1.070
Flack value	–0.030(6)	-
max peak/hole [e Å^{-3}]	1.96/–1.41	4.13/–1.07

Table S2. Crystal data and details of the structure determinations of 3 and 4.

Compound	$[K(crypt\text{-}222)]_3[Tl_2Bi_6\{Ru(cod)\}]\cdot 2tol$ **(3)**	$[K(crypt\text{-}222)]_3(Tl_4Bi_5)\cdot 2en$ **(4)**
empirical formula	$C_{58}H_{100}N_4O_{12}K_2\ Ru_1Tl_2Bi_6$	$C_{58}H_{116}N_{10}O_{18}K_3Tl_4Bi_5$
formula weight [g mol^{-1}]	2887.36	3221.28
crystal color, shape	black block	black block
crystal size [mm^3]	0.08 x 0.08 x 0.12	0.243 x 0.246 x 0.334
crystal system	triclinic	triclinic
space group	$P\bar{1}$ (2)	$P\bar{1}$ (2)
a [Å]	12.7413(3)	14.8838(4)
b [Å]	13.4191(3)	16.2271(5)
c [Å]	25.8672(6)	20.1664(6)
a [°]	75.537(2)	92.802(2)
β [°]	83.410(2)	96.791(2)
γ [°]	62.680(1)	111.678(2)
V [Å^3]	3804.8(2)	4471.7(2)
Z, ρ_{calc} [g cm^{-3}]	2, 2.520	2, 2.392
μ ($Mo_{K\alpha}$) [mm^{-1}]	18.39	17.18
absorption correction type	numerical	numerical
2θ range [°]	3.504 – 53.598	2.84 – 53.54
total reflns	56686	34724
unique reflns [R_{int}]	16103	18809
obs. Reflns [$I > 2\ 4\sigma(I)$]	14077	14371
R_{int}	0.0961	0.1614
parameters	768	847
wR_2 (all data)/ R_1 [$I > 2\sigma(I)$]	0.0515, 0.0242	0.0896, 0.0480
GooF (all data)	1.002	0.921
max peak/hole [e Å^{-3}]	1.892/–1.846	3.65/–3.48

3.2. Details of the Structure Determinations

3.2.1. Structure Determination of [K(crypt-222)]$_2$(TlBi$_3$)·0.58*thf*·0.42*en* (1a)

The structure of **1a** was solved using intrinsic phasing in the non-centro-symmetric space group $P2_1$ (No. 4). The asymmetric unit features one heavy atom cluster anion $(TlBi_3)^{2-}$, two independent $[K(crypt\text{-}222)]^+$ counter ions, one thf, and one en molecule. Both crystal solvent molecules are disordered on one position (see Figure S41), with a refined ratio of 0.58:0.42. The cryptand ligands did not show disorder and anisotropic displacement parameters could be refined for both without the use of restraints. The cluster anion also does not show any sign of disorder. As Tl- and Bi-atom positions cannot be determined from this experiment these were refined with a 0.25:0.75 disorder on all four positions with equal coordinates and atomic displacement parameters. The heavy atom distances are within the narrow range of 3.0459(8) – 3.0772(6) Å. Figures S41 and S42 show the asymmetric unit and the packing in the unit cell.

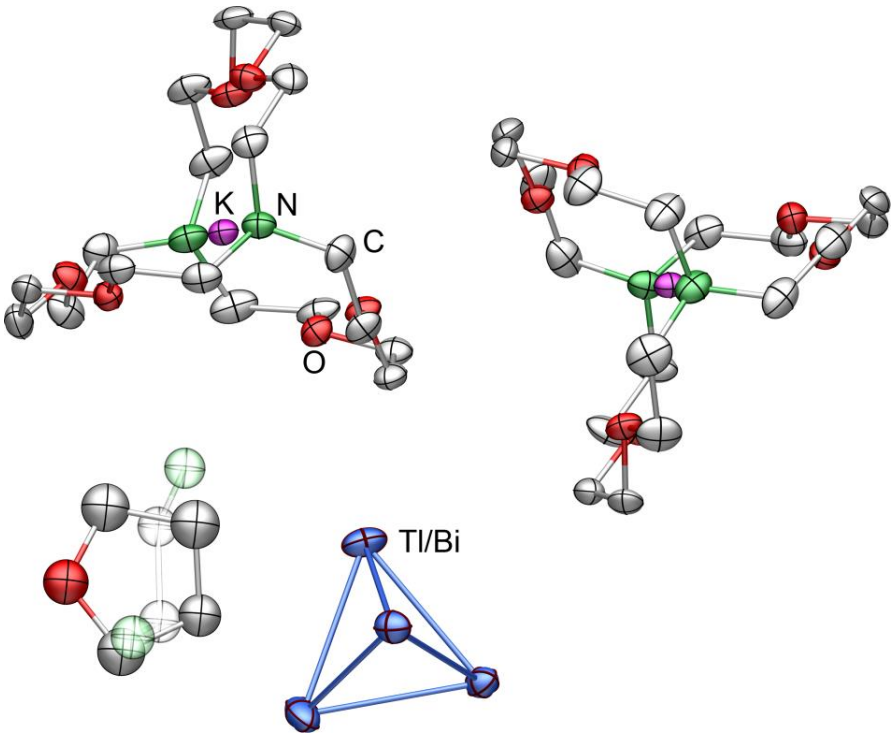

Figure S41. Asymmetric unit of 1a. Displacement ellipsoids are drawn at 50% probability level. Hydrogen atoms are omitted for clarity. Disordered solvent molecules are drawn in transparent mode.

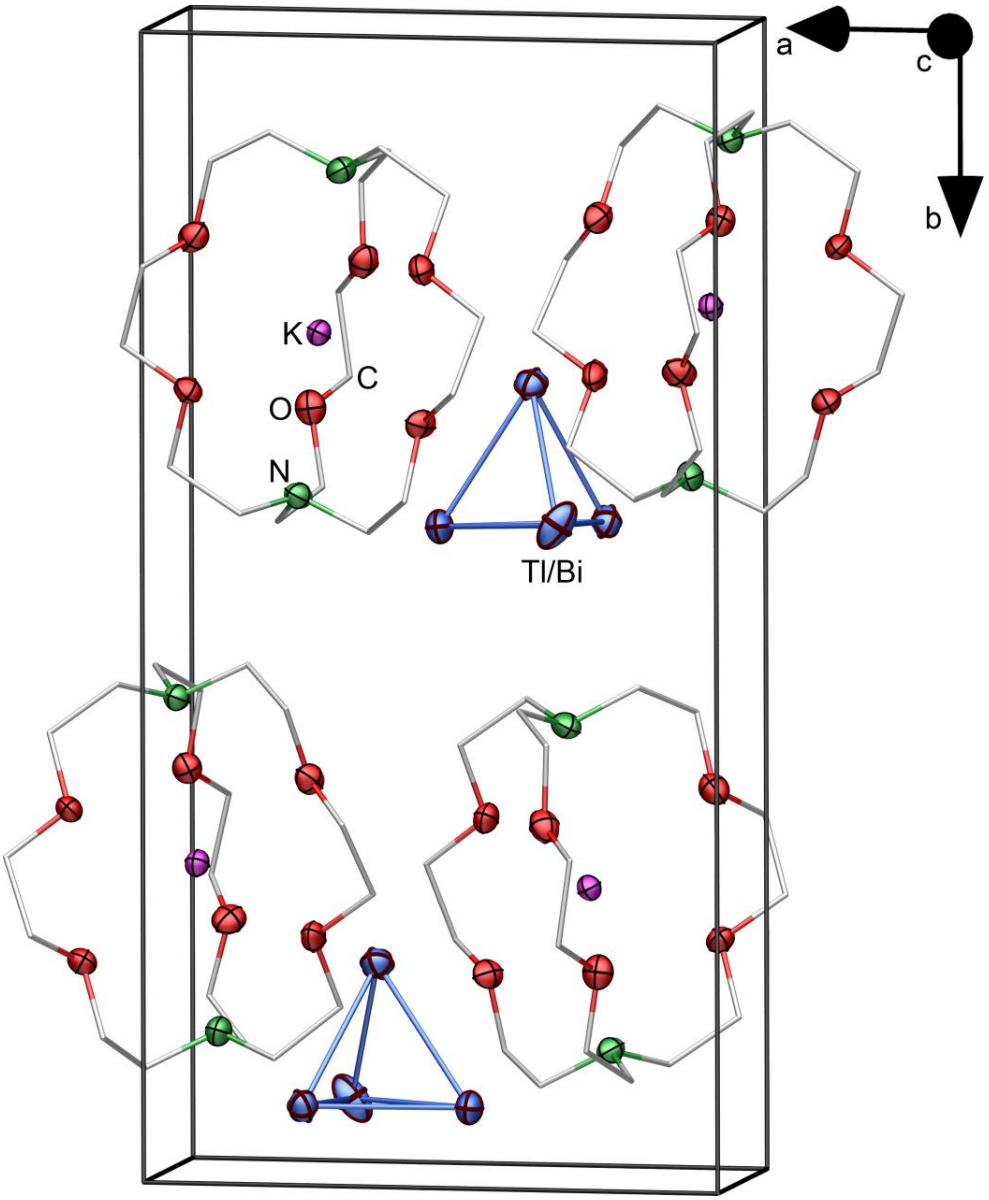

Figure S42. Packing of molecules in the unit cell of 1a. Displacement ellipsoids are drawn at 50% probability level. Hydrogen atoms, incomplete cryptand molecules and crystal solvent molecules are omitted for clarity.

3.2.2. Structure Determination of [K(crypt-222)]$_3$[Bi$_9${Ru(*cod*)}$_2$]·1.5*en* (2)

The structure of **2** was solved using intrinsic phasing in the centro-symmetric space group $P\bar{1}$ (No. 2). The asymmetric unit comprises one heavy atom cluster anion [Bi$_9${Ru(*cod*)}$_2$]$^{3-}$, three independent [K(crypt-222)]$^+$ counter ions, one entire en molecule and another half of an en molecule. The complete molecule is located on a general position while the half molecule sits on special position (0, 0, 0, Wykoff position 1*a*). The cryptand ligands do not show disorder, although some mobility is visible on one of them. Anisotropic displacement parameters could be refined for them without the use of restraints. The cluster anion also does not show any sign of disorder. As the presence of Tl atoms in the cluster cannot be excluded based solely on the single crystals structure data the composition was confirmed via ESI-MS and quantum chemical calculations (see chapters 2.3., 5.2., and 5.3.). Furthermore micro X-ray fluorescence experiments supported the expected absence of Tl atoms in the compound (see chapter 4.).

Figures S43 – S45 show the asymmetric unit, the cluster anion and the packing in the unit cell. Table S3 summarizes all bond lengths within the heavy atom structure.

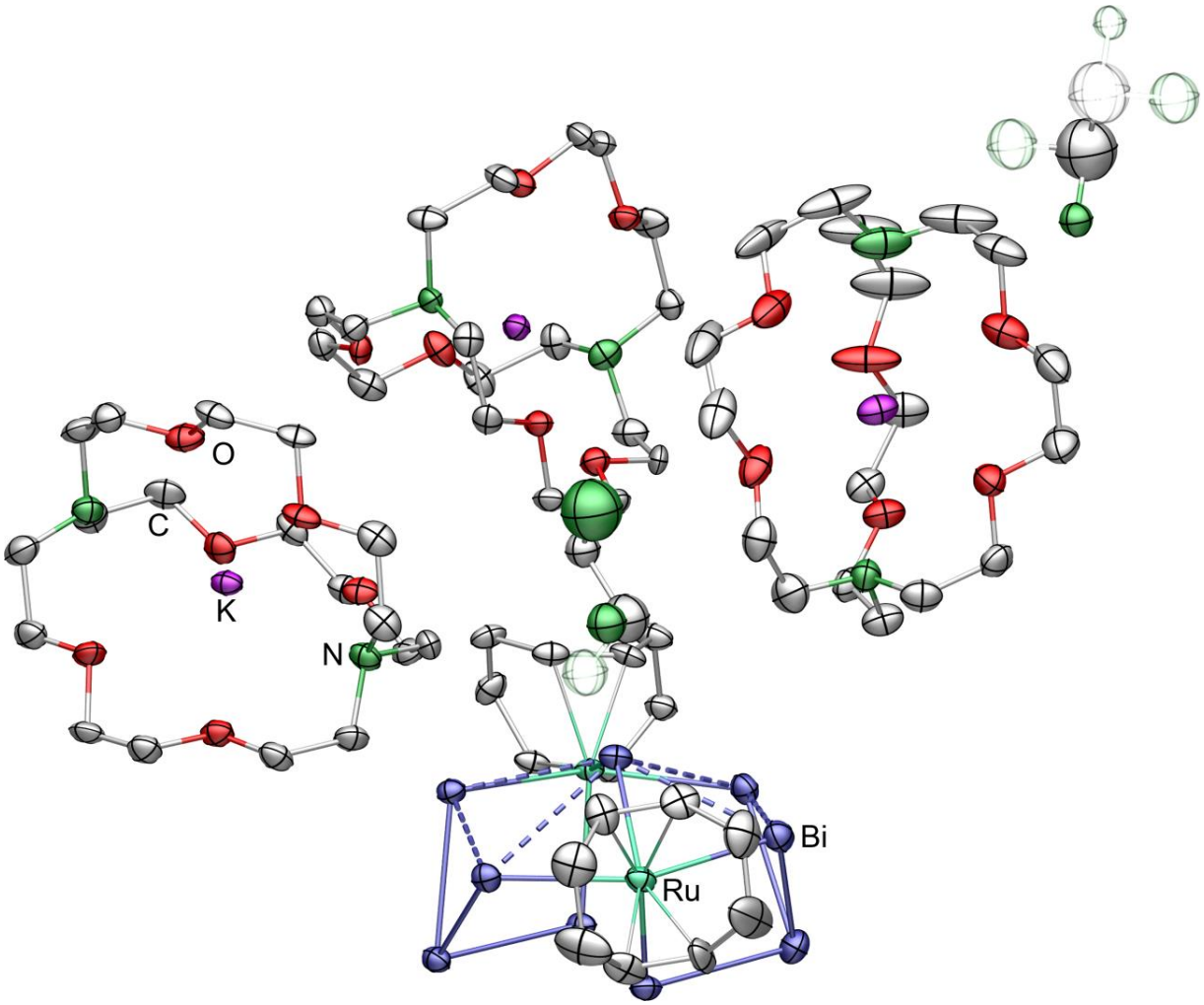

Figure S43. Asymmetric unit of 2. Displacement ellipsoids are drawn at 50% probability level. Hydrogen atoms are omitted for clarity. Disordered and symmetry-generated solvent molecules are drawn in transparent mode.

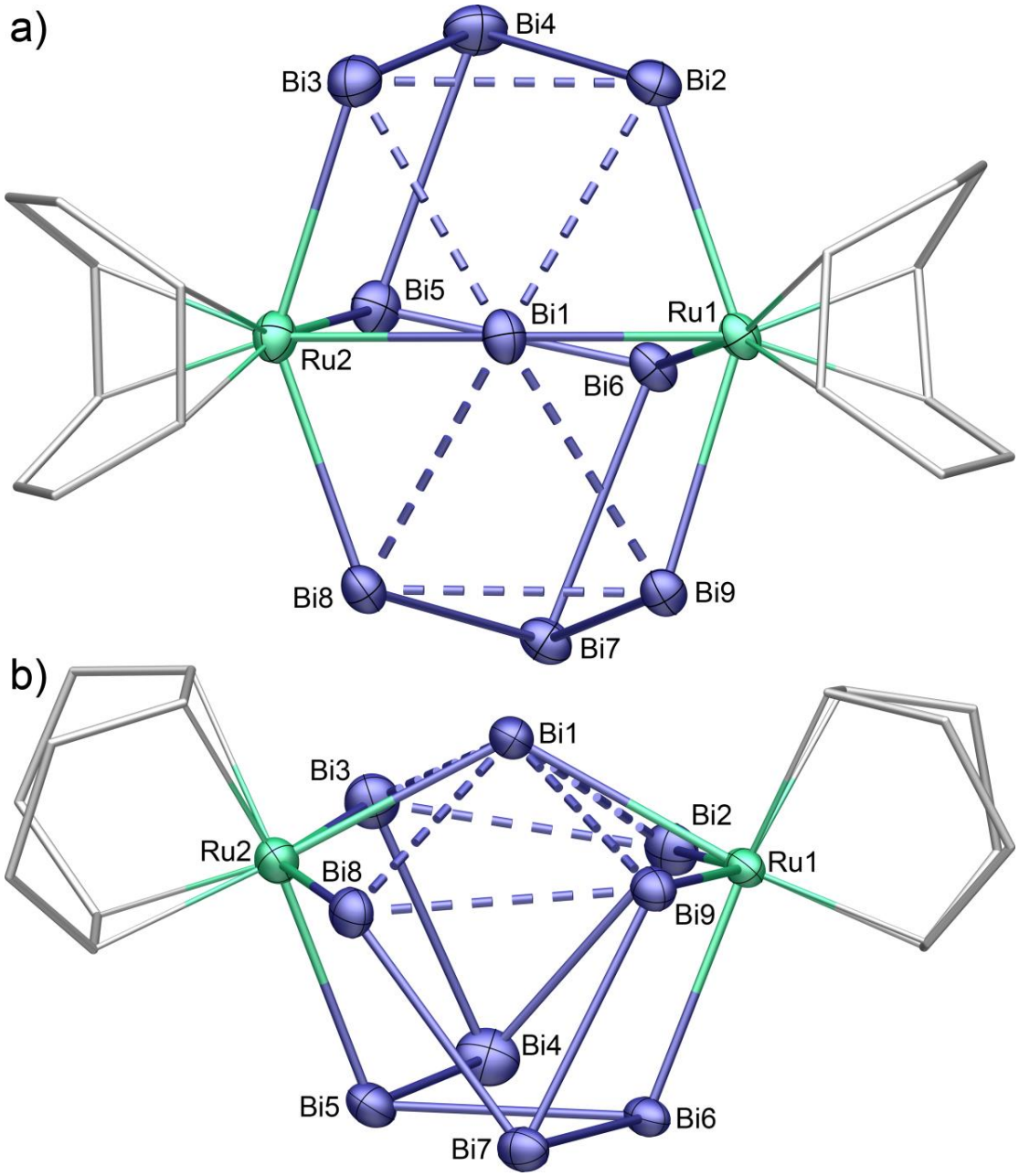

Figure S44. Structure of the cluster anion $[Bi_9\{Ru(cod)\}_2]^{3-}$ in 2. Displacement ellipsoids are drawn at 50% probability level. Only one of the two enantiomers is shown, as the other is created through inversion symmetry in the crystal structure.

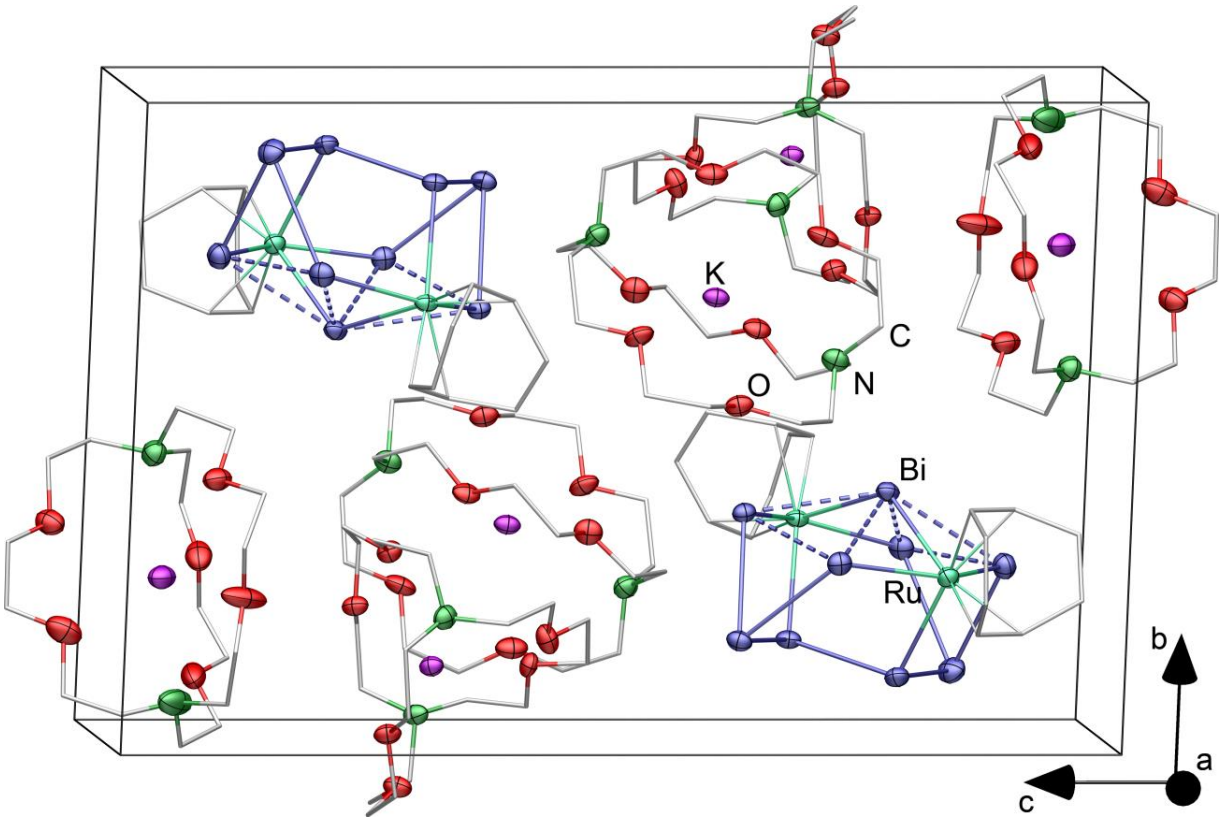

Figure S45. Packing of molecules in the unit cell of 2. Displacement ellipsoids are drawn at 50% probability level. Hydrogen atoms, incomplete cryptand molecules and crystal solvent molecules are omitted for clarity.

Table S3. Interatomic distances in the cluster anion $[Bi_9\{Ru(cod)\}_2]^{3-}$ in 2. Atom numbers are used as in Figure S44.

Atoms	Distance / Å	Atoms	Distance / Å	Atoms	Distance / Å
Bi1 – Bi2	3.3943(8)	Bi2 – Bi4	3.0224(7)	Ru1 – Bi1	2.753(1)
– Bi3	3.2660(7)	Bi3 – Bi4	3.0139(9)	Ru1 – Bi2	2.790(1)
– Bi8	3.3664(7)	Bi8 – Bi7	3.0364(7)	Ru1 – Bi9	2.784(1)
– Bi9	3.3348(7)	Bi9 – Bi7	3.0056(6)	Ru1 – Bi6	2.7629(9)
Bi2 – Bi3	3.1293(7)	Bi4 – Bi5	3.0737(9)	Ru2 – Bi1	2.7518(9)
Bi8 – Bi9	3.1380(6)	Bi6 – Bi7	3.0583(8)	Ru2 – Bi3	2.800(1)
		Bi5 – Bi6	2.9468(6)	Ru2 – Bi8	2.785(1)
				Ru2 – Bi5	2.771(1)

3.2.3. Structure Determination of [K(crypt-222)]$_2$[Tl$_2$Bi$_6$Ru(*cod*)]·2*tol* (3)

Numerous crystals of compound **3** were mounted on the diffractometer and checked for crystal quality and single-crystallinity. Most of these showed signs of multiple twinning and were of an overall poor quality. The crystal that was finally chosen for the structure determination again showed signs of a twin component, however this time only to a very small degree of approximately 4%. Its overall contribution to the detected intensities was very limited and not enough to perform a proper twin refinement. We therefore decided to omit 18 reflections that seemed to be most significantly affected by the twin domain.

The structure of **3** was solved using intrinsic phasing in the centro-symmetric space group $P\bar{1}$ (No. 2). The structure features one heavy atom cluster anion $[Tl_2Bi_6\{Ru(cod)\}]^{2-}$, two independent $[K(crypt\text{-}222)]^+$ counter ions, and two toluene molecules. Both of them are located on general positions. There is no sign of disorder in the whole structure and anisotropic displacement parameters could be refined for all non-hydrogen atoms without the use of restraints. As the cluster composition cannot be determined from the single crystal data it was determined via ESI-MS and quantum chemical calculations (see chapters 2.4., 5.3., and 5.4.). Furthermore micro X-ray fluorescence experiments supported the expected Tl:Bi:Ru atom ratio of 2:6:1 in the compound (see chapter 4.2.).

Figures S46 – S48 show the asymmetric unit, the cluster anion and the packing in the unit cell. Table S4 summarizes all bond lengths within the heavy atom structure.

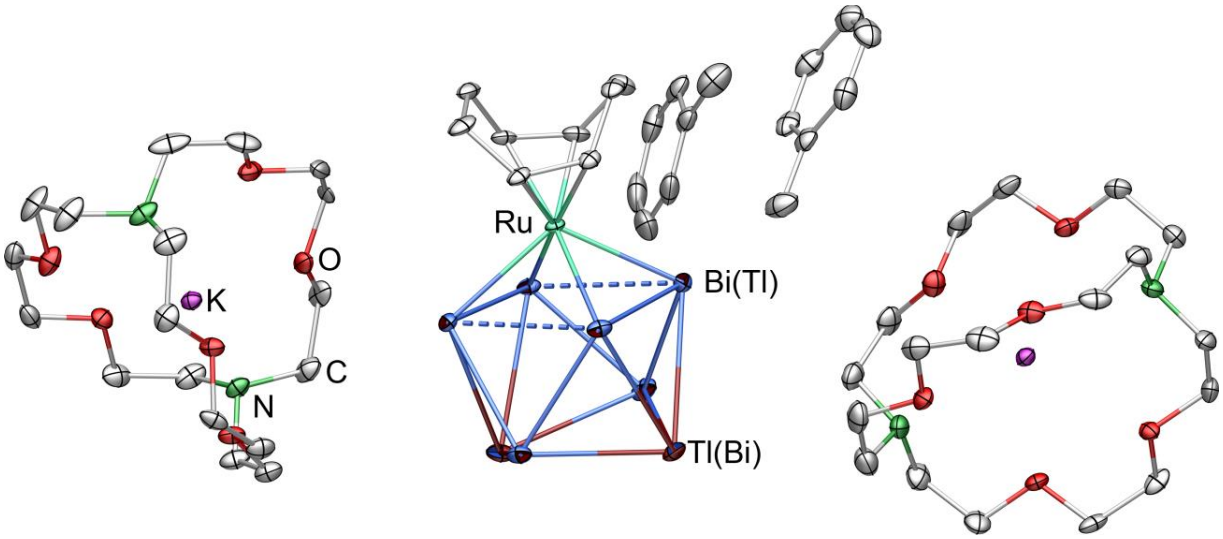

Figure S46. Asymmetric unit of 3. Displacement ellipsoids are drawn at 50% probability level. Hydrogen atoms are omitted for clarity.

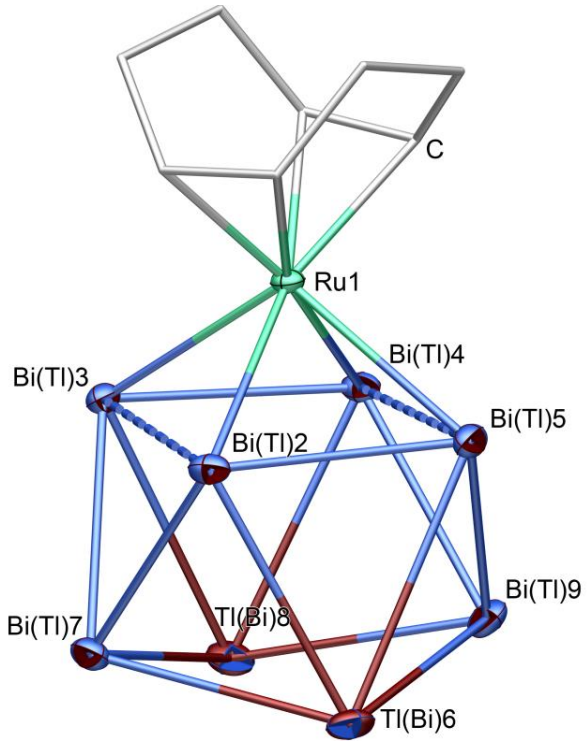

Figure S47. Structure of the cluster anion $[Tl_2Bi_6\{Ru(cod)\}]^{2-}$ in 3. Displacement ellipsoids are drawn at 50% probability level.

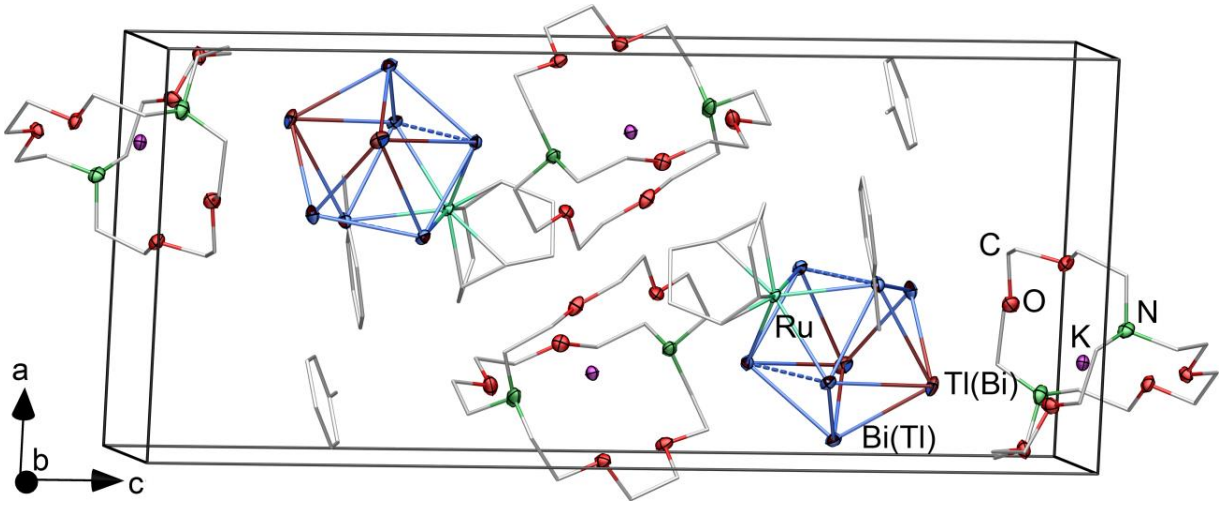

Figure S48. Packing of molecules in the unit cell of 3. Displacement ellipsoids are drawn at 50% probability level. Hydrogen atoms, incomplete cryptand molecules and crystal solvent molecules are omitted for clarity.

Table S4. Interatomic distances in the cluster anion $[Tl_2Bi_6\{Ru(cod)\}]^{2-}$ in 3. Atom numbers are used as in Figure S47. Calculated bond lengths are given in italic (see chapter 5.3. and 5.4.)

Atoms	Distance / Å	Atoms	Distance / Å	Atoms	Distance / Å
Ru1 – Bi2	2.8050(5)	Bi2 – Bi3	3.4846(6)	Bi2 – Bi7	3.0334(5)
	2.817		*3.628*		*3.079*
– Bi3	2.8202(6)	Bi3 – Bi4	2.9677(4)	Bi2 – Tl6	3.2787(6)
	2.841		*2.988*		*3.557*
– Bi4	2.8091(5)	Bi4 – Bi5	3.5623(6)	Bi3 – Bi7	3.1042(6)
	2.817		*3.620*		*3.044*
– Bi5	2.7915(7)	Bi5 – Bi2	2.9817(4)	Bi3 – Tl8	3.4257(5)
	2.840		*2.989*		*3.382*
		Tl6 – Bi7	3.1397(7)	Bi4 – Tl8	3.3138(4)
			3.151		*3.563*
		Bi7 – Tl8	3.0691(3)	Bi4 – Bi9	3.0278(7)
			3.196		*3.081*
		Tl8 – Bi9	3.1240(6)	Bi5 – Bi9	3.0860(4)
			3.149		*3.044*
		Bi9 – Tl6	3.0979(3)	Bi5 – Tl6	3.3668(4)
			3.196		*3.383*

3.2.4. Structure Determination of [K(crypt-222)]$_3$(Tl$_4$Bi$_5$)·2*en* (4)

Numerous crystals of compound **4** were mounted on the diffractometer and checked for crystal quality and single-crystallinity. Most of these showed signs of strong twinning. The crystal that was chosen for the structure determination again showed signs of a twin component, however this time only to a small degree of approximately 10%. Its overall contribution to the detected intensities was very limited and not enough to perform a proper twin refinement. We therefore decided to omit 50 reflections that seemed to be most significantly affected by the twin domain.

The structure of **4** was solved using intrinsic phasing in the centro-symmetric space group $P\bar{1}$ (No. 2). The asymmetric unit features one heavy atom cluster anion $(Tl_4Bi_5)^{3-}$, three independent $[K(crypt\text{-}222)]^+$ counter ions, and a total of two en molecules. One of these is located on a general position while two half molecules sit on special positions (0, 0, ½, and ½, ½, 0, Wykoff positions 1*b* and 1*e*). The cryptand ligands do not show disorder, although some mobility is visible on one of them. Anisotropic displacement parameters could be refined for them without the use of restraints. The cluster anion also does not show any sign of disorder. Higher residual electron density peaks close to the heavy atom cluster are caused by the twin component (~10%). As the overall contribution from the second domain was limited a refinement with a disorder model for the cluster failed. It was only possible with an inappropriate number of restraints and led to significantly higher R-values (R1 + 3%) with unreasonably small thermal displacement ellipsoids for the heavy atoms. The Tl- and Bi-atom positions are assigned based on the isostructural relationship to the previously reported $(In_4Bi_5)^{3-}$ anion, and quantum chemical calculations. We furthermore undertook an additional single crystal structure determination experiment using synchrotron radiation at the Tl-L_{III} absorption edge to obtain an experimental proof. These experimental details and results are discussed in chapter 3.2.5. Figures S49 – S51 show the asymmetric unit, the cluster anion, and the packing in the unit cell.

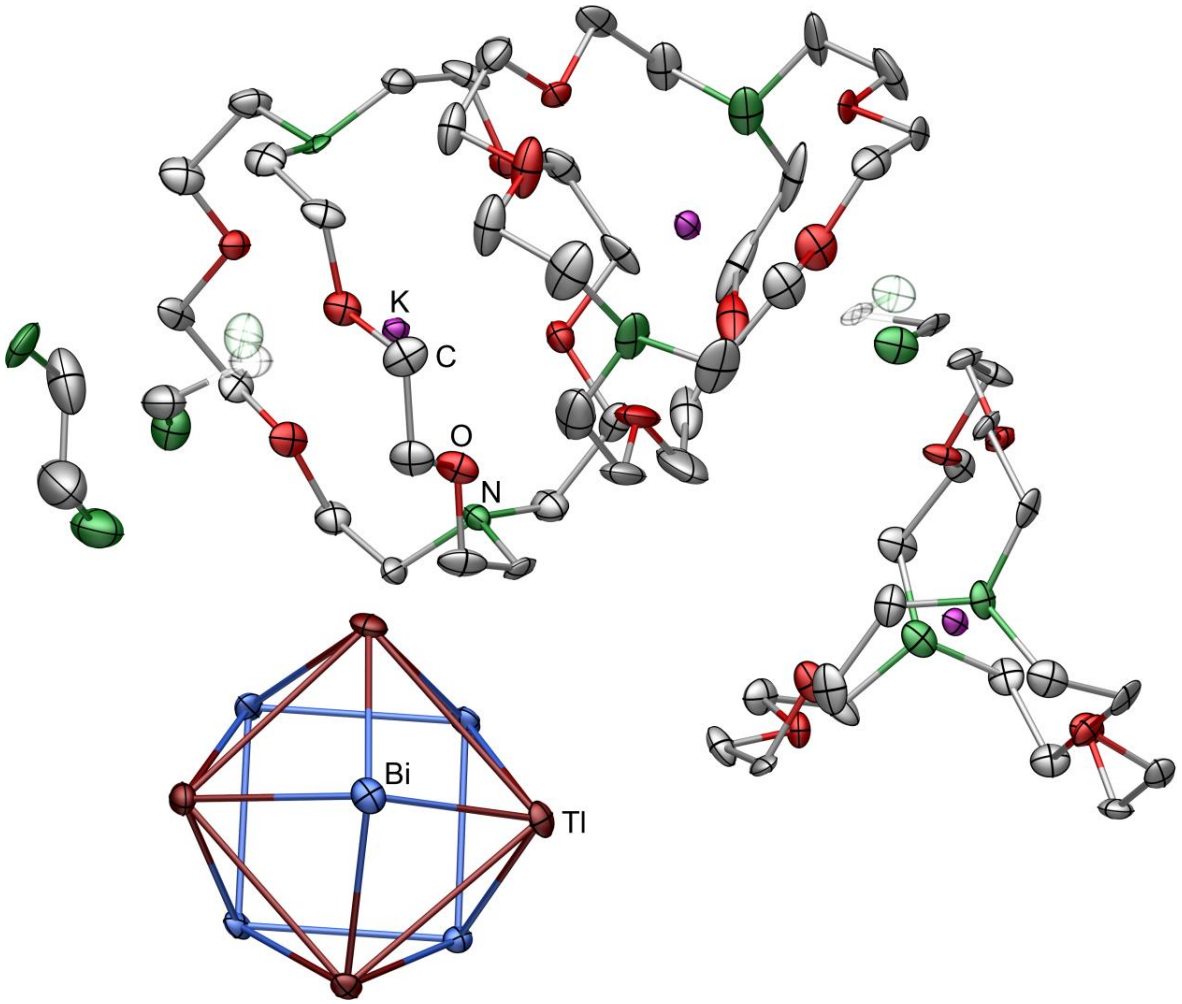

Figure S49. Asymmetric unit of 4. Displacement ellipsoids are drawn at 50% probability level. Hydrogen atoms are omitted for clarity. Symmetry-generated fragments are drawn in transparent mode.

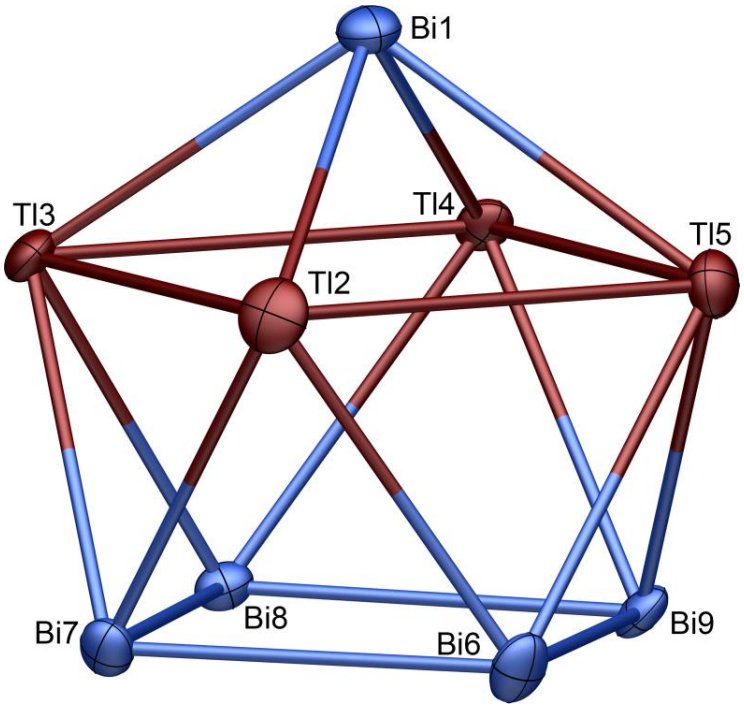

Figure S50. Structure of the cluster anion $(Tl_4Bi_5)^{3-}$ in 4. Displacement ellipsoids are drawn at 50% probability level.

Table S5. Interatomic distances in the cluster anion $(Tl_4Bi_5)^{3-}$ in 4. Atom numbers are used as in Figure S50.

Atoms	Distance / Å	Atoms	Distance / Å	Atoms	Distance / Å
Bi1 – Tl2	3.0639(4)	Tl2 – Tl3	3.6386(5)	Tl2 – Bi6	3.1604(6)
– Tl3	3.0400(6)	Tl3 – Tl4	3.6090(5)	– Bi7	3.1651(6)
– Tl4	3.0669(5)	Tl4 – Tl5	3.4867(5)	Tl3 – Bi7	3.1535(4)
– Tl5	3.0577(6)	Tl5 – Tl2	3.5771(5)	– Bi8	3.1064(5)
		Bi6 – Bi7	3.0450(5)	Tl4 – Bi8	3.1475(5)
		Bi7 – Bi8	3.0702(4)	– Bi9	3.1194(5)
		Bi8 – Bi9	3.0845(5)	Tl5 – Bi9	3.1340(6)
		Bi9 – Bi6	3.0713(4)	– Bi6	3.1630(5)

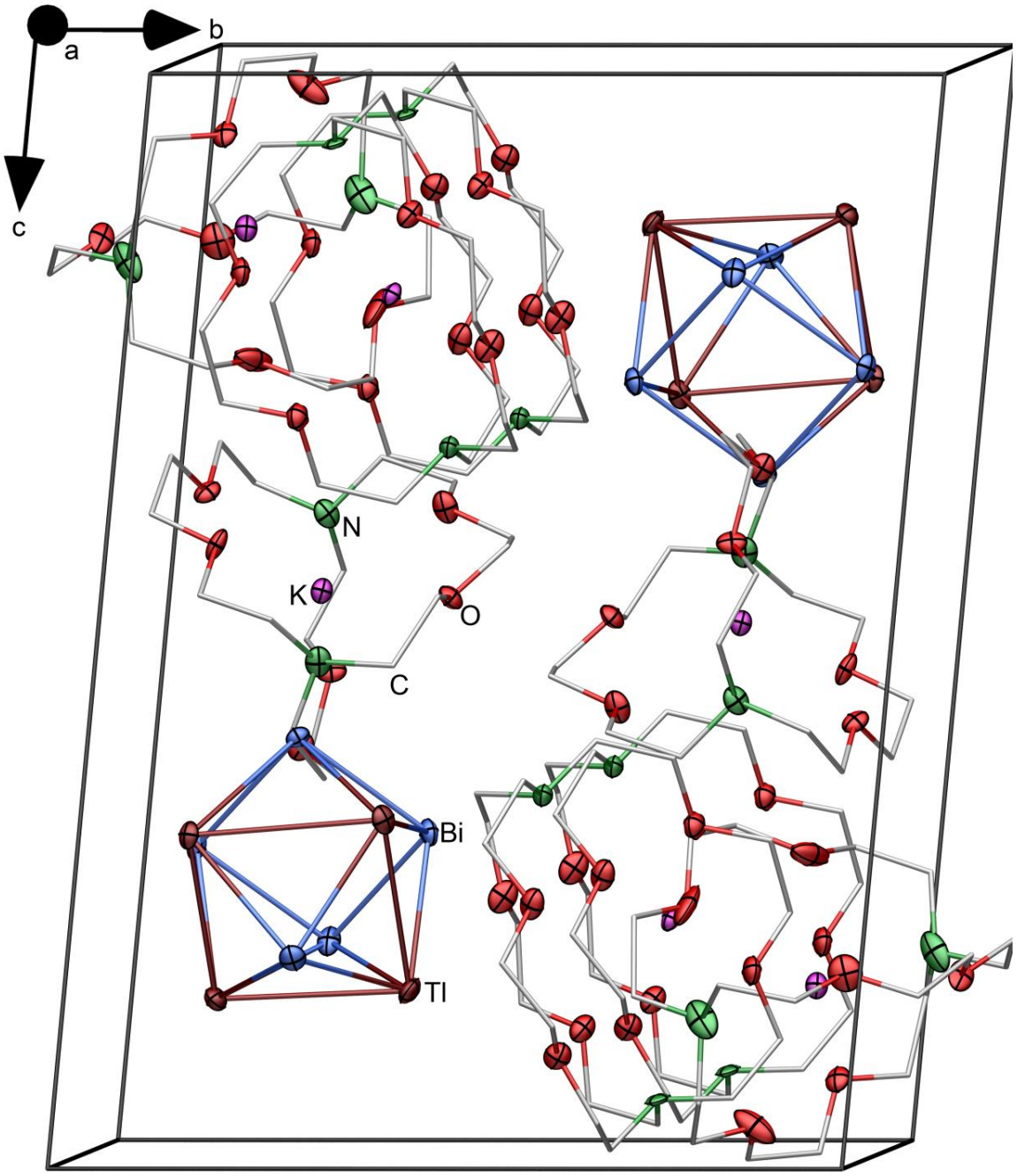

Figure S51. Packing of molecules in the unit cell of 4. Displacement ellipsoids are drawn at 50% probability level. Hydrogen atoms, incomplete cryptand molecules and crystal solvent molecules are omitted for clarity.

3.2.5. Determination of Tl and Bi Atom Positions in [K(crypt-222)]$_3$(Tl$_4$Bi$_5$)·2*en* (4)

A single crystal structure of **4** was measured using the effect of anomalous dispersion close to the Tl-L_{III} absorption edge (λ = 0.97626 Å) at the ANKA synchrotron radiation facility in Karlsruhe.

Atomic form factors for l = 0.97626 Å (12.700 keV) for **4** were obtained by the method of *Brennan* and *Cowan* as implemented on http://skuld.bmsc.washington.edu/scatter/AS_periodic.html.[8]

Two different structure models were refined, one in which the heavily disordered solvent was ignored and one in which its contribution to the overall structure factors was calculated and subtracted by back Fourier transform with the SQUEEZE algorithm in the PLATON program package.[9] Four different position models were refined: All atoms as Tl, all atoms as Bi, four Tl atoms in the open square plane, and four Tl atoms in the capped square plane. The results for all 8 refinements are provided in Table S6.

Table S6. Comparison of *R*1 and *wR*2 values of all 8 refined structure models of 4. The correct atom assignment is evident from significantly lower *R*-values (last row).

	disordered solvent not modeled		disordered solvent treated with SQUEEZE	
	***R*1 / %**	***wR*2 / %**	***R*1 / %**	***wR*2 / %**
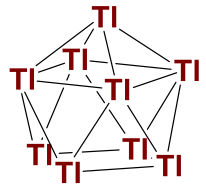	6.35	16.86	6.11	16.86
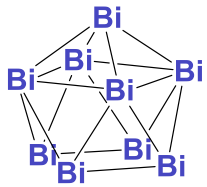	6.44	18.04	6.18	17.09
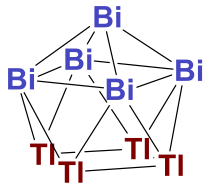	7.08	20.38	6.86	19.40
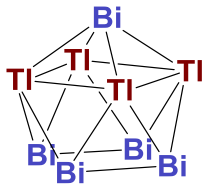	5.77	16.72	5.47	15.22

4. Micro X-ray Fluorescence Spectroscopy (µ-XFS)

4.1. General Procedure

All μ-XFS measurements were performed with a Bruker M4 Tornado, equipped with a Rh-target X-ray tube and a silicon drift detector. The emitted fluorescence photons are detected with an acquisition time of 100 s. Quantification of the elements is achieved through deconvolution of the spectra. Results are summarized in Table S7. Figures S52 – S54 present the measured spectra for **1b**, **3**, and **4** along with the results of the deconvolution algorithm. All spectra are shown with a square-root intensity scale to enable an easier identification of smaller features. For compound **2**, a more detailed study was performed to clarify the origin of the observed Tl content (see below). The data for **1b** was collected on freshly mounted crystals that were immersed in a thin protective coating of non-drying high viscosity oil (21 cSt).

In case of compound **2** the accurate measurement of the micro X-ray fluorescence spectrum is very difficult due to the crystal shape. **2** crystallizes as extremely thin plates that cannot be isolated without traces of the side-products and metal powder when washed with toluene. This leads to contaminations with Tl from the mother liquor, and accounts for the presence of weak Tl signals in the spectrum. The acquisition of a clean micro X-ray fluorescence spectrum on a single crystal that was picked directly from the wall of the Schlenk tube failed, as the sample thickness prevents useful signal intensities. Table S8 provides the results of six different µ-XFS measurements on crystals of **2** and the corresponding spectra are shown in Figures S55 – S60. For each of the measurements, two different data evaluations were performed. The first one includes the Tl content (normalized to two Ru-atoms per cluster, left column in Table S8), while it is omitted from the second one (normalized to the 14 heavy atoms in the asymmetric unit: "$K_3Bi_9Ru_2$", right column in Table S8). As clearly evident from the results, the Tl content of the sample varies with respect to the rest of the quantified elements, as expected for a signal caused by contamination.

In summary, the K:Bi:Ru ratio of **2** was determined correctly, and the overall composition of the compound was unambiguously confirmed by combination of the ESI-MS, SC-XRD, µ-XFS data, and quantum chemical calculations (see chapter 5.3.).

4.2. Results for Compounds 1b, 3, and 4

Table S7. μ-XFS analyses of 1b, 3, and 4 (K, Tl, Bi, Ru). Corresponding spectra are shown in Figure S52 – S54.

[K(crypt-222)]$_2$(TlBi$_3$)·0.5*en* (1b)						
Element	Element wt % (exp)	Element wt % (calc)	Atom % (exp)	Atom % (calc)	Element ratio (exp)	Element ratio (calc)
K	7.92	8.60	31.37	33.33	1.9	2
Tl	22.67	22.47	17.19	16.67	1.0	1
Bi	69.41	68.93	51.45	50.00	3.1	3
Total	100.00	100.00	100.00	100.00	6	6
[K(crypt-222)]$_2$[Tl$_2$Bi$_6${Ru(*cod*)}]·2*tol* (3)						
Element	Element wt % (exp)	Element wt % (calc)	Atom % (exp)	Atom % (calc)	Element ratio (exp)	Element ratio (calc)
K	4.04	4.25	17.13	18.18	1.9	2
Tl	21.73	22.19	17.64	18.18	1.9	2
Bi	66.80	68.08	53.03	54.55	5.8	6
Ru	7.43	5.49	12.20	9.09	1.3	1
Total	100.00	100.01	100.00	100.00	10.9	11
[K(crypt-222)]$_3$(Tl$_4$Bi$_5$)·2*en* (4)						
Element	Element wt % (exp)	Element wt % (calc)	Atom % (exp)	Atom % (calc)	Element ratio (exp)	Element ratio (calc)
K	6.02	5.92	25.31	25.00	3	3
Tl	41.03	41.29	33.02	33.33	4	4
Bi	52.95	52.78	41.67	41.67	5	5
Total	100.00	99.99	100.00	100.00	12	12

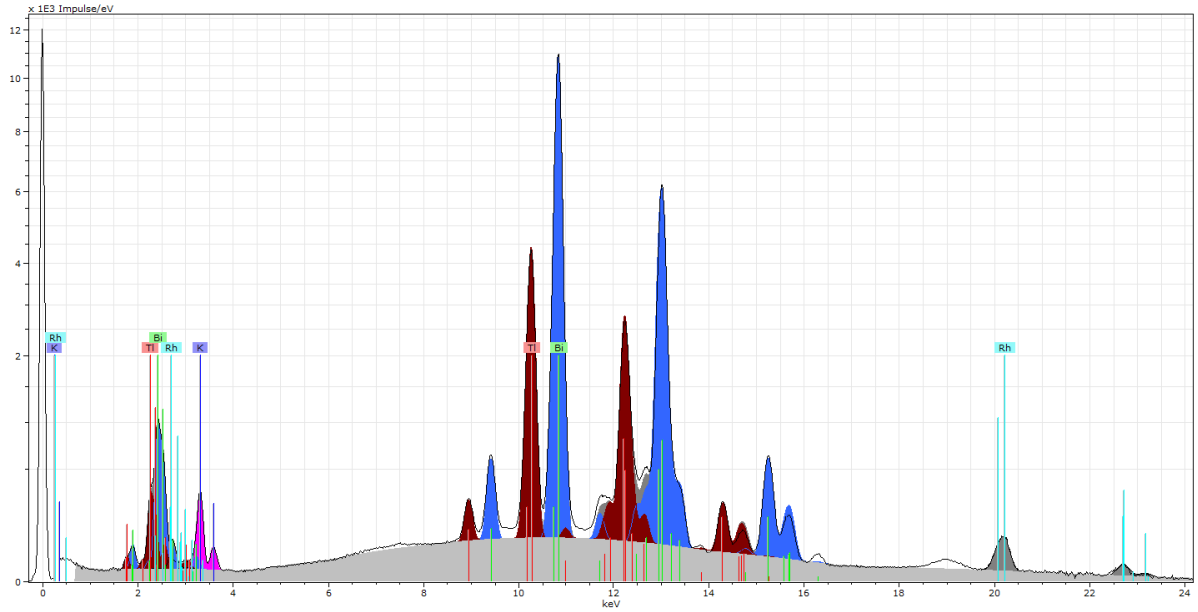

Figure S52. Micro X-ray fluorescence spectrum of [K(crypt-222)]$_2$(TlBi$_3$)·0.5*en* (1b) (line) with the results of the deconvolution algorithm. Colors are used as follows: K (pink), Tl (dark red), Bi (blue), Ru (green), background (grey).

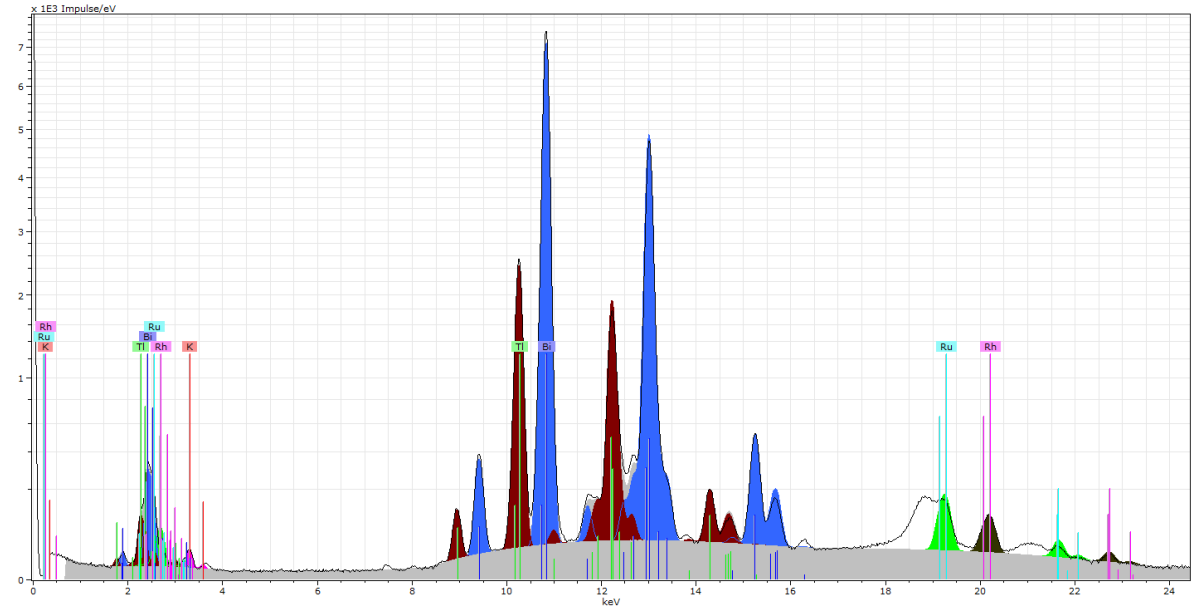

Figure S53. Micro X-ray fluorescence spectrum of [K(crypt-222)]$_2$[Tl$_2$Bi$_6$Ru(*cod*)]·2*tol* (3) (line) with the results of the deconvolution algorithm. Colors are used as follows: K (pink), Tl (dark red), Bi (blue), Ru (green), background (grey).

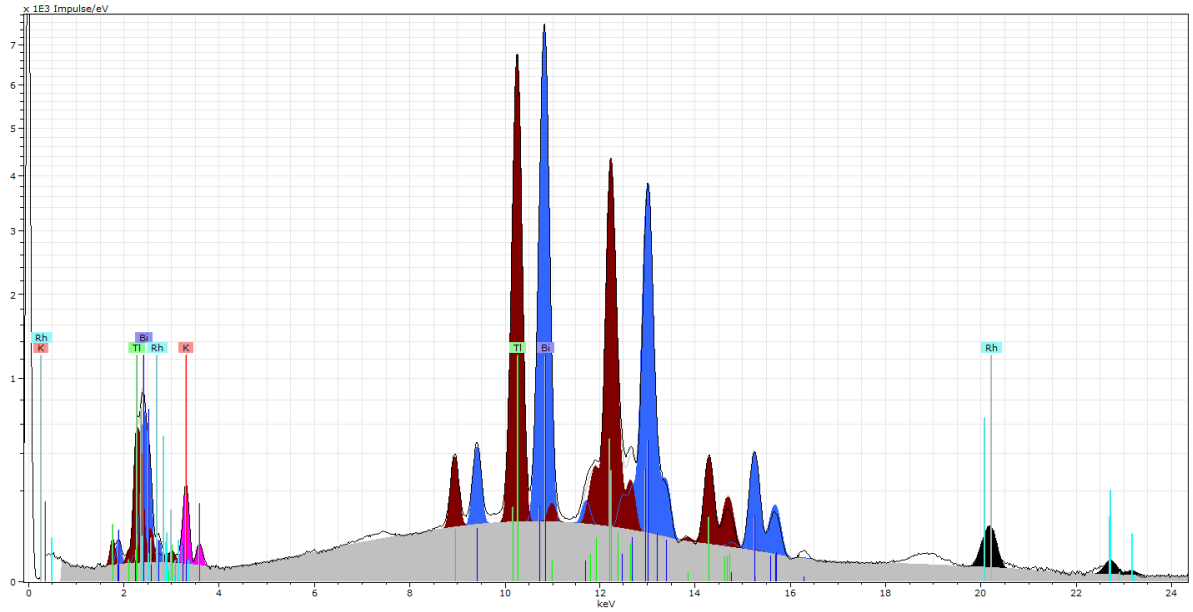

Figure S54. Micro X-ray fluorescence spectrum of [K(crypt-222)]$_3$(Tl_4Bi_5)·2*en* (4) (line) with the results of the deconvolution algorithm. Colors are used as follows: K (pink), Tl (dark red), Bi (blue), Ru (green), background (grey).

4.3. Results for Compound 2

Table S8. μ-XFS analysis of several crystals of 2 (K, Tl, Bi, Ru). Element ratios for all calculations including Tl (denoted with *) are based on the known number of two ruthenium atoms in the cluster anion. The calculations excluding Tl are normalized to the number of heavy 14 atoms in the asymmetric unit. Corresponding spectra are shown in Figures S55 – S60.

	Measurement incl. Tl						Measurement excl. Tl					
Element	Element wt %		Atom %		Element ratio*		Element wt %		Atom %		Element ratio	
Measurement 1												
K	5.08	5.33	20.69	21.4	3.2	3.0	5.72	5.33	22.68	21.4	3.2	3.0
Tl	9.45	0.00	7.37		1.1							
Bi	77.19	85.48	58.88	64.3	9.0	9.0	84.94	85.48	63.00	64.3	8.8	9.0
Ru	8.28	9.19	13.06	14.3	2.0	2.0	9.34	9.19	14.32	14.3	2.0	2.0
Total	100.00	100.00	100.00	100.00	15.1	14.0	100.00	100.00	100.00	100.00	14.0	14.0
Measurement 2												
	exp	calc	exp	calc	exp	calc	exp	calc	exp	calc	exp	calc
K	5.02	5.33	20.50	21.4	3.1	3.0	5.79	5.33	22.87	21.4	3.2	3.0
Tl	11.13	0.00	8.69		1.3							
Bi	75.55	85.48	57.70	64.3	8.8	9.0	84.53	85.48	62.50	64.3	8.8	9.0
Ru	8.30	9.19	13.11	14.3	2.0	2.0	9.58	9.19	14.63	14.3	2.0	2.0
Total	100.00	100.00	100.00	100.00	15.4	14	100.00	100.00	100.00	100.00	14.0	14.0
Measurement 3												
K	4.98	5.33	20.34	21.4	3.0	3.0	5.46	5.33	21.82	21.4	3.1	3.0
Tl	7.21	0.00	5.64		0.8							
Bi	79.30	85.48	60.58	64.3	9.0	9.0	85.22	85.48	63.76	64.3	8.9	9.0
Ru	8.51	9.19	13.44	14.3	2.0	2.0	9.32	9.19	14.42	14.3	2.0	2.0
Total	100.00	100.00	100.00	100.00	14.8	14.0	100.00	100.00	100.00	100.00	14.0	14.0
Measurement 4												
K	4.86	5.33	19.93	21.4	3.0	3.0	5.44	5.33	21.73	21.4	3.0	3.0
Tl	8.80	0.00	6.90		1.0							
Bi	77.93	85.48	59.81	64.3	9.0	9.0	85.12	85.48	63.66	64.3	8.9	9.0
Ru	8.42	9.19	13.35	14.3	2.0	2.0	9.45	9.19	14.61	14.3	2.0	2.0
Total	100.01	100.00	99.99	100.00	15	14	100.01	100.00	100.00	100.00	13.9	14.0
Measurement 5												
K	4.85	5.33	19.86	21.4	2.9	3.0	5.29	5.33	21.24	21.4	3.0	3.0
Tl	6.91	0.00	5.41		0.8							
Bi	79.54	85.48	60.94	64.3	8.8	9.0	85.23	85.48	64.03	64.3	9.0	9.0
Ru	8.28	9.19	13.78	14.3	2.0	2.0	9.49	9.19	14.74	14.3	2.1	2.0
Total	99.99	100.00	99.99	100.00	14.5	14.0	100.01	100.00	100.01	100.00	14.1	14.0
Measurement 5												
K	4.92	5.33	20.12	21.4	3.0	3.0	5.42	5.33	21.68	21.4	3.0	3.0
Tl	7.62	0.00	5.97		0.9							
Bi	78.94	85.48	60.43	64.3	9.0	9.0	85.19	85.48	63.78	64.3	8.9	9.0
Ru	8.52	9.19	13.49	14.3	2.0	2.0	9.39	9.19	14.54	14.3	2.0	2.0
Total	100.00	100.00	100.01	100.00	14.9	14.0	100.00	100.00	100.00	100.00	13.9	14.0

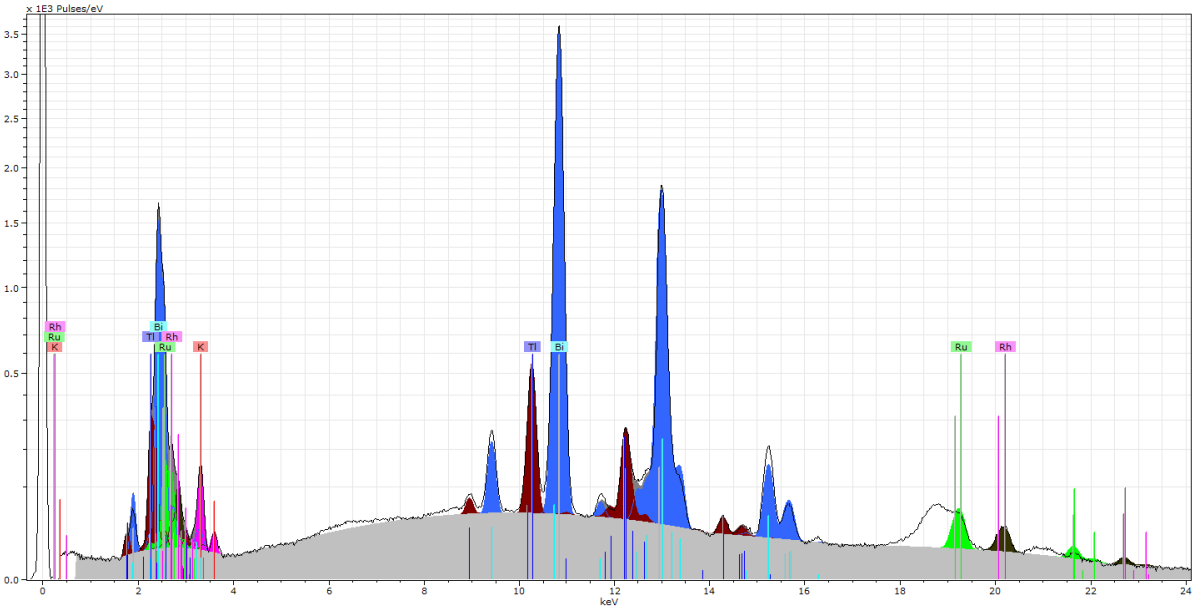

Figure S55. Micro X-ray fluorescence spectrum [K(crypt-222)]$_3$[Bi$_9${Ru(*cod*)}$_2$]·1.5*en* (2) (line) with the results of the deconvolution algorithm. Colors are used as follows: K (pink), Tl (dark red), Bi (blue), Ru (green), background (grey). (Measurement 1, Table S8)

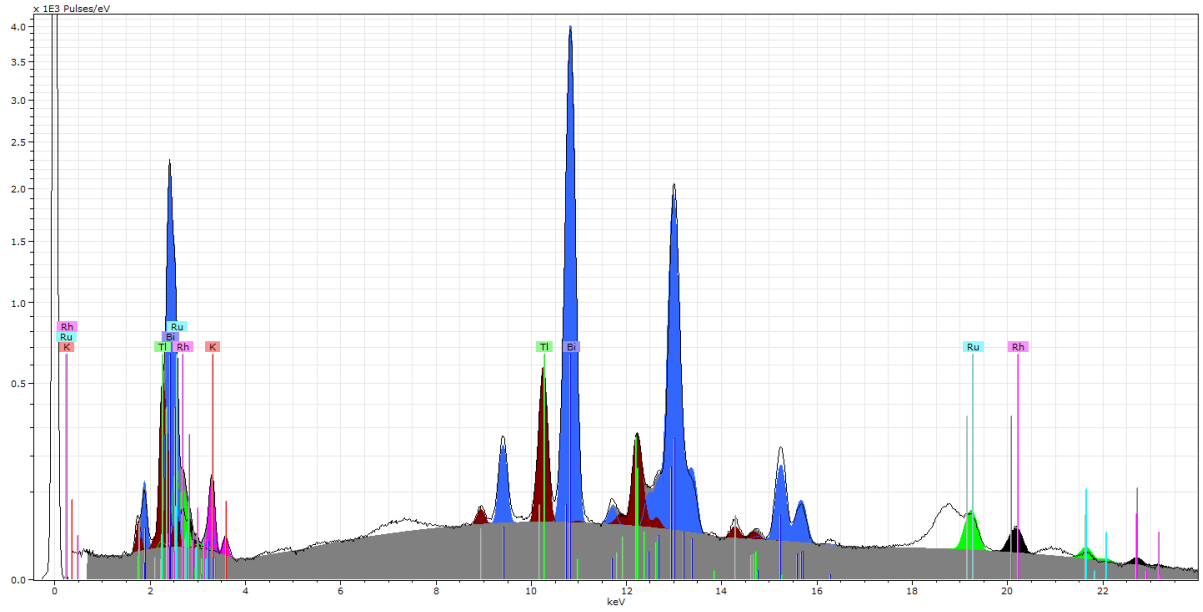

Figure S56. Micro X-ray fluorescence spectrum of[K(crypt-222)]$_3$[Bi$_9${Ru(*cod*)}$_2$]·1.5*en* (2) (line) with the results of the deconvolution algorithm. Colors are used as follows: K (pink), Tl (dark red), Bi (blue), Ru (green), background (grey). (Measurement 2, Table S8)

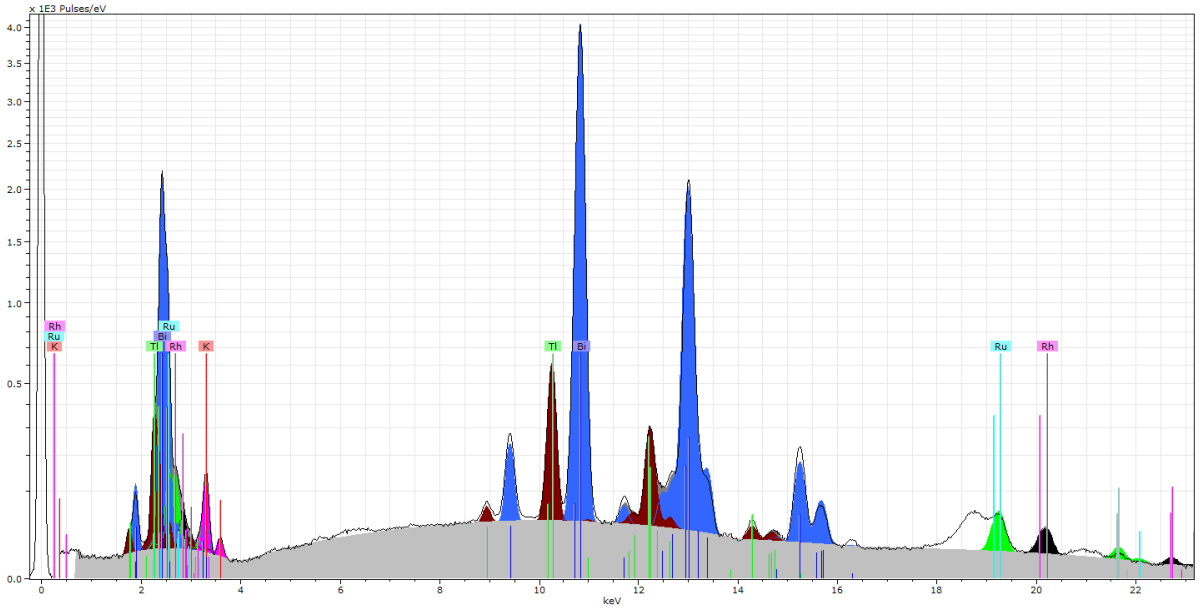

Figure S57. Micro X-ray fluorescence spectrum of [K(crypt-222)]$_3$[Bi$_9${Ru(*cod*)}$_2$]·1.5*en* (2) (line) with the results of the deconvolution algorithm. Colors are used as follows: K (pink), Tl (dark red), Bi (blue), Ru (green), background (grey). (Measurement 3, Table S8)

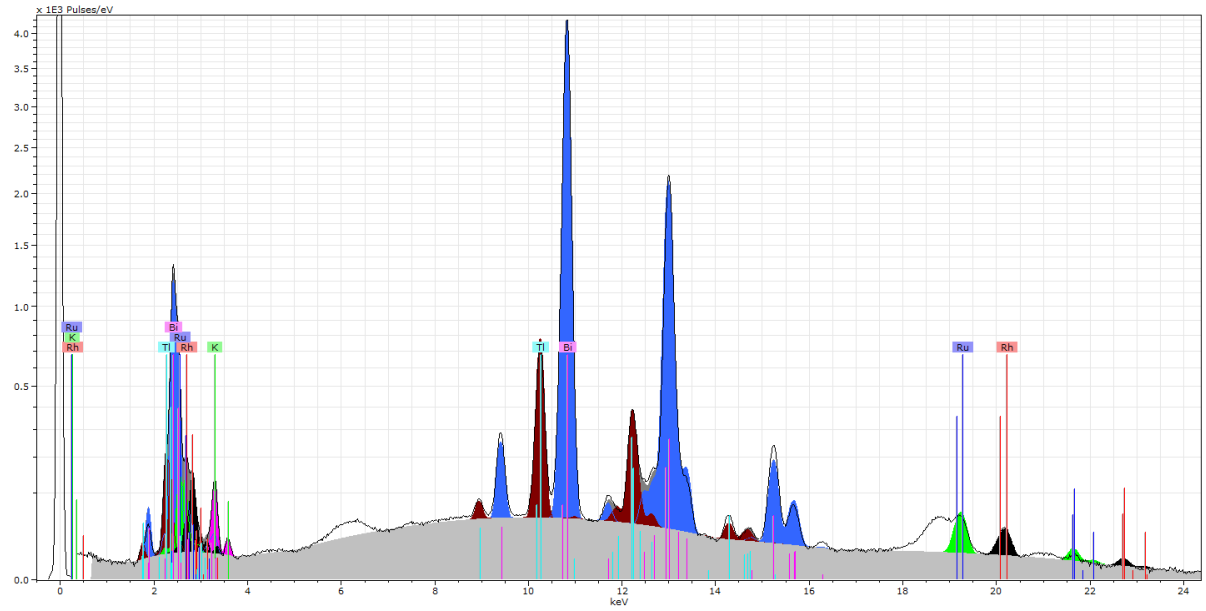

Figure S58. Micro X-ray fluorescence spectrum of [K(crypt-222)]$_3$[Bi$_9${Ru(*cod*)}$_2$]·1.5*en* (2) (line) with the results of the deconvolution algorithm. Colors are used as follows: K (pink), Tl (dark red), Bi (blue), Ru (green), background (grey). (Measurement 4, Table S8)

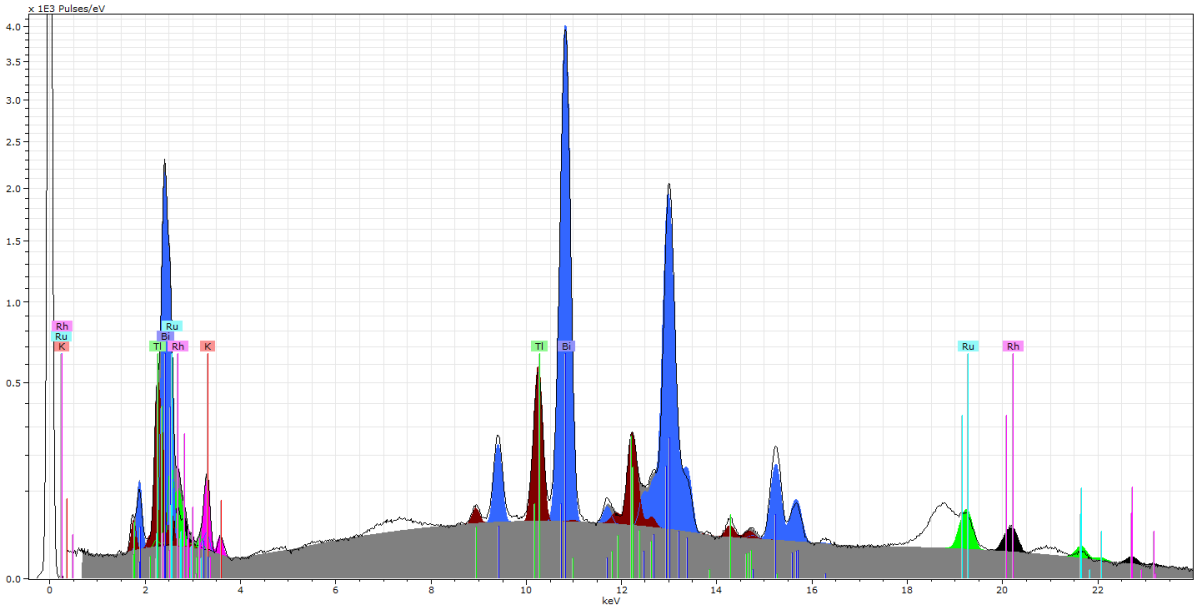

Figure S59. Micro X-ray fluorescence spectrum of [K(crypt-222)]$_3$[Bi$_9${Ru(*cod*)}$_2$]·1.5*en* (2) (line) with the results of the deconvolution algorithm. Colors are used as follows: K (pink), Tl (dark red), Bi (blue), Ru (green), background (grey). (Measurement 5, Table S8)

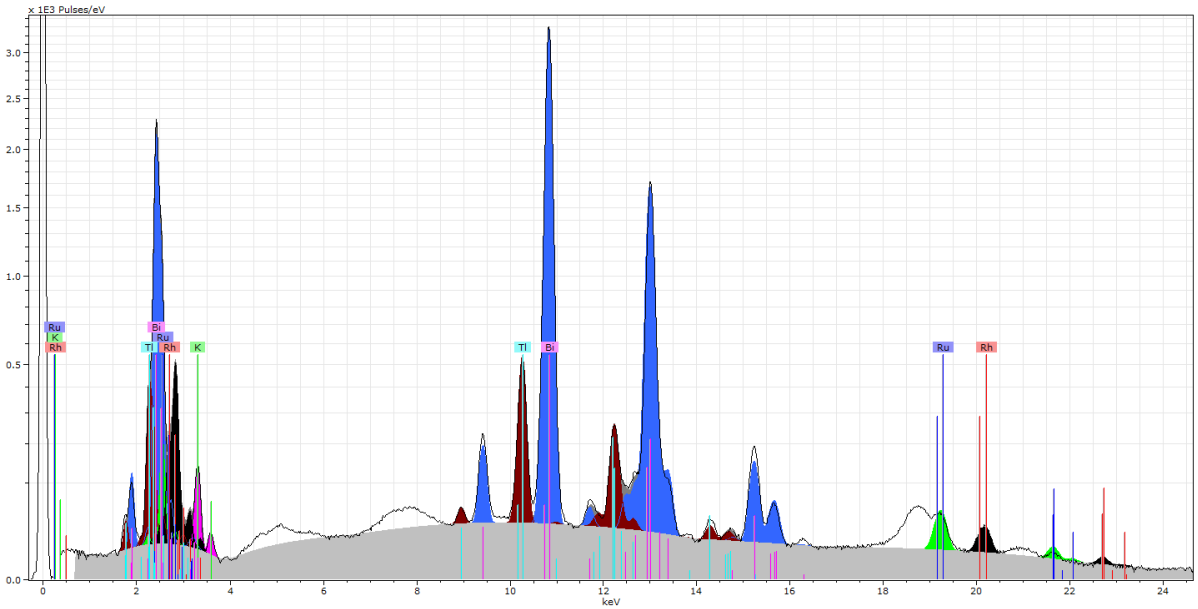

Figure S60. Micro X-ray fluorescence spectrum of [K(crypt-222)]$_3$[Bi$_9${Ru(*cod*)}$_2$]·1.5*en* (2) (line) with the results of the deconvolution algorithm. Colors are used as follows: K (pink), Tl (dark red), Bi (blue), Ru (green), background (grey). (Measurement 6, Table S8)

5. Quantum Chemical Investigations

5.1. Methods

The DFT calculations were performed with the program system Turbomole (v. 6.6).[10] The hybrid functional BP86 was applied.[11] For all elements, the basis sets def2-TZVP[12] with according auxiliary basis sets,[13] and effective core potentials ECP-60 (Ru),[14] and ECP-78 (Tl, Bi)[15] were used. Modelling of counter charges for the anionic compounds was achieved with the COSMO[16] model using the default parameters. The localized orbitals were calculated using the method of *Boys* and *Foster*.[17] Amplitudes in figure 2 in the main document are drawn at ±0.03 a.u. and were created with gOpenMol.[18]

The structures of the cluster $[Ru_2Bi_9]^{3-}$ and $[Ru_2Bi_9]^{-}$ were investigated with a genetic algorithm implemented in Turbomole.[19] For these calculations, the functional BP86 and the basis sets def-SVP[14, 20] were used in combination with the COSMO model. The final structures were optimized with the settings described above to allow for the comparison of energies.

5.2. Bonding Analysis of the Anion $[Bi_9\{Ru(cod)\}_2]^{3-}$

The bonding situation in the anion $[Bi_9\{Ru(cod)\}_2]^{3-}$ was analyzed based on the localized molecular orbitals. Table S9 gives an overview over all LMOs that are directly involved in the cluster bonding and the types of bonds. Furthermore, one lone pair at each Bi atom was found. Two 2e3c bonds are present between Bi1 and the neighboring Bi atoms (Bi2, 3, 8, and 9). No further bonding orbitals between Bi2 and Bi3 (and Bi8 and Bi9 respectively) were found. The remaining Bi-Bi contacts are all best described as covalent bonds, even though in the case of the Bi2/Bi3-Bi4 and Bi7-Bi8/Bi9 bonds some polarization towards the third Bi atom is visible. All Ru-Bi bonds are mainly covalent, again with small degrees of polarization towards one or two Bi atoms.

The bonding situation is therefore best described as follows: The zig-zag Bi_4 chain and the adjacent bonds towards Bi2, 3, 8, and 9 are an electron-precise fragment with covalent Bi-Bi bonds. Both Ru atoms form covalent bonds to all four neighboring Bi atoms. In contrast to this, all Bi1-Bi contacts are strongly delocalized.

The LMOs that represent Bi-Bi bonds are shown in Figure S61. Furthermore all Ru-Bi bonds are shown in Figure S62 while the Bi lone-pairs are represented in Figure S63.

Table S9. Overview over the localized orbitals of the anion $[Bi_9\{Ru(cod)\}_2]^{3-}$ that are directly involved in the cluster bonding.

Ref. to HOMO	Type	atoms	Figure
HOMO	2e3c bond	Bi1-Bi2-Bi3	S25a
HOMO-1		Bi1-Bi8-Bi9	S25b
HOMO-2	covalent bond	Bi2-Bi4	S25c
HOMO-3		Bi7-Bi8	S25d
HOMO-4		Bi4-Bi5	S25e
HOMO-5		Bi6-Bi7	S25f
HOMO-6		Bi3-Bi4	S25g
HOMO-7		Bi7-Bi9	S25h
HOMO-8		Bi5-Bi6	S25i
HOMO-9		Ru1-Bi9	S26a
HOMO-12		Ru2-Bi3	S26d
HOMO-10		Ru1-Bi1	S26b
HOMO-11		Ru2-Bi1	S26c
HOMO-13		Ru1-Bi6	S26e
HOMO-15		Ru2-Bi5	S26g
HOMO-14		Ru1-Bi2	S26f
HOMO-16		Ru2-Bi8	S26h
HOMO-65	lone pair	Bi1	S27a
HOMO-66		Bi5	S27b
HOMO-67		Bi6	S27c
HOMO-68		Bi2	S27d
HOMO-69		Bi8	S27e
HOMO-70		Bi3	S27f
HOMO-71		Bi9	S27f
HOMO-72		Bi4	S27g
HOMO-73		Bi7	S27h

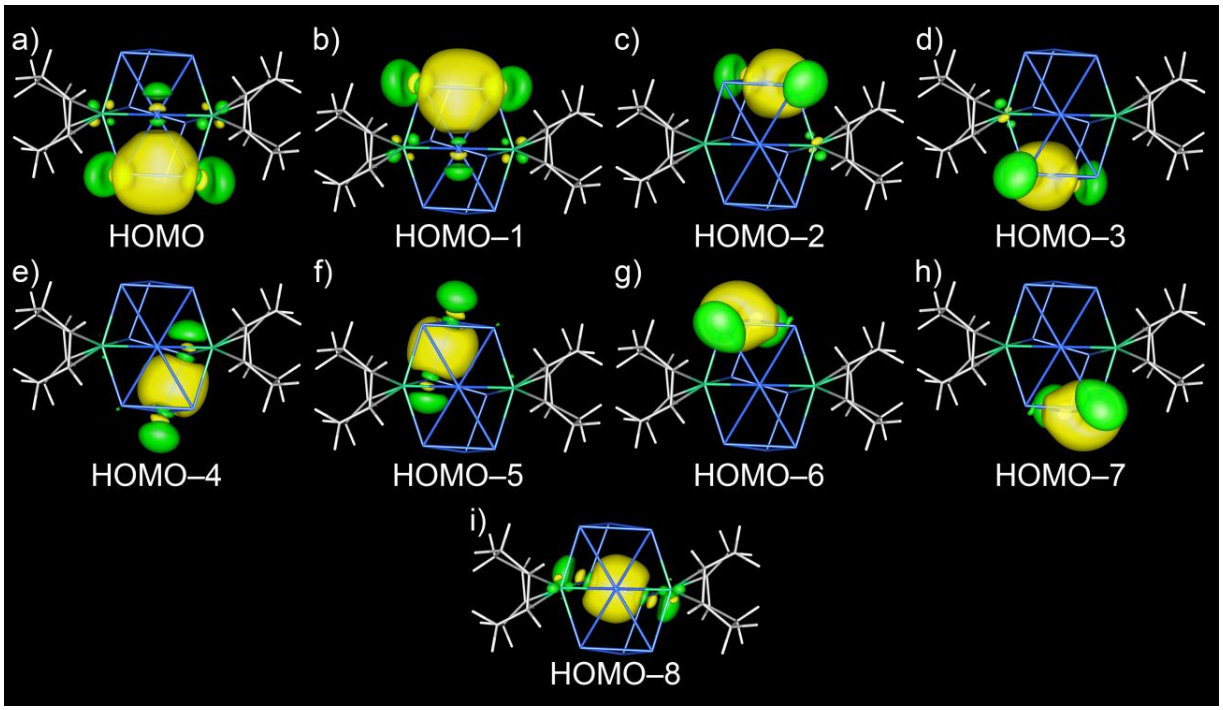

Figure S61. Localized molecular orbitals of $[Bi_9\{Ru(cod)\}_2]^{3-}$ that are Bi-Bi bonding. The color code is the same as in all other figures. Amplitudes are drawn at ±0.03 a.u..

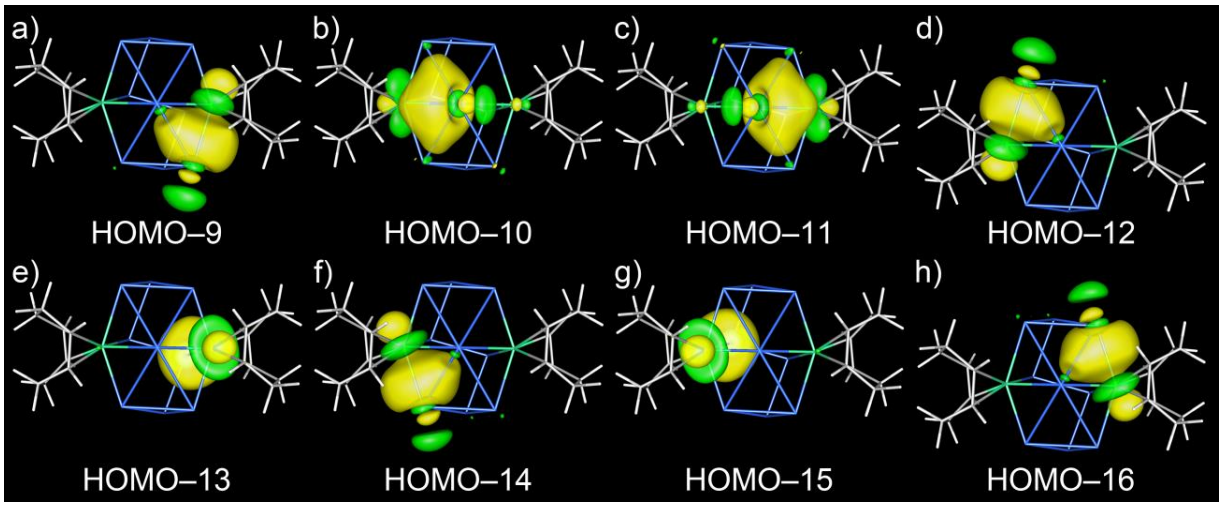

Figure S62. Localized molecular orbitals of $[Bi_9\{Ru(cod)\}_2]^{3-}$ that are Bi-Ru bonding. The color code is the same as in all other figures. Amplitudes are drawn at ±0.03 a.u..

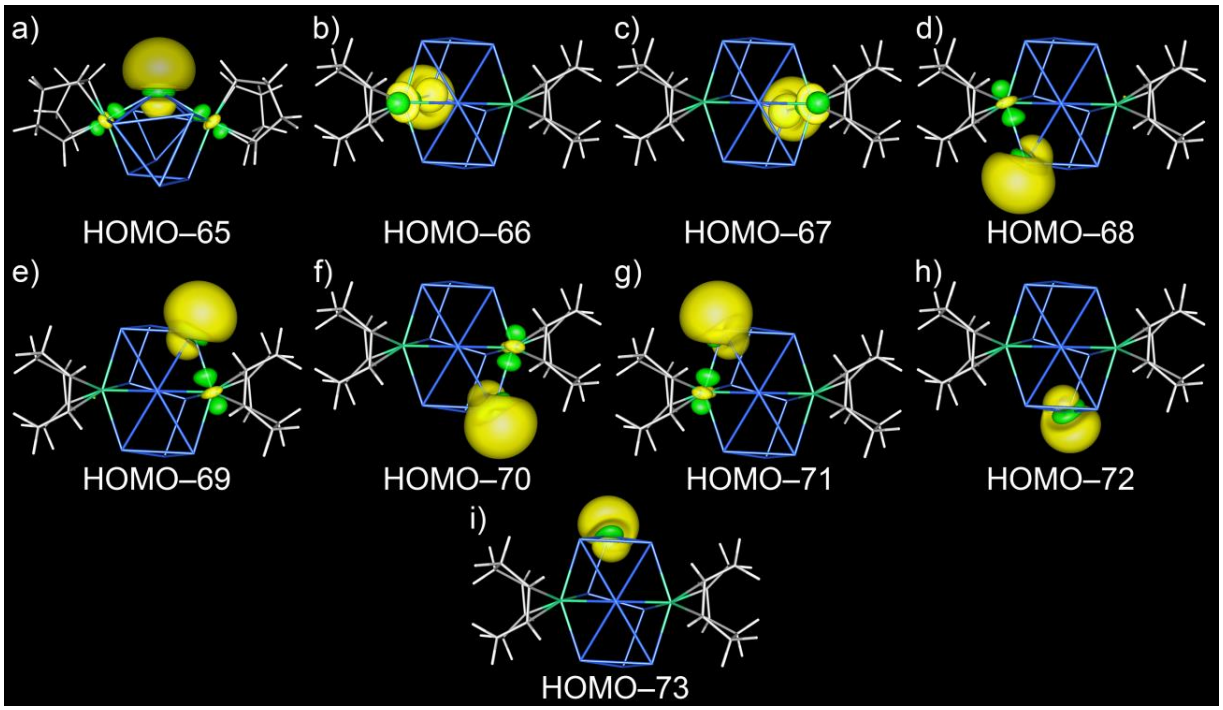

Figure S63. Localized molecular orbitals of $[Bi_9\{Ru(cod)\}_2]^{3-}$ that represent lone pairs located at the Bi atoms. The color code is the same as in all other figures. Amplitudes are drawn at ±0.03 a.u..

5.3. Evaluation of the Cluster Composition in 2

For the synthesis of $[Bi_9\{Ru(cod)\}_2]^{3-}$ in **2**, a binary precursor, $(TlBi_3)^{2-}$ in **1b**, was used as starting material. The inorganic core of the product cluster could therefore be binary (elemental combinations Ru/Bi or Ru/Tl) or ternary (elemental combination Ru/Tl/Bi), in principle. All our analytical methods indicated the absence of Tl atoms and a binary cluster core of the elemental combination Ru/Bi, as given in the formula above.

However, to confirm our data, we investigated a hypothetical anion $[TlBi_8\{Ru(cod)\}_2]^{3-}$ with quantum chemical methods, with a Tl atom placed at the Bi1 position that behaves differently from the other atomic positions (see Figure S64).

The replacement of one Bi atom with one Tl atom reduces the total cluster electron number by 2, such as in the isoelectronic anion "$[Bi_9\{Ru(cod)\}_2]^{-}$", which was also calculated as it occurs as signal in the mass spectrometric investigations (see Figure 3 in the main document).

A comparison of the interatomic distances found in the single-crystal structure of compound **2** with those calculated for $[Bi_9\{Ru(cod)\}_2]^{3-}$, "$[Bi_9\{Ru(cod)\}_2]^{-}$", and "$[TlBi_8\{Ru(cod)\}_2]^{3-}$" and is provided in Table S10. The single-crystal structure of the $[Bi_9\{Ru(cod)\}_2]^{3-}$ cluster in **2** and the structures of all calculated anions are shown and opposed to each other in Figure S64.

The comparison shows the cluster composition to be unambiguously $[Bi_9\{Ru(cod)\}_2]^{3-}$, as the exchange of Bi1 for Tl or the removal of two electrons to form $[Bi_9\{Ru(cod)\}_2]^{-}$ leads to a differently shaped cluster core. The Bi5–Bi6 bond is no longer tilted with respect to the Ru1···Ru2 axis, leading to an idealized cluster symmetry of C_{2v} instead of the C_2 symmetry observed in **2**. This significantly affects some of the interatomic distances, in particular Bi4–Bi5, Bi5–Bi7, Bi4–Bi6, and Bi5–Bi7.

In summary, we note that only for the composition/charge $[Bi_9\{Ru(cod)\}_2]^{3-}$, experimental and calculated structures are matched. This serves as another strong argument that the composition of the anion in **2** is $[Bi_9\{Ru(cod)\}_2]^{3-}$, in agreement with all other experimental data.

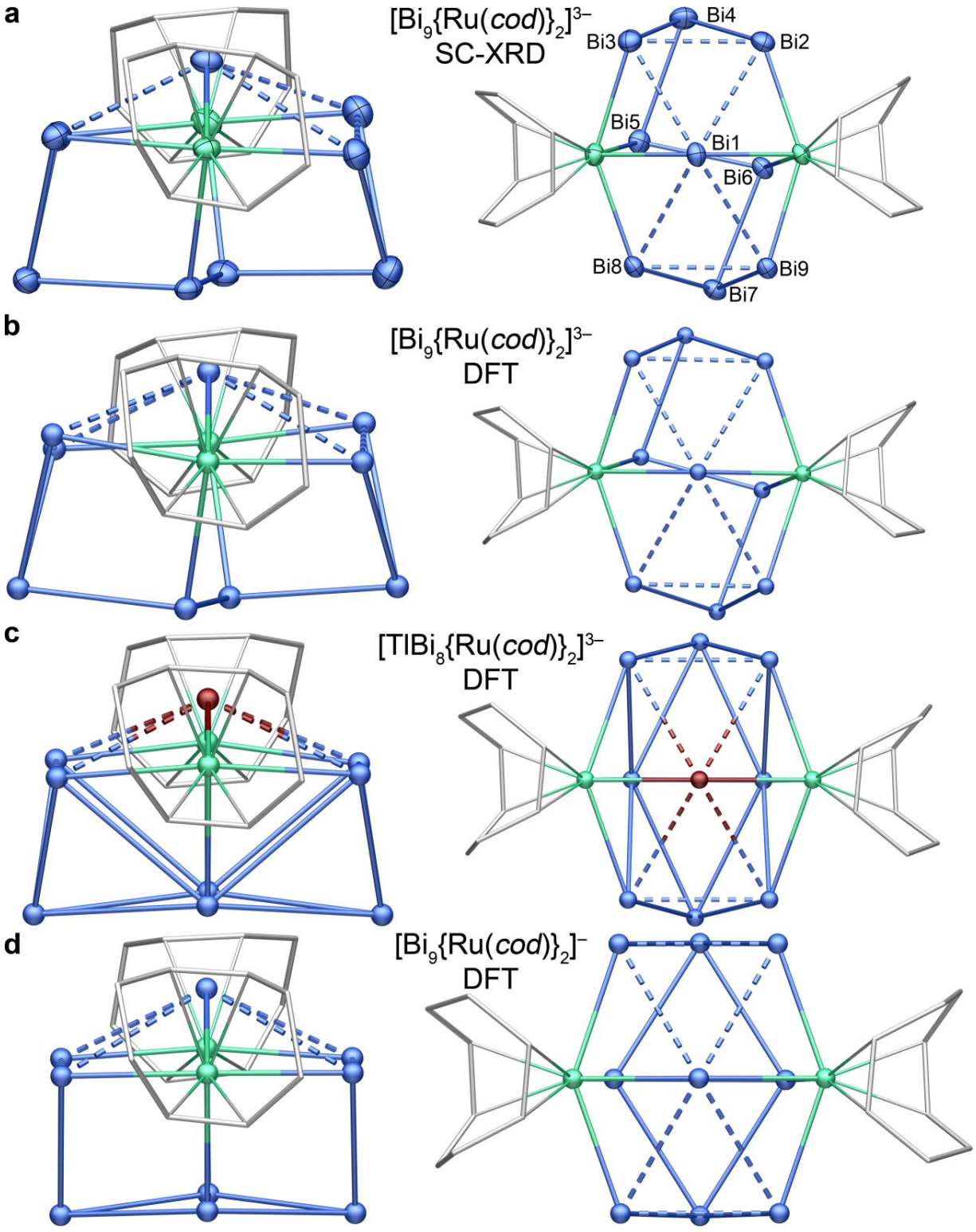

Figure S64. Structural comparison between a) $[Bi_9\{Ru(cod)\}_2]^{3-}$ (SC-XRD), b) $[Bi_9\{Ru(cod)\}_2]^{3-}$ (DFT), c) $[TlBi_8\{Ru(cod)\}_2]^{3-}$ (DFT) and d) $[Bi_9\{Ru(cod)\}_2]^{-}$ (DFT).

Table S10. Comparison of interatomic distances in the cluster anion $[Bi_9\{Ru(cod)\}_2]^{3-}$ in 2 with the structure of the calculated anions $[Bi_9\{Ru(cod)\}_2]^{3-}$ (bold italic), "$[Bi_9\{Ru(cod)\}_2]^{-}$" (bold), and "$[TlBi_8\{Ru(cod)\}_2]^{3-}$" (italic).

Atoms	Distance / Å	Atoms	Distance / Å	Atoms	Distance / Å
Ru1 – **Bi1**	2.753(1)	Bi1 – Bi2	3.3943(8)	Bi4 – Bi5	3.0737(9)
	2.802		***3.370***		***3.065***
	2.782		**3.349**		**3.140**
– Tl1	*2.715*	Tl1 – Bi2	*3.334*		*3.447*
– Bi2	2.790(1)	Bi1 – Bi3	3.2660(7)	Bi4 – Bi6	3.9588(8)
	2.796		***3.265***		***4.071***
	2.782		**3.372**		**3.153**
	2.853	Tl1 – Bi3	*3.356*		*3.412*
– Bi6	2.7629(9)	Bi1 – Bi8	3.3664(7)	Bi5 – Bi6	2.9468(6)
	2.802		***3.370***		***2.959***
	2.687		**3.346**		**3.345**
	2.785	Tl1 – Bi8	*3.336*		*2.954*
– Bi9	2.784(1)	Bi1 – Bi9	3.3348(7)	Bi5 – Bi7	3.7886(8)
	2.822		***3.265***		***4.071***
	2.780		**3.365**		**3.155**
	2.859	Tl1 – Bi9	*3.354*		*3.408*
		Bi2 – Bi3	3.1293(7)	Bi6 – Bi7	3.0583(8)
			3.158		***3.065***
			3.096		**3.138**
			3.158		*3.436*
Ru2 – **Bi1**	2.7518(9)	– Bi4	3.0224(7)		
	2.802		***3.040***		
	2.781		**3.087**		
– Tl1	*2.714*		*3.054*		
– Bi3	2.800(1)	Bi3 – Bi4	3.0139(9)	Bi3 – Bi5	3.6926(7)
	2.822		***3.027***		***3.772***
	2.779		**3.089**		**3.583**
	2.861		*3.059*		*3.507*
– Bi5	2.771(1)	Bi8 – Bi9	3.1380(6)	Bi2 – Bi6	3.7930(7)
	2.802		***3.158***		***3.940***
	2.686		**3.095**		**3.620**
	2.784		*3.157*		*3.564*
– Bi8	2.785(1)	– Bi7	3.0364(7)	Bi5 – Bi8	3.7878(8)
	2.796		***3.040***		***3.940***
	2.781		**3.089**		**3.616**
	2.853		*3.055*		*3.562*
		Bi9 – Bi7	3.0056(6)	Bi6 – Bi9	3.5845(8)
			3.027		***3.772***
			3.084		**3.586**
			3.054		*3.510*

5.3. Isomer Study of the Anion $[Tl_2Bi_6\{Ru(cod)\}]^{2-}$

The atomic coordinates for the cluster were taken from the single crystal structure and used as a starting point for all geometry optimizations. The resulting structures were analyzed with respect to their energies and their conformity with the single crystal data. Only isomer 1 yields a reasonable agreement. Even though isomer 2 is slightly lower in energy the final structure differs significantly from the single crystal data. The study shows that positional occupation of Tl atoms in the open square plane is clearly favorable (>30 kJ/mol). Figure S65 provides an overview over all 6 isomers and their relative energies after the geometry optimization. Note that the structures are schematic drawings and do not represent the final geometries. These are shown in Figure S66.

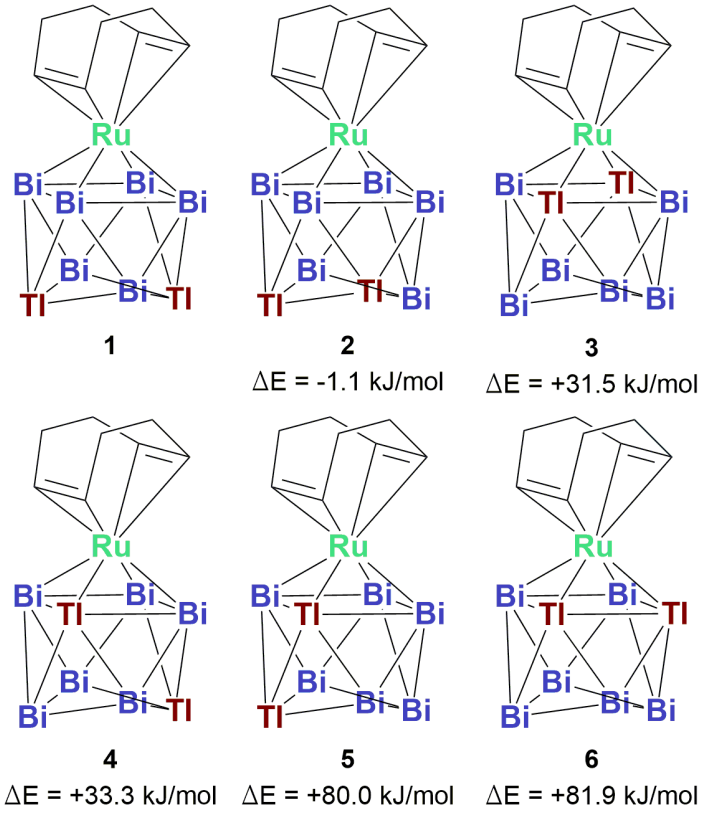

Figure S65. Schematic initial geometries of the 6 isomers of the anion $[Tl_2Bi_6\{Ru(cod)\}]^{2-}$ as used for the geometry optimizations. Only isomer 1 reproduced the structural characteristics of the anion in the crystal structure of 3. The given energies are those of the optimized molecules.

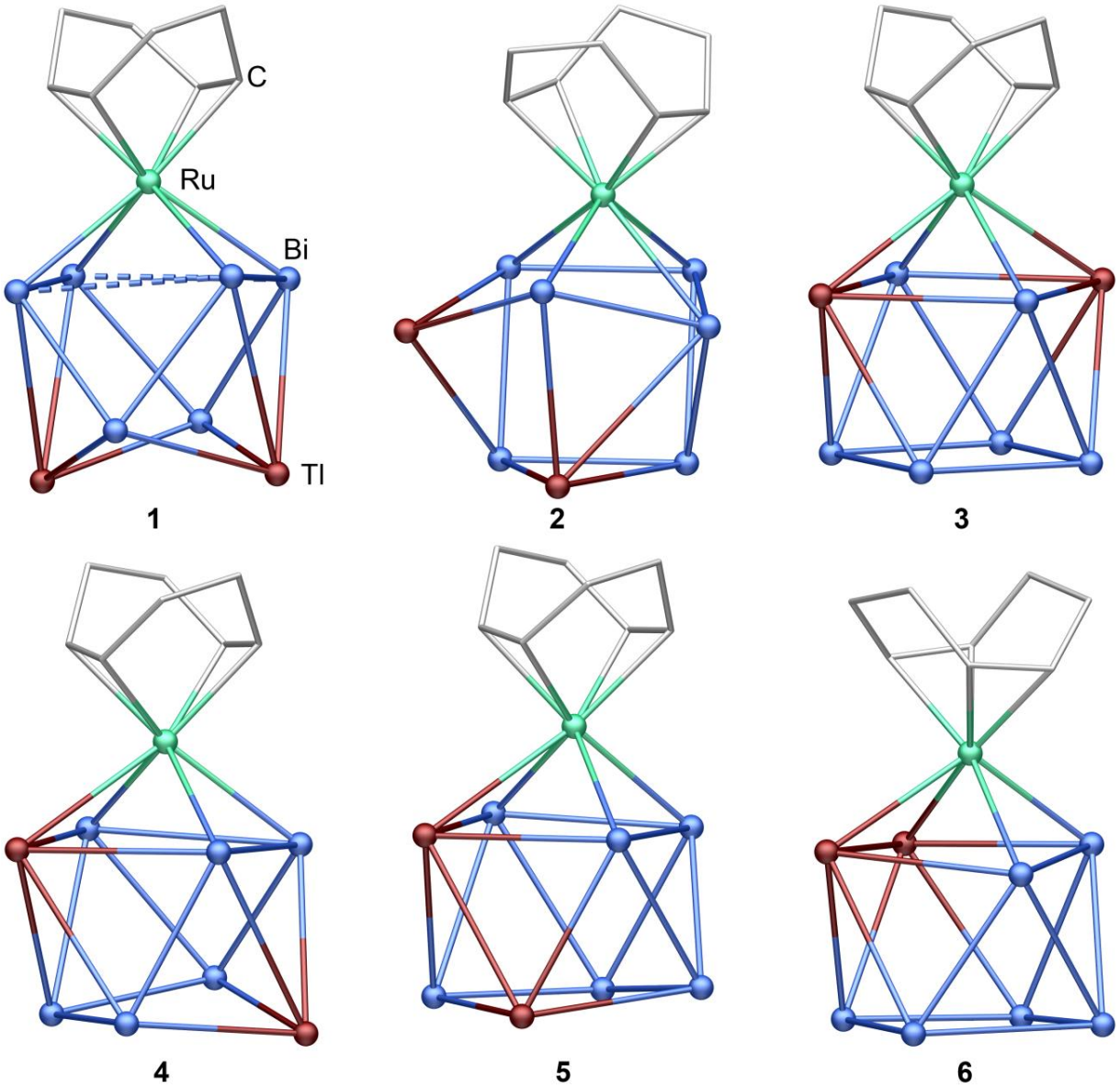

Figure S66. Final geometries of the resulting 6 isomers of the anion $[Tl_2Bi_6\{Ru(cod)\}]^{2-}$ after geometry optimization. The numbers correspond to the numbers given in Figure S65.

5.4. Bonding Analysis of the Anion $[Tl_2Bi_6\{Ru(cod)\}]^{2-}$

The bonding situation in the anion $[Tl_2Bi_6\{Ru(cod)\}]^{2-}$ was analyzed based on the localized molecular orbitals. Table S11 gives an overview over all LMOs that are directly involved in the cluster bonding and the types of bonds. These are shown in Figure S67. The electron count is in accordance with the *Wade-Mingos* rules for a *nido*-type cluster: 8+2·2 (Ru(*cod*) +2·3 (Tl) +6·5 (Bi) +2 (charge) = 50 valence electrons or 50–12–8·2 = 22 = 2n+4 skeletal electrons.

Table S11. Overview over the localized orbitals of the anion $[Tl_2Bi_6\{Ru(cod)\}]^{2-}$ that are directly involved in the cluster bonding.

Ref. to HOMO	Type	Atoms	Figure
0, –1	2e3c bonds	Tl6-Bi2-Bi5, Tl8-Bi3-Bi4	S30a,b
–2 - –5		Bi2-Bi7-(Tl6), Bi5-Bi9-(Tl6) Bi3-Bi7-(Tl8), Bi4-Bi9-(Tl8)	S30c - f
–6 - –9	covalent	Ru1-Bi(2-5)	S30g - j
–10, –11	2e3c bonds	Tl6-Bi7-Tl8, Tl6-Bi9-Tl8	S30k,l

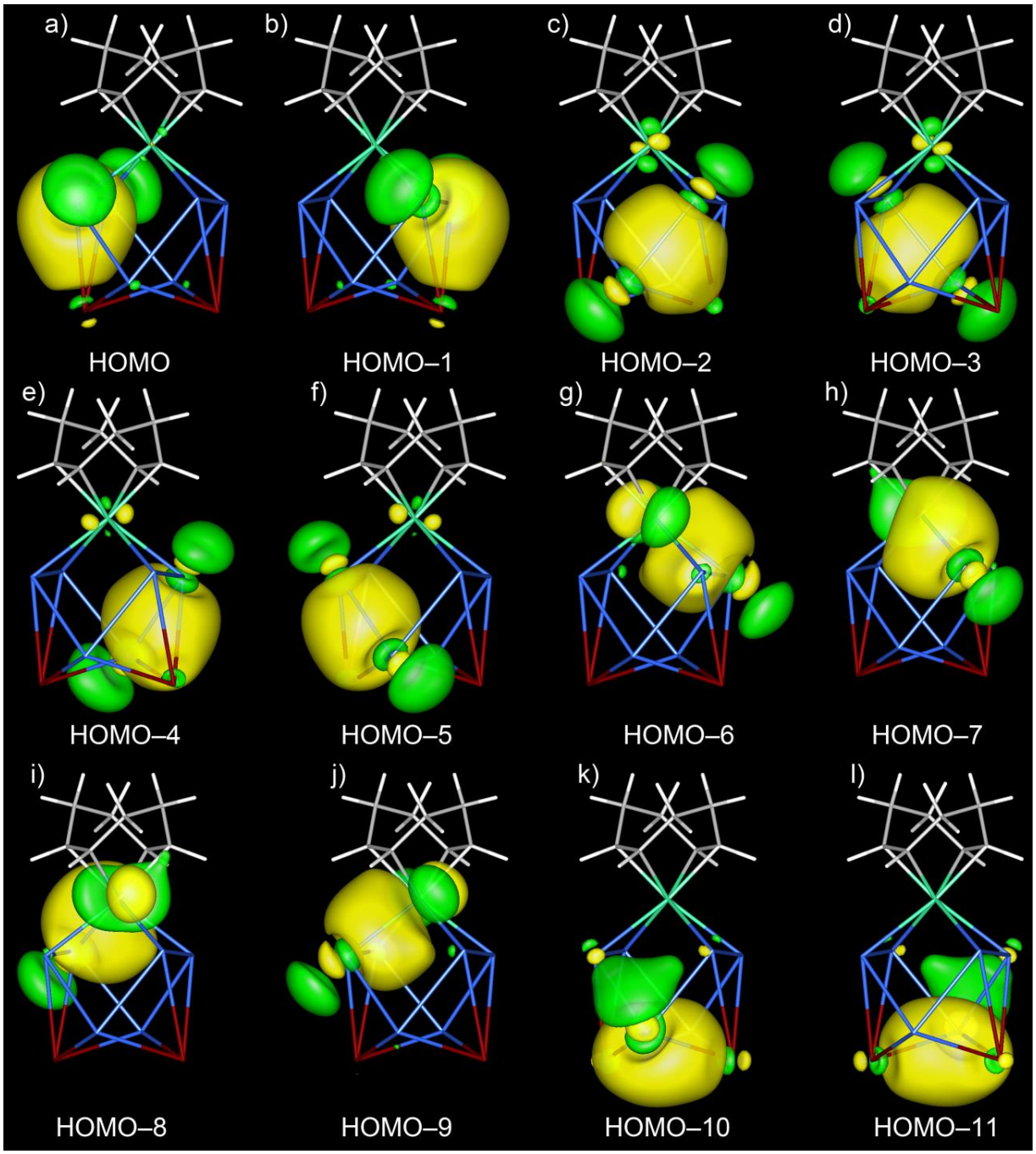

Figure S67. Localized molecular orbitals of $[Tl_2Bi_6\{Ru(cod)\}]^{2-}$ that are directly involved in the cluster bonding. The color code is the same as in all other figures. Amplitudes are drawn at ±0.03 a.u..

5.5. Isomer Study of the Anion $(Tl_4Bi_5)^{3-}$

The atomic coordinates for the cluster were taken from the single crystal structure and used as a starting point for all geometry optimizations. The resulting structures were analyzed with respect to their energies and their conformity with the single crystal data. Only isomer 1 and 15 (which converge into the same geometry) yield a reasonable agreement and are also lowest in energy by 15.8 kJ/mol. Figure S68 provides an overview over all 21 initial isomers. Schematic drawings of the resulting 9 isomers and their relative energies after the geometry optimization are given in Figure S69. Note that the structures are schematic drawings and do not represent the final geometries. These are shown in Figure S70.

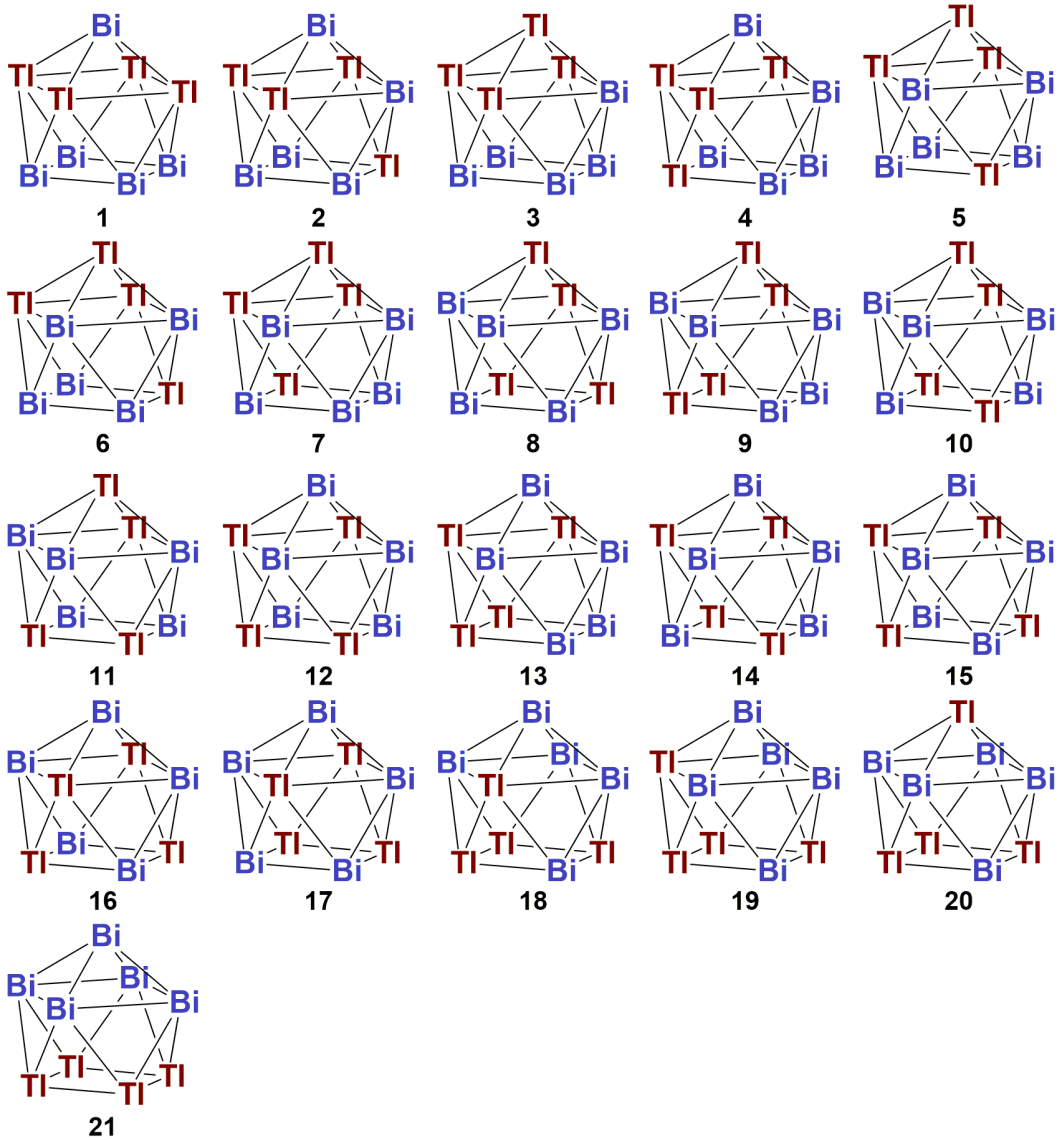

Figure S68. Initial geometries of all 21 isomers of the anion $(Tl_4Bi_5)^{3-}$, as used for the geometry optimizations with their assigned numbers.

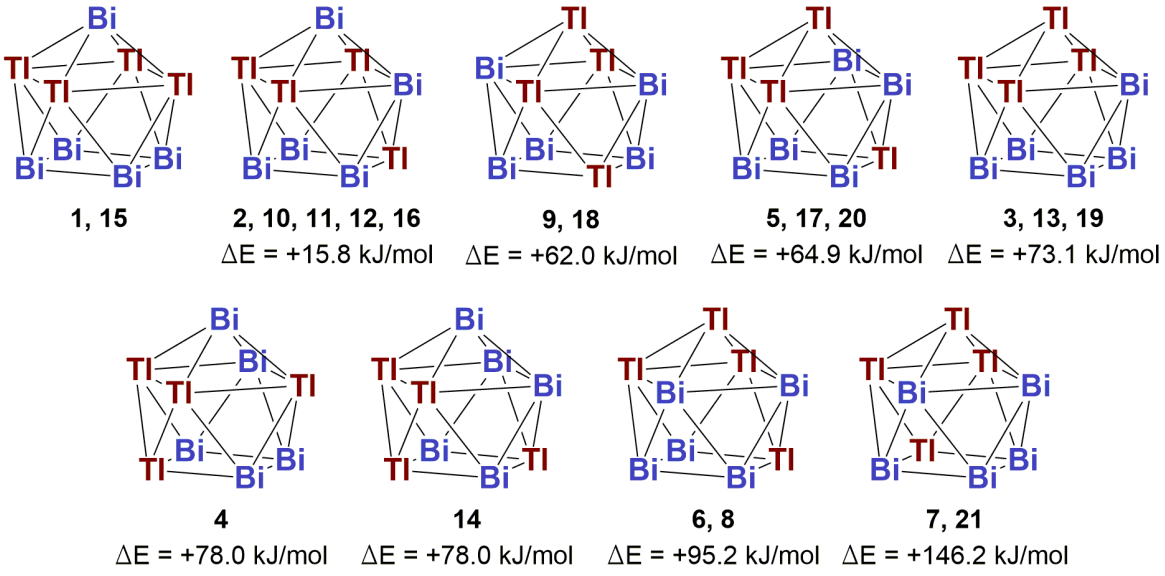

Figure S69. Schematic final geometries of the resulting 9 isomers of the anion $(Tl_4Bi_5)^{3-}$ after geometry optimization. The numbers indicate which isomers converged into these geometries. Note that partially significant distortions occurred during the optimization process that have been omitted for clarity but are shown in Figure S70.

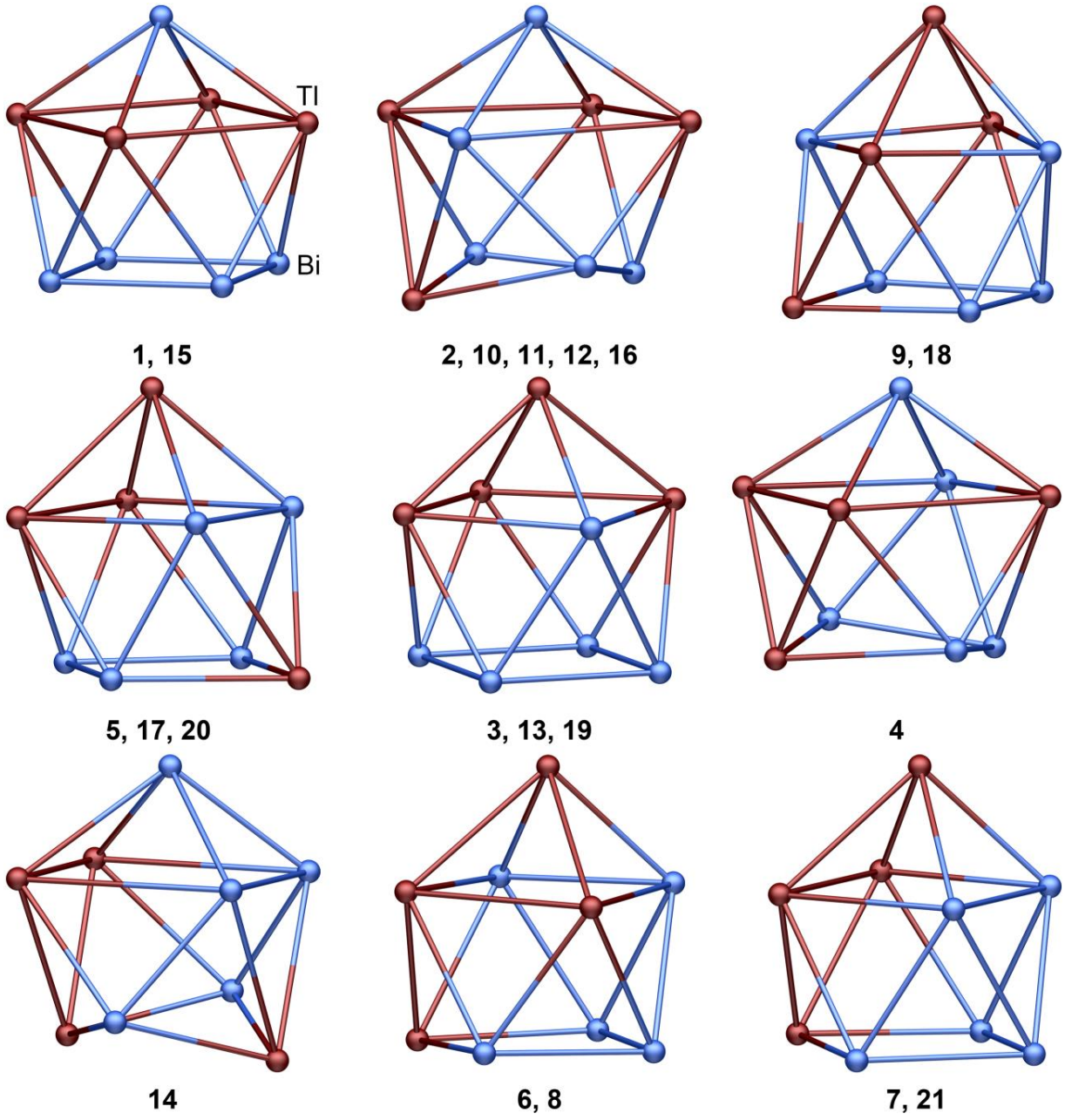

Figure S70. Final geometries of the resulting 9 isomers of the anion $(Tl_4Bi_5)^{3-}$ after geometry optimization. The numbers indicate which isomers converged into these geometries.

6. References for the Supporting Information

[1] crypt-222: 4,7,13,16,21,24-Hexaoxa-1,10-diazabicyclo[8.8.8]hexacosane

[2] M. Strohalm, D. Kavan, P. Novák, M. Volný, V. Havlíček, *Anal. Chem.* **2010**, *82*, 4648-4651.

[3] G. Sheldrick, *Acta Cryst.* **2015**, *A71*, 3-8.

[4] a) G. M. Sheldrick, *Acta Cryst.* **2008**, *A64*, 112-122; b) G. M. Sheldrick, *Acta Cryst.* **2015**, *C71*, 3-8.

[5] O. V. Dolomanov, L. J. Bourhis, R. J. Gildea, J. A. K. Howard, H. Puschmann, *J. Appl. Crystallogr.* **2009**, *42*, 339-341.

[6] Diamond - Crystal and Molecular Structure Visualization, Crystal Impact - Dr. H. Putz & Dr. K. Brandenburg GbR, Kreuzherrenstr. 102, 53227 Bonn, Germany, http://www.crystalimpact.com/diamond

[7] Persistence of Vision Pty. Ltd. (2004) Persistence of Vision Raytracer (Version 3.6) [Computer software]. Retrieved from http://www.povray.org/download/

[8] S. Brennan, P. L. Cowan, *Rev. Sci. Instrum.* **1992**, *63*, 850-853.

[9] a) P. van der Sluis, A. L. Spek, *Acta Cryst.* **1990**, *A46*, 194-201; b) A. Spek, *Acta Cryst.* **2009**, *D65*, 148-155.

[10] TURBOMOLE V6.6 2015, a development of University of Karlsruhe and Forschungszentrum Karlsruhe GmbH, 1989-2007,TURBOMOLE GmbH, since 2007; available from http://www.turbomole.com.

[11] a) A. D. Becke, *J. Chem. Phys.* **1993**, *98*, 5648-5652; b) P. A. M. Dirac, *Proc. R. Soc. A* **1929**, *123*, 714-733; c) J. P. Perdew, *Phys. Rev. B* **1986**, *33*, 8822-8824; d) J. C. Slater, *Phys. Rev.* **1951**, *81*, 385-390; e) S. H. Vosko, L. Wilk, M. Nusair, *Can. J. Phys.* **1980**, *58*, 1200-1211.

[12] F. Weigend, R. Ahlrichs, *Phys. Chem. Chem. Phys.* **2005**, *7*, 3297-3305.

[13] F. Weigend, *Phys. Chem. Chem. Phys.* **2006**, *8*, 1057-1065.

[14] D. Andrae, U. Häußermann, M. Dolg, H. Stoll, H. Preuß, *Theor. Chim. Acta* **1990**, *77*, 123-141.

[15] B. Metz, H. Stoll, M. Dolg, *J. Chem. Phys.* **2000**, *113*, 2563-2569.

[16] A. Klamt, G. Schüürmann, *J. Chem. Soc., Perkin Trans. 2* **1993**, 799-805.

[17] a) S. F. Boys, *Rev. Mod. Phys.* **1960**, *32*, 296-299; b) J. M. Foster, S. F. Boys, *Rev. Mod. Phys.* **1960**, *32*, 300-302.

[18] D. L. Bergman, L. Laaksonen, A. Laaksonen, *J. Mol. Graph. Model.* **1997**, *15*, 301-306, 328-333.

[19] a) D. M. Deaven, K. M. Ho, *Phys. Rev. Lett.* **1995**, *75*, 288-291; b) M. Sierka, J. Dobler, J. Sauer, G. Santambrogio, M. Brummer, L. Woste, E. Janssens, G. Meijer, K. R. Asmis, *Angew. Chem.* **2007**, *119*, 3437-3440; *Angew. Chem. Int. Ed.* **2007**, *46*, 3372-3375.

[20] a) A. Schafer, H. Horn, R. Ahlrichs, *J. Chem. Phys.* **1992**, *97*, 2571-2577; b) K. Eichkorn, F. Weigend, O. Treutler, R. Ahlrichs, *Theor. Chem. Acc.* **1997**, *97*, 119-124.

C.3 The Identity of Ternary A/Tl/Pb or K/Tl/Bi Solid Mixtures and Binary Zintl Anions Isolated From Their Solutions

Supporting Information

The Identity of "Ternary" A/Tl/Pb or K/Tl/Bi Solid Mixtures and Binary *Zintl* Anions Isolated From Their Solutions

Niels Lichtenberger,[a] Yannick J. Franzke,[b] Werner Massa,[a] Florian Weigend,[c] and Stefanie Dehnen*[a]

[a] *Fachbereich Chemie und Wissenschaftliches Zentrum für Materialwissenschaften, Philipps-Universität Marburg, Hans-Meerwein-Straße 4, 35043 Marburg, Germany.*

[b] *Karlsruhe Institute of Technology (KIT), Institute of Physical Chemistry, Kaiserstr. 12, 76131 Karlsruhe, Germany.*

[c] *Karlsruhe Institute of Technology (KIT), Institute of Nanotechnology, Hermann-von-Helmholtz-Platz 1, 76344 Eggenstein-Leopoldshafen, Germany*

Contents

1. Synthesis Details

1.1. General

All manipulations and reactions were performed under dry Ar atmosphere using standard Schlenk or glovebox techniques. All solvents were dried and freshly distilled prior to use. Crypt-222[1] (Merck) was dried *in vacuo* for at least 18 hours. Samples were shielded from ambient light throughout all solution-based syntheses.

1.2. Solid-State Syntheses

1.2.1. General Procedure

All solid state syntheses were carried out according to a standardized procedure. Niobium tubes were cut to size and sealed on one side by arc-welding inside a glovebox. The elements were weighed into beakers, mixed, and afterwards transferred into the Nb containers. These were sealed tight by arc-welding and transferred into quartz tubes. After evacuation and subsequent sealing, they were then placed in a chamber furnace and treated with the desired temperature program.

1.2.2. Syntheses of "A_5TlPb_3" (A = Na (I), K (II))

Samples were heated to 900 °C with 10 K/h, annealed for 48 h and cooled down to 350 °C with 10 K/h. Annealing for 21 d at 350 °C was followed by cooling to room temperature with 2 K/h.

"Na_5TlPb_3" (I)

Element	m / mg	n / mmol	Eq
Na	244.3	10.62	5
Tl	434.4	2.12	1
Pb	1321.2	6.37	3

"K_5TlPb_3" (II)

Element	m / mg	n / mmol	Eq
Na	382.8	9.79	5
Tl	400.2	1.96	1
Pb	1217.1	5.87	3

1.2.3. Synthesis of $Na_{17}Tl_5Pb_7$ (2)

Samples were heated to 900 °C with 10 K/h, annealed for 48 h and cooled down to 350 °C with 10 K/h. Annealing for 21 d at 350 °C was followed by cooling to room temperature with 2 K/h.

Element	m / mg	n / mmol	Eq
Na	682.5	29.7	17
Tl	1.786	8.7	5
Pb	2.533	12.2	7

1.2.4. Synthesis of "$K_5Tl_2Bi_4$" (III)

Samples were heated to 550 °C with 20 K/h, annealed for 7 d and cooled down to room temperature with 5 K/h.

Element	m / g	n / mmol	Eq
K	1.3575	34.72	5
Tl	2.8383	13.89	2
Bi	5.8043	27.77	4

1.2.5. Synthesis of "K_2TlBi" (IV)

Samples were heated to 900 °C with 10 K/h, annealed for 48 h and cooled down to 350 °C with 5 K/h. Annealing for 7d at 350 °C was followed by cooling to room temperature with 2 K/h.

Alternative temperature program:

Samples were heated to 550 °C with 20 K/h, annealed for 7 d and cooled down to room temperature with 5 K/h.

Element	m / g	n / mmol	Eq
K	1.5909	40.69	2
Tl	4.1578	20.34	1
Bi	4.2514	20.34	1

1.2.6. Synthesis of "K_2TlBi_3" (V)

Samples were heated to 550 °C with 20 K/h, annealed for 7 d and cooled down to room temperature with 5 K/h.

Element	m / g	n / mmol	Eq
K	1.7195	43.98	2
Tl	4.4942	21.99	1
Bi	13.7862	65.97	3

1.3. Solution-based Syntheses

1.3.1. Synthesis of $[Na(crypt\text{-}222)]_3(TlSn_9)_{0.8}(TlSn_8)_{0.2}\cdot 0.55en\cdot 0.45thf$ (1)

200 mg (296 µmol, 1 eq) of Na_5TlSn_3[2] and 563 mg (1.50 mmol, 5.05 eq) of crypt-222 were combined in a Schlenk tube and dissolved in 20 mL of en, at first forming a pale brown solution. Upon successive stirring the solution slowly turned intensely brown. It was filtered through a standard glass frit after stirring for 3 days. A total of 10 mL of the solution were transferred into two different Schlenk tubes in which 5 mL of the solution were layered with 10 mL of toluene or THF respectively. The remaining 10 mL were concentrated by slow evaporation of the solvent and then stored at 5 °C. Metallic black single crystals of **1** were obtained from all three experiments, even though they will be different solvates. Under the microscope a dark red color is noticeable at thinner crystal edges.

1.3.2. Synthesis of $[Na(crypt\text{-}222)]_3(TlPb_9)_{0.94}(TlPb_{11})_{0.06}\cdot 0.9thf$ (6)

150 mg (159 µmol, 1 eq) of "Na_5TlPb_3" (I) and 303 mg (805 µmol, 5.05 eq) of crypt-222 were combined in a Schlenk tube and dissolved in 15 mL of en, forming a goldish brown solution. The extraction solution was filtered through a standard glass frit after stirring for 3 days. A total of 10 mL of the solution were transferred into two different Schlenk tubes in which 5 mL of the solution were layered with toluene or THF respectively. The remaining 5 mL were concentrated by slow evaporation of the solvent and then stored at 5 °C. Crystals of $[Na(crypt\text{-}222)]_3(TlPb_9)_{0.94}(TlPb_{11})_{0.06}\cdot solv$ (**6**) were obtained from both diffusion experiments. No crystals of $[Na(crypt\text{-}222)]_2(Pb_5)$ were observed in any of the experiments. As the solutions showed signs of decomposition before the diffusion process was complete we isolated the crystals at that time. Therefore, final yields could not be determined but we estimate that they were never higher than 30% at any given time.

1.3.3. Synthesis of $[K(crypt\text{-}222)]_4[Tl@Tl_4Pb_8]_{0.5}(Tl_2Pb_{10})_{0.1}(Pb_9)_{0.4}\cdot 1.2en$ (7)

200 mg (195 µmol) of "K_5TlPb_3" (**II**) and 372 mg (988 µmol, 5.05 eq) of crypt-222 were combined in a Schlenk tube and dissolved in 20 mL of en, initially forming a goldish brown solution which turned reddish brown after a few hours. The extraction solution was filtered through a standard

glass frit after stirring for 3 days, again yielding a goldish brown solution. A total of 10 mL of the solution were transferred into two different Schlenk tubes in which 5 mL of the solution were layered with toluene or THF respectively. The remaining 10 mL were concentrated by slow evaporation of the solvent and then stored at 5 °C to afford crystals of **7** besides crystals of $[K(crypt\text{-}222)]_2Pb_5$ and metallic powder. A microscopic picture of the substance mixture is given in figure S1. As an inseparable substance mixture is obtained we could not determine the final yields of this reaction. We estimate that these are never higher than 30% at any given time.

Shortening of the extraction time (3 h) and layering of the extraction solution both led to the exclusive formation of $[K(crypt\text{-}222)]_2Pb_5$ as bright red needles. The synthesis is again successful if the extraction time amounts to at least 24 h.

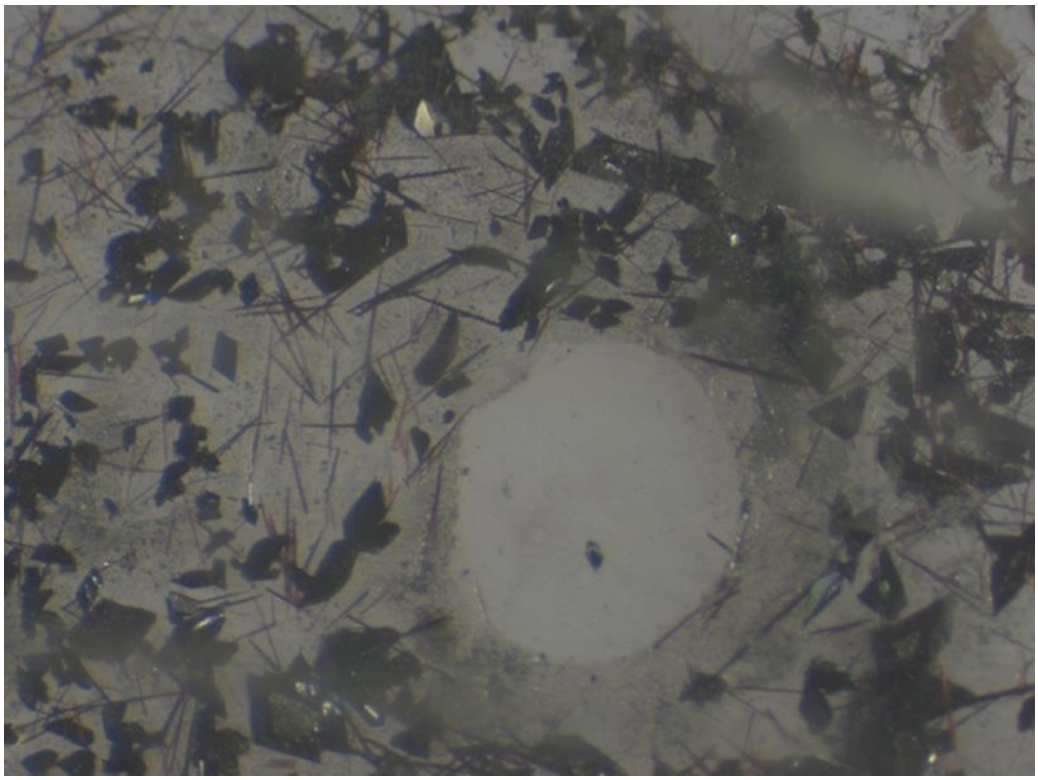

Figure S1. Microscopic picture of the substance mixture of $[K(crypt\text{-}222)]_4[Tl@Tl_4Pb_8]_{0.5}(Tl_2Pb_{10})_{0.1}(Pb_9)_{0.4}\cdot 1.2$*en* (7, black blocks) and $[K(crypt\text{-}222)]_2Pb_5$ (thin red needles).

1.3.4. Synthesis of $[K(crypt\text{-}222)]_3(Tl_4Bi_3)$ (8)

500 mg (1.02 mmol) of "K_2TlBi" (**IV**) and 785 mg (2.09 mmol) of crypt-222 were combined in a Schlenk tube and dissolved in 50 mL of en, forming a intensively colored dark green solution. The extraction solution was filtered through a standard glass frit after stirring for 3 days. Concentration of the solution under reduced pressure to approximately 6 mL and subsequent storing at 5 °C for

several days yielded $[K(crypt\text{-}222)]_3(Tl_4Bi_3)$ (**8**) as black block-shaped crystals along with some metallic powder. The remaining solution was removed and the crystals were washed with toluene. Removal of all volatiles under reduced pressure yielded 511 mg of $[K(crypt\text{-}222)]_3(Tl_4Bi_3)$ (75%).

2. Mass Spectrometry

2.1. General Procedure

All mass spectra were recorded with a Thermo Fischer Scientific Finnigan LTQ-FT spectrometer in negative ion mode. Single crystals of the compounds **1, 6 – 8** were dissolved in freshly distilled DMF inside a glovebox and filtered through 0.2 µm PTFE syringe filters. The solutions were ingested into the spectrometer with gastight 500 µL Hamilton syringes by syringe pump infusion. All capillaries within the system were washed with dry DMF for 2 hours before and at least 10 minutes in between measurements to avoid decomposition reactions and consequent clogging. All simulations were created using the *mMass* software suite.[3]

2.2. Mass Spectrometry of $[Na(crypt\text{-}222)]_3(TlSn_9)_{0.8}(TlSn_8)_{0.2}\cdot 0.55en\cdot 0.45thf$ (1)

Crystals of **1** were obtained from diffusion controled crystallization experiments. After prolonged crystallization times of several weeks the solution was removed with a syringe. The crystals were washed with 10 mL of dry toluene and then dried *in vacuo* for 30 minutes. Figure S2 provides an overview of the obtained mass spectrum. A high resolution view of the $(TlSn_9)^-$ signal is given in figure S3 along with the corresponding simulation.

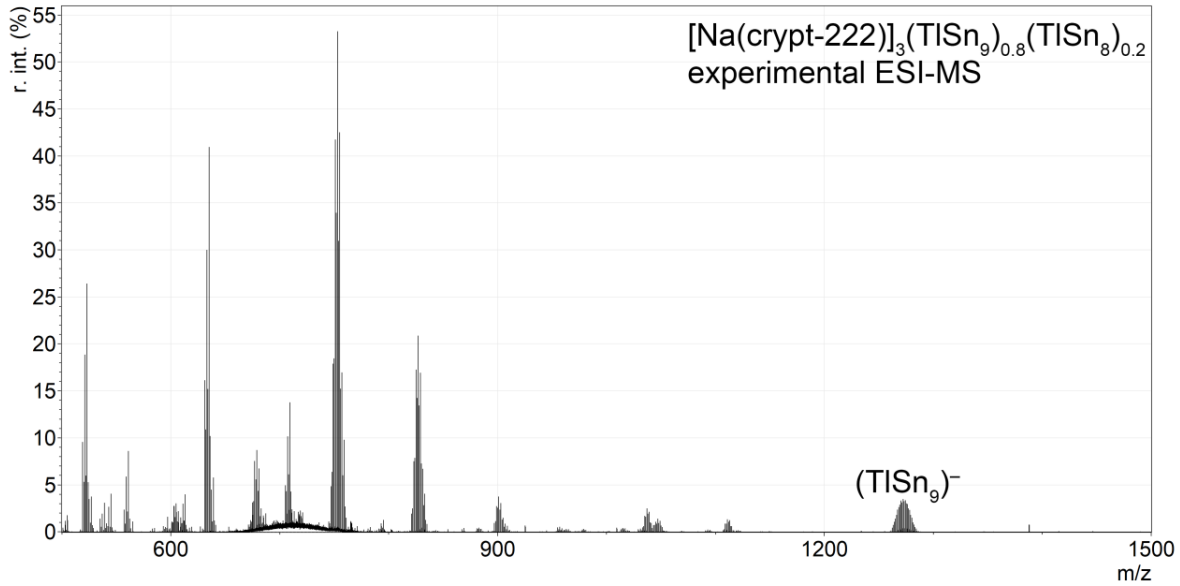

Figure S2. Overview of the ESI-MS of $[Na(crypt\text{-}222)]_3(TlSn_9)_{0.8}(TlSn_8)_{0.2}$ (1) in DMF.

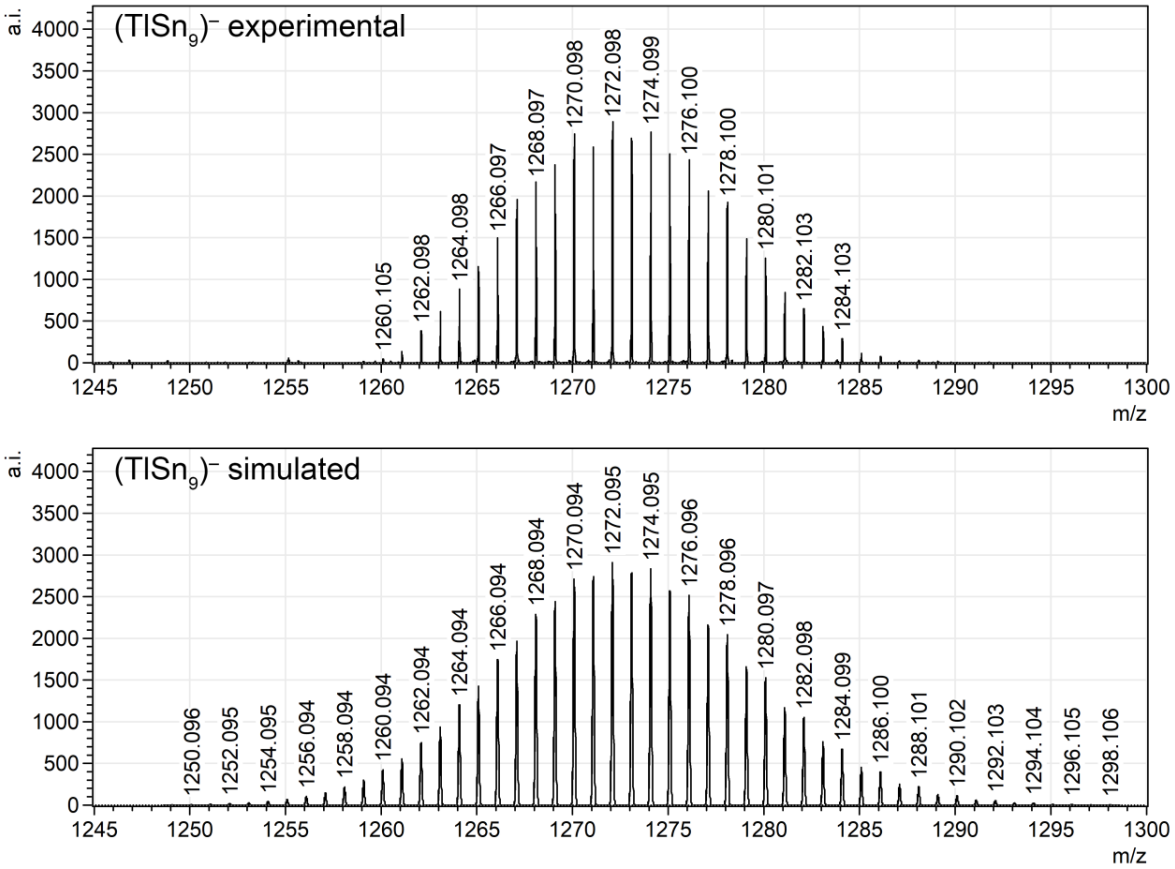

Figure S3. Comparison of experimental (top) and simulated (bottom) signals of $(TlSn_9)^-$ ions.

2.3. Mass Spectrometry of $[Na(crypt\text{-}222)]_3(TlPb_9)_{0.94}(TlPb_{11})_{0.06}$ (6)

Crystals of **6** were obtained from diffusion controled crystallization experiments. After prolonged crystallization times of several weeks the solution was removed with a syringe. The crystals were washed with 10 mL of dry toluene and then dried *in vacuo* for 30 minutes. Figure S4 provides an overview of the obtained mass spectrum. High resolution views of the individual signals are given in the figures S5 – S8 along with the corresponding simulations.

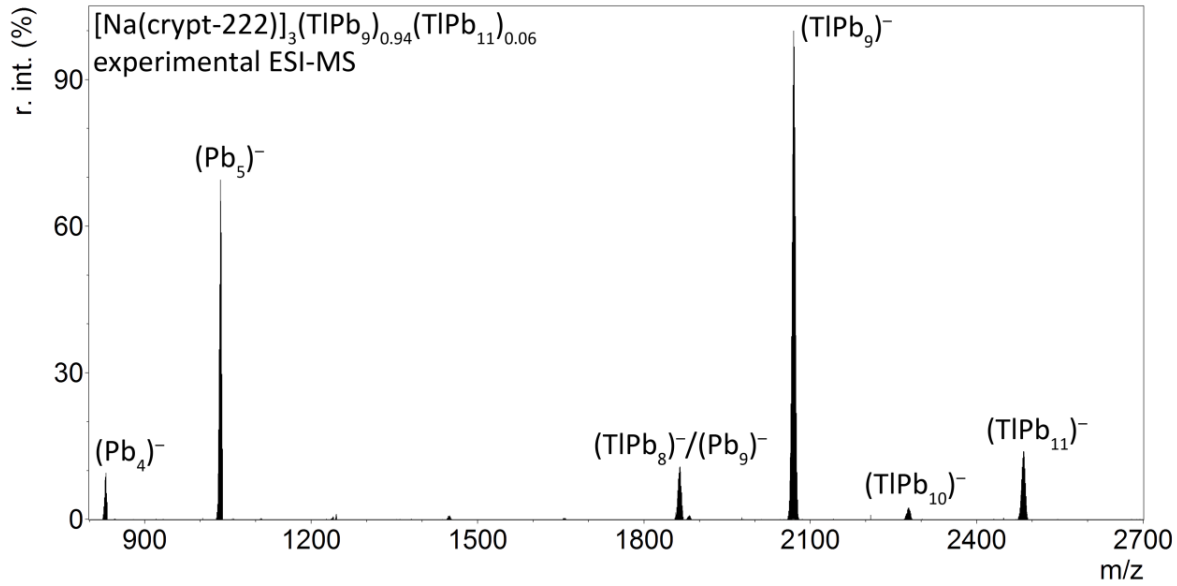

Figure S4. Overview of the ESI-MS of $[Na(crypt\text{-}222)]_3(TlPb_9)_{0.94}(TlPb_{11})_{0.06}$ (6) in DMF.

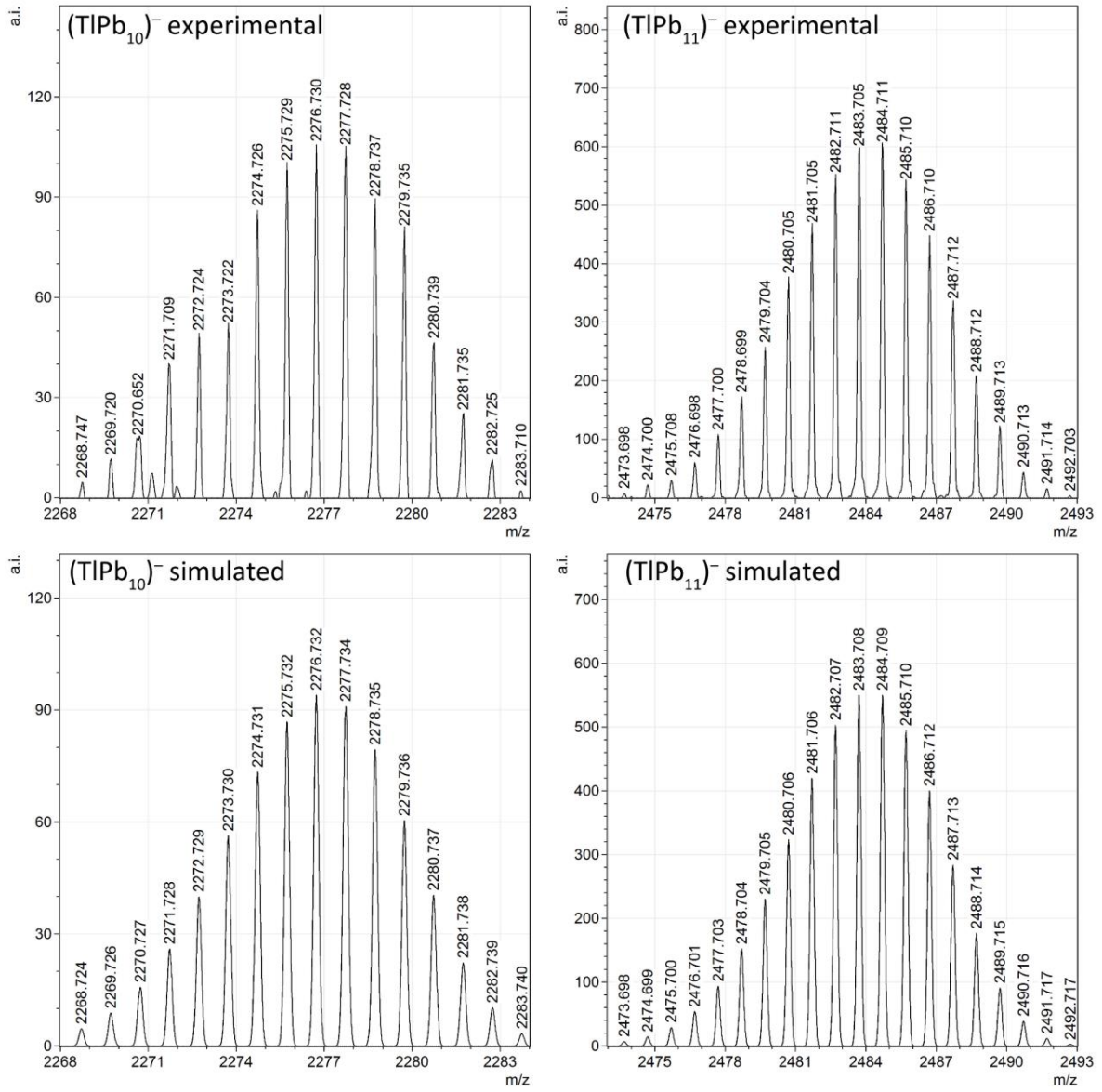

Figure S5. Comparison of experimental (top) and simulated (bottom) signals of $(TlPb_{10})^-$ (left) and $(TlPb_{11})^-$ (right) ions.

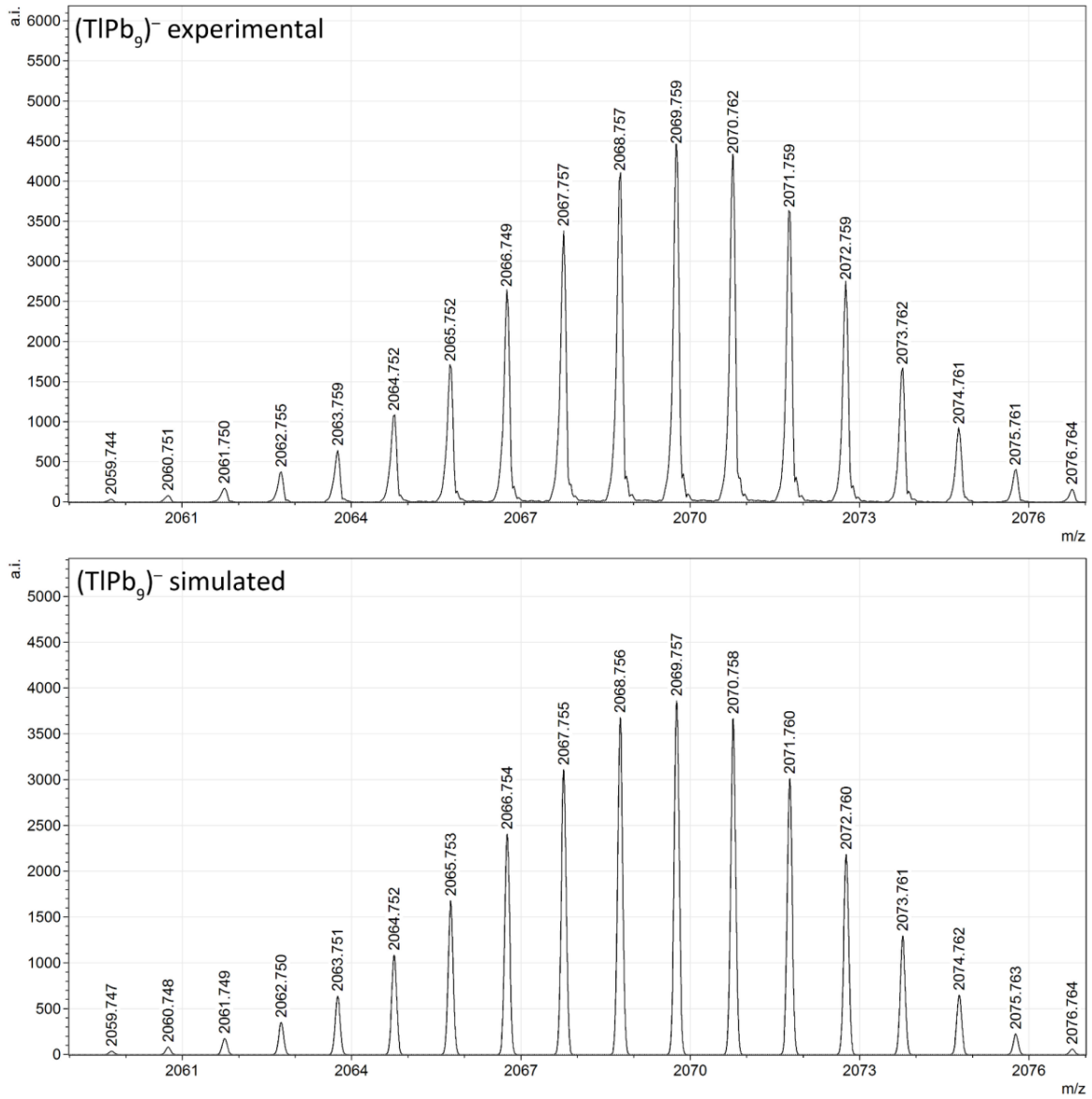

Figure S6. Comparison of experimental (top) and simulated (bottom) signals of $(TlPb_9)^-$ ions.

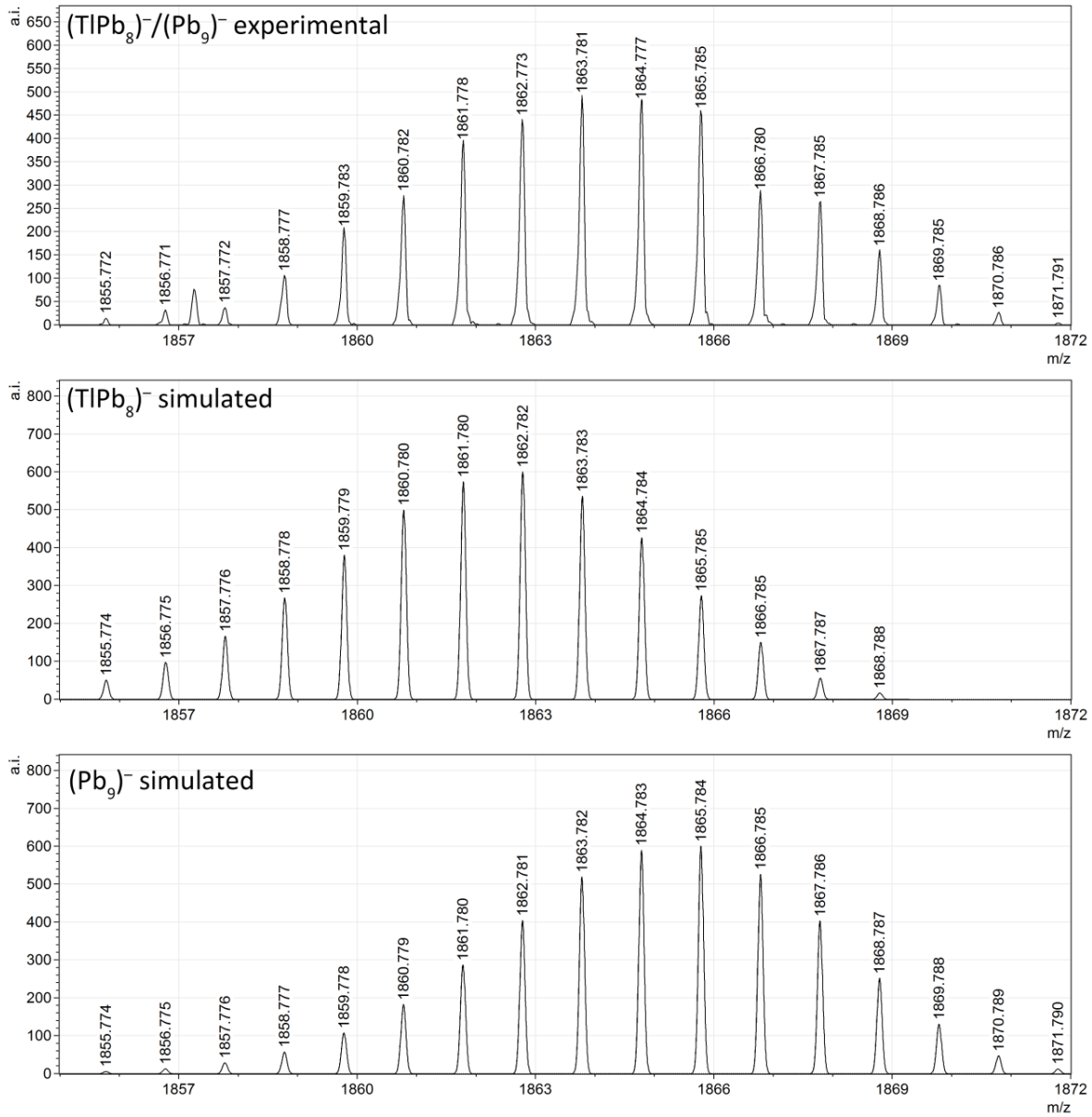

Figure S7. Comparison of experimental (top) and simulated (center, bottom) signals of $(TlPb_8)^-$ (center) and $(Pb_9)^-$ (bottom) ions.

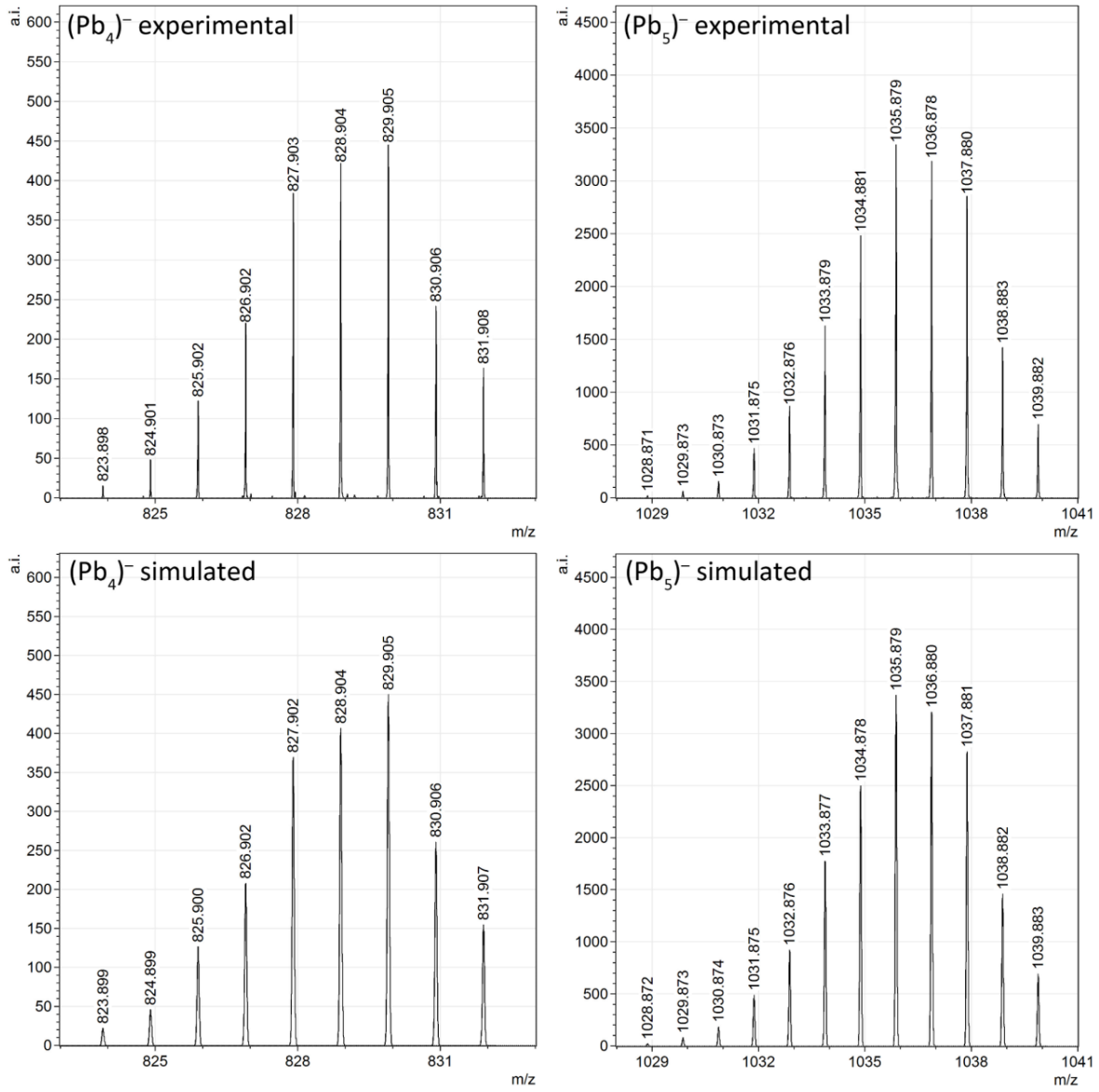

Figure S8. Comparison of experimental (top) and simulated (bottom) signals of $(Pb_4)^-$ (left) and $(Pb_5)^-$ (right) ions.

2.4. Mass Spectrometry of $[K(crypt\text{-}222)]_4[Tl@Tl_4Pb_8]_{0.5}(Tl_2Pb_{10})_{0.1}(Pb_9)_{0.4}$ (7)

Crystals of **7** were obtained from a saturated extraction solution of **7** in *en*. After prolonged crystallization times of several weeks the solution was removed with a syringe. The crystals were washed with 10 mL of dry toluene and then dried *in vacuo* for 30 minutes. Figure S9 provides an overview of the obtained mass spectrum. High resolution views of the individual signals are given in the figures S10 – S21 along with the corresponding simulations.

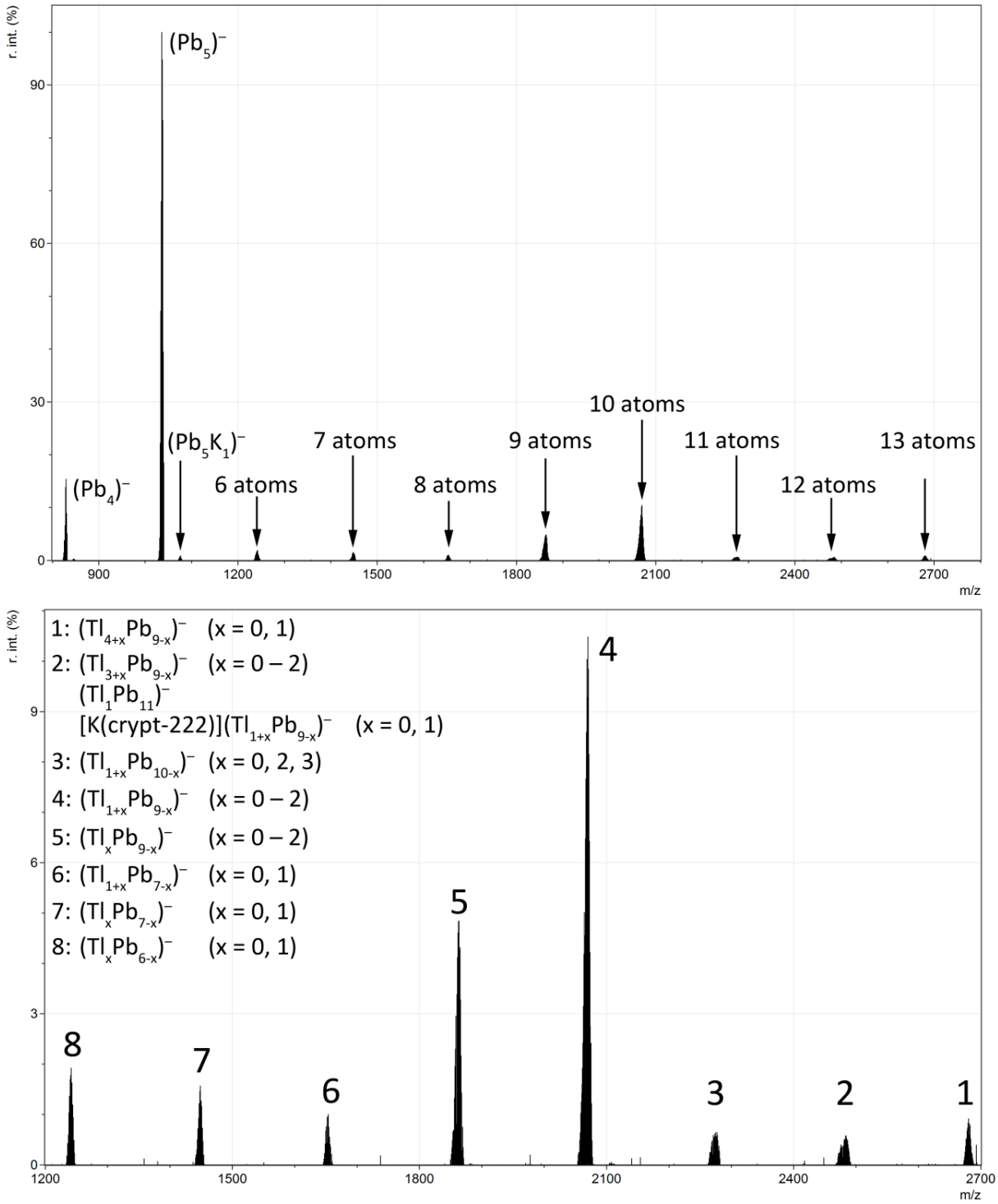

Figure S9. Full ESI-MS of $[K(crypt\text{-}222)]_4[Tl@Tl_4Pb_8]_{0.5}(Tl_2Pb_{10})_{0.1}(Pb_9)_{0.4}$ (7) in DMF (top) and a detailed view of m/z = 1200 – 2700 (bottom).

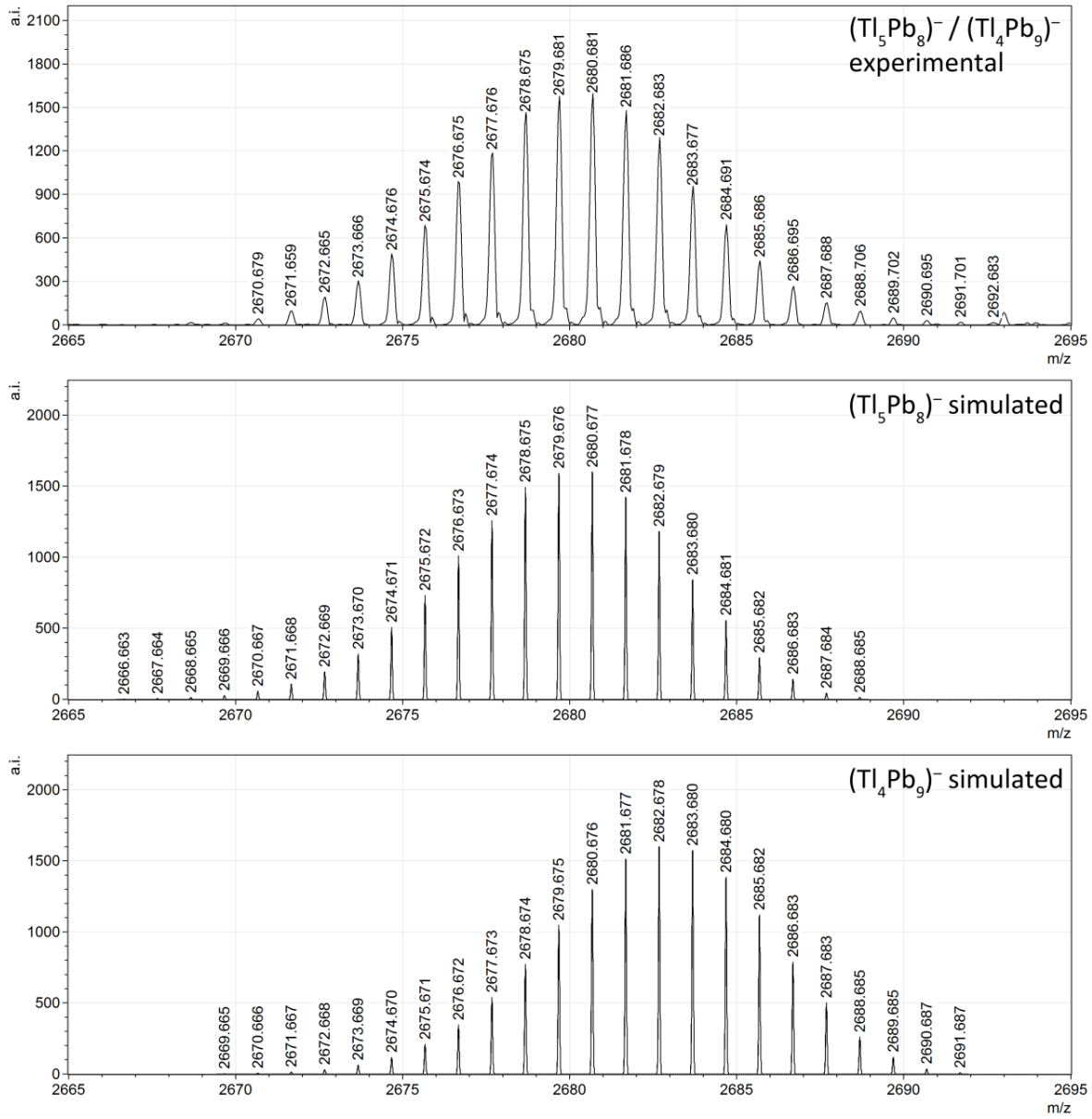

Figure S10. Comparison of experimental (top) and simulated (center, bottom) signals of $(Tl_5Pb_8)^-$ (center) and $(Tl_4Pb_9)^-$ (bottom) ions.

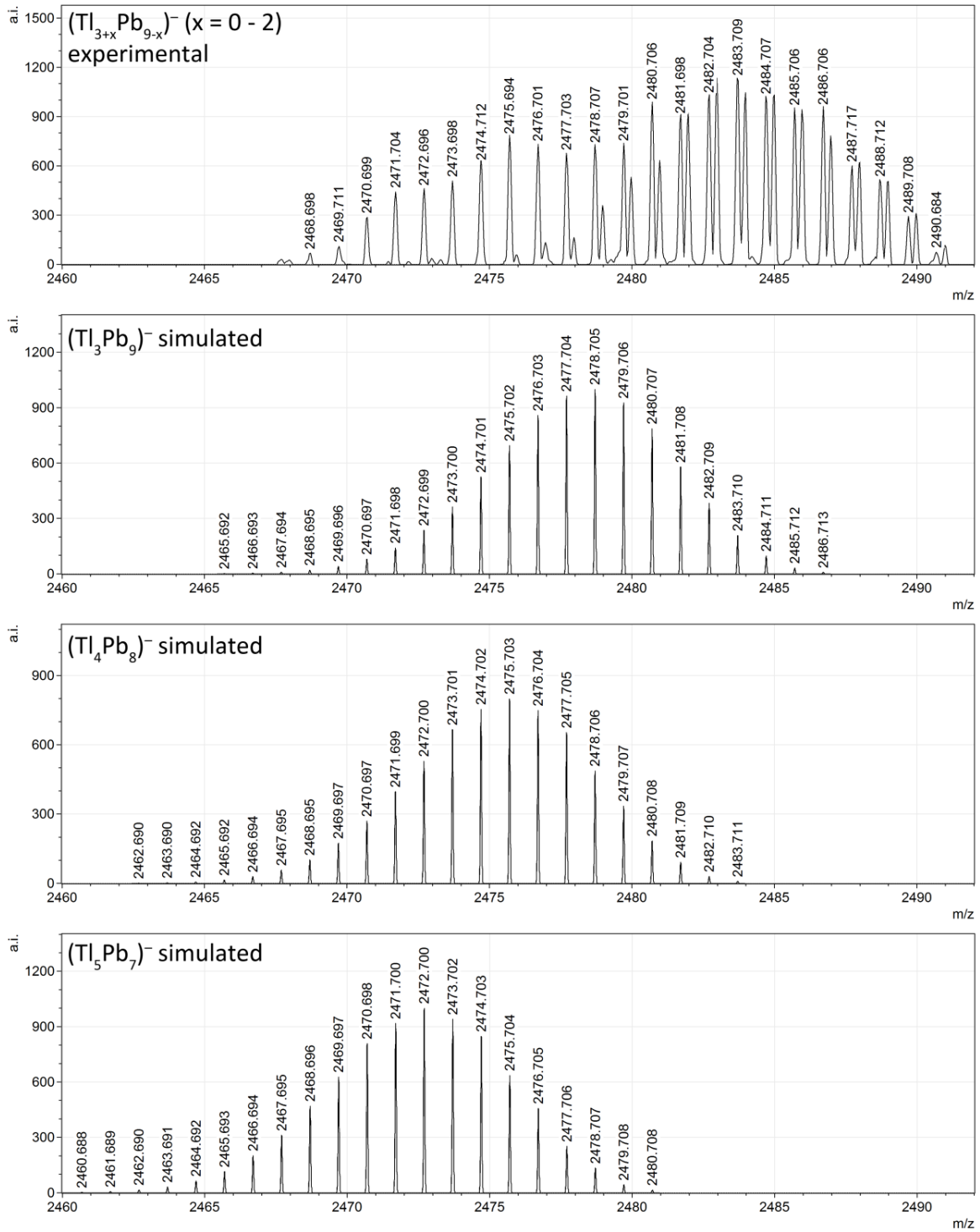

Figure S11. Comparison of experimental (top) and simulated (2nd – 4th) signals of $(Tl_3Pb_9)^-$ (2nd), $(Tl_4Pb_8)^-$ (3rd), and $(Tl_5Pb_7)^-$ (4th) ions.

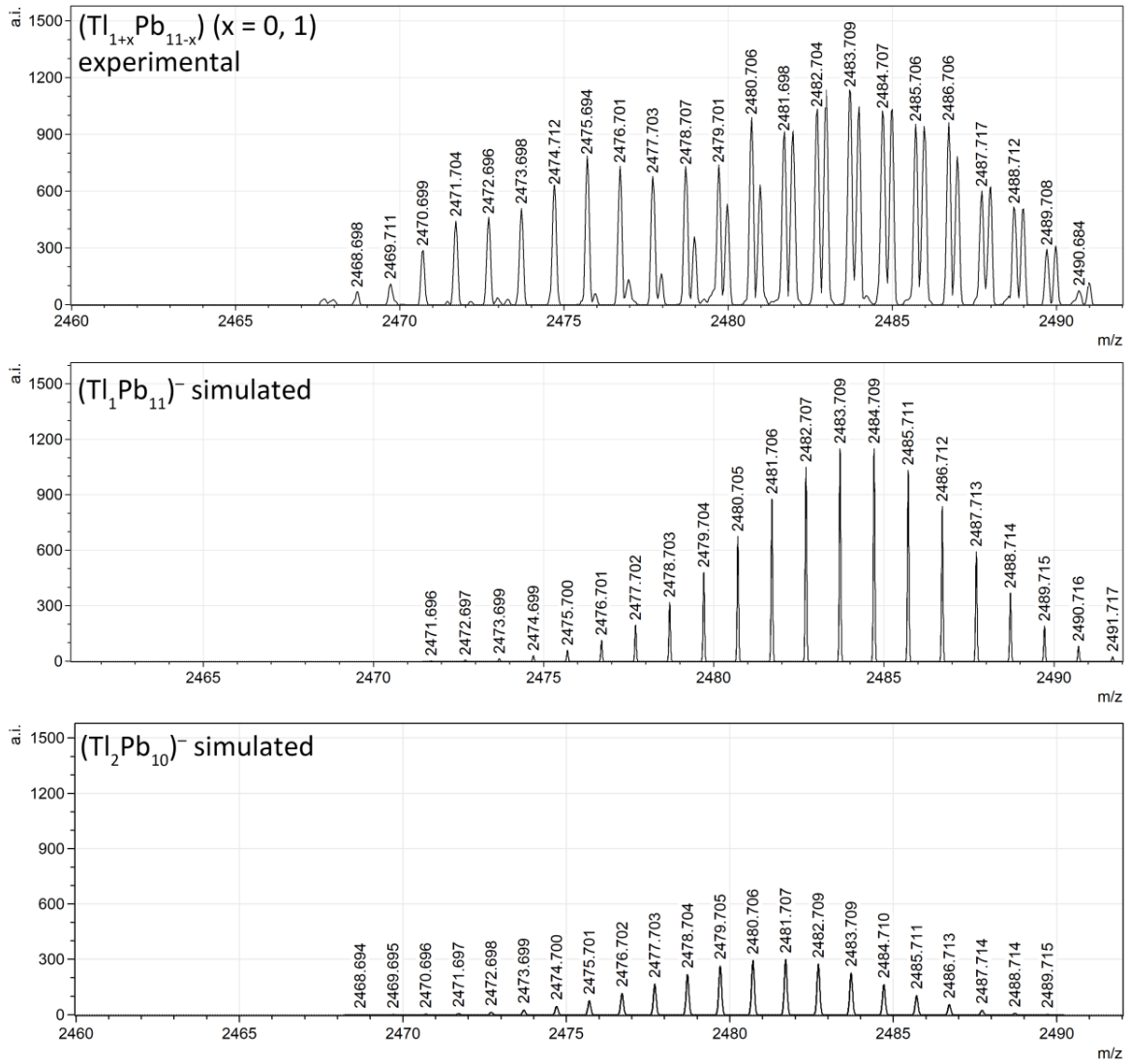

Figure S12. Comparison of experimental (top) and simulated (center, bottom) signals of $(Tl_1Pb_{11})^-$ (center) and $(Tl_2Pb_{10})^-$ (bottom) ions.

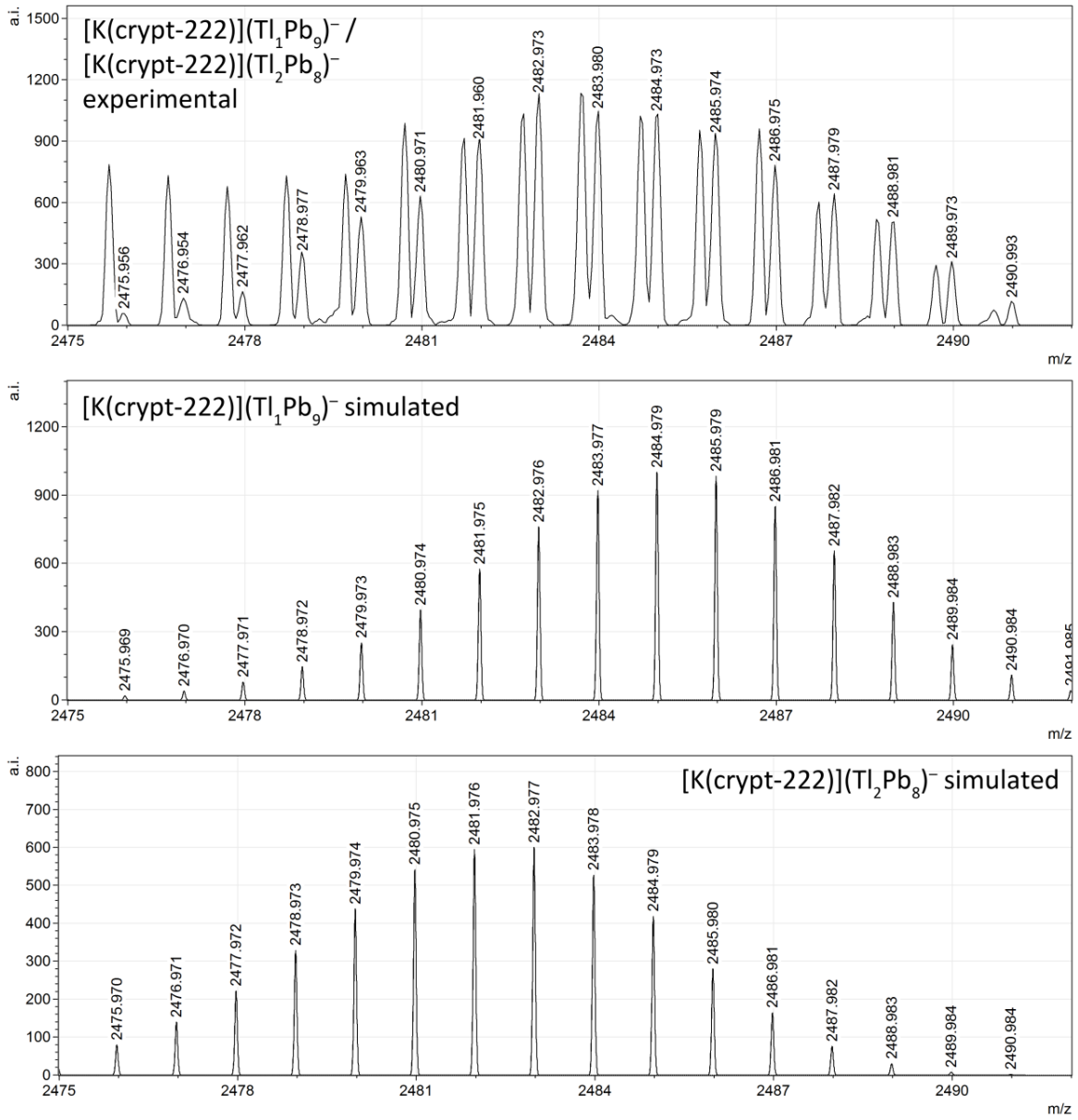

Figure S13. Comparison of experimental (top) and simulated (center, bottom) signals of [K(crypt-222)](TlPb$_9$)$^-$ (center) and [K(crypt-222)](Tl$_2$Pb$_8$)$^-$ (bottom) ions.

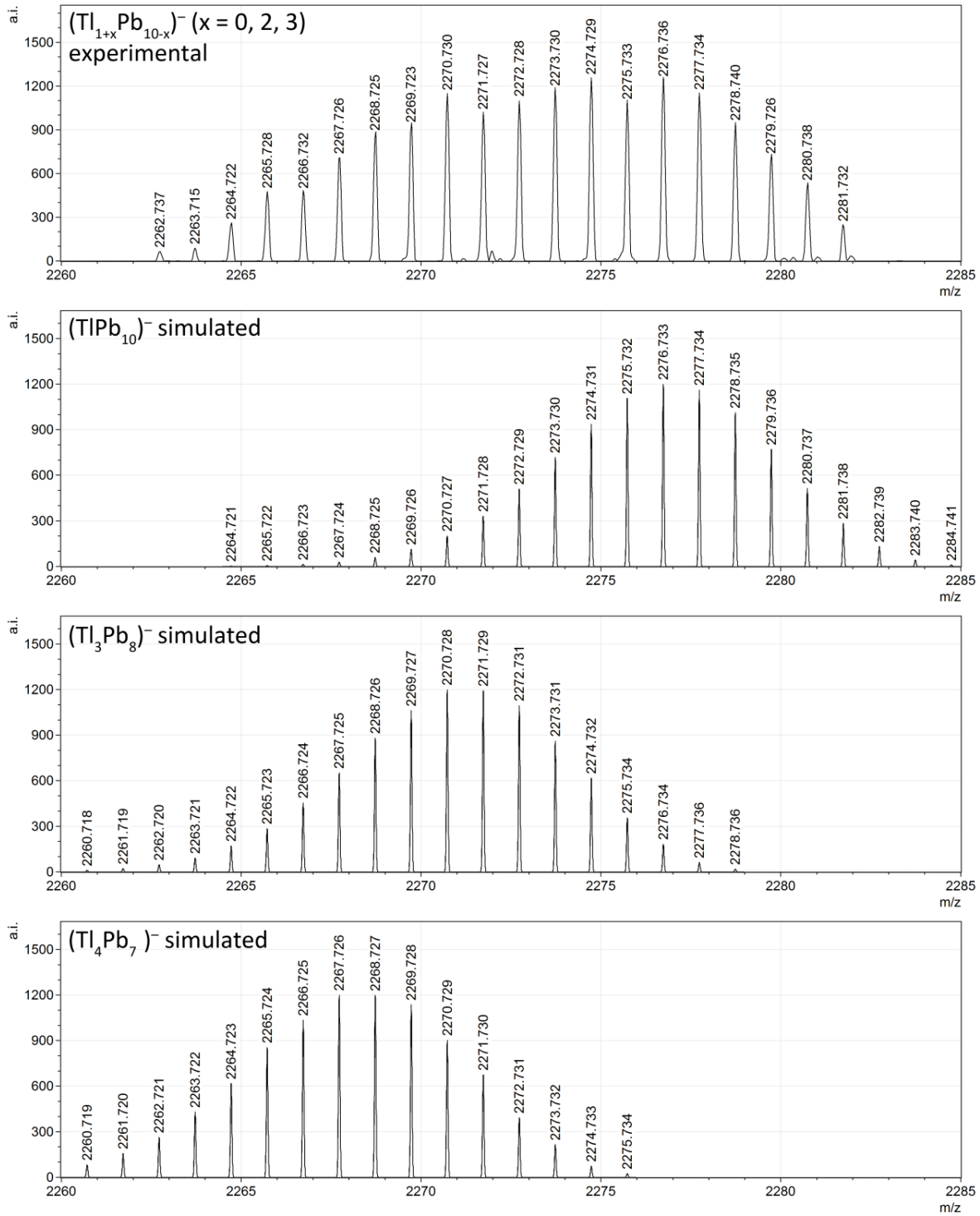

Figure S14. Comparison of experimental (top) and simulated (2^{nd} – 4^{th}) signals of $(TlPb_{10})^-$ (2^{nd}), $(Tl_3Pb_8)^-$ (3^{rd}) and $(Tl_4Pb_7)^-$ (4^{th}) ions.

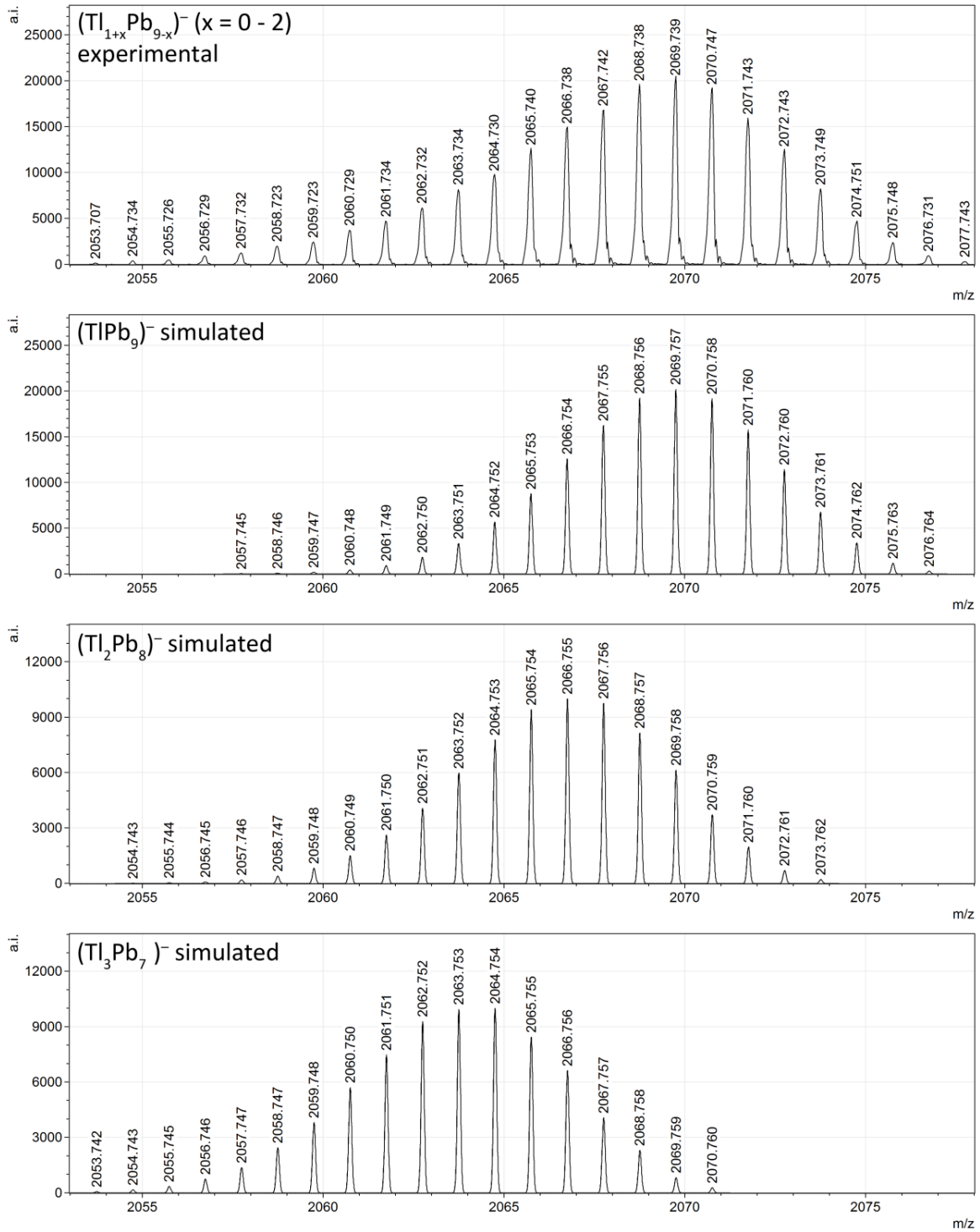

Figure S15. Comparison of experimental (top) and simulated (2nd – 4th) signals of $(TlPb_9)^-$ (2nd), $(Tl_2Pb_8)^-$ (3rd) and $(Tl_3Pb_7)^-$ (4th) ions.

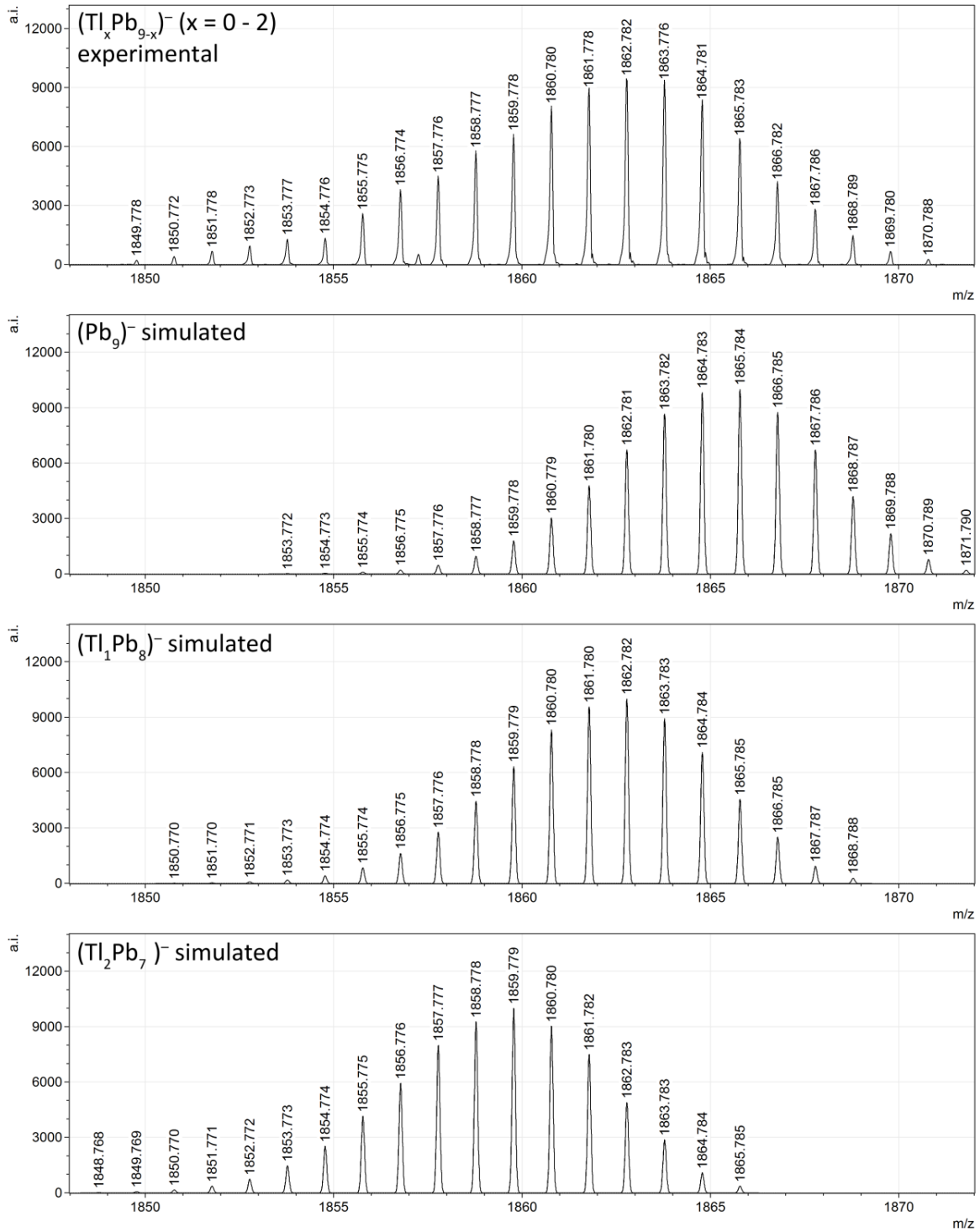

Figure S16. Comparison of experimental (top) and simulated (2^{nd} – 4^{th}) signals of $(Pb_9)^-$ (2^{nd}), $(Tl_1Pb_8)^-$ (3^{rd}) and $(Tl_2Pb_7)^-$ (4^{th}) ions.

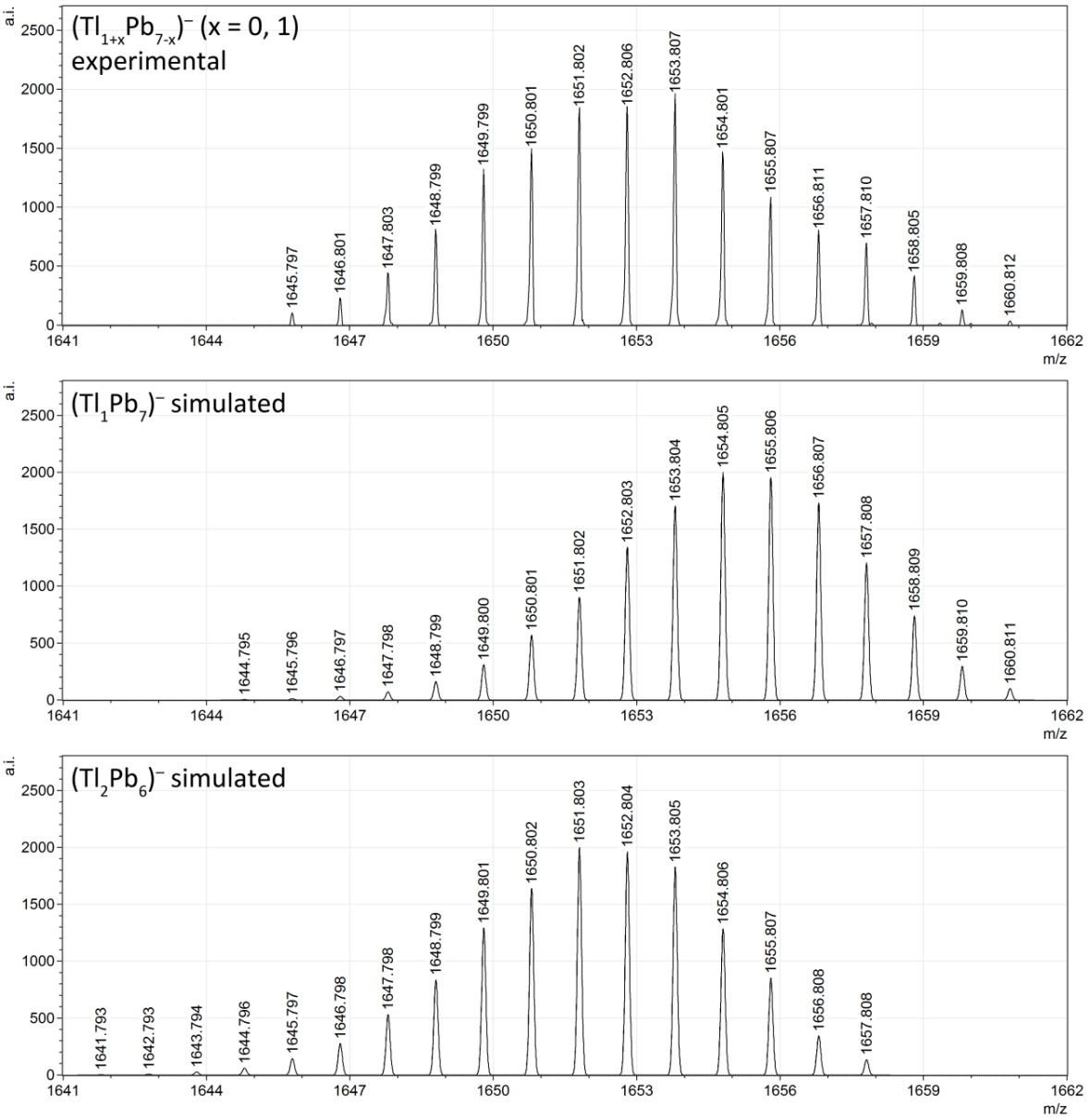

Figure S17. Comparison of experimental (top) and simulated (center, bottom) signals of $(TlPb_7)^-$ (center) and $(Tl_2Pb_6)^-$ (bottom) ions.

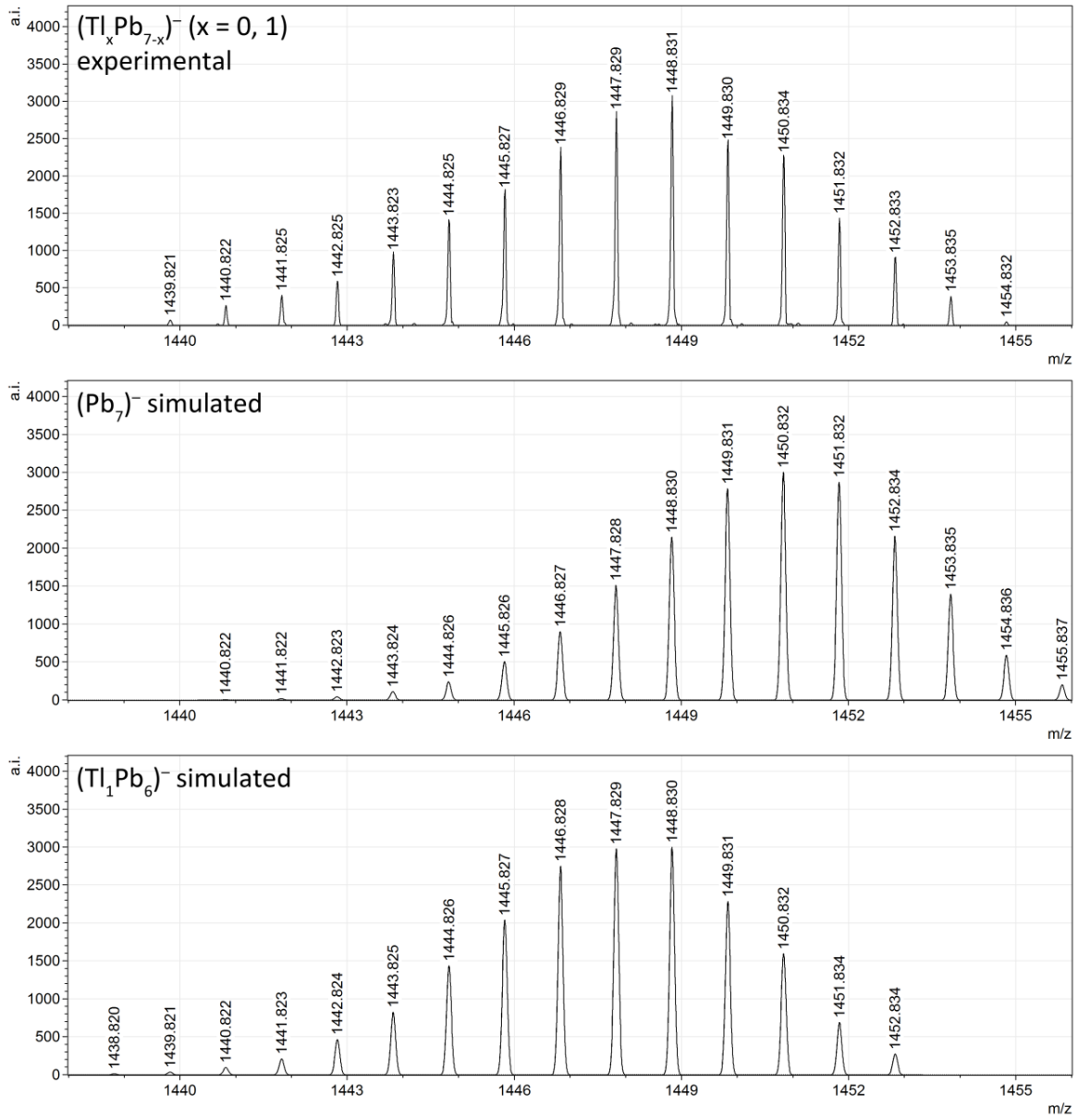

Figure S18. Comparison of experimental (top) and simulated (center, bottom) signals of $(Pb_7)^-$ (center) and $(Tl_1Pb_6)^-$ (bottom) ions.

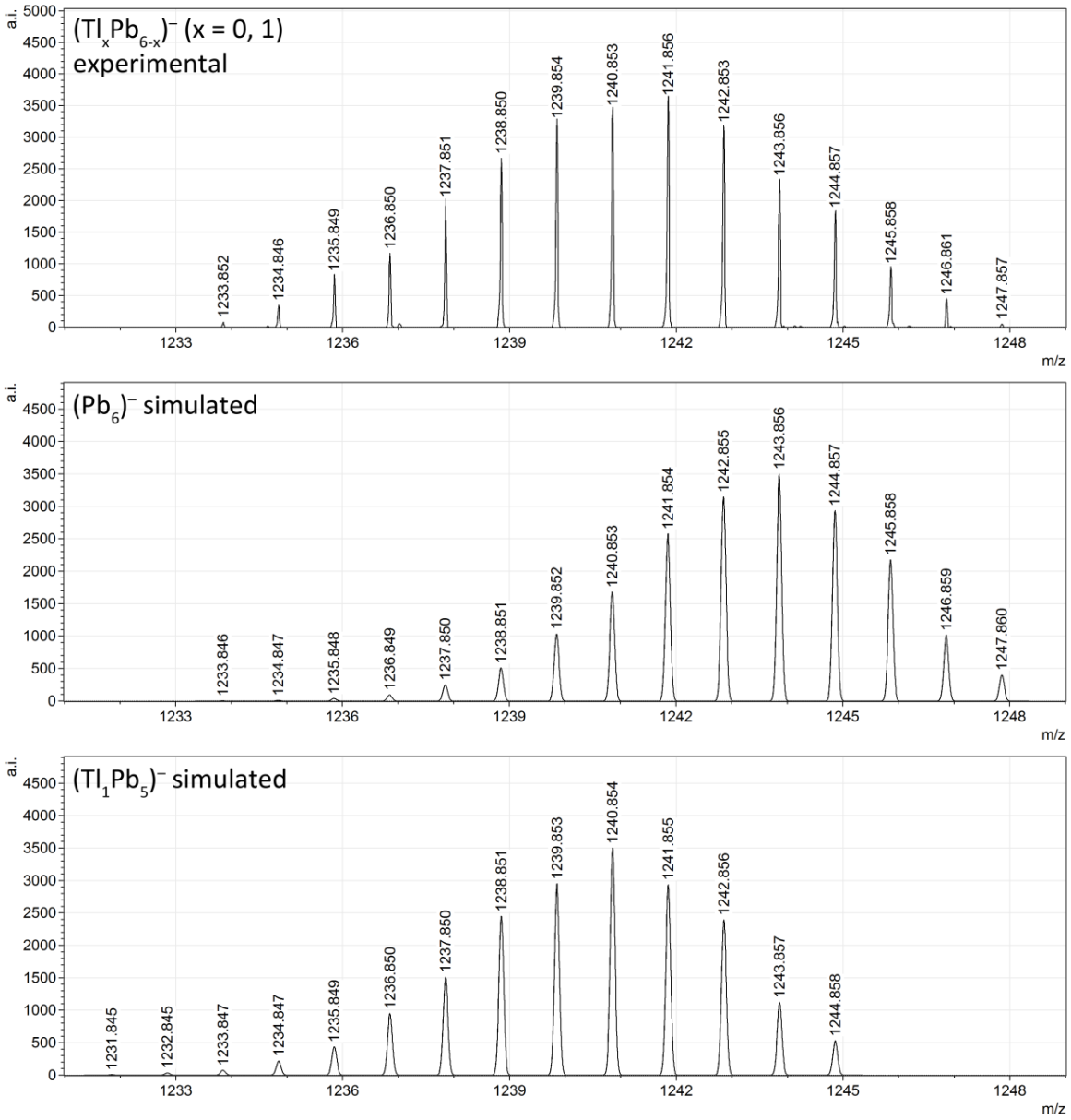

Figure S19. Comparison of experimental (top) and simulated (center, bottom) signals of $(Pb_6)^-$ (center) and $(TlPb_5)^-$ (bottom) ions.

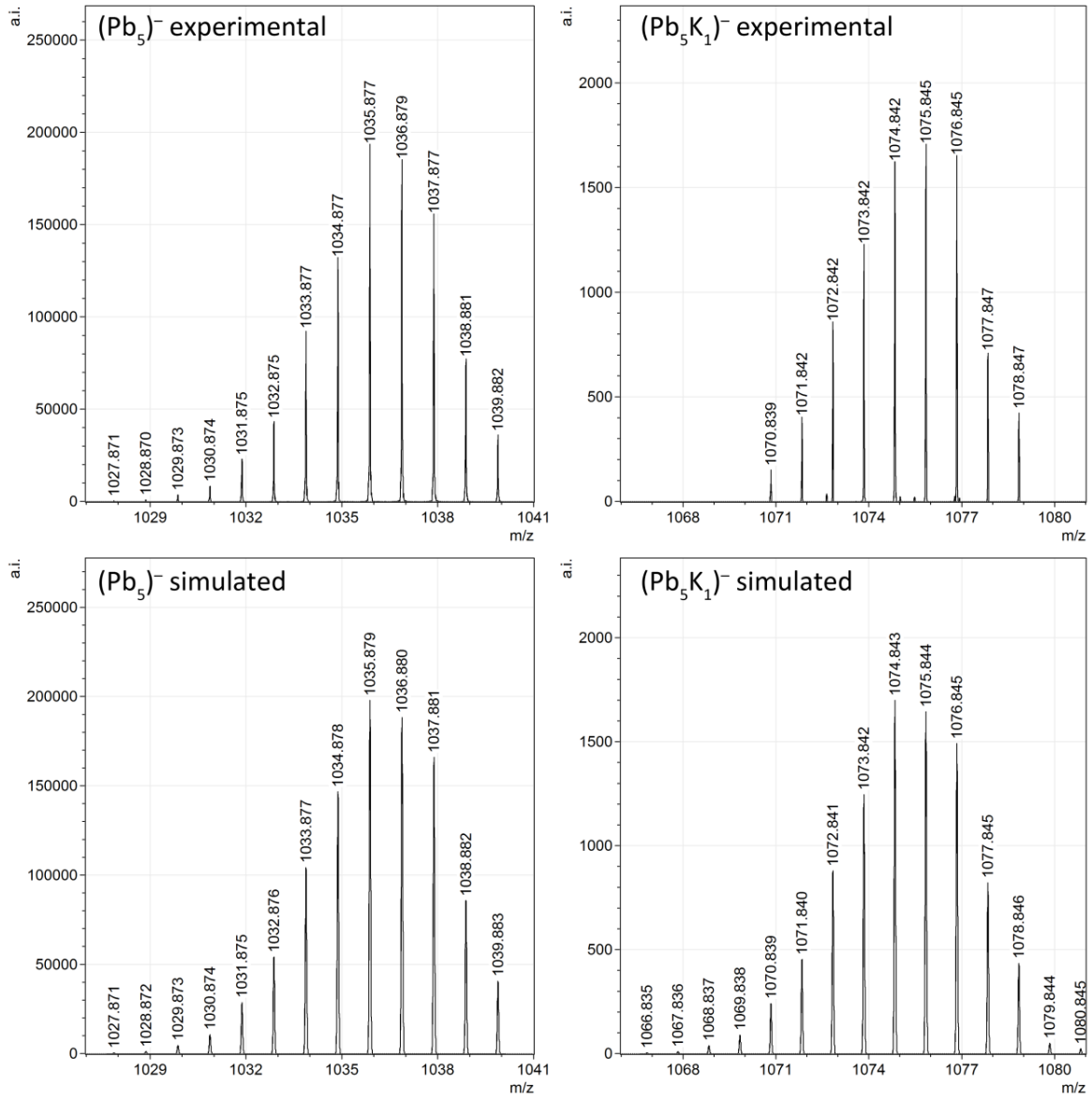

Figure S20. Comparison of experimental (top) and simulated (bottom) signals of $(Pb_5)^-$ (left) and $(Pb_5K)^-$ (right) ions.

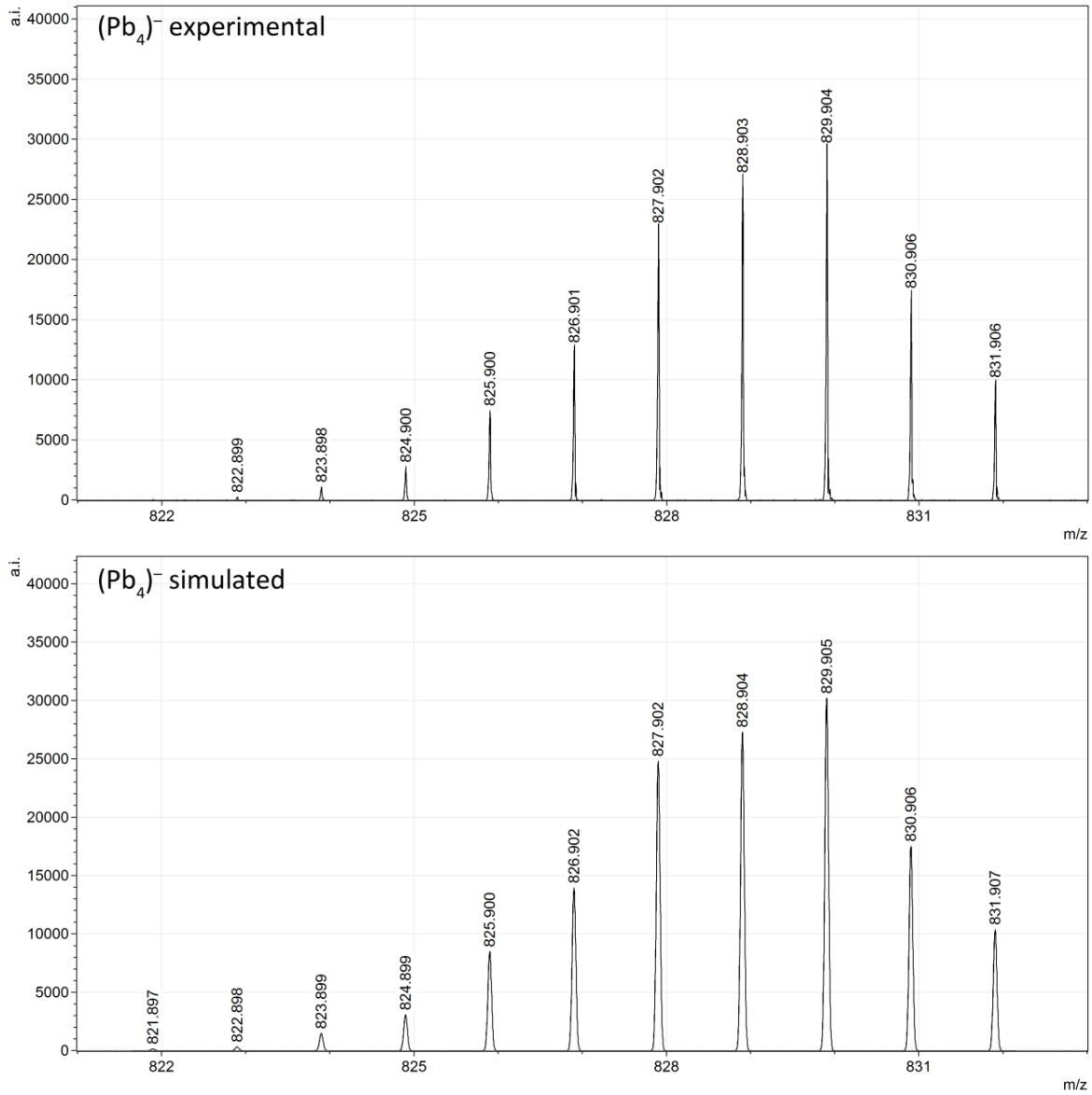

Figure S21. Comparison of experimental (top) and simulated (bottom) signals of $(Pb_4)^-$ ions.

2.5. Mass Spectrometry of $[K(crypt\text{-}222)]_3(Tl_4Bi_3)$ (8)

Crystals of **8** were obtained from a saturated solution in en. After prolonged crystallization times of several weeks the solution was removed with a syringe. The crystals were washed with 10 mL of dry toluene and then dried *in vacuo* for 30 minutes. Figure S22 provides an overview of the obtained mass spectrum and a comparison with the mass spectrum of $[K(crypt\text{-}222)]_3(Tl_4Bi_5)$.[4] High resolution views of the individual signals are given in the figures S23 – S25 along with the corresponding simulations. The presence of $(Tl_3Bi_6)^-/(Tl_4Bi_5)^-$ signals is most likely caused by decompostion reactions of $(Tl_4Bi_3)^{3-}$ ions in solution under ESI-MS conditions. That same decomposition reaction can be observed if samples of **8** are not sufficiently shielded from light or if trace amounts of air are present in the used vessels.

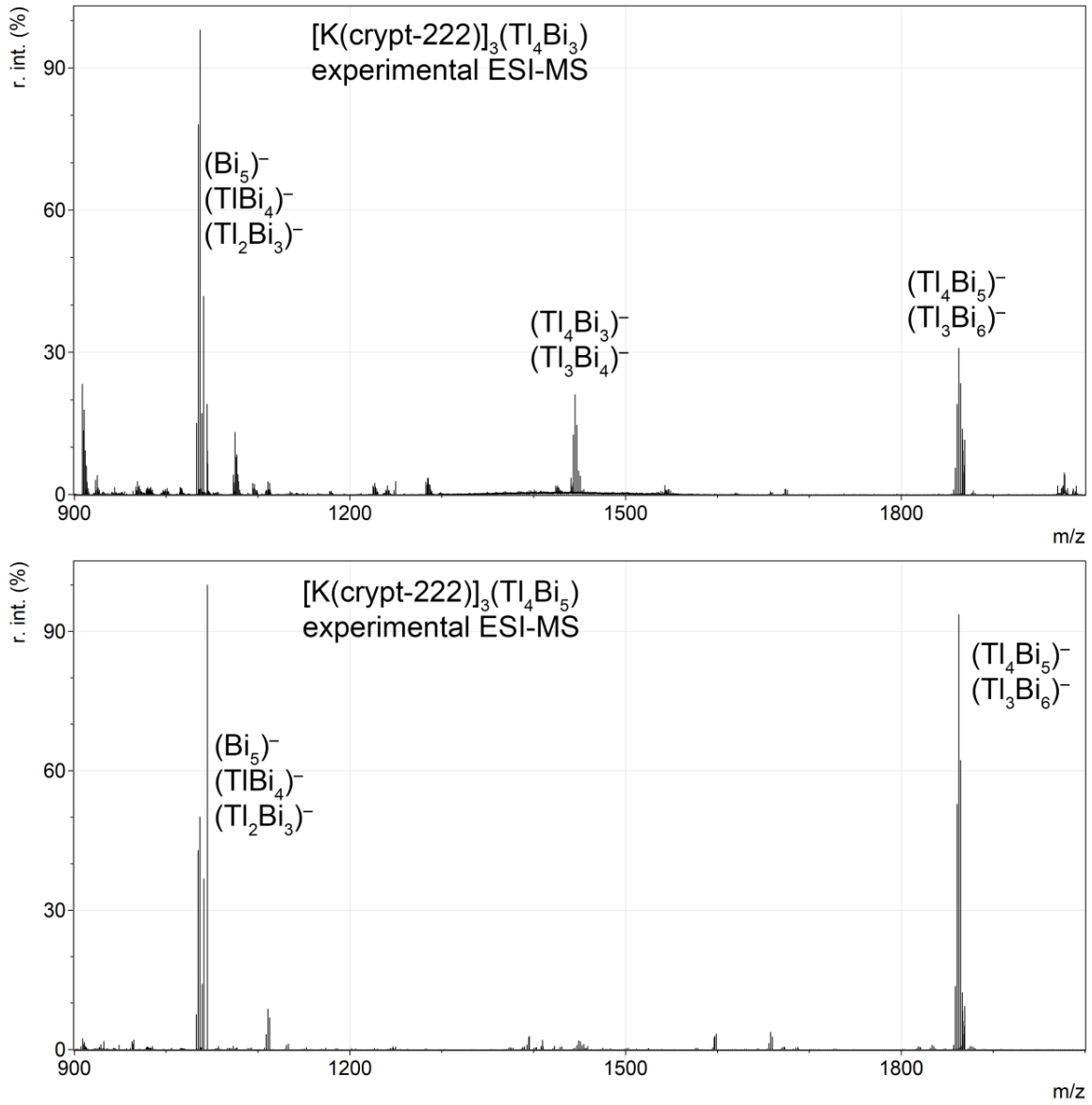

Figure S22. Comparison of the overviews of the ESI-MS of [K(crypt-222)]$_3$(Tl$_4$Bi$_3$) (8, top) and [K(crypt-222)]$_3$(Tl$_4$Bi$_5$) (bottom)[4] in DMF.

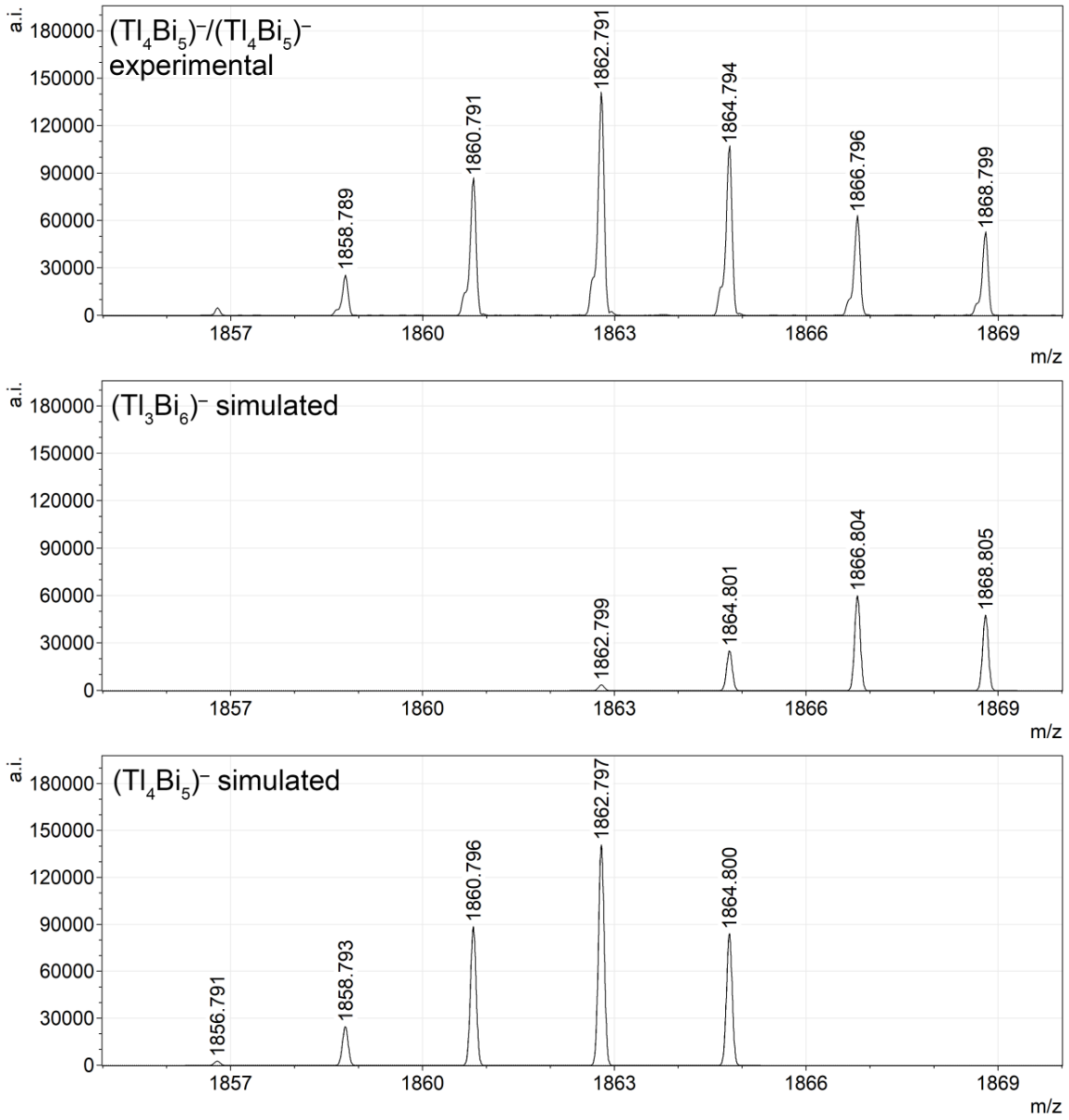

Figure S23. Comparison of experimental (top) and simulated (center, bottom) signals of $(Tl_3Bi_6)^-$ (center) and $(Tl_4Bi_5)^-$ (bottom) ions.

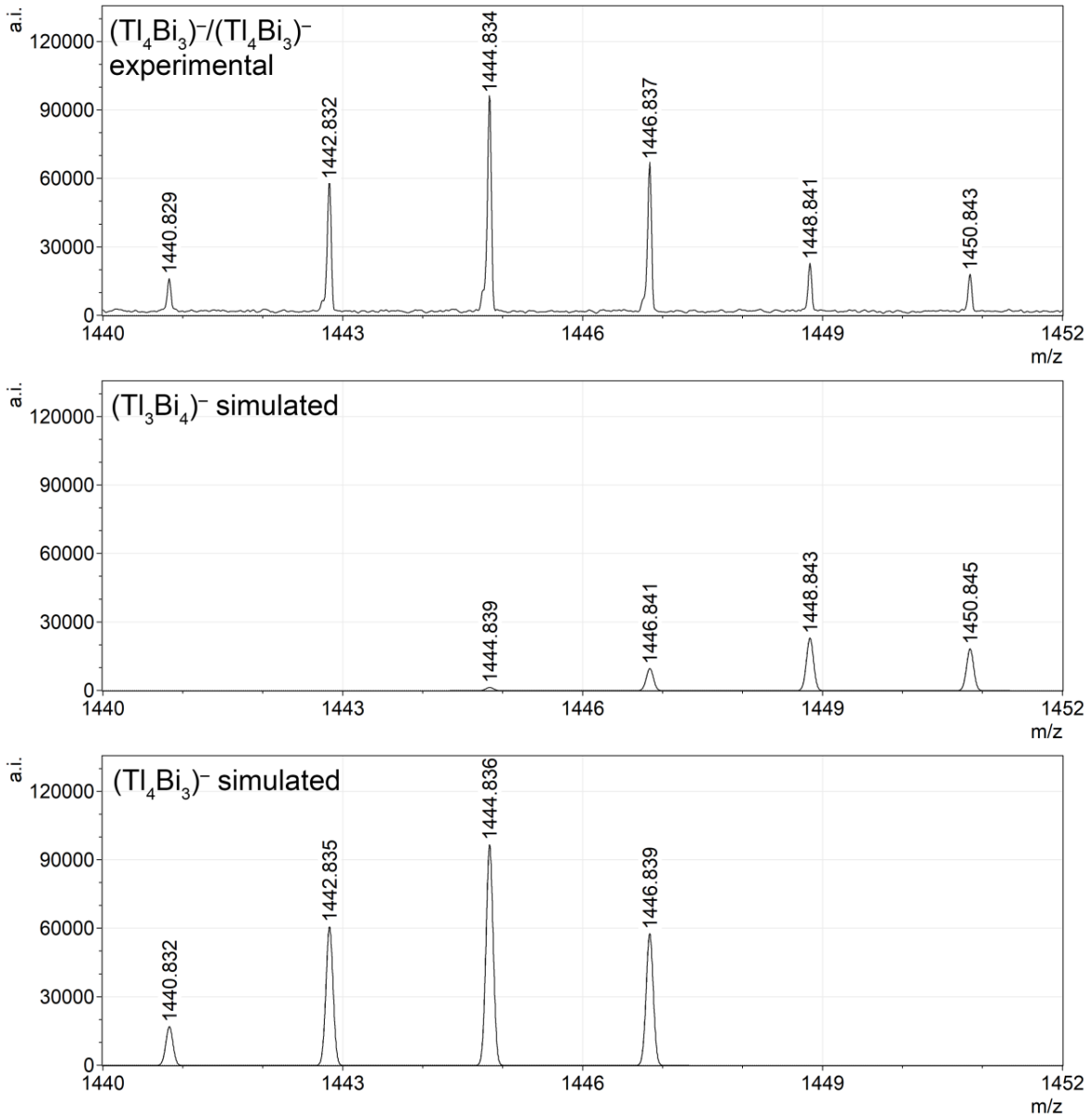

Figure S24. Comparison of experimental (top) and simulated (center, bottom) signals of $(Tl_3Bi_4)^-$ (center) and $(Tl_4Bi_3)^-$ (bottom) ions.

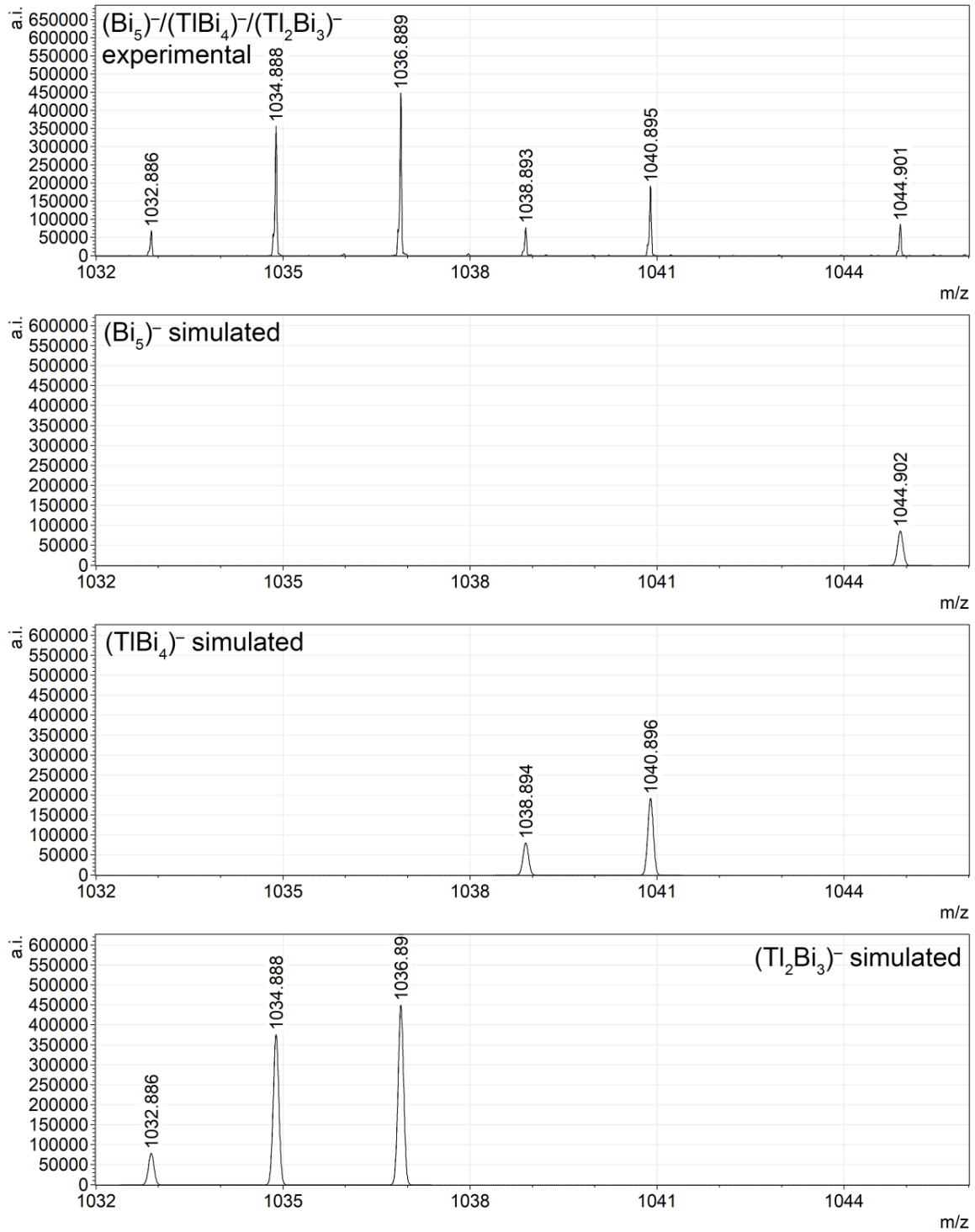

Figure S25. Comparison of experimental (top) and simulated (2^{nd} – 4^{th}) signals of $(Bi_5)^-$ (2^{nd}), $(Tl_1Bi_4)^-$ (3^{rd}) and $(Tl_2Bi_3)^-$ (4^{th}) ions.

3. Single Crystal X-ray Diffraction

3.1. General

The data for the X-ray structural analyses were collected at T = 100(2) K with Mo-K_α-radiation (λ = 0.71073 Å) on area detector systems Stoe IPDS2 for **1 – 3, 7, 8** and Stoe IPDS/2T for **4 – 6**. All structures were solved by intrinsic phasing (SHELXT-2015).[5] The refinement was done by full-matrix-least-squares methods against F^2 with the program SHELXL-2014.[6] All hydrogen atoms were kept riding on calculated positions with isotropic displacement parameters U = 1.2 U_{eq} (or 1.5 U_{eq} for methyl groups) of the bonding partners. The CIFs of the binary and ternary solids (compounds **2**, **3**, **4**, and **5**) were deposited at FIZ Karlsruhe (CSD-434528, -434529, -434520, and -434531) The CIFS of the complex salts (compounds **1**, **6**, **7**, and **8**) were deposited at the Cambridge Crystallographic Data Centre (CCDC 1841189, 1841188, 1841187 and 1841190). These data are provided free of charge upon request. The crystal data and experimental parameters of the structure determinations are collected in Tables S1 and S2. Figures were created with Diamond 4 and rendered with PovRay 3.7.[7]

The growth and collection of single crystals suitable for X-ray diffraction structure analysis is very challenging in the case of the discussed intermetallic phases. The Nb-tubes used for the synthesis were cut open in a glovebox and the usually very brittle phases were removed by careful squeezing with pliers. Typically, bigger blocks are obtained this way which need to be broken down by gentle hits with a pestle. The mixture obtained this way often contains some larger crystals that can be used for diffraction experiments. Several scoops were transferred into a mass vial and stored until needed. The crystals can be examined under inert oil and also picked this way. Usually, they show significant degrees of twinning and are of general poor quality.

Table S1. Crystal structure data and details of the structure determinations of the neat solids 2 – 5.

Compound	2	3	4	5
empirical formula	$Na_{17}Tl_5Pb_7$	K_2TlBi	$K_6Tl_2Bi_3$	KTlBi
formula weight [g mol^{-1}]	2863.01	491.55	1270.28	452.44
crystal color, shape	silver metallic, block	silver metallic, block	silver metallic, block	dark grey, block
crystal size [mm^3]	0.12 x 0.13 x 0.09	0.43 x 0.33 x 0.18	0.14 x 0.23 x 0.11	0.18 x 0.15 x 0.10
crystal system	cubic	orthorhombic	monoclinic	hexagonal
	I-centered	primitive	*C*-centered	primitive
space group (No.)	$I\bar{4}3m$ (217)	*Pbcm* (57)	*C*2/*c* (15)	$P6_3/mmc$ (194)
a [Å]	11.8116(5)	6.8048(5)	10.0799(7)	6.8037(3)
b [Å]		13.4464(9)	17.2809(7)	
c [Å]		6.5212(6)	20.002(1)	10.491(1)
β [°]			103.711(5)	
V [Å^3]	1647.9(2)	596.95(8)	3384.9(4)	420.59(5)
Z, ρ_{calc} [g cm^{-3}]	2, 5.770	4, 5.469	8, 4.985	4, 7.145
μ ($Mo_{K\alpha}$) [mm^{-1}]	60.17	57.65	51.50	80.792
absorption correction type	numerical	numerical	numerical	numerical
2θ range [°]	4.87 – 53.78	5.99 – 53.42	4.78 – 53.99	6.92 – 53.05
total reflns	743	5199	18922	3680
unique reflns [R_{int}]	598	688	3684	200
obs. Reflns [$I > 4\sigma(I)$]	332	607	2331	198
Parameters/restraints	17/0	24/0	101/0	10/0
wR_2 (all data)/	0.2208/	0.1957/	0.1594/	0.0914/
R_1 [$I > 4\sigma(I)$]	0.0879	0.0755	0.0859	0.0527
GooF (all data)	1.097	1.158	0.985	1.303
Flack value	-0.1(5)	-	-	-
max peak/hole [e Å^{-3}]	4.5/-3.42	4.91/-2.53	4.26/-2.55	6.31/-2.09
Depository number	CSD-434528	CSD-434529	CSD-434530	CSD-434531

Table S2. Crystal structure data and details of the structure determinations of the complex salts 1, 6 – 8.

Compound	**1**	**6**	**7**	**8**
empirical formula	$C_{56.9}H_{117}N_{7.1}O_{18.33}Sn_{9.21}Tl_{0.6}$	$C_{57.69}H_{115.38}N_6O_{18.92}Na_3Pb_{9.12}Tl$	$C_{74.48}H_{147.92}N_{10.48}O_{24}K_4Pb_{8.24}Tl_{2.77}$	$C_{54}H_{108}N_6O_{18}Bi_3K_3Tl_4$
formula weight [g mol^{-1}]	2478.13	3358.37	4004.17	2691.18
crystal color, shape	dark red, irregular block	black metallic, block	black metallic, hexagonal plate	black metallic, block
crystal size [mm^3]	0.30 x 0.27 x 0.15	0.21 x 0.24 x 0.22	0.16 x 0.09 x 0.04	0.23 x 0.22 x 0.22
crystal system	monoclinic primitive	monoclinic primitive	triclinic	monoclinic primitive
space group	$P2_1/n$ (14)	$P2_1/c$ (14)	$P\bar{1}$ (2)	$P2_1/n$ (14)
a [Å]	18.9468(5)	14.3233(3)	14.4510(6)	21.2179(5)
b [Å]	20.9559(4)	21.8968(5)	15.3339(6)	33.375(1)
c [Å]	20.9110(6)	28.7725(6)	16.2360(8)	24.2254(6)
α [°]			62.643(3)	
β [°]	93.061(2)	102.798(2)	63.944(3)	90.216(2)
γ [°]			86.421(3)	
V [Å^3]	8290.8(4)	8799.9(3)	2826.4(2)	17155.2(8)
Z, ρ_{calc} [g cm^{-3}]	4, 1.985	4, 2.535	1, 2.352	8, 2.084
μ ($Mo_{K\alpha}$) [mm^{-1}]	3.958	19.27	16.38	13.819
absorption correction type	numerical	numerical	numerical	numerical
2θ range [°]	2.75 – 50.00	2.90 – 54.98	4.76 – 50.48	4.02 – 50.48
total reflns	59001	35386	35930	157591
unique reflns [R_{int}]	14492	20117	9973	30191
obs. Reflns [$I > 4\sigma(I)$]	11268	13760	6395	14573
Parameters/restraints	902/29	926/0	661/59	1125/1297
wR_2 (all data)/ R_1 [$I > 4\sigma(I)$]	0.1950/0.0719	0.1261/0.0505	0.1178/0.0513	0.3109/0.1145
GooF (all data)	1.050	1.054	1.056	1.404
max peak/hole [e Å^{-3}]	2.48/-1.52	2.595/-2.076	2.11/-1.06	2.82/-8.19
Depository number	CCDC 1841189	CCDC 1841188	CCDC 1841187	CCDC 1841190

3.2. Details of the Structure Determinations

3.2.1. Structure Determination of $Na_{17}Tl_5Pb_7$ (2)

The structure of **2** could be solved using intrinsic phasing in the space group $I\bar{4}3m$ (No. 217). Due to the large difference in electron numbers of Na and Pb the atom assignment was evident. The further structure refinement proceeded without problems. As only one symmetry-independent Tl/Pb-position is present equal coordinates and atomic displacement parameters were introduced for the Tl and Pb atoms and their ratio was fixed to 5:7. Owing to the very high absorption coefficient of 60.17 mm^{-1}, refinement of the Na atoms with anisotropic displacement parameters was only possible after a careful numerical absorption correction.

3.2.1.1 Structure description of $Na_{17}Tl_5Pb_7$

The cluster anion $Na_4[Na@Tl_5Pb_7]^{12-}$ forms a Frank-Kasper polyhedron that is depicted in figure S26. These anions are embedded in the cavities of a Na+-network built up from the Na3 atoms (see figure S28) and packed in a cubic I-centered arrangement (see figure S29). The Na3-cations form a network of corner-sharing tetrahedra (figure S28) with their center of gravity located on a special position (¼, ½, 0, 12*d*). This creates a cubeoctahedral arrangement of these centroids (figures S28, and S29), well known as β-cages in zeolites. The structure of **3** can be seen as a closely packed (*c*I) arrangement of these β-cages of which each one contains one cluster in its cavity. Interatomic distances are provided in table S3.

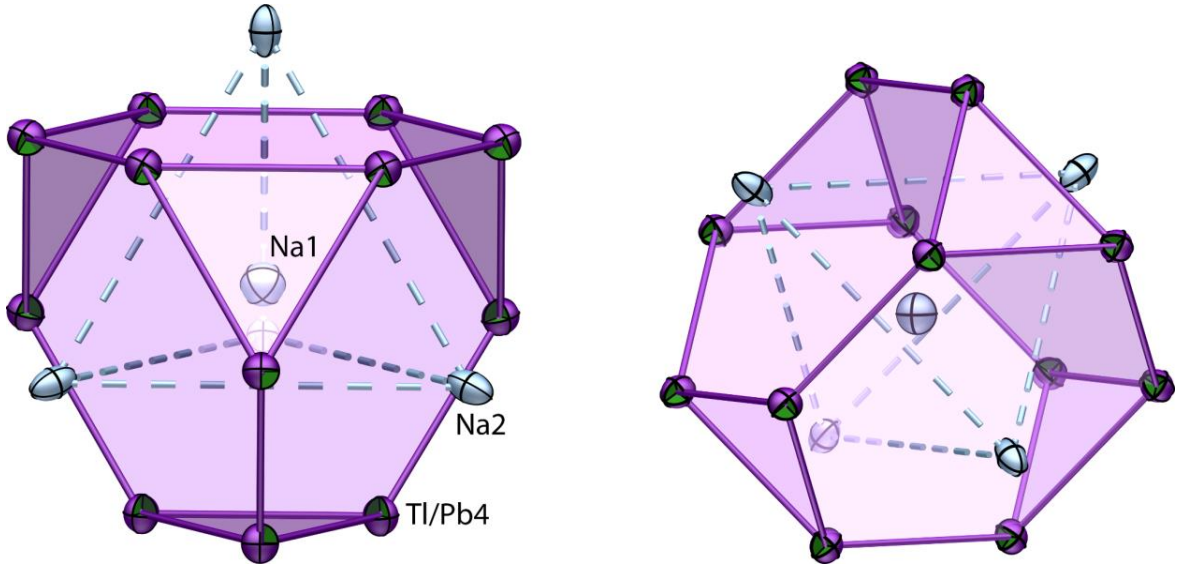

Figure S26. Two orientations of the anionic cluster $Na_4[Na@Tl_5Pb_7]^{12-}$ adapting the shape of a Frank-Kasper polyhedron in 2. Displacement ellipsoids are drawn at 50% probability. Interatomic distances are provided in Table S3.

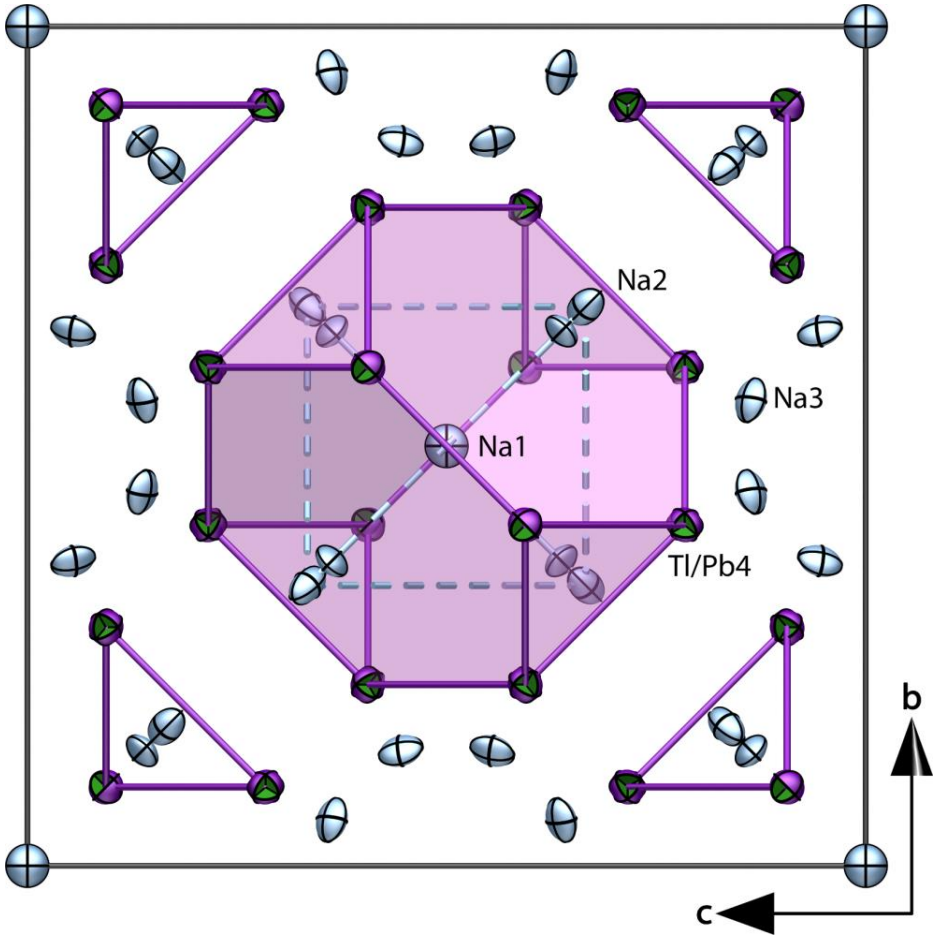

Figure S27. Arrangement of the atoms in the unit cell of 2. Displacement ellipsoids are drawn at 50% probability level.

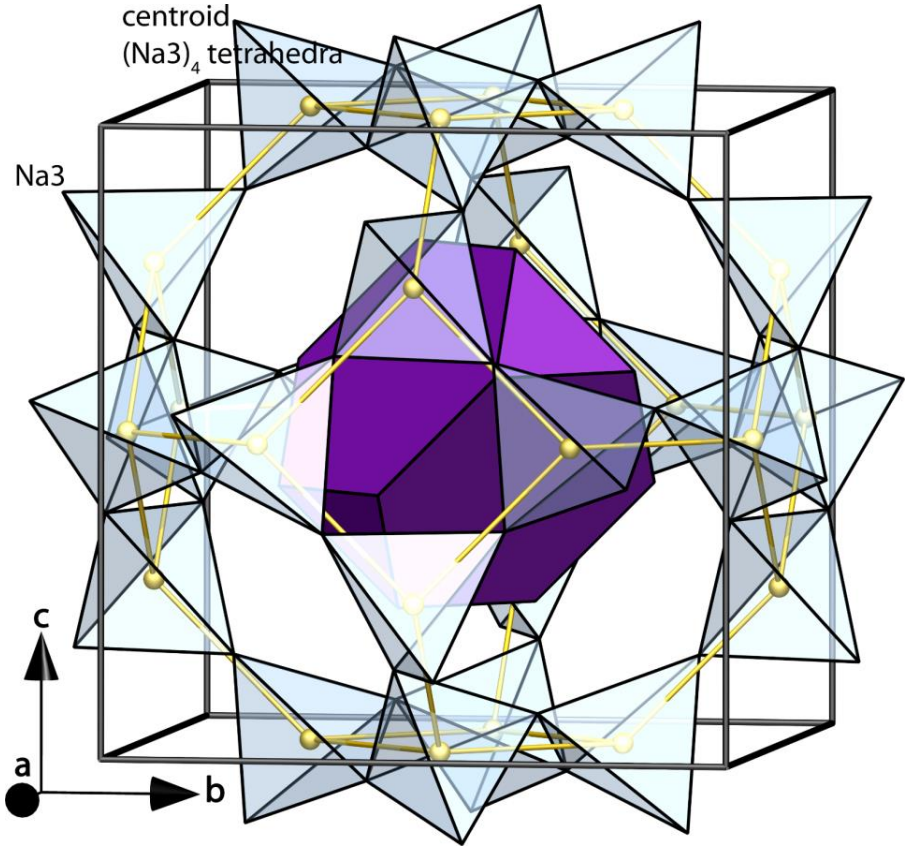

Figure S28. Network of Na3-atoms in 2 with one Na3-atom at each corner of the tetrahedra. The tetrahedra are highlighted in shaded blue. Centroids are drawn in orange. All other Na atoms are omitted for clarity and the $Na_4[Na@Tl_5Pb_7]^{12-}$ is shown in purple.

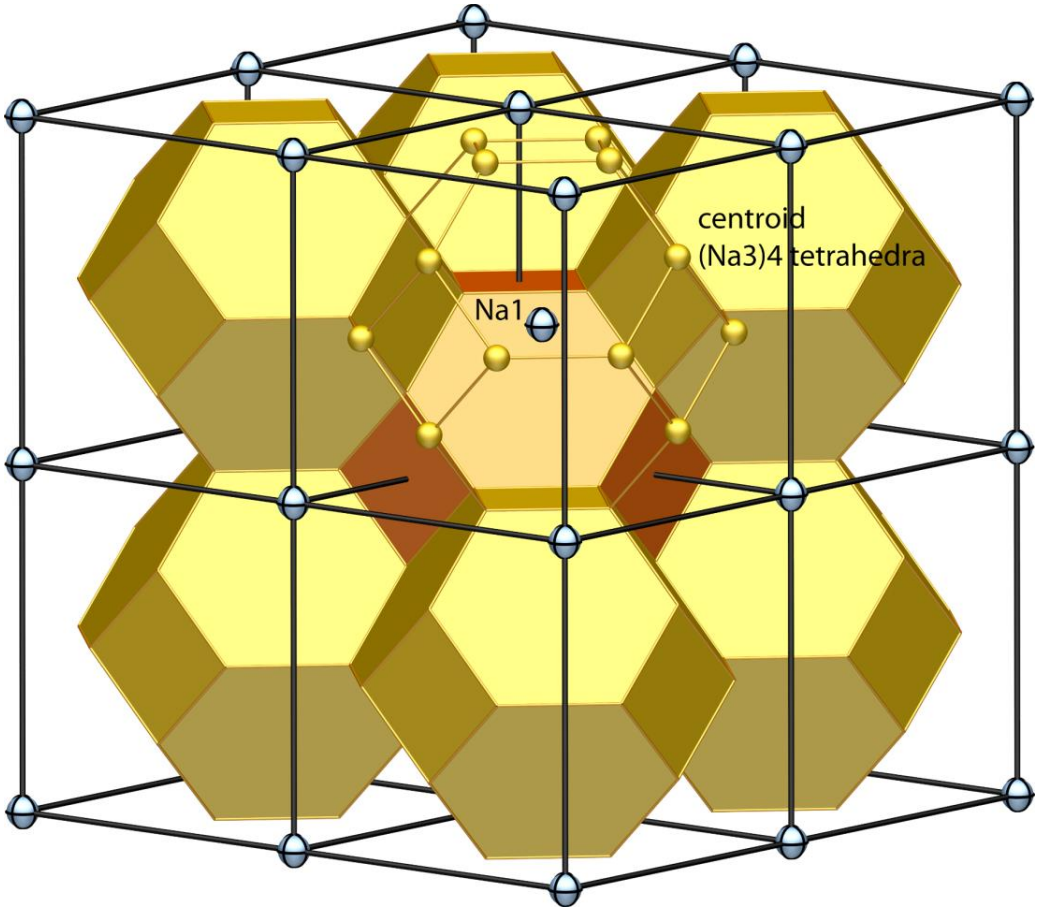

Figure S29. 2x2x2 Supercell of 2 with only the Na1-positions and the centroids of the (Na3)4-tetrahedra centroids forming *β*-cages (solid yellow and orange cuboctahedra). The cubic I-centered arrangement of these cages is highlighted (orange).

Table S3. Bond lengths and interatomic distances in 2.

Atoms	Distance / Å	Atoms	Distance / Å	Atoms	Distance / Å
Tl/Pb-Tl/Pb (triangle)	3.1788(1)	Na1-Tl/Pb	3.7040(1)	Na1-Na2	3.3966(1)
Tl/Pb-Tl/Pb (hexagon)	3.1348(1)	Na2-Tl/Pb	3.4776(1)	Na2-Na2	5.5466(2)
				Na3-Na3	3.4812(1)
					3.6331(1)
				Cent.-cent.	4.1760(1)

3.2.1.2 Structural Relationship between $Na_{17}Tl_5Pb_7$ and α-Mn

The structure of **2** is highly related to that of α-Mn and can be derived by substitution of elements. In the following table atomic positions and general structure information of both structures are provided. See figure S30 for a direct comparison of both structures. In both unit cells, the atom positions are given the same color code.

Table S4. Comparison of atomic positions in α-Mn and $Na_{17}Tl_5Pb_7$.

α-Mn (*c*I58), $I\bar{4}3m$ (a = 8.905 V = 706.2)

Atom name	Atom type	Wyckoff symbol	Site multiplicity	x	y	z	occ.
Mn4	Mn	g	24	0.09081	0.09081	0.28276	1
Mn3	Mn	g	24	0.35776	0.35776	0.03543	1
Mn2	Mn	c	8	0.31836	0.31836	0.31836	1
Mn1	Mn	a	2	0	0	0	1

$Na_{17}Tl_5Pb_7$ (*c*I58), $I\bar{4}3m$ (a = 11.8116(5) V = 1647.8(1))

Atom name	Atom type	Wyckoff symbol	Site multiplicity	x	y	z	occ.
Tl/Pb4	Tl/Pb	g	24	0.09391(14)	0.09391(14)	0.2842(2)	1
Na3	Na	g	24	0.3616(14)	0.3616(14)	0.056(3)	1
Na2	Na	c	8	0.333(4)	0.333(4)	0.333(4)	1
Na1	Na	a	2	0	0	0	1

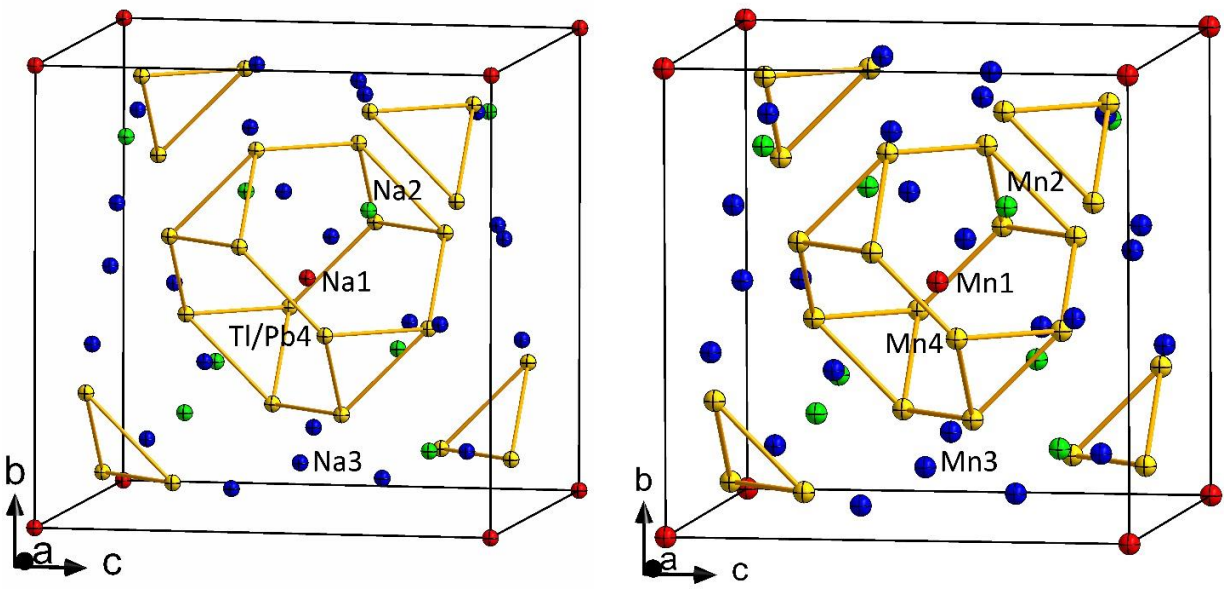

Figure S30. Comparison of the unit cells of $Na_{17}Tl_5Pb_7$ (left) and α-Mn (right). The atom positions are given the same color code

3.2.2. Structure Determination of K_2TlBi (3)

The structure of **3** could be solved using intrinsic phasing in the orthorhombic space group $Pbcm$ (No. 57). It is isostructural to the known phase K_2SnBi and features an infinite 1d TlBi-chain.[8] This chain is best described as a linear Tl-strand with the Bi-atoms positioned in an alternating fashion on both sides with a Bi-Tl-Tl-Bi angle of 96.54(3)°. Despite the exchange of Sn for Tl the structure is almost identical with only a minor elongation of the Tl-Tl distance of 3.2606(3) Å with respect to the Sn-Sn distance of 3.249 Å. If one assumes a charge of –1 for the Bi atoms the Tl atoms also carry a charge of –1. Therefor they should behave like a group 14 element with 4 (or 2) bonds. The Sn atoms in K_2SnBi also carry a charge of –1 and should be pseudo-group 15 elements. An alternative description of the structure can be given by closer inspection of the Tl environment. The linear Tl-Tl strand forms the center of a columnar stack of (K4Bi) rings. These are arranged so that they form stacks of distorted pentagonal antiprisms. The Tl and K4Bi layers lie in the *ab*-plane and are shifted against each other by z = 0.25.
The unit cell is depicted in figure S31. Figure S2 shows the columnar environment of the Tl strands.

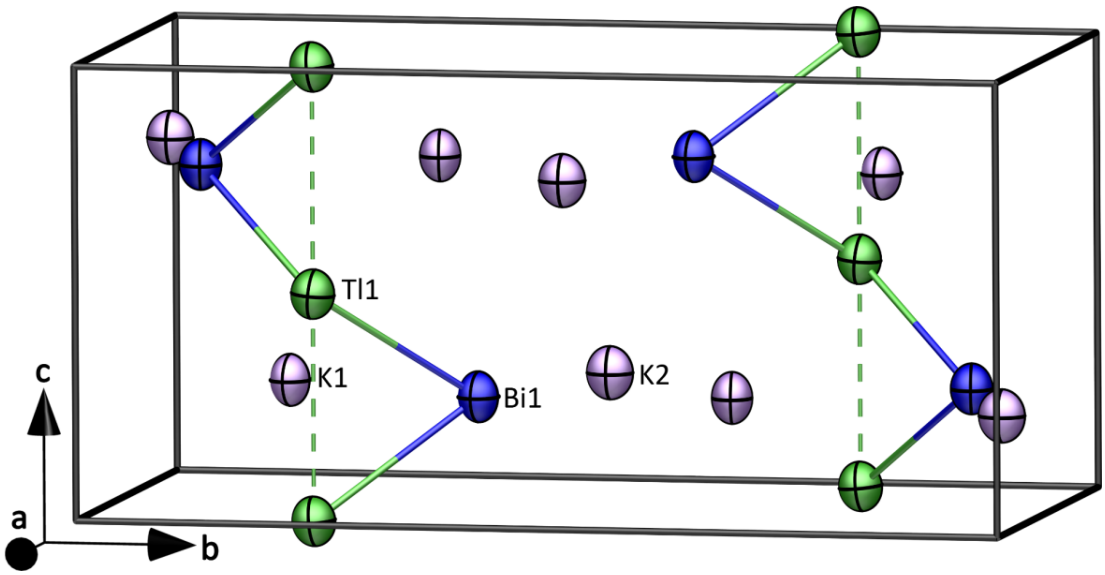

Figure S31. Unit cell packing of 3 with labels given in the asymmetric unit. Two parallel $^{1}_{\infty}[TlBi]^{2-}$ strands run along the crystallographic *c*-axis. Displacement ellipsoids are drawn at 50% probability level.

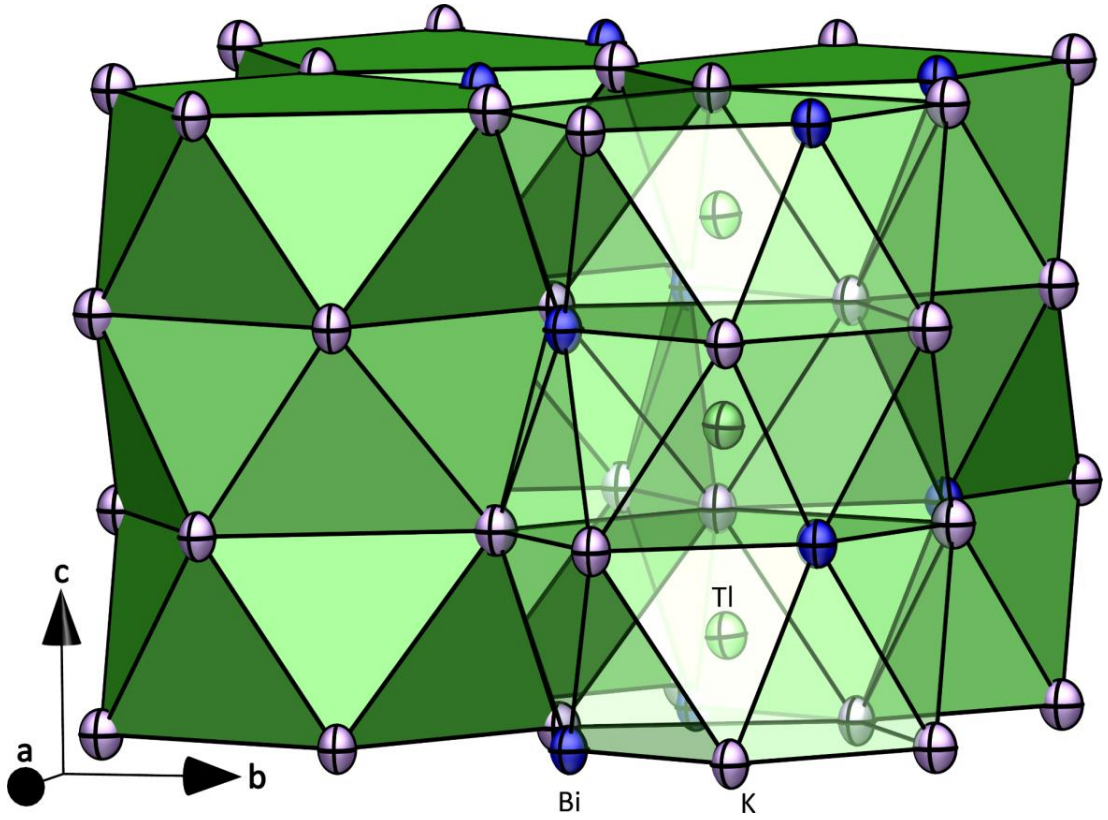

Figure S32. Alternative structure description of 3. The Tl atoms form a linear strand along the crystallographic *c*-axis that is enclosed into a columnar stack of (K4Bi)-rings. These rings are rotated against each other by 96.54(3)°.

3.2.3. Structure Determination of $K_6Tl_2Bi_3$ (4)

The structure of **4** could be solved using intrinsic phasing in the centro-symmetric space group $C2/c$ (No. 15). It features $^{1}_{\infty}[Tl_4Bi_6]^{12-}$ chains that expand along the crystallographic a axis. In the asymmetric unit half a cage (Tl_2Bi_3) and seven independent K atoms are present, two of which sit on special positions with a 0.5 crystallographic occupancy. While the distinction between the Tl/Bi and the K positions is clear the assignment of Tl- and Bi-atoms has to be done on a chemical basis. There are three positions on which the heavy atom is two-bonded, one where it is three bonded, and one where it features four bonds. Employment of the pseudo-element concept with an overall charge of 6– within the asymmetric unit leads to the following result: all two-bonded positions are occupied by Bi^- ions whereas the three- and four-bonded positions are occupied by Tl^{2-} and Tl^- ions respectively. The same atom assignment is found in the phase $K_6Tl_2Sb_3$ which is isostructural.[9] In this phase the atom positions can be distinguished unambiguously due to the difference in electron numbers of Tl and Sb.
In figure S33 a unit cell plot of **4** is given. The infinite chains along the crystallographic a-axis are well visible. A detailed view on the cation environment around one $[Tl_4Bi_6]^{12-}$ cage is given in figure S34. One cage is shown in figure S35 and the relevant bond lengths within the heavy atom framework are provided in table S5.

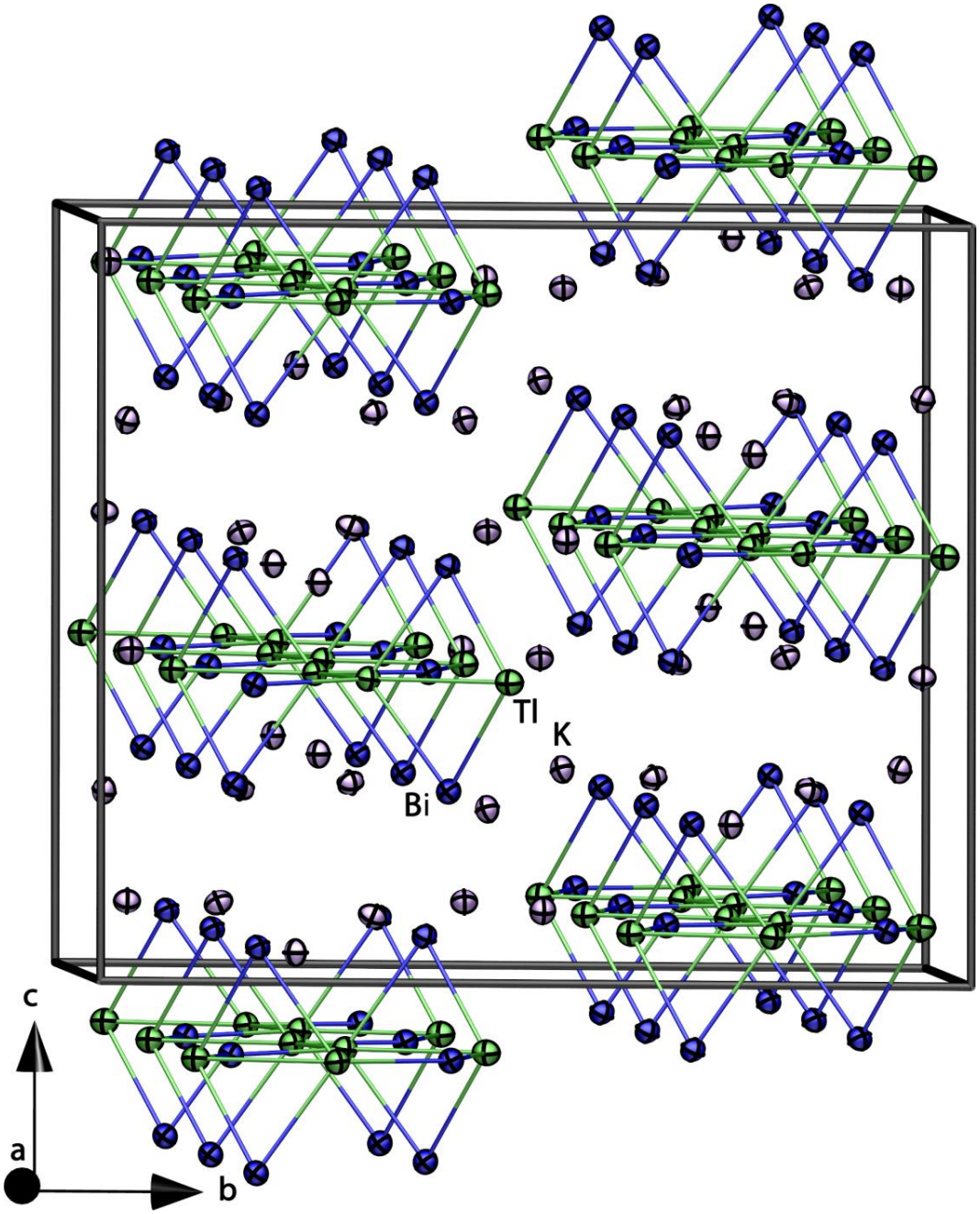

Figure S33. Extended unit cell plot of 3 and the arrangement of the $^{1}_{\infty}[Tl_4Bi_6]^{12-}$. View approximately along the crystallographic a axis. Displacement parameters are drawn at 50% probability level.

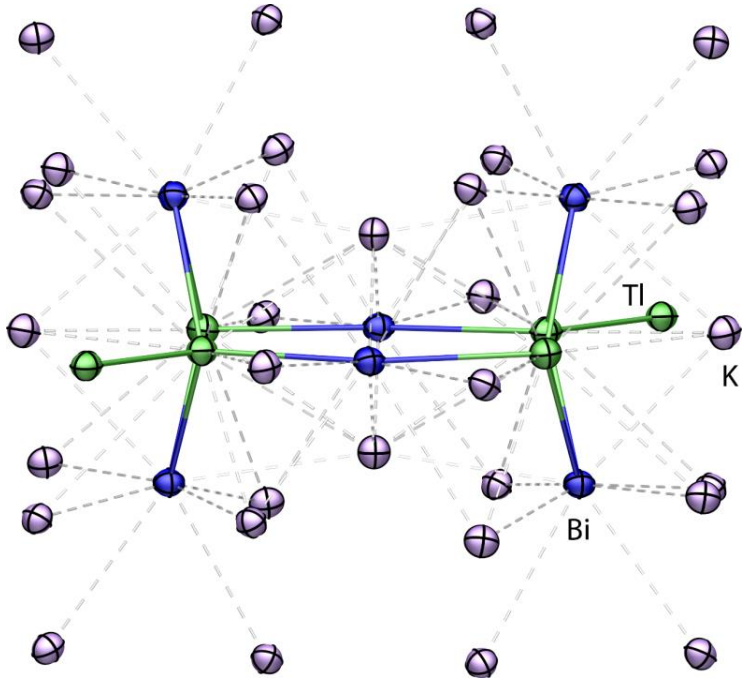

Figure S34. Cation environment around one $[Tl_4Bi_6]^{12-}$ cage in the $^{1}_{\infty}[Tl_4Bi_6]^{12-}$ strand in 3. Displacement ellipsoids are drawn at 50% probability level.

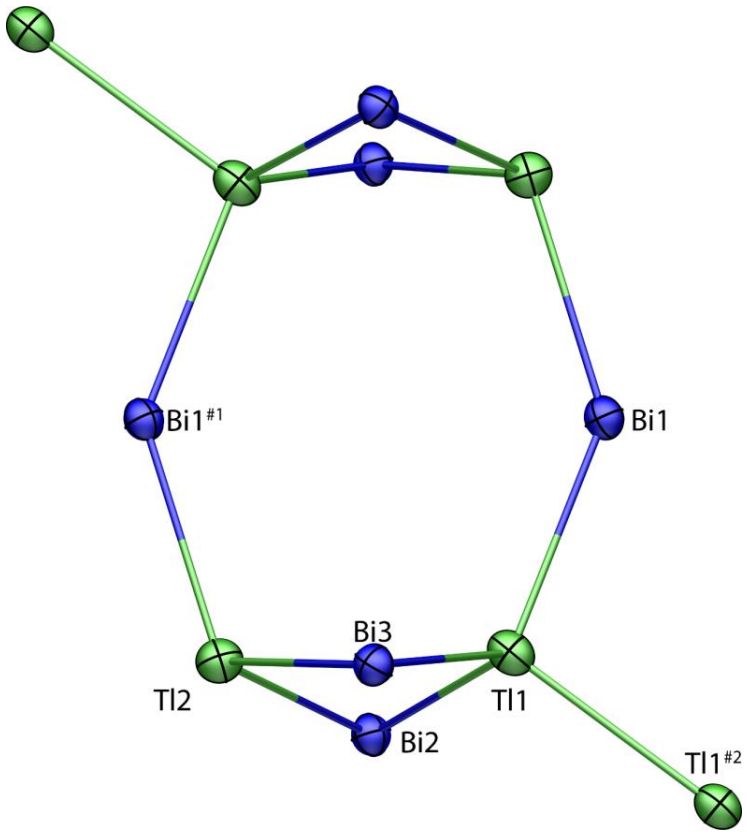

Figure S35. Close-up view of one $[Tl_4Bi_6]^{12-}$ cage in 4. Displacement ellipsoids are drawn at 50% probability level. Bond lengths are given in Table S5. Symmetry operations #1: 2-x, y, 1/2-z; #2: 1-x, y, ½-z.

Table S5. Interatomic distances in the $[Tl_4Bi_6]^{12-}$ cage. Atom labels as given in figure S35. #1: 2-x, y, 1/2-z; #2: 1-x, y, ½-z.

Atoms	Distance / Å	Atoms	Distance / Å
Tl1 – Bi1	3.285(1)	Tl2 – Bi1#1	3.259(1)
– Bi2	3.163(1)	– Bi2	3.253(1)
– Bi3	3.188(1)	– Bi3	3.267(1)
Tl1 – Tl1#2	3.289(1)		

3.2.4. Structure Determination of KTlBi (5)

Several crystals obtained from a solid state reaction were mounted on the diffractometer. Many of them did prove to be KBi_2, which is not surprising.[10] The cell determination of the second type of crystals did suggest a trigonal/hexagonal unit cell with preliminary cell constants of a = 6.80 Å, and c = 1.49 Å. A database search suggested a reasonable agreement with the unit cell of KPb_2, a hexagonal Laves phase with the $MgZn_2$ structure prototype.[11] As no lead was used throughout the synthesis this did hint towards an isoelectronic replacement with the elements Tl and Bi. In fact, this turned out to be exactly the case. Formally K(Tl-)(Bi+) is isoelectronic to KPb_2 and therefore expected to also crystallize in isostructural manner. The structure of **5** thus could be refined in the hexagonal space group $P6_3/mmc$ (No. 194). As Tl- and Bi-positions cannot be distinguished in this experiment the two heavy atom positions were refined with a 1:1 ratio of Tl- and Bi-atoms with equal coordinates and anisotropic displacement parameters, only K-Tl/Bi and Tl/Bi-Tl/Bi-distances can be given. They are in the range of 3.7980(3) – 3.9894(2) Å and 3.1960(1) – 3.6077(2) Å and do not differ drastically from the according distances in KPb_2. As the structure is that of a classical hexagonal Laves-phase a more detailed structure description can be obtained from any solid state chemistry textbook. The unit cell is depicted in figure S36, one Frank-Kasper-Polyhedron is shown in figure S37 and the hexagonal ABCABC layer arrangement is illustrated in figure S38.

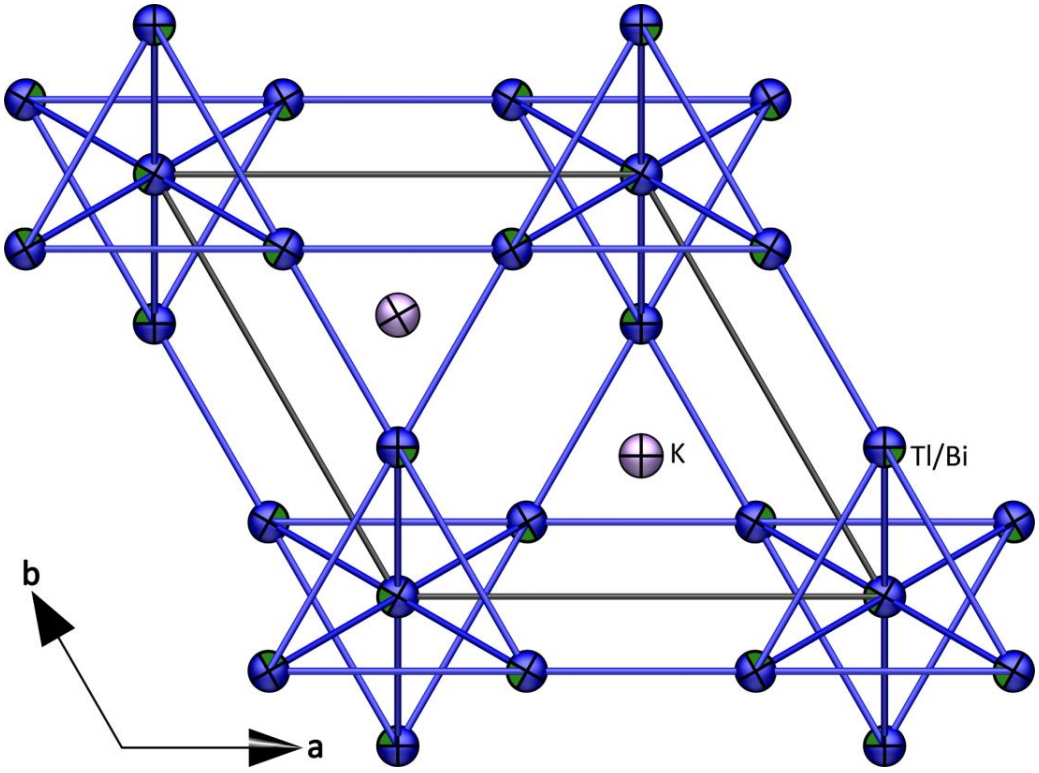

Figure S36. Extended unit cell of 5. Displacement ellipsoids are drawn at 50% probability level.

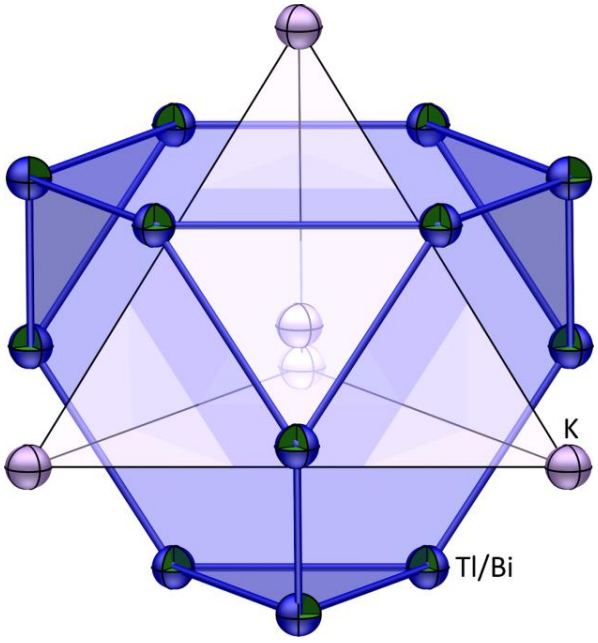

Figure S37. Frank-Kasper-Polyhedron around one central K^+ ion. Displacement ellipsoids are drawn at 50% probability level.

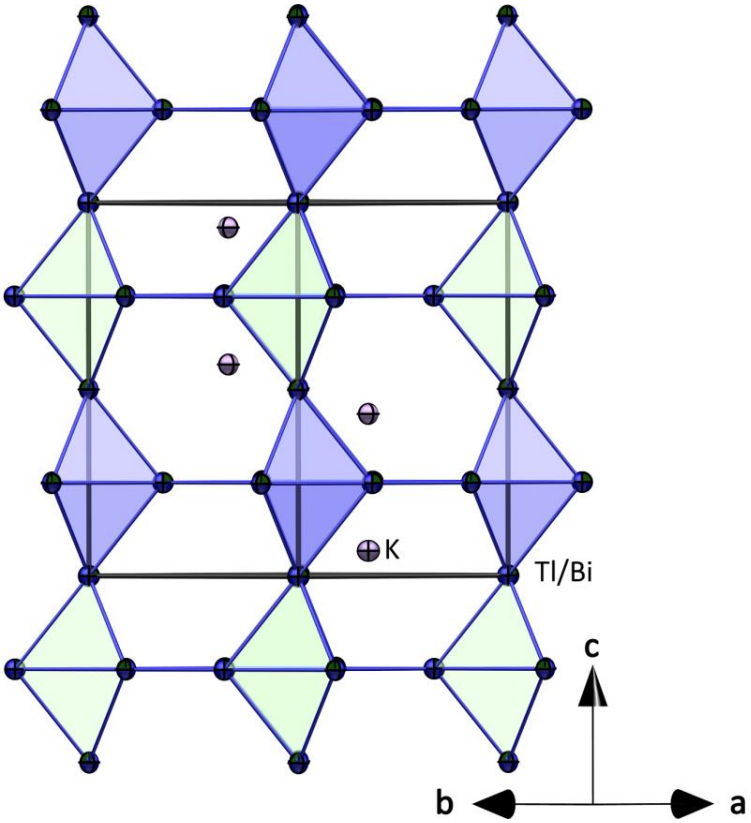

Figure S38. Arrangement of atoms into layers within the *ab*-plane. The ABAB layer repetition of the hexagonal arrangement is visible. Displacement ellipsoids are drawn at 50% probability level.

3.2.5. Structure Determination of $[Na(crypt\text{-}222)]_3(TlSn_9)_{0.8}(TlSn_8)_{0.2}$•0.55*en*•0.45*thf* (1)

The structure of **1** could be solved using intrinsic phasing in the centro-symmetric space group $P\bar{1}$ (No. 2). The structure features two heavy atom cluster anions $(TlSn_9)^{3-}$ and $(TlSn_8)^{3-}$ located on one position, three independent $[Na(crypt\text{-}222)]^+$ counter ions, one ethylene diamine molecule, and one THF molecule, the last two being located on the same position, in the asymmetric unit (see figure SX). The THF molecule was refined using geometrical and bond length restraints created from the DSR library in Olex2 (FragmentDB plugin).[12] The cryptand ligands did not show disorder and anisotropic displacement parameters could be refined for all three without the use of restraints, even though relatively large thermal ellipsoids indicate a dynamic behavior. The two cluster anions are located on one position with an occupancy ratio of approximately 4:1. It was previously reported that these two anions occur alongside each other in the solid state. They were structurally characterized as their respective $[K(crypt\text{-}222)]^+$ salt but with a different kind of disorder.[13] The Tl- and Sn-atom positions in the $(TlSn_9)^{3-}$ anion could not be sufficiently determined from this experiment and were refined with a 1:1 disorder on both capping positions with equal coordinates and atomic displacement parameters. Quantum chemical calculations have shown these to be the favorable positions for a group 13 atom in a 10-atom cluster cage (see chapter 6.2.). The $(TlSn_8)^{3-}$ anion adopts the shape of a tricapped trigonal prism with a disorder of the Tl atom over two of the three capping atom sites. Again, a 1:1 ratio of both elements on these positions was assumed. Figures S39-41 show the asymmetric unit, the heavy atom clusters $(TlSn_9)^{3-}$ and $(TlSn_8)^{3-}$ and their disorder in the crystal. Tables S6 and S7 contain the corresponding interatomic distances in the anions.

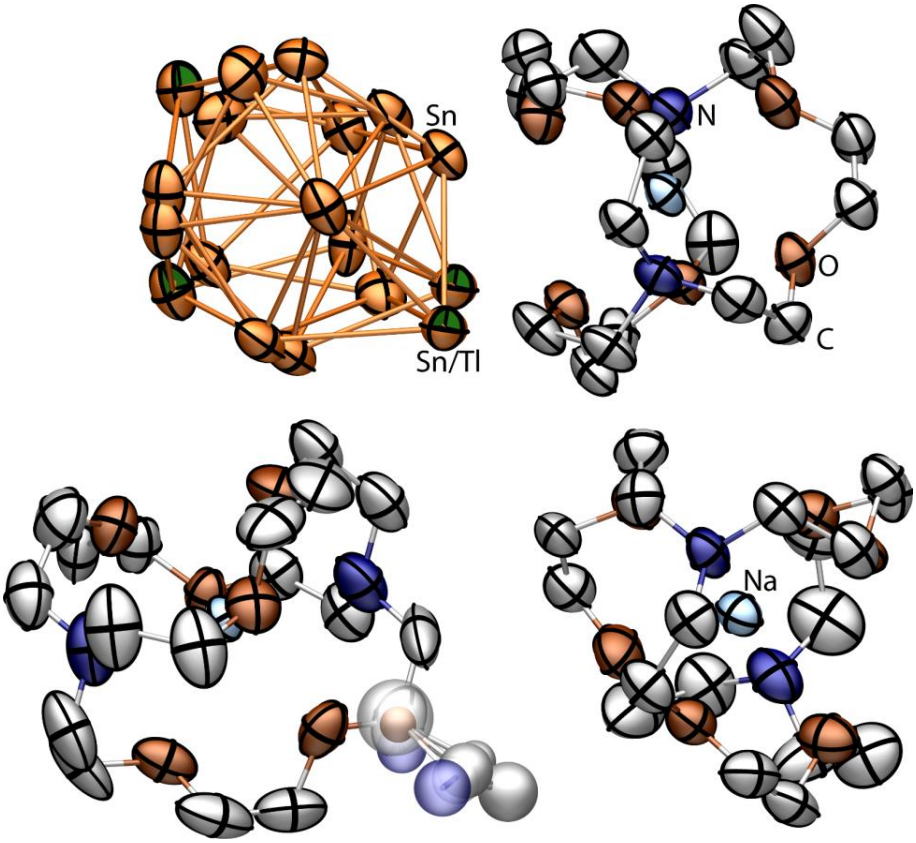

Figure S39. Asymmetric unit of 1. Displacement ellipsoids are drawn at 50% probability level. Hydrogen atoms are omitted for clarity.

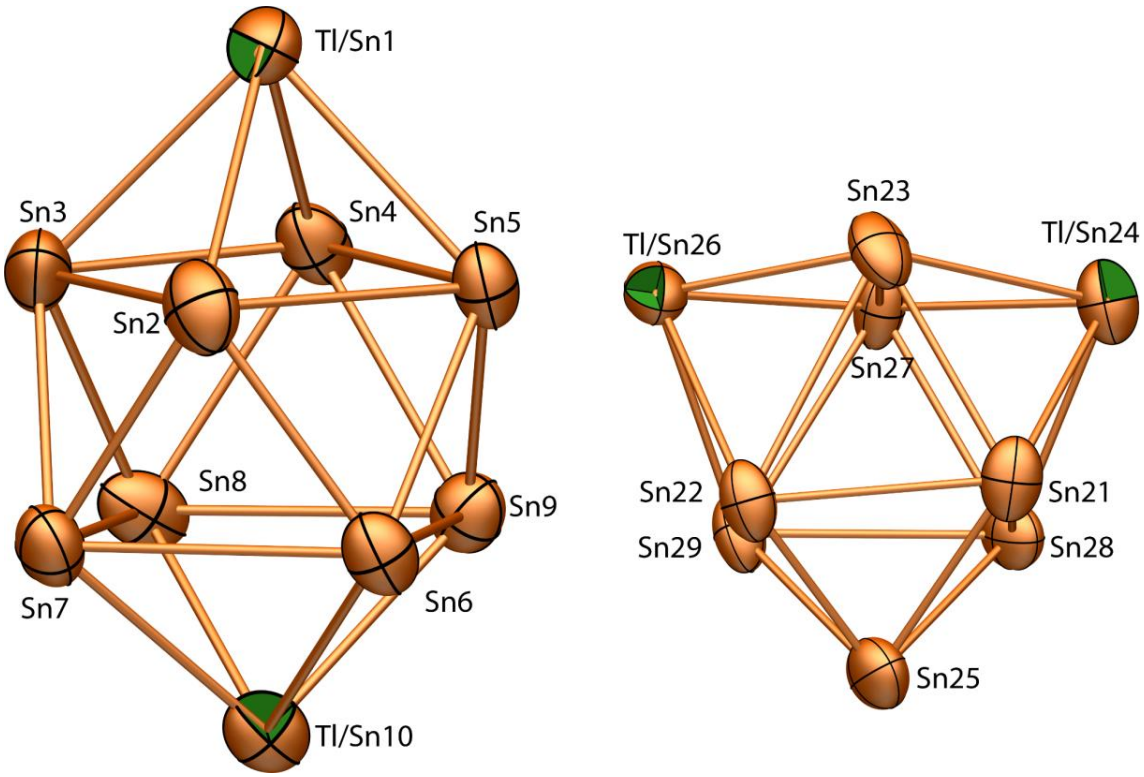

Figure S40. Structures of the anionic clusters $(TlPb_9)^{3-}$ (left) and $(TlPb_8)^{3-}$ (right) in 1. Displacement ellipsoids are drawn at 50% probability. Bond lengths are provided in Table S6 and S7.

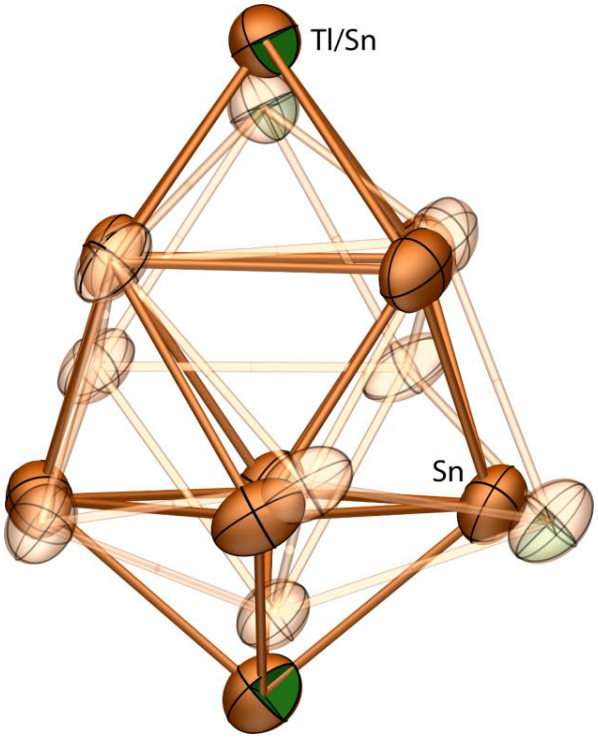

Figure S41. Disorder of the anionic clusters $(TlPb_9)^{3-}$ and $(TlPb_8)^{3-}$ in 1. Displacement ellipsoids are drawn at 50% probability.

Table S6. Interatomic distances in the cluster anion $(TlSn_9)^{3-}$ in 1. Position numbers as given in figure S6.

Atoms	Distance / Å	Atoms	Distance / Å	Atoms	Distance / Å
Tl/Sn1 – Sn2	3.1014(1)	Tl/Sn10 – Sn6	2.9290(1)	Sn2 – Sn6	2.9117(1)
– Sn3	3.1477(1)	– Sn7	2.9866(1)	– Sn7	2.9661(1)
– Sn4	3.0671(1)	– Sn8	2.9750(1)	Sn3 – Sn7	2.9354(1)
– Sn5	3.1010(1)	– Sn9	2.9609(1)	– Sn8	2.9843(1)
average	3.104	average	2.963	Sn4 – Sn8	2.9985(1)
				– Sn9	2.9990(1)
Sn2 – Sn3	3.0919(1)	Sn6 – Sn7	3.2410(1)	Sn5 – Sn6	2.9348(1)
Sn3 – Sn4	3.0232(1)	Sn7 – Sn8	3.1844(1)	– Sn9	2.9167(1)
Sn4 – Sn5	3.1098(1)	Sn8 – Sn9	3.1826(1)	Average	2.956
Sn2 – Sn5	3.1023(1)	Sn9 – Sn6	3.1962(1)		
average	3.082	average	3.201		

Table S7. Interatomic distances in the cluster anion $(TlSn_8)^{3-}$ in 1. Position numbers as given in figure S7.

Atoms	Distance / Å	Atoms	Distance / Å	Atoms	Distance / Å
Tl/Sn24 – Sn21	3.1282(1)	Tl/Sn26 – Sn22	3.2803(1)	Sn21 – Sn22	3.0548(1)
– Sn23	3.0829(1)	– Sn23	2.9589(1)	– Sn23	3.1017(1)
– Sn27	3.0455(1)	– Sn27	3.0907(1)	Sn22 – Sn23	3.3268(1)
– Sn28	3.0648(1)	– Sn29	3.1050(1)	Sn27 – Sn28	3.0909(1)
				– Sn29	3.1405(1)
Sn25 – Sn21	2.9479(1)			Sn28 – Sn29	3.1551(1)
– Sn22	3.3268(1)			Sn21 – Sn28	3.1295(1)
– Sn28	2.9566(1)			Sn22 – Sn29	3.0125(1)
– Sn29	2.9237(1)			Sn23 – Sn27	3.0972(1)

3.2.6. Structure Determination of $[Na(crypt\text{-}222)]_3(TlPb_9)_{0.94}(TlPb_{11})_{0.06}\bullet 0.9thf$ (6)

The structure of **6** could be solved using intrinsic phasing in the centro-symmetric space group $P2_1/c$ (No. 14). The structure features two heavy atom cluster anions $(TlPb_9)^{3-}$, and $(TlPb_{11})^{3-}$ located on one position, three independent $[Na(crypt\text{-}222)]^+$ counter ions, and one thf molecule in the asymmetric unit (see figure SX). The cryptand ligands did not show disorder and anisotropic displacement parameters could be refined for all three without the use of restraints. The two cluster anions are located on one position with an occupancy ratio of approximately 13:1. As the Tl- and Pb-atom positions in the $(TlPb_9)^{3-}$ anion cannot be determined from this experiment they were refined with a 1:1 disorder on both capping positions with equal coordinates and atomic displacement parameters. In the $(TlPb_{11})^{3-}$ anion the Tl atom was treated as disordered over all 12 equal atom positions with equal coordinates and atomic displacement parameters. Figures S42 – 44 show the asymmetric unit, the heavy atom clusters $(TlPb_9)^{3-}$ and $(TlPb_{11})^{3-}$ and their disorder in the crystal. Tables S8 and S9 contain the corresponding interatomic distances in the cluster anion.

Table S8. Interatomic distances in the cluster anion $(TlPb_9)^{3-}$ in 6. Position numbers as given in figure S43.

Atoms	Distance / Å	Atoms	Distance / Å	Atoms	Distance / Å
Tl/Pb1 – Pb2	3.0698(1)	Tl/Pb10 – Pb6	3.1162(1)	Pb2 – Pb6	3.0776(1)
– Pb3	3.0967(1)	– Pb7	3.1755(1)	– Pb7	3.0869(1)
– Pb4	3.0808(1)	– Pb8	3.1977(1)	Pb3 – Pb7	3.0988(1)
– Pb5	3.0660(1)	– Pb9	3.1235(1)	– Pb8	3.0973(1)
avg.:	3.078	avg.:	3.153	Pb4 – Pb8	3.1066(1)
				– Pb9	3.0882(1)
Pb2 – Pb3	3.2825(1)	Pb6 – Pb7	3.2230(1)	Pb5 – Pb6	3.0908(1)
Pb3 – Pb4	3.3191(1)	Pb7 – Pb8	3.1808(1)	– Pb9	3.0916(1)
Pb4 – Pb5	3.3389(1)	Pb8 – Pb9	3.2719(1)	avg.:	3.092
Pb2 – Pb5	3.4024(1)	Pb9 – Pb6	3.2811(1)		
avg.:	3.336	avg.:	3.239		

Table S9. Interatomic distances in the cluster anion $(TlPb_{11})^{3-}$ in 6. Position numbers as given in figure S44.

Atoms	Distance / Å	Atoms	Distance / Å	Atoms	Distance / Å
21 – 22	3.0984(1)	22 – 23	3.1658(1)	22 – 27	3.1430(1)
– 23	3.1521(1)	– 26	3.1704(1)	– 28	3.1247(1)
– 24	3.1413(1)	23 – 24	3.1371(1)	23 – 28	3.1105(1)
– 25	3.1259(1)	24 – 25	3.1460(1)	– 29	3.1468(1)
– 26	3.1521(1)	25 – 26	3.1235(1)	24 – 29	3.1364(1)
32 – 27	3.1709(1)	27 – 28	3.1920(1)	– 30	3.0327(1)
– 28	3.1490(1)	– 31	3.0833(1)	25 – 30	3.1286(1)
– 29	3.1359(1)	28 – 29	3.2623(1)	– 31	3.2212(1)
– 30	3.1529(1)	29 – 30	3.1203(1)	26 – 27	3.1062(1)
– 31	3.1154(1)	30 – 31	3.2289(1)	– 31	3.0833(1)
avg.:			3.142		

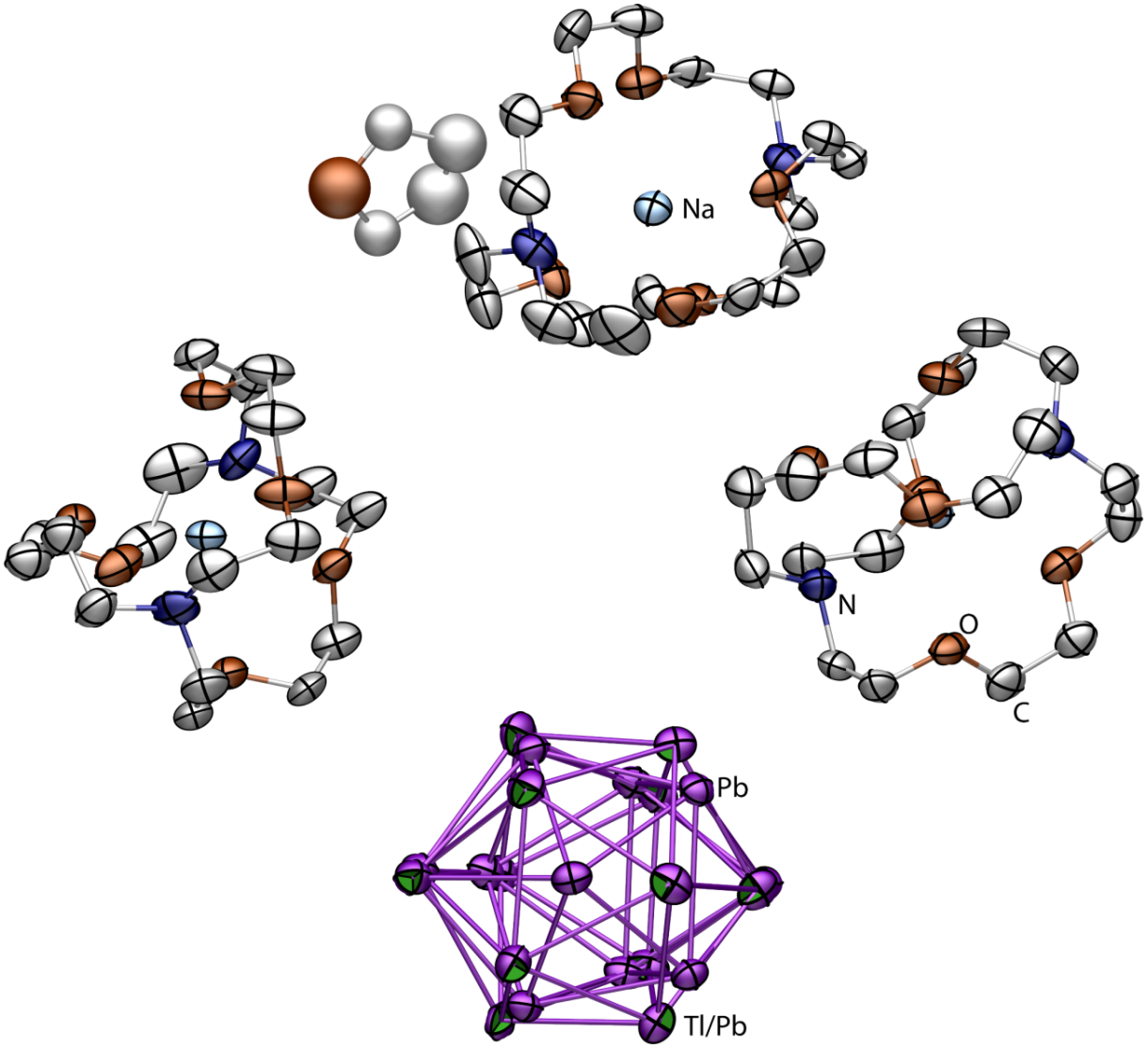

Figure S42. Asymmetric unit of 6. Displacement ellipsoids are drawn at 50% probability level. Hydrogen atoms are omitted for clarity.

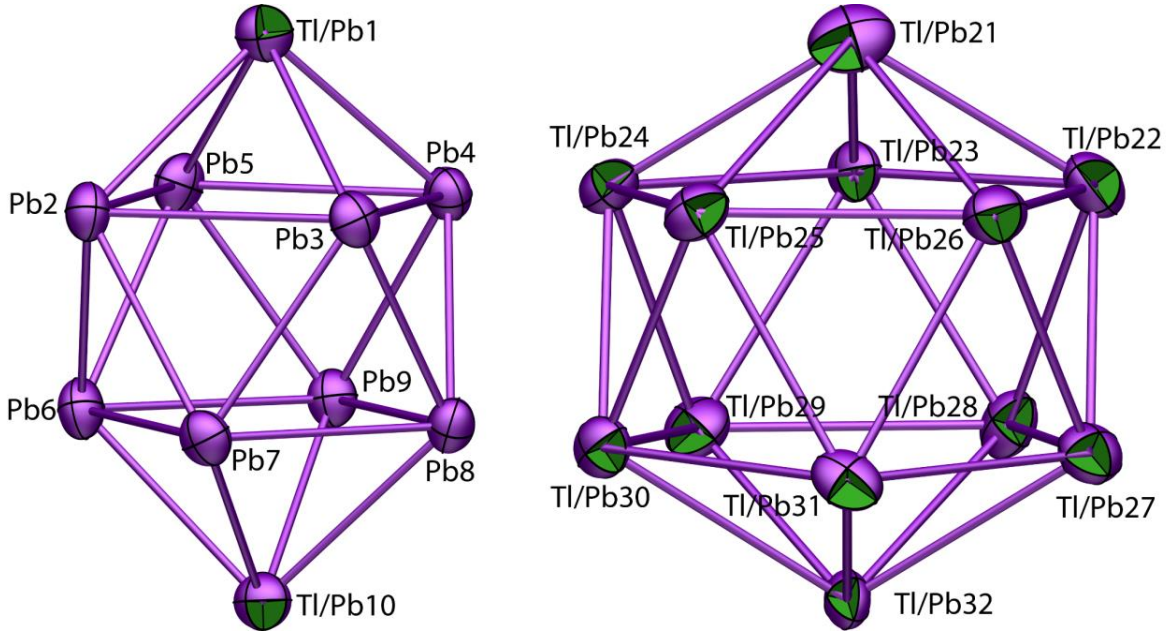

Figure S43. Structure of the anionic clusters $(TlPb_9)^{3-}$ (left) and $(TlPb_{11})^{3-}$ (right) in 6. Displacement ellipsoids are drawn at 50% probability. Bond lengths are provided in Table S8.

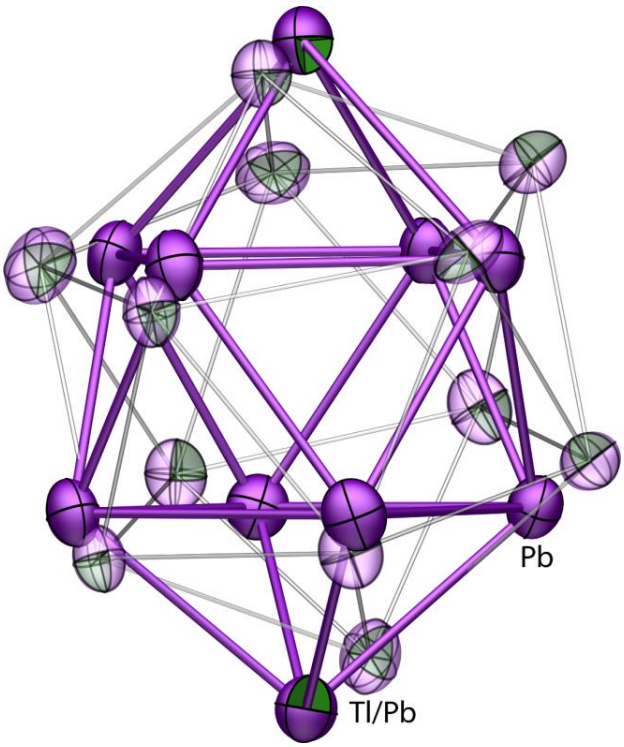

Figure S44. Disorder model of the anionic clusters $(TlPb_9)^{3-}$ and $(TlPb_{11})^{3-}$ (transparent) in 6. Displacement ellipsoids are drawn at 50% probability. Bond lengths are provided in Table S9.

3.2.7. Structure Determination of $[K(crypt\text{-}222)]_4[Pb@Tl_4Pb_8]_{0.5}(Tl_2Pb_{10})_{0.11}(Pb_9)_{0.39}\bullet 1.2\textit{en}$ (7)

The structure of **7** could be solved using intrinsic phasing in the centro-symmetric space group $P\bar{1}$ (No. 2). The structure features three different heavy atom cluster anions $[Pb@Tl_4Pb_8]^{4-}$, $(Tl_2Pb_{10})^{4-}$, (only half of the molecules in the ASU) and $(Pb_9)^{4-}$ located on one position, two independent $[K(crypt\text{-}222)]^+$ counter ions, and one en molecule in the asymmetric unit (see figure S45). The center of gravity of all clusters is located on an inversion center (½, 0, ½, Wyckoff position 1*f*). While the larger, centro-symmetric icosahedral clusters do not show signs of disorder the nine atom cage shows an inversion disorder due to its lower symmetry (figure S48). Besides these three different cluster types significant amounts of residual electron density was found (6% occupancy with Pb) that hints towards another, only partially resolved orientation of one Pb_9^{4-} cluster (see figure S48). The cryptand ligands did not show disorder and anisotropic displacement parameters could be refined without the use of restraints.

The initial structure solution reveals the heavy atom positions of one filled icosahedron that were refined as Pb atoms until the final composition was adjusted in the end. As the cluster is located on an inversion center only six independent atoms are required to describe the cluster shell. Anisotropic displacement parameters can be introduced for all atoms without problems but a high amount of residual electron density remains in the region of the heavy atom structure. Furthermore, a free refinement of all heavy atom occupancies resulted in a significantly lower occupancy for the central atom with respect to the cluster shell. This can be understood with the presence of two different icosahedral clusters, $[Pb@Tl_4Pb_8]^{4-}$, and $(Tl_2Pb_{10})^{4-}$, that are located on the same position. As Tl- and Pb-atoms cannot be distinguished in a classical diffraction experiment with Mo-K_α radiation. The Pb_9^{4-} cluster appears in two different orientations due its position on the inversion center. Due to the number of different clusters on one position their relative ratios could not be refined freely but were restrained to 100% with the use of SUMP and one free variable for each cluster. The occupancy of the $[Pb@Tl_4Pb_8]^{4-}$ cluster was linked to the occupancy of the central Pb atom (50%), attributing the difference between the central atom and the atoms in the icosahedral shell to the $(Tl_2Pb_{10})^{4-}$ cluster (11%). The fully and the partially resolved Pb_9^{4-} clusters refine with 13% and 6%. ESI-MS confirmed the presence of all clusters.

Figures S45 - 49 show the asymmetric unit, packing in the unit cell, the icosahedral cluster anions, the 9-atomic cluster anion and unresolved 9-atom cage, and the disorder of the different anions on one position. Tables S10 and S11 contain relevant interatomic distances in the cluster anions.

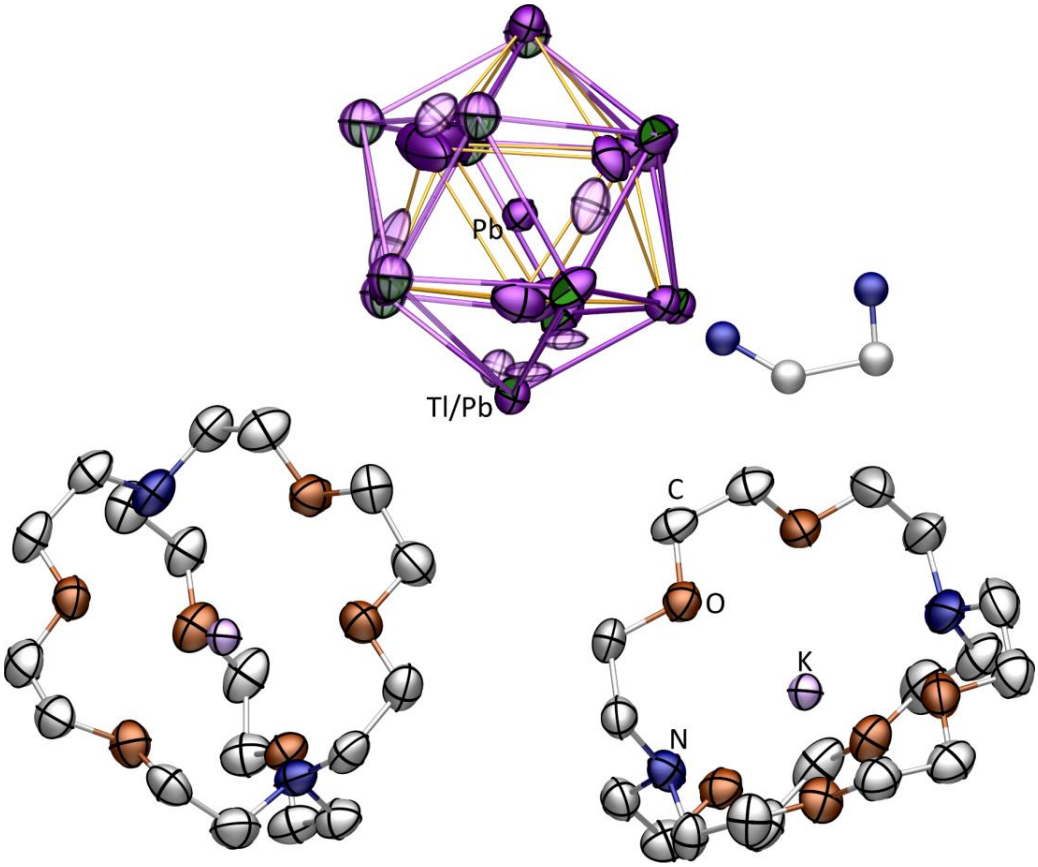

Figure S45. Asymmetric unit of 7 containing half of the cluster anion. The complete cluster anion is created by symmetry through inversion. The symmetry-generated part is shown in transparent colors. Displacement ellipsoids are drawn at 50% probability level. Hydrogen atoms are omitted for clarity.

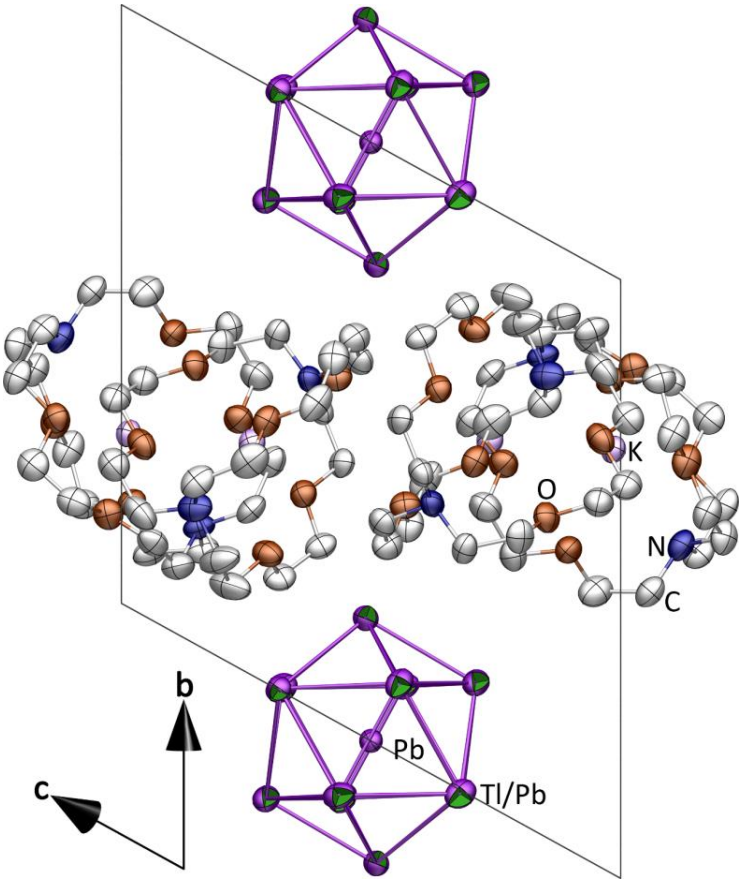

Figure S46. Packing of molecules in the unit cell of 7. View along the crystallographic a axis. Displacement ellipsoids are drawn at 50% probability level. Hydrogen atoms and incomplete cryptand molecules are omitted for clarity.

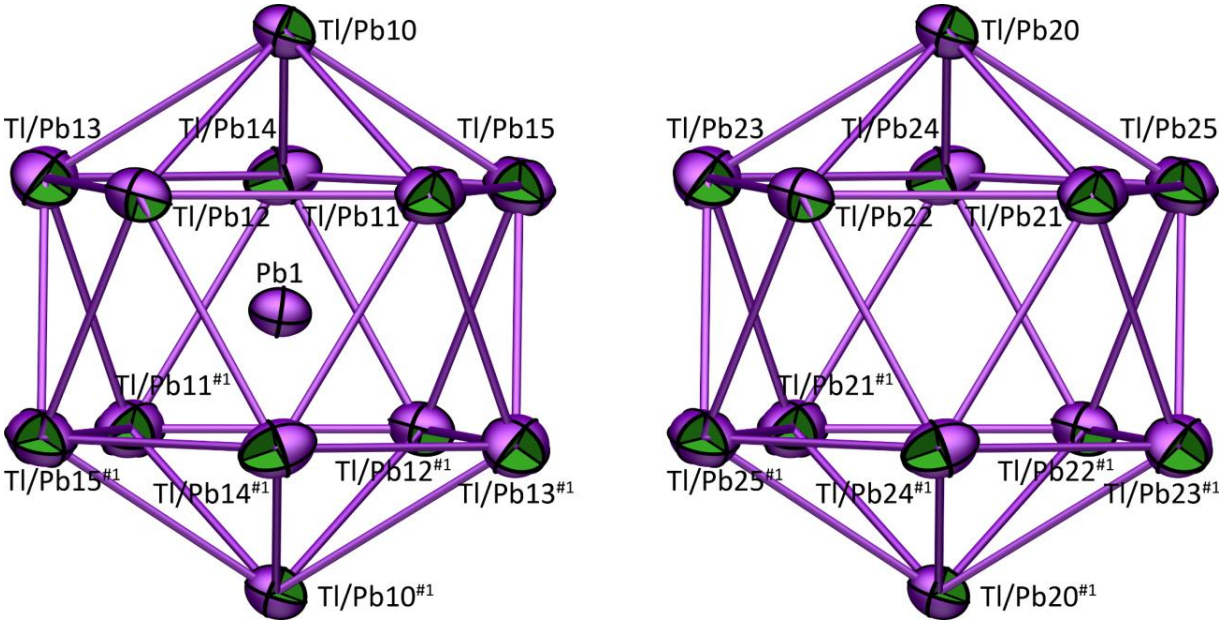

Figure S47. Structure of the anionic clusters $[Pb@Tl_4Pb_8]^{4-}$ (left) and $(Tl_2Pb_{10})^{4-}$ (right) in 7. Displacement ellipsoids are drawn at 50% probability. Bond lengths are provided in Table S10. Symmetry operation #1: 1-x, 2-y, 1-z.

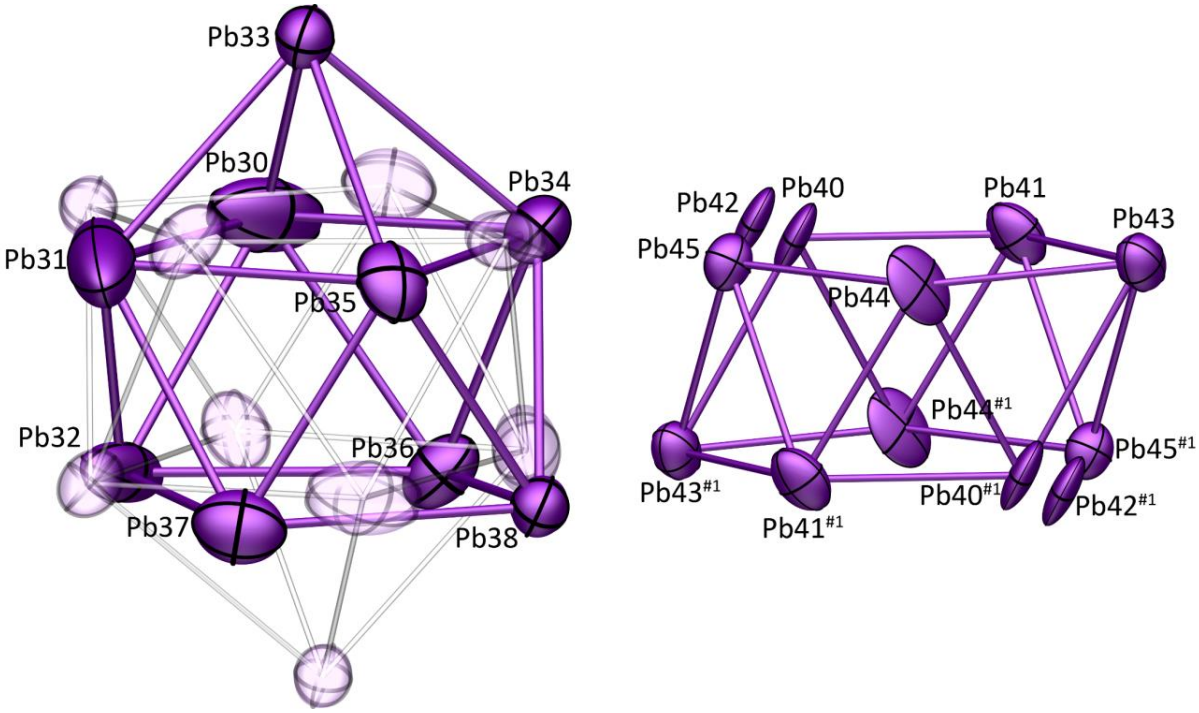

Figure S48. Structure of the anionic cluster Pb_9^{4-} (left, second orientation in transparent colors) and the only partially resolved further orientation (right) in 7. Displacement ellipsoids are drawn at 50% probability. Bond lengths are provided in Table S11.

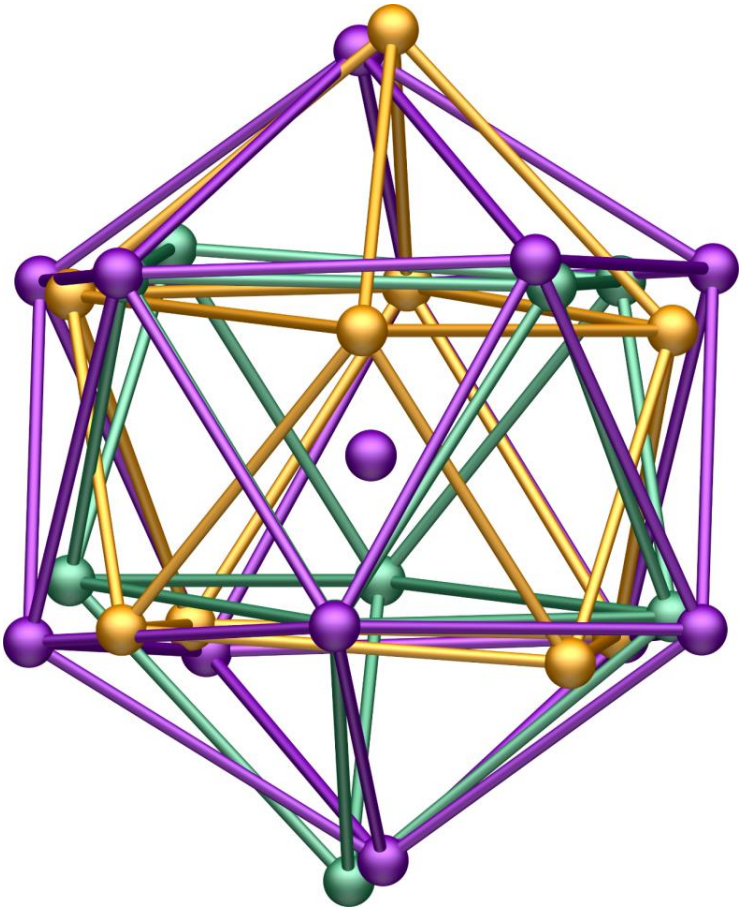

Figure S49. Disorder model for the anionic clusters $[Pb@Tl_4Pb_8]^{4-}$/$(Tl_2Pb_{10})^{4-}$ (purple) and two orientations of Pb_9^{4-} (orange, green) in 7. The unresolved further orientation of a Pb_9^{4-} cluster has been omitted for clarity.

Table S10. Bond lengths in the anions $[Tl@Tl_4Pb_8]^{4-}$ and $(Tl_2Pb_{10})^{4-}$ (italic). Position numbers as given in figure S47. Symmetry operation #1: 1-x, 2-y, 1-z.

Position no.	Distance / Å	Position no.	Distance / Å	Position no.	Distance / Å
Pb1-10	3.1592(1)	11-12/*21-22*	3.2697(2)	11-13#1/*21-23#1*	3.3969(1)
-11	3.1934(2)	12-13/*22-23*	3.2795(2)	11-14#1/*21-24#1*	3.3397(1)
-12	3.1365(1)	13-14/*23-24*	3.2939(1)	12-14#1/*22-24#1*	3.2670(2)
-13	3.1385(2)	14-15/*24-25*	3.2908(2)	12-15#1/*22-25#1*	3.3677(1)
-14	3.0667(2)	15-11/*25-21*	3.2543(2)	13-15#1/*23-25#1*	3.2700(2)
-15	3.1266(1)			13-11#1/*23-21#1*	3.3970(1)
				14-11#1/*24-21#1*	3.3397(1)
				14-12#1/*24-22#1*	3.2670(2)
				15-12#1/*25-22#1*	3.3677(1)
				15-13#1/*25-23#1*	3.2700(2)
Avg.:	3.137	Avg.:		3.311	

Table S11. Bond lengths in the anion Pb_9^{4-} . Position numbers as given in figure S48.

Position no.	Distance / Å	Position no.	Distance / Å	Position no.	Distance / Å
Pb33 – Pb30	3.2225(2)	Pb32 – Pb36	3.3893(1)	Pb30 – Pb32	3.1320(1)
– Pb31	3.1411(1)	– Pb37	3.4973(2)	– Pb36	3.1799(1)
– Pb34	3.2290(1)	Pb36 – Pb38	3.3360(2)	Pb31 – Pb32	3.1931(2)
– Pb35	3.1790(1)	Pb37 – Pb38	3.2349(1)	– Pb37	3.1677(1)
				Pb34 – Pb36	3.1255(2)
Pb30 – Pb31	3.6600(2)			– Pb38	3.2143(1)
– Pb34	3.2111(2)			Pb35 – Pb37	2.9774(1)
Pb31 – Pb35	3.2346(2)			– Pb38	3.0757(1)
Pb34 – Pb35	3.3091(2)				

3.2.8. Structure Determination of [K(crypt-222)]$_3$(Tl$_4$Bi$_3$) (8)

Crystals of compound **8** can be obtained via different routes, all showing the same intrinsic problems that will be discussed below. **8** crystallizes in the form of large black blocks and pyramids. The unit cell determination on these crystals suggested either a monoclinic cell with a = 21.2, b = 33.3, c = 24.2, and β = 90.2° or the according orthorhombic cell. After proceeding to the integration with the lower-symmetric monoclinic unit cell the structure could be solved in the space group $P2_1/n$ (No. 14) with the SHELXT algorithm, revealing three anion positions and six independent $[K(crypt\text{-}222)]^+$ ions. The anions adopt the shape of pentagonal bipyramid that show a significant dynamic even at these low temperatures through rotation around the pseudo C_5-axis. Two of the three anions are located on special positions (*Wyckoff* positions 2*b* (0, ½, ½) and 2*c* (0, 0, ½)), with only half of each anion belonging to the asymmetric unit. The third anion is located on a general position. All three anions are disordered over at least two sites. For the anions on the inversion centers a satisfying model could be created with only two different orientations and a 1:1 ratio. However, the third anion could not be modeled properly. The best result was obtained with a model in which two different orientations of the five-membered ring are refined with a linked occupancy. This results in an occupancy of 70% for the main component and 30% for the second. While the atoms in the first orientation indicate a strong tendency towards the rotation around the *pseudo*-C_5 axis but can overall be described adequately this is not possible for the second orientation. In this one, three of the five atoms in the ring adopt elongated shapes upon introduction of anisotropic displacement parameters that cannot be optimized with according restraints. The thermal displacement parameters of these atoms strongly correlate with each other as well as with some of the other lighter atoms in the structure model. Even though two ring positions are refined already the highest residual electron density still remains close to the heavy atoms in the ring plane, further emphasizing the strong dynamic of the anions. However, all attempts to refine a third orientation of the ring remained unsuccessful. The Tl and Bi atom positions within the anions are based on the results of quantum chemical calculations (see chapter 6.4.). The two apical positions are occupied by Tl-atoms and all atom positions in the five-membered rings are refined with at fixed Tl:Bi ratio of 2:3. In order to further evaluate the quality of the structure model a powder diffraction pattern of the compound was measured. It shows a sufficiently good match with the simulated pattern calculated from our final model. This is shown in chapter 3.8..
In total, the crystal did show several phenomena that influenced the quality of the final model:

1. Due to the heavy atoms in the compound the crystal does show high xray absorption that could only be corrected partially.
2. Reciprocal space plots revealed a fourfold superstructure along the crystallographic *b*-axis. This can be understood well upon inspection of the packed unit cell. Every second layer (parallel to the *ac*-plane, see figure S51) is almost identical which leads to a pseudotranslation along the crystallographic *b*-axis.
3. The crystal turned out to be a pseudomerohedral twin. As the monoclinic angle is close to 90° this can be treated relatively well and should not impair the refinement too much.

4. Severe disorder of the heavy metal polyanions. This is one of the key factors that contribute to the high R-values. As the anions are highly symmetric this problem did occur in every single experiment and could not be avoided through different crystallization methods.

Nevertheless, the individual components of the compound could be identified and also structurally characterized. The discussion of the anion structure will be based solely on the two ones located on special positions, as these are sufficiently modeled. A plot of the asymmetric unit is given in figure S50. The whole unit cell is shown in figure S51 and the three independent anions are shown in figure S52.

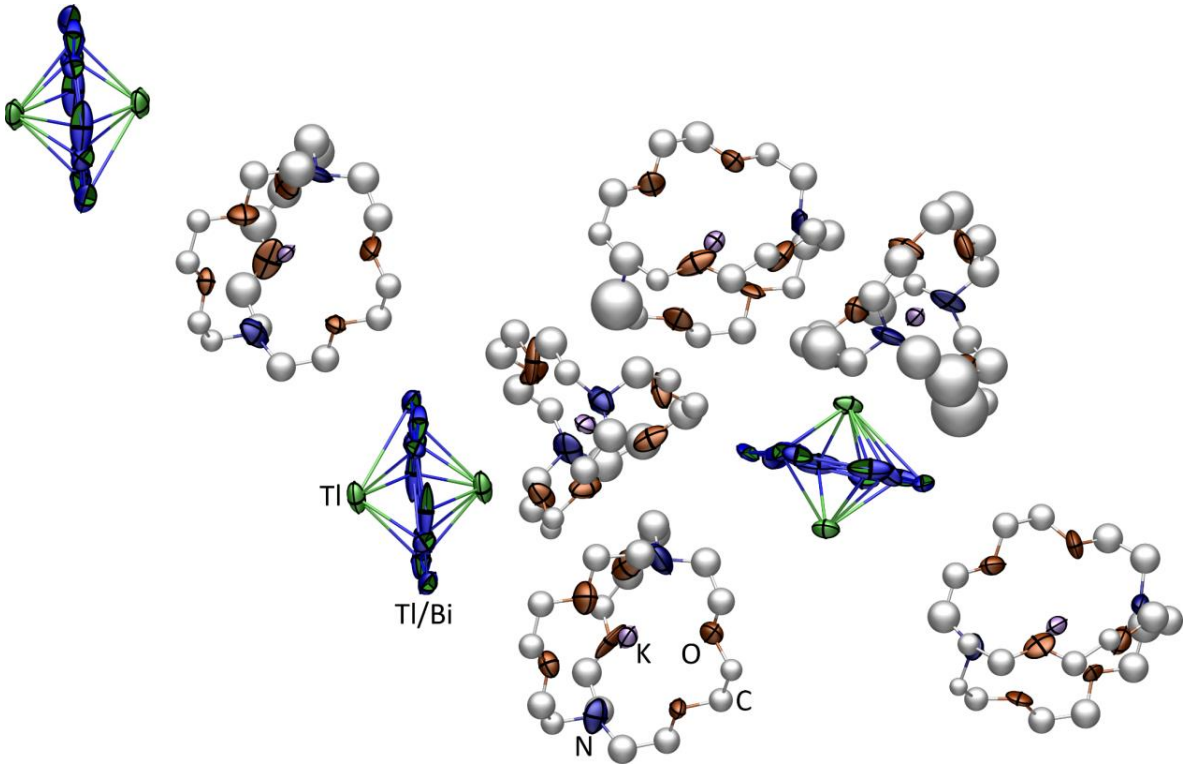

Figure S50. Extended asymmetric unit of 8 with atom labels. Two of the three anions sit on an inversion center with half of their atoms positioned in the ASU. Displacement ellipsoids are drawn at 50% probability level.

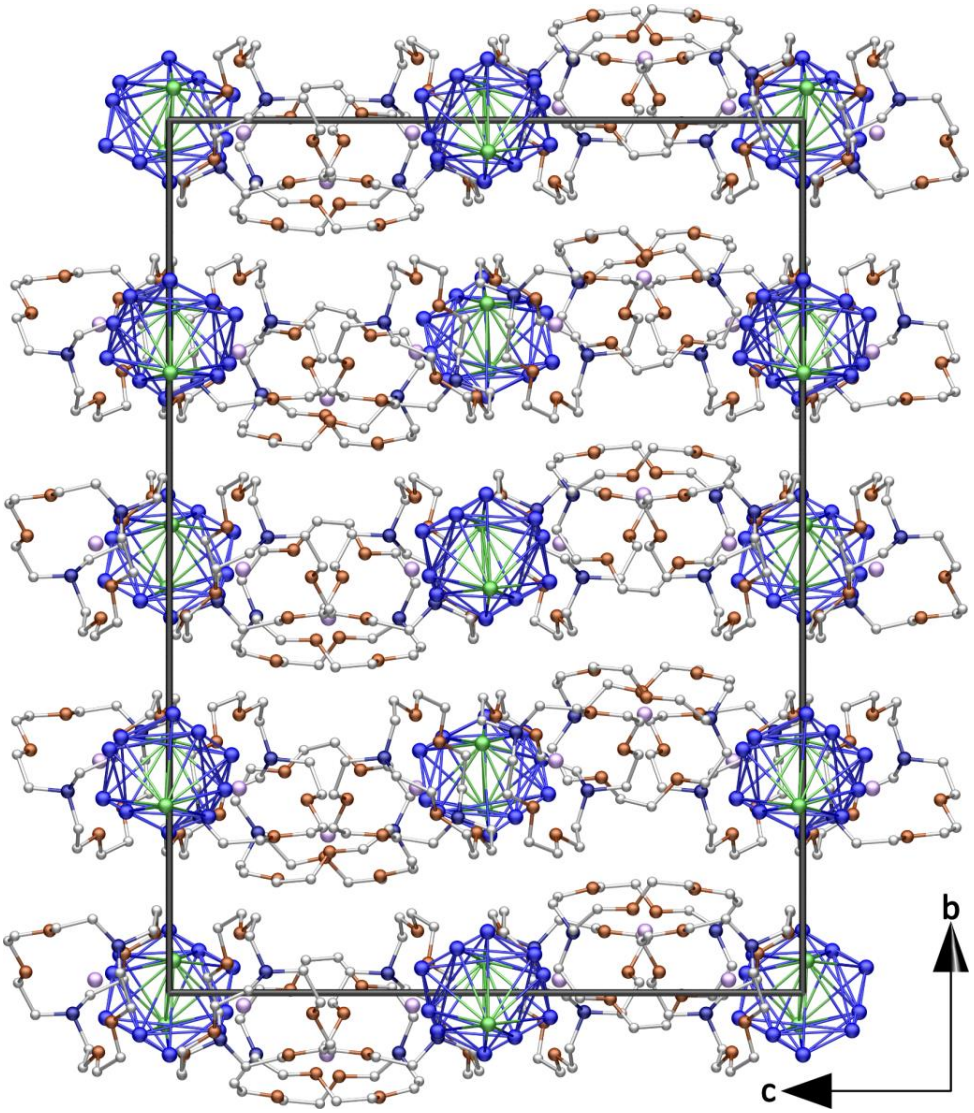

Figure S51. Unit cell packing of 8. The crystals show a fourfold superstructure along the crystallographic *b*-axis, caused by the similarity between every second layer in the *ac*-plane. Displacement ellipsoids are drawn at 50% probability level.

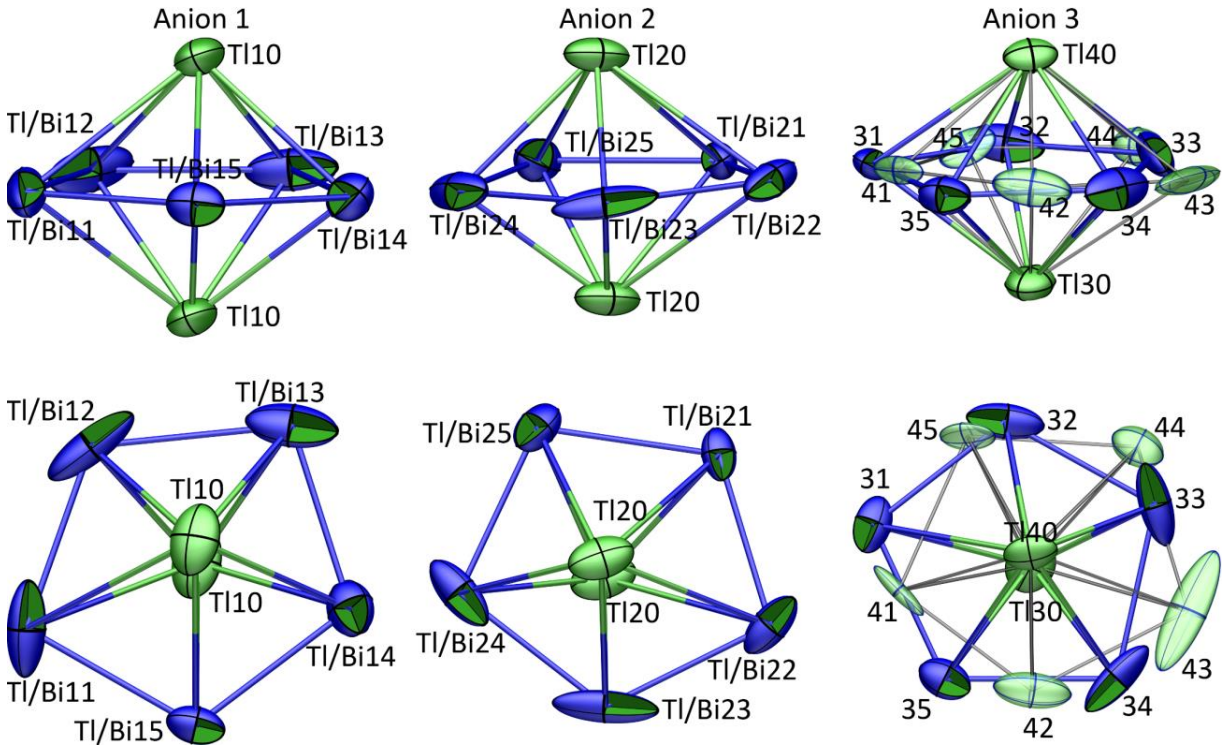

Figure S52. Two different views of the three independent $(Tl_4Bi_3)^{3-}$ anions in 8.

4. Powder X-ray Diffraction (PXRD)

4.1. General Procedure

Powder X-ray diffraction patterns were measured on a Stoe StadiMP diffractometer system equipped with a Mythen 1K silicon strip detector and a Cu-K_α (λ = 1.54056 Å) radiation source. Samples of intermetallic phases showed very high absorption coefficients and could not be measured with standard methods (mark tubes). For these samples, 0.1 mm mark tubes were covered with a thin layer of inert silicon grease and then rolled through the respective finely ground sample. These tubes were then cut to length and placed in a 0.6 mm mark tube serving as a container. Fixation of the inner tube and air-tight sealing of the outer one was achieved with air-tight soft wax. All other samples were ground and directly filled into 0.6 mm tubes. The tubes were then mounted onto the goniometer head using wax (horizontal setup) and rotated throughout the measurement. The pronounced peak asymmetries are caused by the used slit collimator as well as the detector system. Increasing shifts between detected and calculated reflection positions are caused by temperature differences between the single crystal and PXRD measurements and therefor different lattice parameters.

4.2. PXRD Data of "Na_5TlPb_3" (I)

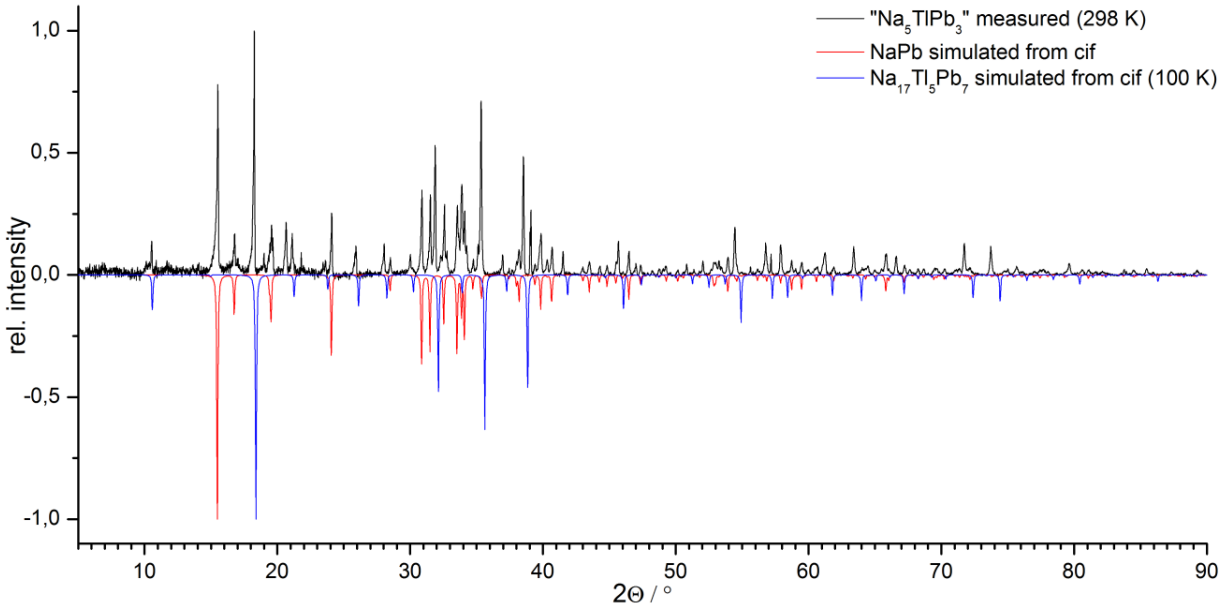

Figure S53. Comparison of the measured diffraction pattern (black line) of "Na5TlPb3" (I) and simulated diffraction patterns of NaPb[14] (red line) and $Na_{17}Tl_5Pb_7$ (2, blue line).

4.3. PXRD Data of $Na_{17}Tl_5Pb_7$

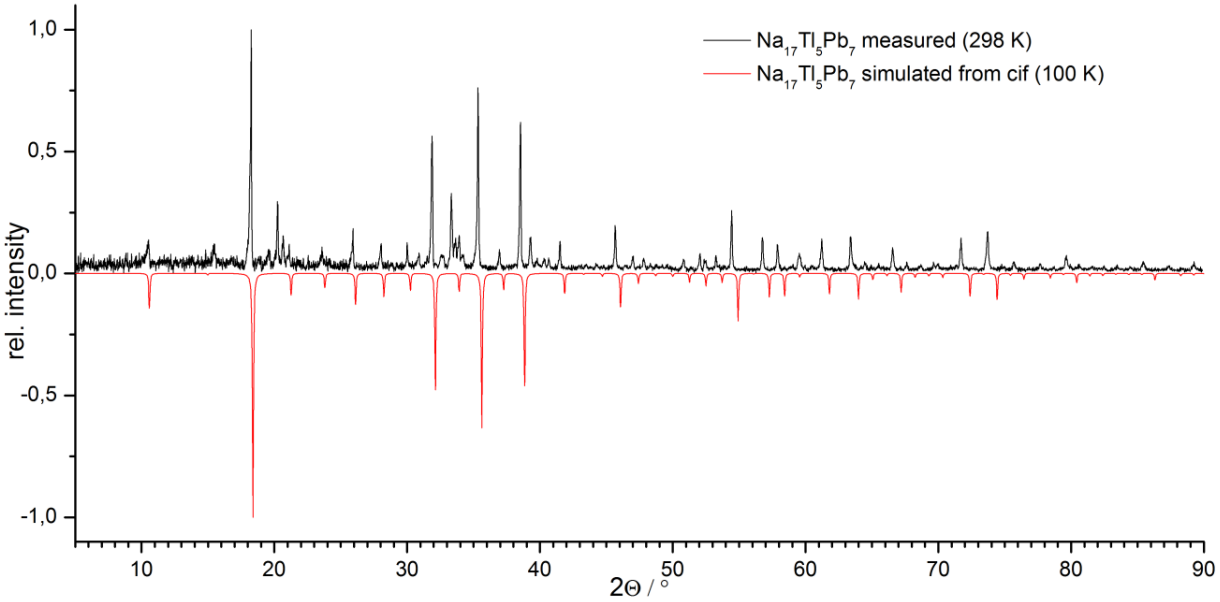

Figure S54. Comparison of the measured diffraction pattern (black line) of "$Na_{17}Tl_5Pb_7$" and simulated diffraction pattern of $Na_{17}Tl_5Pb_7$ (1, red line).

4.4. PXRD Data of "K_5TlPb_3" (II)

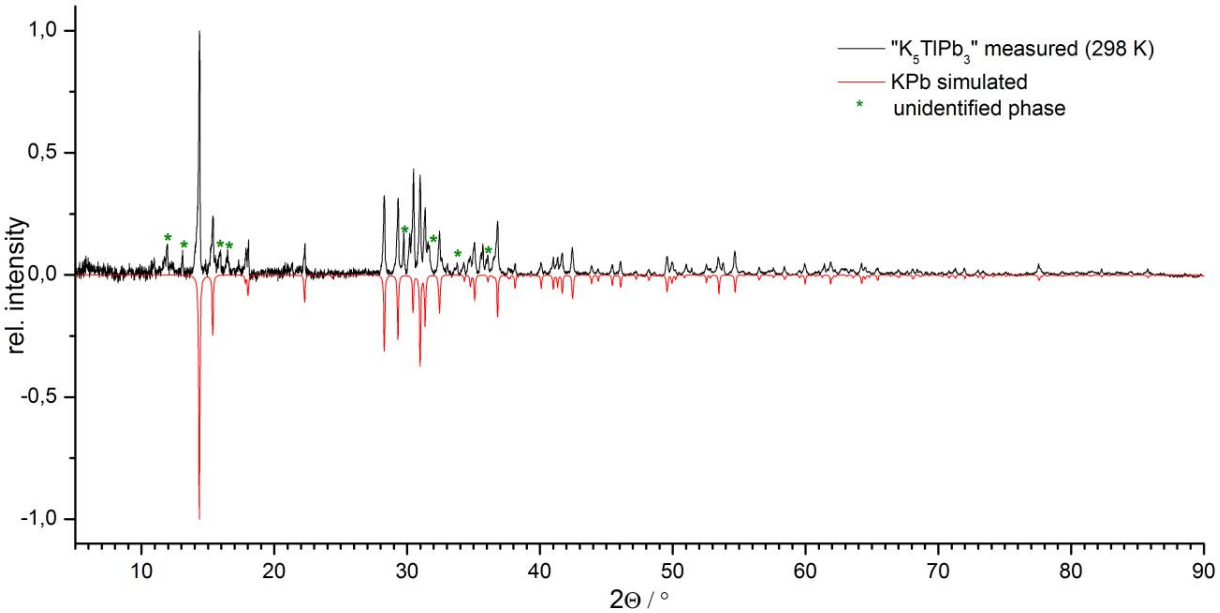

Figure S55. Comparison of the measured diffraction pattern (black line) of "K_5TlPb_3" (II) and simulated diffraction pattern of KPb[15] (red line).

4.5. PXRD Data of "$K_5Tl_2Bi_4$" (III)

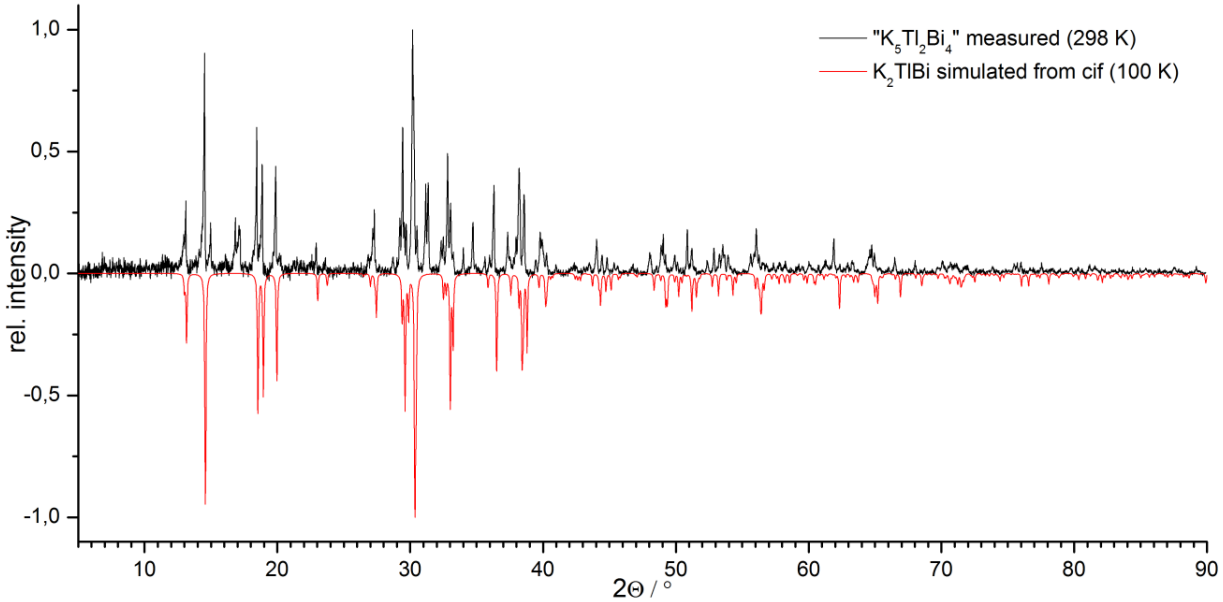

Figure S56. Comparison of the measured diffraction pattern (black line) of "$K_5Tl_2Bi_4$" (III) and simulated diffraction pattern of K_2TlBi (3, red line).

4.6. PXRD Data of "K_2TlBi" (IV)

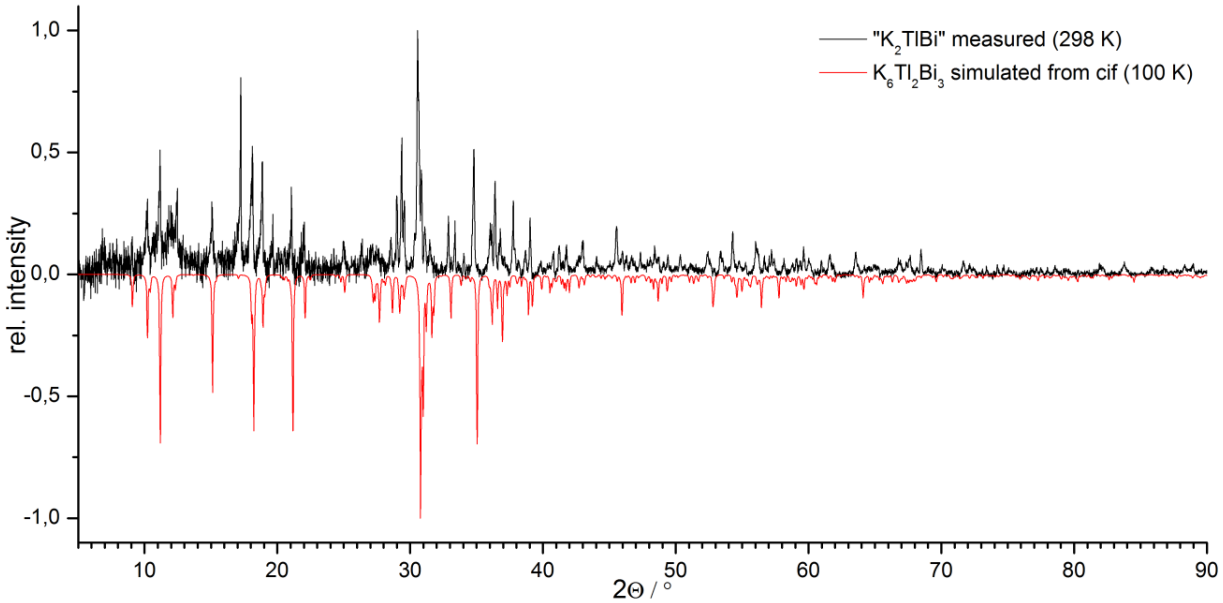

Figure S57. Comparison of the measured diffraction pattern (black line) of "K_2TlBi" (IV) and simulated diffraction pattern of $K_6Tl_2Bi_3$ (4, red line).

4.7. PXRD Data of "K_2TlBi_3" (V)

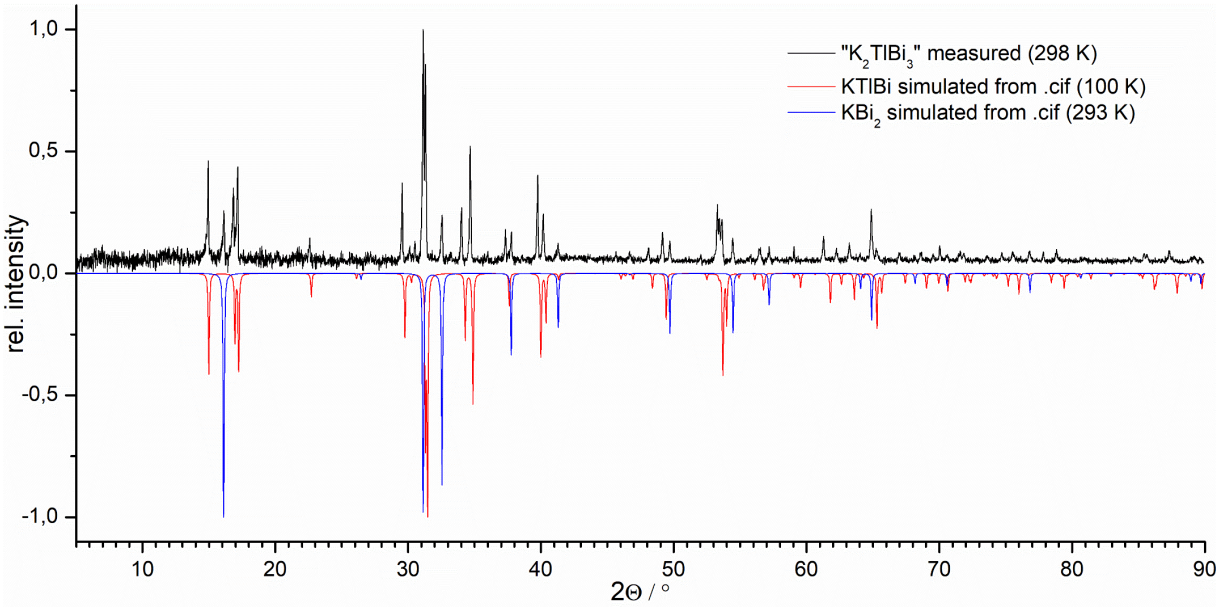

Figure S58. Comparison of the measured diffraction pattern (black line) of "K_2TlBi" (V) and simulated diffraction patterns of KTlBi (5, red line) and KBi_2 (blue line).

4.8. PXRD Data of $[K(crypt\text{-}222)]_3(Tl_4Bi_3)$ (8)

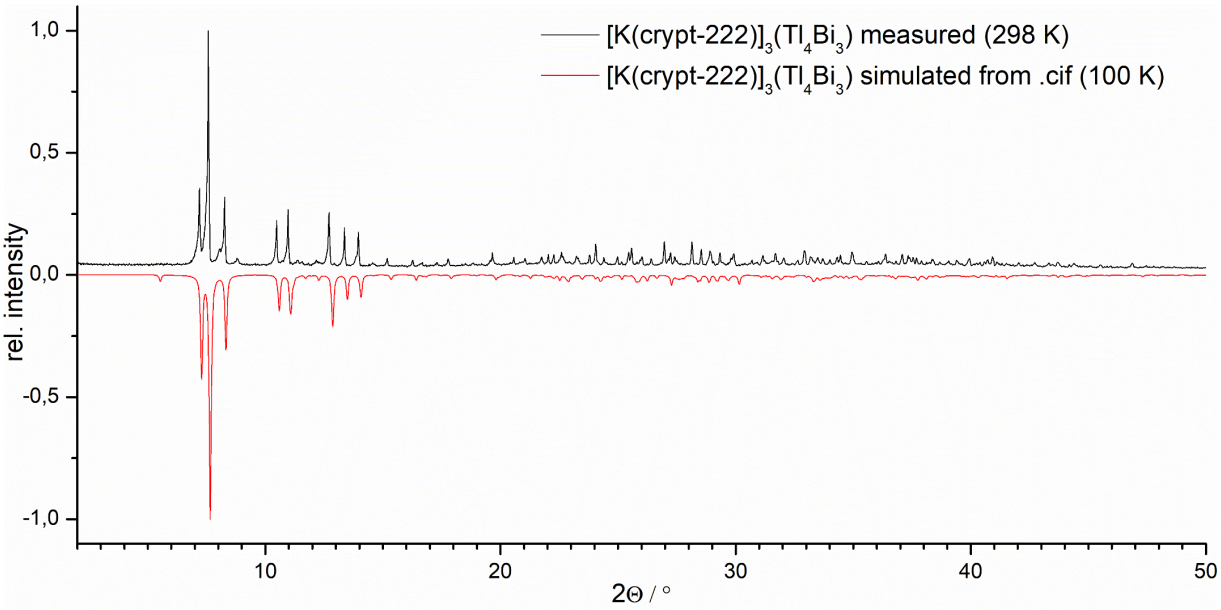

Figure S59. Comparison of the measured (black line) and simulated (red line) diffraction pattern of $[K(crypt\text{-}222)]_3(Tl_4Bi_3)$ (8).

5. Micro-X-ray Fluorescence Spectroscopy (µ-XRF)

5.1. General Procedure

All µ-XRF measurements were performed with a Bruker M4 Tornado, equipped with a Rh-target X-ray tube and a silicon drift detector. The emitted fluorescence photons are detected with an acquisition time of 100 s. Quantification of the elements is achieved through deconvolution of the spectra. Results are summarized in Table S12. Figures S60 – S62 present the measured spectra for **6** – **8** along with the results of the deconvolution algorithm. The data were collected on freshly mounted crystals that were immersed in a thin protective coating of non-drying high viscosity oil (21 cSt).

5.2. Summary of µ-XRF Results for Compounds 6 - 8

Table S12. µ-XRF analysis of 6 – 8 (Na, K, Tl, Pb, Bi).

$[Na(crypt\text{-}222)]_3(TlPb_9)_{0.94}(TlPb_{11})_{0.06}$ (6)

Element	Element wt % (exp)	Element wt % (calc)	Atom % (exp)	Atom % (calc)	Element ratio (exp)	Element ratio (calc)
Na	3.21	3.19	22.98	22.87	3.01	3
Tl	10.98	9.45	8.84	7.62	1.16	1
Pb	85.81	87.36	68.18	69.51	8.95	9.12
Total	100.00	100.00	100.00	100.00	13.12	13.12

$[K(crypt\text{-}222)]_4[Tl@Tl_4Pb_8]$ (7)

Element	Element wt % (exp)	Element wt % (calc)	Atom % (exp)	Atom % (calc)	Element ratio (exp)	Element ratio (calc)
K	5.38	5.51	23.05	23.53	3.92	4
Tl	35.82	36.03	29.37	29.41	4.99	5
Pb	58.81	58.45	47.58	47.06	8.09	8
Total	100.01	99.99	100.00	100.00	17	17

$[K(crypt\text{-}222)]_3(Tl_4Bi_3)$ (8)

Element	Element wt % (exp)	Element wt % (calc)	Atom % (exp)	Atom % (calc)	Element ratio (exp)	Element ratio (calc)
K	7.49	7.51	29.96	30	3.00	3
Tl	51.75	52.35	39.57	40	3.96	4
Bi	40.76	40.14	30.48	30	3.05	3
Total	100.00	100.00	100.01	100	10.01	10

5.3. µ-XF Spectrum of $[Na(crypt\text{-}222)]_3(TlPb_9)_{0.94}(TlPb_{11})_{0.06}$ (6)

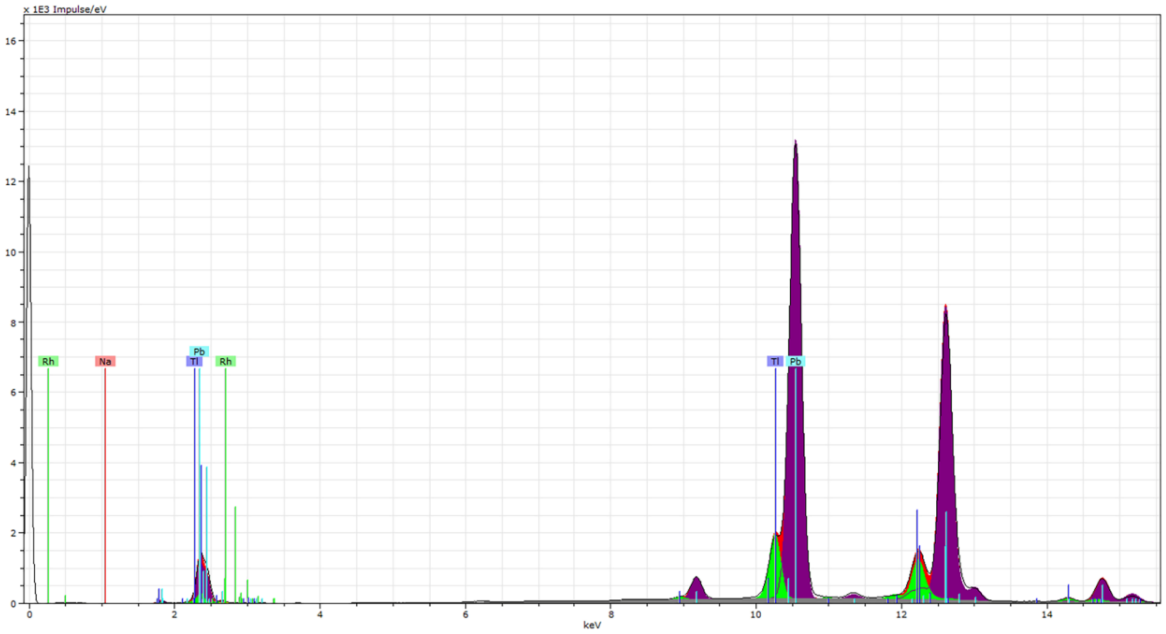

Figure S60. µ-XF spectrum of 6 (line) with the results of the deconvolution algorithm (solid, red). Colors are used as follows: Na (blue), Tl (green), Pb (purple), background (grey).

5.4. µ-XF Spectrum of $[K(crypt\text{-}222)]_4[Tl@Tl_4Pb_8]$ (7)

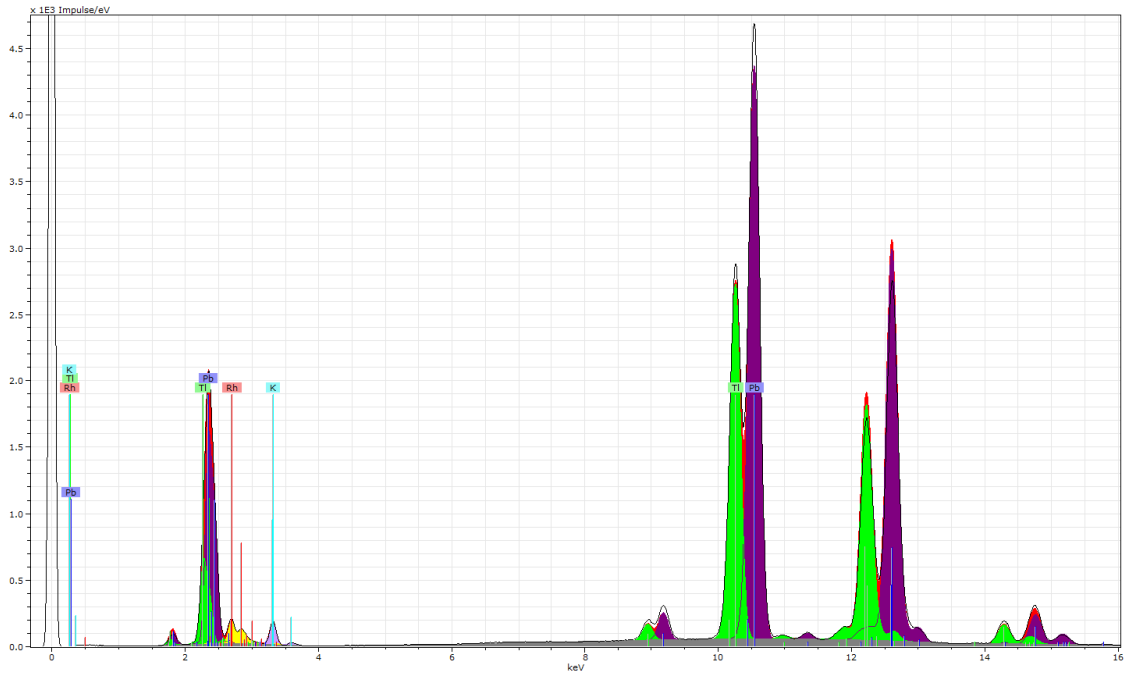

Figure S61. *µ*-XF spectrum of 7 (line) with the results of the deconvolution algorithm (solid, red). Colors are used as follows: K (pink), Tl (green), Pb (purple), background (grey).

5.5. µ-XF Spectrum of $[K(crypt\text{-}222)]_3(Tl_4Bi_3)$ (8)

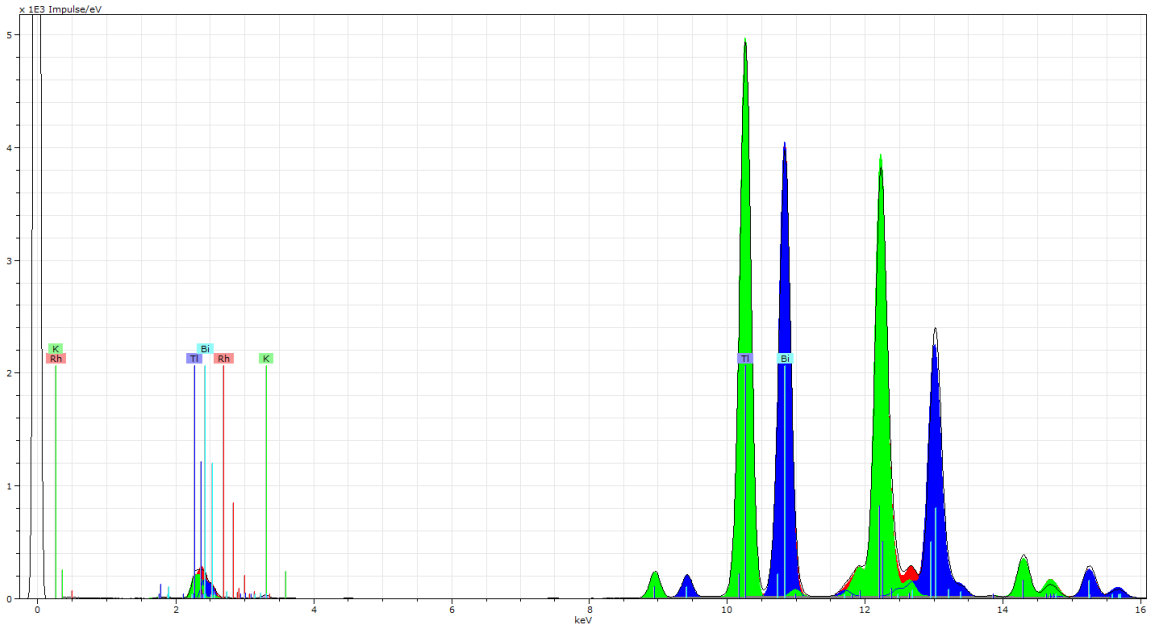

Figure S62. *µ*-XF spectrum of 8 (line) with the results of the deconvolution algorithm (solid, red). Colors are used as follows: K (pink), Tl (green), Bi (blue), background (grey).

6. Quantum Chemical Investigations

6.1. Methods

All quantum chemical calculations presented in this chapter were performed with a pre-version of TURBOMOLE V7.3.[16] The two-component self-consistent relativistic all-electron method X2C[17] was applied, which accounts for spin-orbit interaction in self-consistent manner. We employed the density functional TPSS,[18] optimized basis sets of type x2c-TZVPall-2c[19] and corresponding auxiliary basis sets.[19] The diagonal local approximation to the unitary decoupling transformation (DLU)[20] was applied both for the calculation of energies[21] and gradients.[22] The finite nucleus model based on a Gaussian charge distribution was applied.[22-23] For compensation of the negative charge the conductor-like screening model (COSMO)[24] was employed.

6.2. Isomer analysis of the $(TlPb_9)^{3-}$ anion

In a bi-capped tetragonal antiprismatic geometry there are two different positions one atom can theoretically occupy. Either, the unique atom is located in one of the two capping positions (positions 1 and 10 in figure S43) or in one of the eight ring positions (positions 2 – 9 in figure S43). Optimizations of structural parameters were performed for both isomers. A comparison of the energies of both isomers revealed a preference for the capping position by 17 kJ/mol. Very reasonable agreement of calculated and measured distances is obtained, if the Tl atom is assigned to position 10: For the distances a) apical Pb to upper ring, b) within upper ring, c) upper to lower ring, d) within lower ring and e) lower ring to Tl we calculate 309.5/336.6/312.1/323.0/319.8 pm, which means differences of 1.7/3.0/2.9/-0.9/4.5 pm to the mean values of measured data listed in Table S12.

Table S12. Cartesian coordinates (in atomic units) and total energies (in Hartree) of the two isomers of $(TlPb_9)^{3-}$ with D_{4d}- symmetric topology.

Isomer 1 (E = -208474.2273290 E_h)				**Isomer 2** (E = -208474.2209082 E_h)			
Pb	-0.0000814	2.2836453	1.2543041	Tl	2.4924112	-1.3102043	0.0000675
Tl	-0.0000282	0.0000278	3.4828431	Pb	0.0726526	-3.2353742	0.000041
Pb	-1.6828483	1.6830977	-1.3044308	Pb	1.6496401	1.2302609	1.6424501
Pb	0.0001007	-2.2836608	1.2543289	Pb	-2.3734287	-1.2735052	-0.0000883
Pb	1.6828524	-1.6830988	-1.304437	Pb	-1.7090395	1.2983121	-1.6545549
Pb	1.6830923	1.6830843	-1.3043121	Pb	1.6495953	1.2304164	-1.6426099
Pb	2.2839392	0.0000686	1.2541427	Pb	-0.051256	-1.2608041	-2.3479551
Pb	-1.683076	-1.6831168	-1.3043058	Pb	-1.7089855	1.2982355	1.6546445
Pb	-2.283928	-0.0000892	1.2541364	Pb	-0.0513429	-1.2608426	2.3480498
Pb	-0.0000227	0.0000419	-3.2822696	Pb	0.0297534	3.2835053	-0.0000447

6.3. Isomer analyses and atomic position determinations for icosahedral anions $(Tl_4Pb_9)^{4-}$, $(Tl_5Pb_8)^{4-}$, and $(Tl_6Pb_7)^{4-}$

For all symmetry-non-redundant icosahedral isomers of $(Tl_4Pb_9)^{4-}$ (52 VE), $(Tl_5Pb_8)^{4-}$ (51 VE), and $(Tl_6Pb_7)^{4-}$ (50 VE) optimizations of structure parameters were carried out. The results are summarized in the tables S13 – S15 and illustrated in figure S64. All coordinates of favorable structures (<15 kJ/mol above the most stable isomer) are provided in the tables S16 – S18.

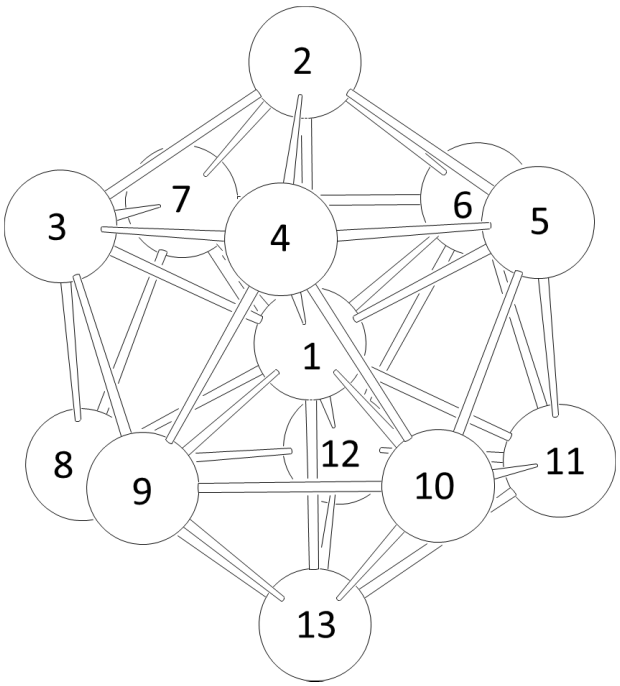

Figure S63. Atom labelling in the filled icosahedral clusters, as referred to in the Tables S13 – S15.

Table S13. Energy and structure data for all symmetry-non-redundant isomers of $(Tl_4Pb_9)^{4-}$, specified by the positions occupied by Tl, column 1; see also Figure S63. *E*, in kJ/mol denotes the energy relative to the most stable isomer; d_{CS} and d_{SS} are the mean values of the distances of the 12 shell atoms to the core atom and the mean values of the 42 distances between the shell atoms in pm. σ_{CS} and σ_{SS} are the corresponding standard deviations.

Tl positions	*E / kJ/mol*	d_{CS} / pm	σ_{CS} / pm	d_{SS} / pm	σ_{SS} / pm
5,6,8,9	0.0	323.18	3.87	339.72	11.30
2,6,8,10	8.5	322.93	5.42	339.59	7.02
2,3,5,8	10.9	323.51	6.65	340.01	13.10
3,5,6,8	11.4	322.86	3.50	339.47	7.05
1,4,6,8	11.5	323.24	18.05	339.55	22.06
2,4,6,8	16.1	322.91	5.33	339.52	6.99
1,2,5,8	18.6	322.70	16.39	339.14	21.00
1,2,3,5	20.8	323.04	18.00	339.51	22.10
3,4,5,6	22.9	322.96	5.37	339.51	8.09
2,3,4,6	29.1	322.97	4.83	339.51	8.86
2,3,4,5	35.7	322.96	4.07	339.44	9.59
1,3,4,6	37.0	323.03	18.26	339.41	21.48
1,2,3,4	38.5	323.13	20.19	339.71	23.83

Table S14. Energy and structure data for all symmetry-non-redundant isomers of $(Tl_5Pb_8)^{4-}$. For details see Table S13.

Tl positions	*E / kJ/mol*	d_{CS} / pm	σ_{CS} / pm	d_{SS} / pm	σ_{SS} / pm
1,5,6,8,9	0.0	319.23	3.02	335.63	7.30
1,2,6,8,10	1.1	319.49	7.33	336.02	7.10
1,3,5,6,8	6.8	319.30	4.45	335.75	5.39
1,2,3,5,8	7.0	319.60	6.30	335.96	8.99
1,2,4,6,8	7.8	319.55	7.07	336.00	6.78
3,5,6,8,10	12.6	321.95	5.15	338.57	5.32
1,3,4,5,6	13.6	319.64	7.07	336.02	7.69
2,5,6,8,9	14.3	321.83	2.69	338.37	5.54
2,3,6,8,10	16.7	322.02	6.36	338.65	4.82
1,2,3,4,6	18.3	319.73	6.73	336.06	8.29
3,4,5,6,8	18.6	321.97	4.76	338.51	5.69
1,2,3,4,5	23.6	319.85	6.44	336.08	8.91
2,3,5,6,8	24.8	322.00	4.19	338.47	5.79
2,3,4,5,8	29.4	322.05	3.76	338.43	6.66
3,4,5,6,7	29.6	322.06	5.53	338.52	4.75
2,3,4,5,6	38.9	322.27	4.89	338.57	6.74

Table S15. Energy and structure data for all symmetry-non-redundant isomers of $(Tl_6Pb_7)^{4-}$. For details see Table S13.

Tl positions	*E / kJ/mol*	d_{CS} / pm	σ_{CS} / pm	d_{SS} / pm	σ_{SS} / pm
1,3,5,6,8,10	0.0	318.10	6.29	334.57	4.08
1,2,3,6,8,10	0.7	318.36	7.62	334.84	4.63
1,2,5,6,8,9	4.4	318.01	4.35	334.36	3.77
1,3,4,5,6,8	6.2	318.16	5.76	334.55	4.00
1,2,3,5,6,8	11.9	318.29	5.45	334.57	4.31
1,3,4,5,6,7	13.4	318.38	5.97	334.72	4.47
1,2,3,4,5,8	16.5	318.48	5.80	334.62	4.82
1,2,3,4,5,6	21.6	318.90	6.78	334.93	5.93
2,4,6,8,9,11	53.7	321.22	6.69	337.85	4.38
2,4,7,8,9,11	56.1	321.44	7.91	338.08	4.96
5,6,7,8,9,10	57.1	320.74	2.43	337.26	2.64
4,5,6,7,8,9	58.3	320.98	4.63	337.52	3.66
2,3,5,6,8,9	58.4	321.14	4.00	337.53	4.71
2,3,5,6,8,10	58.5	321.34	6.63	337.84	4.89
2,3,4,6,8,10	61.1	321.64	8.16	338.14	5.42
3,4,5,6,7,8	64.8	321.29	5.67	337.73	4.84
2,3,4,5,6,8	67.0	321.60	6.24	337.87	5.97
2,3,4,5,7,8	71.8	321.74	5.97	337.89	6.50
2,3,4,6,7,8	73.9	322.03	7.57	338.17	7.06
2,3,4,5,6,7	77.7	322.06	7.00	338.10	7.46

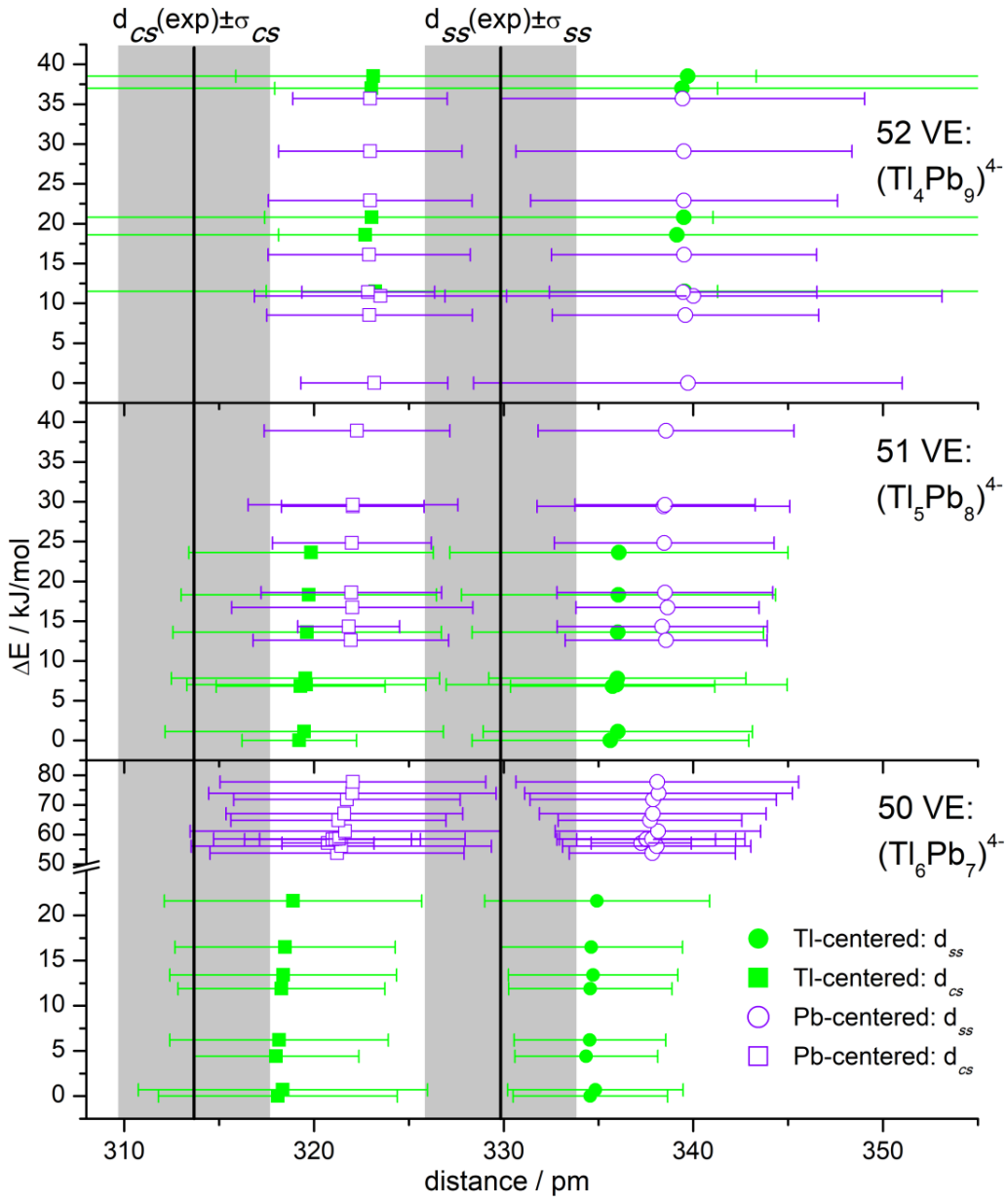

Figure S64. Graphical summary of the isomer analyses for $(Tl_4Pb_9)^{4-}$ (52 VE), $(Tl_5Pb_8)^{4-}$ (51 VE), and $(Tl_6Pb_7)^{4-}$ (50 VE). Shown are the mean values of the average core-shell (*cs*, square), and shell-shell (*ss*, circles) interatomic distances along with the respective standard deviations (bars). Green data points represent Tl-centered isomers and purple data points represent Pb-centered isomers. The according experimental values obtained from the crystal structure of compound 8 are represented as black lines (average) and grey rectangles (std. deviation).

Table S16. Cartesian coordinates (in atomic units) of isomers of $(Tl_4Pb_9)^{4-}$ with relative energies lower than 15 kJ/mol. The total energy of the most stable isomer is -269292.187135 Hartree.

Isomer 1				**Isomer 2** (ΔE = + 8.5 kJ/mol)			
Pb	0.0001948	-0.0000601	-0.0003606	Pb	0.0000336	-0.0002858	0.0055616
Pb	-1.5856027	-0.000112	2.8755762	Tl	-0.0001152	1.7796661	2.7602698
Pb	1.5855748	-0.0000871	2.8758523	Pb	1.6385056	2.7962737	-0.0045365
Pb	-0.0001621	2.6754622	1.7690551	Pb	-1.6384081	2.7964083	-0.0043459
Tl	-2.7032106	1.7189705	0.0001831	Pb	-2.678297	0.0000897	1.6358456
Tl	-2.7032969	-1.718749	0.0002088	Tl	0.000141	-1.7796748	2.7606494
Pb	-0.0000722	-2.6756212	1.7693011	Pb	2.6782961	0.0001804	1.6359419
Tl	2.7032874	-1.7190069	0.0003888	Tl	2.7929001	0.0003173	-1.724729
Tl	2.7034583	1.719048	0.0001069	Pb	0.0000416	1.7486506	-2.6653576
Pb	-0.0001679	2.6757279	-1.7690761	Tl	-2.793039	0.0001669	-1.7247345
Pb	-1.5859249	0.0001789	-2.8758736	Pb	-1.6387669	-2.7963341	-0.0045035
Pb	0.0001866	-2.6757478	-1.7690342	Pb	1.6386699	-2.7966242	-0.0044186
Pb	1.5857357	-0.0000033	-2.8763277	Pb	0.0000383	-1.7488341	-2.6656426
Isomer 3 (ΔE = + 10.9 kJ/mol)				**Isomer 4** (ΔE = + 11.4 kJ/mol)			
Pb	0.0001109	-0.0001488	0.056725	Pb	-0.000136	-0.000275	0.0316745
Tl	-1.3594351	1.0495669	2.731058	Pb	0.4821981	1.5805996	2.754466
Tl	1.3594071	-1.0494259	2.7315544	Tl	2.692217	-0.6899502	1.7643635
Pb	1.941643	2.0894121	1.5726926	Pb	2.3684023	2.1648392	-0.0205534
Tl	-0.9353646	3.0662239	-0.014314	Tl	-0.8734676	3.1101915	-0.0064546
Pb	-3.2791896	0.3318754	-0.0219534	Tl	-2.6920215	0.6904819	1.7644759
Pb	-1.9417408	-2.0894418	1.5727678	Pb	-0.4822513	-1.5807574	2.7550238
Tl	0.9353151	-3.0662843	-0.0144059	Tl	0.8736715	-3.1102283	-0.0064098
Pb	3.2793344	-0.3318522	-0.0220139	Pb	2.5944816	-0.650895	-1.7286496
Pb	1.9475699	2.1065741	-1.6511076	Pb	0.482752	1.5971418	-2.7790435
Pb	-1.2770415	1.0267624	-2.6447183	Pb	-2.5943988	0.6510549	-1.728659
Pb	-1.9476781	-2.1065582	-1.6511623	Pb	-2.3686476	-2.1650722	-0.0207726
Pb	1.2770692	-1.0267036	-2.6451223	Pb	-0.4827997	-1.5971308	-2.7794612

Isomer 5 (ΔE = + 11.5 kJ/mol)			
Tl	-0.0017032	0.0002965	0.1149539
Pb	-0.8955811	-1.5552239	2.8803306
Pb	-0.8954126	1.5547072	2.8810427
Tl	-3.0758468	0.0002416	0.6918744
Pb	-1.4509948	-2.5063648	-0.7574796
Tl	1.5357833	-2.6672519	0.6874772
Pb	1.7989833	-0.0004091	2.8731365
Tl	1.5357191	2.6676883	0.6876825
Pb	-1.4511113	2.5066231	-0.75807
Pb	-1.8192862	-0.0001799	-2.854706
Pb	0.9124354	-1.5784566	-2.847914
Pb	2.8945613	0.0001529	-0.7495559
Pb	0.9124535	1.5781766	-2.8487722

Table S17. Cartesian coordinates (in atomic units)of isomers of $(Tl_5Pb_8)^{4-}$ with relative energies lower than 15 kJ/mol. The total energy of the most stable isomer is -268653.558701 Hartree.

Isomer 1				**Isomer 2** (ΔE = + 1.1 kJ/mol)			
Tl	0.0002396	-0.0000755	-0.0004203	Tl	0.0000799	-0.0003189	0.0117805
Pb	-1.6054231	-0.0003282	2.8047535	Tl	-0.0000145	1.7783826	2.7352884
Pb	1.6054093	-0.0000712	2.8050471	Pb	1.62282	2.7943134	-0.0043256
Pb	-0.0001955	2.6615865	1.7105824	Pb	-1.6231284	2.7943838	-0.0041686
Tl	-2.6958117	1.6873806	0.000197	Pb	-2.6106657	0.0001361	1.6047685
Tl	-2.6958132	-1.6872782	0.0003871	Tl	0.0001836	-1.7782665	2.7357141
Pb	-0.0000634	-2.6618992	1.7112255	Pb	2.6109263	0.0003156	1.6048865
Tl	2.6958276	-1.6874382	0.0004578	Tl	2.7553805	0.0008211	-1.7054526
Tl	2.6960096	1.6875084	0.0002101	Pb	-0.0001741	1.7091855	-2.6318061
Pb	-0.0000876	2.6620184	-1.7109166	Tl	-2.7554366	-0.0007368	-1.7055333
Pb	-1.6056733	0.0004027	-2.8052153	Pb	-1.6232554	-2.7941218	-0.0043836
Pb	0.0000188	-2.6618727	-1.7106386	Pb	1.6233071	-2.7944127	-0.0045139
Pb	1.6055628	0.0000666	-2.8056698	Pb	-0.0000227	-1.7096812	-2.6322543
Isomer 3 (ΔE = + 6.7 kJ/mol)				**Isomer 4** (ΔE = + 7.0 kJ/mol)			
Tl	-0.0004218	0.0000259	0.0358211	Tl	0.0001179	-0.000182	0.066286
Pb	0.4562559	1.5753832	2.7357783	Tl	-1.3180459	1.063321	2.7008252
Tl	2.6578203	-0.7071358	1.7443261	Tl	1.3179406	-1.0631866	2.7013741
Pb	2.3108115	2.1397313	-0.0183412	Pb	1.8670558	2.0722803	1.5803092
Tl	-0.8761646	3.0768137	-0.0107047	Tl	-0.9443388	3.0424256	-0.0145693
Tl	-2.6574887	0.7070457	1.7437411	Pb	-3.2201303	0.3777984	-0.0249393
Pb	-0.4558276	-1.5751805	2.7364738	Pb	-1.8672041	-2.0723358	1.5804247
Tl	0.8765504	-3.0757145	-0.0109174	Tl	0.9443828	-3.0424015	-0.0146517
Pb	2.5457202	-0.6819415	-1.6954355	Pb	3.2202904	-0.3777747	-0.025119
Pb	0.4627129	1.5861882	-2.7730684	Pb	1.8870845	2.0923223	-1.6566913
Pb	-2.5459835	0.6817475	-1.6959514	Pb	-1.2477938	1.0377735	-2.6180362
Pb	-2.3111897	-2.1401103	-0.0189668	Pb	-1.8871745	-2.0923242	-1.6567532
Pb	-0.4627953	-1.5868529	-2.772755	Pb	1.2478154	-1.0377164	-2.6184592
Isomer 5 (ΔE = + 7.8 kJ/mol)				**Isomer 6** (ΔE = + 12.5 kJ/mol)			
Tl	0.0108767	-0.0665438	-0.0001449	Pb	0.0026119	-0.0265526	0.0001576
Tl	0.0615404	-3.2342994	0.000133	Pb	1.6241734	-2.2025373	-1.6741994
Pb	2.3628962	-1.4303029	1.6292106	Tl	3.2875721	0.1875458	0.0000967
Tl	-0.8996684	-1.4260314	2.7461673	Pb	1.6248894	-2.2027974	1.6735289
Pb	-2.8530079	-1.295324	0.000088	Tl	-1.1936452	-2.9932157	-0.0000188
Tl	-0.9000064	-1.4256468	-2.7463053	Tl	-1.3865916	-0.9870051	-2.8075475
Pb	2.3630019	-1.4307354	-1.6292039	Pb	1.3233146	0.9567148	-2.6883199
Tl	2.9776459	1.4281335	0.000214	Tl	1.206374	3.0021694	0.0000946
Pb	0.8431397	1.3925337	2.6190725	Pb	1.32317	0.9569639	2.688411
Pb	-2.3788522	1.4751648	1.6456871	Tl	-1.3868154	-0.9867225	2.8078873
Pb	-2.3789043	1.4750185	-1.6456713	Pb	-3.1560827	-0.1474488	-0.0001379
Pb	0.843319	1.3926449	-2.6191439	Pb	-1.6343579	2.2214322	-1.6694839
Pb	-0.0519806	3.1453883	-0.0001031	Pb	-1.6346126	2.2214534	1.6695313

	Isomer 7 (ΔE = + 13.6 kJ/mol)				**Isomer 8** (ΔE = + 14.3 kJ/mol)		
Tl	0.0314587	0.0762362	-0.0000847	Pb	-0.0055948	-0.0430897	-0.0000187
Pb	-0.1358013	3.1876258	-0.0002622	Tl	0.0702605	-3.2747106	-0.0001115
Tl	-0.9410611	1.4876878	2.7538065	Pb	2.8512643	-1.4752615	0.0001319
Tl	2.324353	1.3959078	1.6900287	Pb	0.901336	-1.4179308	2.7236922
Tl	2.323837	1.3968881	-1.6899924	Tl	-2.3241647	-1.4037348	1.7304912
Tl	-0.9416267	1.4876816	-2.7540417	Tl	-2.3242532	-1.4035	-1.7302533
Pb	-2.8814442	1.5020581	0.000008	Pb	0.9013704	-1.4178415	-2.7238186
Pb	-2.2383701	-1.3782876	1.623592	Tl	2.3303079	1.4311864	-1.7249751
Pb	0.8851255	-1.4747446	2.6286192	Tl	2.3307363	1.4310317	1.7249276
Pb	2.8347136	-1.5428027	0.0003314	Pb	-0.9044832	1.4511428	2.7208061
Pb	0.8855767	-1.4742994	-2.6284008	Pb	-2.8550062	1.5021855	0.0002367
Pb	-2.2383111	-1.3790884	-1.6234592	Pb	-0.9047458	1.4510545	-2.7208791
Pb	0.09155	-3.2848628	-0.0001448	Pb	-0.0670274	3.1694679	-0.0002296

Table S18. Cartesian coordinates (in atomic units) of isomers of $(Tl_6Pb_7)^{4-}$ with relative energies lower than 15 kJ/mol. The total energy of the most stable isomer is -268014.944171 Hartree.

Isomer 1				**Isomer 2** (ΔE = + 0.7 kJ/mol)			
Tl	0.0002396	-0.0000755	-0.0004203	Tl	0.0000799	-0.0003189	0.0117805
Pb	-1.6054231	-0.0003282	2.8047535	Tl	-0.0000145	1.7783826	2.7352884
Pb	1.6054093	-0.0000712	2.8050471	Pb	1.62282	2.7943134	-0.0043256
Pb	-0.0001955	2.6615865	1.7105824	Pb	-1.6231284	2.7943838	-0.0041686
Tl	-2.6958117	1.6873806	0.000197	Pb	-2.6106657	0.0001361	1.6047685
Tl	-2.6958132	-1.6872782	0.0003871	Tl	0.0001836	-1.7782665	2.7357141
Pb	-0.0000634	-2.6618992	1.7112255	Pb	2.6109263	0.0003156	1.6048865
Tl	2.6958276	-1.6874382	0.0004578	Tl	2.7553805	0.0008211	-1.7054526
Tl	2.6960096	1.6875084	0.0002101	Pb	-0.0001741	1.7091855	-2.6318061
Pb	-0.0000876	2.6620184	-1.7109166	Tl	-2.7554366	-0.0007368	-1.7055333
Pb	-1.6056733	0.0004027	-2.8052153	Pb	-1.6232554	-2.7941218	-0.0043836
Pb	0.0000188	-2.6618727	-1.7106386	Pb	1.6233071	-2.7944127	-0.0045139
Pb	1.6055628	0.0000666	-2.8056698	Pb	-0.0000227	-1.7096812	-2.6322543
Isomer 3 (ΔE = + 4.4 kJ/mol)				**Isomer 4** (ΔE = + 6.2 kJ/mol)			
Tl	-0.0004218	0.0000259	0.0358211	Tl	0.0001179	-0.000182	0.066286
Pb	0.4562559	1.5753832	2.7357783	Tl	-1.3180459	1.063321	2.7008252
Tl	2.6578203	-0.7071358	1.7443261	Tl	1.3179406	-1.0631866	2.7013741
Pb	2.3108115	2.1397313	-0.0183412	Pb	1.8670558	2.0722803	1.5803092
Tl	-0.8761646	3.0768137	-0.0107047	Tl	-0.9443388	3.0424256	-0.0145693
Tl	-2.6574887	0.7070457	1.7437411	Pb	-3.2201303	0.3777984	-0.0249393
Pb	-0.4558276	-1.5751805	2.7364738	Pb	-1.8672041	-2.0723358	1.5804247
Tl	0.8765504	-3.0757145	-0.0109174	Tl	0.9443828	-3.0424015	-0.0146517
Pb	2.5457202	-0.6819415	-1.6954355	Pb	3.2202904	-0.3777747	-0.025119
Pb	0.4627129	1.5861882	-2.7730684	Pb	1.8870845	2.0923223	-1.6566913
Pb	-2.5459835	0.6817475	-1.6959514	Pb	-1.2477938	1.0377735	-2.6180362
Pb	-2.3111897	-2.1401103	-0.0189668	Pb	-1.8871745	-2.0923242	-1.6567532
Pb	-0.4627953	-1.5868529	-2.772755	Pb	1.2478154	-1.0377164	-2.6184592
Isomer 5 (ΔE = + 11.9 kJ/mol)				**Isomer 6** (ΔE = + 13.4 kJ/mol)			
Tl	0.0108767	-0.0665438	-0.0001449	Pb	0.0026119	-0.0265526	0.0001576
Tl	0.0615404	-3.2342994	0.000133	Pb	1.6241734	-2.2025373	-1.6741994
Pb	2.3628962	-1.4303029	1.6292106	Tl	3.2875721	0.1875458	0.0000967
Tl	-0.8996684	-1.4260314	2.7461673	Pb	1.6248894	-2.2027974	1.6735289
Pb	-2.8530079	-1.295324	0.000088	Tl	-1.1936452	-2.9932157	-0.0000188
Tl	-0.9000064	-1.4256468	-2.7463053	Tl	-1.3865916	-0.9870051	-2.8075475
Pb	2.3630019	-1.4307354	-1.6292039	Pb	1.3233146	0.9567148	-2.6883199
Tl	2.9776459	1.4281335	0.000214	Tl	1.206374	3.0021694	0.0000946
Pb	0.8431397	1.3925337	2.6190725	Pb	1.32317	0.9569639	2.688411
Pb	-2.3788522	1.4751648	1.6456871	Tl	-1.3868154	-0.9867225	2.8078873
Pb	-2.3789043	1.4750185	-1.6456713	Pb	-3.1560827	-0.1474488	-0.0001379
Pb	0.843319	1.3926449	-2.6191439	Pb	-1.6343579	2.2214322	-1.6694839
Pb	-0.0519806	3.1453883	-0.0001031	Pb	-1.6346126	2.2214534	1.6695313

6.4. Isomer analysis of the $(Tl_4Bi_3)^{3-}$ anion

There are five different possible isomers. Optimizations of structure parameters were performed for all five, starting from the same pentagonal bipyramidal geometry (taken from the Tl_7^{7-} anion in $K_{10}Tl_7$)[25]. The isomers and their final geometries are shown in figure S65, along with the relative energies of the optimized structures. The final structures are rotated in such a way that significant deviations from an idealized pentagonal bipyramidal geometry are visible best. Cartesian coordinates of the final geometries for all five isomers are given in Table S19. For the most stable isomer (isomer 5) distances for the apical Tl atom to the Tl atom in the ring are 3.395 Å, to the Bi atoms in the ring 3.230 Å (2x) and 3.259 Å; in the ring the Bi-Bi distance amounts to 3.087 Å and all Tl-Bi distances to 3.096 Å.

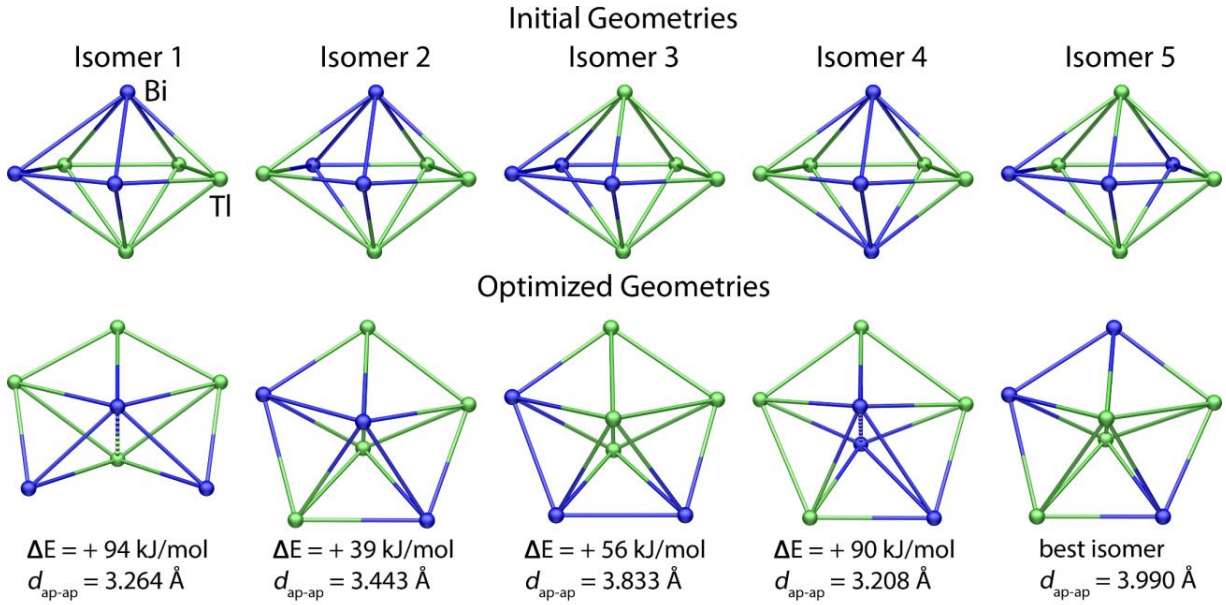

Figure S65. Comparison of the initial and optimized geometries for all five different isomers of the anion $(Tl_4Bi_3)^{3-}$ with their optimized geometries, relative energies and interatomic apical-apical distances (d_{ap-ap}).

Table S19. Cartesian coordinates (in atomic units) of all five isomers of $(Tl_4Bi_3)^{3-}$ with the according relative energies relative to the most stable isomer (5). The total energy of the most stable isomer is -145779.7241188 Hartree.

	Isomer 1 (ΔE = + 94 kJ/mol)				**Isomer 2** (ΔE = + 39 kJ/mol)		
Bi	-0.3269939	1.5308713	0.0008841	Bi	0.0247401	-1.659888	-0.0000617
Tl	-0.4057579	-1.7325254	-0.0008587	Tl	0.0489639	1.7825251	0.0000135
Bi	-1.9375087	0.0190297	2.2687252	Tl	2.7758893	0.0408279	0.0000094
Bi	-1.9374643	0.0212324	-2.2685716	Bi	0.7777659	-0.0726999	-2.6052136
Tl	1.0101359	0.0591733	-2.664847	Tl	-2.2024333	-0.0089498	-1.6122098
Tl	2.5875639	0.0465412	0.0000283	Tl	-2.2025512	-0.0095547	1.6124139
Tl	1.0100251	0.0556775	2.6646397	Bi	0.7776254	-0.0722606	2.6050483
	Isomer 3 (ΔE = + 56 kJ/mol)				**Isomer 4** (ΔE = + 90 kJ/mol)		
Tl	0.0005201	-1.9165241	-0.0921971	Bi	-0.0000128	-1.604323	-0.1778774
Tl	-0.0010081	1.9165527	-0.0914693	Bi	-0.0001772	1.6037102	-0.1769142
Bi	2.6037795	0.0012426	-0.7387968	Bi	0.0001775	0.00079	2.9573911
Bi	0.0003989	-0.0014852	-2.5549506	Tl	2.5331156	0.0001552	1.0194722
Bi	-2.604652	0.0008824	-0.7392541	Tl	1.6459879	-0.0000187	-2.3209863
Tl	-1.6013766	0.0010493	2.1080807	Tl	-1.64575	-0.0000788	-2.3209332
Tl	1.6023381	-0.0017176	2.1085872	Tl	-2.5333411	-0.0002349	1.0198478
	Isomer 5						
Tl	0.0000065	-1.9951674	0.0461516				
Tl	0.0000124	1.9952205	0.0461799				
Bi	-1.5434097	-0.0001933	2.065469				
Bi	1.5433489	0.000248	2.0653549				
Tl	2.5972097	-0.0002133	-0.8460985				
Bi	-0.000033	0.000036	-2.5309929				
Tl	-2.5971348	0.0000696	-0.846064				

7. References for the Supporting Information

[1] crypt-222: 4,7,13,16,21,24-Hexaoxa-1,10-diazabicyclo[8.8.8]hexacosane.

[2] a) W. Blase, G. Cordier, *Z. Kristallogr.* **1991**, *196*, 207-211; b) W. Blase, G. Cordier, *Z. Kristallogr.* **1990**, *193*, 319-320.

[3] M. Strohalm, D. Kavan, P. Novák, M. Volný, V. Havlíček, *Anal. Chem.* **2010**, *82*, 4648-4651.

[4] N. Lichtenberger, N. Spang, A. Eichhöfer, S. Dehnen, *Angew. Chem.* **2017**, *129*, 13436-13442; *Angew. Chem. Int. Ed.* **2017**, *56*, 13253-13258.

[5] G. M. Sheldrick, *Acta Cryst.* **2008**, *A64*, 112-122.

[6] G. M. Sheldrick, *Acta Cryst.* **2015**, *C71*, 3-8.

[7] a) Persistence of Vision Pty. Ltd. (2004) Persistence of Vision Raytracer (Version 3.7) [Computer software]. Retrieved from http://www.povray.org/download/; b) Diamond - Crystal and Molecular Structure Visualization, Crystal Impact - Dr. H. Putz & Dr. K. Brandenburg GbR, Kreuzherrenstr. 102, 53227 Bonn, Germany, http://www.crystalimpact.com/diamond.

[8] M. Asbrand, B. Eisenmann, *Z. Kristallogr.* **1992**, *198*, 283-284.

[9] L. Chi, J. D. Corbett, *Inorg. Chem.* **2001**, *40*, 2705-2708.

[10] S. Ponou, N. Müller, T. F. Fässler, U. Häussermann, *Inorg. Chem.* **2005**, *44*, 7423-7430.

[11] D. Gilde, *Z. Anorg. Allg. Chem.* **1956**, *284*, 142-143.

[12] D. Kratzert, J. J. Holstein, I. Krossing, *J. Appl. Crystallogr.* **2015**, *48*, 933-938.

[13] R. C. Burns, J. D. Corbett, *J. Am. Chem. Soc.* **1982**, *104*, 2804-2810.

[14] R. E. Marsh, D. P. Shoemaker, *Acta Crystallogr.* **1953**, *6*, 197-205.

[15] C. Röhr, *Z. Naturforsch. B: Chem. Sci.* **1995**, *50*, 802-808.

[16] TURBOMOLE V7.3 2018, a development of University of Karlsruhe and Forschungszentrum Karlsruhe GmbH, 1989-2007, TURBOMOLE GmbH, since 2007; available from http://www.turbomole.com.

[17] W. Kutzelnigg, W. J. Liu, *J. Chem. Phys.* **2005**, *123*, 241102.

[18] J. M. Tao, J. P. Perdew, V. N. Staroverov, G. E. Scuseria, *Phys. Rev. Lett.* **2003**, *91*, 146401.

[19] P. Pollak, F. Weigend, *J. Chem. Theory Comput.* **2017**, *13*, 3696-3705.

[20] D. Peng, M. Reiher, *J. Chem. Phys.* **2012**, *136*, 244108.

[21] D. Peng, N. Middendorf, F. Weigend, M. Reiher, *J. Chem. Phys.* **2013**, *138*, 184105.

[22] Y. J. Franzke, N. Middendorf, F. Weigend, *J. Chem. Phys.* **2018**, *148*, 104110.

[23] L. Visscher, K. G. Dyall, *At. Data Nucl. Data Tables* **1997**, *67*, 207-224.

[24] A. Klamt, G. Schüürmann, *J. Chem. Soc., Perkin Trans. 2* **1993**, 799-805.

[25] S. Kaskel, J. D. Corbett, *Inorg. Chem.* **2000**, *39*, 778-782.

C.4 Polybismuthide Anions as Ligands: The Homoleptic Complex $[(Bi_7)Cd(Bi_7)]^{4-}$ and the Ternary Cluster $[(Bi_6)Zn_3(TlBi_5)]^{4-}$

Supporting Information

Polybismuthide Anions as Ligands: The Homoleptic Complex $[(Bi_7)Cd(Bi_7)]^{4-}$ and the Ternary Cluster $[(Bi_6)Zn_3(TlBi_5)]^{4-}$

Niels Lichtenberger, Werner Massa, and Stefanie Dehnen*

* *Fachbereich Chemie und Wissenschaftliches Zentrum für Materialwissenschaften, Philipps-Universität Marburg, Hans-Meerwein-Straße 4, 35043 Marburg, Germany. E-mail: dehnen@chemie.uni-marburg.de*

Contents

1. Synthesis Details

1.1. General

All manipulations and reactions were performed under dry Ar atmosphere using standard Schlenk or glovebox techniques. All solvents were dried and freshly distilled prior to use. Crypt-222[1] (Merck) was dried *in vacuo* for at least 18 hours. Samples were shielded from ambient light throughout all solution-based syntheses. $[K(crypt\text{-}222)]_2(TlBi_3)\cdot 0.5en$ (**A**) was prepared according to a literature procedure.[2] MPh_2 were prepared according to modified literature procedures[3] (M = Zn, Cd, Hg) and purified by sublimation before use.

1.2. Syntheses

1.2.1. Synthesis of $[K(crypt\text{-}222)]_4[(Bi_7)Cd(Bi_7)]\cdot en$ (1)

200 mg (118 µmol, 1 eq) of $[K(crypt\text{-}222)]_2(TlBi_3)\cdot 0.5en$ (**A**) and 11 mg (41 µmol, 0.35 eq) of $CdPh_2$ are combined in a Schlenk tube and dissolved in 5 mL of en. The initially dark green solution quickly turns goldish brown upon stirring. After 3 h of stirring at room temperature the solution is filtered, layered with 5 mL of THF and subsequently stored at 5 °C. Crystals of **1** form as long, black metallic needles besides large, black metallic blocks of $[K(crypt\text{-}222)]_3(Tl_4Bi_5)\cdot 1.5en$ (**B**)[2] on the wall of the Schlenk tube after several days. The determination of a crystalline yield was not possible due to the presence of two different types of crystals which could not be separated in bulk.

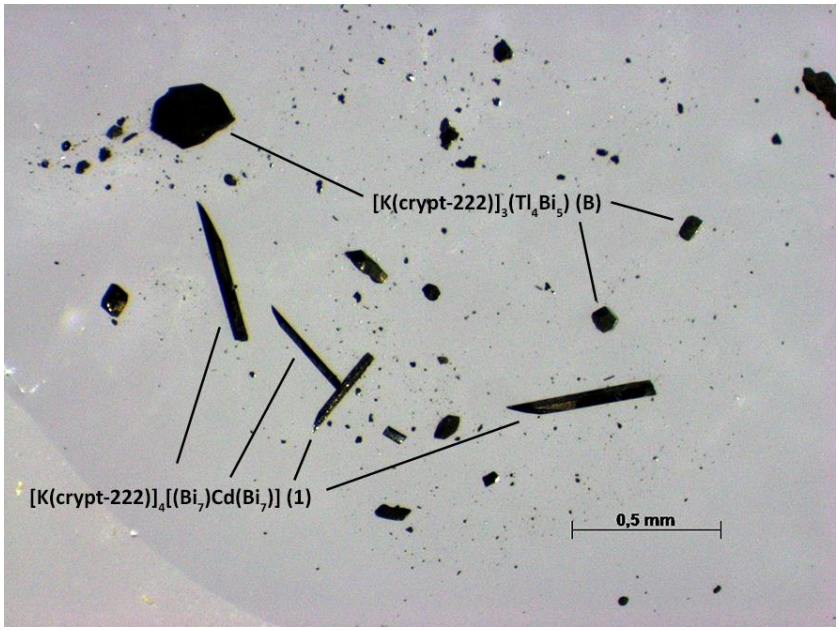

Figure S1. Photography of the crystal mixture of **1** and **B** immersed in oil.

1.2.2. Synthesis of $[K(crypt\text{-}222)]_7[(Bi_6)Zn_3(TlBi_5)](Tl_4Bi_5)_{0.935}(Bi_7)_{0.065}$ (2)

200 mg (118 µmol, 1 eq) of $[K(crypt\text{-}222)]_2(TlBi_3)\cdot 0.5en$ and 18 mg (83 µmol, 0.7 eq) of $ZnPh_2$ are combined in a Schlenk tube and dissolved in 5 mL of en. The initially dark green solution quickly turns goldish brown upon stirring. After 3 h of stirring at room temperature the solution is filtered, layered with 5 mL of THF and subsequently stored at 5 deg. C. Few crystals of **2** formed as tiny, black metallic, hexagonal plates besides a majority of large, black metallic blocks of $[K(crypt\text{-}222)]_3(Tl_4Bi_5)\cdot 1.5en$ (**B**) on the wall of the Schlenk tube after several days. The determination of a crystalline yield was not possible due to the presence of two different types of crystals which could not be separated in bulk.

2. Mass Spectrometry

2.1. General Procedure

All mass spectra were recorded with a Thermo Fischer Scientific Finnigan LTQ-FT spectrometer in negative ion mode. Single crystals of the compound **1** were dissolved in freshly distilled DMF inside a glovebox and filtered through 0.2 µm PTFE syringe filters. Reaction solutions of $[K(crypt\text{-}222)]_2(TlBi_3)$ (**A**)[2] with MPh_2 (M = Zn, Cd, Hg) in en were prepared in a Glovebox, filtered through 0.2 µm PTFE syringe filters, and diluted with en to achieve a suitable concentration for mass spectrometry (noticeable but pale color). All solutions were ingested into the spectrometer with gastight 250 or 500 µL Hamilton syringes by syringe pump infusion. All capillaries within the system were washed with dry DMF or en respectively for 2 hours before and at least 10 minutes in between measurements to avoid decomposition reactions and consequent clogging. Spectra were inspected and simulations created using the *mMass* software suite.[4]

2.2. Results of the Mass Spectrometry

None of the recorded spectra showed parent peaks of the cluster species found in the crystal structures of **1** and **2**. In all cases the most dominant signals were those of the $(Tl_4Bi_5)^-$ anion and its fragmentation products, as expected due to the presence of large amounts of $[K(crypt\text{-}222)]_3(Tl_4Bi_5)$ (**A**) in all samples. The mass spectrum of this compound and the anions fragmentation pathway was reported before.[2]

However, in all cases signals corresponding to the Bi_7^- anion are observed, supporting the presence of Bi_7^{3-} ions in solution. There are no reports of mass spectrometric observations of any of the known $[(E_7)M(E_7)]^{4-}$ clusters, most likely due to a high fragmentation tendency of the (E_7)-M bonds.

All mass spectra of the reaction solutions look almost identical with only slight variations in the relative signal intensities. Again, in no case are fragments with obvious transition metal isotopic patterns observable and the spectra are dominated by the $(Tl_4Bi_5)^-$ anion signal and its fragmentation products.

Overviews over the mass spectra of the reaction solutions are provided in Figure S2. A comparison between the mass spectrum of a crystal mixture of **1** and **B** with that of the according reaction solution is provided in Figure S3. High resolution signals of the Bi_{11}^- and Bi_7^- ions detected in the mass spectrum of **1** and **B** in DMF are shown in Figure S4 along with the corresponding simulations.

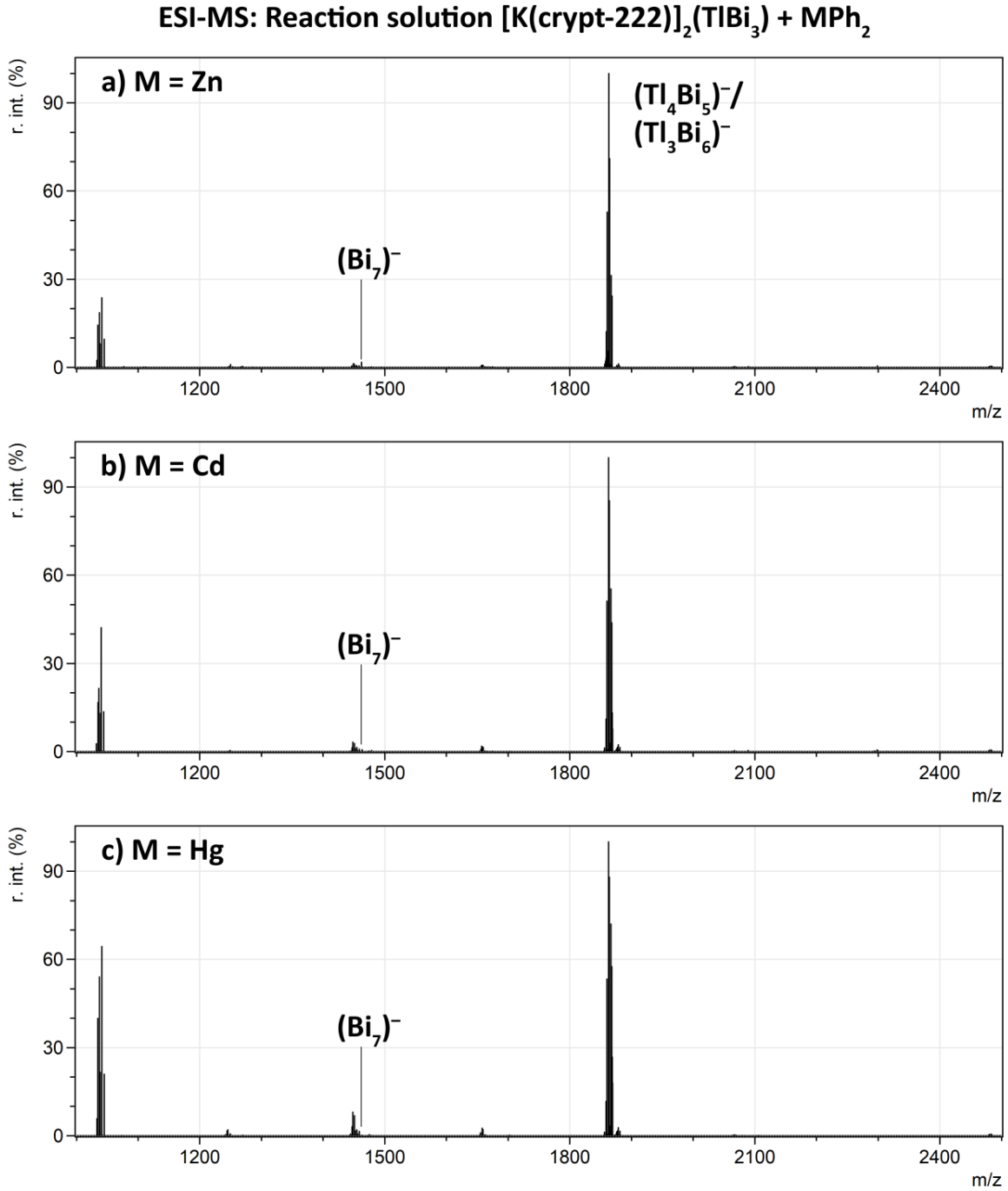

Figure S2. Comparison of recorded mass spectra of the reaction solutions of [K(crypt-222)]$_2$(TlBi$_3$) (**A**) with MPh$_2$ (M = Zn (a), Cd (b), Hg (c)) in the mass range of m/z = 1000 – 2500.

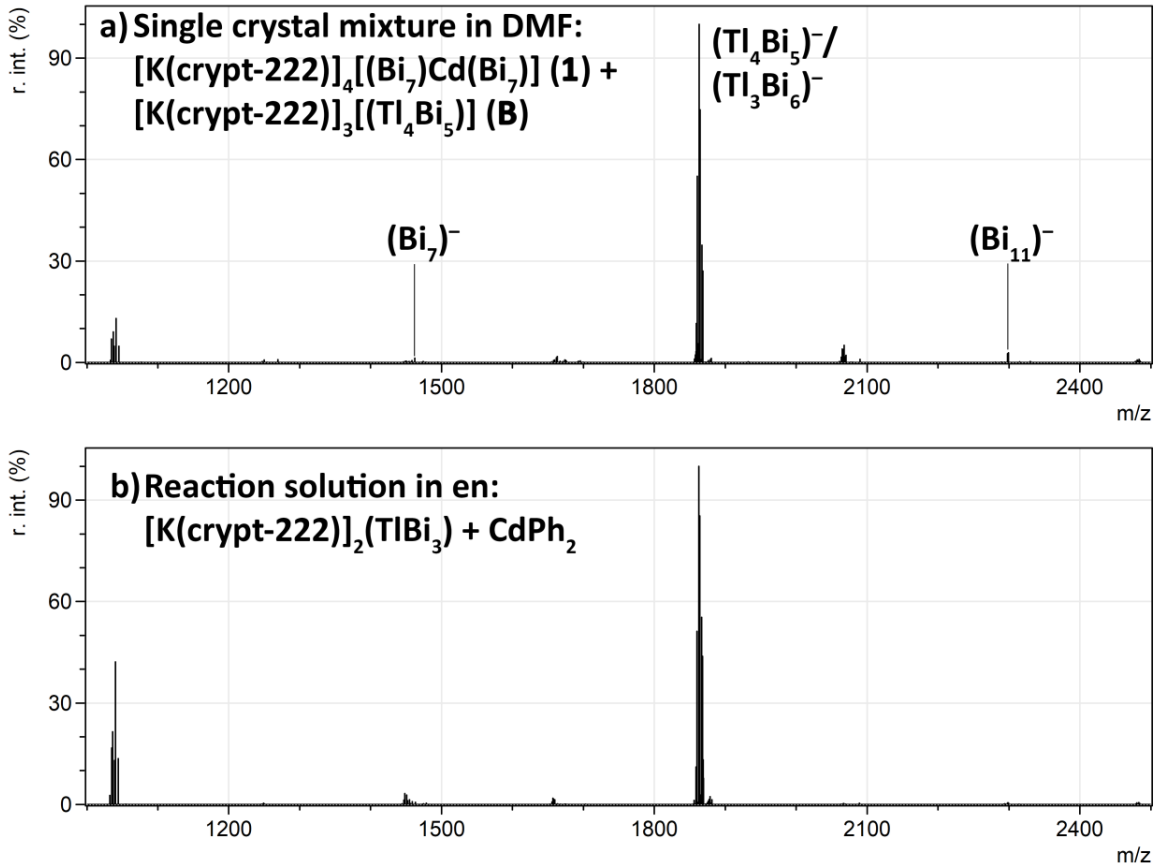

Figure S3. Comparison of recorded mass spectra of a crystal mixture of compounds 1 and B (a) with the reaction solution of $[K(crypt\text{-}222)]_2(TlBi_3)$ (**A**) with $CdPh_2$ in the mass range of m/z = 1000 – 2500.

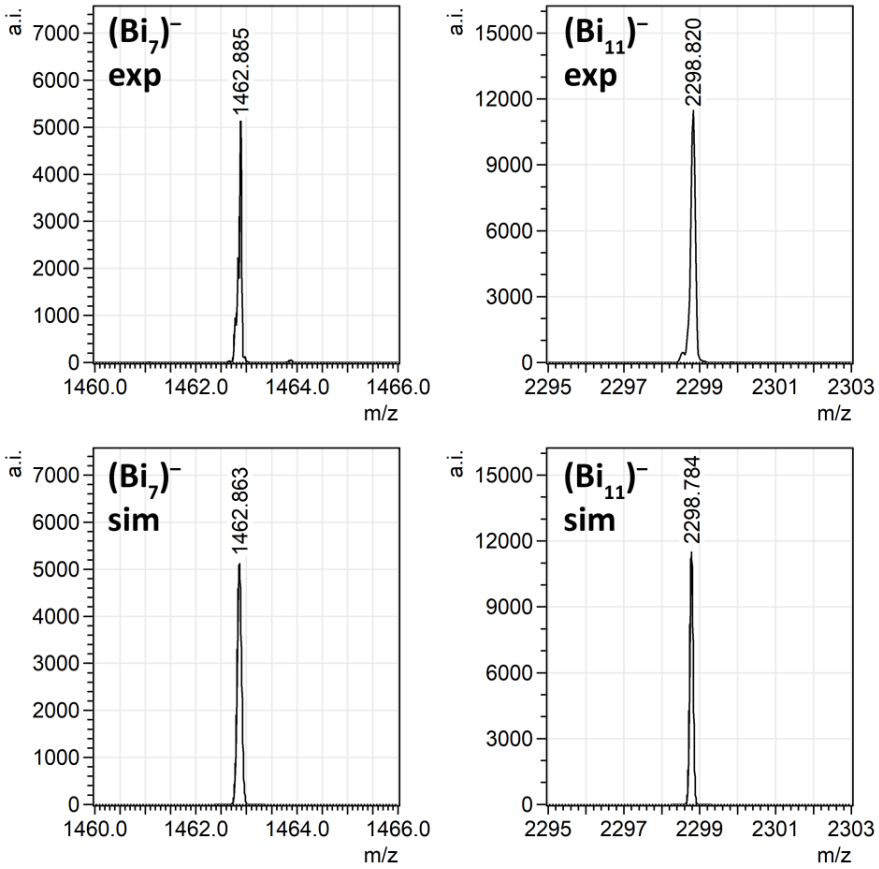

Figure S4. Comparison of experimental (top) and simulated (bottom) signals of the Bi_7^- (left) and Bi_{11}^- (right) ions in the mass spectra of a crystal mixture of compounds **1** and **B**.

3. Single Crystal X-ray Diffraction

3.1. General

The data for the X-ray structural analyses were collected at T = 100(2) K with Mo-K_α-radiation (λ = 0.71073 Å) on area detector systems Stoe StadiVari for **1**, and Stoe IPDS2 for **2**. Structures were solved by intrinsic phasing (**1**, SHELXT-2015)[5] or direct methods (**2**, SHELXS-2008).[6] The refinement was done by full-matrix-least-squares methods against F^2 with the program SHELXL-2014.[7] All hydrogen atoms were kept riding on calculated positions with isotropic displacement parameters U = 1.2 U_{eq} of the bonding partners. The CIFs of compounds **1,** and **2** were deposited at the Cambridge Crystallographic Data Centre (CCDC 1875914 (**1**), and 1875516 (**2**)). These data are provided free of charge upon request. The crystal data and experimental parameters of the structure determinations are collected in Tables S1. Figures were created with Diamond 4 and in part rendered with PovRay 3.7.[8]

Table S1. Crystal structure data and details of the structure determinations of compounds **1** and **2**.

Compound	**1**	**2**
empirical formula	$C_{74}H_{152}Bi_{14}Cd_1K_4N_{10}O_{24}$	$C_{126}H_{252}Bi_{16.13}K_7N_{14}O_{42}Tl_{4.74}Zn_3$
formula weight [g mol^{-1}]	4760.57	7444.76
crystal color, shape	black metallic, long needle	black metallic, tiny needle
crystal size [mm^3]	0.22 x 0.1 x 0.05	0.20 x 0.06 x 0.05
crystal system	triclinic	monoclinic
space group (No.)	$P\bar{1}$ (2)	$P2_1/m$ (11)
a [Å]	14.1287(3)	21.1641(6)
b [Å]	18.1174(4)	41.979(1)
c [Å]	23.9198(4)	23.4301(6)
α [°]	86.423(2)	
β [°]	88.658(2)	93.736(2)
γ [°]	79.936(2)	
V [Å^3]	6016.4(2)	20772(1)
Z, ρ_{calc} [g cm^{-3}]	2, 2.628	4, 2.381
μ ($Mo_{K\alpha}$) [mm^{-1}]	20.760	17.807
absorption correction type	numerical	numerical
2θ range [°]	4.46 – 50.00	4.09 – 50.00
total reflns	114543	143124
unique reflns [R_{int}]	21136	36912
obs. Reflns [$I > 4\sigma(I)$]	15042	11239
Parameters/restraints	1126/156	1091/1197
wR_2 (all data)/ R_1 [$I > 4\sigma(I)$]	0.1308/0.0533	0.1770/0.0721
GooF (all data)	1.029	0.873
max peak/hole [e Å^{-3}]	6.9/−1.72	4.3/−3.4
Depository number	CCDC 1875914	CCDC 1875516

3.2. Details of the Structure Determinations

3.2.1. Structure Determination of [K(crypt-222)]$_4$[Bi$_7$CdBi$_7$]•*en* (1)

The structure of **1** could be solved using intrinsic phasing in the centro-symmetric space group $P\bar{1}$ (No. 2). The structure features one heavy atom cluster anion $[Bi_7CdBi_7]^{4-}$ (Figure S5). Table S2 contains interatomic 1,2-distances of this cluster anion. A comparison to those in the free anion Bi_7^{3-} is provided in Table S3. The asymmetric unit contains further four independent $[K(crypt\text{-}222)]^+$ counter ions, and one ethylene diamine molecule (Figure S6). Three of the four cryptand ligands did not show disorder and anisotropic displacement parameters could be refined for all of them without the use of restraints. One of them (Fig. S6a) showed signs of disorder which could not be resolved to a point which would allow for a refinement of two separate positions. For this reason its structural parameters were restrained to the geometry of the second cryptand molecule (Fig. S6b) with the use of the SHELX SAME instruction and anisotropic displacement parameters were additionally restrained using the ISOR instruction.

The $[Bi_7CdBi_7]^{4-}$ anion is located on a general position. There are several high residual electron density peaks (6.9 – 4.5 e Å^{-3}) located next to the Bi atoms suggesting possible disorder. However, refinement of split positions gave no significant improvement of the residuals, and free refinement of the occupation factors of the original atoms gave no significant deviations from full occupation. Thus we assume that the electron density maxima are spurious peaks caused by non-perfect absorption correction due to a very high absorption coefficient ($\mu(Mo_{K\alpha})$ = 20.76 mm^{-1}) and highly anisotropic crystal shape (long needle).

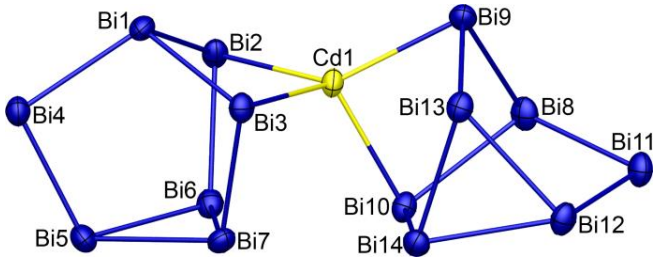

Figure S5. Structure of the cluster anion $[(Bi_7)Cd(Bi_7)]^{4-}$ in **1**. Displacement ellipsoids are drawn at 50% probability level.

Table S2. Interatomic distances in the cluster anion $[(Bi_7)Cd(Bi_7)]^{4-}$ in **1**. Atom labels as given in Figure S5.

Atoms	Distance / Å	Atoms	Distance / Å	Atoms	Distance / Å
Bi1 – Bi2	2.981(1)	Bi5 – Bi6	3.029(1)	Bi2 – Bi6	2.9497(9)
– Bi3	2.9797(9)	– Bi7	3.0528(9)	Bi3 – Bi7	2.9364(9)
– Bi4	2.954(1)	Bi6 – Bi7	3.0486(9)	Bi4 – Bi5	2.930(1)
Bi8 – Bi9	2.994(1)	Bi12 – Bi13	3.044(1)	Bi9 – Bi13	2.936(1)
– Bi10	3.009(1)	– Bi14	3.030(1)	Bi10 – Bi14	2.9335(9)
– Bi11	2.9502(9)	Bi13 – Bi14	3.0723(9)	Bi11 – Bi12	2.923(1)
average	2.978	**average**	3.046	**average**	2.935
Cd1 – Bi2	2.991(1)				
– Bi3	3.007(2)				
– Bi9	2.975(1)				
– Bi10	3.010(2)				
average	2.996				

Table S3. Comparison of interatomic Bi – Bi distances in the cluster anion $[(Bi_7)Cd(Bi_7)]^{4-}$ in **1** to those in Bi_7^{3-}. Position numbers as given in Figure S5.

Atoms	Distance / Å	Atoms	Distance / Å	Atoms	Distance / Å
		$[Bi_7CdBi_7]^{4-}$			
Top - two-bonded		Two-bonded - bottom		bottom	
Bi1 – Bi2	2.981(1)	Bi2 – Bi6	2.9497(9)	Bi5 – Bi6	3.029(1)
– Bi3	2.9797(9)	Bi3 – Bi7	2.9364(9)	– Bi7	3.0528(9)
– Bi4	2.954(1)	Bi4 – Bi5	2.930(1)	Bi6 – Bi7	3.0486(9)
Bi8 – Bi9	2.994(1)	Bi9 – Bi13	2.936(1)	Bi12 – Bi13	3.044(1)
– Bi10	3.009(1)	Bi10 – Bi14	2.9335(9)	– Bi14	3.030(1)
– Bi11	2.9502(9)	Bi11 – Bi12	2.923(1)	Bi13 – Bi14	3.0723(9)
average	2.978	**average**	2.935	**average**	3.046
		Bi_7^{3-}			
Bi1 – Bi2	2.943(5)	Bi2 – Bi6	2.895(5)	Bi5 – Bi6	3.100(5)
– Bi3	2.939(6)	Bi3 – Bi7	2.882(4)	– Bi7	3.085(5)
– Bi4	2.913(5)	Bi4 – Bi5	2.915(6)	Bi6 – Bi7	3.029(5)
average	2.932	**average**	2.897	**average**	3.071

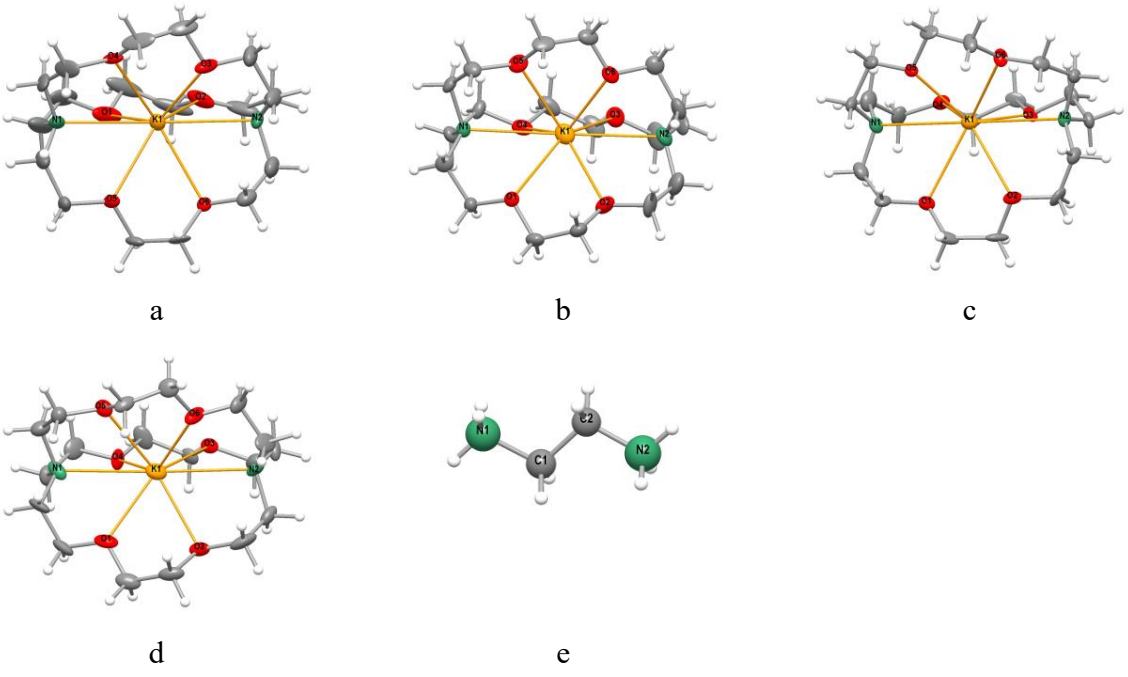

Figure S6. a)-d) The 4 $[K(crypt\text{-}222)]^+$ cations, and the *en* molecule in **1**. Displacement ellipsoids at 30% probability level.

3.2.2. Structure Determination of $[K(crypt\text{-}222)]_7[(Bi_6)Zn_3(TlBi_5)][(Tl_4Bi_5)_{0.935}(Bi_7)_{0.065}]$ (2)

The structure of **2** could be solved with direct methods in the centro-symmetric space group $P2_1/m$ (No. 11). It shows three independent sites with cluster anions: The first one with a $(Tl_4Bi_5)^{3-}$ anion on a mirror plane (Fig. S7), the second one - also on a mirror plane - shows the same anion overlayed by 13% of a Bi_7^{3-} anion (Fig. S8). Owing to strong overlap with the major component, its geometry appears deformed. The third site is occupied by a $[(Bi_6)Zn_3(TlBi_5)]^{4-}$ anion (Fig. S9) with corresponding interatomic distances in Table S4. As Tl and Bi atoms cannot be distinguished with Mo-K_α X-ray diffraction data the assignment was taken based on DFT calculations.
One of the [K(crypt)] cations (No. 1) (Fig. S10a) is on a mirror plane. In reality, small deviations from this symmetry are expected that are averaged by disorder. This may explain that some unrealistic short H...H distances are observed. The second cation shows strong disorder over a mirror plane (Fig. 10b+c). Its atom positions were claimed by a fragment fit based on the geometry of the first cation. The refinement of this and the remaining six cations (Fig. S10d-i) on general sites was done using 1,2- and 1,3-restraints but leaving conformational freedom (SAME option of SHELXL) for all these groups. This is the reason for the large number of restraints. Due to the large structure, poor data quality, and presence of many heavy atoms, all C,N,O atoms could be refined with isotropic displacement parameters only. High displacement parameters in some of the cations indicate high dynamics and/or disorder.

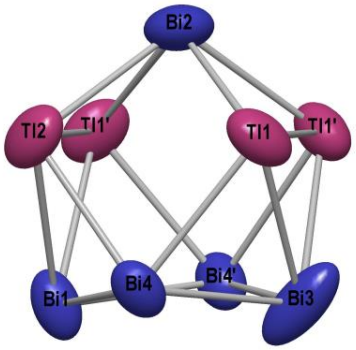

Figure S7. $(Tl_4Bi_5)^{3-}$ anion on cluster site 1 of **2**. Displacement ellipsoids are drawn at 50% probability level.

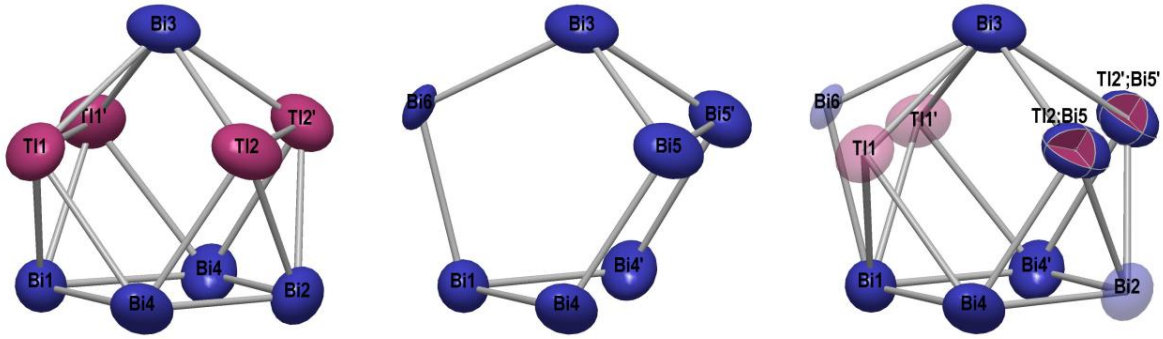

a b c

Figure S8. Disorder on cluster site 2: (a) $(Tl_4Bi_5)^{3-}$ anion (93.5%) b) Bi_7^{3-} anion (6.5%) (c) Superposition. Partially occupied atoms transparent. Displacement ellipsoids are drawn at 50% probability level.

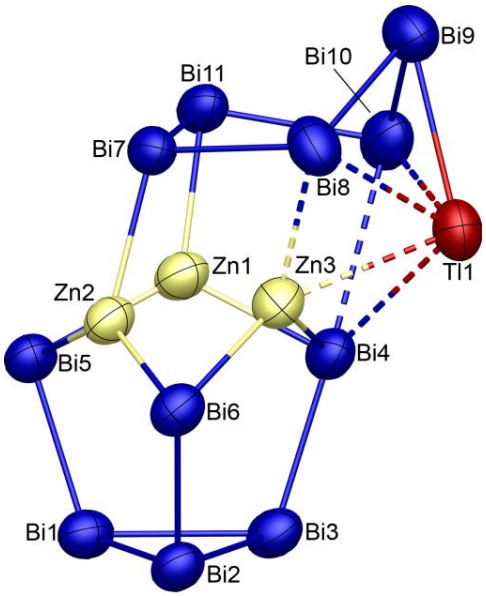

Figure S9. Structure of the ternary cluster anion $[(Bi_6)Zn_3(TlBi_5)]^{4-}$ in **2**. Displacement ellipsoids are drawn at 50% probability level. Note that the deposited original atom parameters refer to the mirror image.

Table S4. Interatomic distances in the cluster anion $[(Bi_6)Zn_3(TlBi_5)]^{4-}$ in **2**. Atom labels as given in figure S9.

Atoms	Distance / Å	Atoms	Distance / Å	Atoms	Distance / Å
Bi – Bi distances				2e-3c bonds	
Bi1 – Bi2	3.056(2)	Bi7 – Bi8	3.013(2)	Bi4 – Bi10	3.603(2)
Bi2 – Bi3	3.028(2)	Bi8 – Bi9	3.048(2)	Tl1 – Bi8	3.199(2)
Bi1 – Bi3	3.020(2)	Bi9 – Bi10	2.978(2)	Tl1 – Bi9	3.236(2)
Bi1 – Bi5	2.955(2)	Bi10 – Bi11	2.993(2)	Tl1 – Bi10	3.139(2)
Bi2 – Bi6	2.963(2)	Bi11 – Bi7	3.017(2)	Tl1 – Bi4	3.410(2)
Bi3 – Bi4	3.012(2)			Tl1 – Zn3	3.160(4)
Zn – Bi distances (bottom)		Zn – Bi distances (top)		Zn – Zn distances	
Zn1 – Bi4	2.720(4)	Zn1 – Bi11	2.717(4)	Zn1 – Zn2	2.784(5)
Zn1 – Bi5	2.756(4)	Zn2 – Bi7	2.809(4)	Zn2 – Zn3	2.762(5)
Zn2 – Bi5	2.666(3)	Zn3 – Bi8	2.827(4)	Zn1 – Zn3	3.317(5)
Zn2 – Bi6	2.682(4)	Zn1 – Bi7	3.272(4)		
Zn3 – Bi4	2.757(4)	Zn3 – Bl7	3.190(4)		
Zn3 – Bi6	2.798(4)				

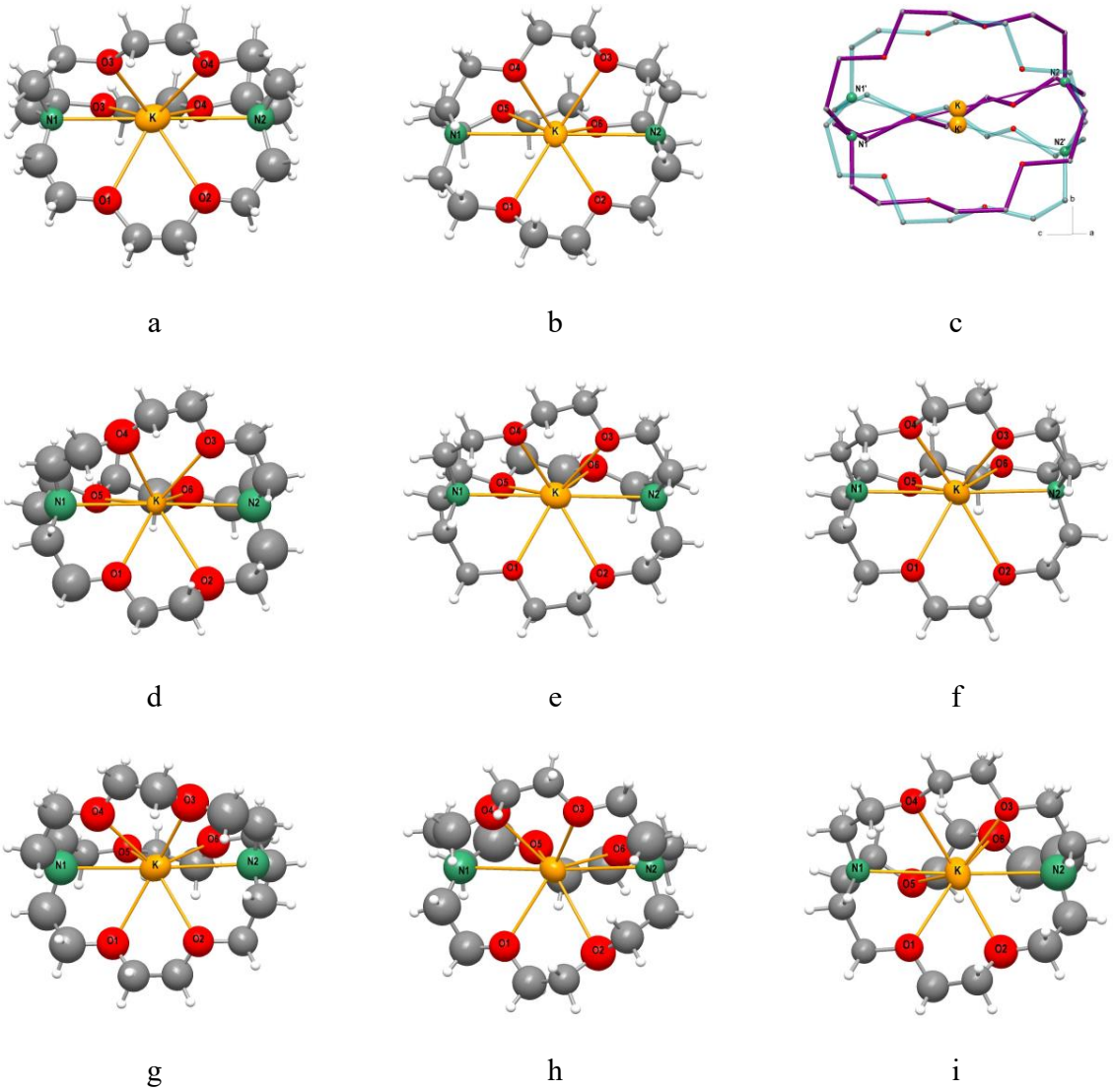

Figure S10. $[K(crypt\text{-}222)]^+$ cations in **2**. a) Cation 1 with *m* (C_S) symmetry, b) Cation 2, c) disorder of cation 2 over a mirror plane. H atoms omitted, wire model. d)-i) $[K(crypt\text{-}222)]^+$ cations 3-8 on general positions. Displacement ellipsoids at 30% probability level.

4. Micro-X-ray Fluorescence Spectroscopy (µ-XRF)

4.1. General Procedure

The µ-XRF measurement were performed with a Bruker M4 Tornado, equipped with a Rh-target X-ray tube and a silicon drift detector. The data were collected through mapping of a freshly mounted crystal that was immersed in a thin protective coating of non-drying high viscosity oil (21 cSt). Mapping was performed with 5 µm spot sizes on a 5 µm x 5 µm grid and emitted fluorescence photons were detected with acquisition times of 5ms/spot. All data points were averaged over three full cycles. Quantification of the elements is achieved through deconvolution of the spectra. Results are summarized in Table S5. Figure S11 presents the measured spectra for **1** along with the results of the deconvolution algorithm. As the sample contains a mixture of **1** and $[K(crypt\text{-}222)]_3(Tl_4Bi_5)$ (**B**) small amounts of Tl are visible in the spectrum that are caused by surface contaminations on the crystal.

4.2. Summary of µ-XRF Results for Compound 1

Table S5. µ-XRF analysis of **1** (K, Bi, Cd).

$[K(crypt\text{-}222)]_4[Bi_7CdBi_7]$•*en* (1)

Element	Element wt % (exp)	Element wt % (calc)	Atom % (exp)	Atom % (calc)	Element ratio (exp)	Element ratio (calc)
K	4.80	4.90	20.73	21.05	3.9	4
Bi	91.86	91.59	74.24	73.68	14.1	14
Cd	3.35	3.52	5.03	5.26	1	1
Total	100.01	100.01	100.00	99.99	19	19

4.3. µ-XF Spectrum of $[K(crypt\text{-}222)]_4[Bi_7CdBi_7]$•*en* (1)

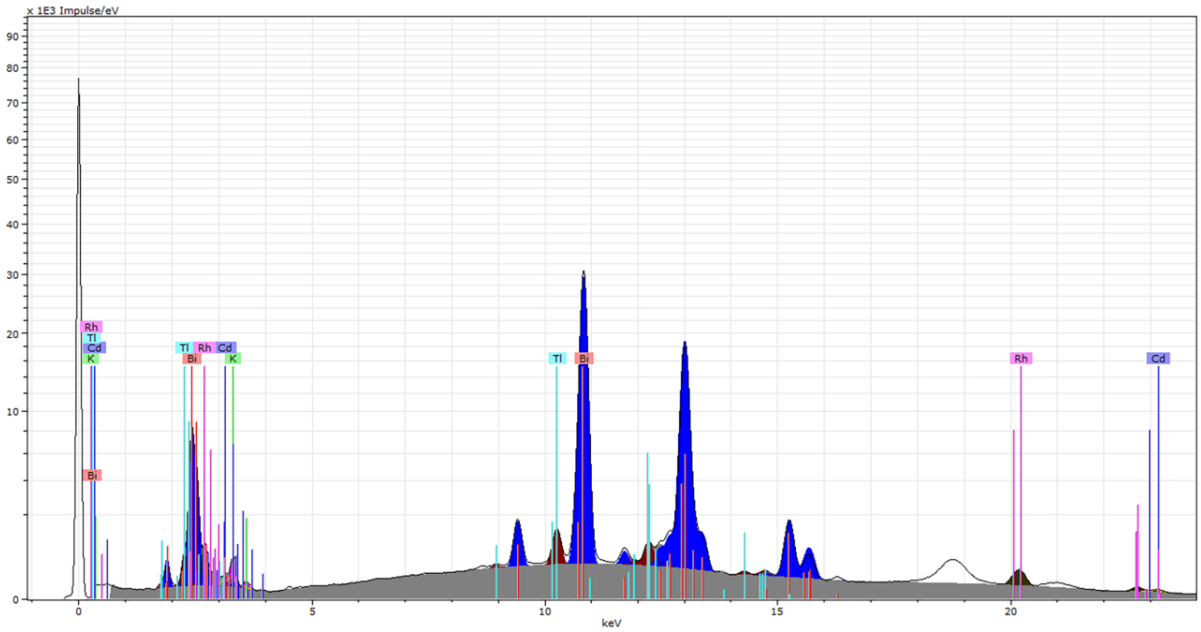

Figure S11. µ-XF spectrum of **1** (line) with the results of the deconvolution algorithm (solid, red). Intensities are shown on a square-root scale. Colors are used as follows: K (purple), Bi (blue), Cd (yellow), Tl (dark red), background (grey).

5. Quantum Chemical Investigations

5.1. Methods

All quantum chemical structure optimizations presented in this chapter were performed with TURBOMOLE V7.2.[9] TURBOMOLE V7.0.1.[10] was used for the analyses of electronic structures through the use of orbital localization via Boys method[11] with orbital contributions calculated from Mulliken population analysis[12] and calculations of shared electron numbers in population analyses based on orbital occupation numbers (PABOON)[13]. We employed the density functional TPSS,[14] def2-TZVP basis sets[15] and corresponding auxiliary basis sets.[16] The ECPs ECP-28 (Cd) and ECP-60 (Hg) were used for the transition metals.[17] For the main group atoms ECPs were used for Sb (ECP-28) and Bi (ECP-60).[18]
For compensation of the negative charge the conductor-like screening model (COSMO)[19] was employed. Orbital representations were created with gOpenMol[20] and the OrbsAtGOP script with cut-off values of ±0.04 a.u..

5.2. Optimized Geometries for E_7^{3-} and $[(E_7)M(E_7)]^{4-}$ cages

The structural parameters for E_7^{3-} cages and $[(E_7)M(E_7)]^{4-}$ cluster anions were optimized. The final Cartesian coordinates of the minimum structures of the E_7^{3-} cages are provided in Table S6. Tables S7 – S10 contain the Cartesian coordinates for the minimum structures of the $[(E_7)M(E_7)]^{4-}$ cluster anions. The optimized structures of the E_7^{3-} cages and the $[(E_7)M(E_7)]^{4-}$ cluster anions are shown in the Figures S12 – S16.

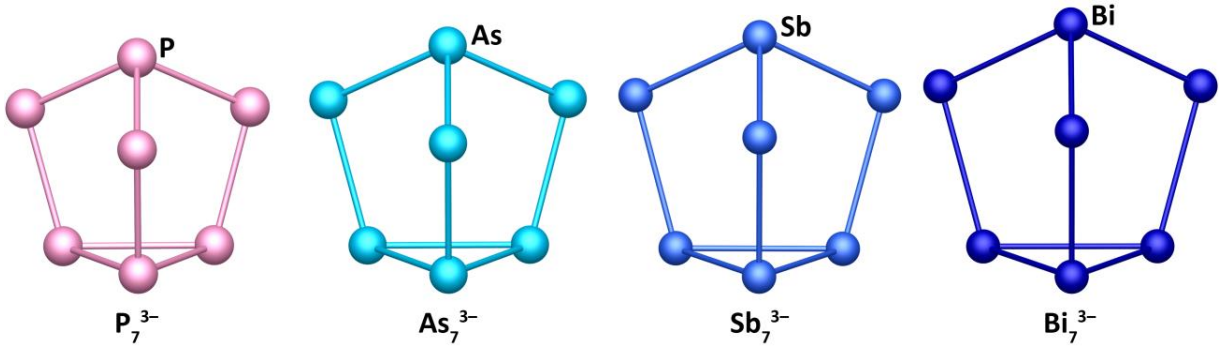

Figure S12. Optimized structures of the E_7^{3-} cages (E = P – Bi) as obtained from the DFT calculations.

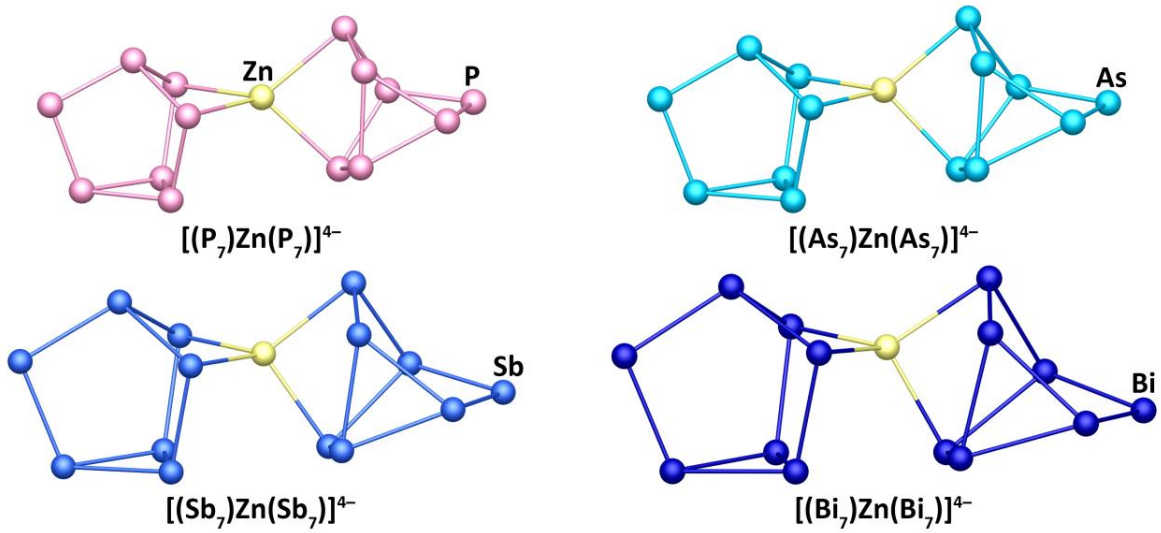

Figure S13. Optimized structures of the $[(E_7)Zn(E_7)]^{4-}$ cages (E = P – Bi) as obtained from the DFT calculations**.**

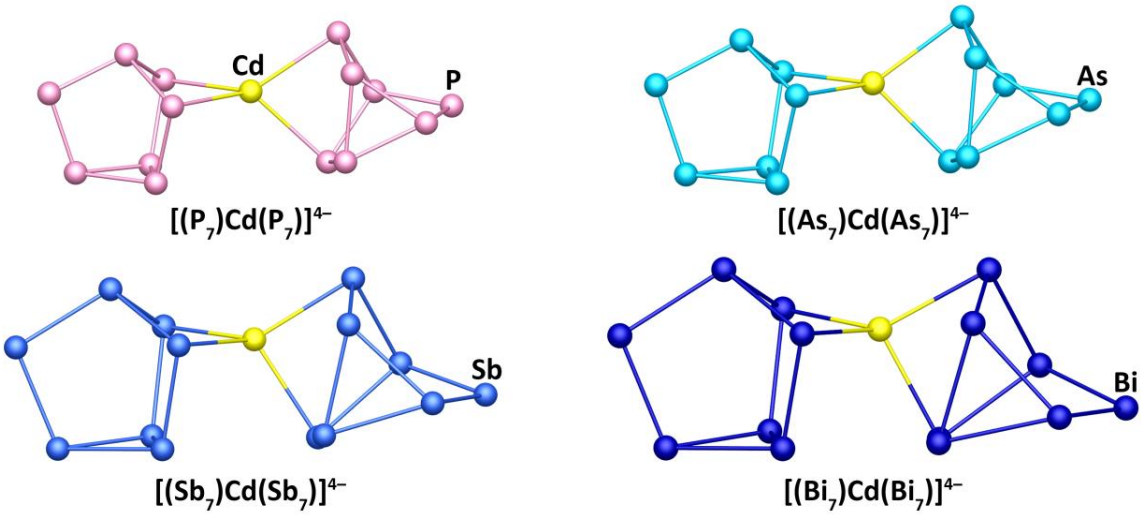

Figure S14. Optimized minimum structures of the $[(E_7)Cd(E_7)]^{4-}$ cages (E = P – Bi) as obtained from the DFT calculations.

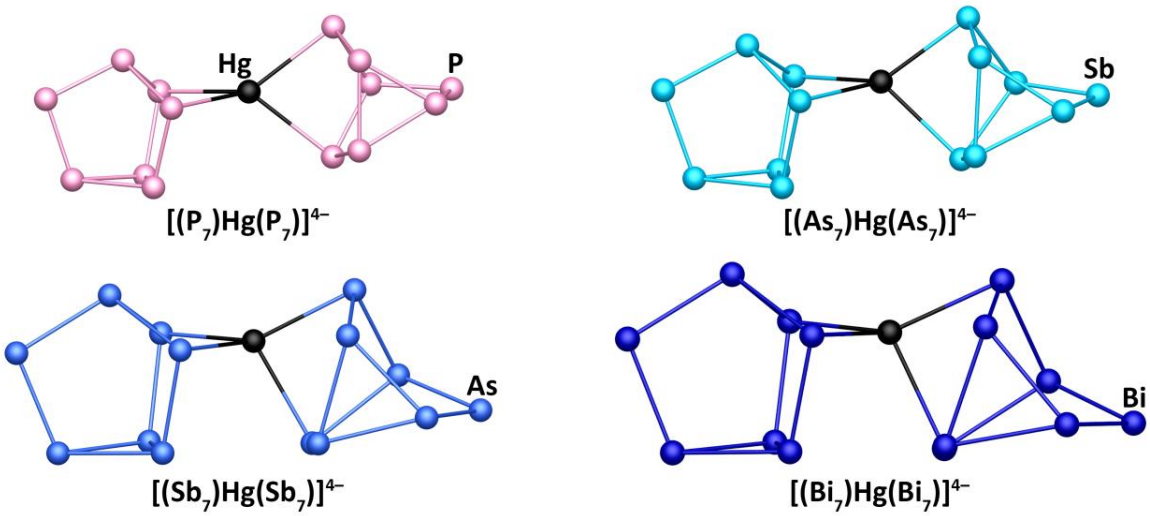

Figure S15. Optimized minimum structures of the $[(E_7)Hg(E_7)]^{4-}$ cages (E = P – Bi) as obtained from the DFT calculations.

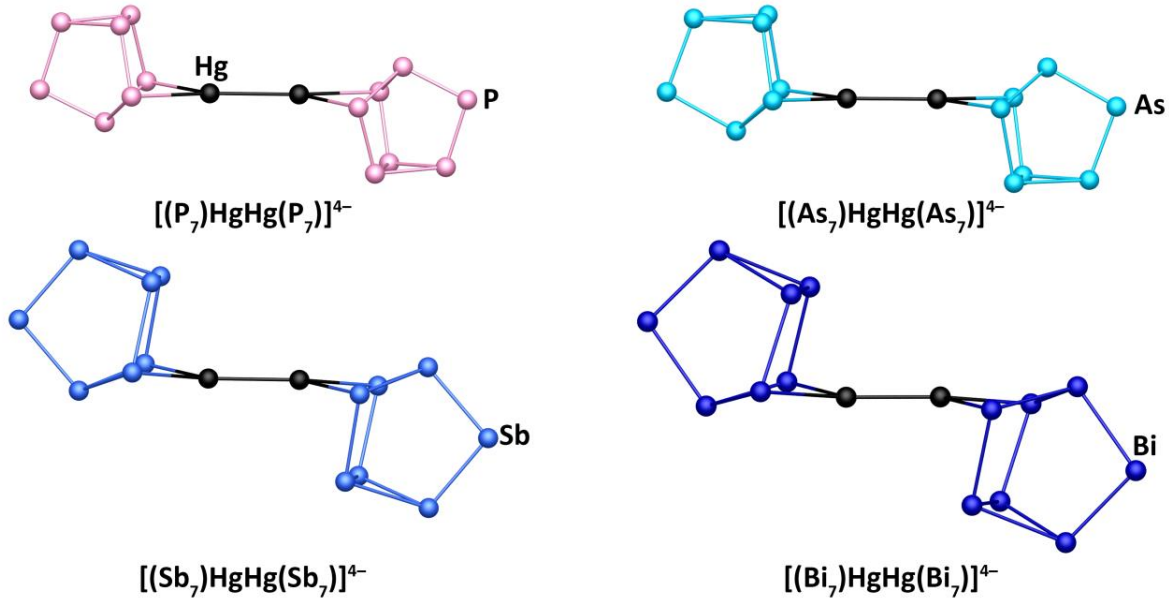

Figure S16. Optimized minimum structures of the $[(E_7)HgHg(E_7)]^{4-}$ cages (E = P – Bi) as obtained from the DFT calculations.

Table S6. Cartesian Coordinates for the E_7^{3-} cages.

		P_7^{3-}				As_7^{3-}	
P	4.9607138	11.2298705	6.518574	As	4.9130332	11.4093036	6.4721558
P	6.7751536	11.0020776	7.7357228	As	6.9169307	11.1396492	7.8145177
P	5.361242	9.8474179	4.8588928	As	5.3555264	9.8691221	4.6492168
P	3.4898629	10.0986485	7.6949377	As	3.2965903	10.1444504	7.7679775
P	4.5715688	8.2603286	7.9011797	As	4.4822143	8.1164377	8.0052802
P	6.7807966	8.8680581	7.9281051	As	6.926158	8.7892687	8.0326993
P	5.8298533	8.0917268	5.993614	As	5.8787381	7.9298963	5.8891787
		Sb_7^{3-}				Bi_7^{3-}	
Sb	4.8311425	11.7057677	6.3939219	Bi	4.7887425	11.839895	6.3534985
Sb	7.1491787	11.3824138	7.9447114	Bi	7.2364986	11.4789484	7.9982604
Sb	5.3510291	9.9168768	4.2905122	Bi	5.3606644	9.936585	4.1453493
Sb	2.9675171	10.2305598	7.8926593	Bi	2.8383424	10.2679175	7.9511842
Sb	4.3555426	7.8695358	8.1678997	Bi	4.3033167	7.7646033	8.2352822
Sb	7.1614938	8.6405263	8.1999306	Bi	7.2628998	8.576456	8.2672786
Sb	5.9532872	7.6524478	5.7413909	Bi	5.9787268	7.5337228	5.6801728

Table S7. Cartesian Coordinates of $[(P_7)M(P_7)]^{4-}$ cages.

$[(P_7)Zn(P_7)]^{4-}$				$[(P_7)Cd(P_7)]^{4-}$			
P	5.5240162	11.8101548	6.5975571	P	5.4960658	11.5853259	6.5754247
P	7.3380338	11.2066848	7.6350783	P	7.3039771	11.0093812	7.6310652
P	5.8145458	10.7004933	4.7017728	P	5.8267192	10.4932762	4.6754467
Zn	6.8256866	13.5388073	5.4128174	Cd	6.8391101	13.5422295	5.3622586
P	8.8884489	11.0541883	5.9759619	P	8.8850598	10.8489679	5.991107
P	7.7777513	11.5903591	4.1837247	P	7.8095461	11.3489992	4.1692353
P	7.8655949	9.1920163	6.7516831	P	7.8512299	8.9910807	6.7659663
P	6.3157349	8.6892222	5.3436105	P	6.3224048	8.4847601	5.3379669
P	5.8026182	15.5910086	4.4412138	P	5.7742466	15.8243009	4.4518883
P	8.1937479	15.1509304	6.6869065	P	8.2316217	15.3948922	6.6810791
P	7.7866396	16.446163	4.9351532	P	7.7689131	16.6677784	4.9269441
P	4.7948471	15.9272458	6.3401397	P	4.8028374	16.111988	6.3753056
P	7.3106309	18.375672	5.8066013	P	7.2825049	18.5865881	5.8221145
P	6.4399916	15.6257663	7.8830958	P	6.4816249	15.8193821	7.8951526
P	5.8499622	17.7121378	7.2430139	P	5.8523888	17.9018997	7.277375
$[(P_7)Hg(P_7)]^{4-}$				$[(P_7)HgHg(P_7)]^{4-}$			
P	5.5645983	11.5023967	6.6168298	P	3.2536677	22.2967588	13.6611994
P	7.3244751	10.7973797	7.6641802	P	6.5895724	22.1243087	13.6255623
P	5.870647	10.4993101	4.6616498	P	3.6862257	20.4223268	14.6548686
Hg	6.8527325	13.5405416	5.4163182	P	5.9869898	20.2940085	14.6227745
P	8.9305681	10.6971003	6.0269507	P	4.8978282	21.0181395	16.4648148
P	7.8784286	11.3514019	4.2456396	P	5.0154678	23.1642632	16.4801564
P	7.8334978	8.8314344	6.6752235	P	4.9931959	23.4908903	14.3314741
P	6.3104074	8.4458187	5.2016816	P	2.8825655	20.4401647	7.0473415
P	5.7105159	15.813471	4.5265538	P	6.2056071	20.1976999	6.8461524
P	8.1707499	15.4790931	6.722426	P	5.7654402	22.0837991	5.8733978
P	7.7206162	16.6732693	4.9077392	P	4.4094988	19.0391244	6.2632532
P	4.7594267	16.250576	6.4267859	P	3.4713188	22.2515663	6.0129038
P	7.2784947	18.6453374	5.6949439	P	4.459963	21.5068058	4.123268
P	6.4654128	16.0195814	7.9449142	P	4.3028217	19.3632608	4.1168078
P	5.857679	18.0641385	7.2064936	Hg	4.9194665	21.6660816	11.5751769
				Hg	4.708651	20.8571515	9.0086583

Table S8. Cartesian Coordinates of $[(As_7)M(As_7)]^{4-}$ cages.

$[(As_7)Zn(As_7)]^{4-}$				$[(As_7)Cd(As_7)]^{4-}$			
As	5.3724889	11.8528647	6.5931201	As	5.3412022	11.6023196	6.5978467
As	7.35721	11.2450531	7.7913876	As	7.3388196	11.0340293	7.7875869
As	5.6910933	10.5158717	4.5575063	As	5.705235	10.3235839	4.5341198
Zn	6.8062429	13.5418758	5.3007532	Cd	6.7968586	13.5397169	5.286024
As	9.0821692	11.0314352	5.977612	As	9.0838585	10.8476703	5.9810221
As	7.8440358	11.5526924	3.9928177	As	7.8711154	11.3364192	3.9737255
As	7.986786	8.9860212	6.9100818	As	7.9958559	8.7876484	6.8936087
As	6.2969764	8.3468298	5.3650144	As	6.3216253	8.1516393	5.333083
As	5.7207242	15.6551603	4.2635018	As	5.6921006	15.8778162	4.274128
As	8.3222296	15.0830488	6.6829828	As	8.3393819	15.3108851	6.7281963
As	7.910029	16.6218632	4.8132895	As	7.9023183	16.7954631	4.8200801
As	4.5961775	15.9781751	6.3558708	As	4.5893603	16.1841673	6.3792275
As	7.3685407	18.7021208	5.8632543	As	7.3687982	18.8901298	5.8519617
As	6.4139657	15.5816811	8.0445938	As	6.4178545	15.8000717	8.0687145
As	5.7595811	17.9161568	7.4265441	As	5.7638656	18.12929	7.4290052
$[(As_7)Hg(As_7)]^{4-}$				$[(As_7)HgHg(As_7)]^{4-}$			
As	5.3966215	11.5628342	6.6133429	As	3.0997584	22.3994263	13.6547354
As	7.368208	10.9381303	7.8023011	As	6.7489782	22.1895136	13.5833142
As	5.7174398	10.2831878	4.5443378	As	3.557518	20.3062035	14.7134456
Hg	6.7877374	13.5435154	5.1967012	As	6.0974827	20.1580475	14.6639941
As	9.1197605	10.7560296	5.9841026	As	4.9062195	20.9250279	16.722357
As	7.8890607	11.3044654	4.0084958	As	5.0442983	23.2907289	16.7775163
As	8.0044553	8.704781	6.8732664	As	5.0206645	23.7190994	14.4207232
As	6.3217828	8.0973934	5.3058873	As	2.7239322	20.3592594	7.0756091
As	5.6755769	15.9089431	4.3076809	As	6.362188	20.1067043	6.8637345
As	8.2800595	15.3421779	6.7477671	As	5.8910618	22.2083135	5.8241823
As	7.8934921	16.831229	4.8339751	As	4.397178	18.8094756	6.1717746
As	4.553369	16.2831154	6.3875076	As	3.3564867	22.3805172	5.9684933
As	7.3751576	18.9440337	5.8283511	As	4.4617031	21.6024402	3.8670601
As	6.3868935	15.8946929	8.09077	As	4.297853	19.238422	3.8169656
As	5.7586353	18.216321	7.413843	Hg	4.8665129	21.7013871	11.5810127
				Hg	4.7164447	20.8217835	9.002892

Table S9. Cartesian Coordinates of $[(Sb_7)M(Sb_7)]^{4-}$ cages.

$[(Sb_7)Zn(Sb_7)]^{4-}$				$[(Sb_7)Cd(Sb_7)]^{4-}$			
Sb	5.1285518	11.9490916	6.5518646	Sb	5.0501617	11.8229687	6.4908211
Sb	7.3889196	11.300353	8.0463248	Sb	7.3374041	11.3344881	7.997217
Sb	5.4887003	10.205354	4.334732	Sb	5.4840427	10.0143145	4.3434091
Zn	6.8186039	13.5555176	5.0794914	Cd	6.8187234	13.5658001	4.9057458
Sb	9.3909989	10.9439785	5.9962663	Sb	9.3674504	10.8872085	5.9838973
Sb	7.9514995	11.4355792	3.664877	Sb	7.9605782	11.1794337	3.5990167
Sb	8.1543538	8.6373518	7.2051265	Sb	8.1495889	8.6363702	7.3125471
Sb	6.1996361	7.7631937	5.4461025	Sb	6.2245428	7.6407081	5.5850416
Sb	5.6175559	15.7995824	3.9467728	Sb	5.6012487	16.0651372	3.8999023
Sb	8.5875534	15.0188601	6.6107602	Sb	8.6626482	15.1532996	6.5540586
Sb	8.1004408	16.9888035	4.61641	Sb	8.1034142	17.1796529	4.6398162
Sb	4.2953619	16.0275437	6.3860335	Sb	4.3190728	16.0859684	6.3701148
Sb	7.4196889	19.2976256	6.0047431	Sb	7.4068837	19.4005168	6.1659748
Sb	6.4076614	15.4807035	8.2787538	Sb	6.4526849	15.4507198	8.21755
Sb	5.578724	18.207312	7.7700715	Sb	5.5898053	18.1942634	7.8732176
$[(Sb_7)Hg(Sb_7)]^{4-}$				$[(Sb_7)HgHg(Sb_7)]^{4-}$			
Sb	5.0699462	11.8664683	6.4264834	Sb	2.855571	22.8365146	13.4777205
Sb	7.3203248	11.4000405	7.9786346	Sb	7.0264332	22.6193211	13.396376
Sb	5.491687	9.9659929	4.3554582	Sb	3.3594343	20.2452154	14.3545218
Hg	6.8205995	13.5776351	4.7018463	Sb	6.2943093	20.0924465	14.3046914
Sb	9.3786478	10.8740496	5.9980181	Sb	4.8900818	20.5896973	16.7642396
Sb	7.9771699	11.1174032	3.6078046	Sb	5.0461127	23.3059146	17.258171
Sb	8.1277126	8.6810429	7.3869482	Sb	5.0425584	24.219213	14.6316131
Sb	6.2231822	7.6275529	5.6645388	Sb	2.4473741	19.9410859	7.2657808
Sb	5.5905803	16.1203102	3.9145535	Sb	6.6018671	19.6441521	7.0310989
Sb	8.6447576	15.1276319	6.4844893	Sb	6.1227593	22.2511008	6.18399
Sb	8.095183	17.2365405	4.6570727	Sb	4.3495402	18.3129062	5.9443415
Sb	4.3099402	16.0864674	6.3818447	Sb	3.1916945	22.4591811	6.3454504
Sb	7.4027341	19.4045089	6.2531068	Sb	4.4949843	21.9518034	3.833993
Sb	6.4728232	15.3877859	8.1900539	Sb	4.2669866	19.2436698	3.3264108
Sb	5.6029616	18.1374198	7.9374768	Hg	4.8679672	21.9255739	11.4843387
				Hg	4.690606	20.5785545	9.1050726

Table S10. Cartesian Coordinates of $[(Bi_7)M(Bi_7)]^{4-}$ cages.

$[(Bi_7)Zn(Bi_7)]^{4-}$				$[(Bi_7)Cd(Bi_7)]^{4-}$			
Bi	4.9620344	12.0228439	6.4324785	Bi	4.8861255	11.8991462	6.4033312
Bi	7.3221922	11.4867093	8.1054122	Bi	7.28742	11.5040855	8.0530662
Bi	5.3728454	9.9795982	4.2440912	Bi	5.3735596	9.8317009	4.2593624
Zn	6.8029536	13.5633613	4.8964425	Cd	6.7992558	13.5678502	4.7586398
Bi	9.4687345	11.0072379	5.9902813	Bi	9.4515166	10.9615669	5.9713123
Bi	7.9435865	11.3315166	3.4976289	Bi	7.9638083	11.1028467	3.436703
Bi	8.2358566	8.6302628	7.4376859	Bi	8.236276	8.6314838	7.5082671
Bi	6.2186876	7.5203257	5.6166692	Bi	6.250977	7.4275124	5.7154626
Bi	5.6094699	15.9287896	3.7885207	Bi	5.581497	16.1598272	3.758718
Bi	8.729667	14.9415136	6.4797988	Bi	8.7897177	15.0561371	6.469675
Bi	8.21696	17.2065918	4.5439846	Bi	8.2214594	17.3337593	4.5742791
Bi	4.2128239	15.9912837	6.3732707	Bi	4.2209052	16.0584856	6.3635741
Bi	7.4479191	19.5050364	6.2137	Bi	7.4536762	19.5727084	6.3245162
Bi	6.4583546	15.2942171	8.3151544	Bi	6.4769772	15.2933241	8.2713242
Bi	5.5261646	18.201562	8.0032111	Bi	5.5350785	18.2104157	8.0700986
$[(Bi_7)Hg(Bi_7)]^{4-}$				$[(Bi_7)HgHg(Bi_7)]^{4-}$			
Bi	4.9330545	11.9312597	6.369726	Bi	2.7841179	22.9908623	13.3381208
Bi	7.3043328	11.5185468	8.041366	Bi	7.1633464	22.7771611	13.3783361
Bi	5.3781267	9.8028559	4.2744257	Bi	3.2888611	20.2240012	14.1897615
Hg	6.8170692	13.5795319	4.5861516	Bi	6.3852661	20.0704091	14.2218617
Bi	9.4815366	10.8982205	5.9757155	Bi	4.8266205	20.4825487	16.7888451
Bi	7.9881288	11.0382115	3.4515317	Bi	4.9852485	23.3391631	17.4253502
Bi	8.2107869	8.6297423	7.5523961	Bi	5.0372732	24.4292791	14.6957207
Bi	6.2266938	7.4103535	5.7619271	Bi	2.3579455	19.782917	7.3862703
Bi	5.5674053	16.2113379	3.7794711	Bi	6.7134074	19.4616889	7.0426055
Bi	8.760363	15.0572386	6.4373193	Bi	6.2218237	22.258246	6.2825034
Bi	8.2084761	17.3835997	4.5931659	Bi	4.3157819	18.1073935	5.8604207
Bi	4.200274	16.0799877	6.3730106	Bi	3.1380067	22.4847025	6.5319539
Bi	7.4420499	19.5941419	6.3736025	Bi	4.4489995	22.0864912	3.8273442
Bi	6.4770513	15.2813559	8.2622883	Bi	4.1987157	19.2464402	3.151708
Bi	5.5329012	18.1944662	8.1062326	Hg	4.945577	21.9796965	11.4457187
				Hg	4.737289	20.4953495	9.1412893

5.3. Reaction Energies for Exchange Reactions in $[(E_7)M(E_7)]^{4-}$ cages

The absolute energy values for all components of these reactions were taken from the optimized geometries and are provided in Table S11. Tables S12 and S13 summarize the exchange reaction energies.

Table S11. Absolute energies of E_7^{3-} cages, M^{2+} ions, and $[(E_7)M(E_7)]^{4-}$ cages used for the calculation of exchange energies (see Tables SX and SX). All energies given in Hartree.

E_7^{3-}		M^{2+}	
P	-2390.18201	Zn	-1779.05452
As	-15651.3567	Cd	-167.230059
Sb	-1681.77019	Hg	-152.883224
Bi	-1502.69349	HgHg	-306.488811

$[(E_7)M(E_7)]^{4-}$				
	M = Zn	M = Cd	M = Hg	M = HgHg
P	-6559.65172	-4947.9288	-4933.65753	-5087.13446
As	-33082.0168	-31470.2989	-31456.0295	-31609.5109
Sb	-5142.81338	-3531.10129	-3516.8366	-3670.31456
Bi	-4784.66594	-3172.95697	-3158.69515	-3312.17081

Table S12. Energies of the exchange reactions of E_7^{3-} cages in the clusters $[(E_7)M(E_7)]^{4-}$. All energies given in kJ/mol.

$[(E_7)M(E_7)]^{4-} + 2\ E'_7{}^{3-} \rightarrow [(E'_7)M(E'_7)]^{4-} + 2\ E_7^{3-}$			
	P → As	P → Sb	P → Bi
Zn	-41	38.6	23
Cd	-54.1	10.2	-13.7
Hg	-59	-7.1	-38.5
HgHg	-70.7	-9.8	-35.1
	As → P	As → Sb	As → Bi
Zn	41	79.7	64
Cd	54.1	64.3	40.4
Hg	59	51.9	20.5
HgHg	70.7	60.9	35.6
	Sb → P	Sb → As	Sb → Bi
Zn	-38.6	-79.7	-15.6
Cd	-10.2	-64.3	-23.8
Hg	7.1	-51.9	-31.4
HgHg	9.8	-60.9	-25.3

Table S13. Energies of the exchange reactions of M^{2+} ions in the clusters $[(E_7)M(E_7)]^{4-}$. All energies given in kJ/mol.

$[(E_7)M(E_7)]^{4-} + M'^{2+} \rightarrow [(E_7)M'(E_7)]^{4-} + M^{2+}$			
	Zn → Cd	Zn → Hg	Zn → HgHg
P	-266.6	-465	-127.2
As	-279.6	-482.9	-156.8
Sb	-295	-510.7	-175.6
Bi	-303.2	-526.4	-185.3
	Cd → Zn	Cd → Hg	Cd → HgHg
P	266.6	-198.4	139.4
As	279.6	-203.2	122.8
Sb	295	-215.7	119.4
Bi	303.2	-223.2	117.9
	Hg → Zn	Hg → Cd	Hg → HgHg
P	465	198.4	337.8
As	482.9	203.2	326.1
Sb	510.7	215.7	335.1
Bi	526.4	223.2	341.1
	HgHg → Zn	HgHg → Cd	HgHg → Hg
P	127.2	-139.4	-337.8
As	156.8	-122.8	-326.1
Sb	175.6	-119.4	-335.1
Bi	185.3	-117.9	-341.1

5.4. Determination of the Cluster Composition for $[(Bi_6)Zn_3(TlBi_5)]^{4-}$

The initial quantum chemical investigations of the cluster anion in compound **2** were performed by C. C. Schmidt as a part of his B.Sc. thesis under supervision of PD. Dr. F. Weigend.[21] Due to the lack of experimental evidence for the cluster composition several hypothetic ones in combination with different charges were analyzed in a first set of calculations. These were $[Zn_3Tl_xBi_{12-x}]^{q-}$ (**a**), $[Zn_1Tl_xBi_{13-x}]^{q-}$ (**b**), and $[Zn_0Tl_xBi_{13-x}]^{q-}$ (**c**) with the atom positions obtained from the SC-XRD data. In all cases the Tl content was varied, x = 0 – 6 for **a** and **c** and 0 – 7 for **b** and the preferred atomic positions for Tl and Bi were derived from perturbation theory.[22] In all cases the cluster charge was varied for q = 2, 4, and 6. The reduced number of Zn atoms was chosen to include the possibility of positional disorder, not necessarily obvious in the SC-XRD data, into the calculations. In all cases a structure optimization was performed using the functional BP86[14b-d,23] with a def-SV(P)[24] basis set.

The only composition that yields a reasonable agreement with the experimentally determined structure is $[(Bi_6)Zn_3(TlBi_5)]^{4-}$. All further structure optimization and the investigations of the electronic structure were performed using the methods given in chapter 5.1 as a part of this work.

5.5. Optimized Structural Parameters for $[(Bi_6)Zn_3(TlBi_5)]^{4-}$

The atomic distribution determined in the quantum chemical studies discussed above in chapter 5.4 was transferred to the SC-XRD data and served as a starting point for another quantum chemical optimization of structural parameters. The Cartesian coordinates of the optimized structure are provided in Table S14. A comparison of the interatomic distances obtained from the DFT calculations to the experimental values is given in Table S15.

Table S14. Cartesian coordinates of the atoms in the $[(Bi_6)Zn_3(TlBi_5)]^{4-}$ cage.

$[(Bi_6)Zn_3(TlBi_5)]^{4-}$			
Zn	5.7953483	20.6385686	5.8187433
Bi	5.7606394	22.2062688	8.4664542
Bi	4.7341467	18.1753829	6.6785206
Bi	4.6777896	22.0424356	3.7242497
Tl	8.0392061	21.6674036	3.8955622
Bi	8.2696972	21.140016	7.1197022
Zn	3.6983438	20.5048918	7.5148763
Bi	5.3214718	24.9141799	7.2202257
Zn	3.7193466	22.8923116	6.196915
Bi	2.4931333	17.7604615	4.7495761
Bi	2.4290325	20.1149265	2.8913271
Bi	6.9010027	24.6049857	4.6913995
Bi	9.3738554	23.7483708	6.124634
Bi	1.3551391	21.7825108	7.2992405
Bi	0.4034174	19.9767358	5.1389335

Table S15. Comparison of the interatomic distances in the cluster anion $[(Bi_6)Zn_3(TlBi_5)]^{4-}$ in **2** with those obtained from the DFT calculations (*italic*). Position numbers as given in Figure S9.

Atoms	**Distance / Å**	**Atoms**	**Distance / Å**	**Atoms**	**Distance / Å**
Bi – Bi				2e-3c bonds	
Bi1 – Bi2	3.056(2) *3.071*	Bi7 – Bi8	3.013(2) *3.041*	Bi4 – Bi10	3.603(2) *3.528*
Bi2 – Bi3	3.028(2) *3.000*	Bi8 – Bi9	3.048(2) *3.002*	Tl1 – Bi8	3.199(2) *3.275*
Bi1 – Bi3	3.020(2) *3.029*	Bi9 – Bi10	2.978(2) *2.984*	Tl1 – Bi9	3.236(2) *3.329*
Bi1 – Bi5	2.955(2) *2.972*	Bi10 – Bi11	2.993(2) *2.998*	Tl1 – Bi10	3.139(2) *3.249*
Bi2 – Bi6	2.963(2) *2.986*	Bi11 – Bi7	3.017(2) *3.013*	Tl1 – Bi4	3.410(2) *3.387*
Bi3 – Bi4	3.012(2) *3.077*			Tl1 – Zn3	3.160(4) *3.129*
Zn – Bi (bottom)		Zn – Bi (top)		Zn – Zn	
Zn1 – Bi4	2.720(4) *2.785*	Zn1 – Bi11	2.717(4) *2.775*	Zn1 – Zn2	2.784(5) *2.727*
Zn1 – Bi5	2.756 (4) *2.835*	Zn2 – Bi7	2.809(3) *2.838*	Zn2 – Zn3	2.762(5) *2.700*
Zn2 – Bi5	2.666 (3) *2.678*	Zn3 – Bi8	2.827(4) *2.840*	Zn1 – Zn3	3.317(5) *3.087*
Zn2 – Bi6	2.682(4) *2.683*	Zn1 – Bi7	3.272(4) *3.129*		
Zn3 – Bi4	2.757(4) *2.758*	Zn3 – Bi7	3.190(4) *3.077*		
Zn3 – Bi6	2.798(4) *2.817*				

5.6. Electronic Structure of the Anion $[(Bi_6)Zn_3(TlBi_5)]^{4-}$

The cluster anion $[(Bi_6)Zn_3(TlBi_5)]^{4-}$ cannot simply be interpreted with the Wade-Mingos rules or the pseudo element concept. Hence, a more detailed analysis of its electronic structure is necessary to understand the bonding situation in the cluster. Localized molecular orbitals were generated using Boys method.[11] Atomic contributions to these orbitals were determined by Mulliken population analysis.[12] The results of the orbital localizations for the valence orbitals (LMO #163 – LMO #184) are summarized in Table S16 and the respective orbitals are shown in Figures S17 – S18.

Table S16. Localized molecular orbitals of the cluster anion $[(Bi_6)Zn_3(TlBi_5)]^{4-}$, localized with Boys method. Mulliken contributions are denoted as absolute values and percentages. The type of bond associated with the respective LMO is given in the last column. The orbitals are shown in Figures S16 and S17. Atom numbers as given in Figure S9 and highlighted in the color code of the respective atom type with respect to the figures below.

LMO	Atoms				Mulliken contributions absolute/**percentage**				Bond type
#	Atom 1	Atom 2	Atom 3	Atom 4	Atom1	Atom2	Atom 3	Atom 4	
163	Tl5	Bi13			0.14725 ***7.81***	1.73866 ***92.19***			Polarized
164	Bi4	Zn9			1.31515 ***69.58***	0.57510 ***30.42***			Ionic
165	Bi14	Bi15			0.94604 ***47.33***	1.05287 ***52.67***			Covalent
166	Bi3	Bi10			0.93789 ***47.01***	1.05713 ***52.99***			Covalent
167	Bi6	Bi13			1.04267 ***53.6***	0.90274 ***46.4***			Covalent
168	Bi2	Bi6			1.98361 ***68.94***	0.89378 ***31.06***			Covalent
169	Bi2	Bi8			1.00191 ***52.37***	0.91111 ***47.63***			Covalent
170	Bi3	Zn7			1.32915 ***67.33***	0.64489 ***32.67***			Ionic
171	Zn9	Bi14			0.50926 ***27.01***	1.37646 ***72.99***			Ionic
172	Zn1	Bi4			0.55394 ***30.14***	1.28425 ***69.86***			Ionic
173	Zn1	Bi2	Zn7	Zn9	0.14423 ***7.16***	1.24780 ***61.95***	0.46909 ***23.29***	0.15 ***7.61***	Ionic
174	Bi8	Bi12			1.04596 ***52.83***	0.93380 ***47.17***			Covalent
175	Bi12	Bi13			0.94224 ***48.43***	1.00326 ***51.57***			Covalent
176	Zn7	Bi14			0.63169 ***32.63***	1.30442 ***67.37***			Ionic
177	Zn1	Bi3			0.54805 ***29.42***	1.31464 ***70.58***			Ionic
178	Bi8	Zn9			1.44640 ***73.7***	0.51626 ***26.3***			Ionic
179	Bi4	Bi11			0.58372 ***30.15***	1.35205 ***69.85***			Covalent
180	Bi10	Bi11			1.01861 ***51.09***	0.97532 ***48.91***			Covalent
181	Bi11	Bi15			0.96069 ***48.26***	1.03009 ***51.74***			Covalent
182	Bi4	Tl5	Bi12		0.17228 ***8.99***	0.23494 ***12.25***	1.51014 ***78.76***		2e-3c
183	Bi10	Bi15			0.99363 ***50***	0.99371 ***50***			Covalent
184	Zn1	Tl5	Bi6		0.4324 ***21.95***	0.25505 ***12.95***	1.28237 ***65.1***		2e-3c

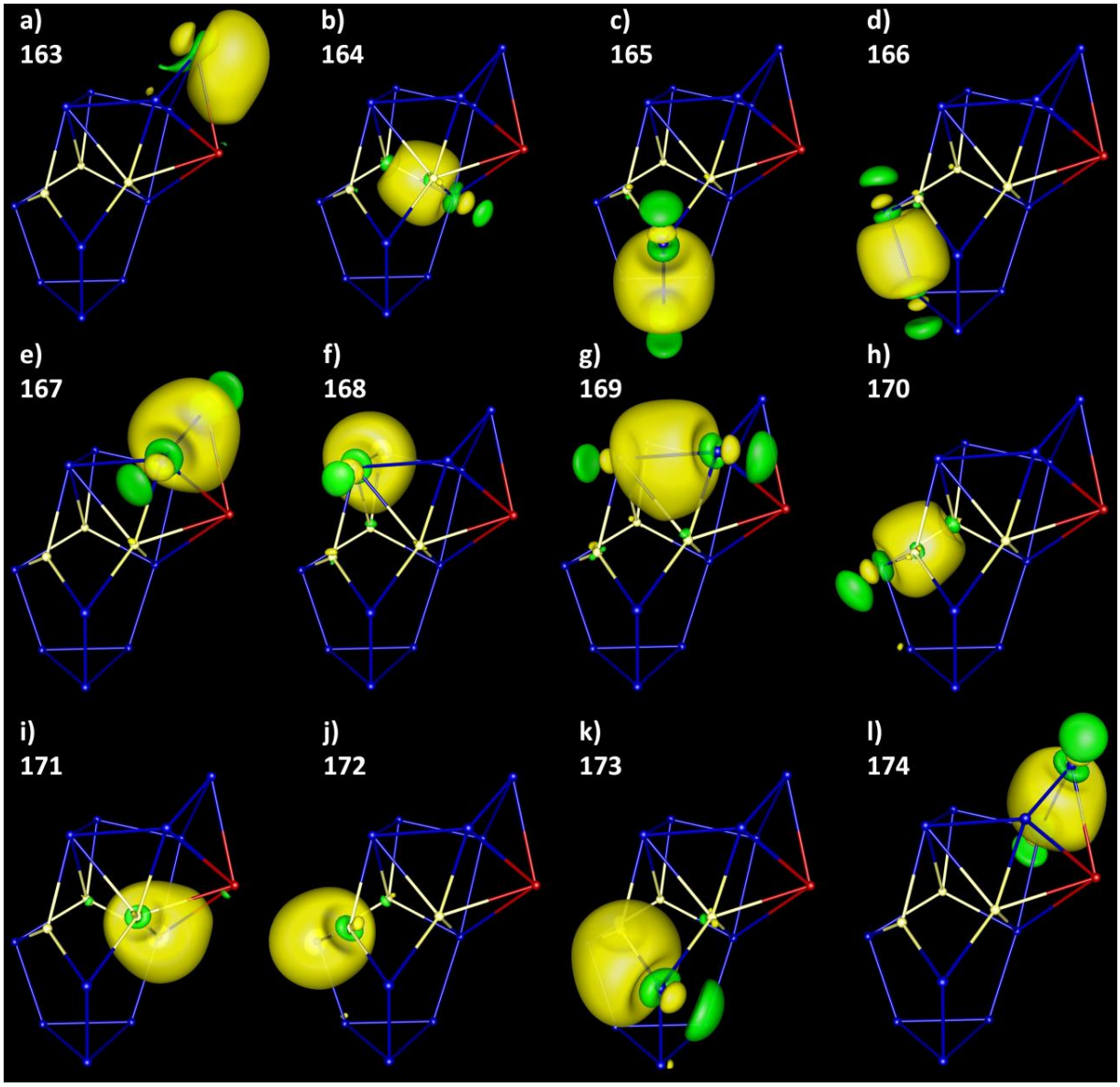

Figure S17. Localized molecular orbitals 163 – 174 of the cluster anion $[(Bi_6)Zn_3(TlBi_5)]^{4-}$, localized with Boys method. Details on orbital contributions are given in Table S16. Contours are drawn at ±0.04 a.u..

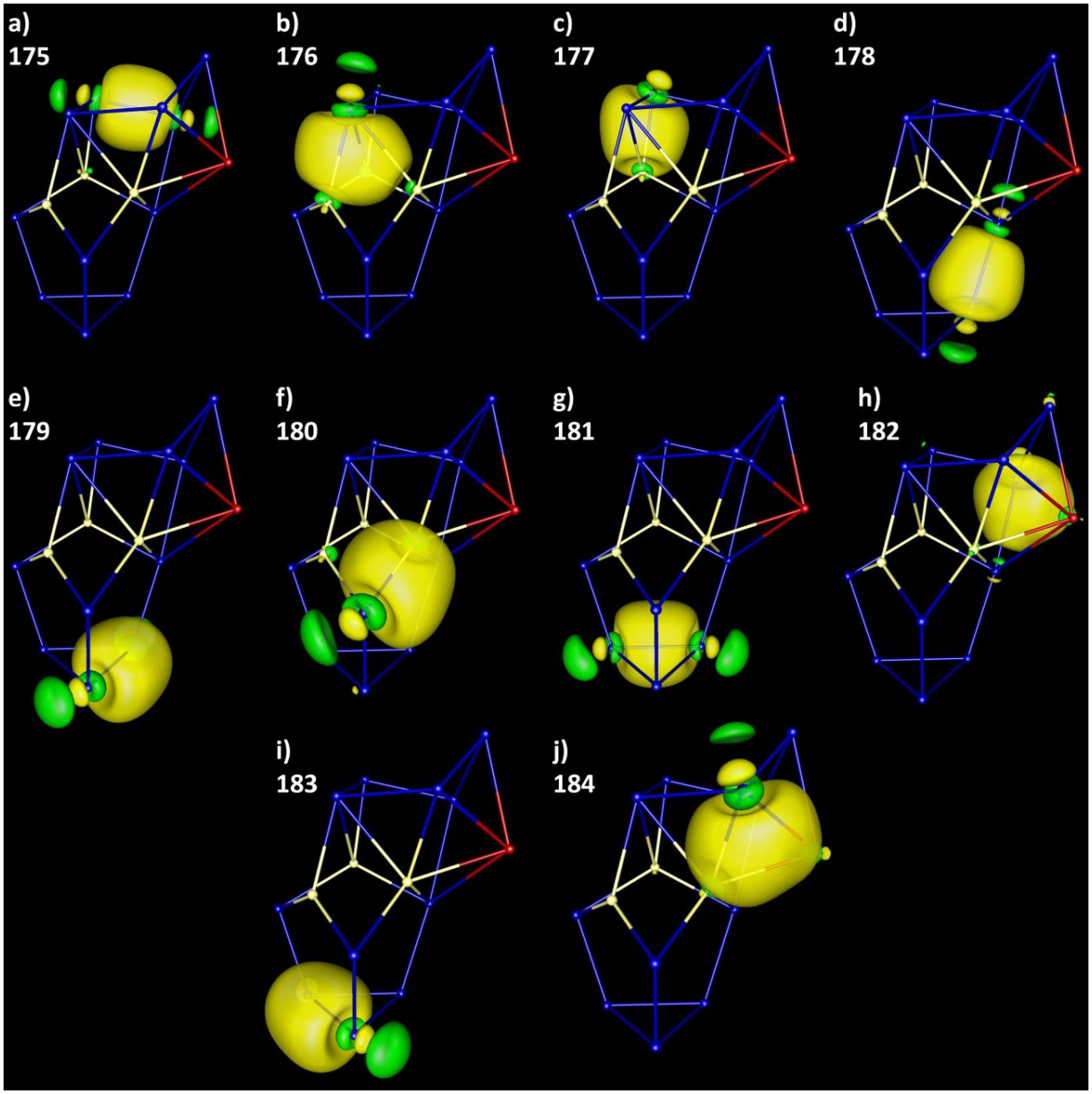

Figure S18. Localized molecular orbitals 175 – 184 of the cluster anion $[(Bi_6)Zn_3(TlBi_5)]^{4-}$, localized with Boys method. Details on orbital contributions are given in Table S16. Contours are drawn at ±0.04 a.u..

6. References for the Supporting Information

[1] crypt-222: 4,7,13,16,21,24-Hexaoxa-1,10-diazabicyclo[8.8.8]hexacosane

[2] N. Lichtenberger, N. Spang, A. Eichhöfer, S. Dehnen, *Angew. Chem.* **2017**, *129*, 13436-13442; *Angew. Chem. Int. Ed.* **2017**, *56*, 13253-13258.

[3] K. Kojima, M. Kimura, S. Ueda, Y. Tamaru, *Tetrahedron* **2006**, *62*, 7512-7520.

[4] M. Strohalm, D. Kavan, P. Novák, M. Volný, V. Havlíček, *Anal. Chem.* **2010**, *82*, 4648-4651.

[5] G. Sheldrick, *Acta Cryst.* **2015**, *A71*, 3-8.

[6] G. M. Sheldrick, *Acta Cryst.* **2008**, *A64*, 112-122.

[7] G. M. Sheldrick, *Acta Cryst.* **2015**, *C71*, 3-8.

[8] a) Diamond - Crystal and Molecular Structure Visualization, Crystal Impact - Dr. H. Putz & Dr. K. Brandenburg GbR, Kreuzherrenstr. 102, 53227 Bonn, Germany, http://www.crystalimpact.com/diamond; b) Persistence of Vision Pty. Ltd. (2004) Persistence of Vision Raytracer (Version 3.7) [Computer software]. Retrieved from http://www.povray.org/download/

[9] TURBOMOLE V7.3 2018, a development of University of Karlsruhe and Forschungszentrum Karlsruhe GmbH, 1989-2007, TURBOMOLE GmbH, since 2007; available from http://www.turbomole.com.

[10] TURBOMOLE V7.0.1 2015, a development of University of Karlsruhe and Forschungszentrum Karlsruhe GmbH, 1989-2007, TURBOMOLE GmbH, since 2007; available from http://www.turbomole.com.

[11] a) S. F. Boys, *Rev. Mod. Phys.* **1960**, *32*, 296-299; b) J. M. Foster, S. F. Boys, *Rev. Mod. Phys.* **1960**, *32*, 300-302.

[12] R. S. Mulliken, *J. Chem. Phys.* **1955**, *23*, 1833-1840.

[13] C. Ehrhardt, R. Ahlrichs, *Theor. Chim. Acta* **1985**, *68*, 231-245.

[14] a) J. M. Tao, J. P. Perdew, V. N. Staroverov, G. E. Scuseria, *Phys. Rev. Lett.* **2003**, *91*, 146401; b) P. A. M. Dirac, *Proc. R. Soc. A* **1929**, *123*, 714-733; c) J. P. Perdew, *Phys. Rev. B* **1986**, *33*, 8822-8824; d) J. C. Slater, *Phys. Rev.* **1951**, *81*, 385-390.

[15] F. Weigend, R. Ahlrichs, *Phys. Chem. Chem. Phys.* **2005**, *7*, 3297-3305.

[16] F. Weigend, *Phys. Chem. Chem. Phys.* **2006**, *8*, 1057-1065.

[17] D. Andrae, U. Häußermann, M. Dolg, H. Stoll, H. Preuß, *Theor. Chim. Acta* **1990**, *77*, 123-141.

[18] B. Metz, H. Stoll, M. Dolg, *J. Chem. Phys.* **2000**, *113*, 2563-2569.

[19] A. Klamt, G. Schüürmann, *J. Chem. Soc., Perkin Trans. 2* **1993**, 799-805.

[20] D. L. Bergman, L. Laaksonen, A. Laaksonen, *J. Mol. Graph. Model.* **1997**, *15*, 301-306.

[21] C. C. Schmidt, B.Sc. thesis, Karlsruhe Institute of Technology **2014**.

[22] a) F. Weigend, C. Schrodt, *Chem. Eur. J.* **2005**, *11*, 3559-3564; b) F. Weigend, C. Schrodt, R. Ahlrichs, *J. Chem. Phys.* **2004**, *121*, 10380-10384.

[23] a) A. D. Becke, *Phys. Rev. A* **1988**, *38*, 3098-3100; b) S. H. Vosko, L. Wilk, M. Nusair, *Can. J. Phys.* **1980**, *58*, 1200-1211.

[24] K. Eichkorn, F. Weigend, O. Treutler, R. Ahlrichs, *Theor. Chem. Acc.* **1997**, *97*, 119-124.

D Genehmigungen zum Abdruck der Publikationen

Die Veröffentlichung „N. Lichtenberger, R. J. Wilson, A. R. Eulenstein, W. Massa, R. Clérac, F. Weigend, S. Dehnen, *J. Am. Chem. Soc.* **2016**, *138*, 9033–9036 “ wurde als open-access-Artikel unter der ACS AuthorChoice-Lizenz publiziert:

Die Genehmigungen zur Verwendung der weiteren Publikationen in dieser Dissertationsschrift sind im Folgenden abgedruckt.

JOHN WILEY AND SONS LICENSE TERMS AND CONDITIONS

Nov 15, 2018

This Agreement between Philipps University of Marburg -- Niels Lichtenberger ("You") and John Wiley and Sons ("John Wiley and Sons") consists of your license details and the terms and conditions provided by John Wiley and Sons and Copyright Clearance Center.

License Number	4470311446426
License date	Nov 15, 2018
Licensed Content Publisher	John Wiley and Sons
Licensed Content Publication	Angewandte Chemie International Edition
Licensed Content Title	Between Localization and Delocalization: Ru(cod)2 Units in the Zintl Clusters [Bi9{Ru(cod)}2]3− and [Tl2Bi6{Ru(cod)}]2−
Licensed Content Author	Niels Lichtenberger, Nils Spang, Andreas Eichhöfer, et al
Licensed Content Date	Sep 13, 2017
Licensed Content Volume	56
Licensed Content Issue	43
Licensed Content Pages	6
Type of use	Dissertation/Thesis
Requestor type	Author of this Wiley article
Format	Print and electronic
Portion	Full article
Will you be translating?	Yes, including English rights
Number of languages	2
Languages	English, German
Title of your thesis / dissertation	Beiträge zur Zintl-Chemie der Elemente der 6. Periode im Festkörper und in Lösung
Expected completion date	Dec 2018
Expected size (number of pages)	350
Requestor Location	Philipps University of Marburg Hans-Meerwein-Straße 4 Marburg, Hessen 35032 Germany Attn: Philipps University of Marburg
Publisher Tax ID	EU826007151
Total	0.00 EUR
Terms and Conditions	

TERMS AND CONDITIONS

This copyrighted material is owned by or exclusively licensed to John Wiley & Sons, Inc. or one of its group companies (each a"Wiley Company") or handled on behalf of a society with

JOHN WILEY AND SONS LICENSE TERMS AND CONDITIONS

Nov 18, 2018

This Agreement between Philipps University of Marburg -- Niels Lichtenberger ("You") and John Wiley and Sons ("John Wiley and Sons") consists of your license details and the terms and conditions provided by John Wiley and Sons and Copyright Clearance Center.

License Number	4471870576856
License date	Nov 18, 2018
Licensed Content Publisher	John Wiley and Sons
Licensed Content Publication	Chemistry - A European Journal
Licensed Content Title	The Identity of "Ternary" A/Tl/Pb or K/Tl/Bi Solid Mixtures and Binary Zintl Anions Isolated From Their Solutions
Licensed Content Author	Niels Lichtenberger, Yannick J. Franzke, Werner Massa, et al
Licensed Content Date	Jul 23, 2018
Licensed Content Volume	24
Licensed Content Issue	46
Licensed Content Pages	9
Type of use	Dissertation/Thesis
Requestor type	Author of this Wiley article
Format	Print and electronic
Portion	Full article
Will you be translating?	Yes, including English rights
Number of languages	2
Languages	German, English
Title of your thesis / dissertation	Beiträge zur Zintl-Chemie der Elemente der 6. Periode im Festkörper und in Lösung
Expected completion date	Dec 2018
Expected size (number of pages)	350
Requestor Location	Philipps University of Marburg Hans-Meerwein-Straße 4 Marburg, Hessen 35032 Germany Attn: Philipps University of Marburg
Publisher Tax ID	EU826007151
Total	0.00 EUR
Terms and Conditions	

TERMS AND CONDITIONS

This copyrighted material is owned by or exclusively licensed to John Wiley & Sons, Inc. or one of its group companies (each a"Wiley Company") or handled on behalf of a society with

Einige Worte des Dankes

Hiermit möchte ich mich ganz herzlich bei all denjenigen bedanken, die mich in den letzten Jahren auf dem Weg zur Promotion begleitet haben. Es war eine wunderschöne Zeit und ich habe immer gerne Zeit auf der Arbeit verbracht. Dies wäre sicherlich anders gewesen, wenn die Atmosphäre im Labor und in der Gruppe nicht so positiv gewesen wäre.

Bei meiner Doktormutter Prof. Dr. Stefanie Dehnen möchte ich mich für das immerwährende Vertrauen, die stete Begeisterung für die Forschung und den Freiraum bei der Bearbeitung des Themas bedanken. Vielen Dank, dass ich in dieser Zeit so viel von dir lernen durfte.
Herrn Prof. Dr. Michael Gottfried danke ich für die Übernahme des Zeitgutachtens dieser Arbeit. Auch für seinen Beitrag zur Unterstützung meines Auslandsaufenthaltes in Los Alamos durch den DAAD möchte ich mich noch einmal herzlichst bedanken. Vielen Dank an Herrn PD. Dr. Ralf Tonner für die spontane Mitwirkung in der Prüfungskommission.
Während meiner Promotionszeit wurde ich durch mehrere Geldgeber finanziell unterstützt: Der MArburg University Research Academy danke ich für die Förderung durch ein Promotionsstipendium. Die Gesellschaft Deutscher Chemiker unterstütze mehrere Konferenzteilnahmen finanziell und hat so dazu beigetragen, dass ich viele großartige Wissenschaftlerinnen und Wissenschaftler treffen durfte. Dem Deutschen Akademischen Austauschdienst möchte ich für die Vergabe eines Kurzstipendiums zur Förderung meines Aufenthalts am Los Alamos National Laboratory und die Unterstützung meiner Teilnahme an der GRC - Inorganic Chemistry 2018 durch ein Kongressreisestipendium danken.
Den Serviceabteilungen des Fachbereichs Chemie, insbesondere den Abteilungen für Kristallstrukturanalyse und Massenspektrometrie sei für die vielen Stunden an Messzeit, die die Charakterisierung meiner Verbindungen ermöglicht haben, gedankt. Herrn Prof. Dr. Werner Massa soll an dieser Stelle noch einmal ausdrücklich für die Hilfestellungen bei besonderen kristallographischen Problemen gedankt sein. Auch die externen Kooperationspartner Florian Weigend, Rodolphe Clérac und Andreas Eichhöfer haben maßgebliche Anteile an der erfolgreichen Publikation der Ergebnisse. Vielen Dank dafür.

Robert „Deutsch-Bob“ Wilson war der beste Laborpartner, den man sich wünschen konnte! Ich werde die Diskussionen über Chemie, Politik und die Absurdität der Welt auf der Arbeit vermissen. Armin Eulenstein und Bastian Weinert, die

weiteren „Zintlaner“, haben immer für eine gute Stimmung im Labor gesorgt und waren gleichzeitig die zuverlässigsten Kooperationspartner.
Herr Doktor Niklas Rinn hat nicht nur, aber insbesondere zu Weihnachten eine gute Stimmung verbreitet. Zudem feiert er legendäre Geburtstage.
Ursula Siepe - dem guten Engel des Arbeitskreises - möchte ich an dieser Stelle noch einmal ganz besonders für ihre unvergleichlich positive Art und alle Hilfestellungen in den letzten Jahren danken. Ohne diese wäre der Arbeitskreis im universitären Verwaltungschaos versunken und wir würden vermutlich noch heute versuchen unseren ersten Dienstreiseantrag einzureichen. Genieß deinen wohlverdienten Ruhestand!
Isabell Nußbruch und Bettina Wagner haben so manche Kaffeepause sehr unterhaltsam gemacht. Vielen Dank dafür, dass ihr die guten Seelen des Arbeitskreises seid!
Lukas Guggolz danke ich für sehr stilvolle Cocktailabende und eine offene Tür bei sämtlichen Fragen zu Turbomole und zur Quantenchemie.
Johanna Heine möchte ich für ein offenes Ohr, hilfreiche Diskussionen und die nötige Portion Ablenkung von der Arbeit danken. Die Gewährung (politischen) Asyls in ihrem Büro war nicht selbstverständlich und hat es mir ermöglicht, mich sehr produktiv auf meine Arbeit zu konzentrieren. Dabei hat die einfache Frage „Kaffee?“ so manchen Morgen erträglicher gemacht. Danke dafür.
Carsten Donsbach danke ich für spannende Diskussionen zu unserem Lieblingsthema Kristallographie und seine verrückten Einfälle bei Laborproblemen. Du bist der vermutlich lustigste Schreibtischnachbar, den man sich vorstellen kann.
Auch allen nicht explizit erwähnten, aktuellen und ehemaligen Mitgliedern des Arbeitskreises und der Nachwuchsgruppen möchte ich für die schöne Atmosphäre in der Gruppe und die gemeinsame Zeit in und außerhalb des Labors danken.
Allen Vertiefern und Bachelorstudenten, die sich über die Jahre für die Freuden der *Zintl*-Chemie - zum Teil sehr zum Leidwesen von Bob - interessiert haben, möchte ich für die fleißige Mitarbeit im Labor danken.

I also want to thank several people at LANL, who have made my stay there as pleasant and enjoyable as it was. A big thank you to Stosh A. Kozimor, the craziest and most genious scientist I have met so far, for letting me join his group for five months. It was a memorable experience and I am very grateful that I was given this chance.
Rhiana Knope helped me to survive in the bureaucratic nightmare that is trying to work at LANL. Thank you, you are amazing! I could not have done it without your help.
A massive thank you to all past and current members of the 'KoMo-team' I had the honor to share the α-wing with: Laura M. Lilley, Ben Stein, Veronika Mocko, Sam Schrell, Kevin Bennett, David Woen, Anastasia Blake, and Sharon Bone. A very special mention has to go to Laura M. Lilley. You were the best roommate I could have asked for! I truly admire your courage to let me stay with you without knowing me at all. Thank you for early morning coffees, bike rides, long and short

climbing days, long lab days, your Spotify playlists, trips to Santa Fe, beers, barbeques, and just hanging out in the evenings. You made my stay in Los Alamos just so much better in every aspect and I look forward to seeing you again! Always remember: Angie (or whoever's in charge next) will always have you.
One big thank you to Andy Gaunt for the academic adoption, for letting me work in his glovebox and for trusting me that I would not put a hole in the glove. Conrad Goodwin for helping me getting started at ARF and in Andys box.
The climbing crew: Erik, Nick, Leslie, Rachel M., Adrian, Bob & Rachel and all the other climbers we met at the crags and the Y.

Allen Freunden, ob in Marburg, Bremen oder über ganz Deutschland verteilt, danke ich für die gemeinsam verbrachte Zeit.
Meiner Familie und insbesondere meinen Eltern möchte ich für die immerwährende Unterstützung danken. Es ist nicht selbstverständlich und bedeutet mir viel, dass ich mich nie sorgen musste.

Meiner Liebe Katharina gebührt ein ganz besonderer Dank!